

# SUPER PORPHYRY COPPER & GOLD DEPOSITS



A Global Perspective

VOLUME 2



**PGC**  
PUBLISHING

AUSTRALASIA | EURASIA

**SUPER PORPHYRY  
COPPER AND GOLD DEPOSITS  
A GLOBAL PERSPECTIVE**

**Volume 2**

Edited  
by  
**T M Porter**

**PGC  
PUBLISHING**

a division of  
**PORTER GEOCONSULTANCY PTY LTD**  
6 Beatty Street, Linden Park, SA 5065 Australia  
[www.portergeo.com.au/publishing](http://www.portergeo.com.au/publishing)

**Other titles in the Global Perspective series:**

- Porphyry and Hydrothermal Copper & Gold Deposits:  
A Global Perspective ISBN 0-908039-71-9
- Hydrothermal Iron Oxide Copper-Gold & Related Deposits:  
A Global Perspective - Volume 1 ISBN 0-9580574-0-0
- Hydrothermal Iron Oxide Copper-Gold & Related Deposits:  
A Global Perspective - Volume 2 ISBN 0-9580574-1-9
- Super Porphyry Copper and Gold Deposits:  
A Global Perspective - Volume 1 ISBN 0-9580574-2-7

Contents and abstracts may be browsed, and copies ordered on-line from:

**[www.portergeo.com.au/bookshop](http://www.portergeo.com.au/bookshop)**

**SUPER PORPHYRY COPPER AND GOLD DEPOSITS:  
A GLOBAL PERSPECTIVE  
Volume 2**

ISBN 0-9580574-3-5

First edition, October, 2005

**PGC  
PUBLISHING**

PORTER GEOCONSULTANCY PTY LTD

ABN 15 075 541 632

Trading as: PGC PUBLISHING

6 Beatty Street

Linden Park SA 5065 Australia

Phone: +61 8 8379 7397 Facsimile: +61 8 8379 7397

E-mail: [publishing@portergeo.com.au](mailto:publishing@portergeo.com.au)

Web page: <http://www.portergeo.com.au/publishing>

Printed in Australia

---

*Inclusion of a paper in this publication does not necessarily reflect endorsement of its contents by PGC Publishing, Porter GeoConsultancy Pty Ltd., their respective employees, officers or agents, or the editor. Readers should use their own judgement before using or applying any information herein. PGC Publishing, Porter GeoConsultancy Pty Ltd., their respective employees, officers and agents, and the editor, accept no responsibility for any damages or losses in any form that might result from the publication of, or as a result of reading or applying the information included in any part of this volume in any way what-so-ever.*

---

**Cover photograph:** *Upper benches of the Grasberg open pit, Papua, Indonesia, 1999. Photograph by T M Porter.*

**Contents**

	Page
<i>DEDICATION</i> .....	281
<i>PREFACE</i>	
<i>T. Michael Porter</i> .....	283
<i>AUSTRALASIA</i> .....	285
<b>The Porphyry Au-Cu Deposits and Related Shoshonitic Magmatism of the Palaeozoic Macquarie Volcanic Arc, Eastern Lachlan Orogen in New South Wales, Australia: A Review</b>	
<i>T. Mike Porter and Richard A. Glen</i> .....	287
<b>Grasberg Porphyry Cu-Au Deposit, Papua, Indonesia: 1. Magmatic History</b>	
<i>John T. Paterson and Mark Cloos</i> .....	313
<b>Grasberg Porphyry Cu-Au Deposit, Papua, Indonesia: 2. Pervasive Hydrothermal Alteration</b>	
<i>John T. Paterson and Mark Cloos</i> .....	331
<b>Porphyry-Style Mineralisation in the Ertzberg Diorite, Gunung Bijih (Ertzberg/Grasberg) District, West Papua, Indonesia</b>	
<i>Kurt C. Friehauf, Spencer R. Titley, and Stacie L. Gibbins</i> .....	357
<i>EURASIA</i> .....	367
<b>Multi-Million-Year Cyclic Ramp-up of Volatiles in a Lower Crustal Magma Reservoir Trapped Below the Tampakan Copper-Gold Deposit by Mio-Pliocene Crustal Compression in the Southern Philippines</b>	
<i>Bruce D. Rohrlach and Robert R. Loucks</i> .....	369
<b>Dexing Porphyry Copper Deposits in Jiangxi, China</b>	
<i>Rui Zongyao, Zhang Lisheng, Wu Chengyu, Wang Longsheng and Sun Xinya</i> .....	409
<b>A Tectonic Model for Porphyry Copper-Molybdenum-Gold Deposits in the Eastern Indo-Asian Collision Zone</b>	
<i>Hou Zengqian, Zhong Dalai, Deng Wanming and Khin Zaw</i> .....	423
<b>Porphyry Copper Deposits of the Urumieh-Dokhtar Magmatic Arc, Iran</b>	
<i>Alireza Zarasvandi, Sassan Liaghat and Marcos Zentilli</i> .....	441
<b>The Majdanpek Cu-Au Porphyry Deposit of Eastern Serbia: A Review</b>	
<i>Robin Armstrong, Dejan Kozelj and Richard Herrington</i> .....	453
<b>The Porphyry Cu-Au/Mo Deposits of Central Eurasia: 1. Tectonic, Geologic &amp; Metallogenic Setting and Significant Deposits</b>	
<i>Reimar Seltmann and T. Mike Porter</i> .....	467
<b>The Porphyry Cu-Au/Mo Deposits of Central Eurasia: 2. The Almalyk (Kal'makyr-Dalnee) and Saukbulak Cu-Au Porphyry Systems, Uzbekistan</b>	
<i>Igor M. Golovanov, Reimar Seltmann and Alexander A. Kremenetsky</i> .....	513
<b>Erdenetiin Ovoo Porphyry Copper-Molybdenum Deposit in Northern Mongolia</b>	
<i>Ochir Gerel and Baatar Munkhtsengel</i> .....	525
<i>BIOGRAPHY</i> .....	545
<b>Biographies of Principal Authors</b> .....	547

**Contents**

	Page
<i>DEDICATION</i> .....	1
<i>PREFACE</i>	
<i>T. Mike Porter</i> .....	3
<i>GENERAL</i> .....	5
<b>Cumulative Factors in the Generation of Giant Calc-Alkaline Porphyry Cu Deposits</b>	
<i>Jeremy P. Richards</i> .....	7
<b>Thermal History Analysis of Selected Chilean, Indonesian and Iranian Porphyry Cu-Mo-Au Deposits</b>	
<i>Brent I.A. McInnes, Noreen J. Evans, Frank Q. Fu, Steve Garwin, Elena Belousova, W.L. Griffin, Alfredo Bertens, Djadjang Sukarna, Sam Permanadewi, Ross L. Andrew and Katja Deckart</i> .....	27
<i>SOUTH AMERICA</i> .....	43
<b>The Andean Porphyry Systems</b>	
<i>Francisco Camus</i> .....	45
<b>Origin of Giant Miocene and Pliocene Cu-Mo Deposits in Central Chile: Role of Ridge Subduction, Decreased Subduction Angle, Subduction Erosion, Crustal Thickening, and Long-Lived, Batholith-Size, Open-System Magma Chambers</b>	
<i>Charles R. Stern and M. Alexandra Skewes</i> .....	65
<b>The El Teniente Megabreccia Deposit, the World's Largest Copper Deposit</b>	
<i>M. Alexandra Skewes, Alejandra Arévalo, Ricardo Floody, Patricio H. Zuñiga and Charles R. Stern</i> .....	83
<b>A Review of the Geology and Mineralisation of the Alumbrera Porphyry Copper-Gold Deposit, Northwestern Argentina.</b>	
<i>Steve C. Brown</i> .....	115
<b>The Escondida Porphyry Copper Deposit, Northern Chile: Discovery, Setting, Geology, Hypogene Mineralisation and Supergene Ore - A Review</b>	
<i>T. Mike Porter</i> .....	133
<b>Chuquicamata, Core of a Planetary Scale Cu-Mo Anomaly</b>	
<i>Alejandro Faunes, Fernando Hintze, Armando Siña, Héctor Véliz, Mario Vivanco and Geological Staff (of 2003)</i> .....	151
<b>Geology and Discovery of Porphyry Cu-Mo-Ag Deposits in the Collahuasi District, Northern Chile</b>	
<i>Glenton J. Masterman, David R. Cooke and Richard L. Moore</i> .....	175
<b>The Geology of the Antamina Copper-Zinc Deposit, Peru, South America</b>	
<i>Eric J. Lipten and Scott W. Smith</i> .....	189
<i>NORTH AMERICA</i> .....	205
<b>The Geologic History of Oxidation and Supergene Enrichment in the Porphyry Copper Deposits of Southwestern North America</b>	
<i>Sterling S. Cook and T. Mike Porter</i> .....	207
<b>Geology of the Bingham Mining District, Salt Lake County, Utah</b>	
<i>Charles H. Phillips, Edward D. Harrison and Tracy W. Smith</i> .....	243
<b>Porphyry Cu-Mo Deposits of the Highland Valley District, Guichon Creek Batholith, British Columbia, Canada</b>	
<i>W.J. McMillan</i> .....	259
<i>BIOGRAPHY</i> .....	275
<b>Biographies of Principal Authors</b> .....	277



### **Ross Lang Andrew 1948-2005**

This volume is dedicated to the memory of Ross Lang Andrew, one of the authors featured in this publication, who died peacefully at his home in Melbourne, Australia, in April 2005.

Ross was born in Hamilton, Scotland, in 1948. He wanted to be a geologist from the age of nine and realised his ambition in 1971, graduating from Glasgow University with a B.Sc. Honours. He completed his PhD in Mining Geology in 1979 at Imperial College, London. His thesis, "The geology, mineralogy and geochemistry of selected metal gossans in southern Africa", was the first of many published contributions to economic geology. Stints with Palabora Mining Company, JCI and Anglovaal added to Ross' southern African experience.

After moving to Australia in 1979, Ross, as a District Manager with CRA Exploration, led the team that discovered the Kintyre uranium deposit in Western Australia, establishing the existence of a new unconformity-vein style uranium province in the Proterozoic of the Great Sandy Desert. Here, in charge of a large team of young geologists and support staff involved in evaluation and regional exploration, Ross proved a much loved mentor of young professionals; a mantle that he carried throughout his life.

From here, his career took him to Melbourne in 1990, as a General Manager and Chief Geologist for CRA, subsequently Rio Tinto, responsible for project generation and evaluation around the world. His growing interest in porphyry style mineralisation led to the discovery of the Wafi Cu-Au Porphyry in PNG and subsequent evaluation over four years and the discovery of outcropping porphyry mineralisation in two locations in Mindanao, Philippines. During the next 15 years on his many excursions in the porphyry belts of the Americas, the Pacific Rim and elsewhere, Ross established himself in the porphyry fraternity as a highly regarded friend and professional.

Ross' diplomatic manner, language skills and respect for fellow professionals naturally lent him to negotiating entry to emerging exploration regions in the Russian Far East, Argentina, Vietnam, China, India and Iran. His passion for music, cycling, golf and cuisine were natural accompaniments to the friendships he formed wherever he went.

Ross met his wife Teri in Ireland in 1971 where, typically, he had been attending a geological conference. Realising very quickly that he had discovered somebody unique, he promptly proposed before leaving for a five month field excursion to Burma. Thus a life-long partnership and pattern were established. Ross and Teri were married in 1972 and their daughter Cath was born in South Africa in 1975. As a family they settled in Australia in 1979, initially in Karratha and Perth, and then in Melbourne.

Ross was enthusiastic about everything he did. His priority in life was his family, followed very closely by his love for playing guitar and listening to music, getting out on his bike, his model planes and hitting the little white ball. His love for the finer things of life, good food, fine wine and quality chocolate, was legendary.

Throughout his life Ross remained an inspiration to many friends and colleagues, particularly young research geologists. He continually encouraged geological enquiry and supported research with open minded generosity. He was a fine mentor, a technical expert and a great leader.

Ross leaves behind Teri, Cath and many friends and colleagues throughout the world. He will be sadly missed and fondly remembered.

**Bruce Harvey**  
*Rio Tinto Limited*



## PREFACE

T. Mike Porter  
Editor

*Porter GeoConsultancy Pty Ltd, Adelaide, South Australia*

Porphyry-style Cu-Au/Mo deposits are among the most sought after targets for both base and precious metal exploration in the world today. Of particular interest are the "super porphyry" copper and or gold deposits, because of their size, grade and ability to support large scale, long life, profitable operations.

The term "super porphyry" is interpreted loosely in this publication, relating in general to the largest deposits in any established porphyry province. For a discussion of the accepted terminology and size classification of large porphyry-style deposits, see the introduction section of Richards, (2005) in this publication.

These two volumes have been designed to provide an overview of the distribution, tectonic, geologic and metallogenic setting, and the characteristics of the world's largest porphyry-style Cu-Au/Mo deposits and the 'provinces' or 'belts' in which they occur. Most of the larger deposits covered contain in excess of 5 Mt, up to more than 75 Mt of Cu (or more than 750 t of Au). The result is a collection of 25 new papers, occupying 550 pages, that include overview papers on the occurrence of large porphyry systems, as well as descriptions of individual porphyry orebodies, districts that contain clusters of porphyry deposits and porphyry 'belts' or 'provinces' that embrace strings of such deposits. This has involved detail of some deposits that many would not rate as "super porphyries", but which provide an insight into the setting of "super porphyries" and the evolution of the provinces that contain such deposits.

Up to the 1960's there was an acceptance by many that porphyry copper deposits were restricted to late Cretaceous to early Tertiary porphyritic textured "granitic" intrusive associations that were localised in the U.S. "South-west", and in northern Chile and southern Peru, and were Cu-Mo orebodies (Gilmour, *et al.*, 1995). Since then however, it has been realised that porphyry-style deposits were formed throughout the geologic record and on all continents. Substantial deposits are found in the Proterozoic e.g., Haib in Namibia, southern Africa; and the 'porphyry affinity' quartz-vein network at Malanjand in India; through the Palaeozoic, e.g., the Ordovician Bozshakol deposit in Kazakhstan (see Seltmann and Porter, in this publication); the Ordovician Cadia deposits in Australia (see Porter and Glen, in this publication); the Devonian Oyu Tolgoi system in southern Mongolia (see Seltmann and Porter, in this publication); the Late Carboniferous Almalyk deposit in Uzbekistan (see Golovanov *et al.*, in this publication);

through the Mesozoic, e.g., the Jurassic Dexing deposit in south-eastern China (see Rui *et al.*, in this publication); during the Cretaceous and the Tertiary, e.g., many of the deposits in western North America in Mexico, the U.S. and Canada (see Phillips *et al.*; McMillan; Cook and Porter; - all in this publication) and in Chile, Argentina and Peru in South America (see Camus; Stern and Skewes; Brown; Skewes *et al.*; Porter; Faunes *et al.*; Masterman *et al.*; and Lipten and Smith; - all in this publication) to giant deposits in very young rocks, e.g., the Pliocene Grasberg system in Papua, Indonesia (see Paterson and Cloos, in this publication) and the similar aged Tampakan deposit in the Philippines (see Rohrlach and Loucks, also in this publication). This list emphasises the wide geographic and temporal spread of significant porphyry-style deposits.

The papers in these two volumes have all been invited, based on the editor's research and design, to provide the global perspective the title promises. They cover a comprehensive and representative selection of the most important deposits throughout the geologic time scale (except the Proterozoic) and the main porphyry belts of the world, and concentrate on descriptive detail. The authors were selected for their expertise and reputation pertinent to the subject of the paper they have been asked to prepare. The background and credentials of the principal authors to contribute, as well as 'corresponding author' contacts are listed in a 'Biography' section at the end of each volume. All papers have been carefully reviewed by the editor, an experienced geologist who has visited and studied most of the deposits included in the two volumes. Selected contributions were also submitted for external review, particularly those in which the editor is an author or co-author.

The papers have been grouped by volume and geographic region, namely those relating to *South America* (the Andean belt) and *North America* (the 'cordilleran' deposits) are in volume 1; while those within *Australasia* (deposits within and on the margins of the current Australian Plate) and *Eurasia* (the Southeast Asian Archipelago, the Tethyan Orogenic Belt and the deposits of central Eurasia) are in volume 2. A general grouping for non-geographic specific contributions, is included in volume 1. Within this framework, papers are arranged by progressive geographic location order along individual belts, while where more than one belt is found within the same region, papers from each belt are grouped consecutively. Specifically, within the Eurasia section, the first two chapters (Rohrlach and Loucks; and Rui *et al.*) relate to deposits on the western



margin of the Pacific Plate, while the next three (Hou *et al.*; Zarisvandi *et al.*; and Armstrong *et al.*) cover three representative segments spanning the length of the Tethyan (or Alpine-Himalayan) Orogenic Belt in the Himalayas of Tibet, in Iran, and the Balkans of south-eastern Europe respectively. The focus of the final three papers is the vast belt of Palaeozoic to Mesozoic deposits that stretches across central Eurasia from the Urals to the Pacific coast (Seltmann and Porter; Golovanov *et al.*; and Gerel and Munkhsengel).

#### *Conventions and Units*

All units are metric, using standard international abbreviations. Mass is expressed in grams (g), kilograms (kg), tonnes (t), thousands of tonnes (Kt), millions of tonnes (Mt) and billions of tonnes (Gt). Similarly, length (width, depth or diameter) is expressed in microns ( $\mu\text{m}$ ), millimetres (mm), metres (m) and kilometres (km). Absolute ages are recorded as millions of years (Ma) or billions of years (Ga) before the present, while age ranges are in millions of years (M.y. or m.y.) or thousands of years (K.y.). Grades are in percent (%) or grams per tonne (g/t). Gold contents are in tonnes (t). For those accustomed to ounces, 1 Moz = 31.10348 tonnes.

Spelling has been standardised in all papers to 'Commonwealth English' as applied in Australia, where the volumes are published, and as used (with some variations) in the majority of English speaking countries. This usage includes 'metres', 'kilometres', 'sulphide', 'mineralisation', 'mineralised', 'colour', 'grey', Archaean, and 'Palaeozoic'.

#### References

Gilmour P, Andrew R L, Bernstein M, Maxwell I, Morrissey C J, 1995 - Porphyry copper deposits: History, recent developments, economics; in Pierce F W, Bolm J G (Eds), *Porphyry Copper Deposits of the American Cordillera, Arizona Geol. Soc., Digest 20*, Tucson, pp 128-155.

For references to papers cited from this publication, see the 'Contents' page of the respective volume. The general reference to the volume(s) is:

Porter, T.M. (Ed.), 2005 - Super Porphyry Copper & Gold Deposits: A Global Perspective; *PGC Publishing*, Adelaide, v. 1 and 2.

# ***Australasia***

---



## **THE PORPHYRY Au-Cu DEPOSITS AND RELATED SHOSHONITIC MAGMATISM OF THE PALAEOZOIC MACQUARIE VOLCANIC ARC, EASTERN LACHLAN OROGEN IN NEW SOUTH WALES, AUSTRALIA, A REVIEW**

<sup>1</sup>T. Mike Porter and <sup>2</sup>Richard A. Glen

<sup>1</sup>*Porter GeoConsultancy Pty Ltd, Adelaide, South Australia*

<sup>2</sup>*Geological Survey of New South Wales, Maitland, NSW, Australia*

**Abstract** - Ordovician volcanic, volcanoclastic and intrusive rocks of calc-alkaline affinity in the Eastern Subprovince of the Lachlan Orogen were formed in the intraoceanic Macquarie Volcanic Arc. The Macquarie Arc was developed in response to west-dipping subduction along part of the boundary between eastern Gondwana and the proto-Pacific Plate and was situated on the Gondwana Plate, some 1000 km east of Precambrian continental crust. The intervening area was occupied by a back arc basin that developed on oceanic crust as the proto-Pacific Plate rolled back eastwards after the Middle Cambrian Delamerian Orogeny. Subsequent extension, strike-slip translation and thin-skinned tectonics have structurally dissected the single arc into four north to NNE trending structural belts of Ordovician calc-alkaline rocks that are separated largely by younger rift basins and in part by coeval craton-derived turbidites.

Two of the belts host substantial porphyry style gold-copper, and epithermal gold deposits. The currently exploited porphyry gold-copper deposits are localised in two tight clusters in the Cadia and Goonumbla districts, which are approximately 100 kilometres apart, and fall within a major, long-lived, NW- to WNW-trending, semi-continental scale, structural corridor known as the Lachlan Transverse Zone.

The Cadia district comprises four porphyry style deposits, Ridgeway, Cadia Hill, Cadia Quarry and Cadia East, which have a combined resource of 1210 Mt @ 0.75 g/t Au, 0.32% Cu with a total of 905 tonnes (29 Moz) of contained gold. These ore deposits are spatially associated with Late Ordovician to Early Silurian, shoshonitic, porphyritic monzonite to quartz-monzonite phases of the Cadia Igneous Complex (CIC), intruding Late Ordovician coarse volcanoclastic rocks of similar composition to the CIC. The intrusive complex is represented as a stock at Cadia Hill and Cadia Quarry, a narrow restricted pipe at Ridgeway and as a series of dykes at Cadia East. The ore deposits occur as a string of mineralised centres within, and elongated parallel to, a 7 km long, NW- to WNW-trending corridor of alteration and mineralisation that is up to 2 km in width and has been intersected by drilling to a depth of more than 1600 m. Mineralisation occurs as sheeted quartz-sulphide veins at Cadia Hill, Cadia Quarry and Cadia East, as stockwork quartz veins at Ridgeway and Cadia Quarry and as disseminations at Cadia East, and, depending on the deposit, is hosted by either the CIC intrusive rocks alone, or by both the intrusive and volcanoclastic wallrocks. Veins are mainly quartz-calcite with bornite, grading outwards to chalcocopyrite and pyrite. Alteration takes the form of an early sodic phase, overprinted by potassic alteration and pervasive propylitisation. Individual veins have selvages of potassic and calc-potassic alteration. Skarn bodies are found in adjacent carbonate bearing units, while phyllic alteration is generally restricted to late stage faults.

The Goonumbla district includes four economic deposits, Endeavour 22, 26, 27 and 48, hosted by Early Silurian shoshonitic intrusive and Late Ordovician volcanoclastic rocks of the Goonumbla Igneous Complex and lie within a 22 km diameter circular structure that embraces a series of mineralised centres. The four deposits had a combined pre-mining resource of 132 Mt @ 1.1% Cu, 0.5 g/t Au. Each is centred on a separate, narrow, pipe-like, vertical, quartz monzonite porphyry complex comprising up to nine intrusive phases. These intrusive complexes have lateral dimensions in the order of 50 to 150 m and minimum vertical extents of 600 to 900 m. The associated ore zones are up to 400 m in diameter at a 0.5% Cu equivalent cutoff. Main stage mineralisation at all four deposits is associated with the same K feldspar quartz monzonite porphyry and augite-K feldspar quartz monzonite porphyry intrusive phases and is characterised by multiple generations of stockwork and sheeted quartz, K feldspar, bornite, chalcocopyrite and gold-bearing veins. Early Stage pervasive biotite-magnetite and propylitic alteration is overprinted by Main Stage mineralised veins that have halos of early K feldspar and later sericite-hematite. Sulphides are zoned from proximal bornite, through bornite and chalcocopyrite, to chalcocopyrite and peripheral pyrite.

## Introduction

Numerous examples of well-preserved porphyry style copper-gold, copper-molybdenum and molybdenum mineralisation have been recognised from the Tasmanides of eastern Australia since the late 1950s. All have been either: i). of lower Palaeozoic age, principally Ordovician to Silurian, in the Lachlan Orogen of New South Wales, ii). associated with upper Palaeozoic intrusives, particularly those of Permo-Carboniferous age, emplaced to the west of the Bowen Basin in north Queensland, or iii). Permian to Triassic in the New England Orogen in northeastern New South Wales (NSW) and eastern Queensland. While the same magmatic episodes also produced epithermal gold deposits that have been economically exploited in all of these regions, none of the known porphyry style mineralisation had been mined on a significant scale until the development in 1993 of the Northparkes operation, based on the Endeavour deposits.

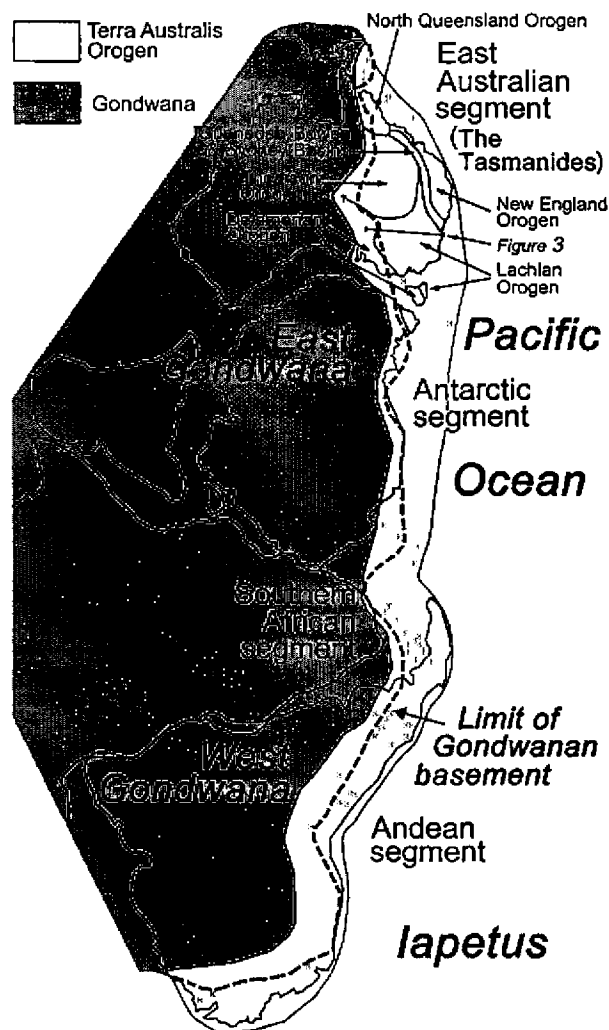
Porphyry gold-copper deposits are currently in commercial production in two districts in eastern Australia. Both have alkalic affiliations and are hosted by monzonitic and monzodioritic intrusions emplaced into Late Ordovician shoshonitic magmatic rocks of the Macquarie Volcanic Arc

in the Eastern Subprovince of the Lachlan Orogen, New South Wales.

The larger of these, the Cadia Valley Operations of Newcrest Mining Limited, is located some 20 km south of the city of Orange in an area of well developed pre-existing infrastructure, 200 km west of Sydney (Figs. 2 and 4). It comprises four deposits, Cadia Hill, Cadia Extended (previously known as Cadia Quarry), Ridgeway and Cadia East, which are embraced by a 7 km long, WNW-trending corridor of alteration and mineralisation. As at June 2004, the combined resource contained within the four deposits was 1210 Mt @ 0.75 g/t Au, 0.32% Cu, for a total of 905 tonnes (29 Moz) of contained gold (Newcrest 2003; Newcrest 2004). These resources place the operation in the top 10 largest known gold-rich porphyry districts in the world (Cooke *et al.*, 2002).

Current operations include: i). a large composite open pit removing over 100 Mt of ore and waste per annum, based on the Cadia Hill and Cadia Extended deposits, including +17 Mt of ore per annum at a head grade of around 0.7 g/t Au, 0.16% Cu, and ii). an underground, sub-level cave mine at Ridgeway, extracting +5 Mt of ore at a head grade of 1.96 g/t Au, 0.67% Cu. The Cadia Hill open pit commenced mining in 1997, while the Ridgeway underground mine was commissioned in 2002 (Newcrest Mining presentation, 2004).

The second district is exploited by Northparkes Mines at Goonumbra, approximately 100 km WNW of the Cadia Valley Operations and 30 km NW of the city of Parkes in NSW. This operation is based on four deposits, Endeavour 22, 26, 27 and 48, which are distributed over an interval of 5 km. Each is associated with a separate, narrow, pipe-like quartz monzonite porphyry complex. These deposits are members of a group of eleven mineralised centres recognised within a 22 km diameter circular feature defined by aeromagnetism and gravity (Heithersay *et al.*, 1990). The pre-mining resource in these four deposits totalled 132 Mt @ 1.1% Cu, 0.5 g/t Au (Lickfold *et al.*, 2003). Following initial open pit operations at Endeavour 22 and 27 beginning in 1993, an underground block cave mine was established at Endeavour 26, which during 2001 produced 5.425 Mt of ore with a head grade of 1.1% Cu, 0.32 g/t Au (Rio Tinto, 2002). Lift 1 of the block cave commenced mining in 1997 and was 'tailed off' in 2002-03, with Lift 2 scheduled to commence operation in 2004 (Rio Tinto, 2003). Endeavour 48 is the subject of a pre-feasibility study which commenced in 2002 (Lickfold *et al.*, 2003).



**Figure 1: Location of the Tasmanides and Lachlan Fold Belt within the late Neoproterozoic to late Palaeozoic Terra Australis Orogen on the margin of the super continent Gondwana. See Fig. 2 for the location of the Macquarie Arc. Modified after Cawood, (2005).**

### Editors Note:

The purpose of this paper is to provide up to date information on the regional and local setting of the most important of the known and mined porphyry gold and copper deposits within the Tasmanides of eastern Australia, and to describe the geology, alteration and mineralisation of each of the districts and individual ore deposits.

While R.A. Glen has contributed original material to the "Tectonic & Geological Setting" section, the remainder of the paper is a review of the most recently published information on the Cadia Valley and Endeavour group of deposits, largely drawn from Holliday *et al.*, (2002), Wilson *et al.*, (2003) and Lickfold *et al.*, (2003), complemented by a range of other sources. Other than the section detailed above, there is **no original input from the authors**, with attribution to the source for all information either within or at the end of each paragraph.

## Tectonic & Geological Setting

The Ordovician Macquarie Volcanic Arc lies within the Eastern Subprovince of the Lachlan Orogen, one of the constituents of the Tasmanides of eastern Australia. The Tasmanides occupy the eastern third of Australia, fringing Precambrian cratons to the west. They record the rifting of a supercontinent in the Neoproterozoic, as the proto-Pacific Ocean opened, followed by convergent margin activity that lasted from the late Middle Cambrian (~520 Ma) until the Middle Triassic (~230 Ma) and the commencement of the Mesozoic Gondwanide Orogeny (Cawood 2005; Glen 2005).

The Tasmanides formed one sector or segment of the proto-Pacific margin of Gondwana that stretched almost 20 000 km, from Papua New Guinea southwards to Tasmania and New Zealand (Tuhua Orogen), into Antarctica (Ross Orogen), and then northwards up the Antarctic Peninsula into the western margin of South America to what is now northern Colombia (Fig. 1) (Cawood 2005, Glen 2005). Cawood (2005) called this the Terra Australis Orogen. It overlapped the Precambrian cratonic masses of Gondwana on one side and was bounded by proto-Pacific Ocean on the other margin (Cawood 2005).

The key point of the Tasmanides is that they record interaction between Gondwana and the proto-Pacific Plate and are therefore accretionary. The proto-Pacific Ocean never closed. Several authors (Crook, 1969; Crawford *et al.*, 2003; Cawood, 2005; Glen, 2005) have recognised that this contrasts with the classical textbook orogenic belt that developed by the opening and closing of an ocean basin (the Wilson cycle with its continent-continent collision).

The Tasmanides are divided into five orogenic belts, as well as the Sydney-Gunnedah-Bowen Basin system (Glen 2005) (Fig. 1). In the south, the Delamerian Orogen occupies eastern South Australia, western New South Wales and Victoria, and western Tasmania (where it is also known as the Tyennan Orogen). It passes eastwards into the Lachlan Orogen, which extends to the Tasman Sea in Victoria and southern New South Wales, and northeast into the Thomson Orogen across a concealed and poorly understood, curvilinear east-west boundary. Further to the northeast, the Lachlan Orogen is bounded by the Sydney and Gunnedah Basins, which in turn pass eastwards into the New England Orogen. The Thomson Orogen is almost completely obscured by the Great Australian Basin. It passes eastwards into the Bowen Basin and northwards into the North Queensland Orogen.

Although there is a general tendency for younger rocks to occur in the east, reflecting a stepping out of orogenic activity (Powell 1983), old strata are found in even the most outboard belts, the New England Orogen and the North Queensland Orogen (Glen 2005). Thus the North Queensland Orogen is built on Neoproterozoic inliers and its evolution extended from the Ordovician into the Triassic. The New England Orogen was probably developed, in part, on Precambrian igneous crust and contains an early Cambrian and Ordovician history, despite its major development as a convergent margin arc-forearc basin-

accretionary complex system from the Late Devonian to the Triassic. Glen (2005) suggested that the early Palaeozoic strata were rifted-off fragments formed during rollback of the proto-Pacific Plate following the Delamerian Orogeny.

The Tasmanides reach a maximum width of ~1600 km in southeastern Australia, but only 200 km in Far North Queensland in the North Queensland Orogen, although rocks of either the North Queensland or northern New England Orogens occur in islands in the Coral Sea (summary in Glen 2005). The greater width in the south has been attributed to i) the opening and filling of a large back-arc basin (the Wagga Basin) in the Ordovician as a consequence of ocean retreat of the proto-Pacific Plate after the Delamerian Orogeny, and ii) to crustal extension leading to rifting and granite emplacement resulting from further ocean retreat of the Pacific Plate following the earliest Silurian Benambran Orogeny (Glen 2005).

### Lachlan Orogen

The Lachlan Orogen extends from eastern Tasmania, through Victoria to New South Wales, where it occupies much of the state. The western boundary with the Delamerian Orogen is largely obscured by the Tertiary Murray Basin and the Great Australian Basin, but is exposed in Western Victoria. Although the east-dipping Moyston Fault has been accepted until recently as the surface expression of the boundary (VandenBerg *et al.*, 2000; Korsch *et al.*, 2002), results of recent Ar-Ar dating by Miller *et al.*, (2004) suggest that the Avoca Fault, ~100 km further east, may be the actual boundary (Glen 2005).

The eastern boundary with the largely younger New England Orogen is obscured by the coal-rich Permian to Triassic Sydney and Gunnedah Basins, although deep seismic reflection profiling indicates that the crust of the Lachlan Orogen extends east under the foreland fold-thrust belt of the New England Orogen (Glen, Korsch *et al.*, 1993; Korsch, Wake-Dyster *et al.*, 1993). The northern margin with the Thomson Orogen (largely in Queensland) lies beneath the Mesozoic sediments of the Great Australian Basin and is inferred to be a suture marked by early Palaeozoic oceanic and island arc igneous rocks (Glen 2005).

The Lachlan Orogen is a complex orogenic belt, different to classical orogenic belts that have a well defined foreland fold-thrust belt inboard of a more complex higher grade internal zone. Its evolution can best be described in terms of cycles.

### Delamerian Cycle

The Delamerian cycle is best represented in the Delamerian Orogen, which underwent development from a rifted and passive margin in the Neoproterozoic, to a convergent margin that involved accretion of boninitic forearc crust and one or more arcs in the late Middle Cambrian (e.g. Crawford and Berry, 1992). The Delamerian Orogeny was followed in western Victoria by post-collisional volcanism and deposition of Late Cambrian turbidites of the Glenthompson and St Arnaud Groups (VandenBerg *et al.*, 2000; Crawford *et al.*, 2003; Miller *et al.*, 2004; Glen 2005).

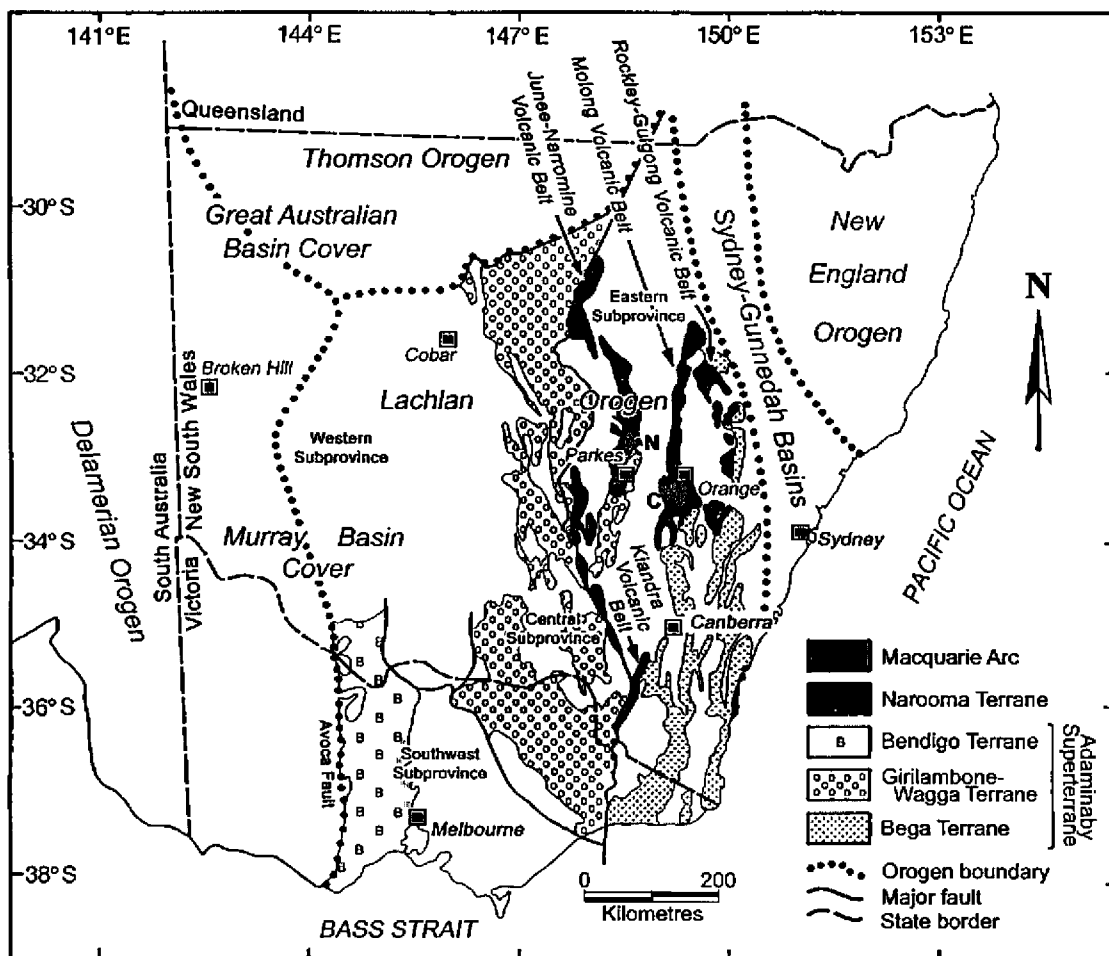


Figure 2: Distribution and setting of the Ordovician to Early Silurian volcanic (and intrusive) rocks of the Macquarie Volcanic Arc in the Eastern Subprovince of the Lachlan Orogen, New South Wales, and their context within the tectonic framework of southeastern Australia. These are represented by the Junee-Narromine, Molong, Rockley-Gulgong, and Kiandra volcanic belts. See Fig. 1 for location and continental scale setting and text for discussion. Cross picks show the Cadia Valley (C) and Northparkes (N) operations.

In the Lachlan Orogen, the Delamerian cycle is represented by Cambrian mafic, ultramafic and related rocks that are found in Victoria as several belts of greenstone that occur in the hangingwall of major thrusts, and underlie Ordovician turbidite packages (VandenBerg *et al.*, 2000).

#### Benambran Cycle

This cycle extends from the base of the Ordovician until the Llandoveryan in the Early Silurian, when it was terminated by the multistage Benambran Orogeny (Glen 2005; Glen *et al.*, 2005). Several contrasting Ordovician lithotectonic associations are divided into separate tectonostratigraphic terranes (e.g. Glen 2004; 2005; Fig. 6).

i) *Adaminaby Superterrane*: This superterrane is spread across the four subprovinces of the Lachlan Orogen and is divided into three terranes that are restricted in outcrop to specific subprovinces. In the Eastern Subprovince, the *Bega Terrane* consists of the Early-Middle Ordovician Adaminaby Group, overlain by the Late Ordovician Bendoc Group, consisting largely of starved shales. In the Central Subprovince, the *Girilambone-Wagga Terrane* comprises the Early-Middle Ordovician Girilambone and Wagga Groups overlain by the Bendoc Group. Late Ordovician shales are largely missing from

the *Bendigo Terrane* of the Southwestern Subprovince, where Early-Middle Ordovician turbidites thin eastwards and are locally overlain by Late Ordovician turbidites (VandenBerg *et al.*, 2000). In all three subprovinces, turbidites consist of slates, local cherts, siltstones and quartz-rich sandstones containing minor amounts of detrital feldspar and white mica, and which were derived from the Delamerian-Ross Craton to the west and south (Turner *et al.*, 1996).

- ii) *Macquarie Arc*: an intraoceanic island arc developed, discontinuously, from the earliest Ordovician through to the Llandoveryan (Early Silurian). This arc is described in more detail below.
- iii) *Narooma Terrane*: A terrane of chert passing up into argillite, siltstone and sandstone that accumulated on the floor of the proto-Pacific Plate from the Middle Cambrian until the late Ordovician, before being accreted to the Bega Terrane in the Benambran Orogeny (Glen *et al.*, 2004)
- iv) Basalt and mafic schists with MORB chemistry, near major faults east and west of the Junee-Narromine Volcanic Belt. This lithotectonic association is inferred to represent MORB-like tholeiitic basalts developed in a back arc setting west of the Macquarie Arc (Glen 2004).

- v) A single outcrop of limestone at Waratah Bay in eastern Victoria (VandenBerg *et al.*, 2000).
- vi) Zoned mafic-ultramafic complexes (Fifield Complexes) of inferred Late Ordovician age, intruding the Girilambone-Wagga Terrane and lying west of the Macquarie Arc (Suppel and Barron, 1986).

#### *Tabberabberan Cycle*

This cycle reflects development of the Lachlan Orogen in a back arc setting, as a consequence of rapid retreat of the proto-Pacific plate to the east after the Benambran Orogeny (e.g. Scheibner & Basden 1998; Glen 2005). The cycle is characterised by the formation of sedimentary basins (some filled with felsic volcanic and volcanoclastic rocks, and limited amounts of mafic volcanic rocks), their flanking shallower-water shelves, and the emplacement of large amounts of granites, many of which are elongated north-south and organised into major batholiths. Silurian to Middle Devonian basins are most common in the Eastern Subprovince. Multiple cycles of basin fill suggest these originated as extensional or transtensional basins. The Tabberabberan Cycle was terminated by the Middle Devonian Tabberabberan Orogeny dated at ~380 Ma. Earlier deformation around the Silurian-Devonian boundary, the Bindi Deformation, flanks the Kiandra Volcanic Belt, and seems to reflect strike-slip movement on major linked faults (Glen 2005).

#### *Kanimblan Cycle*

This cycle was synchronous with convergent margin activity in the New England Orogen to the northeast. High level S- and I-type granites and related volcanic rocks mark the lower part of the cycle in Victoria (VandenBerg *et al.*, 2000). To the north in central NSW, early rifting led to formation of A-type volcanic rocks and emplacement of A-type granites. In both areas, the bulk of the cycle is represented by deposition of a thick (~4 km) blanket of shales, siltstones and sandstones of the dominantly continental Lambie Facies that extends from the South Australian border to the Tasman Sea. The ~340 Ma (Early Carboniferous) Kanimblan Orogeny deformed all older units, but is best deciphered from the Lambie Facies. Deformation varies from kilometre scale wavelength folds in the Central Subprovince, to imbricate tight to isoclinal synclines in the Eastern Subprovince where they lie in the footwalls of major thrusts (Glen 1992). Post-orogenic effects are restricted to the emplacement of the cross-cutting Bathurst granites in the eastern part of the subprovince that were emplaced between 340 and 320 Ma (Glen 2005).

#### *The Macquarie Arc*

The Macquarie Volcanic Arc, which lies within the Eastern Subprovince of the Lachlan Orogen, is an intra-oceanic island arc developed on the Gondwana Plate in response to westwards subduction of the proto-Pacific Plate (Fig. 3) (Glen *et al.*, 1998; Glen *et al.*, 2003). Ordovician andesitic and basaltic rocks, particularly in a meridional zone passing through Orange and Molong, had been interpreted as products of Ordovician subduction in some of the earliest plate tectonic models of the Lachlan Orogen (e.g., Oversby, 1971; Solomon and Griffiths, 1972; Scheibner, 1973).

Wyborn (1988, 1992) documented the shoshonitic character of many of these volcanics, and used their high K- contents to discount previous models of arc formation during Ordovician subduction. He suggested instead, that these volcanics were formed by Ordovician melting (due to asthenospheric upwelling) of lithosphere enriched in incompatible elements during Cambrian subduction. In a different model, Scheibner (1987) and Scheibner & Basden (1998) suggested that the shoshonitic nature of the volcanic rocks indicated the presence of Precambrian continental substrate. However, Glen *et al.*, (1998) showed that only the youngest parts of the arc were shoshonitic and older parts were K-rich calc-alkaline rocks similar to those found in other island arcs.

Intermediate and mafic volcanic, volcanoclastic and intrusive arc rocks occur in four belts in the Eastern Subprovince. Three in central NSW, namely: i). the western most *Junee-Narromine Volcanic Belt*; ii). the central *Molong Volcanic Belt*; and iii). the eastern *Rockley-Gulgong Volcanic Belt*; and one close to the NSW-Victoria border, iv). the *Kiandra Volcanic Belt* (Figs. 3 & 4) (Glen *et al.*, 1998; Holliday, *et al.*, 2002). These are structural belts, reflecting the combined effects of the Benambran, Tabberabberan and Kanimblan contractional orogenies, and importantly, crustal extension from the Early Silurian to the Middle Devonian (Glen *et al.*, 1998).

Whole rock geochemistry from a recent CODES-NSW Geological Survey study (summarised by Glen *et al.*, 2003, Glen *et al.*, 2004) confirmed the suggestion that these belts formed from a single arc (Crawford *et al.*, in press) which has undergone multiple contractional deformation and Palaeozoic extension and dislocation. Glen *et al.*, (1998), suggested that the western Junee-Narromine Volcanic Belt represented the core of the arc and the eastern two belts, the Molong and Rockley-Gulgong, are the visible parts of a large volcanoclastic apron, with lesser centres, and are not primary palaeogeographic features. Data, particularly that from the Junee-Narromine and western and central parts of the Molong Volcanic Belts, show that the arc evolved episodically over a period of ~50 Ma, with three pulses of igneous activity, separated by two significant hiatuses in volcanic activity (Glen *et al.*, 2003; Percival and Glen 2005) (Fig. 3). These are:

- Pulse 1*, Early Ordovician, from ~489 to 474 Ma, followed by a ~8 Ma hiatus;
- Pulse 2*, Middle Ordovician, from 466 Ma, and variably ending between 458 and 455 Ma across the arc, succeeded by a ~5.5 Ma hiatus in the west only; and
- Pulse 3*, Late Ordovician to earliest Silurian, variably commencing between 458 and 450 Ma in different parts of the arc and persisting to ~435 Ma.

In the eastern part of the Molong Volcanic Belt, and in the Rockley-Gulgong Volcanic Belt, pulses 2 and 3 are not separated by a discernible hiatus in volcanism as occurs to the west. While the first pulse has not been recognised in the Rockley-Gulgong Volcanic Belt, ~475 Ma cherts, similar to those in the other belts, were reported by Murray and Stewart (2000).



Lavas from the three igneous pulses have positive  $\epsilon Nd$  values and primitive Pb/Pb ratios (Glen *et al.*, 1998; Carr *et al.*, 1995; Glen *et al.*, 2003), indicating development on igneous substrate and precluding continental basement. Because the pulse 1 volcanics are chemically unlike primitive intra-oceanic arc lavas, basement may consist of a rifted and thinned fragment of forearc igneous crust that was accreted to the Delamerian Orogen during the Delamerian Orogeny (Glen *et al.*, 2003; Crawford *et al.*, 2005) (Fig. 3). The hiatus in volcanism around 470 Ma was interpreted as reflecting back-arc spreading, and the hiatus at 450 Ma as reflecting the effects of either back arc spreading or shallow subduction caused by a buoyant seamount (Glen *et al.*, 1998) being subducted (Fig. 3). The Late Ordovician pulse volcanics are everywhere shoshonitic, representing melting of an enriched mantle source which was apparently absent (or untapped) during the Middle Ordovician (Glen *et al.*, 2003).

*Intrusive Porphyries*

Most gold-copper deposits in the Macquarie Arc are associated with porphyritic intrusives that range in composition from monzonitic to monzodioritic and monzogabbroic. Glen *et al.*, (2003) subdivided the intrusions of the Macquarie Arc into four temporal groups which they related to the evolution of the arc.

**Group 1** - high-K calc-alkaline intrusions aged ~484 Ma, emplaced towards the end of the first pulse of active volcanism in the Junee-Narromine Volcanic Belt, but with no known associated mineralisation.

**Group 2a** - a high-K magmatic suite, comprising mainly

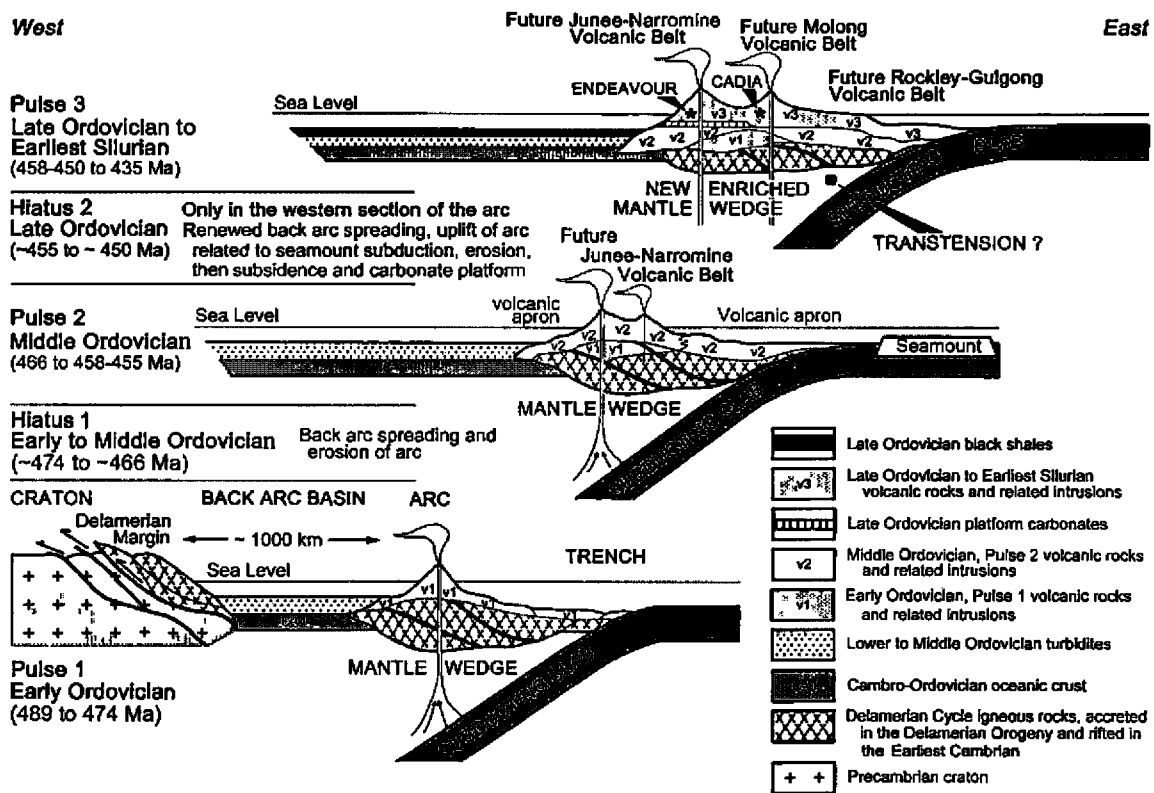
monzogabbroic and monzonitic rocks, chemically little different from Group 1, but emplaced at ~465 Ma in the Junee-Narromine Volcanic Belt, close to the initiation of the second pulse of volcanism.

**Group 2b** - a second group of intrusive rocks in the Junee-Narromine Volcanic Belt that was emplaced towards the end of the second pulse of volcanism at ~455 Ma.

**Group 3** - the Copper Hill Suite, which intruded at ~450 to ~445 Ma, at the beginning of the third pulse of volcanism, is represented in all of the volcanic belts by small, predominantly dacitic porphyries (but with some dioritic and gabbroic examples). They have medium-K calc-alkaline affinities and commonly have quartz and hornblende phenocrysts in porphyries with >60% SiO<sub>2</sub>. This suite is associated with significant mineralisation in the Molong Volcanic Belt (e.g. the Copper Hill and Cargo porphyry prospects) and in the Narromine Igneous Complex of the Junee-Narromine Volcanic Belt.

**Group 4** - emplaced at the end of the third pulse of volcanism in all but the Kiandra Volcanic Belt. These mainly porphyritic intrusions are all high-K, alkalic to shoshonitic, monzodioritic to monzonitic and are comagmatic with most of the Late Ordovician volcanic rocks in the arc. Porphyries belonging to Group 4 host the Cadia Valley gold-copper and Endeavour copper-gold deposits.

Recognition of these different temporal groups suggest that intrusions were not emplaced during steady-state subduction, but during critical events in the evolution of the arc (Glen *et al.*, 2003), when the angle of subduction



**Figure 3:** The plate tectonic evolution of the Macquarie Arc and setting of the Cadia Valley and Endeavour (Goonumbla District) porphyry copper-gold deposits before rifting in the Silurian and Devonian. See Fig. 1 for the section of the Lachlan Orogen this diagram represents.

shallowed, or subduction ceased as a consequence of either back arc spreading, or jamming of the subduction zone. Glen *et al.*, (2003) argued that porphyries were not emplaced at times of maximum tension, when they would have vented to the surface and not fractionated. Rather, they were emplaced in a compressive stress regime that allowed magmas to pond and fractionate in high-level chambers in crust thick which was strong enough to hold such chambers. To form a deposit, these chambers had to subsequently be breached, either by fluid build-up, or by reduction in differential stress, focussed along new or pre-existing fractures. Conditions for breaching established magma chambers were initiated by transient switches in the stress state of the Macquarie Arc during critical events in the evolution of the arc, as listed above. Significantly, the mineralised Group 4 porphyries were emplaced after the cessation of volcanism, during the Benambran Orogeny and during formation of transient extensional or transtensional basins. The regional compression that prevented Llandoverian magmas venting to the surface was provided by deformation within the arc and by the weight of overlying, structurally thickened volcanic and sedimentary rocks (Glen *et al.*, 2003).

Previous workers (Wyborn 1992; Mueller *et al.*, 1992, 1993, 1995) have shown that magmas with a high oxidation state were more likely to produce gold-enriched porphyry systems. This is because highly oxidised magmas transport gold and copper more readily than their reduced counterparts since sulphur is present as  $\text{SO}_2$  rather than  $\text{H}_2\text{S}$ . Magmas containing  $\text{H}_2\text{S}$  tend to form immiscible sulphide liquids that scavenge gold, copper and other metals and retain them in the igneous source regime. Shoshonites are thus an especially favourable oxidised magma composition for the formation of gold rich porphyry copper-gold mineralisation. Such magmas are particularly common in the third pulse of magmatism, and Group 4 porphyries host the known key porphyry copper-gold deposits in the Macquarie Arc. Group 3 porphyries are less well endowed in gold and copper than those of the shoshonitic Group 4, although they have a similar signature to Andean host porphyries in Chile (Glen *et al.*, 2003).

## Distribution of Cu & Au Mineralisation

The Late Ordovician to Early Silurian igneous complexes of the Macquarie Arc host a range of copper-gold and gold mineral occurrences and deposits (see Fig. 4), including both porphyry and epithermal styles.

The largest cluster and most economically significant are the *Cadia Valley* deposits (including *Cadia Hill*, *Cadia Quarry*, *Cadia East* and *Ridgeway*) described later in this paper, which are within the Molong Volcanic Belt (MVB). Other deposits of note in the MVB include the sub-economic, calc-alkaline (not shoshonitic) *Copper Hill* and *Cargo* porphyry prospects and the *Junction Reefs* iron-gold skarn. *Copper Hill* has a resource of 6.6 Mt @ 0.8% Cu, 0.8 g/t Au (Golden Cross Resources web site, 2004) within 34 Mt @ 0.54 g/t Au, 0.43% Cu, embraced in turn by a larger body of porphyry style mineralisation with grades of 0.1 to 0.15% Cu (Scott, 1978, Chivas and Nutter, 1975). *Cargo* (Richardson, 1976) comprises simple gold rich pyrite-chalcocopyrite veins with a current resource of 3.7 Mt @ 1.24 g/t Au (Golden Cross Resources web site, 2004). *Junction Reefs* had an initial reserve of 1.4 Mt @ 4.1 g/t Au prior to mining (Overton, 1990; Gray *et al.*, 1995).

The less well exposed Junee-Narromine Volcanic Belt to the west, also hosts significant deposits and occurrences. These include the *Endeavour* porphyry copper-gold deposits of the Goonumbla District described in this paper (Heithersay *et al.*, 1990; Heithersay & Walshe, 1995; Lickfold *et al.*, 2003 and references cited therein), the high sulphidation *Peak Hill* gold deposit with 16 Mt @ 1.3 g/t Au (Alkane Exploration Ltd web site), the low sulphidation carbonate-base metal-gold *Cowal* or *Endeavour 42* (Miles & Brooker, 1998) deposit with a total reserve+resource of 111 Mt @ 1.13 g/t Au (Barrick Gold web site, 2004), including 66 Mt @ 1.5 g/t Au (McInnes *et al.*, 1998), the high sulphidation *Gidginbung* gold deposit at Temora (Thompson, *et al.*, 1986), which had pre-mining reserves of 4.5 Mt @ 2.5 g/t Au, 5.4 g/t Ag (Lindhorst & Cook, 1990) and the currently sub-economic *Marsden* porphyry prospect with 115 Mt @ 0.3 g/t Au, 0.5% Cu (Newcrest Mining).

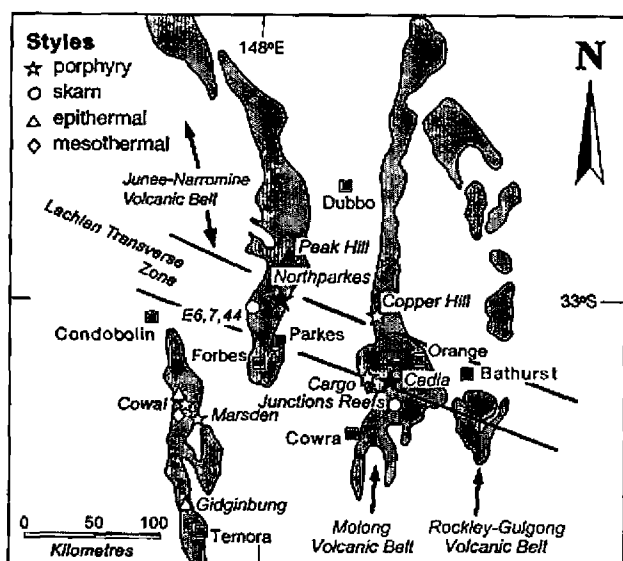


Figure 4: Copper-gold mineral occurrences of the Macquarie Volcanic Arc in the Eastern Subprovince of the Lachlan Orogen (refer to Fig. 2). The Junee-Narromine Volcanic Belt hosts the *Endeavour* 22, 26, 27 & 48 porphyry copper-gold deposits at Northparkes; porphyry copper-gold mineralisation at *Marsden*; high-sulphidation epithermal gold mineralisation at *Peak Hill* and *Gidginbung*; intrusion-related gold-zinc mineralisation at *Lake Cowal*; and lead-zinc skarn deposits at *E6*, *E7* & *E44*. The Molong Volcanic Belt hosts the *Cadia-Ridgeway* cluster of gold-copper deposits at *Cadia* and the *Copper Hill* and *Cargo* porphyry gold-copper deposits. Filled symbols = mines; outline symbols = prospects. The Lachlan Transverse Zone is a crustal linear feature that appears to have controlled Late Ordovician igneous complexes and also the distribution of the Late Ordovician porphyry copper-gold deposits (Glen and Walshe, 1999). Based on information from Holliday *et al.*, (2001), Wilson *et al.*, (2003) and Lickfold *et al.*, (2003).

Table 1: Published resources at the Newcrest Mining Cadia Valley Operations deposits

Deposit	Mt of ore	Au (g/t)	Cu %	Contained Au (t)	Contained Cu (Mt)	Mined from
<b>Cadia Hill</b>						1997
Pre-mine total resource <sup>1</sup>	352	0.63	0.16	221.3	0.56	
Total resource, June 2003 <sup>3</sup>	260	0.7	0.16	180.4	0.42	
<b>Ridgeway</b>						2002
Pre-mine total resource <sup>2</sup>	54	2.5	0.77	132.6	0.42	
Total resource, June 2003 <sup>3</sup>	78	1.96	0.67	149.3	0.52	
<b>Cadia Quarry</b>						2001
Pre-mine total resource <sup>2</sup>	40	0.40	0.21	16.0	0.08	
Total resource, June 2003 <sup>3</sup>	50	0.40	0.23	21.7	0.11	
<b>Cadia East – Open pit</b>						Un-mined
Total resource, June 2004 <sup>4</sup>	300	0.46	0.37	133.7	1.11	
<b>Cadia East – Underground</b>						Un-mined
Total resource, June 2004 <sup>4</sup>	530	0.81	0.33	435.0	1.8	
<b>Total Resource, June 2004</b>	<b>1210</b>	<b>0.75</b>	<b>0.32</b>	<b>905.4</b>	<b>3.89</b>	

Total resource = Measured + Indicated + Inferred resource, calculated to the specifications of the Australian JORC Code for reporting of 'ore reserves'.

<sup>1</sup> Newcrest Mining Limited (1997); <sup>2</sup> Newcrest Mining Limited (2000); <sup>3</sup> Newcrest Mining Limited (2003); <sup>4</sup> Newcrest Mining Limited (2004).

Mt = Million tonnes; t = tonnes (1 Moz = 31.10348 tonnes); g/t = grams/tonne.

Although significant historical gold was mined in parts of the Rockley-Gulgong Volcanic Belt, no mineralisation of economic importance has been recorded recently.

The main porphyry copper-gold deposits and prospects associated with the Molong Volcanic Belt, as listed above, and a number of the key deposits in the Junee-Narromine Volcanic Belt, all fall within a broad NW- to WNW-trending structural corridor, the Lachlan Transverse Zone (Fig. 4) (Glen, *et al.*, 2003). This zone is a key arc-normal structure that can be recognised stretching across NSW from the current Pacific coastline to the western half of the state, where it marks the boundary between the Kanmantoo and Thompson Orogens. In its western sections it is marked by a series of WNW trending faults, while in the Eastern Lachlan Orogen it is defined by a corridor of WNW-trending folds and faults that disrupt the major folds and faults defining the orogen's regional grain. This structure has been active throughout the development of the Lachlan Orogen, from at least the Late Ordovician, and has influenced the partitioning of upper crustal extension and contractional deformation, the emplacement of igneous bodies and the distribution of copper and gold mineralisation (Glen and Walshe, 1999).

In the structurally restored Macquarie Volcanic Arc, the Cadia Intrusive Complex falls within, and is elongated parallel to, the Lachlan Transverse Zone (LTZ), as is the markedly elongate mineralised corridor defined by the deposits of the Cadia Valley, which are also individually elongated NW to WNW. The LTZ underwent (apparently repeated) dilation during the Ordovician, particularly near the termination of, or intersection with, arc parallel structures. It apparently established a regional differential stress regime with WNW  $\sigma_1$  and NNE  $\sigma_3$ , which influenced the emplacement of NW to WNW elongate intrusives. As well as the Cadia Valley deposits, both Cargo and Copper Hill were developed within the zone, as are the Endeavour deposits in the Junee-Narromine Volcanic Belt, although the latter are not elongated parallel to the structure, but follow the grain of the orogen. Deposits such as Cowal, Marsden and Gidginbung are outside of the LTZ.

## Cadia Valley Gold-Copper Deposits

Four porphyry gold-copper deposits have been delineated within the 7 km long Cadia-Ridgeway mineralised corridor, hosted by a suite of Late Ordovician shoshonitic intrusives and broadly coeval volcanoclastics and lavas, on the western margin of the Molong Volcanic Belt. These deposits are the Ridgeway, Cadia Hill, Cadia Quarry and Cadia East-Far East deposits, which together accounted for an original combined resource of 1210 Mt @ 0.75 g/t Au, 0.32% Cu, and a total of 905 tonnes of contained gold (Table 1).

### Geological Setting

The Cadia Valley porphyry gold-copper deposits are hosted by the Late Ordovician to Early Silurian Cadia Intrusive Complex (CIC) and by the Late Ordovician Forest Reef Volcanics and underlying Weemalla Formation, towards the western margin of the Molong Volcanic Belt. The CIC is a product of magmatic pulse 3 of the Macquarie Arc (Fig. 5). The deposits and their hosts are in part discordantly overlain by siltstones and sandstones of the Silurian Waugoola Group and by a relatively thin layer of Tertiary basalt and gravel (Holliday *et al.*, 2002).

The *Weemalla Formation* is the lowest stratigraphic unit exposed in the Cadia district. It is at least 1000 m in thickness and comprises a fine grained unit of thinly laminated, carbonaceous to volcanic siltstones, with minor arenaceous volcanic beds (Holliday *et al.*, 2002).

The *Forest Reefs Volcanics* (FRV) conformably overlie, but are partly coeval with, the Weemalla Formation with a 40 to 50 m thick transitional contact comprising a gradual upwards coarsening of grain size from volcanic siltstones to lapilli volcanoclastics (Holliday *et al.*, 2002). Five lithofacies have been recognised within the FRV in the Cadia district (Wilson *et al.*, 2003), as follows:

- i) Intermediate volcanic lithic conglomerates, breccias and sandstones, comprising the bulk of the FRV. At Ridgeway, this facies is composed of massive bands

that are >50 m thick of intercalated volcanic lithic conglomerates to breccias, and bedded volcanic sandstone. Clasts in the coarse units are well rounded clinopyroxene- and hornblende-phyric basaltic to feldspar-phyric basaltic-andesites supported by volcanic sandstones of the same composition as the clasts. Intercalated with these bands are packages up to 100 m thick of plagioclase crystal rich volcanic sandstones that normally show graded bedding on scales of metres to tens of metres.

- ii) Bedded calcareous volcanic sandstone, largely confined to the east and north where it occurs near the top of the FRV and has been altered to host both the Big Cadia and Little Cadia skarns.
- iii) Laminated siliceous volcanic siltstone, which occurs in minor amounts in the upper part of the FRV on the eastern end of the district at Cadia East, where it stratigraphically overlies lithofacies 2.
- iv) Massive basaltic to basaltic-andesite flows which occur throughout the district, but are more abundant to the east.
- v) Basaltic to andesitic hypabyssal to sub-volcanic intrusions, locally termed pyroxene- or plagioclase-porphyrries, depending upon the dominant phenocryst (Wilson *et al.*, 2003).

In the Ridgeway area, the FRV, particularly lithofacies 1, are "predominantly intermediate" in composition, characterised by feldspar- and hornblende-phyric clasts within the fragmental volcanic rocks. To the east of the Cadiangullong Fault (Figs. 5 and 6), at Cadia Hill and Cadia East, the volcanoclastics are more "intermediate to basic", with predominantly pyroxene- and lesser feldspar-phyric clasts. The relationship between these two volcanoclastic facies has not been established. However, the "predominantly intermediate" facies at Ridgeway, which immediately overlie the Weemalla Formation, are assumed to in turn be stratigraphically overlain by the "intermediate to basic" facies found to the east of the Cadiangullong Fault, where the Weemalla Formation is at a depth below the current limit of drilling (see Fig. 6) (Holliday *et al.*, 2002).

The subvolcanic intrusions and possible related extrusives of lithofacies 5 are more frequent in the upper part of the sequence to the east of the Cadiangullong Fault. At Cadia East and near Little Cadia, the local globular peperitic margins of these intrusives suggest they were emplaced as shallow sills and dykes in soft, unconsolidated, wet volcanoclastics and sediments of the Forest Reefs Volcanics (Wilson *et al.*, 2003; Ian Tedder, Newcrest Mining, pers. comm., 2004). These intrusions, which include pyroxene-

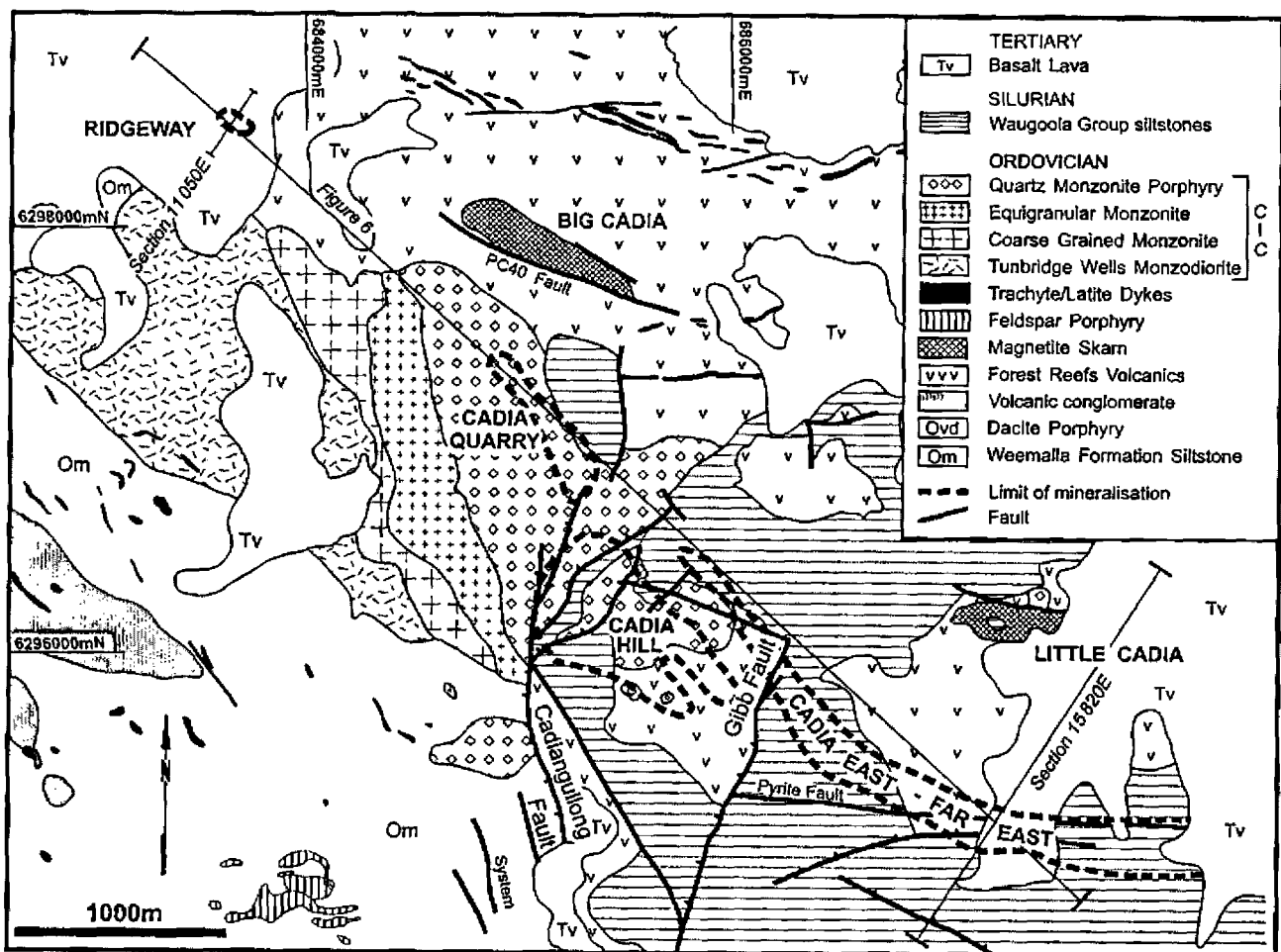


Figure 5: *Geology of the Cadia-Ridgeway district* and location of the principal zones of porphyry- and skarn-related gold-copper mineralisation. The locations of sections 11 050E at Ridgeway, 15 820E at Cadia East and the longitudinal section in Figure 6 are also shown. Abbreviations: CIC = Cadia Intrusive Complex. Modified from Tedder *et al.*, (2001), with information from Holliday *et al.* (2002) and Wilson *et al.*, (2003).

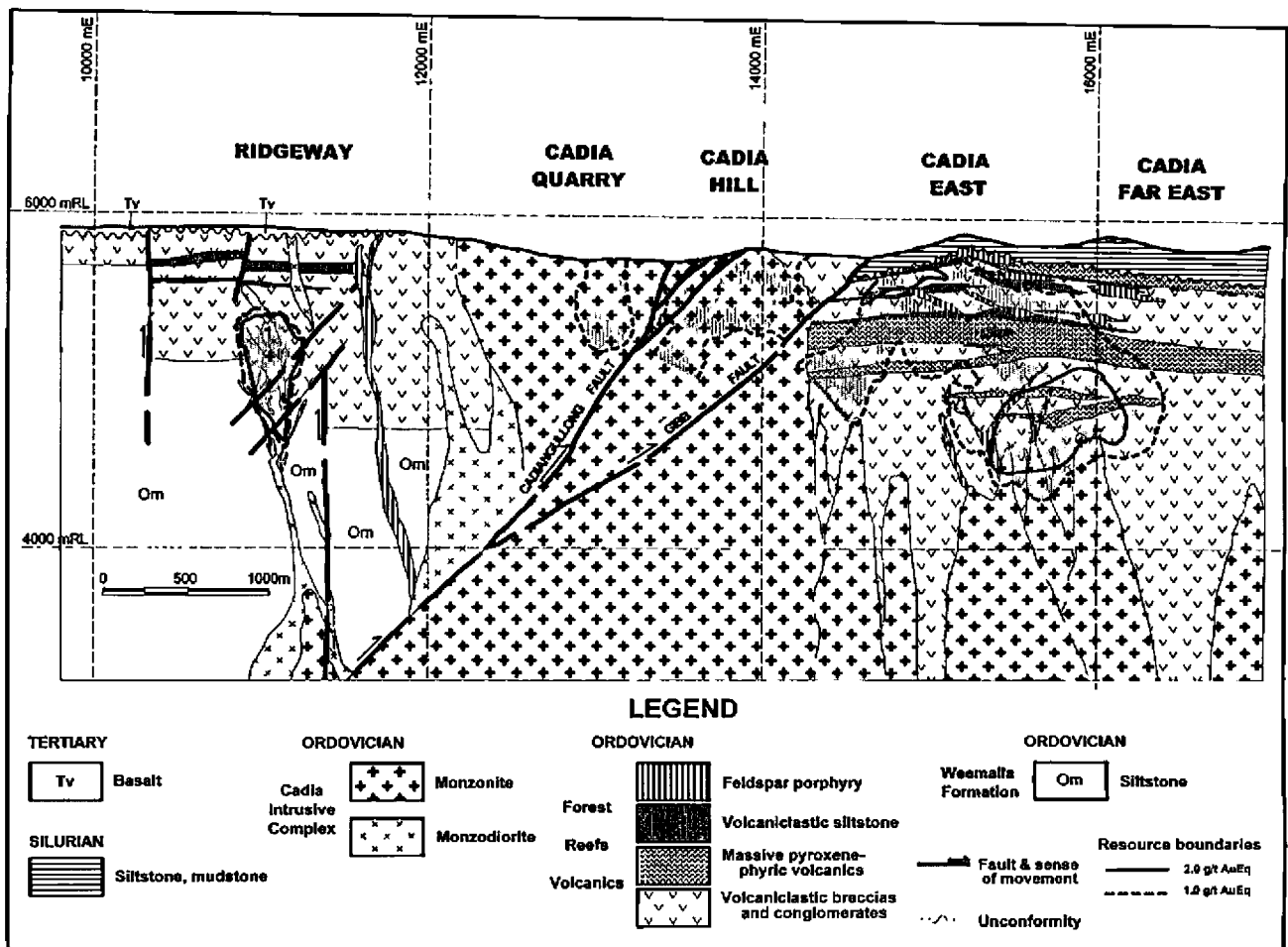


Figure 6: Schematic geological long section of the Cadia-Ridgeway mineralised corridor showing projected ore deposit outlines. See Fig. 5 for location. Note that the lithologies of the Forest Range Volcanics differentiated on this figure are subdivided differently to lithofacies units 1 to 5 described in the text. Modified from Tedder *et al.*, (2001).

phyric basalt to basaltic andesite dykes and younger plagioclase-phyric andesite dykes, cut all Ordovician lithologies in the Cadia district with the exception of the Late Ordovician Cadia Igneous Complex and the Silurian cover sequence (Holliday *et al.*, 2002).

Lithofacies 2 is high in the volcaniclastic suite to the east of the Cadiangullong Fault, where it is a carbonate-rich, sandy volcaniclastic that marks the upper limit of the pyroxene-phyric suite and is host to the Big Cadia and Little Cadia gold-copper-hematite-magnetite skarns. Fauna from these carbonates have yielded similar palaeontological ages to the host Weemalla Formation at Junction Reefs, 20 km south. This has been taken to imply that the Weemalla Formation may in part be a distal lateral facies equivalent of the Forest Reef Volcanics (Holliday *et al.*, 2002).

The unconformably overlying Silurian *Waugoola Group* is predominantly composed of dark grey to green, fine-grained siltstones with wispy bedding laminations, subunits of fine grained, light grey quartz sandstone and a pink crinoidal limestone band with latest Llandovery age fauna. It is at least 200 m thick at Cadia East, thickening to the east. The base of the unit is marked by a one to two metre thick calc-rudite composed of coral fragments and volcanic grit. To the north, the sequence is covered by 50 to 80 m of *middle Miocene basalts*, comprising at least two layers.

To the south, at a lower elevation, *Tertiary gravels* predominate (Packham *et al.*, 1999; Holliday *et al.*, 2002).

The *Cadia Intrusive Complex* (CIC) occurs as a NW- to WNW-elongated, 3x1.5 km, composite stock which comprises the mafic Tunbridge Wells Diorite in its western end, while phases of the Cadia Hill Monzonite occupying the remainder of the complex. There is a strong compositional zonation within the complex, ranging from pre-mineralisation monzodiorite, diorite and minor gabbro to the west, to coarsely orthoclase- and plagioclase-phyric quartz monzonite porphyry at the eastern extremity. The boss of quartz monzonite at Cadia Hill, the monzodiorite and monzonite encountered at depth in drilling on the eastern end of Cadia East and at Ridgeway to the west (described below), are petrographically and compositionally identical to the exposed CIC, while a swarm of latite/trachyte dykes to the north of the main exposed CIC are believed to be differentiates of the CIC. All of these observations have been taken to indicate the presence of an extensive magma chamber at depth (Holliday *et al.*, 2002, Wilson, *et al.*, 2003).

The Lachlan Transverse Zone (as described above) appears to have influenced the structural grain of the Cadia Valley district, as expressed by faulting and fracturing which trends NW to WNW, and generally dips steeply to the SW. This

structural grain has facilitated and localised the emplacement and elongation of the CIC, as well as strongly influencing the mineralising event, as is evidenced by the dominant orientation of mineralised sheeted veins at Cadia Hill, Cadia Quarry and Cadia East. On a broader scale, the mineralised corridor of the Cadia Valley District, as defined by the distribution of alteration and mineralisation that envelopes the string of ore deposits from Ridgeway to Cadia East, also parallels to this same structural trend. In addition, post-mineral faults, such as the PC40 which offsets the Big Cadia skarn (Fig. 5) and the Purple Faults which offset the North Fault at Ridgeway (Fig. 7), have the same NW- to WNW-orientation. Extension, that was orthogonal to this trend, accompanied the formation of sheeted veins (Holliday *et al.*, 2002; Wilson, *et al.*, 2003).

An additional, north-south striking, west dipping, set of post-Silurian faults, including the Cadiangullong and Gibb Faults, with west-over-east reverse movement, have dismembered and juxtaposed different parts of the Cadia hydrothermal system and orebodies. Specifically, the Cadia Quarry, Cadia Hill and Cadia East deposits have been telescoped together (Fig. 6), while the lower sections of the Forest Reefs Volcanics have been faulted over upper lithofacies of the same sequence to the east. These faults represent the northern extremity of the regional Werribee Fault system (Holliday *et al.*, 2002, Wilson *et al.*, 2003).

#### *Petrology & Geochemistry of the Cadia Intrusive Complex*

Holliday *et al.*, (2002) reported on a petrographic and geochemical study of 53 drill core and outcrop samples collected from different parts of the Cadia Intrusive Complex (CIC). Additional descriptions from the Ridgeway intrusives were contributed from work by Wilson *et al.*, (2003).

These reports show that the mafic phases of the main CIC are composed of 1-4 mm laths of euhedral plagioclase, 2-3 mm calcic pyroxenes and magnetite, all of which are partially or wholly enclosed by larger alkali feldspar crystals. Apatite and magmatic titanite are also present. Magmatic biotite is usually altered to secondary chlorite, epidote and titanite, while amphibole has been replaced by pyroxene. There are petrographic characteristics indicating both pyroxene and plagioclase accumulation and modestly developed layering (Holliday *et al.*, 2002).

With increasing differentiation of the magma and transition from the mafic to felsic phases, the pyroxene abundance decreases and magmatic amphibole appears, while the alkali feldspar:plagioclase ratio increases, but not systematically. The grain size of the rock decreases from coarse equigranular to medium grained, with the accompanying appearance of porphyritic orthoclase and lesser plagioclase in the monzonites and quartz-monzonites. The monzonites are salmon pink to green in hand specimen, with phenocrysts up to 20 mm across of pink orthoclase within a seriate textured groundmass of plagioclase and mafics. With the exception of thin (generally <200 mm thick) syenogranite-aplite dykes, there are no crosscutting relationships observed in the main CIC (Holliday *et al.*, 2002).

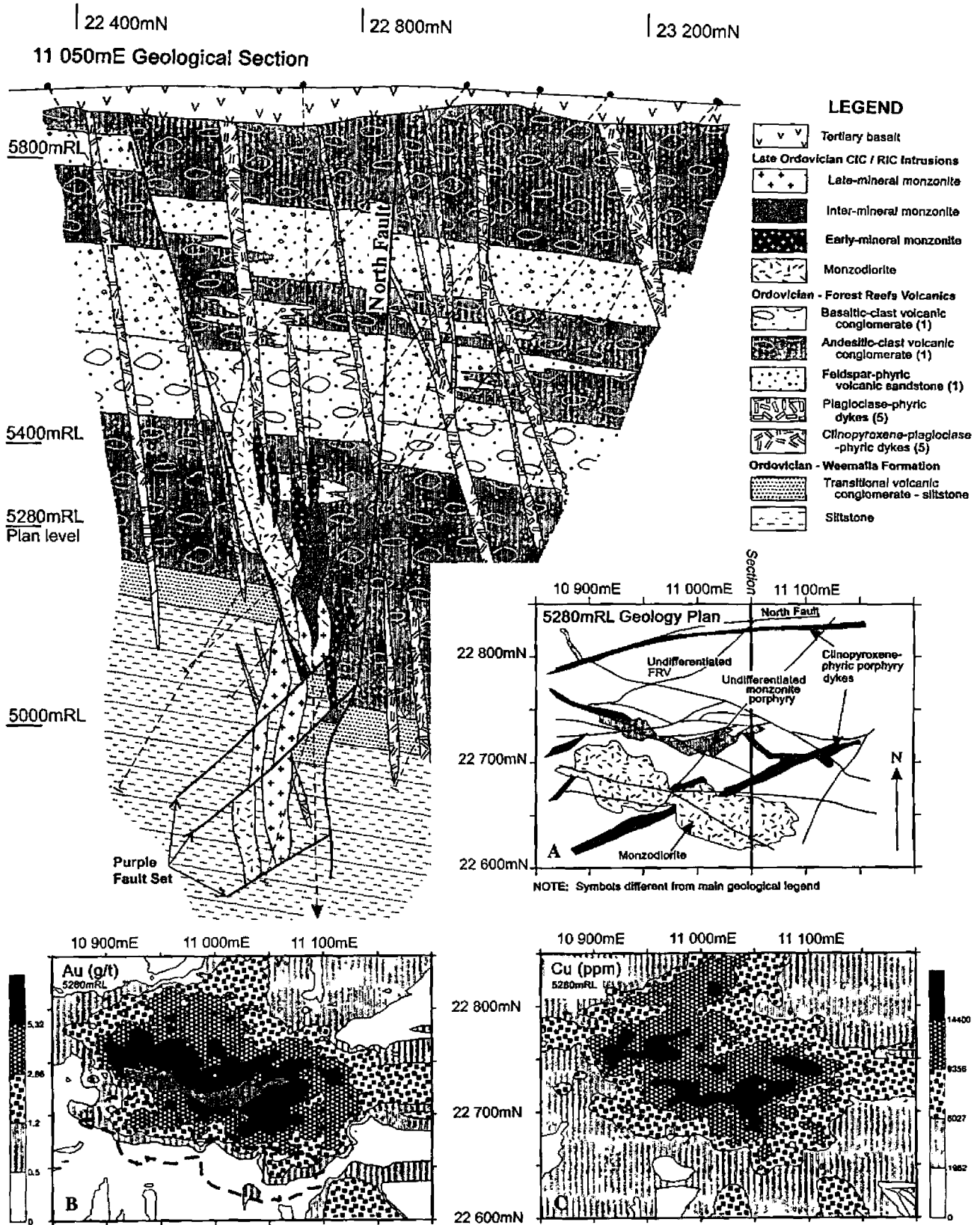
At the physically separated and smaller intrusive complex at Ridgeway, the earliest phase is an equigranular monzodiorite, comprising an equigranular mass of intergrown plagioclase, orthoclase and clinopyroxene, minor biotite and magnetite with accessory apatite and titanite. The monzodiorite at Ridgeway was succeeded by three groups of monzonite intrusions (early-, inter- and late-mineral), all of which are post-monzodiorite. The early-mineral monzonite is typically green to dark green, characterised by the presence of rare orthoclase phenocrysts in a fine grained, highly altered groundmass, although all primary igneous textures have been obliterated by intense actinolite-magnetite-biotite (calc-potassic) alteration. This phase hosts the most densely developed quartz vein stockwork and highest gold-copper grades. The inter- and late-mineral monzonites are compositionally and texturally similar, but are more fractionated than the early-mineral phase. They are pale pink to cream, with abundant plagioclase, and lesser orthoclase and chlorite altered clinopyroxene phenocrysts, in an orthoclase rich groundmass, with accessory and trace magnetite, biotite, quartz, apatite and zircon. In contrast to the main CIC, multiple intrusion and mineralising phases are indicated by the truncation of intrusive contacts and veins within the smaller Ridgeway intrusive (Wilson *et al.*, 2003).

Holliday *et al.*, (2002) considered that early magmatic biotite, replacement of pyroxene by amphibole and the occurrence of aplites, pegmatites and vapour cavities filled by interstitial melts are all consistent with rapid build up of water within the melt during differentiation.

Holliday *et al.*, (2002) reported that petrographic and textural evidence indicate that the CIC crystallised under strongly oxidising conditions. The more mafic units contain 1 to 2 modal percent early crystallised magnetite, while magmatic biotite has high Mg/(Mg+Fe) ratios of 0.59 to 0.65. They also noted that whole rock Fe<sub>2</sub>O<sub>3</sub>/FeO ratios are elevated in the range 1.0 to 1.5, which they say are typical of intermediate igneous complexes associated with porphyry style mineralisation.

A series of analyses reported by Holliday *et al.*, (2002) shows SiO<sub>2</sub> values in the CIC range from 48 to 65%, with the more mafic end monzodiorites and diorites varying from 48 to 54%, while the mafic monzonites extend from 52 to 54% and the monzonites contain 58 to 65% SiO<sub>2</sub>. The CIC is characterised by high (3.5 to 6.5%) K<sub>2</sub>O, falling within the shoshonite field on K<sub>2</sub>O-SiO<sub>2</sub> diagrams, while the complex exhibits a well defined trend from trachybasalt to trachyte fields on the alkali-SiO<sub>2</sub> diagrams with 5 to 11% K<sub>2</sub>O+Na<sub>2</sub>O. In addition, the molecular K/Na ratio for all unaltered samples is >1, i.e. they are potassic (Müller and Groves, 1995). Holliday *et al.*, (2002) also note that the high alkalis to SiO<sub>2</sub> ratio allows the CIC to be defined as *alkalic* (after MacDonald and Katsura, 1964).

Holliday *et al.*, (2002) also stated that calculated CIPW normative proportions for the CIC range from olivine normative (quartz saturated) to quartz normative (silica over-saturated). The absence of a strongly alkaline or peralkaline character is confirmed by the petrographic absence of late interstitial magmatic quartz throughout the



**Figure 7: Interpreted geology and structure of section 11050mE through the Ridgeway deposit.** Mineralisation is intimately associated with monzonitic intrusions of the Ridgeway Intrusive Complex. Variations in stratigraphic thicknesses across the North Fault suggest it was in extension during deposition of at least part of the Forest Reefs Volcanics and may have influenced localisation of the Ridgeway Intrusive Complex. Numbers after the Forest Reefs Volcanics lithology in the legend refer to the lithofacies association discussed in the text. Inset A - *Geology plan of the 5280mRL* of the Ridgeway underground mine, showing the principal pyroxene porphyry dykes, the monzodiorite intrusion (pre- to early-mineral) and the un-differentiated monzonite porphyry complex (early- to late-mineral). The pyroxene porphyry dykes occupy ENE- and WNW-trending faults, the latter set possibly controlling the localisation of the monzodiorite and monzonite intrusions. Inset B - *5280mRL gold grade* - the monzodiorite intrusion (thick dashed line) is marginal to the main body of mineralisation, but the monzonite intrusive (grey polygon at the centre of the mineralisation) is partially coincident with the high-grade portion of the deposit. Inset C - *5280mRL copper grade* - a close spatial association between Au, Cu and the monzonite intrusions is evident. The highest Au/Cu ratios are along the southern flank of the monzonite intrusion, where early-mineral monzonites have been logged. Abbreviations: FRV = Forest Reefs Volcanics. Contour intervals on insets B & C are at 75th, 90th, 95th, and 98th percentile values. Modified from Wilson et al., 2003, *Economic Geology*, v98:8, p1642 Fig. 4 and p1645 Fig. 6.

complex, the lack of "alkaline" chemical characteristics (eg. very high HFSE enrichments in elements such as Zr, Nb, etc.) and the absence of peralkaline mineral phases (eg. high Ti and/or sodic pyroxenes or amphiboles, etc.). Compositionally the complex conforms to the definition of shoshonite based on major element geochemistry and its modal mineralogy and textures. The CIC samples all fall within the shoshonite field on Ce/Yb-Ta/Yb and Th/Yb-Ta/Yb plots of Pierce (1982) and Müller *et al.*, (1992).

### Mineralisation Styles & Deposits

The ore deposits and associated mineralisation in the Cadia Valley are spatially associated with high-K, alkalic affinity, shoshonitic, porphyritic monzonite to quartz-monzonite phases of the Cadia Igneous Complex (CIC). This mineralisation is interpreted to be genetically related to crystallisation of deeper portions of the CIC. The majority of the exposed porphyries of the complex and the adjacent wallrocks are hydrothermally altered and mineralised to some extent. This resultant alteration-mineralisation system defines a NW-trending mineralised corridor some 7 km long and up to 2 km in width, which has been intersected by drilling to a depth of more than 1600 m on the eastern end at Cadia East/Far East. The mineralised corridor embraces a string of elongate orebodies, both within the CIC and its hydrothermally altered wallrocks. The Ridgeway orebody to the NW is believed to have been emplaced at the deepest level in the porphyry system, and Cadia East, which is mainly in the wall rock of the CIC, at the shallowest (Holliday *et al.*, 2002).

Holliday *et al.*, (2002) have described six variations in the occurrence of ore and mineralisation within the Cadia-Ridgeway mineralised corridor, (Figs. 5 & 6) listed below from the deepest formed in the intrusive-hydrothermal system to the shallowest and from predominantly intrusion-hosted to predominantly wall rock volcanic-hosted:

- i) intrusion- and wallrock volcanic-hosted stockwork quartz vein mineralisation at *Ridgeway*, closely associated with a separate intrusive plug of the CIC, developed at the base of the Forest Reefs Volcanics;
- ii) intrusion-hosted, mainly sheeted quartz vein mineralisation at *Cadia Quarry*;
- iii) intrusion- and wallrock volcanic-hosted, mainly sheeted quartz vein mineralisation at *Cadia Hill*;
- iv) wallrock volcanic- and intrusion-hosted, mainly sheeted quartz vein mineralisation at *Cadia Far East (Cadia East Underground)*;
- v) wallrock volcanic-hosted disseminated and sheeted quartz vein mineralisation at *Cadia East*; and
- vi) iron rich skarns at *Big and Little Cadia*, hosted by wallrock calcareous volcanic sandstone at the top of the Forest Reefs Volcanics.

The following summarises the main ore deposits and corresponding mineralisation styles encountered to date within the Cadia-Ridgeway mineralised corridor.

### Ridgeway

Ridgeway is a high grade gold-copper porphyry deposit. It is the deepest formed and highest grade of the four main deposits within the Cadia-Ridgeway mineralised corridor.

It is also, at present, the most northwesterly of the economic resources that has been defined. Mineralisation and alteration are zoned around a small, vertically attenuated, alkalic intrusive complex of monzodioritic to quartz monzonitic composition that is part of the CIC, but some 500 m NW of exposures of the main CIC body, and concealed at a depth of 450 m below the present surface (Wilson *et al.*, 2003). At June 30 2003, the resource at Ridgeway amounted to 78 Mt @ 1.96 g/t Au, 0.67% Cu for a total of 149 tonnes (4.8 Moz) of contained gold (Newcrest Mining, 2003). The deposit is currently in production as an underground, sub-level cave mine.

Mineralisation and alteration at Ridgeway are hosted both by the intrusive complex and by the surrounding volcanics of the Forest Reefs Volcanics, at and just above, the contact with the underlying Weemalla Formation (Fig.7). Of the five main lithofacies of the Forest Reefs Volcanics, only lithofacies 1, 4 and 5 are represented at Ridgeway (described in "Geological Setting" above). Of these, lithofacies 1 is dominant, comprising massive bands that are >50 m thick of intercalated volcanic lithic conglomerates to breccias, and bedded volcanic sandstone. Clasts in the coarse units are well-rounded, clinopyroxene- and hornblende-phyric basaltic, to distinctly feldspar-phyric basaltic-andesites. They are supported by volcanic sandstones of the same composition as the clasts. Intercalated with these bands are packages up to 100 m thick of plagioclase, crystal-rich volcanic sandstones that may locally, but not commonly, show graded bedding on scales of metres to tens of metres. Lithofacies 4 is only a minor component at Ridgeway, where it comprises clinopyroxene-phyric basaltic to basaltic andesite flows. Lithofacies 5 is represented by a series of steeply north to NE dipping clinopyroxene-phyric basaltic to plagioclase-phyric andesitic dykes (Wilson *et al.*, 2003).

The Ridgeway Intrusive Complex is physically separated from, but is petrographically and compositionally identical to, and is believed to be connected at depth to, the main Cadia Igneous Complex (CIC). The top of the monzodioritic to monzonitic Ridgeway Intrusive Complex is 450 m below the present day surface. It comprises a thin, subvertical composite pipe, with a vertical extent in excess of 1 km, similar in size to those at Northparkes (described later in this paper). The earliest phase is an equigranular monzodiorite (described in the petrography section above) occurring as a WNW elongated, steep north dipping, 200x50x500 m body with an elliptical cross section, located on the southern margin of the Ridgeway orebody. In detail it occurs as two lobes, cut by the mineralisation, and is interpreted to be pre-mineral (Wilson *et al.*, 2003).

The main mineralisation at Ridgeway is spatially related to three groups of monzonite intrusions (early-, inter- and late-mineral), all of which are post-monzodiorite. They form an irregularly shaped composite plug with dimensions of 70x100x600, immediately to the north of the monzodiorite. The individual bodies of the composite mass having dimensions from metres to tens of metres horizontally and up to 200 m vertically. Multiple intrusion



and mineralising phases are indicated by truncation of contacts and veins (Wilson *et al.*, 2003).

The most significant structure in the deposit area is the east to ENE trending, steeply south-dipping, North Fault, which appears to have been active during deposition of the Forest Reefs Volcanics and during intrusion. It bounds the northern margin of the orebody, although only minimal offset of the alteration envelope is indicated. Another fault set orientated NW to WNW and SW dipping, truncates both mineralisation and the intrusives of the Ridgeway Igneous Complex (Wilson *et al.*, 2003).

The top of the Ridgeway deposit (as defined by the 0.2 g/t Au cut-off) is some 500 m below the current surface. It takes the form of a subvertical, pipe like, quartz-sulphide vein stockwork body, with a WNW elongated axis and an elliptical 150x250 m horizontal shape which persists over a vertical interval of more than 600 m. Distinct styles of veining and alteration are related to each of the three monzonitic intrusive phases of the igneous complex. The metal grades and intensity of alteration decrease from the early- to the late-mineral phases of the intrusive (Wilson *et al.*, 2003).

Early-mineral stage intrusion is accompanied by intense actinolite-magnetite-biotite (calc-potassic) alteration and up to four stages of high grade quartz-magnetite-sulphide veins, all of which contain abundant magnetite, actinolite and bornite with variable amounts of chlorite, biotite, chalcopryrite, pyrite, quartz and orthoclase. Bornite, which is the most abundant sulphide, correlates closely with gold. Magnetite dominates in the earliest vein stage, while in the last, chalcopryrite becomes more important. Some of these veins persist for up to 350 m outwards from the Ridgeway Igneous Complex (Wilson *et al.*, 2003).

Moderate- to weak-intensity potassic alteration as orthoclase-biotite  $\pm$  magnetite accompanies both the inter- and late-mineral intrusions and is associated with chalcopryrite- and pyrite-rich quartz-orthoclase veining. The veining and alteration accompanying the inter-mineral phase intrusives is referred to as transitional-stage veining and transitional-stage alteration respectively. Transitional-stage alteration assemblages are characterised by orthoclase, biotite (mostly retrograde altered to chlorite) and magnetite with minor quartz, titanite and apatite. The transitional-stage veining occurs as up to 4 styles which contain variable amounts of magnetite, chalcopryrite and pyrite with quartz and orthoclase, while bornite is rare to absent. The late-mineral monzonite intrusives is accompanied by weak late-stage alteration, occurring as weak pervasive potassic (orthoclase) development around late-stage veins, and chlorite alteration of mafic components of the monzonite. The late-stage veins are characterised by pyrite  $\pm$  chalcopryrite with fluorite, but no bornite or actinolite, and gangue progressing from quartz to sericite to chlorite-calcite from early to late phases (Wilson *et al.*, 2003).

Three discrete and partially zoned hydrothermal alteration suites are found on the periphery of the Ridgeway deposit, namely: i) an inner propylitic; ii) an outer propylitic; and iii) a sodic assemblage. These are peripheral to, and locally

overprint, the potassic phase. Peripheral veins are characterised by epidote, prehnite, quartz and calcite in varying proportions with varying sulphides, depending on the position within the deposit. Some of the outer veins, up to 200 m beyond the inner propylitic zone, carry chlorite/calcite-sphalerite-chalcopryrite  $\pm$  galena. Phyllic alteration is only found on the margins of late stage faults (Wilson *et al.*, 2003).

### *Cadia Hill*

Cadia Hill was the first of the deposits to be mined on a large scale as part of the present Newcrest Mining Ltd Cadia Valley Operations. The ore grade mineralisation is predominantly hosted by a quartz monzonite porphyry phase of the CIC, although a small portion cuts a roof pendant of Forest Reefs Volcanics at the eastern end of the deposit (Holliday *et al.*, 2002). The total pre-mine resource at Cadia Hill was 352 Mt @ 0.63 g/t Au, 0.16% Cu for 221.3 tonnes of contained gold (Newcrest Mining, 1997). In June 2003, the remaining total measured + indicated + inferred resource was 260 Mt @ 0.70 g/t Au, 0.16% Cu for 180 tonnes of contained gold (Newcrest Mining, 2003). The deposit is currently being exploited via a large tonnage low grade open pit mine.

The Cadia Hill deposit is bounded on three sides by post-mineral faulting. To the west, a west-dipping reverse imbricate system, the Cadiangullong Fault (Figs. 5, 6 and 8), which encloses slivers of the Silurian Waugoola Group, truncates the ore and juxtaposes a block of quartz monzonite porphyry hosting the Cadia Quarry deposit over the Cadia Hill mineralisation. On its eastern margin, the quartz monzonite porphyry hosting the Cadia Hill deposit is thrust over Forest Reefs Volcanics carrying the Cadia East mineralisation, by the west dipping reverse Gibb Fault (Figs. 5 and 6) which has a displacement of at least 300 m. The northern side of the deposit is bounded by a NE-striking, steeply NW-dipping fault (Fig. 8). Fault dislocation is also evident within the deposit where disparate ore zones with varying metal ratios, grades and vein densities are juxtaposed across fault planes (Holliday *et al.*, 2002).

Mineralisation is present as chalcopryrite, native gold, lesser pyrite and bornite, which are disseminated within and immediately adjacent to the quartz-carbonate veins of a low density sheeted vein array (Fig. 8). This array forms a broadly tabular envelope that is approximately 300 m wide, dips SW at around 60° and strikes NW. The sheeted vein envelope persists over a length of some 900 m and to a depth of at least 800 m beneath the surface, although grades decrease below 600 m (Holliday *et al.*, 2002). Within the envelope, veins range from a millimetre to 10 centimetres in width with densities from 2 to 10 per metre, but locally in the core of the deposit may exceed 15 per metre (Newcrest Mining presentation). Gold grades can be broadly correlated with the intensity of chalcopryrite bearing veins, irrespective of the host lithology. In general, the higher copper grades are found in the core of the deposit where chalcopryrite dominates over pyrite. This zone is flanked by decreasing chalcopryrite:pyrite ratios, both outwards from the core and down dip/plunge. The

chalcopyrite:pyrite ratio, however increases up dip and to the NW where zones carrying bornite become increasingly abundant. A higher grade copper zone is localised at the northwestern end of the deposit, with grades of up to 0.5% Cu being encountered in an interval where bornite and chalcopyrite occur as minor infill in a crackle brecciated quartz monzonite porphyry (Holliday *et al.*, 2002).

A pervasive, rarely texture destructive, propylitic alteration comprising a chlorite, albite, epidote and calcite assemblage is the most widespread overprint. The quartz monzonite porphyry has a pervasive pink colouration due to disseminated, sub-microscopic, hematite in both feldspar phenocrysts and in the groundmass, a feature common to the CIC in the Cadia Valley deposits. Potassic (orthoclase) alteration is manifested as narrow selvages to chalcopyrite and bornite bearing quartz veins and as ragged patches partially replacing some plagioclase phenocrysts and overprinting the earlier albite and chlorite phase and its associated magnetite veining. In addition, late- to post-mineral, milled, jigsaw-fit breccias have chlorite altered rock flour cement. Sericite-pyrite alteration, with localised sphalerite and galena is also found, in association with NW-striking late mineral faults, while weakly developed post-mineral crackle breccias have a laumontite-epidote-calcite-orthoclase ± fluorite cement and are found throughout the deposit (Holliday *et al.*, 2002).

#### Cadia Quarry

The Cadia Quarry deposit (now known as *Cadia Extended*) lies in the hangingwall block of the west-dipping Cadiangullong reverse fault (Figs. 5 and 6) and is located immediately to the NW of the Cadia Hill pit. It is almost entirely hosted by quartz monzonite porphyry (Holliday *et al.*, 2002). The total pre-mine resource at Cadia Quarry

was 40 Mt @ 0.40 g/t Au, 0.21% Cu for 16.0 tonnes of contained gold (Newcrest Mining, 2000). In June 2003 the remaining total measured + indicated + inferred resource was 50 Mt @ 0.40 g/t Au, 0.23% Cu for 21.8 tonnes of contained gold (Newcrest Mining, 2003). The deposit is currently being exploited via a high tonnage, low grade open pit, which is an extension of the Cadia Hill mine.

Mineralisation and alteration is largely similar to that described above for Cadia Hill. However, in addition to the sheeted quartz-carbonate vein mineralisation, there are locally high copper-molybdenum zones containing coarse grained chalcopyrite and molybdenite, which are intergrown with quartz-orthoclase-biotite-calcite-pyrite as cement in open space pegmatitic breccias within the host quartz monzonite porphyry. The breccias follow the NW- to NNW-structural grain of the Cadia district and take the form of elongate pipes/dykes up to 150 m long and 10 m wide, which persist to depths of as much as 500 m. The clasts within the breccias are strongly sericite altered quartz monzonite porphyry, while the pegmatitic textures and the mineralogy are suggestive of high temperature formation (Holliday *et al.*, 2002).

The Cadia Quarry mineralisation has a grade boundary to the west, where its tenor decreases to that of a geochemical anomaly which persists under cover for some 2 km to the west, to beyond the Ridgeway deposit. To the north, the deposit is terminated at the steep intrusive contact between the host quartz monzonite porphyry and the Forest Reefs Volcanics. This contact contains some localised, weakly gold-copper mineralised epidote-garnet-magnetite skarn. To the south, copper and gold grades gradually decrease as the quartz monzonite porphyry grades into a more mafic phase of the CIC (Holliday *et al.*, 2002).

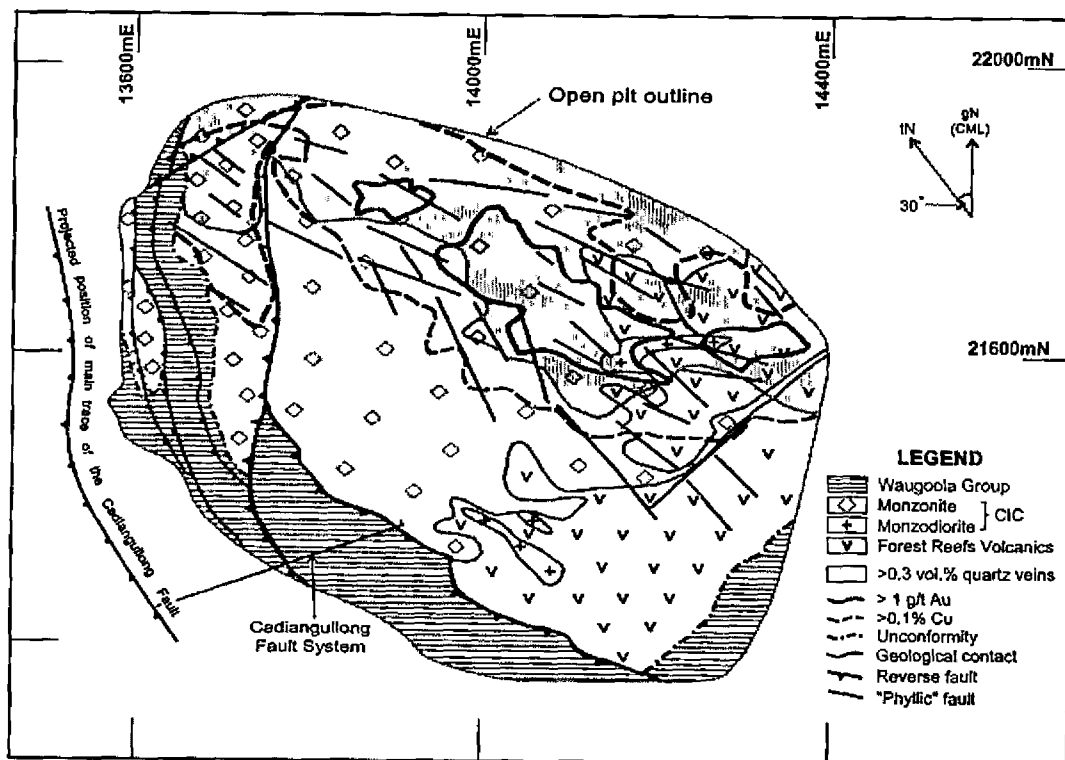


Figure 8: Simplified geology, grade, quartz vein intensity and structure of the Cadia Hill deposit, level plan at 5715mRL. Abbreviation: CIC = Cadia Intrinsic Complex Modified from Holliday *et al.*, (2002).

### Cadia East & Cadia Far East

The Cadia East deposit and its continuation, Cadia Far East, extend SE to ESE over an interval of approximately 1.7 km in length, 300 m in width and at least 1600 m down dip, plunging to the SE. Inferred open pit resources at Cadia East in June 2004 were 300 Mt @ 0.46 g/t Au, 0.37% Cu for 134 tonnes of contained gold (Newcrest Mining, 2004). Cadia Far East (now Cadia East Underground) has a resource of 530 Mt @ 0.81 g/t Au, 0.33% Cu for 435 tonnes of contained gold (Newcrest Mining, 2004).

The composite deposit is hosted by a more than 2000 m thick, shallow to flat dipping sequence of the Forest Reefs Volcanics, comprising predominantly volcanoclastic breccias and conglomerates of lithofacies 1 (see "Geological Setting" above) and lesser pyroxene- and feldspar-phyric lavas of lithofacies 4. Minor monzodiorite to quartz monzonite stocks and dykes belonging to the CIC intrude these Forest Reefs Volcanics units, and in part host mineralisation at depth in Cadia Far East. The Ordovician rocks and the mineralisation are unconformably overlain by up to 200 m of the Silurian Waugoola Group (Holliday *et al.*, 2002).

Mineralisation occurs in two broad, overlapping zones, namely:

- i) An upper zone of disseminated, copper dominant mineralisation within a 200 to 300 m thick, shallow

dipping, unit of volcanoclastic breccia (lithofacies 1) where it is sandwiched between two coherent porphyritic volcanic bands (of lithofacies 4) - an upper feldspar porphyry and a lower pyroxene-phyric unit. This zone comprises the shallow western sections of the Cadia East open pit deposit. Within this zone, disseminated chalcopyrite-bornite forms a core zone, capped by chalcopyrite-pyrite mineralisation (Holliday *et al.*, 2002).

- ii) A deeper, central gold rich zone with sheeted veins, which is localised around a core of steeply dipping sheeted quartz-calcite-bornite-chalcopyrite-molybdenite  $\pm$  covellite  $\pm$  magnetite veins. The highest grade gold is associated with the widest bornite-bearing veins, where native gold is commonly intergrown with bornite (Holliday *et al.*, 2002).

Elevated molybdenite levels are mostly associated with the upper disseminated copper zone, although molybdenum continues below this zone at depth, where it also occurs along both the hangingwall and footwall of the gold rich sheeted vein interval (Holliday *et al.*, 2002).

Three alteration styles and zones were recognised by Holliday *et al.*, (2002), as follows:

- i) Intense silica-albite  $\pm$  orthoclase  $\pm$  tourmaline, with a late sericite-carbonate overprint. Pyrite and minor fluorite are observed, although no magnetite remains.

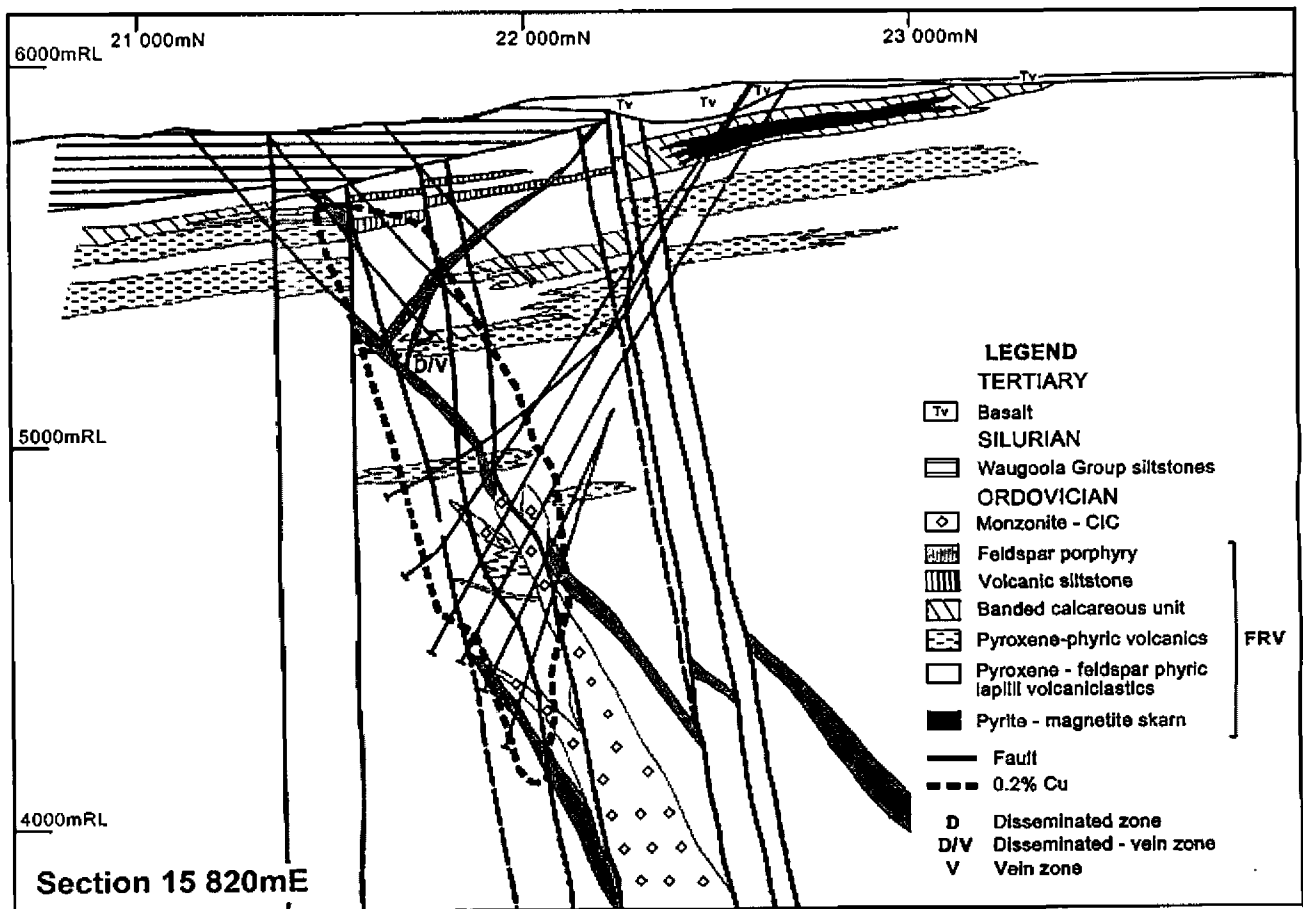


Figure 9: *Interpreted geology and structure of the Cadia East deposit along section 15 820mE (see Fig. 5). The relative location of disseminated and vein-hosted copper mineralisation is also shown on the diagram. Abbreviation: CIC = Cadia Intrusive Complex, FRV = Forest Reefs Volcanics. From Holliday *et al.*, (2002).*

This zone forms a layer at shallower depths, that is semi-conformable with the Forest Reefs Volcanics stratigraphy, replacing more permeable volcanoclastic breccias. It is mainly the product of late sericite-carbonate and tourmaline overprinting of zone 2 type alteration and the destruction of magnetite. The upper disseminated copper rich mineralisation falls within this alteration zone.

- ii) Moderate to intense, grey, silica-albite-orthoclase flooding with minor hematite staining. Hydrothermal magnetite is common and chlorite occurs as a late overprint. This style of alteration grades into an outer propylitic zone of chlorite-epidote  $\pm$  actinolite  $\pm$  calcite.
- iii) Pervasive potassic alteration comprising albite-orthoclase-quartz-biotite-actinolite-epidote-magnetite with sulphides. Late chlorite is an overprint on biotite. Albite replaces magmatic plagioclase, while orthoclase occurs as an alteration selvage to mineralised veins. This zone occurs at greater depths, and overprints and passes out and upward into zone 2. The mineralised sheeted veins, particularly the gold rich zone, are accompanied by the most intense developments of this potassic zone, although the sheeted veins also persist into zone 2 alteration.

Cadia East and Cadia Far East have been dislocated by at least three significant fault zones. Reverse movement on the major NE-trending, west dipping, Gibb Fault truncates the mineralised system and juxtaposes the Cadia Hill deposit over the Cadia East mineralisation on its western margin. A second, un-named, east trending reverse fault with a steep north dip occurs around 1 km to the east of the Gibb Fault and has displaced mineralisation by at least 100 m. A third significant fault is the east trending Pyrite Fault Zone which lies parallel to the main mineralisation direction at Cadia Far East, and has both syn- and post-mineralisation movement as indicated by milled clasts of pyrite, quartz and carbonate within a locally sericitic fault gouge (Holliday *et al.*, 2002).

#### **Cadia Skarns**

Two gold-copper-hematite-magnetite skarns, Big Cadia (also previously known as Iron Duke) and Little Cadia, have long been known in the Cadia Valley. Prior to the discovery of Cadia Hill, Iron Duke (Big Cadia) had been by far the largest producer in the district, having yielded more than 100 000 t of secondary copper ore @ 5 to 7% Cu from underground operations from 1882 to 1898 and 1905 and 1917, and 1.5 Mt of iron ore @ approximately 50% Fe from 1918 to 1929 and 1941-1943 (Welsh, 1975). Based on drilling during the 1960's, there is an estimated potential of 30 Mt @ 0.4 g/t Au, 0.5% Cu for 12 tonnes of contained gold at Big Cadia and 8 Mt @ 0.3 g/t Au, 0.4% Cu for 2.4 tonnes of contained gold at Little Cadia (Holliday *et al.*, 2002).

Big Cadia lies about 100 m north of the drill intersected contact of CIC monzonite and is some 200 m north of Cadia Quarry, while Little Cadia is some 800 m north of the Cadia Far East deposit (Holliday *et al.*, 2002) and 2 km SE of Big Cadia (Holliday *et al.*, 2002). Both skarn zones are around 1000 m long, 250 m wide and average 40 m thick,

although in the centre of Big Cadia it reaches 70 m and is 50 to 85 m thick at Little Cadia. Weathering has resulted in the oxidation and slight secondary enrichment of each of the skarns (Welsh, 1975; Holliday *et al.*, 2002). Primary gold-copper mineralisation at both occurs in association with the hematite-magnetite skarn that formed in the impure bedded calcareous volcanic sandstones of lithofacies 2, at the top of the Forest Reefs Volcanics (see "Geological Setting" above). Elevated copper and gold grades are found in both the skarn and in a surrounding alteration envelope of epidote-quartz-actinolite-chlorite-sericite-calcite-rutile imposed on volcanic conglomerates of the underlying lithofacies 1 of the Forest Reefs Volcanics. Where best developed, the skarn comprises intergrowths of fine to coarse bladed hematite (partially replaced by magnetite) with interstitial calcite  $\pm$  chlorite  $\pm$  pyrite/chalcopyrite. Green (1999) presented mineralogic and isotopic evidence that suggested fluids infiltrated northwards from the CIC, along the volcanoclastic unit, to form Big Cadia. At Little Cadia many drill holes have intersected monzonite possibly belonging to the CIC below the skarn (Holliday *et al.*, 2002).

## **Endeavour Copper-Gold Deposits**

Four economic porphyry copper-gold deposits have been delineated within the Goonumbla district, some 100 km WNW of Cadia. All lie within the Late Ordovician shoshonitic Goonumbla Igneous Complex of the Junee-Narromine Volcanic Belt and are the reserve base of the Northparkes mining operation (Figs. 2 and 4). They are the Endeavour 22, 26, 27 and 48 deposits, which together had a combined pre-production resource of 130.6 Mt @ 1.1% Cu, 0.5 g/t Au. Each is centred on a separate narrow, pipe-like shoshonitic, quartz monzonite porphyry intrusive complex.

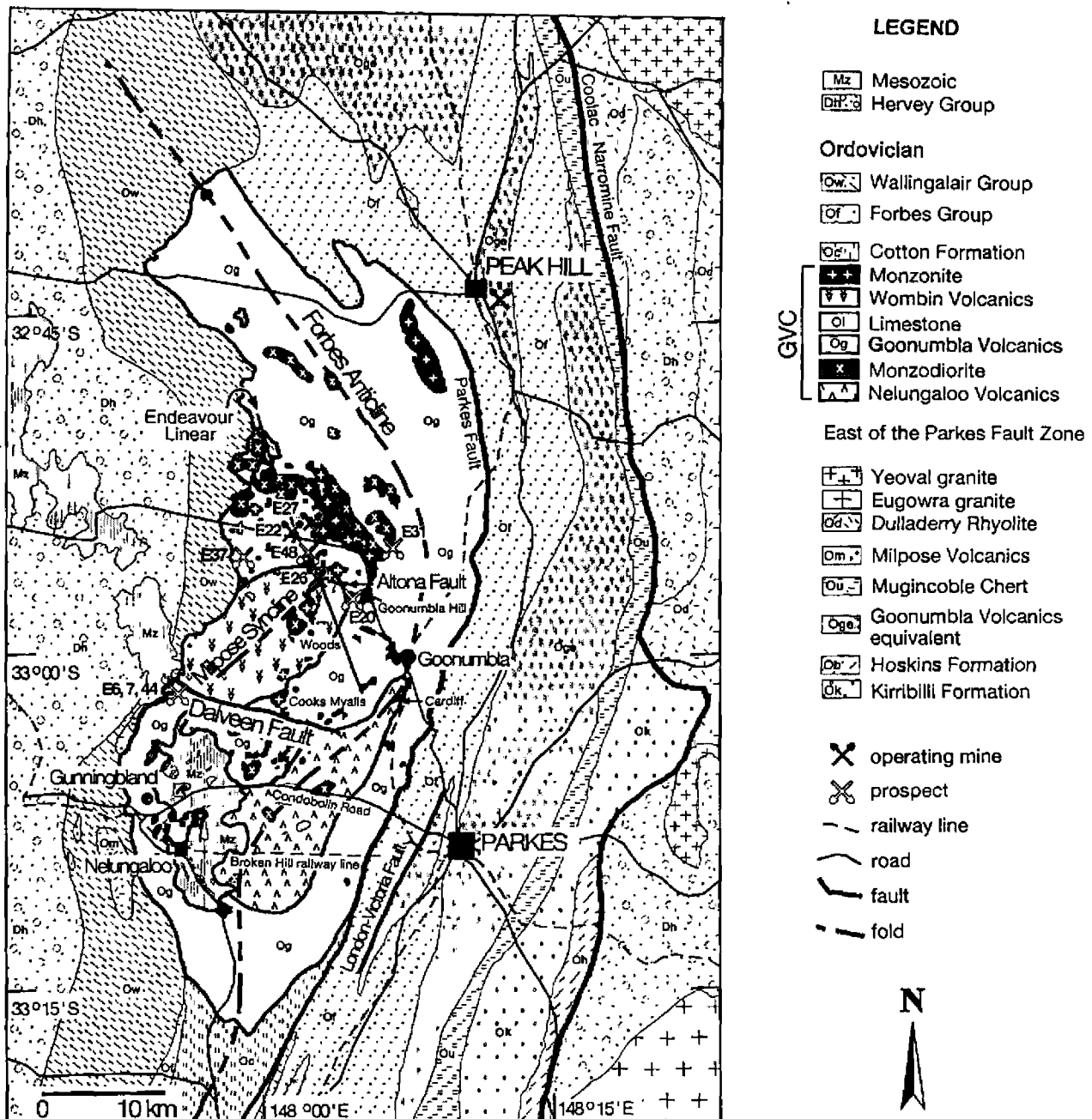
#### **Geological Setting**

The Goonumbla Igneous Complex, which hosts the Endeavour deposits, is part of the Ordovician to Early Silurian Junee-Narromine Volcanic Belt, a remnant of the Macquarie Volcanic Arc. The complex is divided into two parts (see references in Lickfold *et al.*, 2003), both products of the third pulse of arc volcanism, namely the:

**Goonumbla Volcanics**, which are 2500 to 4000 m thick and comprise a Middle to Late Ordovician sequence of coherent basaltic andesitic to trachyandesitic volcanic rocks, including lavas and shallow sills with peperitic margins, volcanoclastic rocks of similar composition, and minor intercalated limestones. A monzodiorite intrusion cutting the lower sections of the Goonumbla Volcanics has been dated at  $450.8 \pm 4.2$  Ma.

**Wombin Volcanics**, which are 700 to 1000 m thick and of Late Ordovician age, are typically dark red hematite-dusted glassy lavas, ignimbrites, polymictic volcanic breccias and other volcanic sediments, with less abundant porphyritic trachyandesitic and flow banded trachytic lavas.

Basement to the Goonumbla Igneous Complex occurs a short distance to the south and consists of the Nelungaloo Volcanics overlain by the Early Ordovician Yarrimbah



**Figure 10: Local geology of the Goonumbla region.** Abbreviations: GVC = Goonumbla Volcanic Complex; E22, E27, E28, E48, = Endeavour 22, 26, 27 and 48 respectively. Modified from Lickfold *et al.*, 2003, *Economic Geology*, v98:8, p1612 Fig. 5; (after Heithersay *et al.*, 1990 and Heithersay and Walshe, 1995).

Formation. These two units are manifestations of pulse 1 of arc magmatism and consist of andesitic lavas and volcaniclastic sedimentary rocks overlain by an upward fining-sequence of volcanic-derived conglomerate, sandstone and siltstone.

Lickfold *et al.*, (2003) quoted Simpson *et al.*, (2000) as having interpreted the Goonumbla and Wombin Volcanics as a 'several kilometre' thick subaqueous volcaniclastic apron that formed on the flanks of a shallow marine, to possibly sub-aerial, largely Late Ordovician strato-volcano. They argue that the ignimbrites and trachytic lavas indicate voluminous explosive eruptions and sector collapse on the subaerial sections of the volcano.

Both the Goonumbla and Wombin Volcanics have been intruded by numerous monzonite and quartz monzonite bodies, including the mineralised quartz monzonite

porphyry pipes associated with the Endeavour ore deposits. These intrusions typically have a microcrystalline to aphanitic, dark red K feldspar + quartz groundmass. Dating of two samples of zircon from quartz monzonite porphyries 3 km apart (see Lickfold *et al.*, 2003 for details), yielded ages of  $439.1 \pm 4.5$  Ma and  $438.9 \pm 4.7$  Ma respectively, and dating of white mica alteration from Endeavour 26 returned an age of  $439.2 \pm 1.4$  Ma (Perkins *et al.*, 1990), suggesting the quartz monzonite porphyries and alteration are essentially coeval. Other age data confirm this hypothesis (Lickfold *et al.*, 2003).

Pre- and syn-mineralisation brittle structures are interpreted to have localised the emplacement of intrusives, including the NNW-trending Endeavour Linear, as well as several other NW- and NE-trending fracture sets. Minor brittle movement on certain post quartz monzonite porphyry

structures resulted in mostly small-scale disruption and some dislocation of the Endeavour mineralisation (Lickfold *et al.*, 2003).

#### **Intrusives**

Lickfold *et al.*, (2003) described the Endeavour deposits as being concentrically zoned, cylindrical bodies of quartz-sulphide stockwork veining centred on pipe-like, multiphase, quartz monzonite porphyry complexes. These intrusive bodies have lateral dimensions in the order of 50 to 150 m and a minimum vertical extent of 600 to 900 m (Fig. 11). The associated ore zones are up to 400 m in diameter based on a 0.5% Cu equivalent cutoff.

The quartz monzonite porphyry (QMP) intrusions in all four Endeavour deposits have ubiquitous phenocrysts of plagioclase and K feldspar, the former typically rimmed by fine-grained, anhedral K feldspar. Primary and secondary magnetite are found in all of the intrusive phases, where the primary phenocrysts are distinguished from the secondary specks by their large (>50 µm) euhedral shape. Similarly, both primary and secondary biotite are also present in all intrusive phases. Apatite, sphene and lesser zircon are accessory micro-phenocrysts in most intrusions (Lickfold *et al.*, 2003).

Lickfold *et al.*, (2003) have recognised and described at least nine intrusive phases within the complexes that are associated with the Endeavour deposits, divided into pre-, early-, syn-, late- and post-mineral intrusions, as detailed below.

**Pre-mineral Intrusions** - represented by an *equigranular monzodiorite* which is found at deeper than 1300 m beneath the surface at Endeavour 26 and in outcrop 500 to 1000 m to the north. It contains 10 to 20% mafic minerals, including, in decreasing order of abundance: augite, biotite, magnetite and hornblende. K feldspar is intergrown with quartz, while rarely, primary(?) anhydrite is interstitial to plagioclase phenocrysts. No primary disseminated sulphides or quartz-sulphide veins are recorded within this lithology, although sericitised clasts of it are found in the biotite quartz monzonite (Lickfold *et al.*, 2003).

**Early-mineral Intrusions** - which are *biotite quartz monzonites* (BQM) that are found adjacent to, or beneath, each of the four deposits at depths of more than 650 m below surface. They are commonly brick red in colour, medium- to coarse-grained, and equigranular to semi-porphyrific, with 1 to 2 mm euhedral plagioclase, K feldspar and biotite crystals, and interstitial, fine-grained granular subhedral K feldspar, anhedral quartz and minor (<1%) anhydrite. Blebs of disseminated bornite, chalcopyrite and rarely chalcocite are found within the BQM at Endeavour 26, 27 and 48, as are minor 2 to 5 mm thick, straight walled quartz-sulphide veins with K feldspar ± biotite selvages.

The first of the three varieties of QMP that comprise the 50 to 200 m diameter complexes central to each of the Endeavour deposits are the early, volumetrically minor *biotite quartz monzonite porphyry* (B-QMP) intrusions. They comprise un-crowded (20 to 30%

phenocrysts) to crowded (50 to 60% phenocrysts) porphyritic rocks containing plagioclase, K feldspar, biotite, augite and magnetite phenocrysts in an aphanitic to fine-grained granular groundmass of K feldspar and quartz, typically with around 5% quartz. Fine (10 to 50 µm) copper sulphides (~1%) are disseminated through the groundmass with coarse (11 to 80 mm) clots of bornite and chalcopyrite and minor (usually <1%) bornite-quartz veins in some deposits.

**Syn-mineral Intrusions** - primarily represented by *K feldspar quartz monzonite porphyry* intrusions (K-QMP, the second of the QMP phases), ranging in colour from pale to salmon pink to dark orange-red. It occurs in the central parts of the QMP complexes at all four Endeavour deposits and is volumetrically the most abundant phase. The hydrothermal alteration zones and high-grade ore at each deposit are centred on, and most intensely developed within, the K-QMP and the immediately adjacent volcanic rocks. Disseminated sulphides generally account for about 2%, and stockwork veins 5 to 20%, of the volume of the K-QMP respectively, although the density of veining diminishes in intensity with distance from the outer margin of the intrusive. K-QMP intrusions have an uncrowded porphyritic texture with 30 to 40% phenocrysts of plagioclase, K feldspar and minor (<2%) magnetite +biotite +hornblende, set in a mainly aphanitic K feldspar-quartz groundmass.

**Late-mineral Intrusions** - represented by dark orange-red *augite-biotite-K feldspar quartz monzonite porphyry* intrusions (KA-QMP, the third of the QMP phases) are found over much of the vertical extent of the four deposits, close to both the syn-mineral K-QMP and the following late-mineral B-QMP (see below). The KA-QMP intrusions are volumetrically the second most abundant intrusive phase and have a markedly diminished level of associated alteration and copper-gold mineralisation compared to the K-QMP. In addition, veins within K-QMP intrusions are truncated at the mutual contacts with KA-QMP. Certain of the KA-QMP examples contain xenoliths of volcanic rocks that have truncated quartz veins and clasts of the K-QMP phase. The KA-QMP intrusions are uncrowded to crowded porphyries with plagioclase, K feldspar and minor augite +biotite +magnetite +hornblende phenocrysts set in a fine-grained groundmass ranging from 10 to 50%, averaging 30 to 40% quartz. Bornite and chalcopyrite comprise up to 1% as disseminations through the groundmass. Mineralised quartz veins, with or without central K feldspar cores, locally comprise 5 to 10% of the KA-QMP in all four deposits.

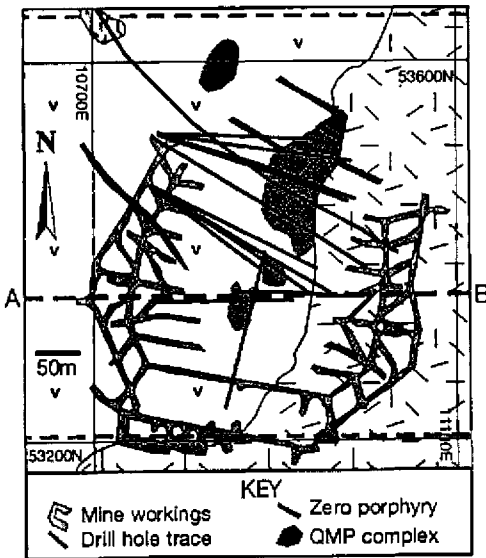
A second, but late-mineral phase of the *biotite quartz monzonite porphyry* (B-QMP), which followed the KA-QMP, is texturally and geochemically indistinguishable from the early-mineral intrusive with the same designation, although a late mineral timing is indicated by vein truncation where it cuts the K-QMP at Endeavour 22 and 26. At Endeavour 27 however, this latter intrusive phase is only found outside of the complex.

*Post-mineral Intrusions* - are present in volumetrically minor amounts and include dykes of *basaltic trachyandesite, mafic monzonite porphyry* and *basalt*. The most significant of these are the "Zero Porphyry" dykes, so named because of their very low ('zero') metal contents. These brownish-red, crowded (40 to 50%) porphyries contain K feldspar, augite +biotite +hornblende and anhydrite phenocrysts in an aphanitic groundmass of predominantly (~95%) K feldspar.





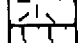
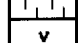

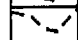

Where trachyandesite dykes are present, they occur at the edges of the Zero Porphyries.

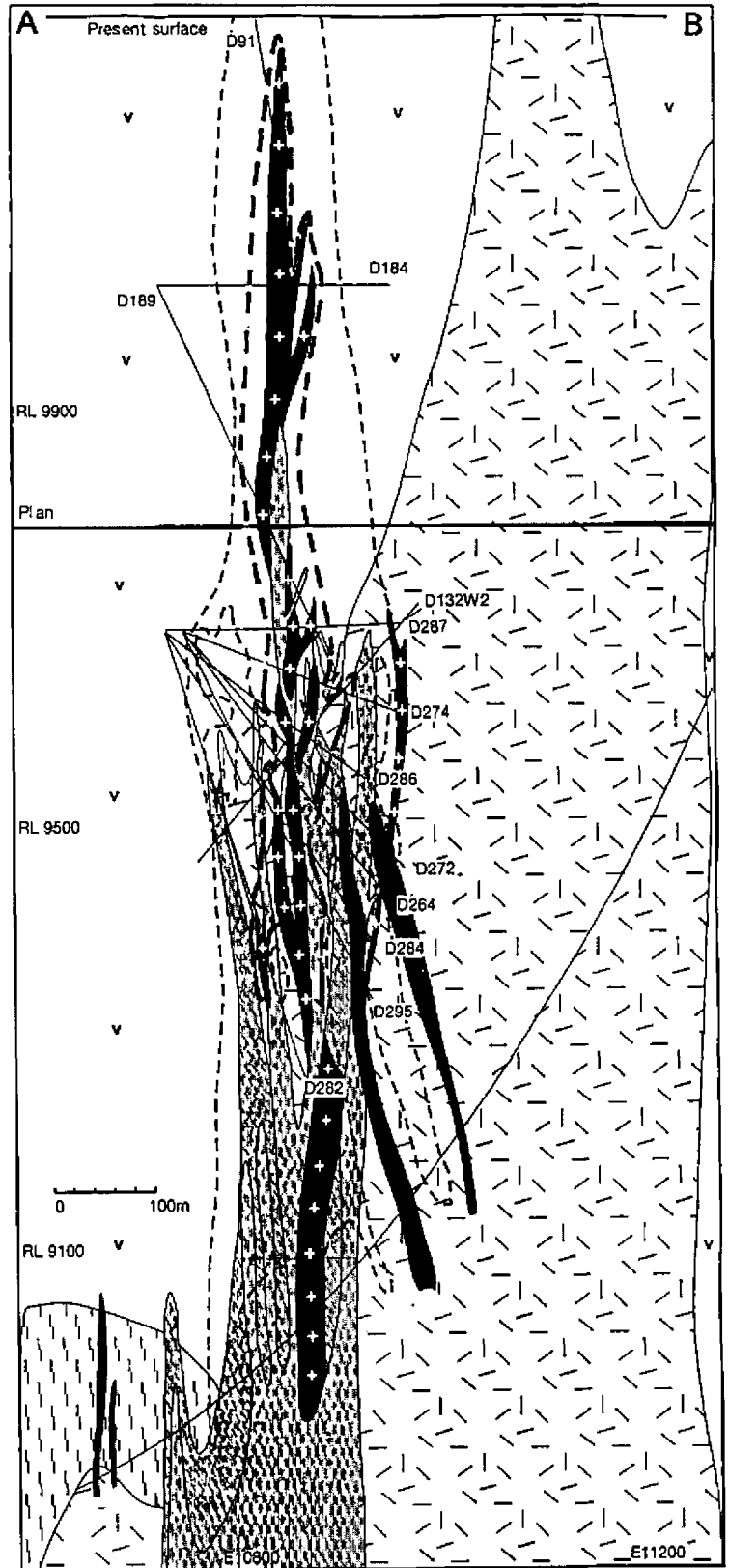
Several basaltic dykes around 1 m thick were emplaced at some of the deposits. The exact age of these dykes is unknown, although some may have intruded the porphyry complexes during the waning stages of volcanism associated with the Goonumbla Volcanic Complex: others may be Tertiary in age.

Figure 11: *Interpreted east-west section through the Endeavour 26 deposit at Northparkes. Modified from Lickfold et al., 2003, Economic Geology, v98:8, p1613 Fig. 6.*



Legend

-  Zero porphyry
-  Augite-biotite K-feldspar QMP
-  K-feldspar QMP
-  Biotite QMP
-  Biotite quartz monzonite
-  Monzoniorite
-  Wombin Volcanics
-  2% copper contour
-  0.5% copper contour



### Mineralisation & Alteration

Hydrothermal alteration and mineralisation at each of the four Endeavour deposits are centred on the QMP intrusive pipes and generally do not persist beyond 750 m from the margins of the intrusive complexes into the surrounding volcanic rocks (Lickfold *et al.*, 2003).

The sulphides in each of the mineralisation stages of the Endeavour ore deposits, as described below, are zoned outwards from the cores of the QMP intrusive complexes. They grade from proximal bornite-rich zones, to intervals with equal amounts of bornite and chalcopyrite, to chalcopyrite-dominant, to distal pyrite-dominated assemblages. Gold is typically present as <25 µm inclusions along fractures within bornite grains, along bornite grain boundaries, and on rare occasions, as inclusions in chalcocite. Silver is also found in association with bornite, with average grades of between 3 and 4 g/t in each of the four deposits. Bornite and chalcocite are intergrown where they are found together, while chalcopyrite occurs either along fractures and cleavage planes within bornite, or as mutual intergrowths where the two minerals coexist. Minor tellurides, selenides, tennantite-tetrahedrite and enargite are found as inclusions in bornite and chalcopyrite, as intergrowths in bornite, and less commonly in chalcopyrite and chalcocite. In the main stage veining, bornite and chalcopyrite are intergrown with anhydrite. Bornite also occurs as clots in the B-QMP, K-QMP and KA-QMP at each of the Endeavour deposits, generally accounting for <1% of the total sulphides. These clots are spherical to irregular in shape and contain ~98% bornite, with only traces of the other sulphides and silicates. They have no obvious connection with veining and occur in rocks that have been overprinted by K silicate alteration only; sericite alteration assemblages are absent (Lickfold *et al.*, 2003).

Lickfold *et al.*, (2003), and authors cited therein, noted that alteration assemblages are generally both discontinuous and non-symmetrical, and vary from deposit to deposit due to the multiplicity and geometry of intrusion and alteration/mineralisation. They also point out that while the pattern at each deposit is therefore unique, there are common features that have combined to produce the overall result, as summarised below.

**Pre-mineral Stage** - an early halo of vein-like K feldspar + quartz dykes containing weak copper mineralisation appears to predate early K-silicate alteration and possibly to have been related to the BQM intrusions. Pre-mineral weak to intense alteration occurs mainly in the volcanic wall rocks and BQM intrusions and comprises albitisation and sericitisation of plagioclase and K feldspar, as well as alteration of magmatic magnetite to chlorite + quartz + carbonate ± fluorite.

**Early Stage** alteration and mineralisation, which followed the pre-mineral stage, resulted in the formation of 50-200 m wide alteration aureoles around all four of the QMP complexes central to the Endeavour deposits. These aureoles contain moderate to intense biotite-magnetite and K feldspar alteration and abundant quartz-sulphide veins at their cores, and grade outwards

to epidote-bearing propylitic alteration at Endeavour 48. Inwards, towards the core of the deposits, there is a transition from biotite + magnetite to K feldspar, characterised by K feldspar ± anhydrite ± magnetite alteration assemblages, hematite dusting of the wall rocks, and irregular discontinuous veins of quartz + K feldspar, ± biotite ± chalcopyrite ± bornite ± magnetite ± anhydrite ± calcite. This alteration assemblage and veining is interpreted to have accompanied the early-mineral B-QMP intrusions.

**Transitional Stage**, unidirectional solidification textures (continuous to discontinuous alternating bands of comb quartz and aplite porphyry containing disseminated sulphides and occasional, plagioclase and/or K feldspar phenocrysts) and related anisotropic textures (such as miarolitic cavities, spherical aggregates of quartz and K feldspar) occur in both the K-QMP and KA-QMP phases. They have been interpreted to have accompanied each phase as discrete "magmatic to hydrothermal" transition episodes.

**Main Stage M1 and M2 veins**, associated with the K-QMP and KA-QMP intrusives respectively, were responsible for the main episodes of mineralisation in the Endeavour deposits. The bulk of the sulphide mineralisation in all four deposits occurs in the M1 veins, which vary in character with time. Early M1 veins have K feldspar halos, while those emplaced later are fringed by sericite-hematite. Early *M1a veins* and veinlets are thin (<10 mm) and comprise quartz + sulphide + K feldspar ± anhydrite ± calcite ± apatite ± rutile with thin (<5 mm) quartz-K feldspar selvages. The *M1b stockwork or sheeted veins*, which are characteristically linear and vary from 5 to 20 mm in thickness, comprise quartz + sulphide ± anhydrite + carbonate + K feldspar, enclosed by a halo of pervasive, locally mottled, sericite + quartz ± hematite alteration. Minor tetrahedrite-tennantite, covellite, chalcocite, tellurides and/or lead selenides are also found within these veins. M1b veins contain the bulk of the sulphides in the Endeavour deposits. The *M1c veins* comprise milky quartz + chalcopyrite > bornite + calcite which are found ~50 m outboard of the QMP complexes in volcanic wall rocks; they are characterised by higher calcite and lower quartz, and are enriched in chalcopyrite and bornite compared to M1b veins.

The *M2a and M2b stage veins* are associated with the KA-QMP intrusive phase in each of the Endeavour deposits and are broadly similar to M1a and M1b, although the M2a and M2b veins carry more chalcopyrite than bornite.

**Late Stage** mineralisation and alteration are represented by three sericite alteration assemblages and associated veining, although only one, L1, is strongly mineralised. L1 alteration comprises intense to moderate, pervasive quartz + sericite + carbonate ± hematite replacement of feldspar phenocrysts and groundmass to produce a fine-grained mass that preserves the original texture of the host and is best developed in the K-QMP and KA-QMP intrusions in the core of the Endeavour deposits. Chalcopyrite and minor bornite are disseminated in the



Deposit	Host intrusion	Coeval volcanics	Ore- related alteration	Sulphide zonation - from core	Quartz stockwork	Au (t)	Au/ Cu (g/ t:%)	Abundant magnetite	References
Ajax-Ajax, British Columbia, Canada	Diorite, monzodiorite	Yes	Albite- diopside-epidote	Chalcopyrite- pyrite	No	31	0.6: 1	No	Ross <i>et al.</i> , 1995, Dawson <i>et al.</i> , 1991
Copper Mountain, Ingerbelle & Similkameen, British Columbia, Canada	Diorite- monzonite-syenite	No	(1) Albite- diopside-epidote- calcite; (2) Orthoclase- biotite- epidote- magnetite	Bornite-chalcopyrite → chalcopyrite- pyrite	No	55	0.36: 1	No	Dawson <i>et al.</i> , 1991 Stanley <i>et al.</i> , 1995
Galore Creek, Stikine, British Columbia, Canada	Syenite	Yes	Garnet- biotite-orthoclase- anhydrite	Chalcopyrite-bornite → pyrite	No	164	0.76: 1	Yes	Enns <i>et al.</i> , 1995
Mount Milligan, British Columbia, Canada	Monzonite, diorite	Yes	Biotite- magnetite-orthoclase	Chalcopyrite-bornite → pyrite	No	205	2.2: 1	Yes	Sketchley <i>et al.</i> , 1995, Dawson <i>et al.</i> , 1991
Mount Polley, Caribou Bell, British Columbia, Canada	Diorite- monzonite	Yes	Orthoclase- diopside- actinolite- magnetite-biotite	Chalcopyrite-bornite → pyrite	No	88	1.3: 1	Yes	Fraser <i>et al.</i> , 1995
Red Chris, British Columbia, Canada	Monzonite, quartz monzodiorite	No	Orthoclase- albite-quartz- magnetite-biotite	Chalcopyrite-bornite → pyrite	Yes	141	0.77: 1	No	Newell and Peatfield, 1995; Baker <i>et al.</i> , 1997
Skouries, Greece	Monzonite, syenite	No	Biotite- magnetite-orthoclase- quartz	Bornite → chalcopyrite → pyrite	Yes	>250	1.3: 1	Yes	Tobey <i>et al.</i> , 1998; Kroll <i>et al.</i> , 2002
Dinkidi, Philippines	Quartz-monzonite, syenite	Yes	(1) Orthoclase- actinolite- magnetite; (2) sericite-carbonate	Bornite-chalcopyrite → chalcopyrite-pyrite	Yes	132	2.4: 1	Yes	Wolfe <i>et al.</i> , 1999
Endeavour 26, New South Wales, Australia	Quartz monzonite	Yes	Orthoclase- biotite-quartz- magnetite	Bornite → chalcopyrite → pyrite	Yes	65	0.45: 1	Yes	Heithersay and Walshe, 1995; Lickfold <i>et al.</i> , 2003
Cadia Hill, Cadia Quarry, Cadia East, & Ridgeway, New South Wales, Australia	Quartz monzonite	Yes	Orthoclase- quartz- calcite- biotite	Chalcopyrite → pyrite	Yes	639	3.8: 1	No	Newcrest Mining., 1997, 2003, 2004
	Monzodiorite, quartz monzonite	Yes	Actinolite- biotite- magnetite- quartz	Bornite chalcopyrite → pyrite	Yes	149	3.2: 1	Yes	Newcrest Mining., 2003

Table modified and updated after Sillitoe, 2000 and Wilson *et al.*, 2003

Table 2: Comparison of the principal features of alkalic gold-copper porphyry deposits

altered matrix of these intrusive complexes at Endeavour 22, 26 and 27, while chalcocite + bornite + tennantite-tetrahedrite are evenly distributed in the similarly altered groundmass at Endeavour 48. Away from the pervasive alteration, L1 quartz + carbonate + sericite + chalcopyrite and/or pyrite veins are distinguished from other veins by their sericite-carbonate-pyrite selvages.

Late stage L2 alteration takes the form of fracture- and fault-controlled sericite (phyllic) assemblages that contain sericite + carbonate + quartz + pyrite  $\pm$  anhydrite.

L3 veins are less abundant and comprises carbonate + sericite + quartz + gypsum +/or anhydrite + base metal sulphides  $\pm$  fluorite, with selvages of the same non-metallic minerals. The base metal sulphides vary widely in quantity and type and are mainly pyrite  $\pm$  sphalerite  $\pm$  galena  $\pm$  chalcopyrite.

*Post-mineral alteration* takes the form of weak to moderate propylitic alteration, where feldspars and mafic minerals have been selectively replaced by carbonate  $\pm$  hematite  $\pm$  pyrite. This alteration episode overprinted the "Zero Porphyry" dykes.

#### Conditions of Deposition

Lickfold *et al.*, (2003) reported microthermometric analyses of fluid inclusions from early-, transitional-, main- and late-stage veins indicating that the Endeavour deposits were formed at depths between 1000 and 1700 m below the palaeosurface, where lithostatic pressure regimes prevailed during early- to main-stages, and near hydrostatic during late-stage events. They note that the data suggest the early-, transitional- and main-stages were subjected to high-temperature (460 to 550°C) magmatic-hydrothermal fluids with salinities of ~55 to 60 wt percent NaCl  $\pm$  KCl equivalent. Although the late stage fluids were cooler (350 to 450°C) and less saline (~40 wt % NaCl equiv.), their compositions are consistent with magmatic-hydrothermal origins. They conclude that the Endeavour porphyry deposits are representative of the orthomagmatic end member of the porphyry continuum.

#### Comparison of Alkalic Deposits

Wilson *et al.*, (2003) observed that the Ridgeway deposit in the Cadia district, and by association, the other shoshonite-related ore deposits in the Cadia district and the Endeavour group, have features that are distinctive of alkalic porphyry gold-copper deposits (Table 2). Gold and copper in such deposits are typically associated with alteration assemblages rich in calcic, potassic or sodic hydrothermal minerals (Lang *et al.*, 1995b). Similar calc-potassic assemblages occur at Dinkidi in the Philippines (Wolfe *et al.*, 1999), and sodic alteration similar to that at Cadia-Ridgeway occurs in association with mineralisation at Ajax and Afton in Canada (Ross *et al.*, 1995). The lack of pervasive phyllic alteration at Ridgeway is also characteristic of alkalic porphyry deposits globally (Lang *et al.*, 1995a). One of the main differences between the deposits of the Macquarie Arc and those of British Columbia (Canada) is the presence of abundant quartz veins

in the former and the correspondence between the density of veining and the gold and copper grades. Mineralised fractures in the Canadian deposits are characteristically devoid of quartz (Lang *et al.*, 1995b). The Red Chris alkalic porphyry deposit in northwestern British Columbia is an exception, with mineralisation being hosted by quartz-rich stockworks, while sericitic alteration is also widespread (Baker *et al.*, 1997). Based on these features and on the whole rock geochemistry of the related intrusions, Baker *et al.*, (1997) suggest that Red Chris is transitional between calc-alkalic and alkalic end members of porphyry-style deposits, a position Wilson *et al.*, (2003) suggest may be the case at Cadia Ridgeway and Endeavour. All of the discussion above is drawn directly from Wilson *et al.*, (2003).

#### Acknowledgements

Authors of the key papers that were the main source of information recorded in this review paper for the Cadia and Endeavour groups of deposits, are thanked for reviewing the paper and ensuring that it faithfully represents their original work and conclusions. These include John Holliday, Alan Wilson and Ian Tedder of Newcrest Mining Limited and Vanessa Lickfold, now of Kumba Resources. Their comments and suggestions have improved the quality of the paper. Thanks are also due to *Economic Geology*, *Mineralium Deposita*, Newcrest Mining Limited and the authors listed above for approving the use of various of the figures within the paper. Richard Glen publishes with the permission of the Director-General, NSW Department of Primary Industries. Work referred to in the papers by Crawford *et al.*, (2005), Percival & Glen (2005) and Glen *et al.*, (2005) was carried out in a project financed by CODES-University of Tasmania, the Geological Survey of New South Wales (NSW Department of Mineral Resources), six sponsoring mining- exploration companies and the Australian Research Council under a SPIRT grant.

#### References

- Baker, T. and Thompson, J.F.H., 1997, Carbonate alteration at the Red Chris porphyry Cu-Au deposit, northwestern British Columbia; *Geological Society of America*, Abstracts, p. A446.
- Blevin, P.L. and Morrison, G.W., 1997 - Magmatic and hydrothermal evolution of major intrusive related gold deposits in eastern Australia; *AMIRA P425 Final Report*, Canberra.
- Carr, G.R., Dean, J.A., Suppel, D.W. and Heithersay, P.S., 1995 - Precise lead isotope fingerprinting of hydrothermal activity associated with Ordovician to Carboniferous metallogenic events in the Lachlan Fold Belt of New South Wales; *Economic Geology*, v. 90, pp. 1467-1505.
- Cawood, P.A., 2005 - Terra Australis Orogen: Rodinia breakup and development of the Pacific and Iapetus margins of Gondwana during the Neoproterozoic and Paleozoic; *Earth-Science Reviews*, v. 69, pp. 249-279.
- Chappell, B.W., 1994 - Lachlan and New England: fold belts of contrasting magmatic and tectonic

- development; *Journal of the Proceedings of the Royal Society of NSW*, v. 127, pp. 47-59.
- Chappell, B.W., White, A.J.R. and Hine, R., 1988 - Granite provinces and basement terranes in the Lachlan fold belt, southeastern Australia; *Australian Journal of Earth Sciences*, v. 35, pp. 505-521.
- Chivas, A.R. and Nutter, A.H., 1975 - Copper Hill porphyry copper prospect; in Knight C.L., (Ed.) *Economic Geology of Australia and Papua New Guinea*, AusIMM, Melbourne, pp. 716-720.
- Collins, W.J. and Vernon, R.H., 1992 - Palaeozoic arc growth, deformation and migration across the Lachlan fold belt, southeastern Australia. *Tectonophysics*, v. 214, pp. 381-400.
- Cooke, D.R., Wilson, A.J., Lickfold, V. and Crawford, A.J., 2002 - The alkalic Au-Cu porphyry province of NSW; AusIMM 2002 - 150 Years of Mining, Auckland, Sept. 1-4, 2002, Proceedings, *AusIMM Publication Series*, no. 6/02, pp. 197-202.
- Crawford, A.J., Meffre, S. and Symonds, P.A., 2003 - 120 to 0 Ma tectonic evolution of the southwest Pacific and analogous geological evolution of the 600 to 220 Ma Tasman Fold Belt System; in Hillis, R.R. and Müller, R.D. (Eds.), *Evolution and Dynamics of the Australian Plate*; *Geological Society of Australia Special Publication 22 and Geological Society of America, Special Paper 372*, pp. 383-403.
- Crook, K.A.W., 1969 - Contrasts between Atlantic and Pacific geosynclines; *Earth and Planetary Science Letters*, v. 5, pp. 429-438.
- Dawson, K.M., Panteleyev, A., Sutherland Brown, A., Woodsworth, G.J., 1991 - Regional metallogeny; in Gabrielse, H., Yorath, C.J., (Eds), *Geology of Canada*, No. 4, *Geology of the Cordilleran Orogen in Canada*, *Geological Survey of Canada* (also *Geological Society of America*), *The Geology of North America*, DNAG Series, v. G-2), Ch. 19, pp. 709-767.
- Enns, S.G., Thompson, J.F.H., Stanley, C.R. and Yarrow, E.W., 1995 - The Galore Creek porphyry copper-gold deposits, northwestern British Columbia; in Schroeter, T.G., (Ed.), *Porphyry deposits of the Northwestern Cordillera of North America*; *CIMM Spec. Vol. 46*, p. 630-644.
- Fraser, T.M., Stanley, C.R., Nikic, Z.T., Pesalj, R., and Gorc, D., 1995 - The Mount Polley alkalic porphyry copper-gold deposit, south-central British Columbia; in Schroeter, T.G., (Ed.), *Porphyry deposits of the Northwestern Cordillera of North America*; *CIMM Spec. vol. 46*, pp. 609-622.
- Glen, R.A., 2004 - Plate tectonics of the Lachlan Orogen: A framework for understanding its metallogenesis; *Abstracts of the Geological Society of Australia*, v. 74, pp. 33-36.
- Glen, R.A., 2005 - The Tasmanides of eastern Australia; in Vaughan, A.P.M., Leat, P.T. and Pankhurst, R.J., (Eds.), *Terran Processes at the Margins of Gondwana*, Special Publication of the *Geological Society*, London, 246p. (in press).
- Glen, R.A., Crawford, A.J. and Cooke, D.R., 2003 - Tectonic setting of porphyry copper-gold mineralisation in the Macquarie Arc. Magmas to Mineralisation: the Ishihara Symposium. Sydney, *Geoscience Australia*, Record 2003/14, pp. 65-68.
- Glen, R.A., Crawford, A.J., Cook, D.R., Percival, I.G., Meffre, S., Scott, R.J., Squire, R. and Barron, L.M., 2004 - The Macquarie Arc: a key component of the Ordovician and earliest Silurian tectonics of the Lachlan Orogen; *Abstracts of the Geological Society of Australia*, v. 73, p. 162.
- Glen, R.A., Korsch, R.J. and Wake-Dyster, K.D., 1993 - A deep seismic cross section through the Tamworth Belt: Preliminary interpretation of 4 seconds two-way time data; in Flood, P.G. and Aitchison, J.C. (Eds), *Conference on the New England Orogen, Eastern Australia*, University of New England, Armidale, Abstract Volume, pp. 102-104.
- Glen, R.A., Scott, R.J., and Meffre, S., 2005 - The Benambran Orogeny in the eastern Lachlan Orogen; *Australian Journal of Earth Sciences* (in press).
- Glen, R.A., Walshe, J.L., Barron L.M. and Watkins, J.J., 1998 - Ordovician convergent-margin volcanism and tectonism in the Lachlan sector of East Gondwana; *Geology*, v. 26, pp. 751-754.
- Glen, R.A. and Walshe, J.L., 1999 - Cross-structures in the Lachlan Orogen: the Lachlan Transverse Zone example; *Australian Journal of Earth Sciences*, v. 46, pp. 641-658.
- Gray, N., Mandyczewsky, A. and Hine, R., 1995 - Geology of the zoned gold skarn system at Junction Reefs, New South Wales; *Economic Geology*, v. 90, pp. 1533-1552.
- Green, D., 1999 - Geology, geochemistry and genesis of the Big Cadia deposit, NSW; Honours Thesis, *University of Tasmania* (unpublished).
- Heithersay, P.S. and Walshe, J.L., 1995 - Endeavour 26 North: a porphyry copper-gold deposit in the Late Ordovician, shoshonitic Goonumbla Volcanic Complex, New South Wales, Australia; *Economic Geology*, v. 90, pp. 1506-1532.
- Heithersay, P.S., Neill, W.J.O., van der Helder, P., Moore, C.R. and Harbon, P.G., 1990 - Goonumbla porphyry copper district: Endeavour 26 North, Endeavour 22 and Endeavour 27 copper-gold deposits; in: Hughes, F.E., (Ed.) *Geology of the mineral deposits of Australia and Papua New Guinea*, *AusIMM, Melbourne*, v. 2, pp. 1385-1398.
- Holliday, J.R., Wilson, A.J., Blevin, P.L., Tedder, I.J., Dunham, P.D. and Pfitzner M., 2002 - Porphyry gold-copper, mineralisation in the Cadia district, eastern Lachlan Fold Belt, New South Wales, and its relationship to shoshonitic magmatism; *Mineralium Deposita*, v. 37, pp. 100-116.
- Korsch, R.J., Barton, T.J., Gray, D.R., Owen, A.J. and Foster D.A., 2002 - Geological interpretation of the deep seismic-reflection transect across the boundary between the Delamerian and Lachlan Orogens, in the vicinity of the Grampians, Western Victoria; *Australian Journal of Earth Sciences* v. 49(6),

- pp. 1057-1075.
- Korsch, R.J., Wake-Dyster, K.D. and Johnstone, D.W., 1993 - The Gunnedah Basin-New England Orogen deep seismic reflection profile: implications for New England tectonics; in Flood, P.G. and Aitchison, J.C. (Eds), *Conference on the New England Orogen, Eastern Australia*, University of New England, Armidale, Abstract Volume, pp. 85-100.
- Kroll, T., Müller, D., Seifert, T., Herzig, P.M. and Schneider, A., 2002 - Petrology and geochemistry of the shoshonite-hosted Scouries porphyry Cu-Au deposit, Chalkidiki, Greece; *Mineralium Deposita*, v. 37, no. 1, pp. 137-144.
- Lang, J.R., Stanley, C.R. and Thompson, J.F.H., 1995a - Porphyry copper-gold deposits related to alkalic igneous rocks in the Triassic-Jurassic arc terranes of British Columbia; *Arizona Geological Society Digest*, v. 20, pp. 219-236.
- Lang, J.R., Stanley, C.R., Thompson, J.F.H. and Dunne, K.P.E., 1995b - Na-K-Ca magmatic-hydrothermal alteration in alkalic porphyry Cu-Au deposits, British Columbia; *Mineralogical Association of Canada Short Course*, v.23, pp. 339-366.
- Lickfold, V., Cooke, D.R., Smith S.G. and Ullrich, T.D., 2003 - Endeavour copper-gold porphyry deposits, Northparkes, New South Wales: intrusive history and fluid evolution; *Economic Geology*, v. 98:8, pp. 1607-1636.
- Lindhorst, J.W. and Cook, W.G., 1990 - Gidginbung gold-silver deposit, Temora; in: Hughes, F.E., (Ed.) *Geology of the mineral deposits of Australia and Papua New Guinea*, v. 2. *AusIMM, Melbourne, Australia*, pp. 1365-1370.
- Macdonald, G.A. and Katsura, T., 1964 - Chemical composition of Hawaiian lavas; *Journal of Petrology*, v. 5, pp. 82-133.
- McInnes, P., Miles, I., Radclyffe, D. and Brooker, M., 1998 - Endeavour 42 (E42) gold deposit, Lake Cowal; in, Berkman D.A. and Mackenzie, D.H., (Ed.s) *Geology of Australian and Papua New Guinean Mineral Deposits*, *AusIMM, Melbourne*, pp. 581-586.
- Miles, I.N. and Brooker, M.R., 1998 - Endeavour 42 deposit, Lake Cowal, New South Wales; a structurally controlled gold deposit. *Australian Journal of Earth Sciences*, v. 45, pp. 837-847.
- Miller, J.M., Phillips, D., Wilson, C.J.L. and Dugdale, L.J., 2004 - A new tectonic model for the Delamerian and western Lachlan orogens; *Abstracts of the Geological Society of Australia*, v. 73, p. 174.
- Müller, D., Rock, N.M.S. and Groves, D.I., 1992 - Geochemical discrimination between shoshonitic and potassic volcanic rocks from different tectonic settings: a pilot study; *Mineralogy and Petrology* v. 46, pp. 259-289.
- Müller, D. and Groves, D.I., 1993 - Direct and indirect associations between potassic igneous rocks, shoshonites and gold-copper deposits; *Ore Geology Reviews*, v. 8, pp. 383-406.
- Müller, D. and Groves, D.I., 1995 - Potassic igneous rocks and associated gold-copper mineralisation; *Springer, Berlin, Heidelberg, New York*
- Murray, S.I. and Stewart I.R., 2000 - Palaeogeographic significance of Ordovician conodonts from the Lachlan Fold Belt, southeastern Australia; *Historical Biology*, v. 15, pp. 145-170.
- Newcrest Mining Limited, 1997 - Annual Report.
- Newcrest Mining Limited, 2000 - Annual Report.
- Newcrest Mining Limited, 2003 - Annual Report.
- Newcrest Mining Limited, 2004 - Annual Report.
- Newell, J.M. and Peatfield, G.R., 1995 - The Red Chris porphyry copper-gold deposit, northwestern British Columbia; in Schroeter, T.G., (Ed.), *Porphyry deposits of the Northwestern Cordillera of North America: CIMM Spec. Vol. 46*, pp. 674-688.
- Oversby, B., 1971 - Palaeozoic plate tectonics in the southern Tasman Geosyncline; *Nature (Physical Sciences)*, v. 234, pp. 45-48.
- Overton, R., 1990 - Sheahan-Grants gold deposit, Junction Reefs; in Hughes, F.E., (Ed.) *Geology of the mineral deposits of Australia and Papua New Guinea*, *AusIMM, Melbourne*, v. 2, pp 1403-1407.
- Packham, G., Percival, I. and Bischoff, G., 1999 - Age constraints on strata enclosing the Cadia and Junction Reefs ore deposits of central NSW and tectonic implications; *Geological Survey of NSW, Quarterly Notes* 110, pp. 1-12.
- Pearce, J.A., 1982 - Trace element characteristics of lavas from destructive plate boundaries; in Thorpe, R.S., (Ed), *Andesites*. *Wiley, Chichester*, pp. 525-548.
- Percival, I.G. and Glen, R.A., 2005 - Ordovician to earliest Silurian history of the Macquarie Arc, Lachlan Orogen, New South Wales; *Australian Journal of Earth Sciences*, v. 52, in press.
- Perkins, C., McDougall, I. and Clauqué-Long, J., 1990 -  $^{40}\text{Ar}/^{39}\text{Ar}$  and U-Pb geochronology of the Goonumbla porphyry Cu-Au deposits, New South Wales, Australia; *Economic Geology*, v. 85, pp. 1808-1824.
- Powell, C.M., 1983 - Tectonic relationships between the Late Ordovician and Late Silurian palaeogeographies of southeastern Australia; *Journal of the Geological Society of Australia*, v. 30, pp. 353-373.
- Ramsay, W.R.H. and VandenBerg, A.H.M, 1990 - Lachlan Fold Belt in Victoria - regional geology and mineralisation; in Hughes F.E., (Ed.) *Geology of the Mineral Deposits of Australia and Papua New Guinea*, *AusIMM, Melbourne*, v. 2, pp. 1269-1273.
- Richardson, S., 1976 - Geology and mineralization of the Cargo area. *International Geological Congress - ore deposits of the Lachlan fold belt, New South Wales, Sydney*, pp. 10-12.
- Rio Tinto, 2003 - Annual Report and Financial Statements.
- Ross, K.V., Godwin, C.I., Bond, L. and Dawson, K.M., 1995 - Geology, alteration, and mineralization of the Ajax East and Ajax West copper-gold alkalic porphyry deposits, southern Iron Mask batholith, Kamloops, British Columbia; *CIMM, Special*

Volume 46, pp. 565–580.

- Rutland, R.W.R., Etheridge, M.A. and Solomon, M., 1990 - The stratigraphic and tectonic setting of the ore deposits of Australia; *in* Hughes F.E., (Ed.) *Geology of the Mineral Deposits of Australia and Papua New Guinea, AusIMM*, Melbourne, v. 1, pp. 15-26.
- Scheibner, E., 1973 - A plate tectonic model of the Palaeozoic tectonic history of New South Wales; *Journal of the Geological Society of Australia*, v. 20, pp. 405-426.
- Scheibner, E., 1987 - Paleozoic tectonic development of eastern Australia in relation to the Pacific region; *in* Monger, J.W.H. and Francheteau, J., (Eds.) *Circum-Pacific orogenic belts and evolution of the Pacific Ocean basin, American Geophysical Union, Geodynamic Series*, 18, pp. 133-165.
- Scheibner, E. and Basden, H., 1998 - Geology of New South Wales - synthesis; *Memoir of the Geological Survey of New South Wales*, 13 (2), 666p.
- Scott, K.M., 1978 - Geochemical aspects of the alteration-mineralization at Copper Hill, New South Wales, Australia; *Economic Geology*, v. 73, pp. 966-976.
- Sillitoe, R.H., 2000 - Gold-rich porphyry deposits: Descriptive and genetic models and their role in exploration and discovery; *Reviews in Economic Geology*, v. 13, pp. 315-345.
- Simpson, C., Cas, R.A.F. and Arundell, M.C., 2000 - The Goonumbla caldera, Parkes, NSW: fact or fiction; *Abstracts of the Geological Society of Australia*, v. 59, p. 452.
- Sketchley, D.A., Rebogliati, C.M., and De Long, C., 1995 - Geology, alteration and zoning patterns of the Mt. Milligan copper-gold deposits; *in* Schroeter, T.G., (Ed.), *Porphyry deposits of the Northwestern Cordillera of North America, CIMM, Spec. Vol. 46*, pp. 650–655.
- Soesoo, A., Bons, P.D., Gray, D.R. and Foster, D.A., 1997 - Divergent double subduction; tectonic and petrologic consequences; *Geology*, v. 25, pp. 755-758.
- Solomon, M. and Griffiths, J. R., 1972 - Tectonic evolution of the Tasman Orogenic Zone, Eastern Australia; *Nature (Physical Sciences)*, v. 237, pp. 3-6.
- Stanley, C.R., Holbek, P.M., Huyck, H.L.O., Lang, J.R., Preto, V.A.G., Blower, S.J. and Bottaro, J.C., 1995 - Geology of the Copper Mountain alkalic porphyry copper-gold deposits, Princeton, British Columbia; *in* Schroeter, T.G., (Ed.), *Porphyry deposits of the Northwestern Cordillera of North America: CIMM, Spec. vol. 46*, pp. 537–563.
- Stuart-Smith, P.G., 1990 - Evidence for extensional tectonics in the Tumut Trough, Lachlan Fold Belt, NSW; *Australian Journal of Earth Sciences*, v. 37, pp. 147-167.
- Suppel, D.W. and Barron, L. M., 1986 - Platinum in basic to ultrabasic intrusive complexes at Fifield: A preliminary report; *Quarterly Notes of the Geological Survey of New South Wales*, v. 65, pp. 1-8.
- Suppel, D.W. and Scheibner, E., 1990 - Lachlan Fold Belt in New South Wales - regional geology and mineral deposits, *in* Hughes F.E., (Ed.) *Geology of the Mineral Deposits of Australia and Papua New Guinea, AusIMM*, Melbourne, pp. 1321-1327.
- Tedder, I.J., Holiday, J. and Hayward, S., 2001 - Discovery and evaluation drilling of the Cadia Far East gold-copper deposit. *Proceeds, NewGenGold 2001 Conference, Case Histories of Discovery*, Perth, 26-27 Nov., 2001, *Australian Mineral Foundation*, Adelaide, pp. 171-184.
- Thompson, J.F.H., Lessman, J. and Thompson, A.J.B., 1986 - The Temora gold-silver deposit; a newly recognized style of high sulfur mineralization in the lower Paleozoic of Australia; *Economic Geology*, v. 81, pp. 732–738.
- Tobey, E., Schneider, A., Alegria, A., Olcay, L., Perantonis, G. and Quiroga, J., 1999 - Skouries porphyry copper-gold deposit, Chalkidiki, Greece: setting, mineralisation and resources; *in* Porter, T.M., (Ed.), *Porphyry and hydrothermal copper & gold deposits - a global perspective, PGC Publishing, Adelaide*, pp.159-168
- Turner, S.P., Kelley, S.P., VandenBerg, A.H.M., Foden, J.D., Sandiford, M. and Flöttmann, T., 1996 - Source of the Lachlan fold belt flysch linked to convective removal of the lithospheric mantle and rapid exhumation of the Delamerian-Ross fold belt; *Geology*, v. 24, pp. 941-944.
- VandenBerg, A.H.M., Willman, C.E., Maher, S., Simons, B.A., Cayley, R.A., Taylor, D.H., Morand, V.J., Moore, D.H. and Radojkovic, A., 2000 - The Tasman Fold Belt System in Victoria; *Geological Survey of Victoria, Special Publication*.
- Welsh, T.C., 1975 - Cadia copper-gold deposits; *in* Knight C.L., (Ed.) *Economic Geology of Australia and Papua New Guinea, AusIMM*, Melbourne, pp. 711-716.
- Wilson, A.J., Cooke, D.R. and Harper, B.L., 2003 - The Ridgeway gold-copper deposits: a high-grade alkalic porphyry deposit in the Lachlan Fold Belt, New South Wales, Australia; *Economic Geology*, v. 98 (8), pp. 1637-1666.
- Wolfe, R.C., Cooke, D.R. and Joyce, P., 1999 - Geology, mineralisation, and genesis of the alkaline Dinkidi Cu-Au porphyry, north Luzon, Philippines; PACRIM '99 Congress, International Congress on Earth Science, Exploration, and Mining around the Pacific Rim, Bali, Indonesia, October 10–13, 1999, *AusIMM*, Melbourne, Publication Series no 4/99, pp. 509–516.
- Wyborn, D. 1988 - Ordovician magmatism, gold mineralisation, and an integrated tectonic model for the Ordovician and Silurian history of the Lachlan Fold Belt in NSW; *BMR Research Newsletter* 8, pp. 13-14.
- Wyborn, D., 1992 - The tectonic significance of Ordovician magmatism in the eastern Lachlan fold belt; *Tectonophysics*, v. 214, pp. 177-192.

## **GRASBERG PORPHYRY Cu-Au DEPOSIT, PAPUA, INDONESIA: 1. MAGMATIC HISTORY**

John T. Paterson and Mark Cloos

*Department of Geological Sciences, University of Texas at Austin, USA*

**Abstract** - The Grasberg Igneous Complex, which formed at ~3 Ma, is host to one of the largest copper and gold porphyry-type ore deposits discovered on Earth. This study focuses on the magmatic characteristics of the three main phases of intrusion at the level of the open pit mine: the Dalam, subdivided into the Dalam Andesite, Dalam Volcanic and Dalam Fragmental, the Main Grasberg Intrusion (MGI), and the Kali (Early and Late). A sample suite consisting of 225 polished slabs and thin sections shows all units contain plagioclase and biotite as the dominant phenocryst phases. The Dalam Andesite, MGI and Late Kali contain(ed) hornblende as well. The Late Kali and the MGI also contained minor amounts of clinopyroxene. Apatite is ubiquitous as a trace phase. Magmatic magnetite is identifiable in the Late Kali. The magmatic groundmass in the Kali, MGI, and Dalam Andesite was potassium feldspar, albitic plagioclase, quartz and biotite. A similar groundmass assemblage probably existed in the other Dalam phase rocks, but hydrothermal alteration caused complete replacement. The phenocryst assemblages record no profound changes in magma chemistry over time, but the parent chamber was probably recharged at least twice, and possibly many times.

The porphyritic Dalam Andesite, comparatively equigranular MGI, and porphyritic Kali units are texturally distinct. The Dalam Volcanic and Dalam Fragmental units are, respectively, polymict and monomict matrix-supported breccias, typically containing 5% to 10%, but locally up to 30% clasts. Broken phenocrysts are common in the Dalam phase rocks. Dalam phase magmas only became volatile-saturated and explosive when intruded to near the surface. The monomict fragmental unit formed near the centre and the polymict volcanic unit along the edges. The geologic setting is interpreted to be a maar caldera. The MGI passively intruded as a cone shaped plug into the still hot core of the Dalam. The volumetrically minor Early Kali appears to be a small plug into the centre of the MGI whereas the Late Kali is a large wedge-shaped dyke that cuts all units.

### **Introduction**

The Grasberg Igneous Complex (GIC), located in the Ertsberg (Gunung Bijih) Mining District (Fig. 1), is situated in the western half of the island of New Guinea, the Indonesian province of Papua (formerly Irian Jaya). In both areal extent and volume the GIC is limited, with a pre-mine surficial footprint of less than 3 km<sup>2</sup>. Ore-grade mineralisation extends to a depth of more than 2 km. Notable about the Grasberg is the quantity of hypogene ore, both disseminated and vein-hosted and a lack of significant supergene enrichment. Currently producing roughly 6% of the world's copper supply, as well as containing significant quantities of gold, this copper-gold porphyry system is one of the most extraordinary mineral systems on Earth. Production since 1989 occurs as open pit mining with underground operations by block caving to begin in 2014. The projected mine life is at least 45 years. The deposit contains more than two billion tonnes of ore grading an average 1 wt. % copper and 1 gram per tonne gold.

### **Regional Setting**

The rocks into which the GIC and other intrusions within the Ertsberg District were intruded are Mesozoic and Cenozoic passive-margin strata deposited on the northern margin of the Australian continent (Martoyojo *et al.*, 1975; Dow *et al.*, 1988). The oldest unit cropping out in the district is the Kembelangan Group (Cretaceous), a siliciclastic sequence which underlies the New Guinea Limestone Group (Quarles van Ufford, 1996). Most of the mineralisation in the district is spatially associated with the largest plutons: the Ertsberg and Grasberg intrusions.

The island of New Guinea is largely composed of passive margin strata that were "bulldozed" during continental margin-oceanic forearc collisional orogenesis into a spectacular mountain belt, the Central Range, whose maximum height is found next to the Ertsberg District at Puncak Jaya (4884 m) (Hamilton, 1979; Dow *et al.*, 1988). Quarles van Ufford (1996) proposed the Cenozoic tectonic history of the island is the product of two collisions; an

earlier event, the Oligocene "Peninsular orogeny" affected only the eastern part of the island whereas the latest Miocene event, the "Central Range orogeny," created most of the mountainous topography that forms the spine of the island. Near the Ertsberg district, the southern slope of the Central Range is the northern limb of a giant fold, the Mapenduma anticline (Nash *et al.*, 1993). Owing to this structure, which is cored in outcrop by Precambrian slates, the access road from the southern portion of the district to the Ertsberg district contains a nearly continuous stratigraphic record capped by the aforementioned New Guinea Limestone Group. The Central Range orogeny in western New Guinea is bracketed in age by carbonate shelf deposition continuing until at least 15 Ma, and the change to siliciclastic deposition at approximately 12 Ma, which marks the beginning of "unroofing" related to Central Range development (Quarles van Ufford, 1996; Quarles van Ufford and Cloos, in press). Igneous activity associated with collisional tectonism dates between 7.1 and 2.5 Ma (O'Connor *et al.*, 1994).

Within this regional context, several investigators have studied the specifics of the geologic history of the greater Ertsberg District and, particularly, the Grasberg Igneous Complex.

### Previous Work

#### Geology of the Ertsberg District

The first descriptions of the geology of the area are those of Dozy (1939) who prepared them at the behest of Royal Dutch Shell, his employer. This report contained descriptions of the Ertsberg pluton and associated copper skarn mineralisation that led to the exploration and development of the district (Wilson, 1981). Work carried out by PT Freeport Indonesia (PTFI) exploration and mine geologists on the igneous rocks, ore deposits, stratigraphic and structural relationships of the district led to the 1988 discovery that a giant ore deposit underlay the Grasberg, a large grass covered rounded hill peaking at 4200 m (Mealy, 1996; Potter, 1996).

The geology of the Ertsberg district has been mapped in great detail by the PTFI geological staff (Fig. 2). Petrologic studies by McMahon (1994a) delineated 16 Pliocene intrusions. McDowell *et al.*, (1996) reported 13 K-Ar ages that indicate magmatic activity in the district ranged from

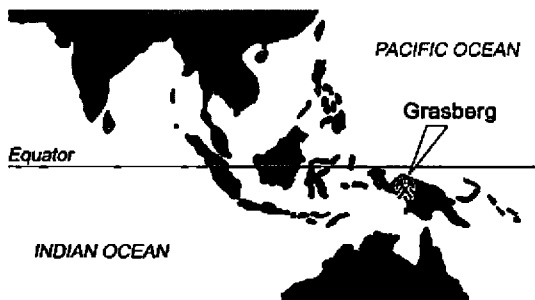
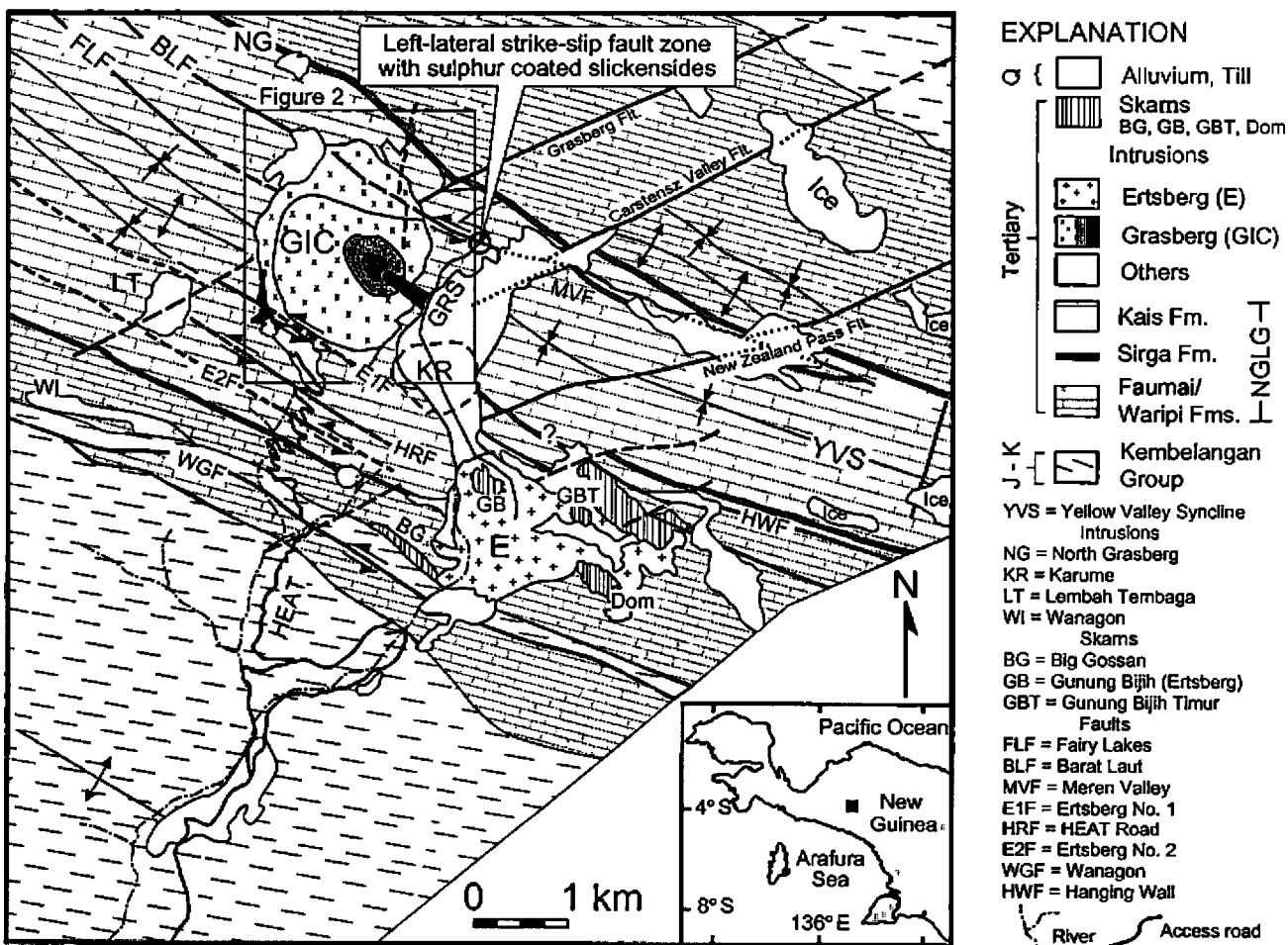


Figure 1: Geologic map of the Ertsberg Mining District, Papua, Indonesia.



4.4 to 2.6 Ma. Most of the intrusions are dykes, sills or plugs with areas of outcrop ranging from a few to several hundred square metres. The Ertsberg and Grasberg are the largest plutons with areas of a few square kilometres. These intrusions have similar chemistries, but the Grasberg is largely porphyritic whereas the bulk of the Ertsberg is equigranular. The mineralogy is dominated by plagioclase, biotite and hornblende with some of the intrusions additionally containing clinopyroxene and small amounts of magnetite and sulphides (McMahon, 1994a, b, c). The potassium contents of intrusives in the district are bimodal, with one population (which includes both the Ertsberg and the Grasberg) of "high-K" latites, trachydacites and trachytes, and the other (small dykes, sills and plugs) composed of "low-K" andesites and dacites.

Pb, Nd, and Sr isotopic analysis (Housh and McMahon, 2000; James *et al.*, in prep.) indicates that the intrusions in the Ertsberg District are the product of a two-stage evolution of mantle-derived magmatism: i) intrusion and ponding in the deep crust with significant chemical modification

from assimilation of Precambrian wallrock, and ii) emplacement into the shallow crust and sedimentary cover with minimal chemical modification from interaction with the wallrock. McMahon (1999) proposed that the equigranular texture of the Ertsberg pluton is the result of near-surface intrusion of an ~20 km<sup>3</sup> mass of phenocryst-poor melt. The scarcity of hornblende and presence of clinopyroxene is a manifestation that most of the crystallisation occurred at low pressure. In contrast, the GIC was emplaced as several small pulses of "crystal-rich" (20 to 40% phenocrysts) magma totalling a few cubic kilometres. Hornblende is common because deep-seated (several kb) crystallisation was substantial.

Two distinct styles of mineralisation are present in the district: i) skarn and ii) porphyry copper-type systems. The former, typified by mineralisation near the Ertsberg pluton (Dozy, 1939; Katchan, 1982; Soeparman and Budijono, 1989; Mertig *et al.*, 1994; Rubin, 1996; Meinert *et al.*, 1997; Coutts *et al.*, 1999) are Cu-Au skarn orebodies that formed as a result of extensive hydrothermal reaction of magmatic

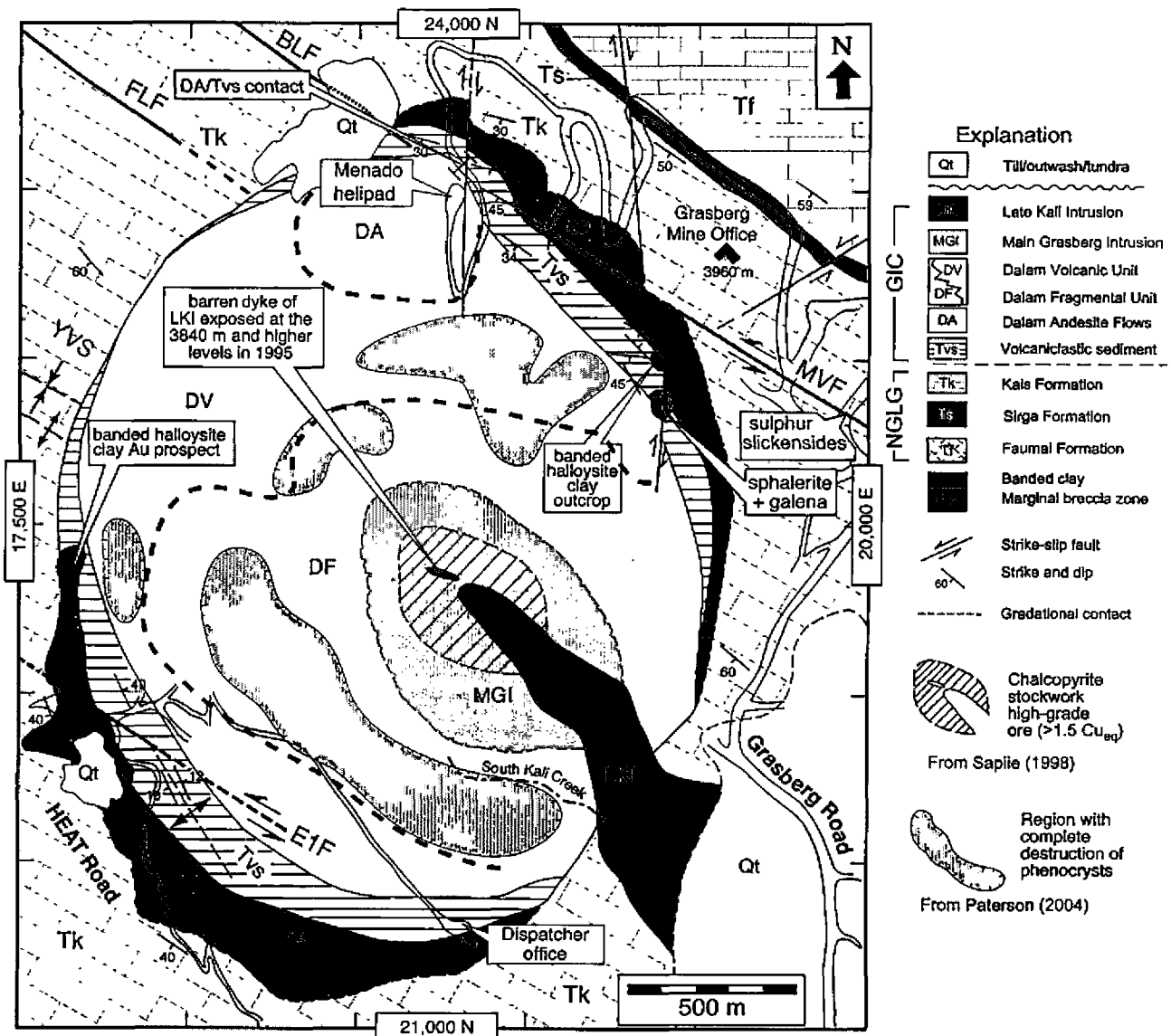


Figure 2: Geology of the Grasberg Igneous Complex (GIC) at the ~3900 m elevation. Modified from Suwardy (1995) and Sapiic (1998). The Mcren Valley Fault (MVF) and Ertsberg #1 Faults (EIF) are left-lateral strike-slip faults. Sapiic (1998) concluded the GIC was emplaced into a pull-apart connecting these fault zones.



fluids with the host carbonate rock. An important Cu-Au skarn, Kucing Liar, is near the Grasberg (Widodo *et al.*, 1999). Ore mineralisation in the district is, however, dominated by the porphyry copper-type Grasberg system. The deposit, which appears to have many geologic similarities to the classical copper porphyries of the American Southwest (Beane and Titley, 1981; Titley, 1982), formed via large scale fluid invasion.

### Geology of the Grasberg Igneous Complex (GIC)

Van Nort *et al.*, (1991) presented the first general description of the Grasberg system. MacDonald and Arnold (1994) published the first detailed descriptions of the three-dimensional geometry of the GIC as well as an igneous history of three distinct phases of magmatism. The GIC is an upward flaring funnel-shaped body that is about 800 m wide at 3000 m elevation and 2000 m wide at 4000 m (Fig. 3). The earliest magmatic phase, the Dalam, was followed by the Main Grasberg Intrusion (MGI) and, finally, the Kali phase. K-Ar ages obtained by McDowell *et al.*, (1996) on very fresh samples from the Grasberg, range from 3.2 to 2.8 Ma. Pollard *et al.*, (2001) reported Ar-Ar ages for Grasberg samples in the range of 3.33 to 3.02 Ma. The Dalam remains undated.

MacDonald and Arnold (1994) classified the Dalam into an assemblage of rocks they called the Dalam Diatreme, including within it two principal phases, both of which are fragmental intrusive breccias: i) an upper andesitic phase, and ii) a lower dioritic phase. On the margins, they differentiated a bedded volcanic unit (Tvs) and a unit of coarse andesite porphyry flows cut by dykes and sills, the Dalam Andesite. Clasts of these units are found in the Dalam Volcanic. They concluded that a major episode of pervasive alteration and disseminated Cu-Au mineralisation occurred in the Dalam that pre-dated the intrusion of the MGI.

At pit levels, much of the MGI is intensively veined by quartz and magnetite forming a stockwork. The MGI is distinguished from the Dalam by the coarse, relatively equigranular textures and a near lack of fragments. MacDonald and Arnold (1994) and subsequent workers all agree the MGI was passively emplaced as a plug into the centre of Dalam phase rocks. MacDonald and Arnold (1994) state that a second major episode of Cu-Au mineralisation was post-MGI and pre-Kali emplacement. This event caused moderately intense alteration and ore mineralisation that was largely veinlet-hosted.

MacDonald and Arnold (1994) report that the Kali phase rocks are a nest of porphyritic dykes, with plagioclase phenocrysts and hornblende comprising 35% to 70% of the rock volume, 5% biotite phenocrysts and 1% to 2% disseminated magnetite set in a finer groundmass of quartz, feldspar and biotite. They report at least two phases of Kali magmatism: one predating or contemporaneous with limited veinlet mineralisation and a later phase, essentially barren of economic mineralisation. McMahon (1994a), in his petrographic observations on the freshest Kali samples, found clinopyroxene, partially altered to actinolite, at a maximum of 5% by volume.

A fundamental question for understanding the magmatic history of the GIC is the physical means of pluton emplacement. As the phrase Dalam Diatreme implies, MacDonald and Arnold (1994, p. 149) hypothesised that the Dalam phase of magmatism included an explosive gas-driven, space-generating eruption. Forceful ejection of sedimentary rock was invoked to explain the funnel-shaped profile of the GIC. The petrographic analysis in the present study found no pieces of sedimentary wall rock (xenoliths) in any part of the GIC. Furthermore, Pb, Sr, and Nd isotopic signatures of the host rocks and the intrusions in the district are very distinct (James *et al.*, in prep.). For the GIC in

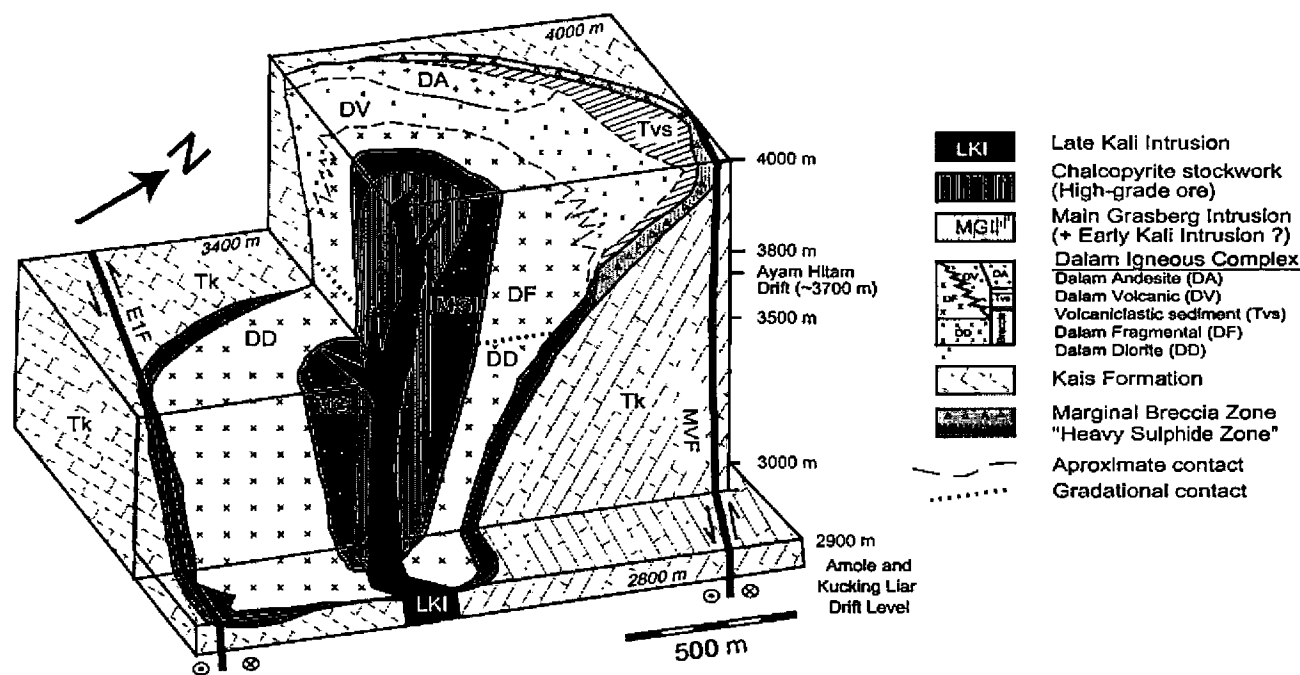


Figure 3: Schematic block diagram of the Grasberg Igneous Complex (GIC). Modified from MacDonald and Arnold (1994) and Sapiic (1998).

particular, and across the district in general, remarkably little isotopic evidence has been detected that indicate the magmas chemically interacted with the sedimentary wall rock column that extends to depths of 10 to 15 km. Emplacement models which invoke any phase of magma generating space by assimilating near-surface wall rock are not plausible.

McMahon (1994a) was the first to speculate that the emplacement of the GIC was fundamentally controlled by space-generating tectonic movements rather than the pressure of intruding magma. The critical study was that of Sapiie (1998), who discovered abundant evidence for strike-slip faulting near and in the GIC. He concluded the fundamental control for Grasberg intrusion and mineralisation involved a dilatational jog, or pull-apart, between two 300° trending, left-lateral strike slip faults (EIF and MVF on Figs. 2 and 3) (Sapiie and Cloos, 2004, in review).

Sapiie (1998) also concluded the marginal breccia that encircles the GIC at outcrop levels was the product of a large amount of solution/collapse of carbonate wall rock by acidic magmatic fluids. With this realisation, it became apparent that the origin of the funnel shape of the GIC has another explanation. The University of Texas investigators replaced the general term Dalam Diatreme with purely descriptive names: the Dalam Andesite (DA), a sequence of thick, massive porphyritic flows, perhaps once forming an extrusive dome, the Dalam Volcanic (DV), a polymict breccia, and the Dalam Fragmental (DF), a monomict

breccia. The sub-surface part of the Dalam (not part of this study), which is more equigranular and has few clasts, is the Dalam Diorite. This nomenclature is used in this study.

The abundance and diversity of clasts in the Dalam Volcanic and Dalam Fragmental units is highly variable. At the ten metre scale, clasts commonly form 5% to 10% of the rock volume, but locally occur in abundance up to about 30%. Most clasts are rounded to subrounded indicating significant movement after fragmentation. The inner boundary of the DV is mapped based upon the last occurrence of polymict breccia (Fig. 4). The inner boundary of the DF with the MGI is mapped based upon the last occurrence of monomict breccia. The contacts are gradational, in that parts of the DV are monomict, and parts of the DF lack clasts. Despite intensely pervasive alteration, outlines of replaced clasts are commonly quite distinct. In the open pit mine benches, the boundaries between these map units were typically localised within distances of several tens of metres. Indistinct contacts are explainable as the result of magma intruding still hot rock.

Sapiie (1998) concluded the Dalam phase magmas intruded to less than ~1 km depth prior to water saturation and explosive auto-fragmentation. He concurred with MacDonald and Arnold (1994) who concluded that the Dalam was emplaced in a setting of low relief, a maar volcano. The DF, which formed in the centre, is probably largely an intrusive unit, whereas the DV is probably largely extrusive. For explosive fragmentation to have only

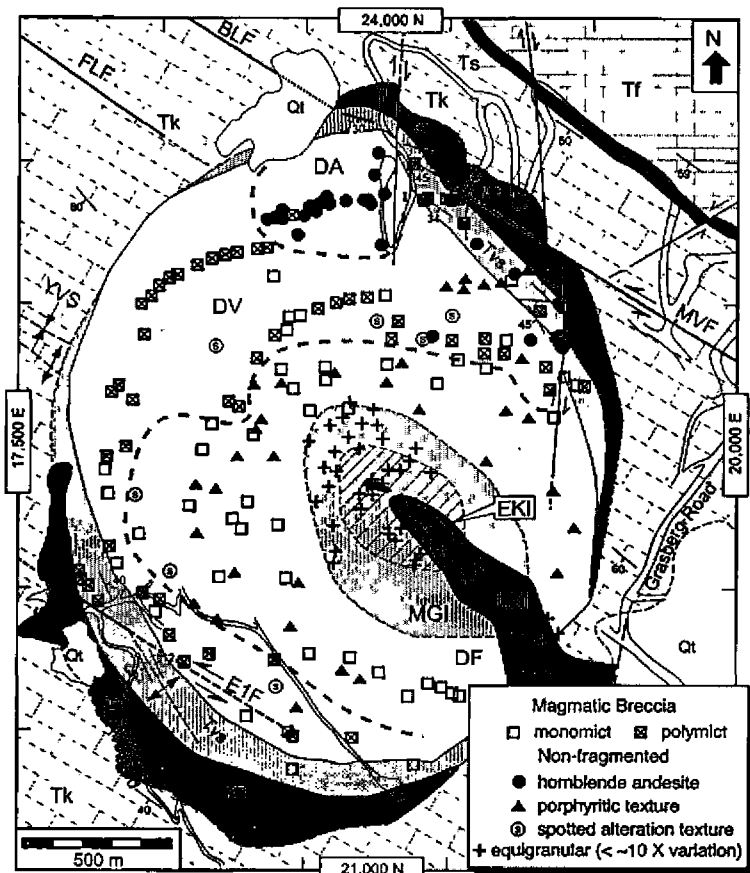


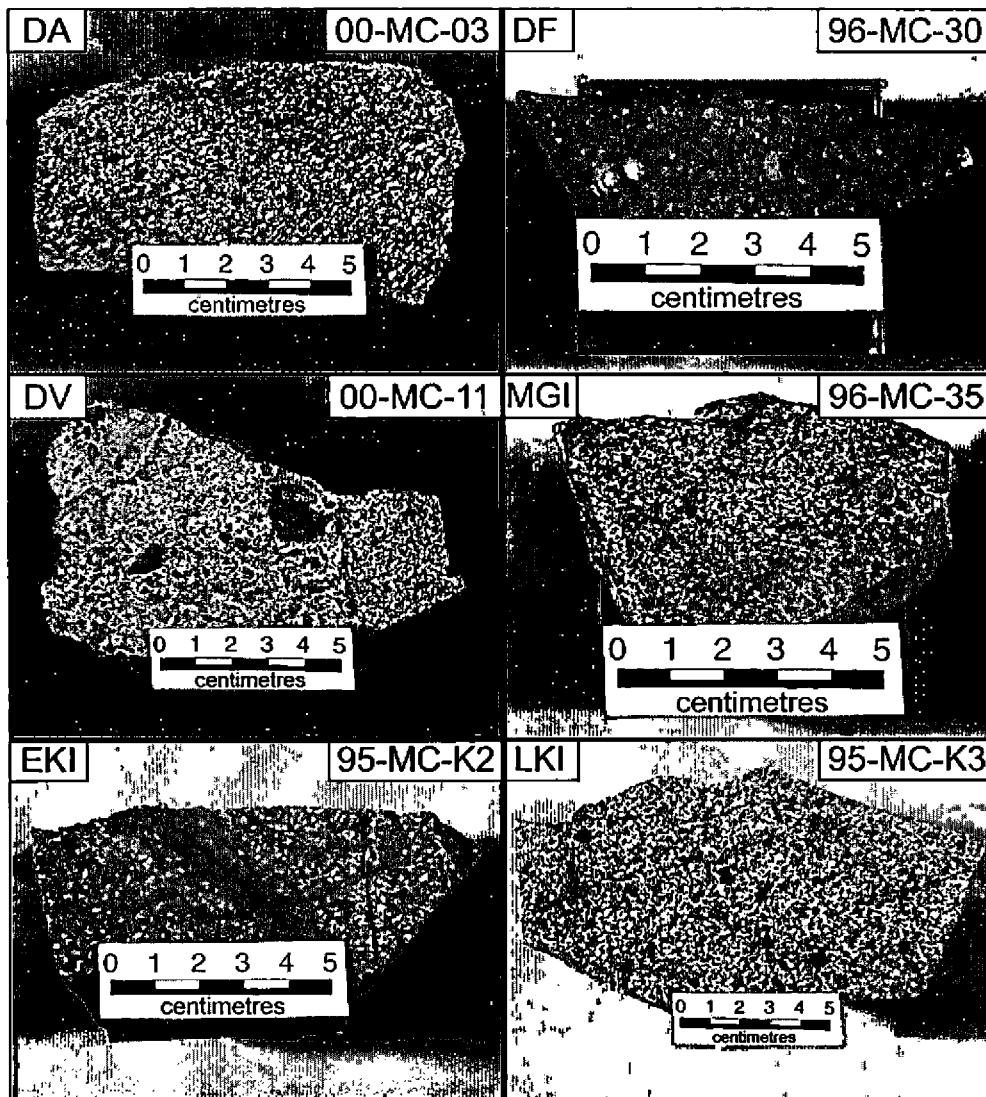
Figure 4: Brecciated and non-fragmented hand specimens. See Figure 2 for explanation of map abbreviations.

occurred at shallow depths, the volatile content of the magma must have been modest, about 2 wt.%. In this interpretation, the rise of the Dalam-phase magma was also relatively passive, except very near the surface.

Porphyry copper deposits, of which the GIC is a supergiant example, have a distinctive mineralogic zonation of alteration that results from pervasive fluid flow. This pattern is most easily explained as alteration by magmatic fluids emanating from a point source - a fluid-charged cupola at the top of a solidifying stock (see Cloos, 2001). This paper concerns the magmatic mineralogy of the GIC based upon the analysis of a suite of 225 hand specimens that were prepared into polished slabs and thin sections. The Grasberg was a hill and the samples were collected in the open pit mine between 1994 and 2002 and at elevations between 3700 m and 4200 m. Most samples are from the elevation interval of 3800 m to 4100 m. The sample suite is the basis for constructing a set of maps that depict mineralogic

and textural variations in the GIC at the ~3900 m level. An accompanying paper (Paterson and Cloos, this volume) concerns the effects of pervasive alteration in the sample suite by diffuse fluid flow.

No volcanic deposits extend beyond the mapped limits of the GIC (Fig. 1) as would be expected if the Grasberg deposit were to underlay a 2 or 3 km tall composite volcano. A small part of the GIC consists of bedded, water-lain volcanoclastic sediments (the Tvs) along the northeast and southwest edges (Fig. 2). The most diagnostic evidence of only shallow burial comes from the presence of small areas of contorted, gold-bearing halloysite clay, the "banded clay unit," on the southwest and northeast sides of the GIC (Fig. 2). These deposits are remnants of a once extensive field of boiling mudpots. It is believed that the sample suite in this investigation was located at positions that were less than 1 km, most probably several hundred metres, from the surface at the time of mineralisation.



**Figure 5:** *Representative polished slabs of igneous units in the Grasberg Igneous complex.* DA = Dalam Andesitic. DF = Dalam Fragmental. DV = Dalam Volcanic. MGI = Main Grasberg Intrusion. EKI = Early Kali Intrusion. LKI = Late Kali Intrusion.

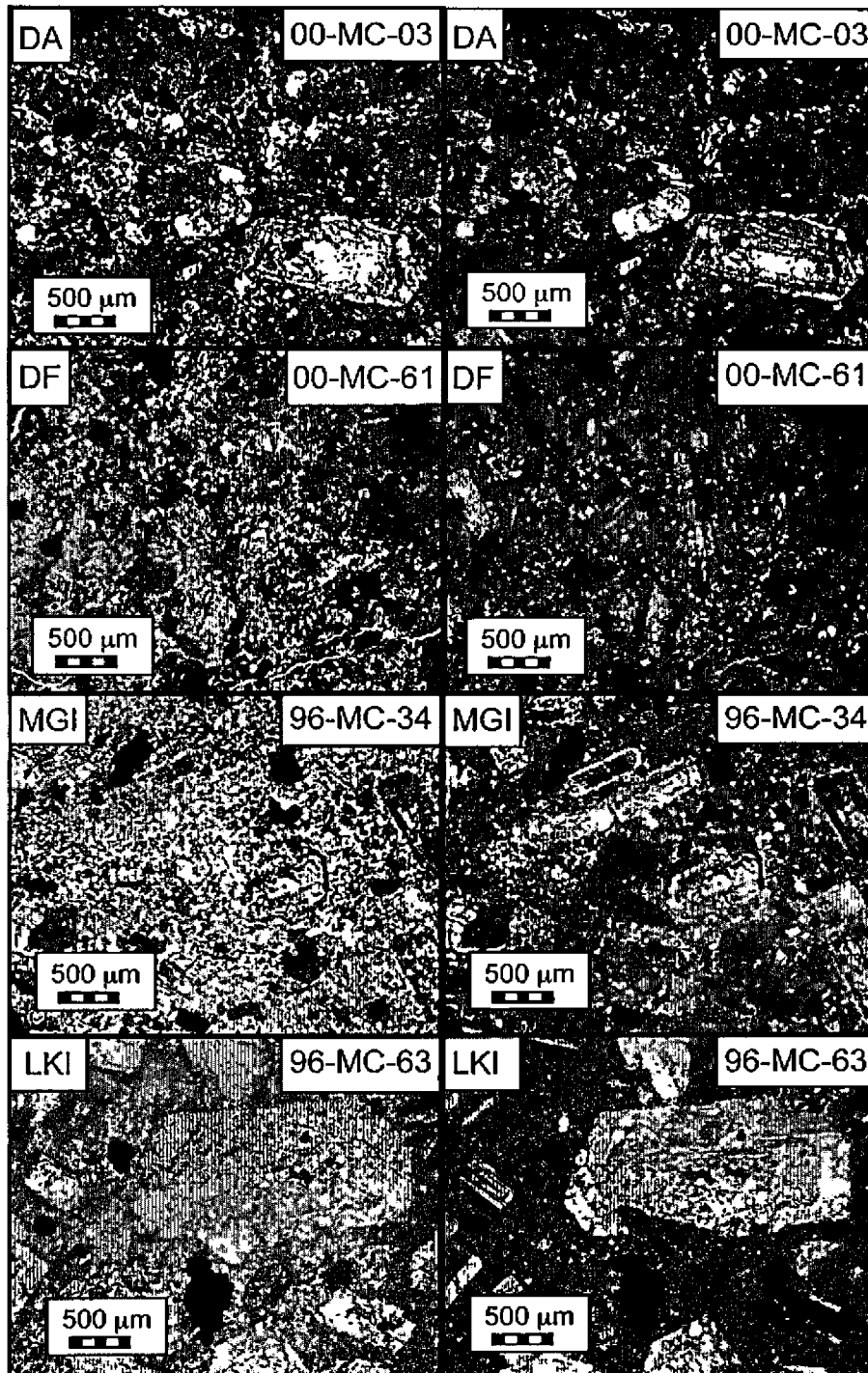
## Magmatic Mineralogy of the GIC

The magmatic mineralogy of each igneous unit must be characterised to gain insight into the evolution of the parent magma chamber and to fully recognise the effects of fluid infiltration and pervasive alteration. Samples from across the GIC vary greatly in their degree of textural reconstitution. In some parts of the deposit, all igneous minerals and textures are destroyed. This report centres on the analysis of the freshest examples of each igneous unit. One point is evident from even casual hand-specimen

observations; most of the Kali phase rocks, even from the centre of the GIC, are relatively unaltered when compared to the Dalam and MGI phase rocks. Photographs of polished slabs of "fresh" examples from each igneous unit are shown in Fig. 5.

### Plagioclase Phenocrysts

Plagioclase is the most obvious and volumetrically abundant phenocryst in fresh to moderately altered rocks. Representative thin-section examples of plagioclase phenocrysts are shown in Fig. 6. Abundances typically



**Figure 6:** Representative thin section photomicrographs of Dalam Andesite (DA), Dalam Fragmental (DF), Main Grasberg Intrusion (MGI) and Late Kali Intrusion (LKI). Left, plane polarized light. Right, cross polarized light.

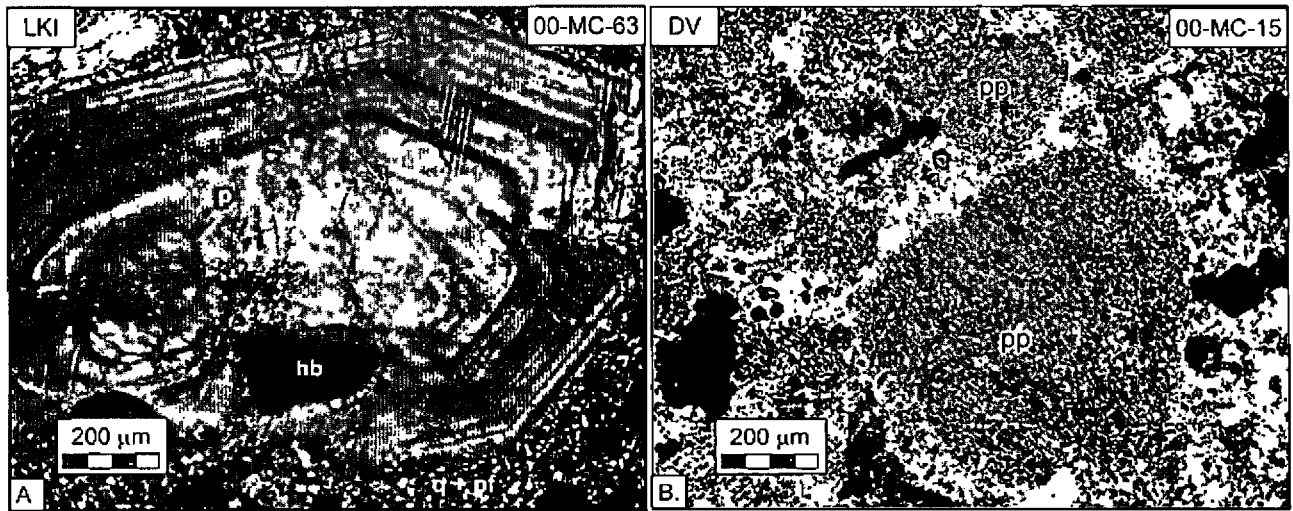


Figure 7: A. Plagioclase phenocryst with oscillatory zoning in the Late Kali Intrusion. p = plagioclase. hb = hornblende. B. Plagioclase phenocryst replaced by sericite in Dalam Volcanic unit. pp = plagioclase pseudomorph.

range from 10% to as much as 50% of the volume of the rock, although alteration has locally caused complete destruction of plagioclase phenocrysts. The DA has a range from approximately 10% to a maximum of 35% by volume, the DV and DF range from 0% (because of alteration) to 45%, commonly approximately 20%. The abundance of plagioclase phenocrysts in the MGI ranges from 20% to 40% and those in the Kali range from 20% to 65%. Fresh plagioclase phenocrysts, which are abundant in the Kali, are strongly oscillatory-zoned (Fig. 7a). Many of the larger phenocrysts in the fresher samples have distinct core zones that indicate a cessation in growth or resorption.

Two features are apparent from the distribution of plagioclase phenocrysts (Fig. 8). In the Kali, MGI and DA

units, relict plagioclase phenocrysts are commonplace, but in the DV and DF units, many samples only contain pseudomorphs (Fig. 7b) and in some areas clusters of samples lack any evidence for the former presence of any magmatic phases (plagioclase, biotite, or hornblende). The largest area with complete textural destruction covers approximately 250 x 1300 m in the DF in the southwestern part of the complex (Fig. 8). Pseudomorphs of plagioclase phenocrysts are typically almost entirely composed of hydrothermal biotite in the interior, and sericite in the exterior part of the complex.

A subtle, but distinctive attribute of the GIC that was discovered during petrographic analysis is the distribution of broken plagioclase phenocrysts (Fig. 9). Broken

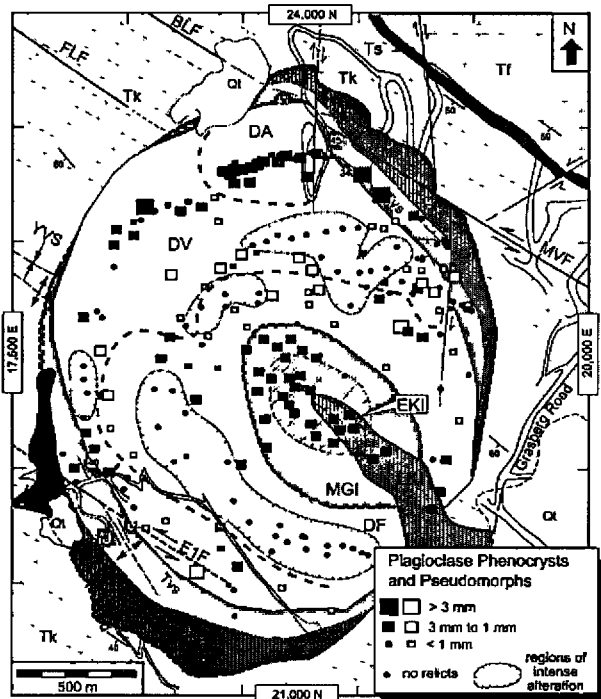


Figure 8: Distribution and size of plagioclase phenocrysts and pseudomorphs.

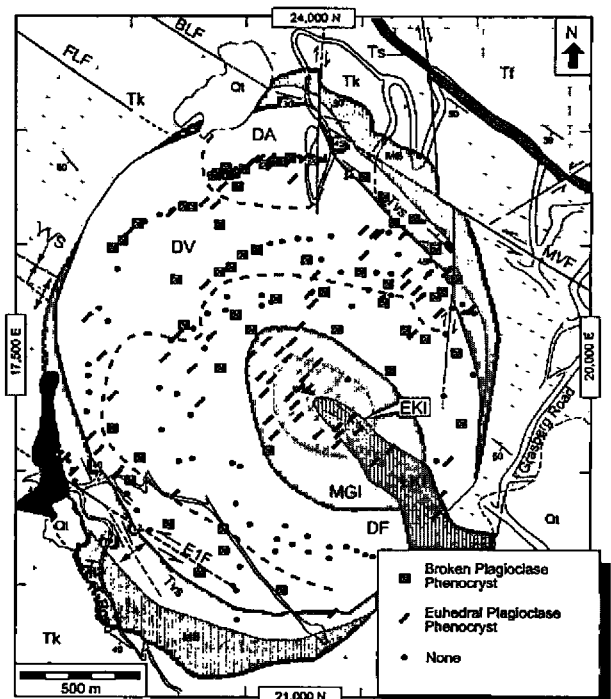


Figure 9: Samples containing broken plagioclase phenocrysts identified from truncated oscillatory zoning.

phenocrysts, recognised from the truncation of oscillatory zoning, are common in the Dalam. They are absent in the MGI and Kali phase rocks.

#### ***Biotite Phenocrysts***

The distinction between magmatic and hydrothermal biotite has been based upon crystal morphology. Fresh magmatic biotites are large euhedral grains with clean and sharp edges (Fig. 10a). Hydrothermal biotites occur as distinctive 'shreddy' aggregates of fine grains (Fig. 10b). Whereas relict igneous plagioclase is present in most samples, magmatic biotite is commonly only recognised as pseudomorphic replacements (Fig. 11). The main alteration products of biotite are shreddy hydrothermal biotite in the interior, and sericite in the exterior, parts of the complex.

In many samples, the former abundance of magmatic biotite is estimated from pseudomorphic outlines. Overall, it appears that biotite typically composed about 15% of the phenocryst population. In both the MGI and the DA, biotite abundance ranges from 5% to 25%. In the Kali, biotite abundance ranges from 10% to 20%. In the DV and DF relict magmatic biotite preservation is patchy, but pseudomorph outlines indicate the abundance ranged from at least 3% to 20%.

#### ***Hornblende Phenocrysts***

Hornblende is much more highly susceptible to alteration than is plagioclase or biotite. Hornblende phenocrysts are only present in parts of the DA and most of the LKI. In the freshest Late Kali, the abundance of hornblende ranges from 3% to 15%. In the freshest DA samples, hornblende phenocryst contents are typically about 10%, but in nearby altered samples, hornblende pseudomorphs typically comprise less than 3% of the rock. From this, it is evident that the volume of pseudomorphs is only an indicator of the minimum former abundance of hornblende. Hornblende has been replaced by shreddy biotite in the interior and sericite where present in the outer parts of the complex.

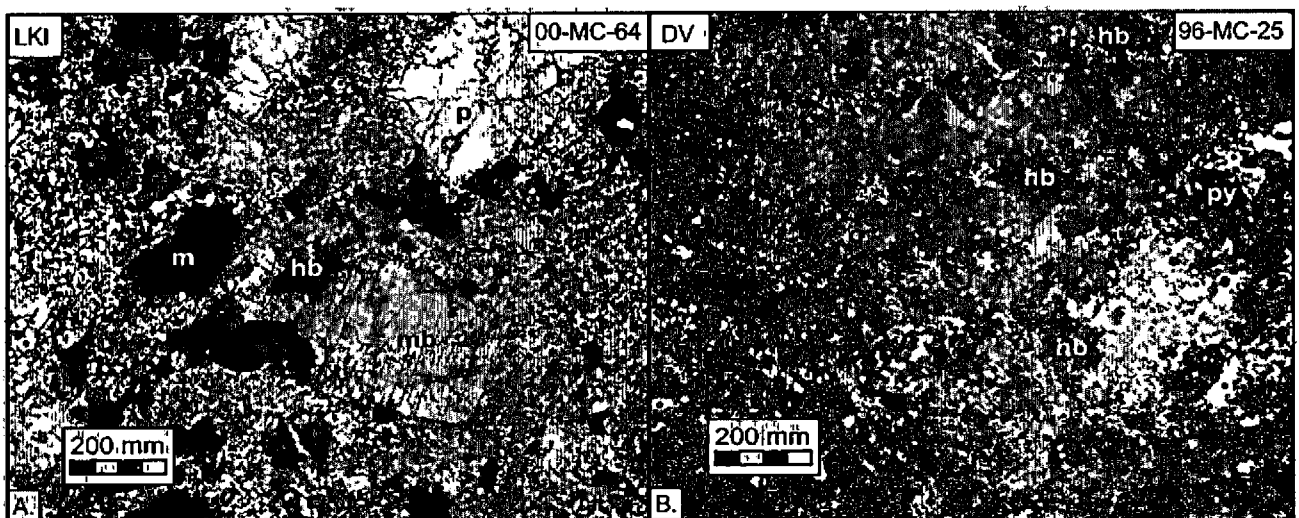
MacDonald and Arnold (1994) concluded there was a two-stage division of the Kali phase of magmatism based upon the degree of mineralisation/alteration wherein a late stage of the Kali postdated nearly all hydrothermal activity. Hornblende is lacking in parts of the Kali. Based upon field observations in the open pit mine and thin sections from eight sample locations, it appears that the Kali can be subdivided into hornblende-bearing and hornblende-absent. The samples lacking hornblende are located in the interior and near the contact of Kali with the MGI (Fig. 12). Because petrographic analysis is needed for confirmation, the boundaries of the two Kalis is very poorly constrained. Drill core relationships indicate they probably interfinger at depth (MacDonald and Arnold, 1994). Their location, combined with observations on the hydrothermal mineralogy, indicate the hornblende-absent Kali is earlier (Early Kali Intrusion, EKI), whereas the hornblende-bearing Kali is the later phase (Late Kali Intrusion, LKI). More work on sub-surface samples is needed to properly understand the phases of Kali magmatism.

Hornblende was a common component of the Dalam Andesite and petrographic analysis indicates it was probably ubiquitous. In striking contrast, only four samples of the Dalam Volcanic and three of the Dalam Fragmental contain pseudomorphic evidence for hornblende. It is certain that alteration is intense enough in many samples to destroy all evidence, but it appears that hornblende was absent or at most a sparse component during most of Dalam phase magmatism.

In the MGI, amphibole pseudomorphs replaced by hydrothermal biotite are common. The former abundance of hornblende was probably up to 5%.

#### ***Clinopyroxene and Actinolite***

Some samples of the Late Kali Intrusion contain as much as 2% of optically identifiable clinopyroxene. In these rocks, actinolite is observed to topotactically replace clinopyroxene (Fig. 12; McMahan, 1994a). Clinopyroxene/actinolite was not found in all samples of the Late Kali



**Figure 10:** A. Magmatic biotite in Late Kali Intrusion. B. Magmatic biotite pseudomorphed by hydrothermal shreddy biotite in Dalam Volcanic. mb = magmatic biotite, p = plagioclase, m = magnetite, hb = hydrothermal biotite, py = pyrite, q = quartz.

examined, and it is absent in the few samples of the Early Kali examined in this study. None of the Dalam samples contain actinolite, indicating the former presence of clinopyroxene.

In the MGI, alteration is extensive and petrographic investigation aided by BSE images reveals that the only amphibole now present in most samples is actinolite. Hornblende was completely replaced by an aggregate of biotite grains in most samples. Actinolite, on the other hand, commonly occurs as irregular, but optically continuous single grains. The critical observation comes from Kali samples in which hornblende is partially to totally replaced by hydrothermal biotite and clinopyroxene is replaced by actinolite. Extrapolating these observations to the MGI, indicates that both hornblende and clinopyroxene existed in abundances of about 5%, with the former replaced by clusters of hydrothermal biotite and the latter via a largely topotactic replacement by actinolite.

#### *Magnetite*

Magnetite (+biotite) is a major alteration product in the interior of the GIC. Veins of magnetite are common, indicating direct precipitation from fluid in fractures. Disseminated magnetite locally comprises as much as 10% of intensely altered rocks. As the morphology of primary and secondary disseminated magnetite is the same, it is not possible to petrographically differentiate most of the magnetite in the MGI and Dalam phases into a magmatic or hydrothermal assemblage. However, the abundance is so great in many of the samples, that the bulk of the magnetite must be hydrothermal. Magmatic magnetite was probably present in all of the igneous units, but it is only evident in the freshest Kali samples. Several samples of Late Kali that lack evidence of hydrothermal alteration contain 1% to 2% magnetite.

#### *Apatite*

Apatite of small grain size is ubiquitous. X-ray mapping with an electron microprobe reveals trace volume concentrations (<1%). Apatite abundance and textures appear similar in fresh and altered rocks. As apatite is a common trace phase in igneous rocks, its occurrence in the GIC is thought to be magmatic.

### Mineral Chemistry

The occurrence of plagioclase and biotite phenocrysts in all units necessitates an investigation into potential compositional differences that could record cryptic chemical changes in the parent magma chamber. The freshest samples identified during petrographic analysis from across the GIC were selected for microprobe analysis of plagioclase and biotite. Standard analytical procedures were followed and described in Paterson (2004). Two forms of compositional mapping were utilised by scanning thin sections with the electron beam: backscattered electron (BSE) imaging and x-ray mapping of major elements. The magnitude of the electron backscattering is a measure of the average atomic number of elements in scanned areas (Potts *et al.*, 1995), hence variations in brightness on a BSE image indicate a variation in composition. X-ray mapping involves setting a spectrometer to detect x-rays characteristic of a particular element. Eight samples containing fresh plagioclase and biotite along with five samples containing only fresh plagioclase were selected for substantial analytical work with the electron microprobe.

#### *Plagioclase Phenocrysts*

Fig. 13a shows the results of quantitative analysis of the Ca-rich cores of plagioclase phenocrysts. The ternary plot indicates that there is no systematic variation in the core compositions of plagioclase between the analysed samples

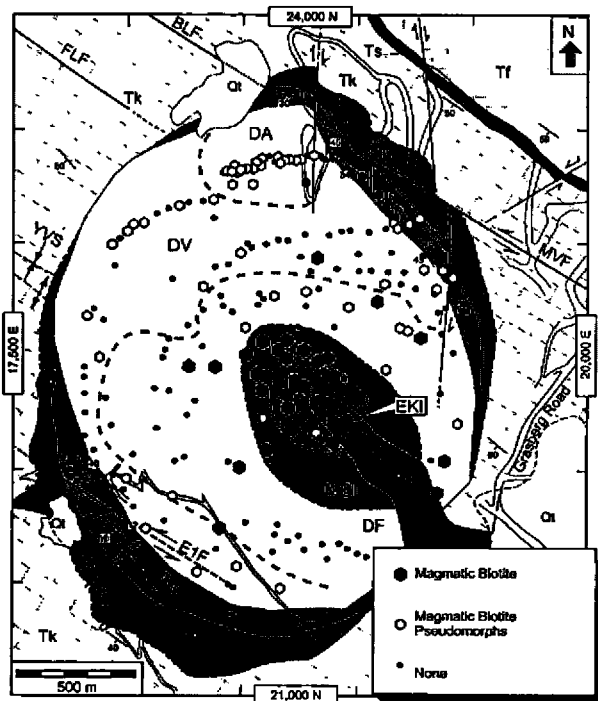


Figure 11: *Distribution of magmatic biotite phenocrysts and pseudomorphs.*

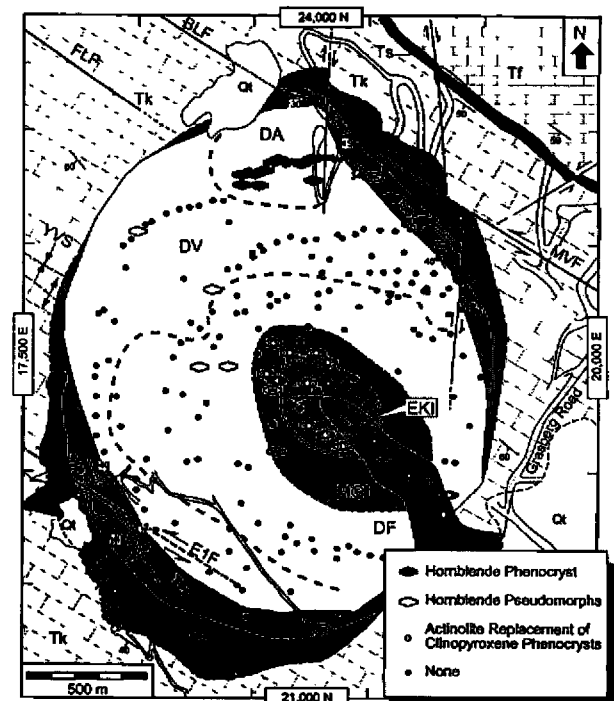


Figure 12: *Distribution of hornblende phenocrysts and pseudomorphs, and actinolite.*

from the Dalam Andesite, MGI or Kali. Nearly all of the core analyses range between An<sub>50</sub> to An<sub>25</sub>. The lower values are probably from crystals that are not central sections.

The oscillatory zoning in plagioclase phenocrysts that is observed optically is readily detectable with both BSE imaging and x-ray mapping. Most of the zoning appears to range between An<sub>35</sub> to An<sub>10</sub> (Fig. 13b). X-ray mapping shows the margins of plagioclase phenocrysts are albitic and, not surprisingly, very similar in composition to plagioclase in the groundmass (Fig. 14a).

Both BSE imaging and x-ray mapping revealed small masses of potassium feldspar inside many plagioclase phenocrysts (see small bright spots Fig. 16a and b). The compositions of the inclusions are similar to potassium feldspar in the groundmass (Fig. 14). They are found in plagioclase from the freshest samples of the Kali and thus at least some of these masses do not appear to be products of alteration. It is possible that they are exsolution phenomenon, but their irregular orientations suggests they are small inclusions. Potassium feldspar inclusions in the interior of plagioclase grains could be relicts of phenocrysts that were largely remelted during a magma mixing event at depth. Alternatively, potassium feldspar inclusions may be slowly growing phenocrysts that were engulfed by more rapidly growing plagioclase.

**Biotite Phenocrysts**

Biotite is second only to plagioclase in terms of volumetric significance in the phenocryst population. BSE imaging of biotites revealed few differences within individual grains or between separate grains. Magmatic biotite was far more susceptible to alteration than plagioclase, and few thin sections contained large, unaltered grains. Reported biotite compositions are an average of four spot analyses per grain.

Variations in biotite chemistry commonly involve the substitution of Ti, Mg, Fe and Al (Spear, 1993). A useful method for describing variations in biotite chemistry is plotting the number of Ti cations against both magnesium number and the number of Si cations (Fig. 15). Analysed biotites show considerable variation in Ti concentration, as much as 60%.

The magnesium numbers ( $Mg \# = Mg/(Fe+Mg)$ ) for biotite show up to 10% variation within a unit. As with the quantitative analysis of plagioclase, the results from the biotite study detected no systematic differences between the different units, although the data set is small.

**Groundmass**

MacDonald and Arnold (1994) stated that, where preserved, the magmatic groundmass of the GIC rocks is a combination of potassium feldspar, plagioclase and quartz. The volume of groundmass is commonly about 40% of the rock volume. Petrographic identification of groundmass phases is extremely difficult because grain sizes are extremely small and the optical properties of un-twinned feldspars and quartz are very similar. X-ray element maps produced with a microprobe enable quick identification of feldspars and distinction from quartz.

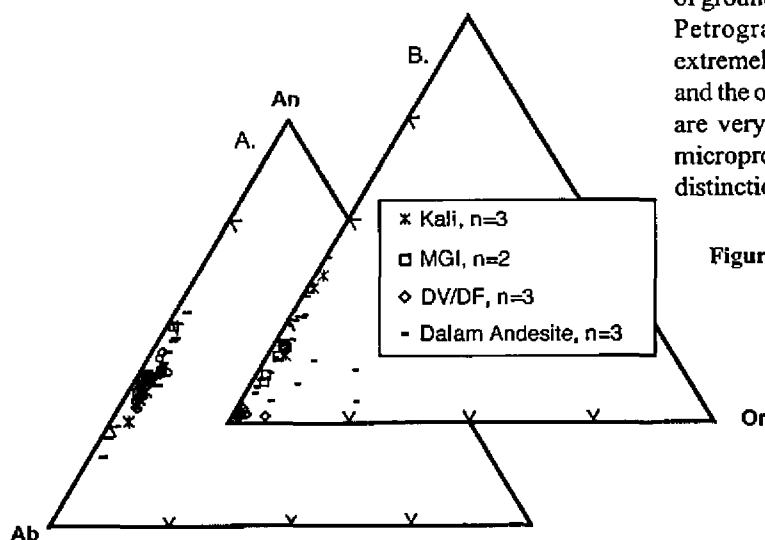


Figure 13: A. Compositions of the cores of plagioclase phenocrysts. B. Compositional variations of oscillatory zones in plagioclase. n = number of samples with analyzed grains.

Figure 14: A. Analyses of feldspar grains in the groundmass. B. Analyses of potassium feldspar inclusions within plagioclase. n = number of samples with analyzed grains.

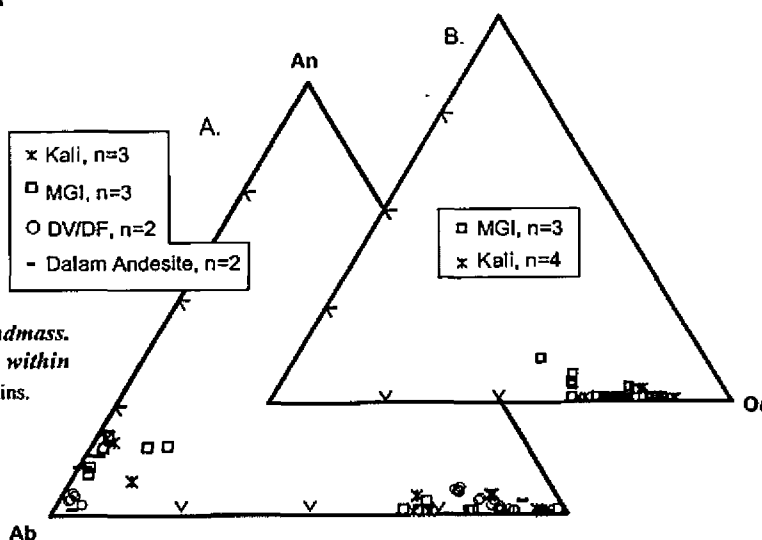




Table 1: Magmatic mineralogy of the igneous units in the Grasberg Igneous Complex

youngest	<b>Late Kali Intrusion (LKI)</b>	
	<b>phenocrysts</b>	plagioclase (20% to 65%) + biotite (10% to 20%) + hornblende (3% to 15%) ± clinopyroxene (altered to actinolite) (~2%)
	<b>groundmass</b>	potassium feldspar (10% to 30%), quartz (10% to 30%), biotite (~5%), albitic plagioclase (~5%), magnetite (~2%) and apatite (tr.)
	<b>texture</b>	porphyritic: ~100x variation in grain size
	<b>Early Kali Intrusion (EKI)</b>	
	<b>phenocrysts</b>	plagioclase (20% to 65%) + biotite (10% to 20%)
	<b>groundmass</b>	potassium feldspar (10% to 30%), quartz (10% to 30%), biotite (~10%), albitic plagioclase (~5%), and apatite (tr.)
	<b>texture</b>	porphyritic: ~100x variation in grain size
	<b>Main Grasberg Intrusion (MGI)</b>	
	<b>phenocrysts</b>	plagioclase (20% to 40%) + biotite (5% to 25%) + hornblende (3% to 15%) + clinopyroxene (altered to actinolite) (~5%)
	<b>groundmass</b>	potassium feldspar (~15%), quartz (~15%), biotite (~5%), albitic plagioclase (~5%), and apatite (tr.)
	<b>Dalam Andesite (DA)</b>	
	<b>phenocrysts</b>	plagioclase (10% to 35%) + biotite (5% to 25%) + hornblende (3% to 15%)
	<b>groundmass</b>	potassium feldspar (~10%), quartz (~20%), biotite (~10%), albitic plagioclase (~5%), and apatite (tr.)
	<b>Dalam Volcanic/Dalam Fragmental (DV/DF)</b>	
	<b>phenocrysts</b>	plagioclase (up to 45%) and biotite (3% to 20%) +/- hornblende (< 2%)
	<b>groundmass</b>	thoroughly altered in almost all samples, may have been glassy, apatite (tr.)
oldest	<b>texture</b>	brecciated, with broken plagioclase crystals

X-ray mapping shows the freshest rocks from the Kali and the least altered samples from the MGI and Dalam Andesite contain potassium feldspar and quartz that occur in a roughly two to one ratio and together comprise 20% to 30% of the rock volume (Fig. 16). The groundmass in the Kali and less altered MGI and Dalam Andesite also contains small grains of magmatic biotite (<30 microns) and plagioclase grains, each approximately 5% of the volume. Magnetite and apatite are common, minor components of the groundmass of the LKI.

Analyses of the groundmass (Fig. 14a) from the least altered samples show albitic plagioclase ( $Ab_5$  to  $Ab_{15}$ ) and potassium feldspar ( $Or_{65}$  to  $Or_{95}$ ) are coexisting. Notably, the compositions of groundmass potassium feldspar overlap

the field on the ternary plot for the potassic feldspar inclusions ( $Or_{95}$  to  $Or_{75}$ ) in the plagioclase feldspar (Fig. 14b).

The groundmass of all samples of the DV and DF are highly recrystallised in nearly all thin sections. Nonetheless, the feldspars in the groundmass from two of the less recrystallised samples of DF were analysed (Fig. 14a). Near end-member albite is present suggesting the co-existing feldspars are probably secondary. In most samples from the outer part of the GIC, potassium feldspar does not occur in the groundmass, because of extensive alteration to sericite. A likely explanation for the thorough recrystallisation of the Dalam phase rocks is that the groundmass was originally glassy.

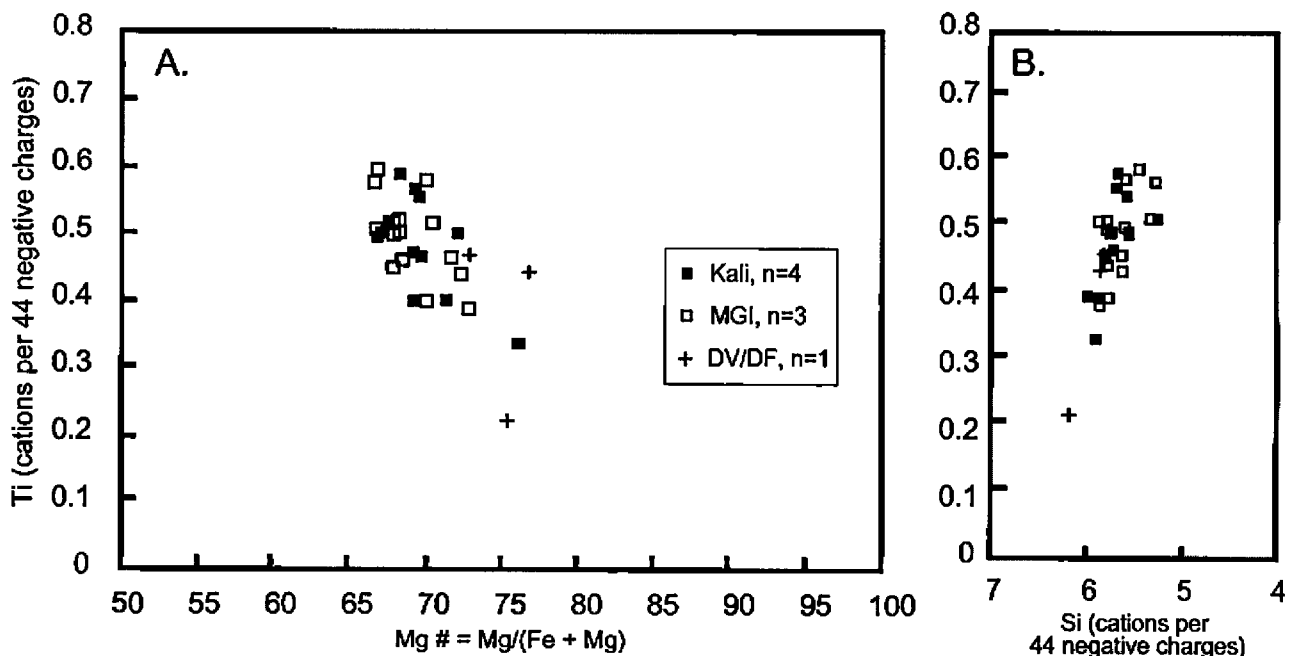


Figure 15: Composition of magmatic biotite. A. Ti versus Mg number. B. Ti versus Si content. n = number samples with analyzed grains.

## Discussion

Table 1 summarises the magmatic mineralogy and textural characteristics for the units forming the GIC based upon the systematic petrographic analysis supplemented by electron microprobe analysis. The mineralogic differences

record evidence on the behaviour of the parent magma chamber and the rates of cooling after intrusion to shallow depths. The gross textural differences between each unit primarily reflect differences in emplacement processes.

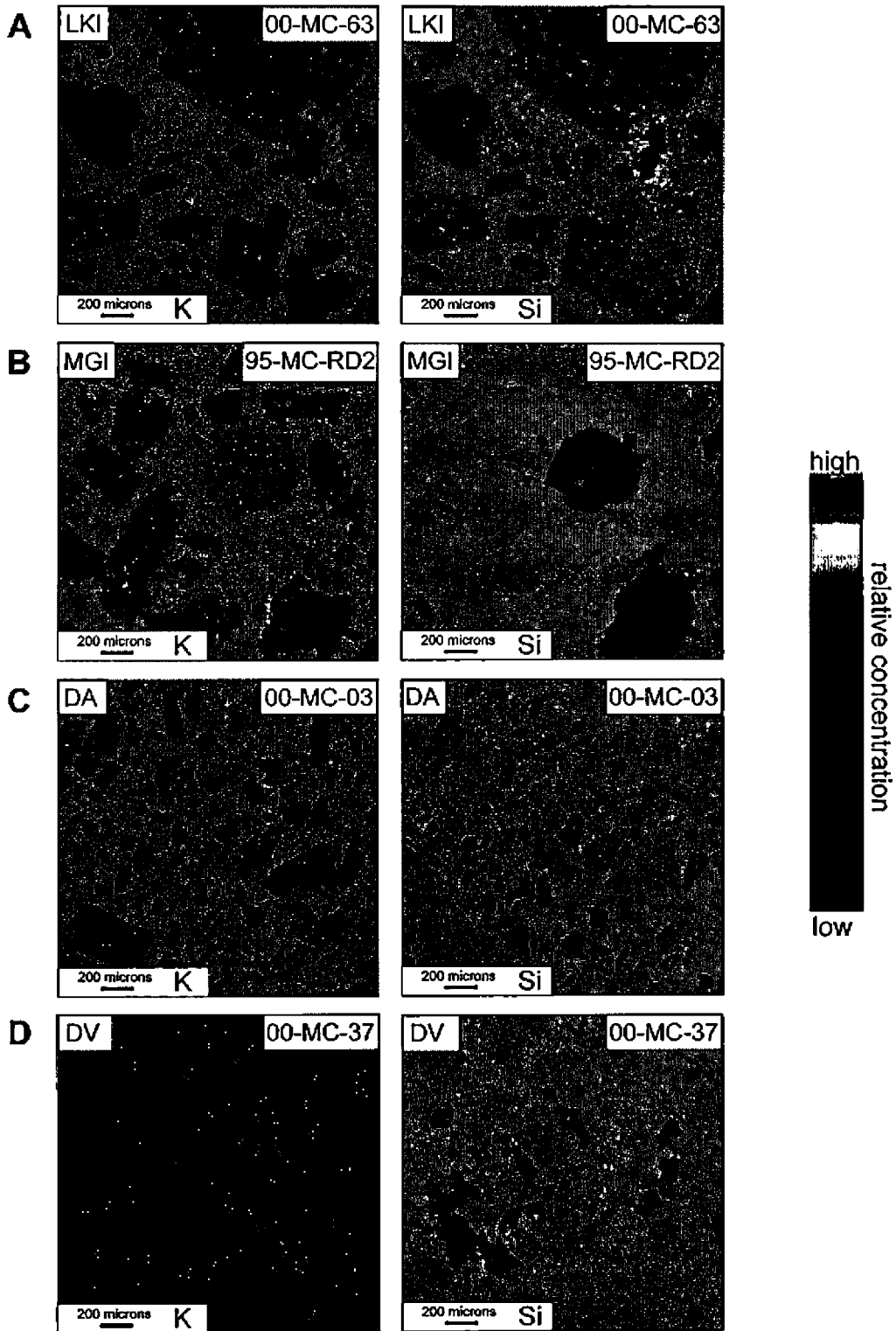


Figure 16: Potassium (left) and silicon (right) x-ray maps of the groundmass of representative samples. Note abundance of potassium feldspar in the groundmass of the LKI (A), MGI (B), and DA (C). Complete replacement of groundmass potassium feldspar is evident in the DV (D).

### *Evolution of the Parent Magma Chamber*

The phenocryst mineral assemblages in each phase of magmatism are similar, indicating no profound differences in the pressure and temperature conditions during crystallisation of the magmas forming the GIC. Plagioclase and biotite phenocrysts are ubiquitous and the chemical analysis reported in this investigation, albeit limited, indicate compositional variations within units are overlapping. These observations suggest, but do not prove, the three phases of magmatism were sourced from the same chamber. However, the differentiation trend defined by mineralogy or by chemical data is not unidirectional. This could be interpreted to indicate tapping of different levels of the parent chamber or that the parent chamber was recharged by compositionally similar magmas.

Cryptic evidence for recharging is suggested by the presence of plagioclase phenocrysts in the DA, MGI and Kali with cores that record two distinct stages of growth. The petrographic observations suggest the parent magma chamber was recharged during the Dalam magmatism and between MGI and Kali intrusive activity.

The major mineralogic differences are the presence or lack of hornblende and clinopyroxene in the different units. This is explainable by differences in the depth of crystallisation. In intermediate composition magmas, higher pressure conditions (>2-3 kb) stabilise hornblende as a phenocryst phase whereas lower pressure conditions stabilise clinopyroxene (Naney, 1983).

The fact that hornblende is abundant in the DA but apparently sparse or lacking in most of the DV and DF suggests recharging of the parent magma chamber or some other fundamental change during Dalam phase magmatism. In the northern part of the complex, the DA overlies the Tvs (Sapiie, 1998). Clasts identical to the DA are found in the DV indicating at least some, probably most, DV magmatism post-dates the DA. This indicates Dalam magmatism tapped a chamber that was differentiated to varying degrees (more crystallised, cooler, sidewall zones, versus a hotter, less crystallised interior) or that the parent chamber for the Dalam was recharged at least once. The lack of clinopyroxene indicates rapid solidification at low pressures suggesting the DF and DV units are composites of magma batches emplaced in small pulses.

The presence of hornblende and clinopyroxene in the MGI indicates substantial growth of mafic phases at both high and low pressures. The comparatively equigranular texture indicates the MGI cooled much more slowly than the Dalam phase magmas. This suggests the cone-shaped plug of MGI was intruded as one large batch (~1 km<sup>3</sup>) into fully solidified, but still hot, Dalam wall rocks.

The Kali phase of magmatism post-dates essentially all of the economic copper mineralisation. Hornblende and clinopyroxene appear to be absent in the small, porphyritic Early Kali plug in the centre. This indicates either less recrystallised, probably deeper parts of the parent magma chamber were tapped than which supplied the MGI and/or the parent chamber was recharged with the addition of heat destabilising the hornblende. The lack of clinopyroxene is

attributed to the small size of the batch of the Early Kali magma (~0.1 km<sup>3</sup>) that intruded the core of MGI after substantial cooling.

Hornblende and clinopyroxene are abundant in the large, wedge-shaped Late Kali dyke that extends outwards from the centre of the GIC. The presence of hornblende indicates substantially more crystallised batches of magma escaped from the parent magma chamber. The growth of clinopyroxene largely resulted from the relatively slow cooling of the Late Kali magma which was emplaced as several large batches (totalling ~1 km<sup>3</sup>).

In summary, the phenocryst mineralogy of the GIC (plagioclase + biotite ± hornblende) requires only one parent magma chamber at depths of greater than about 8 km, most probably located near the interface between crystalline basement and passive margin sedimentary layers at depths of at least 12 km. However, the volume of copper in the Grasberg orebody indicates that the parent chamber supplying the fluids causing mineralisation had a volume of several hundred cubic kilometres; that is a chamber with batholithic dimensions. Isotopic studies (Housh and McMahon, 2000) indicate the chamber was supplied by magmas that assimilated substantial volumes of lower Precambrian continental crust. Hence, it appears that the magmas that resupplied the parent stock/batholith chamber came from a still deeper chamber, probably near the crust/mantle boundary.

### *Emplacement of the Dalam, MGI and Kali*

The Dalam unit has been described by previous authors (MacDonald and Arnold, 1994; Pollard and Taylor, 2002) as a diatreme. A space-generating explosive emplacement of the unit into the carbonate host rock is implied. A distinctive attribute of forceful intrusion and diatreme formation is the incorporation of wall rock clasts, commonly voluminous, into the magmatic breccia (Hack, 1942; Lorenz, 1975; 1986; Philpotts, 1990, p. 57; Best and Christiansen, 2001, p. 232).

Sapiie (1998) suggested and Luck (1999) developed a model of GIC formation that did not invoke an explosive, space-generating event for Dalam emplacement. A 100 m or so wide zone of brecciated carbonate rocks occur along the margins of the GIC. The clasts are rounded by dissolution, rather than explosively fragmented (Sapiie, 1998). The critical field observation is that clasts of the sedimentary wall rock have not been found in the magmatic breccia units. The dense sample coverage and petrographic analysis of this study has failed to reveal fragments of sedimentary wall rock within the Dalam Volcanic or Fragmental units. The only exception to this generalisation is found in two samples of LKI from near the southeasternmost edge of the complex. These samples, which are otherwise very fresh, contain a few grains of epidote that could be replaced micro-xenoliths of carbonate wall rock.

Within the Dalam, there are areas of outcrop from which we collected hand samples that contain clasts with layering (Fig. 17). However, these layered clasts are all fragments similar to the bedded volcanic units (Tvs) along the

northeast and southwest edges of the GIC (Fig. 2). Moreover, these samples with relicts of volcanic layering are confined to the periphery of the complex. They are particularly abundant in the Dalam Andesite near where they overlay the bedded volcanics (Tvs) in the northern part of the GIC (Sapiie, 1998).

The igneous processes that generated the Dalam were not entirely passive. Broken plagioclase phenocrysts recognised from the abrupt truncation of oscillatory zoning are present in many samples (Fig. 9). Most of the Dalam samples that do not contain broken grains are from locations that do not contain any plagioclase phenocrysts owing to intense hydrothermal alteration.

The absence of clasts of sedimentary wall rock fragments at the outcrop, hand-sample and now petrographic scale, strongly argues against a model of Dalam magmatism involving a space generating, diatreme-forming explosion. Broken phenocrysts are lacking in the MGI and Kali phases. Either phenocryst breakage was associated with very near-surface eruptive process or the conduit for magma intrusion at depth was much narrower during Dalam magmatism. The petrology and structure of the Dalam is most consistent with a model wherein volatile saturation of rising magma was only a near-surface (<1 km) phenomenon. The DA overlies the Tvs and clasts of DA are present in the DV which is, in turn, clearly genetically related to the DF in the centre of the complex. The small area of the three million year old GIC, and the presence of bedded volcanoclastic sediments along the margins, leads to the conclusion that the Dalam phase of magmatism occurred in a low-relief maar volcano setting, rather than in the throat of a tall composite volcano. The overall structural relationship of the DF with the DV suggests the igneous activity in the centre of the system was concurrent with

subsidence along the edges. A caldera in the maar volcano is inferred.

In striking contrast to the Dalam phase, broken phenocrysts are absent in the MGI and Kali indicating a different flow process during their emplacement. The Kali units are distinctly porphyritic with a variation in grain size between phenocrysts and groundmass of roughly 100-fold, whereas the MGI is comparatively equigranular with a typical variation of grain size between phenocrysts and groundmass of 10-fold or less. These textural differences are interpreted to indicate the MGI cooled more slowly than the Kali. These relations are most simply explained as the passive emplacement of the MGI into the still hot core of the Dalam phase rocks. This was followed by the similarly passive intrusion of the Early Kali as a very small plug into the centre of the substantially cooled MGI followed by the later, larger intrusion of the Late Kali as a wedge-shaped dyke splitting the substantial cooled intrusive complex.

## Conclusions

Based on 225 hand samples, polished slabs and thin sections from the Grasberg open pit mine, this study confirms that the tripartite division of the GIC reported by MacDonald and Arnold (1994) into the Dalam, MGI and Kali phases is robust. Petrologic refinements include:

- i) The phenocryst mineralogy in all Dalam phase rock is plagioclase and biotite. Hornblende is a sparse constituent except in the Dalam Andesite, a massive unit restricted to the northern part of the GIC.
- ii) The MGI had a magmatic mineralogy of plagioclase, biotite, hornblende and clinopyroxene.
- iii) The Kali can be subdivided into an Early and a Late phase. Both are relatively unaltered in comparison to the MGI, Dalam Andesite, Dalam Volcanic and Fragmental units. The mafic phases in the Early Kali are biotite and probably magnetite. The mafic phases in the Late Kali are biotite, hornblende, clinopyroxene and magnetite.
- iv) Broken plagioclase crystals are very common in the Dalam Volcanic and Fragmental units, resulting from flow processes which are probably related to near-surface volatile saturation. Broken plagioclase crystals are absent from the MGI and Kali phase intrusions, indicating their comparatively passive intrusion.
- v) Clasts of sedimentary wall rock are absent. Layered clasts that are present, are all similar to the bedded volcanoclastic unit along the margins the complex. Intrusion of all units occurred without detectable physical interaction with the sedimentary wall rocks exposed in the district.
- vi) In reconnaissance microprobe analysis, no systematic variation in plagioclase or biotite phenocryst chemistry was detected among the three igneous phases.
- vii) The magmatic groundmass in the Dalam Andesite, MGI and Kali was a combination of potassium feldspar, albite, quartz and biotite. Destruction of the magmatic groundmass was complete in the Dalam Volcanic/Dalam Fragmental units. The groundmass in the Dalam units was probably glassy.

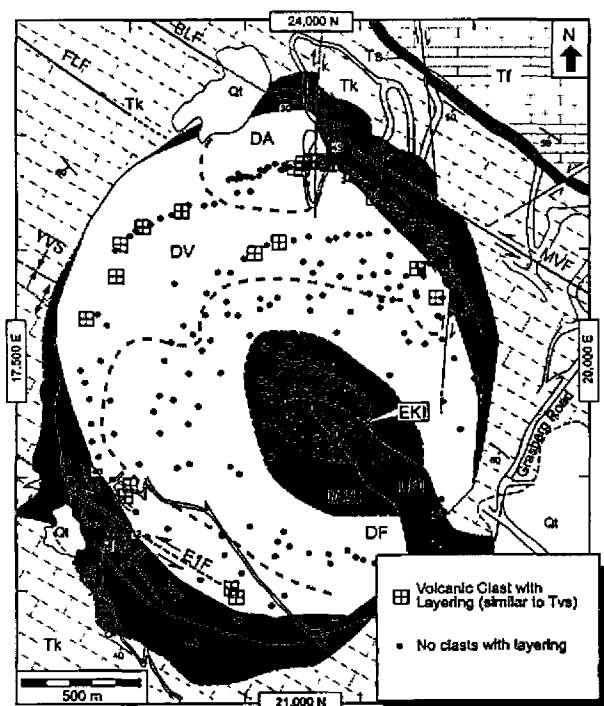


Figure 17: Distribution of layered volcanic clasts. Most layered clasts are very similar to the Tvs.

- viii) There are areas in the Dalam Fragmental/Dalam Volcanic with complete textural destruction of all phenocryst phases by hydrothermal alteration. The largest of these areas, in the southwest part of the GIC, covers approximately 250 x 1300 m.
- ix) Magmatism probably occurred in a low relief maar-caldera. The parent chamber was recharged at least twice, and possibly many times with magma of similar composition.

## Acknowledgments

From logistical to financial support, none of this work would have been possible without a large number of people from Freeport-McMoRan, Inc. and PT Freeport Indonesia: James R. Moffett, Dave Potter, George MacDonald, Wahyu Sunyoto, Sugeng Widodo, Noris Belluz, Keith Parris, Paul Warren, Clyde Leys, Herry Susanto, Chris Christenson, Bambang Irawan, Ben Coutts, Stephen Hughes, Nico Sambur, Aditya Pringgoprawiro, Boedijono, Yahul and Bambang Antoro. A special thanks goes to Benyamin Sapiie. Ertzberg Project Contribution No. 23.

## References

- Beane, R.E. and Titley, S.R., 1981 - Porphyry copper deposits, part II, hydrothermal alteration and mineralization: *Economic Geology* 75<sup>th</sup> Anniversary Volume, pp. 235-269.
- Best, M. G. and Christiansen, E. H., 2001 - Igneous Petrology, *Blackwell Science*, 458p.
- Cloos, M., 2001 - Bubbling magma chambers, cupolas, and porphyry copper deposits: *International Geology Review*, v. 43, pp. 285-311.
- Cloos, M. and Sapiie, B., 2005 - Porphyry copper deposits: Strike-slip faulting and throttling cupolas; Geological Society of America Abstracts with Programs, Vol. 37, No. 7, p. 97.
- Coutts, B. P., Susanto, H., Belluz, N., Flint, D. and Edwards, A., 1999 - Geology of the Deep Ore Zone, Ertzberg East Skarn System, Irian Jaya: Proceedings of the International Congress on Earth Science, Exploration and Mining Around the Pacific Rim (PacRim '99), *Australasian Institute of Mining and Metallurgy, Melbourne*, Publication Series, No. 4, pp. 539-547.
- Dow, D.B., Robinson, G.P., Hartono, U. and Ratman, N., 1988 - Geology of Irian Jaya: Irian Jaya Geological Mapping Project, Geological Research and Development Center, Indonesia, in cooperation with the Bureau of Mineral Resources, Australia, on behalf of the Department of Mines and Energy, Indonesia, and the Australian Development and Assistance Bureau, 298p.
- Dozy, J.J., 1939 - A. General Stratigraphy, tectonics, in J.J. Dozy, ed., Geological results of the Carstensen expedition: *Leidsche Geologische Mededelingen*, v. 11, pp. 68-95.
- Hack, J.T., 1942 - Sedimentation and volcanism in the Hopi Buttes, Arizona: *Geological Society of America Bulletin*, v. 53, pp 335-372.
- Hamilton, W., 1979 - Tectonics of the Indonesian region: *U.S. Geological Survey Professional Paper* 1078, 345p.
- Housh, T. and McMahon, T. P., 2000 - Ancient isotopic characteristics of Neogene potassic magmatism in western New Guinea (Irian Jaya, Indonesia): *Lithos*, v. 50, pp. 217-239.
- Katchan, G., 1982 - Mineralogy and geochemistry of the Ertzberg (Gunung Bijih) and Ertzberg East (Gunung Bijih Timur) skarns, Irian Jaya, Indonesia and the Ok Tedi skarns, Papua New Guinea [Ph.D. dissertation]: *The University of Sydney, Australia*, 498p.
- Lorenz, V., 1975 - Formation of phreatomagmatic maar-diatreme volcanoes and its relevance to kimberlite diatremes: *Physics and Chemistry of the Earth*, v. 9, 940p.
- Lorenz, V., 1986 - On the growth of maars and diatreme and its' relevance to the formation of tuff rings: *Bulletin of Volcanology*, v. 48, pp. 265-274.
- Luck, R. B., 1999 - Structural geology of the Grasberg Lime Operation and Amole Drift: Implications for emplacement of the Grasberg Igneous Complex, Irian Jaya, Indonesia [M.S. Thesis]: *The University of Texas at Austin*, 276p.
- MacDonald, G.D. and Arnold, L.C., 1994 - Geological and geochemical zoning of the Grasberg Igneous Complex, Irian Jaya, Indonesia: *Journal of Geochemical Exploration*, v. 50, pp. 143-178.
- Martojojo, S., Sudradjat, D. Subandrio, E. and Luckman, A., 1975, The geology and stratigraphy along the road cut, Tembagapura, Irian Jaya, Volume 1: *Unpublished report*, 51p.
- McDowell, F.W., McMahon, T.P., Warren, P.Q. and Cloos, M., 1996 - Pliocene Cu-Au bearing igneous intrusions of the Gunung Bijih (Ertzberg) District, Irian Jaya, Indonesia: K-Ar Geochronology: *Journal of Geology*, v. 104, pp. 327-340.
- McMahon, T.P., 1994a - Pliocene intrusions in the Gunung Bijih (Ertzberg) Mining District, Irian Jaya, Indonesia: Petrography and mineral chemistry: *International Geology Review*, v. 36, pp. 820-849.
- McMahon, T.P., 1994b - Pliocene intrusions in the Ertzberg (Gunung Bijih) Mining District, Irian Jaya, Indonesia: Petrography, geochemistry and tectonic setting [Ph.D. Dissertation]: *The University of Texas at Austin*, 298p.
- McMahon, T.P., 1994c - Pliocene intrusions in the Gunung Bijih (Ertzberg) Mining District, Irian Jaya, Indonesia: Major- and trace-element chemistry: *International Geology Review*, v. 36, pp. 925-946.
- McMahon, T.P., 1999 - The Ertzberg Intrusion and the Grasberg Complex: Contrasting styles of magmatic evolution and Cu-Au mineralization in the Gunung Bijih (Ertzberg) Mining District, Irian Jaya, Indonesia: *Bulletin Geologi*, v. 31, (3), pp. 123-132.
- Mealy, G. A., 1996 - Grasberg: Mining the Richest and Most Remote Deposit of Copper and Gold in the

- World, in the Mountains of Irian Jaya, Indonesia: *Freeport-McMoRan Copper & Gold Inc.*, 384p.
- Meinert, L. D., Hefton, K. K., Mayes, D. and Tasiran, L., 1997 - Geology, zonation, and fluid evolution of the Big Gossan Cu-Au skarn deposit, Ertsberg District, Irian Jaya: *Economic Geology*, v. 92, pp. 509-533.
- Mertig, H.J., Rubin, J.N. and Kyle, J.R., 1994 - Skarn Cu-Au orebodies of the Gunung Bijih (Ertsberg) district, Irian Jaya, Indonesia: *Journal of Geochemical Exploration*, v. 50, pp. 179-202.
- Naney, M. T., 1983 - Phase equilibria of rock-forming ferromagnesian silicates in granitic systems: *American Journal of Science*, v. 283, pp. 993-1033.
- Nash, C.R., Artmont, G., Lennie, D., O' Connor, G. and Parris, K.R., 1993 - Structure of the Irian Jaya mobile belt, Irian Jaya, Indonesia: *Tectonics*, v. 12, pp. 519-535.
- O' Connor, G. V., Soebari, L. and Widodo S., 1994 - Upper Miocene-Pliocene magmatism of the Central Range Mobile Belt, Irian Jaya, Indonesia, *Fourth Asia/Pacific Mining Conference*, pp. 1-27.
- Philpotts, A. R., 1990 - Principles of Igneous and Metamorphic Petrology, *Prentice Hall*, 498p.
- Pollard, P. J., Taylor, R. G. and Widodo, S., 2001 - Geochronology of intrusive rocks and Cu-Au mineralization in the Ertsberg Mining District, Irian Jaya, Indonesia: in *A Hydrothermal Odyssey*, Townsville, May 17-19, 2001, Extended Conference Abstracts, Williams, P. J., (Ed.), *James Cook University, Economic Geology Research Unit Contribution 59*, pp. 166-167.
- Pollard, P.J. and Taylor, R.G., 2002 - Paragenesis of the Grasberg Cu-Au deposit, Irian Jaya, Indonesia: Results from logging section 13: *Mineralium Deposita*, v. 37, pp. 117-136.
- Potter, D., 1996 - What makes Grasberg anomalous, Implications for future exploration: in *Porphyry Related Copper and Gold Deposits of the Asia Pacific Region, Conference Proceedings, 12-13 August 1996*, Cairns, *Australian Mineral Foundation*, Adelaide, pp 10.1-10.13.
- Potts, J.P., Bowles, J.F.W., Reed, S.J.B. and Cave, M.R., 1995 - Microprobe Techniques in the Earth Sciences: *Chapman and Hall*, 419p.
- Quarles van Ufford, A., 1996 - Stratigraphy, structural geology, and tectonics of a young forearc-continent collision, western Central Range (western New Guinea), Indonesia [Ph.D. Dissertation]: *The University of Texas at Austin*, 420p.
- Quarles van Ufford, A. and Cloos, M., in press - Cenozoic Tectonics of New Guinea: *American Association of Petroleum Geologists Bulletin*.
- Rubin, J. N., 1996 - Skarn formation and ore deposition, Gunung Bijih Timur complex, Ertsberg district, Irian Jaya, Indonesia: [Ph.D. dissertation], *The University of Texas at Austin*, 310p.
- Sapiie, B., 1988 - Strike-slip faulting, breccia formation and porphyry Cu-Au mineralization in the Gunung Bijih (Ertsberg) Mining District, Irian Jaya, Indonesia [Ph.D. Dissertation]: *The University of Texas at Austin*, 304p.
- Sapiie, B. and Cloos, M., 2004 - Strike-slip faulting in the core of the Central Range of west New Guinea: Ertsberg Mining District, Indonesia: *Geological Society of America Bulletin*: v. 116, pp. 277-293.
- Sapiie, B. and Cloos, M., in review - Strike-slip faulting and veining in the Grasberg giant Porphyry Cu-Au deposit, Gunung Bijih (Ertsberg) mining district, Irian Jaya, Indonesia.
- Soeparman, S. and Budijono, 1989 - Cu-skarn deposits in the Ertsberg mine area, Irian Jaya, *Geologi Indonesia*, v. 12, pp. 359-374.
- Spear, F. S., 1993 - Metamorphic Phase Equilibria and Pressure-Temperature-Time Paths: *Mineralogical Society of America Monograph Series*, 799p.
- Titley, S.R., 1982 - The style and progress of mineralization and alteration in porphyry copper systems, American southwest, in *Advances in Geology of the Porphyry Copper Deposits in Southwestern North America: University of Arizona Press*, Tucson, pp. 117-137.
- Van Nort, S.D., Atwood, G.W., Collinson, T.B., Flint, D.C. and Potter, D.R., 1991 - Geology and mineralization of the Grasberg copper-gold deposit: *Mining Engineering*, v. 43, pp. 300-303.
- Widodo, S., Manning, P., Wiwoho, N., Johnson, L., Belluz, N., Kusnanto, B., MacDonald, G. and Edwards, A., 1999 - Progress in understanding and developing the Kucing Liar orebody, Irian Jaya, Indonesia: Proceedings of the International Congress on Earth Science, Exploration and Mining Around the Pacific Rim (PacRim '99), *Australasian Institute of Mining and Metallurgy, Melbourne*, Publication Series, No. 4, pp. 499-507.
- Wilson, F., 1981 - *The Conquest of Copper Mountain: Atheneum*, New York, 244p.



## **GRASBERG PORPHYRY Cu-Au DEPOSIT, PAPUA, INDONESIA: 2. PERVASIVE HYDROTHERMAL ALTERATION**

John T. Paterson and Mark Cloos

*Department of Geological Sciences, University of Texas at Austin, USA*

**Abstract** - The Grasberg Igneous Complex (GIC) is host to one of the largest copper and gold porphyry-type ore deposits discovered on Earth. Much of the rock volume in the GIC has been pervasively altered by the infiltration of hot, magmatic fluids. In parts of the deposit, alteration destroyed all igneous phases. Petrography reveals that two zones characterise almost the entire complex at the level of the open pit mine. The 1 km-wide core of the deposit is dominated by biotite + magnetite with an inner ~500 m-wide sub-zone containing andalusite. The exterior annular zone, ~500 m across, is dominated by sericite + anhydrite + pyrite with small amounts of kaolinite. Pockets of rock contain epidote with chlorite in the distal portions of the GIC.

The pattern of hydrothermal alteration indicates an intense episode of pervasive fluid flow post-dated the Main Grasberg Intrusion and predated the Late Kali Intrusion. The overall pattern indicates the interior was hot and acid-producing and the exterior was cooler and acid-consuming. In the core of the GIC, the precipitation of abundant magnetite caused outwards moving fluids to become acidic. In the cooler, outer parts of the complex, these acidic fluids caused the hydrolysis of plagioclase and other minerals into sericite. The cooling of outwards flowing fluids also caused the hydrolysis of SO<sub>2</sub> to H<sub>2</sub>S and H<sub>2</sub>SO<sub>4</sub> which, in turn, caused the precipitation of sulphide minerals and anhydrite. The overprint of sericite + anhydrite + pyrite upon the biotite + magnetite zone is limited in area and of minor intensity. Compared to most other porphyry copper deposits, the pervasive infiltration of magmatic fluid ended rather abruptly.

### **Introduction**

A concentric pattern of mineralogic zones is such a distinctive feature of copper porphyry deposits that recognition has long been used in the search for porphyry copper-type mineralisation and as a guide for exploration drilling (Lowell, 1995). Pervasive infiltration and hydrothermal alteration that emanates from a point source is the simple explanation for the bullseye pattern of zonation that characterises these deposits. The basic zonation was first recognised by Sales and Meyer (1950), but it was Lowell and Guilbert (1970) who provided an extensive review of porphyry copper systems that focused on the mineralogic commonalities of the alteration zoning. They described the San Manuel-Kalamazoo deposit in the southwestern United States as the type example. In this deposit, a central core of potassic alteration, with a mineral assemblage characterised by quartz, potassium feldspar, and hydrothermal biotite, grades outwards to a phyllic 'shell' of quartz, sericite and pyrite, which in turn grades into a 'shell' of propylitic alteration, characterised by chlorite, epidote, and albite. More irregularly developed, but concentrated on the outer margins is argillic alteration, characterised by quartz, kaolinite, and chlorite. Lowell and Guilbert (1970) proposed that following the intrusion of a stock, the concentric alteration zones form as a result of a continuum of conditions as hot magmatic fluids in the core

of the system cool as they move outwards. Gustafson and Hunt (1975) proposed, following a study of the El Salvador deposit in Chile, that magmatic-fluid dominated alteration (potassic alteration) in the core of the deposit grades into alteration that is dominated by meteoric fluid (phyllic alteration, or feldspar-destructive). As the system cools, the hydrothermal system collapses and phyllic alteration is superimposed on the potassic zone. The superposition of alteration zones is reported for many deposits.

Mineralisation in copper porphyry systems arises from two fundamentally different forms of fluid flow (Burnham, 1979; Rose and Burt, 1979), namely: 1) extension fractures with mineral precipitation forming veins, and 2) diffuse infiltration causing pervasive alteration and disseminated mineralisation. It is the diffuse infiltration that defines the concentric zones and involves volumes of rock on the scale of cubic kilometres. To some extent, these processes are overlapping. Most veins are tabular with no obvious alteration of the enclosing wall rocks, but some are accompanied by alteration 'halos' that indicate centimetre-scale infiltration and locally intense alteration of the wall rock.

The Grasberg porphyry Cu-Au deposit, which formed at ~3 Ma, is one of the largest on Earth. A brief discussion of the regional geology and characterisation of the primary



magmatic mineralogy is presented in a companion paper (Paterson and Cloos, this volume). This paper focuses on the pervasive alteration history of the GIC caused by the pervasive infiltration of hydrothermal fluid.

**Previous Work on the Grasberg System**

Van Nort et al. (1991) presented a general description of the Grasberg Igneous Complex (GIC) and the contained Cu-Au ore body (Fig. 1). MacDonal and Arnold (1994) provided the first detailed examination of magmatic mineralogy, alteration and mineralisation. In their study, they described a genetic model for alteration in which different stages of alteration and associated mineralisation follow the intrusion of the three main magmatic phases: Dalam, Main Grasberg Intrusion (MGI), and Kali (Fig. 2). They proposed that pervasive alteration and disseminated mineralisation in the GIC dominates in the Dalam phase rocks, with an outer zone of phyllic alteration (sericite +

quartz + pyrite) that transitions inwards to the core zone of potassic alteration (potassium feldspar + biotite + magnetite). Propylitic alteration (epidote ± chlorite) is limited to the extreme periphery of the GIC and argillic alteration (clays) is only locally developed in the phyllic zone. The authors reported only weak pervasive alteration in the MGI and noted minimal alteration in the Kali.

Previous studies of alteration/mineralisation at the University of Texas at Austin (Penniston-Dorland, 1997; Sapiie, 1998) concentrated upon the pattern and orientation of veins in the open pit mine. A concentric zonation of veining is evident centred on the core of the deposit. Penniston-Dorland (1997) provided an analysis of vein mineralogies, concluding that two main stages of veining occurred: post Dalam and MGI, and post Late Kali Intrusion (LKI). The first stage (confined to the Dalam and MGI) was volumetrically abundant and stockwork-forming (networks of veins indicating a three-dimensional dilatation) in the core of the GIC. Stage 1a magnetite + quartz veining was overprinted by Stage 1b chalcopyrite veining. Stage 2 veining was volumetrically minor, postdated the Late Kali Intrusion, and was chemically distinctive forming biotite with little associated copper sulphide mineralisation. Cross-cutting veins are common, but there are very few veins (<1%) re-opened to become lined with more than one generation of minerals (Sapiie, 1998).

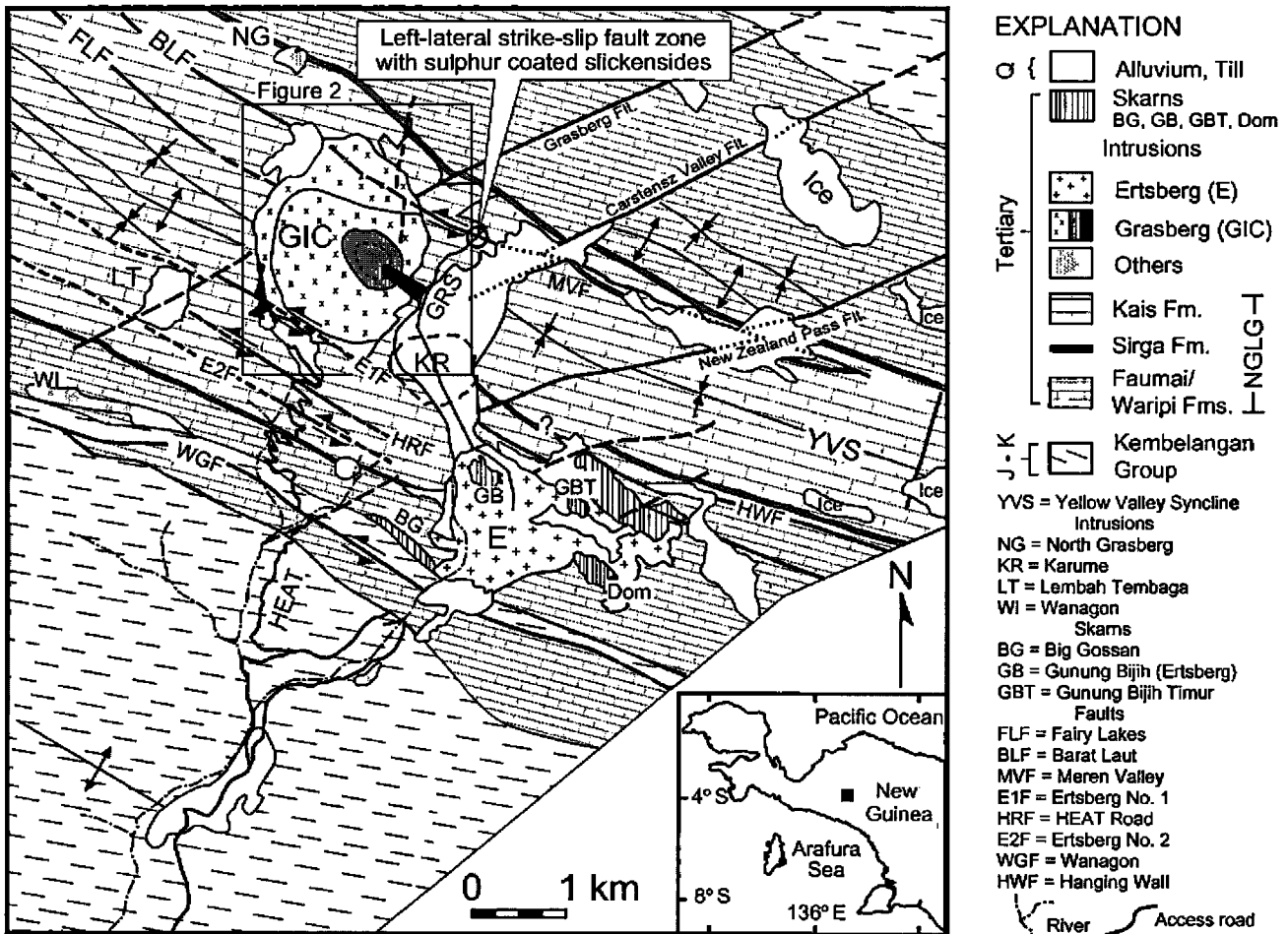
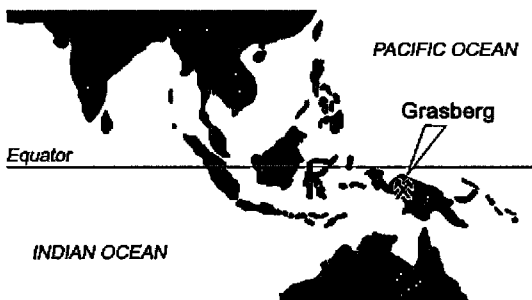


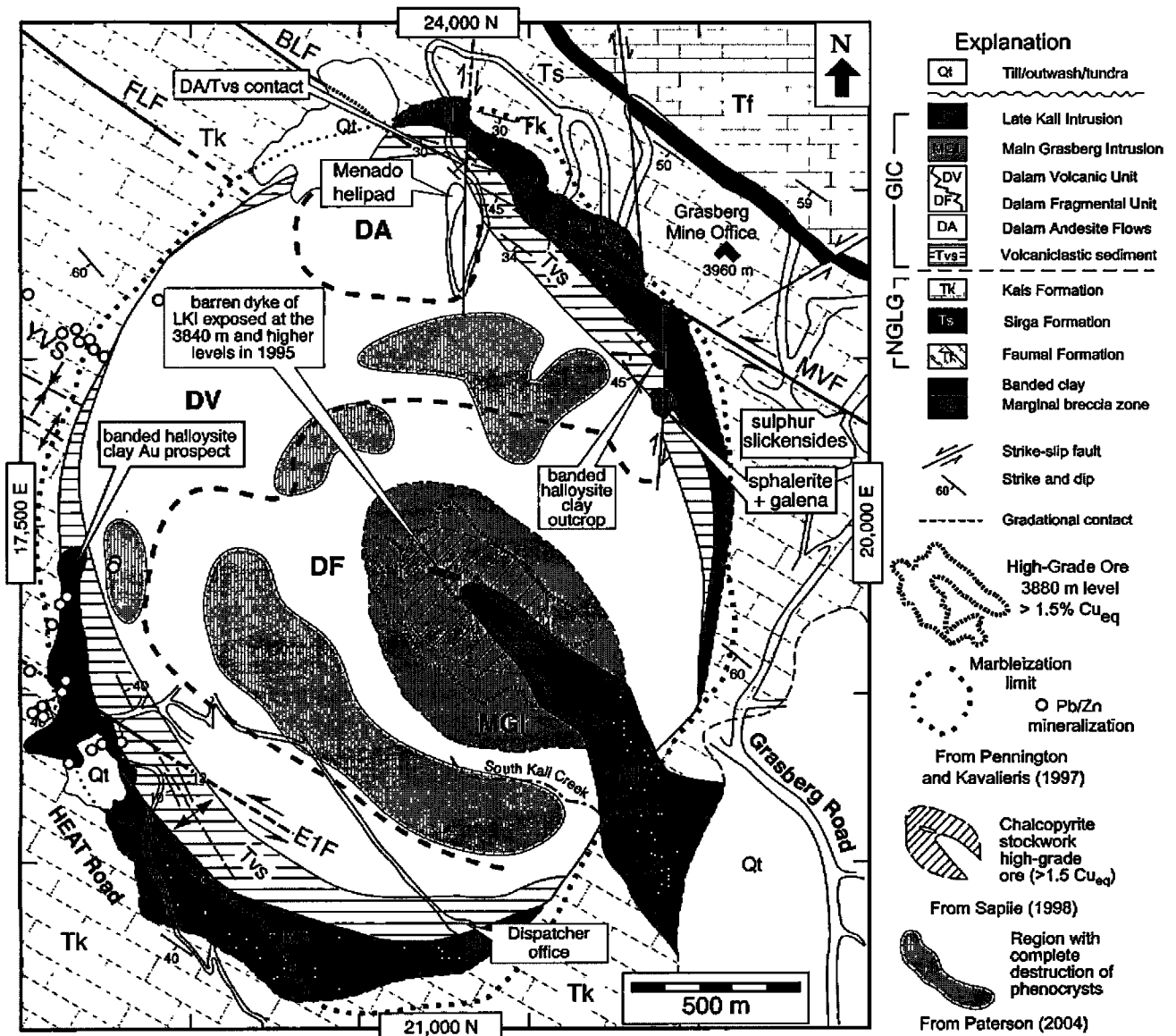
Figure 1: Geologic map of Ertzberg Mining District, Papua, Indonesia.

Millimetre to centimetre-scale sericitic alteration halos are associated with some of the pyrite ± quartz veins. The whitish halos are especially distinct where they cut rock that is black because of abundant magnetite and biotite. Penniston-Dorland (1997) found that geochemical changes in the alteration halos involve the removal of major oxides such as Na<sub>2</sub>O, MgO and CaO as well as trace elements such as Cu, Rb and Sr. She concluded that the alteration forming the halos was the result of acid consumption, or of acid attack on the silicate host rock by the pyrite vein-forming fluid. In doing so, she showed that the alteration halos in the GIC have mineralogies very similar to those commonly reported in the phyllic zone of pervasive alteration. In addition, Penniston-Dorland (2001) used cathodoluminescence analysis to show that the quartz veins were the product of a single opening, fluid infiltration and mineral precipitation event.

Sapiie (1998) mapped the pattern of faulting and vein zonation in the open pit mine (Fig. 3). He divided the GIC into three 300°-trending zones dominated by strike-slip

faults that cross-cut the veins. Sapiie (1998) concluded that the GIC formed in a 2 km-wide pull-apart, or extensional jog, connecting the Meren Valley and Ertsberg No. 1 left-lateral strike-slip faults. Based upon 1996 mapping in the open pit mine, vein abundance is greatest in a slightly elongated 400 x 500 m zone centred on the MGI. Sapiie (1998) mapped the boundaries of the abundant chalcopyrite veining forming most of the highest grade ore (a stockwork zone of Stage 1b) superimposed upon the quartz-magnetite stockwork of Stage 1a (Fig. 3). Inner and outer limits were mapped for vein populations such as quartz + pyrite + anhydrite and pyrite ± quartz veins with alteration envelopes. Most importantly, he deduced that strike-slip faulting, pull-apart extension and veining were causally related.

In striking contrast to the two-stage model for extension fracturing/veining discussed above, Pollard and Taylor (2002) identified 35 temporally and chemically distinct generations of veining and alteration, several of which were also spatially distinct. Their analysis was based on a 'fan'



**Figure 2: Geology of the Grasberg Igneous Complex (GIC) at the ~3900 m elevation.** Modified from Suwardy (1995) and Sapiie (1998). The Meren Valley Fault (MVF) and Ertsberg #1 Faults (E1F) are left-lateral strike-slip faults. Sapiie (1998) concluded the GIC was emplaced into a pull-apart connecting these fault zones.

of drill cores representing a vertical section trending NE-SW through the centre of the deposit from approximately 2600 to 4000 m. Thus, at the beginning of this investigation there were two distinct pictures for alteration and mineralisation: two distinct alteration/mineralisation events and the Pollard and Taylor perspective of many pulses of chemically distinct fluid flow and associated mineralisation.

this study focuses on evaluating the pervasive alteration and disseminated mineralisation in the Grasberg system via the analysis of hand specimens, polished slabs and thin sections of a suite of 225 samples collected in the open pit mine between 1994 to 2002. The samples were located between the elevations of 3700 m and 4200 m, most between 3800 m to 4100 m. Because the Grasberg was a hill prior to mining, the effect of sampling over time resulted in a suite that constitutes a roughly horizontal cross section at ~3900 m elevation. These samples are the basis for constructing a set of maps that depict mineralogic and textural variations of pervasive alteration in the GIC.

### Hydrothermal Mineralogy

The petrographic study of hydrothermally altered rocks is difficult owing to the fine grain size produced by pervasive alteration. Petrographic analysis revealed cryptic micro-

textures that were used as the basis for selecting samples for standard x-ray diffraction and electron microprobe analysis to confirm the identification of fine-grained minerals. See Paterson (2004) for analytical details.

### Hand Specimen Observations

The magmatic mineralogy of the igneous units in the GIC is summarised in Table 1. From the fresh LKI through to the highly altered Dalam phase rocks, photographs of polished slabs (Fig. 4) illustrate the nature of pervasive alteration which is locally severe enough to completely destroy all magmatic phenocrysts (shaded regions on Fig. 2).

### Hydrothermal Biotite

Biotite comprises 3 to 25%, typically 15%, of the magmatic phenocryst population (Paterson and Cloos, this volume) and is a major alteration product. Although in principle differentiation could be difficult, hydrothermal biotite is petrographically very distinct from magmatic biotite due to the marked contrast in morphology. Phenocrystic (magmatic) biotite commonly has a euhedral shape with crystal sizes typically 0.5 to 2 mm across. Groundmass magmatic biotite occurs as solitary grains typically about 0.2 mm across. Hydrothermal biotite, in striking contrast,

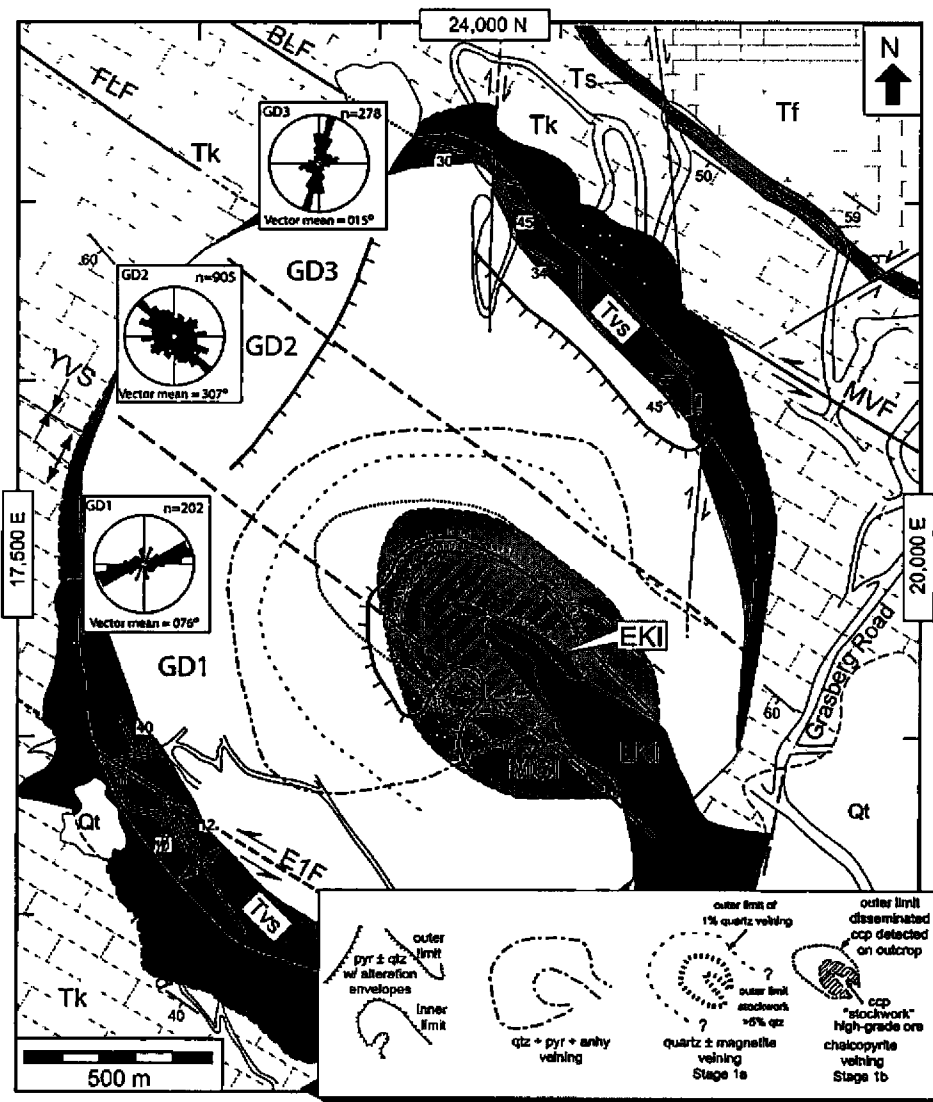


Figure 3: Vein type and density, and structural domains identified by Sapiie (1998). Grasberg Structural Domain 1, GD1, is dominated by 76° trending left-lateral strike-slip faults. GD2 is dominated by 307° trending left-lateral strike-slip faults. GD3 is dominated by 15° trending, right-lateral strike slip faults.

Table 1: Magmatic mineralogy of the igneous units in the Grasberg Igneous Complex

youngest	<b>Late Kali Intrusion (LKI)</b>	
	<b>phenocrysts</b>	plagioclase (20% to 65%) + biotite (10% to 20%) + hornblende (3% to 15%) ± clinopyroxene (altered to actinolite) (~2%)
	<b>groundmass</b>	potassium feldspar (10% to 30%), quartz (10% to 30%), biotite (~5%), albitic plagioclase (~5%), magnetite (~2%) and apatite (tr.)
	<b>texture</b>	porphyritic: ~100x variation in grain size
	<b>Early Kali Intrusion (EKI)</b>	
	<b>phenocrysts</b>	plagioclase (20% to 65%) + biotite (10% to 20%)
	<b>groundmass</b>	potassium feldspar (10% to 30%), quartz (10 to 30%), biotite (~10%), albitic plagioclase (~5%), and apatite (tr.)
	<b>texture</b>	porphyritic: ~100x variation in grain size
	<b>Main Grasberg Intrusion (MGI)</b>	
	<b>phenocrysts</b>	plagioclase (20% to 40%) + biotite (5% to 25%) + hornblende (3% to 15%) + clinopyroxene (altered to actinolite) (~5%)
	<b>groundmass</b>	potassium feldspar (~15%), quartz (~15%), biotite (~5%), albitic plagioclase (~5%), and apatite (tr.)
	<b>texture</b>	comparatively equigranular: ~10x variation in grain size
	<b>Dalam Andesite (DA)</b>	
	<b>phenocrysts</b>	plagioclase (10% to 35%) + biotite (5% to 25%) + hornblende (3% to 15%)
	<b>groundmass</b>	potassium feldspar (~10%), quartz (~20%), biotite (~10%), albitic plagioclase (~5%), and apatite (tr.)
	<b>texture</b>	porphyritic: ~100x variation in grain size
oldest	<b>Dalam Volcanic/Dalam Fragmental (DV/DF)</b>	
	<b>phenocrysts</b>	plagioclase (up to 45%) and biotite (3% to 20%) +/- hornblende (< 2%)
	<b>groundmass</b>	thoroughly altered in almost all samples, may have been glassy, apatite (tr.)
	<b>texture</b>	brecciated, with broken plagioclase crystals

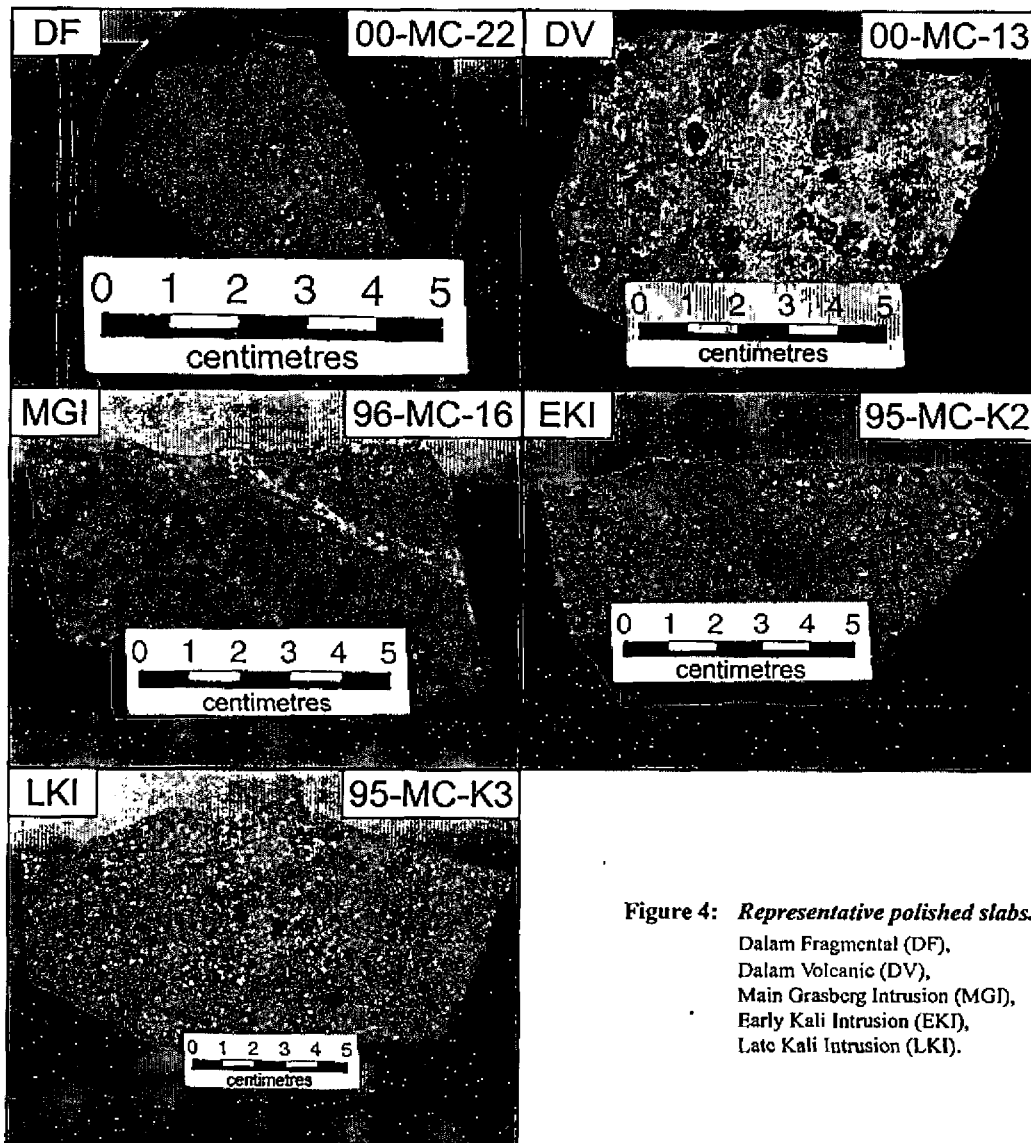


Figure 4: Representative polished slabs. Dalam Fragmental (DF), Dalam Volcanic (DV), Main Grasberg Intrusion (MGI), Early Kali Intrusion (EKI), Late Kali Intrusion (LKI).

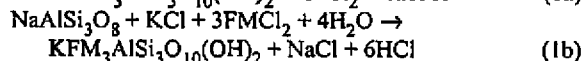
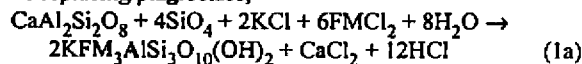
occurs as "shreddy" aggregates of grains that are most commonly smaller than 0.1 mm across. Similar habits for biotite are reported in many copper-porphyry systems (Creasey, 1966; Dilles and Einaudi, 1992).

Hydrothermal biotite is abundant in the core, but absent in the outer portions of the GIC (Fig. 5). The Late Kali (LKI) has little (typically trace to 5%) hydrothermal biotite compared to the Early Kali (EKI) (5 to 15%). This indicates that the emplacement of the LKI occurred after pervasive hydrothermal alteration had essentially ended. In the interior of the GIC, near the northwestern border of the MGI and DF, trace amounts of green biotite is present as replacement rims on hydrothermal, brown biotite. Petrographically it looks similar to green phlogopite.

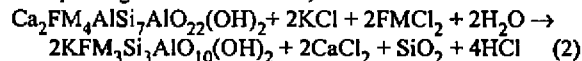
Pseudomorphic relationships indicate much of the hydrothermal brown biotite formed from replacement of plagioclase, hornblende and biotite phenocrysts. It is commonly intimately associated with magnetite. The infiltration of potassic, metal-rich brines can account for the alteration. The products are acidic, Ca-rich, fluids.

Idealised end-member reaction chemistries (with FM= Fe, Mg) for these pseudomorphic reactions are:

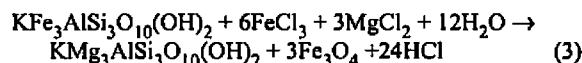
biotite replacing plagioclase,



biotite replacing calcic hornblende,



Microprobe analysis shows brown hydrothermal biotite has a higher Mg content than magmatic biotite. The idealised exchange reaction below also accounts for the intimate association of magnetite with replacement biotite:



The compositional difference between magmatic and hydrothermal biotite (Fe, Mg, Ti) is relatively small (Fig. 6). This is interpreted to indicate the thermal and chemical conditions under which both types formed were similar.

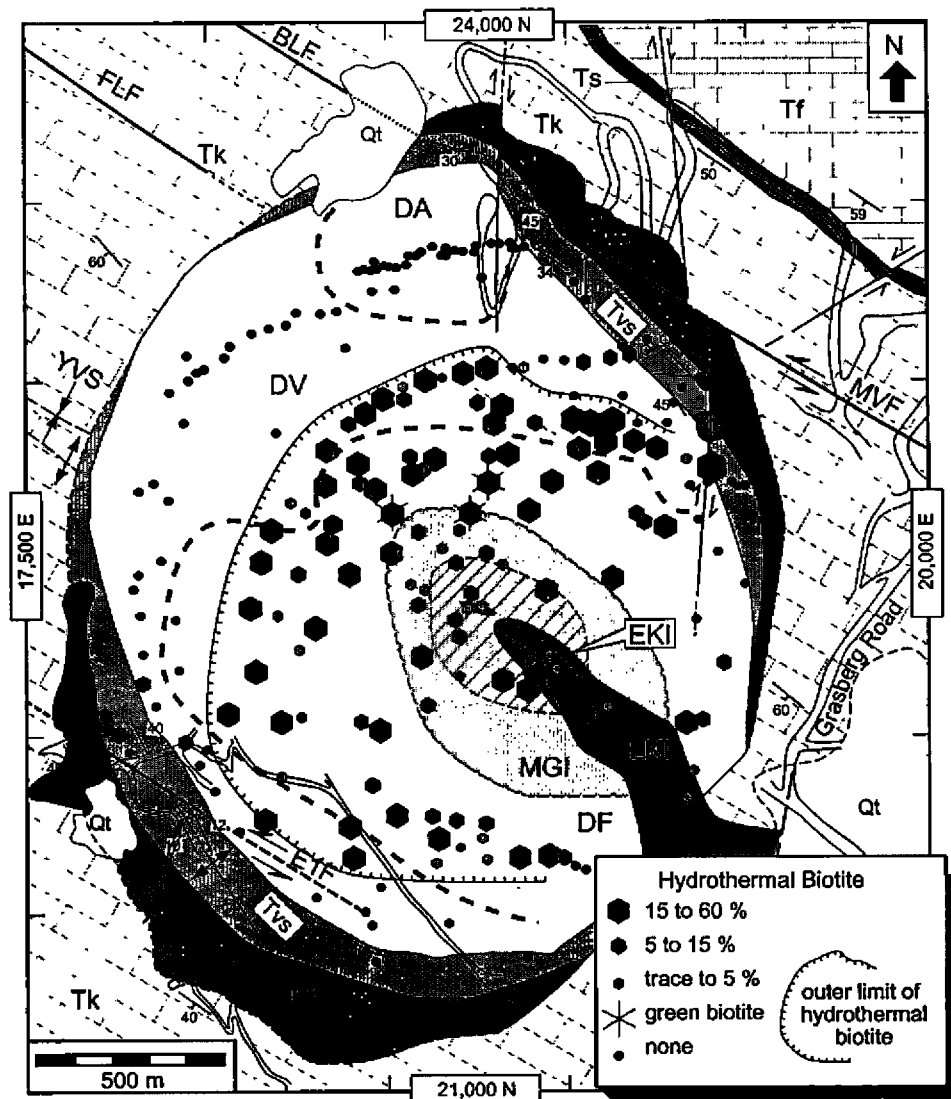


Figure 5: Distribution and abundance of hydrothermal biotite.

Magmatic biotite equilibrated with a melt. Hydrothermal biotite in the core of the GIC equilibrated with a magmatic fluid that was not substantially cooler than the temperature of total magmatic solidification.

Green biotite crystals were only coarse enough for analysis in one sample (94-MC-D2). They differ markedly in composition from magmatic biotite or hydrothermal brown biotite. Using normalisation schemes for biotite (Yavuz and Oztas, 1997), the brown biotite is relatively Mg and Ti-rich whereas the green biotite is relatively Al and Fe<sup>3+</sup>-rich. Therefore, the green biotite crystals appear to record equilibration with either a Mg- and Ti-poor fluid (the latter a strong indicator of lower temperature) and/or a more oxidised fluid during the waning of the hydrothermal system. An important feature of the occurrence of green biotite is that it is localised to near the centre of the GIC.

**Sericite (Fine-Grained Muscovite)**

Unlike hydrothermal biotite, there is no magmatic muscovite. Fine-grained hydrothermal muscovite (sericite) is typically very easy to identify in thin section, but in large parts of many thin sections, sericite is below petrographic resolution. Sericite is typically associated with pyrite, anhydrite/gypsum/porosity, and quartz.

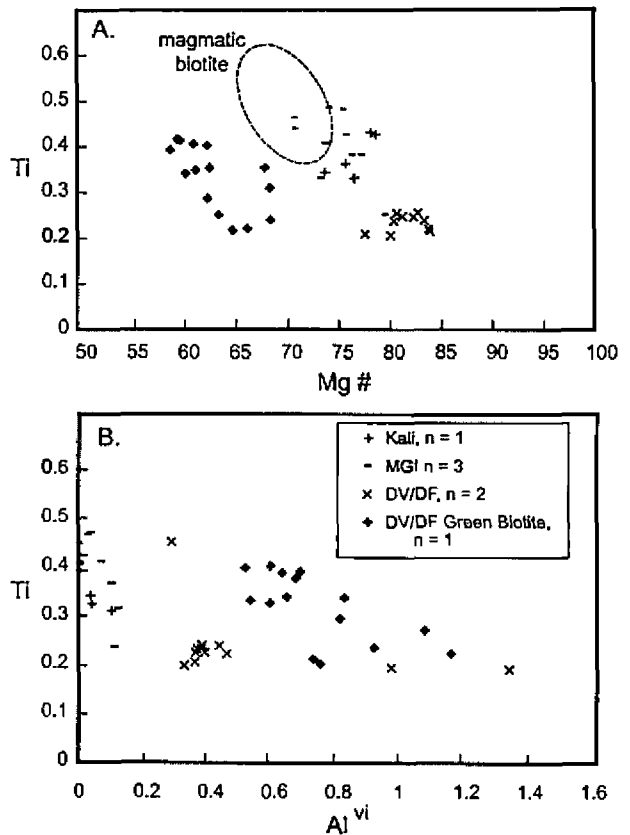


Figure 6 (above): *Composition of shreddy, hydrothermal biotite.*

- A. Ti versus Mg # = Mg/(Fc+Mg).
- B. Ti versus Al in six-fold coordination. Ti and Al cations calculated on basis of 44 negative charges.

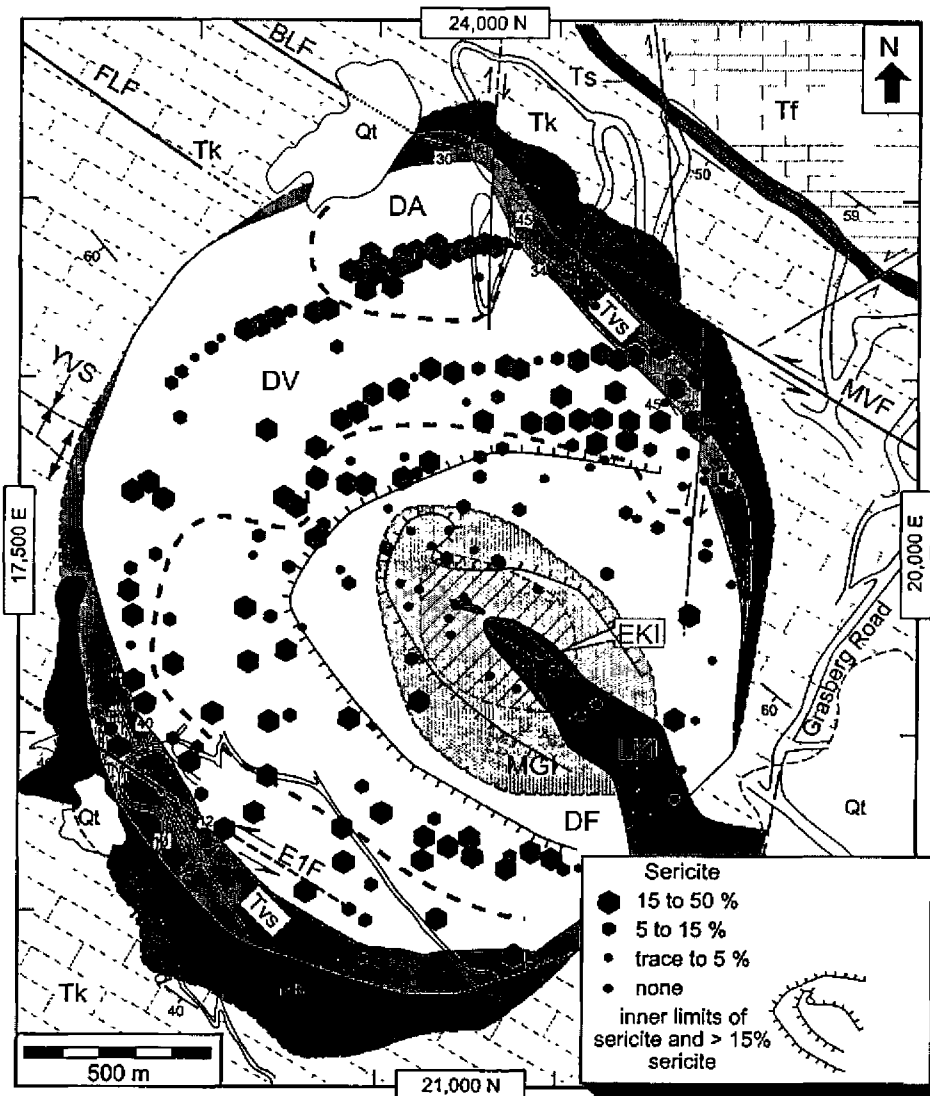


Figure 7 (left): *Distribution and abundance of sericite (fine-grained muscovite).*

In marked contrast to the pattern of hydrothermal biotite, which is only present in the interior of the GIC, sericite is, with the exception of bleached alteration halos along pyrite  $\pm$  quartz veins, only present in the outer portion of the GIC (Fig. 7). Noticeably, there are also regions, or pockets, in the exterior of the GIC where sericite is minor or absent and the mineral assemblage is dominated by epidote  $\pm$  chlorite (see below). Comparison of Figs. 5 and 7 shows the portion of the GIC dominated by sericite is an annular

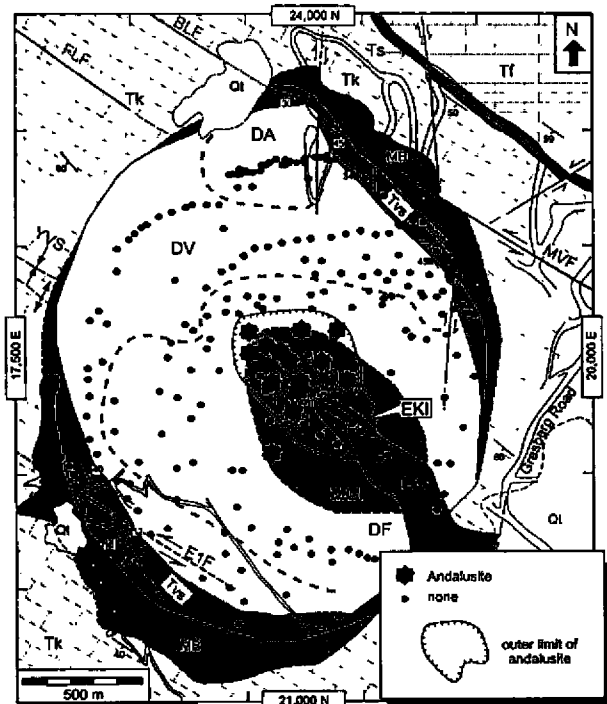


Figure 8: Distribution of andalusite. Note the occurrences are isolated to the interior of the Grasberg Igneous Complex.

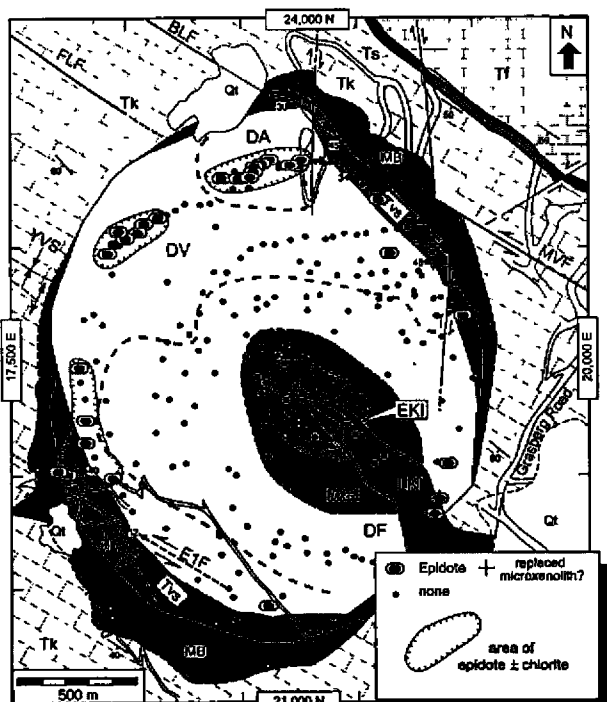
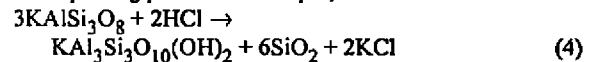


Figure 9: Distribution of epidote. Note the occurrences are isolated to the margins of the Grasberg Igneous Complex.

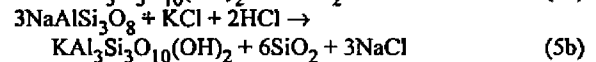
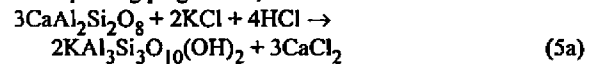
region (with an inner radius of approximately 500 m) in which hydrothermal biotite is minor or absent.

Sericite commonly occurs as a pseudomorphic replacement of groundmass potassium feldspar, and of plagioclase and biotite phenocrysts. Idealised reactions (with FM=Fe, Mg) for the replacements are all acid-consuming:

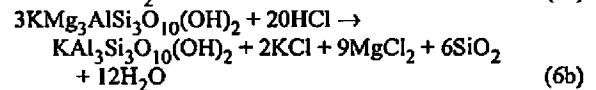
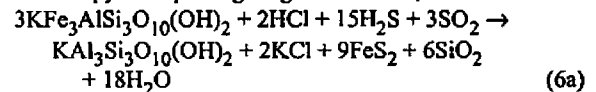
sericite replacing potassium feldspar;



sericite replacing plagioclase,



sericite and pyrite replacing magmatic biotite,



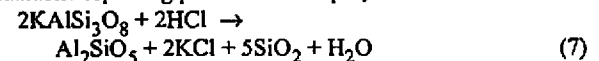
### Andalusite

Andalusite was discovered in the GIC by Penniston-Dorland (1997). The grain size is typically less than 30 microns. Petrographic identification of andalusite is based on the high relief and birefringence and confirmed with energy-dispersive analysis on the electron microprobe.

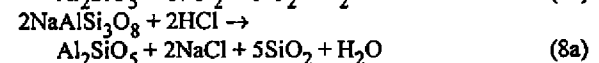
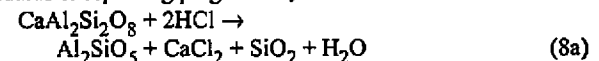
Fig. 8 shows that andalusite is only present in the interior of the GIC. Andalusite was not found in any of the Kali samples. It is spatially associated with magnetite and hydrothermal biotite. No replacement reaction is apparent for andalusite and most appears to be in the groundmass.

It is hypothesised that andalusite is a replacement of potassium feldspar and plagioclase. The idealised reactions are:

andalusite replacing potassium feldspar;



andalusite replacing plagioclase;



Thermodynamic modeling (Paterson, 2004) indicates that andalusite is a high-temperature aluminosilicate alteration product ( $T > 425^\circ\text{C}$ ). The distribution of andalusite indicates the centre of highest-temperature pervasive alteration was located about 250 m to the northwest of the tip of the wedge-shaped Kali intrusion.

### Epidote

Epidote is relatively easy to identify petrographically owing to its pale yellow-green colour and high relief. Fig. 9 shows epidote occurs near the edges of the deposit, in patches that are surrounded by rock altered to sericite and pyrite. Moreover, the occurrences of epidote is also discontinuous at the cm scale of thin sections.

Epidote-bearing samples are associated with chlorite and albite, a common low-temperature (~200 to 300°C) greenschist facies mineral assemblage. The occurrence of epidote delineates portions of the GIC that underwent more of an isochemical thermal metamorphism rather than one of pervasive invasion by chemically destructive acidic fluids.

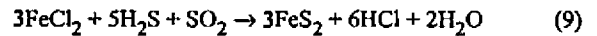
### Pyrite

Pyrite is easily identifiable in hand specimen and reflected light microscopy owing to its pale-yellow colour. It is found with euhedral crystal shapes, but most typically occurs as grain aggregates associated with sericite.

In a limited band, pyrite also occurs (trace to 1%) as overgrowths, intergrowths, or replacements of magnetite (discussed below).

Fig. 10 shows pyrite is disseminated throughout the outer portions of the GIC. It is abundant (5% to 10%) in an annular-shaped region roughly congruent with the greatest abundances of sericite (compare with Fig. 8).

An idealised reaction for the precipitation of pyrite from hydrothermal fluid is:



The precipitation of pyrite requires the presence of reduced sulphur and generates acid.

### Magnetite

Magnetite is readily identifiable in reflected light microscopy owing to its characteristic steel-grey colour. Magnetite does not exhibit a characteristic crystal shape and is only unambiguously identifiable as a member of the magmatic assemblage in the most unaltered portions of the Late Kali (Paterson and Cloos, this volume) where it comprises 1% to 2% of the rock.

There is a fundamental problem of differentiating magmatic magnetite from hydrothermal magnetite. In the portions of the Early Kali, MGI, and Dalam where magnetite veins are common, the abundance of disseminated magnetite is generally 5% to 10% and locally greater.

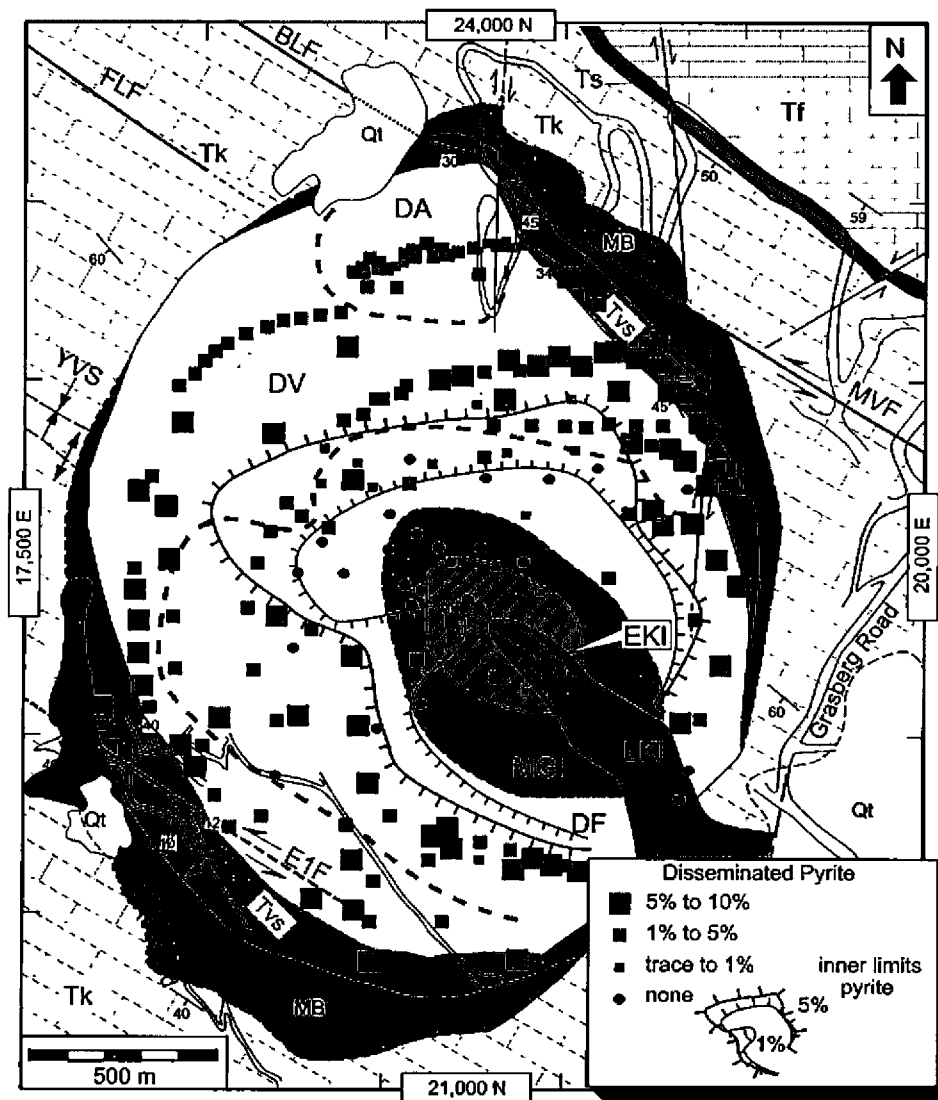


Figure 10: *Distribution and abundance of disseminated pyrite.* Note pyrite is lacking in some samples from the interior of the complex.



Fig. 11 shows disseminated magnetite is abundant in the core of the GIC and has only scattered occurrences in the exterior, where pyrite is abundant. Where abundant, magnetite is intimately associated with hydrothermal biotite. The minor, scattered occurrences in the periphery of the deposit may be relict igneous magnetite. The biotite + magnetite association is locally overprinted by the sericite + anhydrite + pyrite assemblage (discussed below).

An idealised reaction for the precipitation of hydrothermal magnetite from oxidising (high  $\text{Fe}^{+3}/\text{Fe}^{+2}$  ratio) hydrothermal fluid are:



The precipitation of magnetite causes fluid to become acidic. As magnetite is abundant in the core of the GIC, the acidity must have increased substantially as fluid moved outwards and upwards.

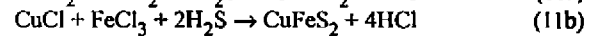
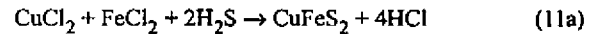
### Chalcopyrite

Chalcopyrite is the dominant ore mineral in the open pit mine. Disseminated chalcopyrite has no distinctive crystal shape and has abundances as great as 3%. Even trace

occurrences of chalcopyrite are readily detectable in thin section because of its distinctive yellow-gold colour.

At the ~3900 m elevation, the highest-grade ore occurs in a zone that is approximately 500 m-long by 400 m-wide. This ore zone contains a stockwork of chalcopyrite veins (marked with a hachured pattern on Fig. 13) that are locally up to 1 to 2 centimetres thick. The limit of disseminated chalcopyrite occurrence is at about 750 m from the centre. Notably, Fig. 12 shows that disseminated chalcopyrite is scarce in the part of the MGI where chalcopyrite veining is most abundant.

Chalcopyrite has a spatial association with both disseminated magnetite and hydrothermal biotite, and was precipitated at higher temperatures than most of the pyrite. Idealised reactions for the precipitation of chalcopyrite from hydrothermal fluid are:



As with the precipitation of magnetite, the precipitation of chalcopyrite increases the acidity of the hydrothermal fluids passing through the rocks.

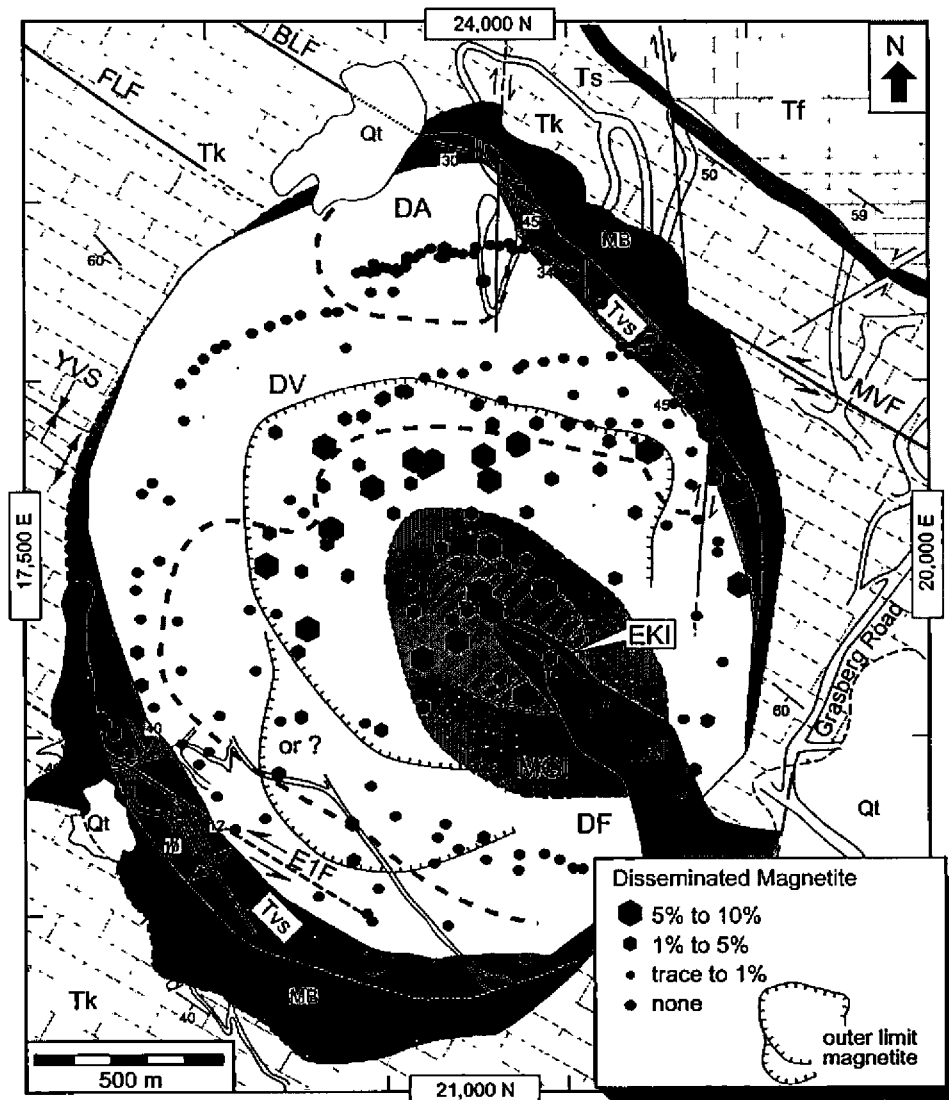


Figure 11: *Distribution and abundance of disseminated magnetite.* Note magnetite is not present in many samples from the exterior of the complex.

**Anhydrite**

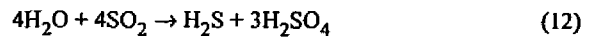
Anhydrite has high solubility in ground water, and hence was readily leached as meteoric water invaded the deposit. Consequently, a lack of anhydrite in thin section is not a basis for inferring an original absence from the rock volume. Where anhydrite is dissolved, porosity is generated and its former presence is commonly indicated by very thin rinds of anhydrite/gypsum along the margins of vuggy pores. Anhydrite is very distinct in thin section owing to its excellent cleavage and very high birefringence. It ranges from very small individual grains (<30 microns) to large poly-crystalline patches, locally comprising up to 10% of the rock volume.

Anhydrite (Fig. 13) and vuggy porosity (Fig. 14) occur in an annular region starting about 500 m from the centre of the GIC. Only trace amounts of anhydrite (<1%) were ever present in the interior where hydrothermal biotite and magnetite dominate. Anhydrite appears to have been most abundant at about 750 m from the centre of the GIC and decreases towards the edges. This relationship is

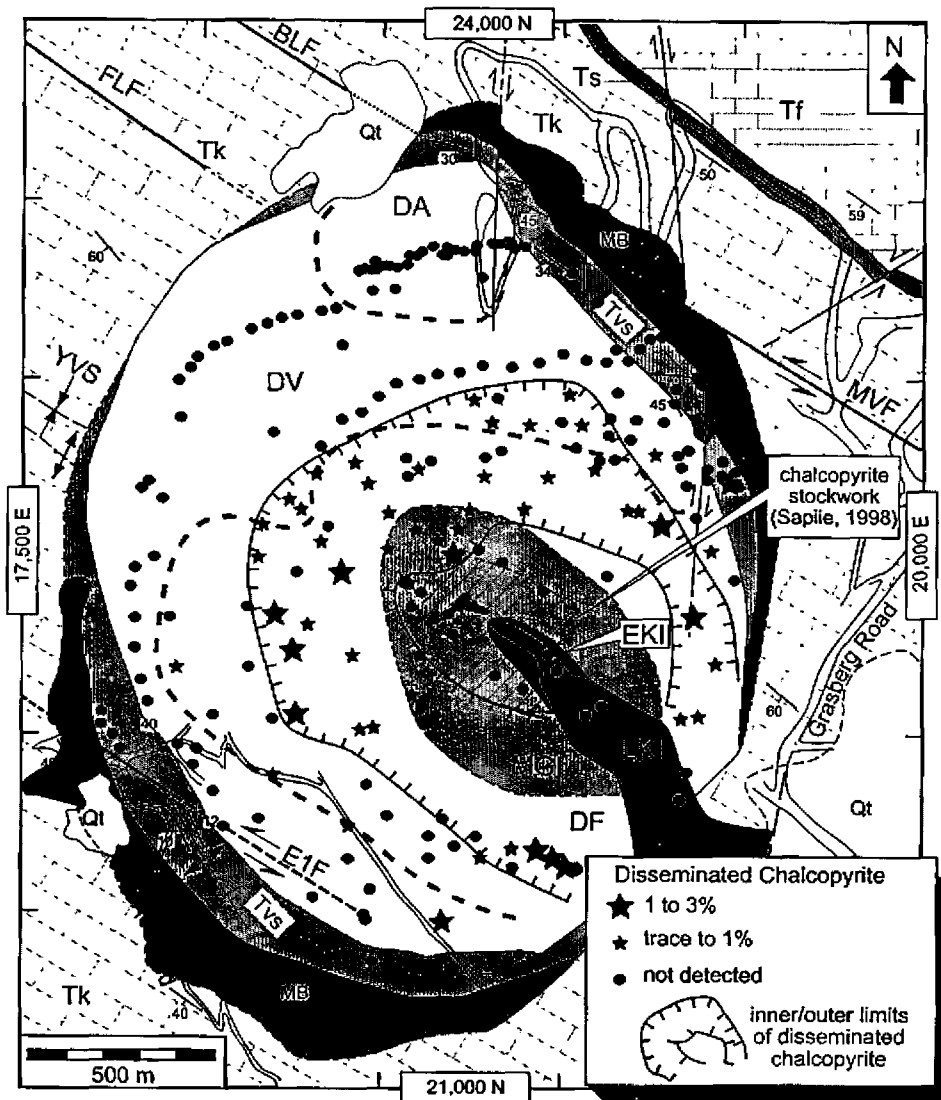
particularly pronounced at depth where it is essentially absent from the edges of the GIC and in the Heavy Sulphide Zone (Lambert, 2000).

A comparison between Fig. 13 and Fig. 14 highlights the variable preservation of anhydrite and the effect of ground water dissolution. Anhydrite/gypsum/vuggy porosity, together with sericite and pyrite, define the outer zone of alteration in the GIC.

The character of sulphur species in solution is of utmost importance in determining the mineralogies of alteration. The near-lack of anhydrite in the interior of the deposit requires explanation. Sulphur dioxide (the dominant sulphur phase in magmatic fluids discharged from erupting volcanoes) undergoes hydrolysis in cooling hydrothermal fluids:



The importance of this reaction was first recognised by Holland (1965) and subsequent studies indicates SO<sub>2</sub> is the dominate sulphur species exsolved from cooling magmas.



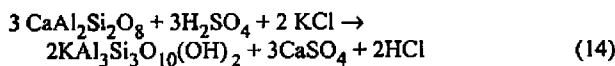
**Figure 12: Distribution and abundance of disseminated chalcopyrite.** Note the chalcopyritic stockwork zone mapped by Sapitje (1998) is denoted by hatched pattern. Disseminated chalcopyrite is sparse or lacking in most samples from the interior of the deposit where abundant chalcopyrite veining makes the rock high-grade ore

Holland and Malinin (1979) concluded that the reaction typically begins at about 600°C and is complete at temperatures of around 400°C. This oxidation/reduction reaction so profoundly changes the chemical behaviour of cooling magmatic fluids that it can cause the precipitation of coexisting sulphide (pyrite, chalcopyrite, bornite) and sulphate (anhydrite) minerals (Burnham and Ohmoto, 1980; Wood, 1998). The solubility of sulphide minerals is very small and cooling brines containing metal chloride complexes will react to precipitate sulphide minerals as fast as the reaction proceeds (Barnes, 1979). This, in turn drives the build-up of  $H_2SO_4$  and the precipitation of anhydrite once saturation concentrations are attained.

The precipitation of anhydrite from solution is dependent upon the concentration of Ca as well as on the activity of sulphate in solution. As evident from pseudomorphic reactions, the Ca content of the outwards flowing fluids increases because Ca is released by the alteration of plagioclase phenocrysts to biotite (reaction 1) in the core of the GIC and to sericite (reaction 4) towards the periphery. Anhydrite is precipitated from solution via the following reaction:



Along the margins of the GIC, anhydrite and sericite replace plagioclase by the reaction:



Blount and Dickson (1969) discovered that anhydrite exhibits the phenomenon of retrograde solubility over a wide range of salinities (Fig. 15). The solubility of

anhydrite is a minimum at approximately 300°C and increases sharply with decreasing temperature (see also Moller, 1988; He and Morse, 1993). Thus, hydrothermal fluids cooling from temperatures higher than the solubility minimum (fluids moving outwards through the deposit) will precipitate anhydrite upon cooling until the temperature of the solubility minimum. From that point onwards, fluids can continue to move outwards and/or upwards without precipitating anhydrite. For rocks containing anhydrite, the flow of cooler fluid, or later influx of meteoric waters, will cause dissolution forming porosity.

Thus, first attaining saturation and retrograde solubility are first-order physical explanations for the distribution and abundance of anhydrite in the GIC. Furthermore, this discussion underscores that precipitation of hydrothermal minerals can be attributed to spatial changes in the physical conditions (in this case, primarily temperature), rather than a series of alteration events invoking pulses of different fluid composition in different parts of the deposit.

### XRD Analysis of Powdered Samples

Copper porphyry systems typically have an abundance of minerals with a very fine (<30 microns in this study) grain size (Creasey, 1966) and the GIC is no exception (Fig. 16). Clay-sized minerals are abundant towards the periphery of the deposit and only minor components of the interior. Thirty-eight samples distributed around the deposit and representing all units were chosen for analysis of bulk rock powders by x-ray diffraction analysis (XRD). Clay mineral identifications are based upon criteria in Thorez (1976). Analytical techniques are discussed in Paterson (2004).

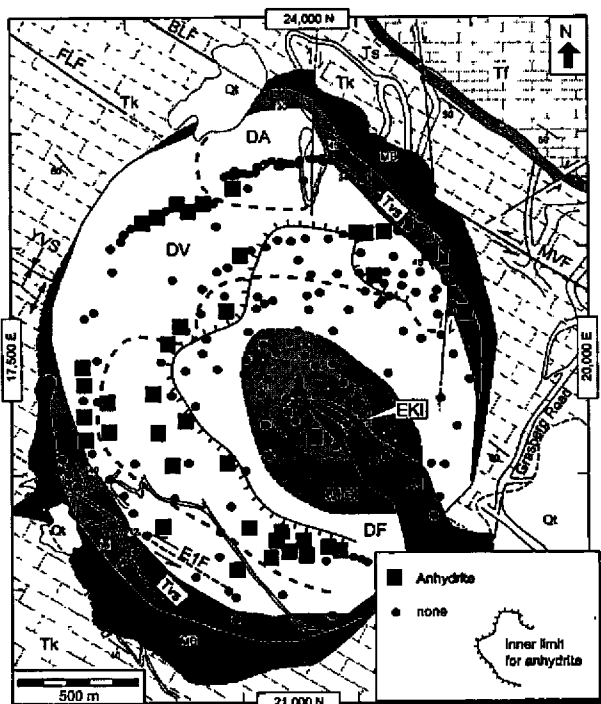


Figure 13: *Distribution of anhydrite.* Anhydrite is lacking in the interior of the Grasberg Igneous Complex because it was never present and has been removed from many samples in the exterior as evident from vuggy porosity.

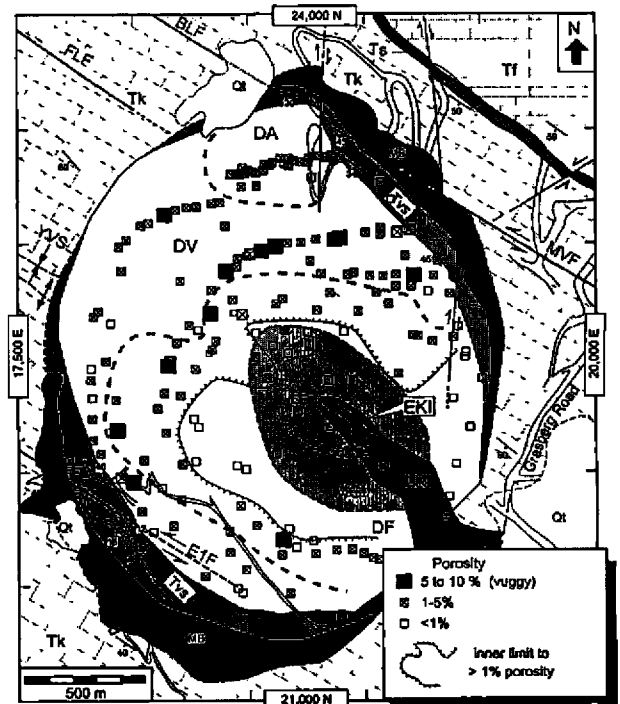
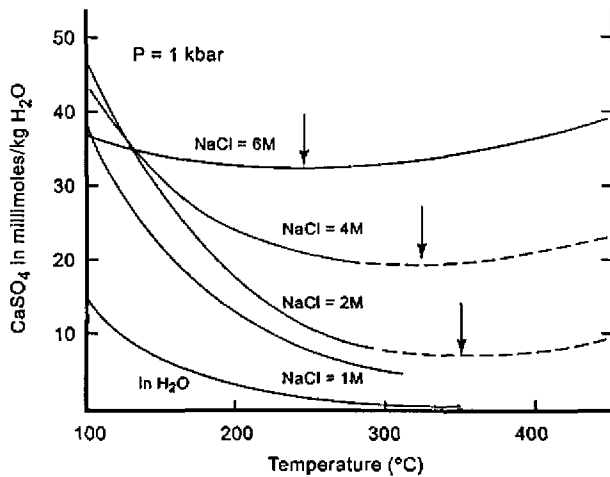


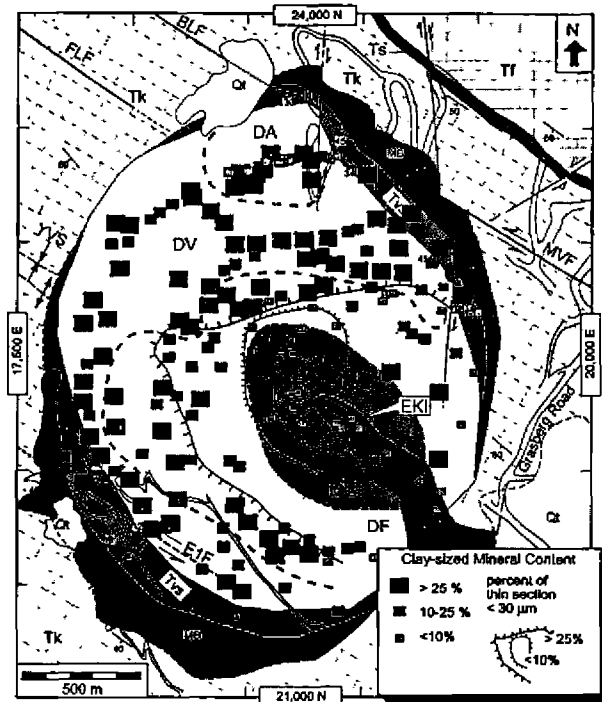
Figure 14: *Porosity variability.* Most of the porosity is probably due to the dissolution of anhydrite. Note the low porosities in the centre and the band of high porosities for samples located about 500 m from the centre of the Grasberg Igneous Complex.



**Figure 15: Solubility of anhydrite in saline fluids.** Note the solubility minimum at about 300° C. From Blount and Dickson (1969).

Fig. 17 shows the location of samples and the clay-sized minerals systematically searched for with XRD. Except for some samples containing epidote, sericite is present in all samples located more than about 500 m from the centre of the GIC. As illite is a mica-like clay mineral that is similar to muscovite/sericite but having less potassium and more water, it is not surprising that illite was detected in almost all XRD patterns.

Most importantly, smectite was not detected in the XRD patterns, indicating that, if present, it occurs in quantities below approximately 5%. This is significant because smectite typifies the argillic zone of copper porphyry systems (Hemley and Jones, 1964; Beane and Titley, 1981; Beane, 1982). Smectite is not entirely absent, however. Sapiie (1998) found that clay dykes which extend into the



**Figure 16: Distribution and abundance of clay-sized minerals.** This is a visual estimate of the percentage of a thin section occupied by minerals <30 microns across.

deposit contain abundant smectite. Using techniques to concentrate clay-sized mineral fractions, Penniston-Dorland (1997) detected small amounts of smectite in alteration halos around pyrite veins. It is clear that smectite is not a significant product of pervasive hydrothermal fluid alteration in the open pit samples included in this study.

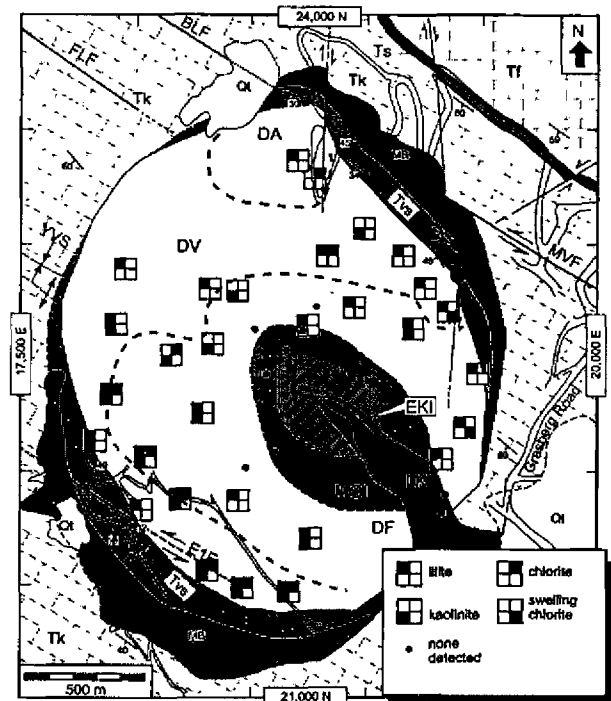
Illite, chlorite, and kaolinite were not detected in the samples from the interior of the GIC. Chlorite was detected in nine samples, mostly in the southwest part of the GIC. Swelling chlorite was detected in two samples from near the northeast margin. Kaolinite was detected in 14 samples and is most abundant near the margins of the deposit. Most samples that contain kaolinite also contain illite (11 of 15 samples), but only about half of the samples that contain illite also contain kaolinite (11 of 23 samples).

### Overprinting Hydrothermal Replacements

Direct evidence for the thermal and chemical evolution of the GIC comes from the observation of hydrothermal minerals that are themselves replaced by other hydrothermal minerals. The most common is sericite replacement of biotite. Another distinctive relationship is chlorite replacement of biotite. Pyrite is found to overgrow or replace magnetite in many samples.

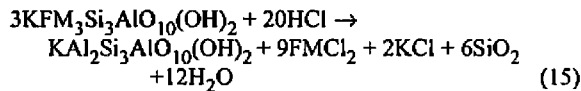
#### Sericite Replacing Hydrothermal Biotite

The petrographic observation of sericite replacing hydrothermal biotite is distinctive but volumetrically minor with replacement of never more than about 1% by volume



**Figure 17: Diagram showing samples selected for x-ray diffraction analysis of bulk powders to detect the presence of illite, kaolinite, smectite, and chlorite.** Note that the samples from the interior lack these minerals. Swelling chlorite was detected in two samples. Smectite was not detected in any sample, but is probably present in trace amounts.

of the biotite present. The spatial distribution of sericite replacing biotite (Fig. 18) defines an annular region about 500 m wide that surrounds the core of the deposit. A critical observation is that sericite always replaces hydrothermal biotite and never the opposite. The idealised replacement reaction is:

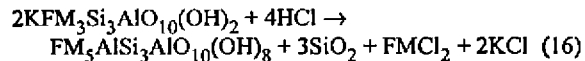


This is an acid-consuming, metal-releasing reaction.

### Chlorite Replacing Biotite

Chlorite (commonly with trace amounts of pyrite) is widely distributed as thin coatings on joint surfaces in most of the GIC (Sapiie, 1988). However, chlorite identifiable in thin section is absent from most of the deposit. Thin rims of chlorite mantle hydrothermal biotite in a zone about 500 x 800 m zone centred about 250 m northwest of the centre of the deposit (Fig. 19).

In these rocks, chlorite is coarse enough to identify petrographically, but too low in abundance to be detected with x-ray diffraction methods. Much like the replacement of hydrothermal biotite by sericite, this alteration never replaces more than about 1% of the volume of biotite. Only the replacement of hydrothermal biotite by chlorite is observed, not the opposite. The idealised chemistry of this replacement is:



The replacement of biotite by chlorite in the interior and sericite in the exterior are both late-stage, acid-consuming,

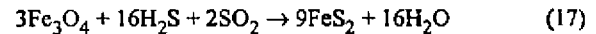
metal-releasing reactions that are unidirectional in their occurrence. They are both manifestations of the final stage of pervasive fluid flow when the hydrothermal system was cooling.

### Pyrite and Magnetite

Pyrite rims, intergrowths, or replacements of magnetite are readily apparent in many thin sections from a horseshoe-shaped region about 200 to 400 m wide, centred about 500 m from the centre of the GIC (Fig. 20). There are scattered occurrences of this phenomenon in samples of the Dalam.

As magnetite occurs in irregular masses, there is no obvious distinction between overgrowths (with a discontinuous growth history), intergrowths (co-existing growth), and replacement by pyrite. However, as sericite is found replacing biotite in most of the same thin sections, it seems certain that some, if not most, of these masses are pyrite replacements of magnetite.

An idealised chemistry for the replacement of magnetite by pyrite is:



In contrast to the acid-consuming reactions previously identified, this reaction requires a high activity of reduced sulphur to proceed. The abundance of magnetite in the core of the deposit and pyrite in the exterior indicates that hydrogen sulphide only became abundant as the infiltrating fluids moved outwards, consistent with the concept that cooling and hydrolysis of  $\text{SO}_2$ -rich fluids caused sulphide mineral and anhydrite precipitation.

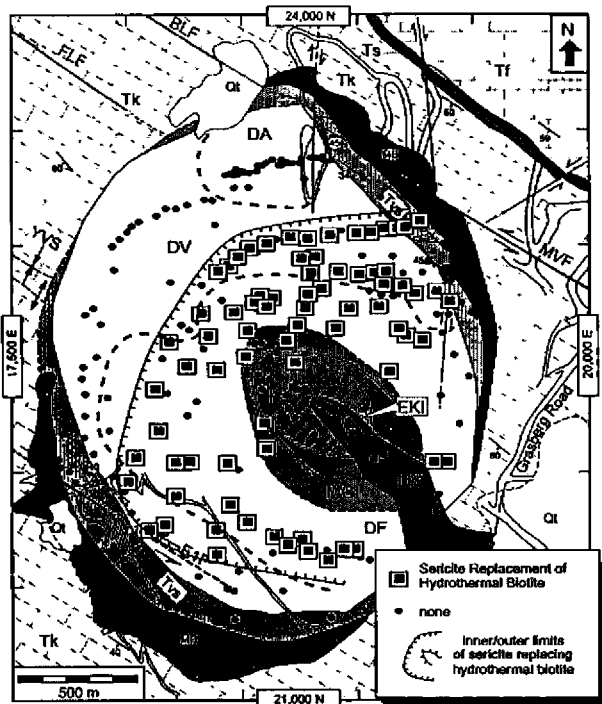


Figure 18: *Distribution of sericite replacing hydrothermal biotite.* In most samples in the interior of the deposits, only trace amounts of sericite are present.

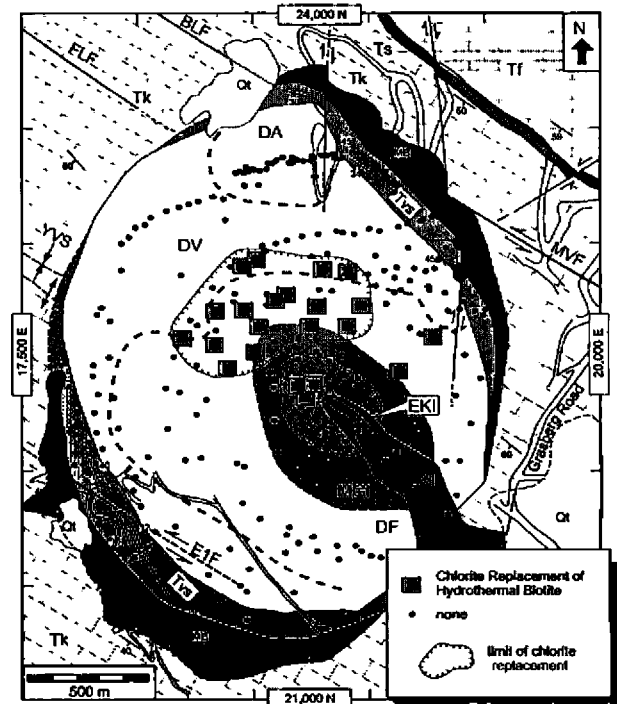


Figure 19: *Distribution of chlorite replacement of hydrothermal biotite.* This replacement typically only occurs in trace amounts.

### Trace Heavy Metal Phases

Reflected light petrography of 225 samples combined with microprobe x-ray mapping of the groundmass in 18 samples revealed remarkably little evidence for opaque phases other than magnetite, pyrite and chalcopyrite. Enargite, an arsenic-bearing phase was found in one sample (00-MC-37) and a few grains of Zn-bearing sulphide were noted in another (00-MC-03). Heavy-metal-bearing trace phases containing Pb, Zn, As, Hg, etc., are widely noted in other copper porphyry deposits; their scarcity in the GIC requires an explanation and is discussed below.

### Alteration Zones

The Grasberg copper-gold orebody displays mineral alteration zoning that is overall very similar to that reported in other copper porphyry systems. In this study, alteration zones in the Grasberg are named in terms of the major mineral assemblages, as is common practice in characterising metamorphic terranes. The lateral mineralogic zonation is summarised in Fig. 21. Fig. 22 is

a summary map which shows that the limits to alteration zones form roughly concentric rings within the Dalam and MGI, centred on the core of the GIC.

#### *Biotite + Magnetite Zone ≈ Potassic Alteration*

“Potassic” alteration dominates the interior portions of many porphyry copper deposits. In most classifications, the requisite assemblage is potassium feldspar + biotite (Lowell and Guilbert, 1970; Titley, 1982). This mineralogic criteria becomes problematic when applied to potassic magmatic rocks. McMahon (1994a, b, c) placed all of the igneous rocks in the GIC into a high-K suite. Potassium feldspar is abundant in the magmatic groundmass of the Kali (Paterson and Cloos, this volume). Thus the presence of potassium feldspar in the GIC is not, by itself, diagnostic of alteration. The same problem applies to magnetite, which is only confirmed as a magmatic phase in Kali phase intrusions, but probably was present in other units as well. The centre of the GIC hydrothermal system also produced andalusite, a mineral not widely reported in most similar deposits.

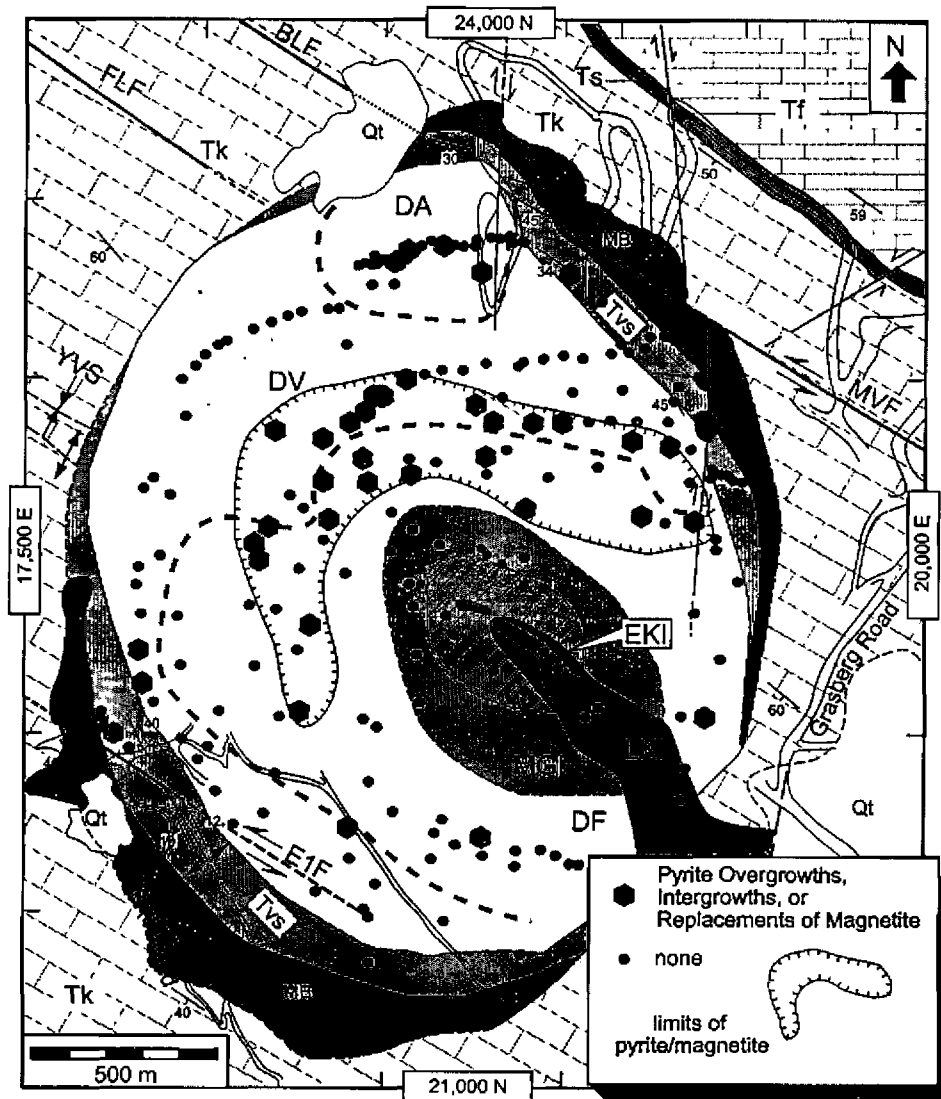


Figure 20: *Distribution of pyrite overgrowths, intergrowths or replacements of magnetite. Where present, pyrite is present on the exterior of the magnetite grains.*

Shreddy biotite is the only diagnostic alteration mineral in the high temperature interior of the deposit. Disseminated magnetite is so abundant and intimately intergrown with shreddy biotite that it also must be an alteration product. That fluids precipitated magnetite, is directly evident from the abundant veins of quartz + magnetite in the core of the deposit, and the less common, but widely occurring magnetite-only veins. Outside of the Kali phase intrusions, the association of hydrothermal biotite with magnetite comprises as much as 60% of the innermost Dalam (DF) and MGI. In the GIC, the mineral assemblage biotite + magnetite with an inner sub-zone containing andalusite is the equivalent of the potassic zone. Fluid infiltration and alteration in the core of the GIC was pervasive to the finest scales of observation.

#### Sericite + Anhydrite + Pyrite Zone ≈ Phyllic Alteration

“Phyllic” alteration comprises large areas in the outer part of many porphyry copper deposits. The requisite assemblage is sericite + quartz + pyrite (Lowell and Guilbert, 1970; Tittley, 1982). In the GIC, quartz is not diagnostic of conditions as it is ubiquitous. Moreover, in much of this deposit, it is clear that sericite and pyrite are intimately associated with anhydrite (compare Fig. 13 [anhydrite] and Fig. 14 [porosity] with Fig. 7 [sericite] and Fig. 10 [pyrite]). In the GIC, the mineral assemblage sericite + anhydrite + pyrite is the equivalent of the phyllic zone.

The degree of alteration in the sericite + anhydrite + pyrite zone is variable. About 500 m from the centre of the deposit, it is locally so intense that all evidence of the original igneous mineralogy is destroyed (Fig. 2). This style of alteration is locally weak or absent in the outer part of the GIC indicating fluid infiltration was not as pervasive as in the interior near the fluid source.

#### Alteration Zone Overlap/Overprint Phyllic

A phyllic overprinting of the potassic zone is reported in almost all copper porphyry deposits (Beane, 1982), while in some, there is a near total overprint of the potassic zone by the phyllic alteration. Examples include the Superior District, Arizona (Manske and Paul, 2002), and Island Copper Porphyry, British Columbia (Arancibia and Clark 1996).

Gustafson and Hunt (1975) proposed that the original alteration assemblage at El Salvador, Chile, graded outwards from potassic directly into propylitic alteration. Only upon the later invasion of meteoric water into the deposit did phyllic alteration overprint the potassic zone. A persistent concept has been the notion that phyllic alteration is the product of the invasion of meteoric water into the system (Taylor, 1974). However, increasing evidence indicates the contrary, that phyllic alteration fluids are magmatically derived (Hedenquist *et al.*, 1998; Richards *et al.*, 1998). Harris and Golding (2002) reported oxygen and hydrogen isotope compositions of vein quartz from the Endeavour 26N Cu-Au porphyry in Australia, and compared their results to published data from El Salvador, Chile, Panguna and Porgera, Papua New Guinea, and Far Southeast, Philippines. They concluded that magmatic fluids caused phyllic-type alteration in all of these deposits.

Fig. 23 shows that there is a 150 to 300 m wide, horseshoe-shaped zone where the sericite + pyrite + anhydrite zone overlaps the biotite + magnetite zone. Some overlap of these zones is expected because the transition from one to the other should not be abrupt because both solid and fluid solutions are involved. Two mapped textural relationships are clear recorders of replacement: i) sericite and pyrite replacing biotite (Fig. 18; reaction 6), and ii) pyrite

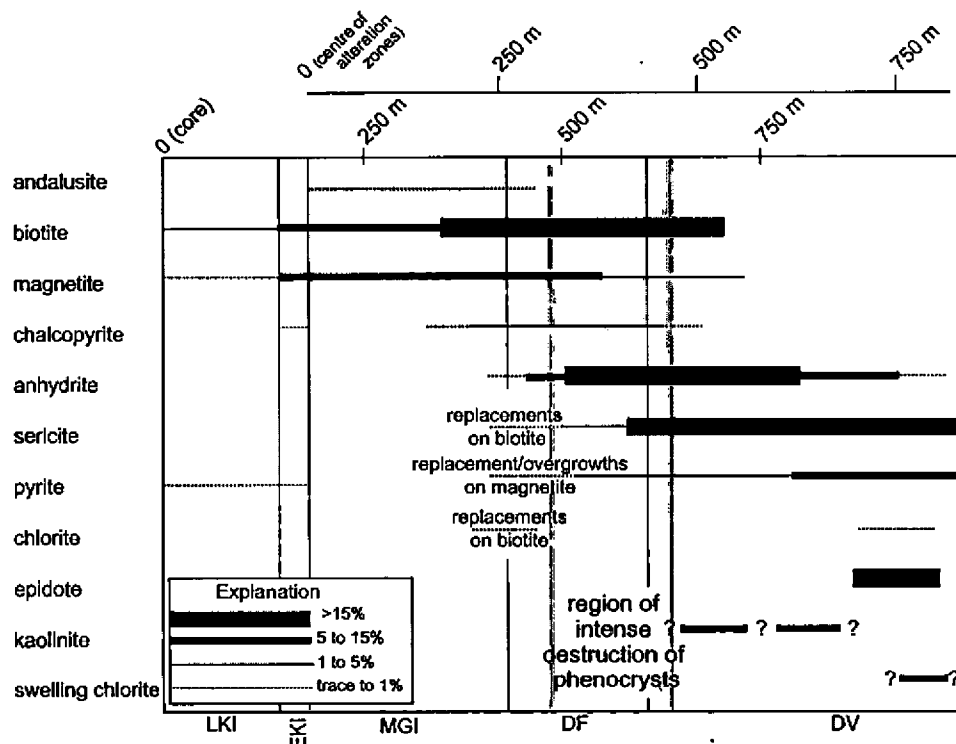


Figure 21: Schematic pattern of mineral replacements due to pervasive alteration.

replacing magnetite (Fig. 20; reaction 17). Samples containing pyrite that is probably replacing magnetite show a similar pattern.

Cooling of chlorine-rich, SO<sub>2</sub>-bearing magmatic fluid will cause an increase in the activity of acid and hydrogen sulphide that would drive these replacements. Consequently, cooling of the system because heat advection into it was lessened by the slowing of hydrothermal fluid flow will cause a mineralogic overprint near the boundary between the two zones of alteration. It is notable that no petrographic evidence (biotite + magnetite replacing sericite + anhydrite + pyrite) was found for an increase in temperature and flow rate.

The temperature of the fluid is the primary control on the mineral assemblage that develops, although it is the volume of flow that determines the extent of reaction. The minor

extent of alteration overprint in the GIC indicates hydrothermal flow rates must have decreased dramatically once substantial cooling of the system had begun. The simplest explanation for the observed overprinting relationships is that the outflow of magmatic fluids did not slowly wane, but instead ended rather abruptly.

**Epidote ± Chlorite Zone ≈ Propylitic Zone**

Epidote is confined to the periphery of the GIC where it replaces plagioclase. In the samples that contain(ed) abundant biotite or amphibole, chlorite is abundant. At the deposit scale, epidote ± chlorite alteration occurs in patches forming islands surrounded by sericite + anhydrite + pyrite alteration (Fig. 9). Some thin sections that contain epidote ± chlorite, have sericite and pyrite in the groundmass. However, no direct evidence of the replacement of epidote ± chlorite by the sericite and pyrite assemblage was found.

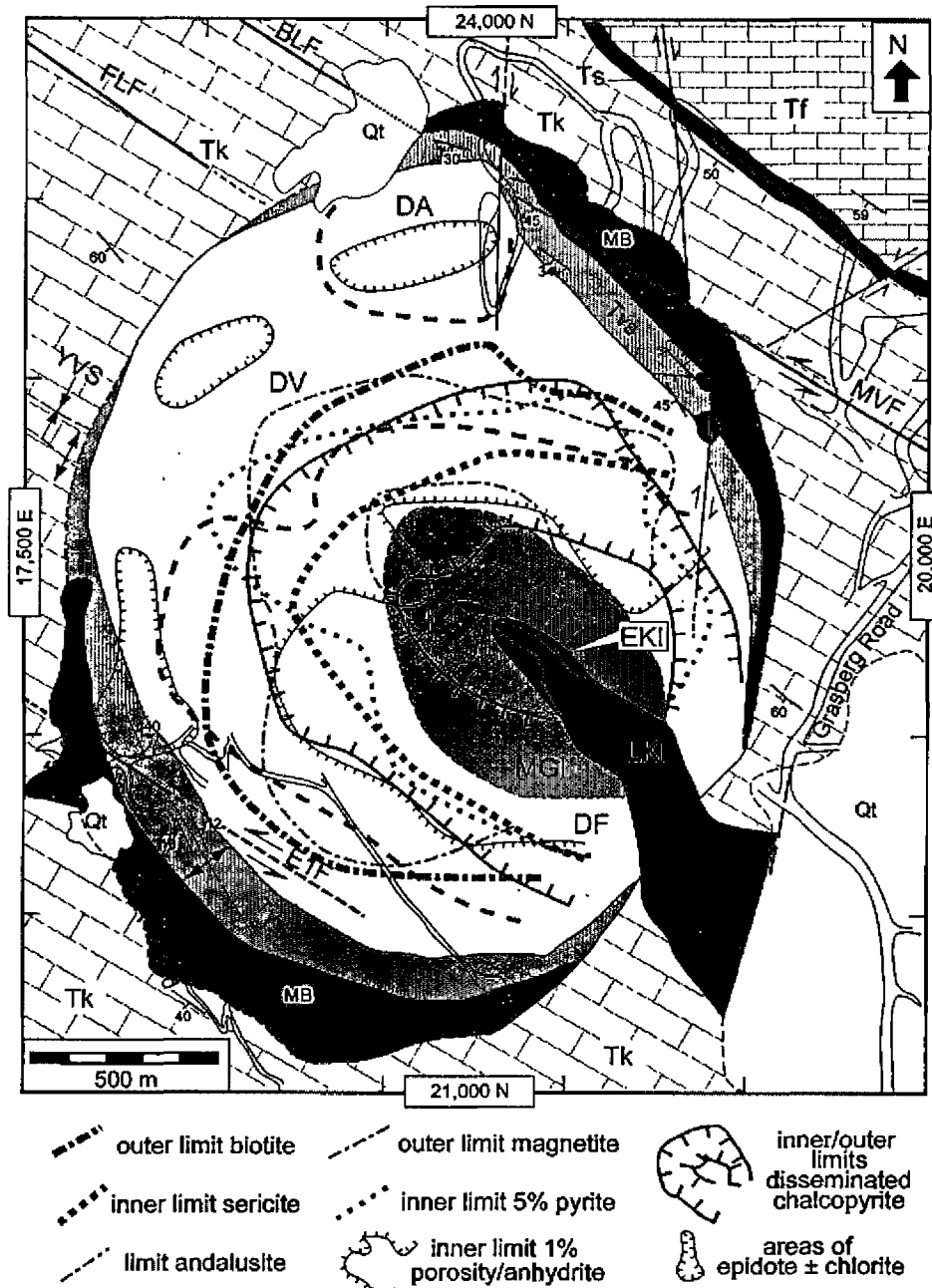


Figure 22: Spatial limits of pervasive alteration zones.



Epidote, chlorite and albite are products of near-isochemical metamorphism under greenschist facies conditions (~300°C) (Beane, 1982; Berger and Velde, 1992). The islands of epidote ± chlorite along the edges of the GIC are regions where the igneous rock was kept at elevated temperatures for a prolonged period without the invasion of acidic hydrothermal fluids. This indicates the hydrothermal flow causing alteration was less pervasive along the edges of the deposit.

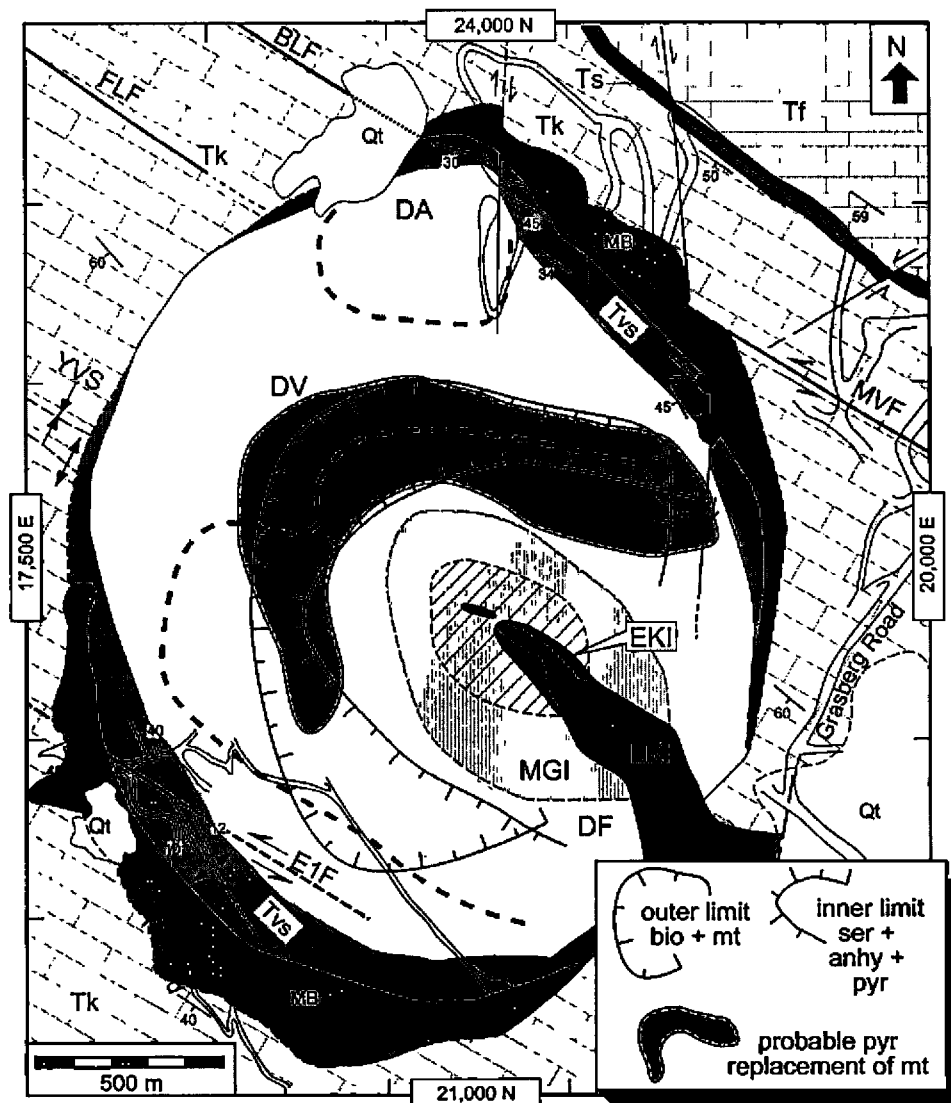
#### ***Kaolinite Occurrence ≈ Argillic Alteration***

The simplest criteria for argillic alteration is the presence of abundant clay minerals, commonly smectite or kaolinite (Creasey, 1966). Advanced argillic alteration (higher temperature) is characterised as abundant quartz in association with kaolinite, pyrophyllite and alunite (Reed, 1997). The formation of clays from feldspars involves the leaching of alkalis at low (<200°C) temperatures. In some deposits, the mapping of the extent of argillic alteration has proven problematic. Recently, Williams and Forrester (1995, p. 26) stated that "the so-called argillic zone is virtually a myth because detailed work on clays from

'magmatic argillic zones' invariably demonstrates the clay to be sericite."

The XRD analyses in this investigation of bulk rock powders revealed small amounts of kaolinite in many samples. Most notably, smectite was not detected in any of the bulk powders. Penniston-Dorland (1997) performed clay-size separations and analysed the clay fraction of several samples, finding kaolinite along with trace amounts of smectite in the alteration halos that border some of the pyrite ± quartz veins. Sapiie (1998) reported that smectite is the major component of clay dykes, that were a volumetrically minor, but common, feature in the Grasberg open pit prior to 1996 (locations higher than about 3700 m elevation). If the presence of smectite is considered essential to document argillic alteration, the GIC has no systematically developed argillic zone.

Using the presence of kaolinite as the criterion, "argillic" alteration is widely developed in the GIC, but of trivial volume. Kaolinite should form from feldspars wherever cool (<200°C), acidic fluid is present. Hence, the minor development of kaolinite is another indicator that cooling



**Figure 23:** *Region where sericite + anhydrite + pyrite alteration overlaps biotite + magnetite alteration. Area where pyrite overlaps magnetite is shaded. Note the horseshoe-shaped regions of mineralogic overlap at the ~3900 m elevation of the open pit mine.*

of the deposit to ambient thermal gradients was not concurrent with the flow of substantial volumes of hydrothermal fluid.

### *Scarcity of Heavy Metal Phases*

Grasberg ore has very low contents of elements such as Pb, Zn, As and Hg (MacDonald and Arnold, 1994). There are two explanations for their scarcity: i) the initial concentration of these species in the mineralising fluids was lower than other systems, and/or, ii) final cooling of the system to ambient thermal gradients was not concurrent with substantial fluid flow.

The solubilities of Pb, Zn, As, Hg and many other trace metals increase exponentially with increasing temperature (Barnes, 1979; Wood and Samson, 1998). For common abundances in magmatic fluids, these metals typically do not form phases at temperatures of 300°C or higher. Sphalerite and galena are present in scattered veins and pods outside the Grasberg. Several examples outcrop along the HEAT road (Sapiie, 1998). Small amounts of sphalerite and galena are present along the outer edges of the cylindrical body of massive pyrite (the "Heavy Sulphide Zone") at the 3045 m elevation of the Kucing Liar and Amole Drifts (Lambert, 2000). Larger pods are present at the surface in the marginal breccias (Fig. 2, northeast corner of the GIC, Sapiie, 1998). The deposition of Pb and Zn at these locations is not surprising, as the fluids reaching the edges of the deposit would have been at temperatures much less than 300°C. The key observation is that Grasberg system fluids did contain Pb and Zn in sufficient quantities to form scattered deposits of base metals.

More diagnostically, Ulrich *et al.*, (1999) analysed a few fluid inclusions from a Grasberg sample and found that their concentrations of zinc and lead significantly exceeded that found in the bulk ore. From this observation and their detailed study of inclusions from the Bajo de La Alumbrera deposit (see Ulrich and Heinrich, 2001), they concluded that: "very large quantities of ore metals are flushed through ore deposits, and ultimately become dispersed unless steep thermal and chemical gradients provide a driving force for efficient mineral precipitation" (p. 678).

The trace-metal contents of Grasberg system fluids may have been lower than other systems, but there is no reason to believe these fluids had exceptionally low trace-metal contents compared to other deposits. The conclusion is that Zn, Pb, As, Hg and other trace metals flushed through the system as large volumes of Cu and Au were precipitating. The scarcity of trace metals is yet another indicator that cooling of the deposit to ambient thermal gradients was not concurrent with the flow of substantial volumes of hydrothermal fluid.

## **Discussion**

Petrography combined with x-ray diffraction analysis shows that the pervasive fluid flow that affected the Dalam and MGI phases of intrusion at the ~3900 m elevation generated mineral assemblages that define several roughly circular alteration zones (Fig. 22). The Late Kali phase postdates essentially all pervasive fluid flow, whereas the Early Kali phase, which is veined and locally altered, but

much less so than the MGI, postdates all but the final stage of pervasive fluid flow.

Biotite + magnetite alteration, with an inner sub-zone containing andalusite affected the MGI and the innermost Dalam whereas sericite + anhydrite + pyrite alteration dominates alteration in the exterior of the deposit. The widespread, but minor occurrence of kaolinite and the local replacement of biotite by chlorite are products of the cooling of the Grasberg system to ambient thermal gradients. The "islands" of epidote ± chlorite near the edges of the GIC delineate areas where thermal metamorphism occurred, but thoroughly pervasive fluid infiltration did not. The chemistry of the hydrothermal mineral-forming reactions can be divided into two groups: i) an inner zone dominated by biotite + magnetite that is hot and acid generating, and ii) an outer zone of sericite + anhydrite + pyrite that is cooler and acid-consuming.

### *Acid Production and Consumption – The Chemistry of Fluid Flow*

Intense acid attack is a long-known and widely described characteristic of hydrothermal alteration in the phyllic zone of copper porphyry systems (Guilbert and Park, 1985). Beane and Bodnar (1995) conclude that fluids in all copper systems increase in acidity as they move from the potassic to phyllic to argillic zones. Acid production in the inner part and consumption in the outer part explains the overall pattern of alteration in the GIC as well.

Significant acid production in the core of the deposit would have resulted from the high-temperature precipitation of abundant magnetite (reaction 10). At slightly lower temperatures, the precipitation of chalcopyrite (reaction 11) added to the acidity of the fluid. Associated silicate alteration reactions, producing hydrothermal biotite in the interior of the deposit, were also acid-producing (reactions 1, 2, and 3). It is most likely that the magmatic fluids altering the core of the GIC only become acidic (by forming HCl which dissociates into H<sup>+</sup> and Cl<sup>-</sup> complexes) after magnetite precipitation begins.

Temperature variations in the Grasberg hydrothermal system are broadly constrained. The fluids are magmatic and would have been exsolved at temperatures of 800 to 1000°C. The best direct petrologic indicator of the highest temperature conditions during pervasive infiltration comes from the presence of andalusite in a zone approximately 500 m across centred on the core of the deposit (Fig. 9). Andalusite, however only indicates temperatures were greater than 425°C (Paterson, 2004). Fluid-inclusion homogenisation temperatures for quartz from the stockwork zone indicate temperatures in the centre of the GIC were actually much hotter, 600°C and higher (Harrison 1999). Maximum temperatures in the marginal breccias that outcrop at the surface were mostly less than 200°C (Sapiie, 1998). Halloysite, which has an upper thermal stability of 110°C, is present in the banded clay unit that outcrops on the southwest and northeast edges of the deposit.

Magmatic fluids can incorporate large amounts of sulphur as SO<sub>2</sub>. The precipitation of sulphide minerals and anhydrite can only begin after SO<sub>2</sub> in the fluid begins to

hydrolyse (reaction 12). As discussed in the section on anhydrite, the production of  $H_2S$  and  $H_2SO_4$  occurs across the temperature range from about 600 to 400°C (Holland and Malinin, 1979). The local concentration of sulphide and sulphate species in the fluid reflects the primary  $SO_2$  content, the thermal gradient along the flow path, and the solubilities of sulphide and sulphate mineral species.

The scarcity of disseminated sulphide minerals in the core of the GIC, where biotite + magnetite alteration is extensive, is explainable as the infiltrating fluids were too hot to hydrolyse  $SO_2$ . Upon cooling to about 600°C, the first reduced sulphur is generated. Chalcopyrite precipitation begins and continues until the fluids became depleted in copper at temperatures of about 400°C. Pyrite precipitation begins where temperatures have cooled to about 450°C. Pyrite mineralisation continues to the edge of the deposit, in part because iron is steadily released by the replacement of mafic phases by sericite (reaction 6). Reduced sulphur would have been steadily removed from the fluid by the growth and precipitation of chalcopyrite and pyrite. In contrast, the sulphate content of the fluid would have steadily increased until the point where anhydrite precipitation begins (Fig. 25).

The replacement of plagioclase by biotite (reaction 1) and sericite (reaction 5) liberates Ca to the fluids (reaction 1). Consequently, the calcium ion content in the migrating fluids must have steadily increased as the fluids migrated outwards. Disseminated anhydrite is essentially absent in the core of the open pit mine (Figs. 13 and 14) and it is thus evident that anhydrite saturation did not occur until the temperatures decreased to about 450°C. Once this occurred, the alteration assemblage became sericite + anhydrite + pyrite. Where temperatures were less than about 300°C, retrograde solubility prevented further precipitation of anhydrite.

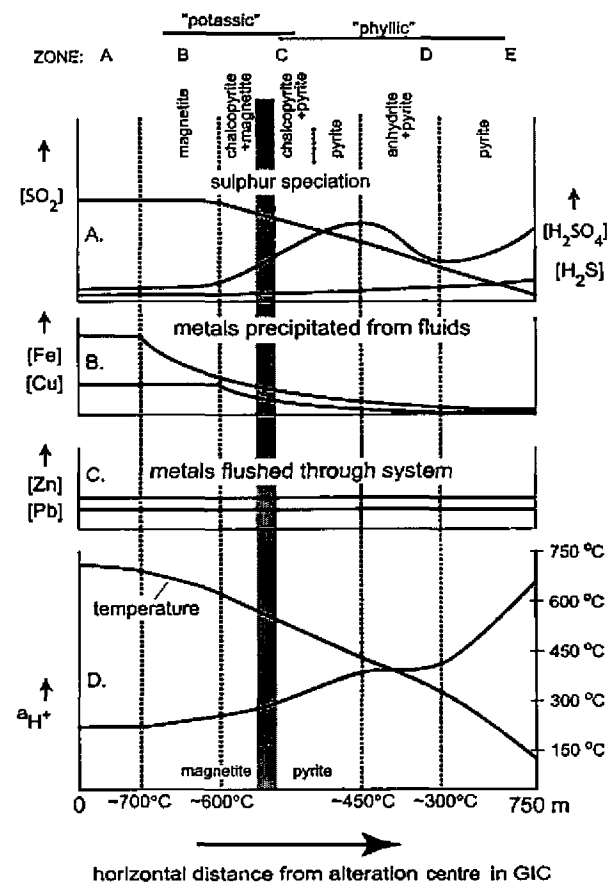
The chemical evolution of the fluids migrating outwards from the core of the system can be summarised as a sequence of zones (Fig. 24). Zone A (not exposed) is primary, near-neutral magmatic fluid at 800°C or so that is little modified by interaction with cooler rock. Zone B is where magnetite precipitation occurs, thereby beginning the increase in the acidity of the fluid. Temperatures were probably about 700°C when magnetite precipitation begins. Zone C begins where temperatures of about 600°C were attained, and the hydrolysis of  $SO_2$  produces  $H_2SO_4$  and  $H_2S$ . While the concentration of  $H_2SO_4$  increases with further cooling, the concentration of  $H_2S$  remains low because chalcopyrite (bomite at depth) and then pyrite precipitate about as fast as  $H_2S$  is produced in solution. The precipitation of abundant pyrite generates substantial HCl that along with the build-up of  $H_2SO_4$  causes attack of the wall rock. Zone D, beginning at temperatures of about 450°C, is where  $H_2SO_4$  reacts with  $CaCl_2$  (abundant Ca was released from the replacement of plagioclase) to precipitate anhydrite. Acid attack of the host rock, locally so strong that all magmatic textures are destroyed, was strongest in the inner part of zone D. Zone E, at temperatures of about 300°C, is where anhydrite precipitation lessens because of the retrograde solubility

of anhydrite. From this point to the edge of the GIC, the concentration of  $H_2SO_4$  in the fluid increases. Alteration is more heterogeneous in the other part of the GIC because the fluid pressure gradients driving the flow are small. When the highly acidic fluids reached the edges of the GIC, they were neutralised by dissolution of carbonate wall rock which formed the extensive zone of marginal breccias (Figs. 2 and 3).

#### *Continuity of Alteration and Copper Mineralisation*

MacDonald and Arnold (1994) previously stated that pervasive hydrothermal alteration in the Dalam was the most laterally and vertically extensive. As they believed the MGI was less altered, they concluded that substantial alteration predated the MGI. This study concludes that there is a continuity of pervasive alteration from the MGI to Dalam phase rocks. Alteration in the MGI appears less intense because the host rocks were still very hot when infiltrated by near-neutral fluids at near-magmatic temperatures. In other words, most of the fluids infiltrating the MGI were nearly in equilibrium with the igneous rock.

The apparently greater intensity of Dalam alteration versus the MGI is primarily due to increased acidity and lower temperatures of the fluids as they moved outwards. Another likely factor is that Dalam phase rocks probably had a



**Figure 24:** *Interpreted evolution of chemistry of fluids causing pervasive alteration.*

- A. Sulphur speciation.
- B. Fe and Cu concentrations.
- C. Zn and Pb concentrations.
- D. Temperature and acidity ( $a_{H^+}$ ).

glassy, highly reactive groundmass. The MGI, which solidified more slowly, was fully crystalline and thus somewhat less reactive.

Most of the copper mineralisation in the Dalam is disseminated while that in the MGI is in veins. Much of the high-grade MGI ore in the core of the deposit contains a stockwork of chalcopyrite veins that are millimetres to centimetres across (limits identified on Fig. 2). This difference in the dominant style of copper mineralisation was interpreted by MacDonald and Arnold (1994) to indicate two distinct phases of mineralisation. Instead, we believe the difference is explainable by differences in the chemical behaviour of fluids flowing in fractures versus those infiltrating the rock. Precipitation of minerals in veins is primarily controlled by fluid chemistry and solubility relationships (fluid-buffered reactions). Growth of disseminated minerals because of pervasive fluid infiltration is primarily controlled by the chemistry of the host rock and the fluid which had exchanged with rock it has previously flowed through (rock-buffered reactions).

No petrographic evidence was detected for a pervasive alteration event that only affected the Dalam phase rocks, but admittedly, the alteration and copper mineralisation event that affected the MGI and Dalam is so intense that an earlier mild event may have been obliterated.

#### *Interpreted History of Intrusion and Mineralisation*

The interpreted history of intrusion, pervasive hydrothermal alteration and mineralisation in the Grasberg is as follows. i) Emplacement of the Dalam phase rocks. ii) Intrusion of MGI as a plug into the still-hot core of the Dalam. iii) Intense fracturing in the MGI core of the system, first forming a stockwork of quartz + magnetite veins (Stage 1a), and then chalcopyrite veins (Stage 1b). This stockwork-forming event in the core of the system was concurrent with the massive outflow of fluid that caused disseminated copper mineralisation. Pervasive infiltration formed a concentric mineralogic zonation in which andalusite + biotite + magnetite and then biotite + magnetite was surrounded by sericite + anhydrite + pyrite. Islands of epidote ± chlorite are the result of isochemical thermal metamorphism and indicate fluid flow was not thoroughly pervasive in the outermost parts of the GIC. iv) Emplacement of the Kali phase intrusions. The LKI postdates essentially all pervasive alteration and most veining. The EKI was intruded very near the end of alteration/mineralisation. Stage 2 veining is a comparatively minor event that began after Kali phase intrusion. These fluids were Cu-poor, but also so Al-rich that many veins of biotite were formed.

#### *Final Cooling Without Substantial Fluid Flow*

The overprint of the cooler sericite + anhydrite + pyrite zone on the hotter biotite + magnetite zone is of limited width and of very minor intensity. This observation, along with the trivial generation of sericite near the core of the deposit and kaolinite across the deposit, as well as the scarcity of trace metal phases, all indicate the fluid flow system forming the Grasberg did not slowly wane, but rather shutdown abruptly. Cooling of the core of the Grasberg

system to temperatures of less than 300°C or so, was not concurrent with significant fluid flow.

It appears that the system cooled to near ambient before emplacement of the Kali phase intrusion, but this is uncertain. Ongoing studies on samples of Kali phase intrusions from the Amole Drift level should enable better understanding of how the EKI relates to alteration and mineralisation.

#### *Centre and Size of the Fluid Source*

The centre of the pervasive flow system was near the tip of the wedge-shaped Kali intrusion. Pervasive alteration to biotite + magnetite affected an area about 1200 m across. The inner sub-zone containing andalusite is about 500 m across. Intense quartz/magnetite stockwork veining (Stage 1a) and superimposed chalcopyrite veining (Stage 1b) define a slightly smaller area. As discharging fluid would disperse outward, 500 m is a maximum width for the source of the fluid feeding the system.

Notably, the centre of the alteration as defined by andalusite (Fig. 8), abundant clay-sized minerals (Fig. 16), and chlorite replacing biotite (Fig. 19), are located about 250 m to the northwest. It thus appears that the centre of hydrothermal alteration migrated slightly northwest over time, but this may be an illusion based upon sample distribution.

#### *Reconstruction of the Mineralising System*

The fact is, pervasive alteration and veining in the GIC delineates a series of rings that indicates rock-altering fluids emanated from a small source area. Consistent with the picture of Cloos and Sapiie (in review) and Sapiie and Cloos (in press) and the magmatic history deduced in this study (Paterson and Cloos, this volume), the underlying fluid source was the apex of a cupola at the top of an intrusive stock (Fig. 25). If the stockwork veining delineates regions where the roof episodically collapsed over a fluid-charged cupola, a width of 200 to 300 m is indicated. The ceiling of the cupola probably first became fluid charged at an elevation of about 3200 to 3400 m, at a depth below the surface of less than 1000 m. As the system cooled, the cupola would have migrated downwards over time. The pervasive fluid infiltration that formed the concentric alteration zones was driven outwards by a difference in fluid pressure from lithostatic near the cupola to hydrostatic near the surface. Pervasive fluid flow was continuous in space and time and caused steady draining of the cupola that was continuously recharged from below (Cloos, 2001). Superimposed on this "background" flow, causing pervasive alteration, were tectonically-induced extension fracturing events that episodically drained much, if not all, of the accumulated fluid. Fracturing and the upwards jetting of magmatic fluids formed veins with mineralogies that varied because of changes in fluid pressure, temperature, and fluid composition along the flow path (Cloos and Sapiie, in review).

It is evident that lateral thermal gradients in the Grasberg system were very high, on the order of 500°C/km. The near-surface vertical thermal gradient was probably even greater. Extreme thermal gradients and low confining

pressures were important factors that localised precipitation of copper and gold. Fluids at near magmatic temperatures have been detected discharging at the bottom of lakes filling calderas (Giggenbach, 1992), and it seems likely that a bubbling lake in a maar caldera was once atop the Grasberg system (Fig. 25). The banded clay deposits on the southern and northern edges of the GIC are relicts of a field of boiling mud pots. The preservation of the evidence for the extreme lateral thermal gradients indicates that the flow system was probably only active for several tens of thousands of years.

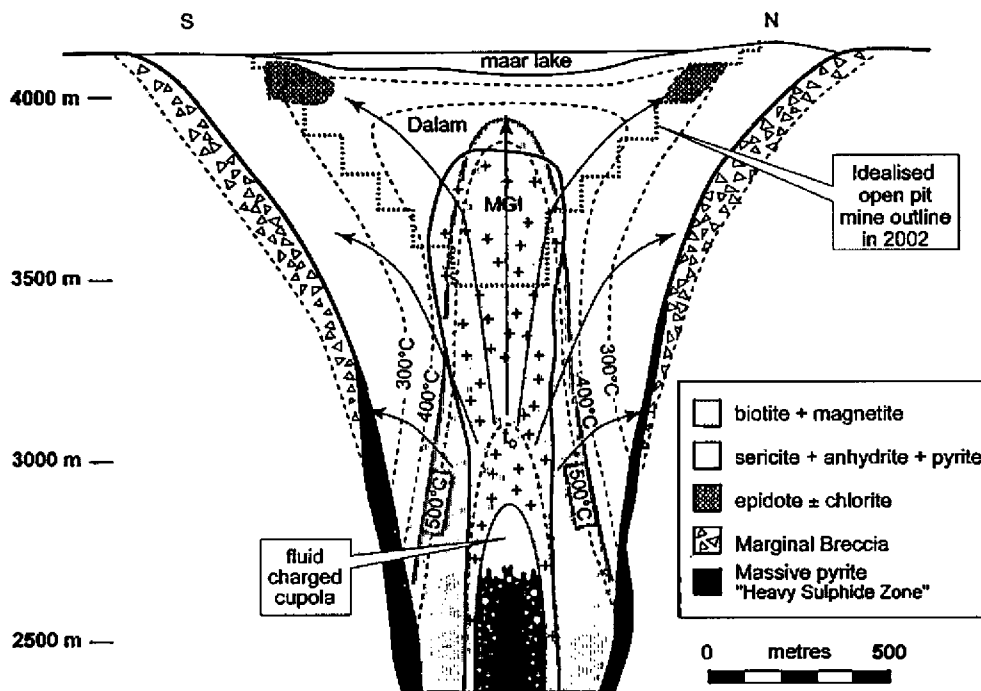
## Conclusions

This study documents that pervasive fluid flow in the Grasberg Igneous Complex generated a hydrothermal mineralogy and pattern similar to that in many copper porphyry systems. New to the study of the GIC are the following observations:

- i) Andalusite occurs in a ~500 m wide zone in the centre of the GIC.
- ii) The replacement of magmatic minerals by later hydrothermal minerals is recorded by phenocryst replacement relationships, and idealised reaction relationships can be identified for all common replacements.
- iii) Anhydrite is almost absent in the core of the deposit, and most abundant in a band about 500 m from the centre. The inner and outer limits to anhydrite occurrence were determined by the hydrolysis of  $\text{SO}_2$  in the fluids and the retrograde solubility of anhydrite.
- iv) Epidote  $\pm$  chlorite, representing nearly isochemical thermal metamorphism, is confined to discontinuous regions (tens to hundreds of metres across) that are

- v) Smectite is not detectable in bulk powders in the GIC, and kaolinite is only present as a minor constituent indicating the flow of acidic fluids at low temperatures was very limited.
- vi) X-ray mapping of 18 samples indicated that heavy metal (Pb, Zn, As, Hg) phases are very scarce. These metals, almost certainly present in significant quantities, were steadily flushed through the system.
- vii) Lateral thermal gradients were on the order of  $500^\circ\text{C}/\text{km}$ . Vertical thermal gradients in the centre of the system were probably even greater. Extreme thermal gradients and low confining pressures combined to localise precipitation of copper and gold.
- viii) Alteration is explicable by a model of acid production/consumption in which magnetite precipitation in the core of the GIC generated abundant acid that caused phyllic alteration in the periphery.
- ix) The limited overprint of the sericite + anhydrite + pyrite zone on the biotite + magnetite zone, minor development of kaolinite, and scarcity of trace metal phases, all indicate the hydrothermal system did not slowly wane, but instead shut down rather abruptly.

The Grasberg Cu-Au deposit is petrologically anomalous only in regard to grade and tonnage. The pervasive alteration (and vein) mineralogy of the Grasberg system is relatively simple compared to other copper porphyry systems because overprinting relationships are minor. The deviations from idealised models of porphyry copper deposits include the presence of andalusite in the core, the scarcity of smectite, and the minor overprint of the sericite + anhydrite + pyrite zone upon the biotite + magnetite zone.



**Figure 25:** *Interpretation of the Grasberg hydrothermal system.* Magmatism in a maar-caldera. Pervasive hydrothermal alteration and ore mineralisation caused by the infiltration of magmatic fluids that emanate from the top of a fluid-charged cupola. When the system was active, the maar lake was a field of boiling halloysite clay mud pots.

The exceptional grade and tonnage of the Grasberg Cu-Au orebody is most likely accountable by a large steady flow up the centre of the system combined with extreme thermal gradients that focused the precipitation of copper and gold. The abrupt shutdown of the hydrothermal flow system indicates something profound occurred at depth. Most likely the area of fluid accumulation jumped to a different cupola – a phenomenon leading to the formation of major mineralisation elsewhere in the district.

## Acknowledgements

From logistical to financial support, none of this work would have been possible without a large number of people from Freeport-McMoRan, Inc. and PT Freeport Indonesia: James R. Moffett, Dave Potter, George MacDonald, Wahyu Sunyoto, Sugeng Widodo, Noris Belluz, Keith Parris, Paul Warren, Clyde Leys, Herry Susanto, Chris Christenson, Bambang Irawan, Ben Coutts, Stephen Hughes, Nico Sambur, Aditya Pringgoprawiro, Boedijono, Yahul, and Bambang Antoro. A special thanks goes to Benyamin Sapiie. Ertsgberg Project Contribution No. 24.

## References

- Arancibia, O.N. and Clark, A.H., 1996 - Early magnetite-amphibole-plagioclase alteration-mineralization in the Island Copper Porphyry copper-gold-molybdenum deposit, British Columbia: *Economic Geology*, v. 91, pp. 402-438.
- Barnes, H.L., 1979 - Solubilities of ore minerals: in Barnes, H.L., (Ed.), *Geochemistry of Hydrothermal Ore Deposits: Wiley Interscience*, New York, 798p.
- Beane, R.E., 1982 - Hydrothermal alteration in silicate rocks, southwestern North America: in Titley, S.R., (Ed.), *Advances in Geology of the Porphyry Copper Deposits in Southwestern North America: University of Arizona Press*, Tucson, pp. 117-137.
- Beane, R.E. and Bodnar, R.J., 1995 - Hydrothermal fluids and hydrothermal alteration in porphyry copper deposits: in, Pierce, F.W. and Bolm, J.G., (Eds.), *Porphyry Copper Deposits of the American Cordillera: American Geological Society Digest* v. 20, pp. 83-93.
- Beane, R.E. and Titley, S.R., 1981 - Porphyry copper deposits, part II, hydrothermal alteration and mineralization: *Economic Geology* 75<sup>th</sup> Anniversary Volume, pp. 235-269.
- Berger, G. and Velde, B., 1992 - Chemical parameters controlling the propylitic and argillic alteration process: *European Journal of Mineralogy*, v. 4, pp. 1439-1454.
- Blount, C.W. and Dickson, F.W., 1969 - The solubility of anhydrite (CaSO<sub>4</sub>) in NaCl-H<sub>2</sub>O from 100 to 450°C and 1 to 1000 bars: *Geochimica et Cosmochimica Acta*, v. 33, pp. 227-245.
- Burnham, C.W., 1979 - Magmas and hydrothermal fluids: in Barnes, H.L., (Ed.), *Geochemistry of Hydrothermal Ore Deposits*, 2<sup>nd</sup> ed., *Wiley Interscience*, New York, pp. 71-136.
- Burnham, C.W. and Ohmoto, H., 1980 - Late stage processes of felsic magmatism: in Ishihara, S. and Takenouchi, S., (Eds.), *Granitic Magmatism and Related Mineralization: Society of Mineralogy and Geology of Japan, Special Issue 8*, pp. 1-11.
- Cloos, M., 2001, - Bubbling magma chambers, cupolas, and porphyry copper deposits: *International Geology Review*, v. 43, pp. 285-311.
- Cloos, M. and Sapiie, B., 2005 - Porphyry copper deposits: Strike-slip faulting and throttling cupolas; Geological Society of America Abstracts with Programs, Vol. 37, No. 7, p. 97.
- Creasey, S.C., 1966 - Hydrothermal alteration: in Titley, S.R. and Hicks, C.L., (Eds.), *Geology of the porphyry copper deposits: Southwestern North America: University of Arizona Press*, Tucson, pp. 51-74.
- Dilles, J.H. and Einaudi, M.T., 1992 - Wall-rock alteration and hydrothermal flow paths about the Ann Mason porphyry copper deposit, Nevada-A 6 km vertical reconstruction: *Economic Geology*, v. 87, pp. 1963-2001.
- Giggenbach, W. F., 1992 - Magma degassing and mineral deposition in hydrothermal systems along convergent plate boundaries: *Economic Geology*, v. 87, pp. 1927-1944.
- Guilbert, J.M. and Park, C.F., 1985 - *The Geology of Ore Deposits: W.H. Freeman and Co.*, New York, 985p.
- Gustafson, L.B. and Hunt, J.P., 1975 - The porphyry copper deposit at El Salvador, Chile: *Economic Geology*, v. 70, pp. 875-912.
- Harris, A.C. and Golding, S.D., 2002 - New evidence of magmatic-fluid-related phyllic alteration: Implications for the genesis of porphyry Cu deposits: *Geology*, v. 30, pp. 335-338.
- Harrison, J.S., 1999 - Hydrothermal alteration and fluid evolution of the Grasberg porphyry Cu-Au deposit, Irian Jaya, Indonesia: [M.S. Thesis]: *The University of Texas at Austin*, 205p.
- He, S. and Morse, J.W., 1993 - Prediction of halite, gypsum and anhydrite solubility in natural brines under sub surface conditions: *Computers and Geosciences*, v. 19, pp. 1-22.
- Hedenquist, J.W., Arribas, A. and Reynolds, T.J., 1998 - Evolution of a intrusion-centered hydrothermal system: Far Southeast Lepanto porphyry and epithermal Cu-Au deposits, Philippines: *Economic Geology*, v. 90, pp. 1506-1532.
- Hedenquist, J.W. and Richards, J.P., 1998 - The influence of geochemical techniques on the development of genetic models for porphyry copper deposits: in *Techniques in Hydrothermal Ore Deposits Geology: Reviews in Economic Geology*, v. 10, pp. 235-256.
- Hemley, J.J. and Jones, W.R., 1964 - Chemical aspects of hydrothermal alteration with emphasis on hydrogen metasomatism: *Economic Geology*, v. 59, pp. 538-569.
- Holland, H.D., 1965 - Some applications of thermochemical data to problems of ore deposits, II. Mineral

- assemblages and the composition of ore-forming fluids: *Economic Geology*, v. 60, pp. 1101-1166.
- Holland, H.D. and Malinin, S.D., 1979 - The solubility and occurrence of non-ore minerals: in Barnes, H.L., (Ed.), *Geochemistry of Hydrothermal Ore Deposits*, 2<sup>nd</sup> ed.: *Wiley Interscience*, New York, pp. 461-508.
- Lambert, C.A., 2000 - Subsurface meso-scale structural geology of the Kucing Liar and Amole Drifts and petrology of the Heavy Sulfide Zone, South Grasberg Igneous Complex, Irian Jaya, Indonesia: [M.S. Thesis]: *The University of Texas at Austin*, 253p.
- Lowell, J.D., 1995 - The Richard and Coutright era and why some exploration programs are successful: in Pierce, F.W. and Bolm, J.G., (Eds.), *Porphyry Copper Deposits of the American Cordillera: American Geological Society Digest* v. 20, pp. 3-5.
- Lowell, J.D. and Guilbert, J.M., 1970 - Lateral and vertical alteration-mineralization zoning in porphyry ore deposits: *Economic Geology*, v. 65, pp. 373-408.
- MacDonald, G.D. and Arnold, L.C., 1994 - Geological and geochemical zoning of the Grasberg Igneous Complex, Irian Jaya, Indonesia: *Journal of Geochemical Exploration*, v. 50, pp. 143-178.
- Manske, S.L. and Paul, A.H., 2002 - Geology of a major new porphyry copper center in the Superior (Pioneer) District, Arizona: *Economic Geology*, v. 97, pp. 197-220.
- McMahon, T.P., 1994a - Pliocene intrusions in the Gunung Bijih (Ertsberg) Mining District, Irian Jaya, Indonesia: Petrography and mineral chemistry: *International Geology Reviews*, v. 36, pp. 820-849.
- McMahon, T.P., 1994b - Pliocene intrusions in the Ertsberg (Gunung Bijih) Mining District, Irian Jaya, Indonesia: Petrography, geochemistry and tectonic setting [Ph.D. Dissertation]: *The University of Texas at Austin*, 298p.
- McMahon, T.P., 1994c - Pliocene intrusions in the Gunung Bijih (Ertsberg) Mining District, Irian Jaya, Indonesia: Major- and trace-element chemistry: *International Geology Review*, v. 36, pp. 925-946.
- Moller, N., 1988 - The prediction of mineral solubilities in natural waters: A chemical equilibrium model for the Na-Ca-Cl-SO<sub>4</sub>-H<sub>2</sub>O system, to high temperature and concentration: *Geochimica et Cosmochimica Acta*, v. 52, pp. 821-837.
- Paterson, J. T., 2004 - Magmatic and pervasive hydrothermal mineralogy of the Grasberg porphyry Cu-Au deposit (west New Guinea): [M.S. Thesis]: *The University of Texas at Austin*, 332p.
- Pennington, J. and Kavalieris, I., 1997 - New advances in the understanding of the Grasberg copper-gold porphyry system, Irian Jaya, Indonesia: Pacific Treasure Trove - Copper-Gold Deposits of the Pacific Rim: *Annual Convention and Trade Show of the Prospectors and Developers Association of Canada*, pp. 79-97.
- Penniston-Dorland, S., 1997 - Veins and alteration envelopes in the Grasberg Igneous Complex, Gunung Bijih (Ertsberg) District, Irian Jaya, Indonesia: [M.S. Thesis]: *The University of Texas at Austin*, 402p.
- Penniston-Dorland, S., 2001 - Illumination of vein quartz textures in a porphyry copper ore deposit using scanned cathodoluminescence: Grasberg Igneous Complex, Irian Jaya, Indonesia: *American Mineralogist*, v. 86, pp. 652-666
- Pollard, P.J. and Taylor, R.G., 2002 - Paragenesis of the Grasberg Cu-Au deposit, Irian Jaya, Indonesia: Results from logging section 13: *Mineralium Deposita*, v. 37, pp. 117-136.
- Reed, M.H., 1997 - Hydrothermal alteration and its relationship to ore fluid composition: in Barnes, H.L., (Ed.), *Geochemistry of Hydrothermal Ore Deposits*, 2<sup>nd</sup> ed.: *Wiley Interscience*, New York, 798p.
- Richards, J.P., Ronacher, E. and Johnston, M., 1998 - New mineralization styles at the Porgera gold deposit, Papua New Guinea: *Geological Society of America*, Abstracts with Programs, v. 30, pp. 302.
- Rose, A.W. and Burt, D.W., 1979 - Hydrothermal Alteration: in Barnes, H.L., (Ed.), *Geochemistry of Hydrothermal Ore Deposits*, 2<sup>nd</sup> ed.: *Wiley Interscience*, New York, 798p.
- Rubright, R.D. and Hart, O.J., 1968 - Non-porphyry ores of the Bingham district, Utah: in *Ore Deposits of the United States, 1933-1967*: v.1, pp. 886-908.
- Sales, R.H. and Meyer, C., 1950 - Interpretation of wall-rock alteration at Butte-Montana: *Colorado School of Mines Quarterly*, v. 45, pp. 261-273.
- Sapiie, B., 1988 - Strike-slip faulting, breccia formation and porphyry Cu-Au mineralization in the Gunung Bijih (Ertsberg) Mining District, Irian Jaya, Indonesia: [Ph.D. Dissertation]: *The University of Texas at Austin*, 304p.
- Taylor, H.P., 1974 - The application of oxygen and hydrothermal isotope studies to problems of hydrothermal alteration and ore deposition: *Economic Geology*, v. 69, p. 229-302.
- Thorez, J., 1976 - Practical Identification of Clay Minerals: Belgium, 90p.
- Titley, S.R., 1982 - The style and progress of mineralization and alteration in porphyry copper systems, American southwest: in Titley, S.R., (Ed.), *Advances in Geology of the Porphyry Copper Deposits in Southwestern North America: University of Arizona Press*, Tucson, pp. 117-137.
- Ulrich, T., Guenther, D. and Heinrich, C.A., 1999 - Gold concentrations of magmatic brines and the metal budget of porphyry copper deposits: *Nature (London)*, v. 399, pp. 676-679.
- Ulrich, T. and Heinrich, C.A., 2001 - Geology and alteration geochemistry of the porphyry Cu-Au deposit at Bajo de la Alumbrera, Argentina: *Economic Geology*, v. 96, pp. 1719-1742.
- Van Nort, S.D., Atwood, G.W., Collinson, T.B., Flint, D.C. and Potter, D.R., 1991 - Geology and mineralization of the Grasberg copper-gold deposit: *Mining Engineering*, v. 43, pp. 300-303.

- Williams, S.A. and Forrester, J.D., 1995 - Characteristics of porphyry copper deposits: *in* Pierce, F.W., and Bolm, J.G., (Eds.), Porphyry Copper Deposits of the American Cordillera: *American Geological Society Digest* v. 20, pp. 21-34.
- Wood, S.A., 1998 - Calculation of activity-activity and log  $fO_2$ -pH diagrams: *in* Techniques in Hydrothermal Ore Deposits Geology: *Reviews in Economic Geology*, v. 10, pp. 81-96.
- Wood, S.A. and Samson, I.M., 1998 - Solubility of ore minerals and complexation of ore metals in hydrothermal solutions: *in* Techniques in Hydrothermal Ore Deposits Geology: *Reviews in Economic Geology*, v. 10, pp. 33-80.
- Yavuz, F. and Oztas, T., 1997 - BIOTERM-A program for evaluating and plotting microprobe analyses of biotite from barren and mineralized magmatic suites: *Computers and Geosciences*, v. 23, pp. 897-907.





## PORPHYRY-STYLE MINERALISATION IN THE ERTSBERG DIORITE, GUNUNG BIJIH (ERTSBERG/GRASBERG) DISTRICT, WEST PAPUA, INDONESIA

<sup>1</sup>Kurt C. Frieauf, <sup>2</sup>Spencer R. Titley, and <sup>2</sup>Stacie L. Gibbins

<sup>1</sup>*Dept. of Physical Sciences, Kutztown University, Kutztown PA USA*

<sup>2</sup>*Dept. of Geosciences, University of Arizona, Tucson AZ USA*

**Abstract** - Newly-recognised porphyry-style mineralisation within the Ertzberg intrusion displays significant differences from porphyry mineralisation at the Grasberg porphyry Cu-Au deposit. Stockwork mineralisation in the Ertzberg occurs near the giant East Ertzberg Skarn System, close to the northern margin of the intrusion. Stockwork mineralisation in the diorite is spatially associated with 5-15 m wide, E-striking, dykes of porphyritic hornblende monzonite that cut equigranular Ertzberg diorite. The porphyry dykes strike parallel to major district structures and occur where those structures project into the Ertzberg intrusion. Hornblende abundance greater than biotite, the much greater content of sphene, a paucity of broken phenocrysts, and the aplitic groundmass distinguish the porphyry dykes in the Ertzberg Stockwork Zone from the finer-grained groundmass Kali dykes of the Grasberg deposit.

Hydrothermal alteration in the Ertzberg Stockwork Zone proceeded through three main stages with little repetition: i) early feldspar-stable alteration, ii) transitional stage characterised by green sericite veins and endoskarn development, and iii) a late stage quartz-sericite-pyrite alteration. Feldspar-stable mineralisation pre-dates the Ertzberg porphyry dykes, but feldspar-destructive alteration post-dates the porphyry. Although economically-important, early, hairline bornite veinlets and zones of pervasive shreddy biotite alteration of mafic minerals cut equigranular diorite, but not adjacent porphyry, while garnet-bearing endoskarn and sericitic alteration types both cut the porphyry dykes, suggesting the dykes intruded during mineralisation. Transitional stage bornite-chalcopyrite and chalcopyrite-pyrite-green sericite veinlets which are important contributors to both copper and gold grades, have magnetite-bearing halos where they cut endoskarn, and quartz-green sericite selvages in diorite. Late-stage veins contribute little to no grade, contain quartz-sericite-pyrite ±chalcopyrite filling and have white sericite selvages.

Compared with rocks from the nearby Grasberg orebody, the Ertzberg porphyry deposit has a coarser grained groundmass in the porphyritic phases, a much weaker development of hydrolytic alteration styles, an absence of very high sulphidation state mineralisation / advanced argillic alteration, and an absence of breccias in igneous rocks, suggesting the physiochemical conditions of mineralisation for the two deposits differed significantly.

The calcic nature of the endoskarn veins, their spatial relationship with regional structures and the porphyry dykes, and their coincidence with a change in mineralisation style from feldspar-stable to feldspar-destructive hydrolytic assemblages suggests porphyry dyke and endoskarn formation correspond to a major shift in mineralising conditions in the Ertzberg Stockwork Zone.

### Introduction

The Gunung Bijih mining district is well known for the giant Grasberg porphyry deposit (MacDonald and Arnold, 1994; McMahon, 1994 a, b; Harrison, 1999; Penniston-Dorland, 1997, 2001; Pollard and Taylor, 2002) and associated copper-gold skarn deposits (Widodo *et al.*, 1998, 1999; New *et al.*, 1999; Gibbins, 2000; Gibbins *et al.*, 2000). The large Ertzberg diorite pluton, located approximately 1.5 km to the southeast of the Grasberg deposit, is known primarily for several large Cu-Au skarn deposits, including the original Ertzberg orebody, Dom (Mertig *et al.*, 1994;

Mertig, 1995), Big Gossan (Meinert *et al.*, 1997; Prendergast, 2002), and the East Ertzberg Skarn System (EESS), which includes the GBT, IOZ, DOZ, and MLZ skarn deposits (Rubin and Kyle, 1997, 1998; Coutts *et al.*, 1999, Clarke, 2002 - Fig. 1). The total reserve and resource estimates for the Ertzberg skarns alone are over 450 Mt (P.T. Freeport Indonesia, 2003 - Table 1).

Exploration within diorite along the northern margins of the Ertzberg pluton near the EESS, identified a body of

**Table 1: Summary of Production and Reserve Data**

Source: P.T. Freeport Indonesia (Ertsberg only, Grasberg not included)  
**Aggregate Proved & Probable Reserves, Dec. 31, 2002**

	Million Tonnes	Copper (%)	Gold ppm	Silver ppm
Mill Level Zone (MLZ)	50	1.40	1.04	4.88
Deep Ore Zone (DOZ)	184	0.96	0.65	5.11
Intermediate Ore Zone (IOZ)	2	1.14	0.15	9.45
Ertsberg Stockwork Zone	121	0.54	0.90	1.64
Big Gossan	33	2.81	1.00	16.85
Dom	71	1.37	0.36	7.33
<b>Total Reserves</b>	<b>461</b>	<b>1.09</b>	<b>0.74</b>	<b>5.38</b>

#### Aggregate Geologic Resources, Dec. 31, 2002

	Million Tonnes	Copper (%)	Gold ppm	Silver ppm
Mill Level Zone (MLZ)	139	0.58	0.65	3.30
Deep Ore Zone (DOZ)	58	0.48	0.53	2.29
Intermediate Ore Zone (IOZ)				
Gunung Bijih (GB)	3	1.67	0.47	7.87
Ertsberg Stockwork Zone	122	0.44	0.58	1.22
Big Gossan	14	1.72	0.90	11.28
Dom	21	1.11	0.29	10.01
<b>Total Geological Resources</b>	<b>357</b>	<b>0.60</b>	<b>0.59</b>	<b>3.17</b>

#### Total Reserves & Resources

Million Tonnes	Copper (%)	Gold ppm	Silver ppm
<b>818</b>	<b>0.88</b>	<b>0.67</b>	<b>4.41</b>

stockwork-type ore roughly centred on the access ramps to the EESS skarn deposits (Pennington, 1993). The disseminated ore in the Ertsberg diorite, called the Ertsberg Stockwork Zone deposit, is part of a classic porphyry copper system that is quite distinct from the Grasberg porphyry deposit both spatially, temporally, and geologically. As of December 2002, the Ertsberg Stockwork Zone contains 121 Mt of proven and probable ore reserves averaging over 1% copper equivalent with a high Au:Cu ratio (>1.5) plus an additional 122 Mt resource with similar copper, but lower gold grades (P.T. Freeport Indonesia, 2003). This paper reports on our studies of this mineralised zone based on underground mapping, examination of drill core, and petrographic analysis during the period 1999-2002.

### District setting

Intermediate composition magmas began intruding the tightly-folded Mesozoic and Cenozoic strata in the Ertsberg mining district - the siliciclastic Kembelangan Group and Tertiary New Guinea Carbonate Group - at roughly 4 Ma, peaking between 3.2 and 2.6 Ma (McDowell *et al.*, 1996).

Major district faults and the axial planés of folds in the sedimentary rocks strike 110°, with fold limbs typically dipping between 50° and 80° to the north and south. Although reverse faults dominate the 110° set, Sapie and Cloos (1995) report evidence of significant strike-slip

offsets. Porphyry dykes intruded the 110° fault set and zones of mineralisation follow this trend.

Although not mapped within the intrusions of the district, zones of poor drill core recovery and leaching of anhydrite-filled veins in the Ertsberg diorite roughly align with the large 110° fault set, suggesting at least minor post-intrusive movement. A second set of generally northeast-oriented left-lateral strike-slip faults offset the 110° faults. In contrast to the 110° fault set, the NE-striking faults only locally affected skarn formation (Glover, 2001) and do not appear to direct dyke emplacement.

### Rock Types

#### Equigranular Diorite Phases

Two main phases of equigranular diorite occur within the Ertsberg pluton: the main clinopyroxene-dominant- and a biotite-clinopyroxene-diorite (Table 2).

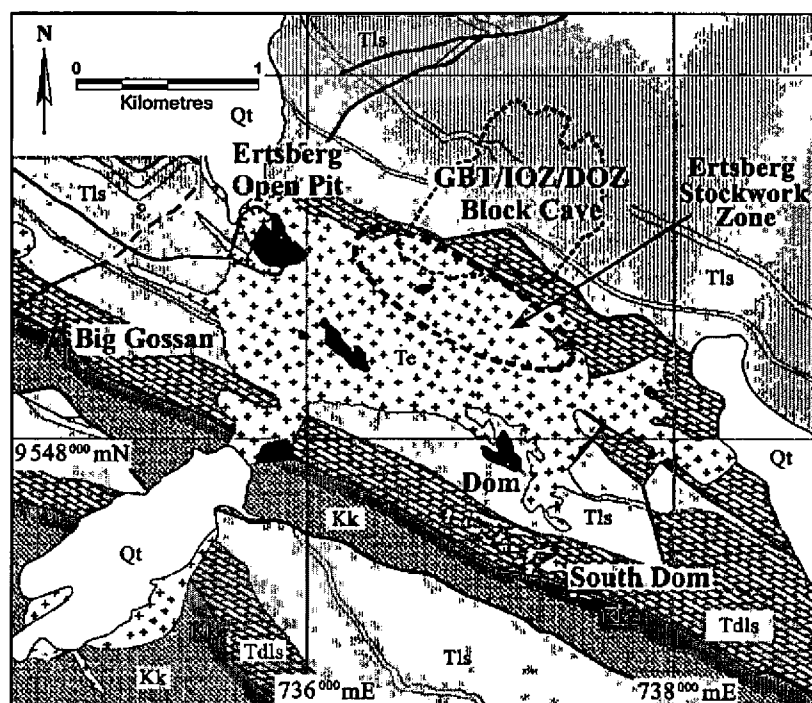
Most of the Ertsberg pluton consists of the "Main Diorite," a quartz monzodiorite that contains 13-18% 2-6 mm clinopyroxene and < 1% biotite set in a sea of plagioclase that commonly exhibits flow foliation (Fig. 2). The Main Diorite constitutes most of the Ertsberg intrusion and is relatively homogeneous.

The biotite-clinopyroxene diorite, hereafter referred to as the Biotite-CPX Diorite, occurs as a large body of uncertain dimensions within the Main Diorite and contains only 10-13% mafic minerals, with 1-4 mm biotite and clinopyroxene in approximately equal proportions (Fig. 2). Clinopyroxene locally exceeds biotite abundance and develops a sieve-like texture in some biotite-rich samples. In contrast to the Main Diorite, the Biotite-CPX Diorite lacks magmatic foliation. Contacts between Main Diorite and Biotite-CPX Diorite are generally sharp, occurring over a 0-5 cm transition zone.

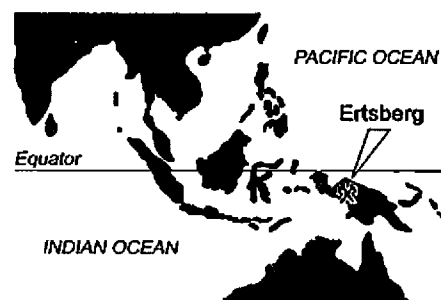
Titanite, magnetite, and zircon occur as common accessory minerals in both equigranular phases. Titanite commonly clusters near mafic sites, suggesting some titanite may have formed as a by-product of propylitic alteration of mafic minerals. Widespread partial alteration of clinopyroxene to actinolite is common throughout the entire pluton.

#### Porphyry Dykes

Porphyry-style mineralisation in the Ertsberg pluton is spatially associated with 5-15 metre wide, east-striking dykes of porphyritic quartz-monzonite that cut both the Main Diorite and the Biotite-CPX Diorite (Fig. 3). Three types of porphyritic dykes have been mapped to date in underground exposures, namely: two "porphyry" phases with sugary, aplitic groundmass, and one porphyritic diorite dyke with an aphanitic groundmass. Several variants of porphyry dykes also occur in the southern part of the Ertsberg intrusion near the Dom deposit. The porphyry most closely related spatially and temporally to mineralisation contains phenocrysts of 40% 1.5-3 mm plagioclase, 3-5% 1-3 mm hornblende, and 1% 1.5 mm biotite set in a sugary, aplitic groundmass (Fig. 2). Although titanite also occurs in the equigranular Ertsberg phases, titanite is conspicuous in the porphyry dykes in hand specimen due to the fine-grained nature of the groundmass.



**Figure 1: Geologic map of the Ertsberg pluton and adjacent sedimentary rocks** showing the locations of major skarn deposits and the general location of diorite-hosted Ertsberg Stockwork Zone mineralisation (outlined in dashed line). Skarn outcrops shown in black. Bold lines indicate faults. Qt = glacial till, Te = Tertiary Ertsberg intrusion, Tls = Tertiary limestones, Tdlis = Tertiary dolomitic limestones, Kk = Cretaceous Kembelangan Fm., and Kke = Cretaceous Ekmai sandy limestone.



Geochemically, porphyry rocks plot in the trachyte-trachyandesite field.

Porphyry dykes differ significantly from the equigranular phases of the Ertsberg intrusion in that the porphyry dykes contain hornblende as the dominant mafic mineral rather than clinopyroxene. The occurrence of hornblende rather than clinopyroxene-biotite suggests a temporal change in the water saturation state in the magma.

Most of the porphyry dykes observed by these authors occur within the Ertsberg Stockwork Zone, along-strike with one of the major 110°-striking district faults. As noted above, evidence exists for post-mineral movement along these faults. The majority of offset along the 110° fault set, however, predates intrusion of the Ertsberg pluton. The coincidence of the dykes with these major faults both spatially and in strike orientation suggests either the faults remained active during mineralisation or at least focused stress on the main body of crystallised Ertsberg diorite along their strike, thereby controlling dyke emplacement. No dykes are known to intrude the younger northeast-striking fault set.

### Comparison of Igneous Rocks at Ertsberg & Grasberg

The Kali dykes of the Grasberg Igneous Complex intruded in multiple stages, with some dykes being affected by weak, very late stage alteration and pyrite mineralisation and others clearly post-dating all mineralisation. The Kali dyke samples we studied for this comparison are of part of the earlier set, being sericite-chlorite altered and having disseminated pyrite. The Ertsberg porphyry dykes differ petrographically from the Kali dykes of the Grasberg deposit in several ways. Ertsberg porphyry dykes have hornblende abundance greater than biotite, a much greater abundance of sphene, and a coarser-grained aplitic (sugary) groundmass compared to the Kali dykes samples studied

by these authors (Fig. 4). The Kali samples have approximately equal biotite and hornblende phenocryst populations, a paucity of sphene, abundant broken phenocrysts, and a distinctly finer-grained groundmass. Of all of the Kali dyke samples observed by these authors, none closely resemble the porphyry dykes in the Ertsberg.

The abundance of sphene in the Ertsberg porphyry dykes, though, is also characteristic of the main equigranular Ertsberg diorite phases, suggesting the equigranular phases and the porphyry dykes may be genetically related. The temporal transition from the Main Diorite to Biotite-CPX Diorite to hornblende-biotite porphyries may reflect a progressive saturation of the underlying magma chamber with respect to water that culminated in the hydrothermal event responsible for mineralisation.

### Alteration/Mineralisation

Hydrothermal alteration in the Ertsberg Stockwork Zone appears to be relatively simple compared to many porphyry deposits. Feldspar-stable mineralisation pre-dates intrusion of the Ertsberg porphyry dykes, whereas feldspar-destructive alteration types dominate alteration that post-dates the porphyry intrusions (Table 3). Broadly, alteration and mineralisation proceeded through three stages: i) early feldspar-stable alteration, ii) transitional stage characterised by green sericite veins and endoskarn development, and iii) late stage quartz-sericite-pyrite alteration.

Early magnetite veins associated with actinolite alteration of clinopyroxene and white, albitic alteration of feldspar (Fig. 5) predate all other vein types. These veins contribute no copper or gold to the ore and probably reflect the earliest prograde development of the hydrothermal system that was later overprinted by the mineralising fluids.

Hairline bornite veinlets with selvages of biotitised clinopyroxene and zones of pervasive shreddy biotite

	Phase	Texture	Magmatic minerals			Mafics Align ?	Feldspar phenocrysts	Key recognition features	Shape	
			Ino-silicate %	Size (mm)	Biotite					
					%					Size (mm)
1.	Main CPX- equigranular diorite	equigranular	10	2-3	< 1	2	No	Equigranular, magmatic biotite books rare, slightly more mafic than equigranular biotite-hornblende	Irregular stock	
2.	Biotite = CPX equigranular diorite	equigranular	8	2	4	3	No	Big magmatic biotite books, equigranular	Irregular stock within the CPX-dominant phase	
3a.	Hornblende porphyry diorite	porphyritic	3-5	2-3	0	0	Common	Low mafic content, feldspar phenocryst cleavage glints, sphene	E-striking 10 m thick dykes	
3b.	"Mafic" hornblende diorite porphyry	porphyritic	5-8	2-3	0	0	Common	Mafic variant of 3a	E-striking 10 m thick dykes	
3c.	"White" hornblende diorite porphyry	porphyritic	1-2	2	0	0	No	Mafic-poor variant of 3a	E-striking 10 m thick dykes	
4.	Fine-grained porphyritic biotite diorite	porphyritic	0	0	3-5	2	No	Finer grain size, darker mafic groundmass, conspicuous biotite phenocrysts	1 m dyke of uncertain orientation	

After Fricke and Soebari, 1999

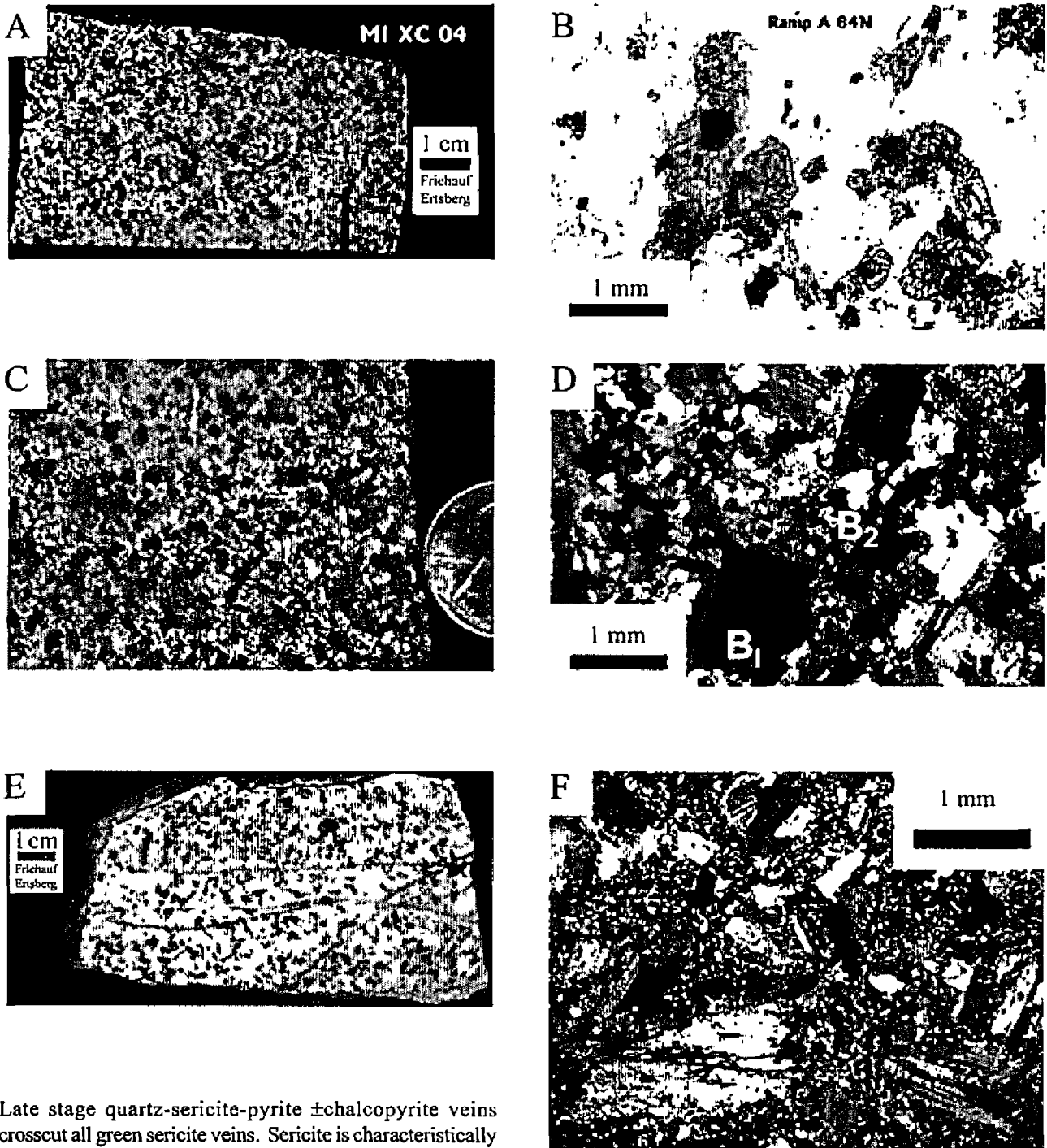
Table 2: Ertzberg Diorite Phases

alteration of mafic sites cut and offset early magnetite-actinolite-albite veins. The early, hairline veins are not strictly planar, commonly curving over their cm-scale strike lengths. Vein filling in early hairline veins ranges from simple biotite-only types to bornite-chalcopyrite-magnetite-anhydrite  $\pm$  quartz types. Total sulphide content is very low, with bornite and chalcopyrite grains occurring only as sporadically distributed, isolated blebs on an otherwise inconspicuous fracture. Anhydrite fills thicker veins, but sulphide content is low, regardless of vein thickness. Within the ore zone, mafic minerals are completely altered to shreddy hydrothermal biotite, but secondary biotite alteration grades laterally to isolated one-cm wide vein selvages peripheral to ore zones. Alteration of plagioclase to hard, pink K-feldspar is restricted to deeper, central portions of the ore zone where the quartz content of veins increases, locally forming quartz veins up to one centimetre in width. Bornite in thicker, quartz-rich veins associated with potassic alteration typically occurs as large, isolated blebs in addition to the finer disseminated grains and gold grades are typically high (>2 ppm) in intervals cut by these veins. Although no vein truncations by dykes have yet been documented, these early, hairline veins cut equigranular diorite, but only extremely rarely cut adjacent porphyry, and pervasive alteration of mafic minerals to shreddy hydrothermal biotite does not affect the dykes, indicating the dykes post-date most potassic alteration.

Both equigranular diorite and porphyry dykes were altered to garnet-bearing endoskarn, commonly, but not exclusively along the margins of the porphyry dykes. Endoskarn veins are texture-destructive near the centre, but have texture-preservative replacement zones interior to the sharp contact with feldspar-bearing rock. Massive brown garnet near the centres of endoskarn veins locally contains voids that are completely filled with anhydrite  $\pm$  bornite, suggesting endoskarn-forming fluids transported some copper. Most endoskarn, however, is very low-grade to barren.

Transitional-stage green sericite veins crosscut endoskarn, developing magnetite-bearing halos where they cut endoskarn and green sericite selvages in diorite. The green sericite veins are important contributors of both copper and gold grade in the Ertzberg Stockwork Zone, especially those containing bornite. Transitional green sericite veins show a systematic variation in mineralogy from bornite-chalcopyrite-anhydrite-quartz filled veins with magnetite-stable dark green sericite selvages to pyrite-anhydrite-quartz  $\pm$  chalcopyrite or bornite with lighter green, magnetite-destructive green sericite selvages. The bornite-bearing, magnetite-stable type of green sericite vein correlates best with copper and gold grades. The transition from bornite-chalcopyrite to chalcopyrite-pyrite assemblages certainly constitutes a change in the Cu:Fe ratio of the sulphide mineralogy and coincides with sulphidation of magnetite to pyrite in vein selvages. In the absence of bornite-pyrite assemblage, however, this transition does not necessarily indicate an increase in sulphidation state because chalcopyrite is stable in both end members of the transition. Temporally, magnetite-destructive pyrite-chalcopyrite-bearing green sericite veins crosscut magnetite-stable, bornite-bearing green sericite veins.

Figure 2: *Main Diorite* in A) *hand specimen*, and B) *plane-polars photomicrograph* (CPX partially altered to actinolite). *Bio-CPX Diorite* in C) *hand specimen*, and D) *crossed-polars photomicrograph* (CPX altered to shreddy biotite). *Ertsberg porphyry* dyke rock in E) *hand specimen* (cut by anhydrite veins), and F) *crossed-polars photomicrograph* (hornblende bottom left). Note there are significantly fewer mafic mineral sites, zoned phenocrysts, and sugary groundmass in the Ertsberg porphyry compared to the Ertsberg equigranular phases.



Late stage quartz-sericite-pyrite  $\pm$ chalcopyrite veins crosscut all green sericite veins. Sericite is characteristically a bleached white colour and disseminated magmatic magnetite in the selvages is sulphidised to pyrite. These late-stage veins are straight, continuous, and typical of "QSP" ("phyllitic") veins in many other porphyry copper deposits.

Very late-stage anhydrite veins and chlorite veins (Table 3) crosscut all other vein types. These generally lack sulphides or contain only minor amounts of pyrite. Chlorite veins represent classic propylitic alteration in many porphyry districts, occurring in rocks with epidote,

actinolite, and calcite alteration. These veins probably represent cooler, propylitic remobilisation of sulphate from earlier veins.

Preliminary SEM studies of early potassic-, transitional-, and late-stage veins demonstrate gold occurs in all three stages (Cook *et al.*, 2003). Gold occurs both as electrum and telluride, most closely associated with bornite grains in bornite-bearing veins and with chalcopyrite where bornite was not present.

	Vein type	Vein filling	Alteration halo in diorite	Diorite phases that host vein
<b>Feldspar-stable</b>	1. Magnetite-actinolite	Magnetite	CPX altered to actinolite + feldspar altered to albite	Equigranular phases only
	2. Biotite	Biotite	Pervasive shreddy biotite	Equigranular phases only
	3. Hairline bornite-biotite	Quartz-biotite-bornite-chalcopyrite	Slight pinkening of feldspar on fracture surface, CPX within 1 cm of veins altered to shreddy biotite	Equigranular phases only
	X*. Molybdenite	Molybdenite-pyrite-anhydrite	None, <i>or</i> 1 cm bleached zone with sericitic wash	Equigranular phases only
<b>Feldspar-destructive</b>	4. Endoskarn	Garnet $\pm$ anhydrite	Inner zone of texture-destructive dark brown garnet + anhydrite $\pm$ epidote $\pm$ pyroxene Outer zone of texture-preserving light brown garnet with pyroxene pseudomorphs of mafic minerals Minor epidote-chlorite alteration of feldspar	Equigranular phases and porphyry
	5. Bornite-anhydrite-green sericite	Quartz-anhydrite-bornite-chalcopyrite	1 cm thick magnetite-stable green sericite zone with disseminated bornite-chalcopyrite; locally develops inner halo of magnetite-destructive tan sericite with disseminated sulphides	Equigranular phases and porphyry (?)
	6. Pyrite-chalcopyrite-sericite	Quartz-pyrite-chalcopyrite $\pm$ anhydrite	1 cm pale green to white sericite, magnetite-destructive <5 mm chloritic outer halo	Equigranular phases and porphyry (?)
	7. Quartz-sericite-pyrite	Quartz-pyrite	1 cm tan to white sericite, magnetite-destructive <5 mm green sericite outer halo	Equigranular phases and porphyry (?)
	8. Purple anhydrite-pyrite	Quartz-pyrite	1 cm tan to white sericite, magnetite-destructive	All
<b>Very late</b>	9a. Chlorite	Chlorite $\pm$ pyrite	None	All
	9b. Anhydrite	Purple / white anhydrite	None	All

\* These veins not noted by number since relative timing inconclusive at present (i.e., no cross-cutting relationships *with offset of vein*).

Table 3: Summary of Vein Types in the Ertzberg Stockwork Zone

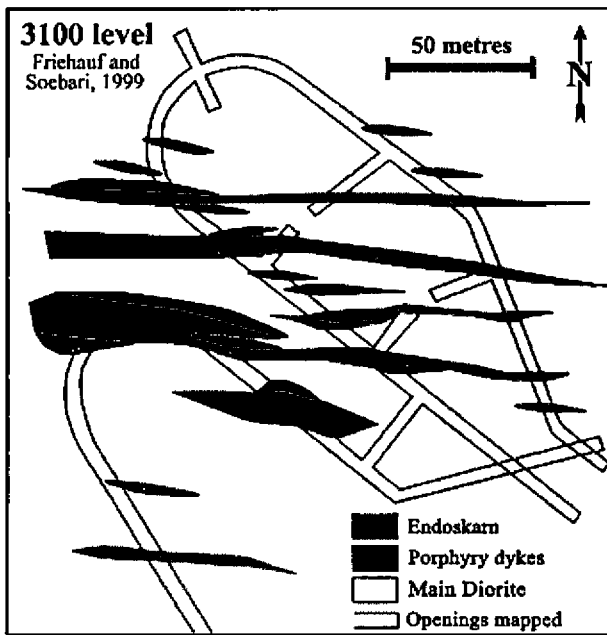


Figure 3: Geologic map showing relationship between porphyry dykes and endoskarn exposed in the access ramps to the EESS deposits based on mapping by Frichauf and Soebari, 1999.

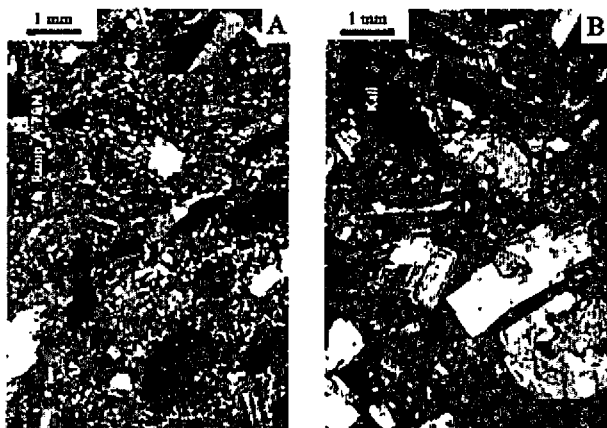


Figure 4: Comparison of A) Ertsberg porphyry dyke, and B) Kali dyke from Grasberg (shown at the same scale). Note how the Grasberg Kali sample contains strongly-zoned, broken phenocrysts set in an aphanitic groundmass.

## Discussion

The observation that the porphyry dykes post-date early bornite mineralisation, but predate later mineralisation styles is important for two reasons. From a production perspective, dykes commonly constitute slightly lower grade intercepts in drill core because they post-date some copper mineralisation. The implication of this is that dyke-parallel drilling may not provide an accurate representation of grade as a whole. The geological evidence that the dykes were coeval with mineralisation, and their broad spatial coincidence with porphyry-type mineralisation, suggests the dykes may have been sourced from the magma chamber that was genetically related to mineralisation.

The coincidence of porphyry dyke emplacement with the change in mineralisation style suggests a major change in the geological/geochemical environment. Mineralisation

prior to dyke emplacement occurred as discontinuous hairline veins that one would expect to form in a hot, approximately isotropic stress environment and/or under slow strain rate conditions. A change to more through-going rock fracture is suggested by the introduction of dyke-shaped intrusions, formation of laterally continuous vein types, initiation of long-distance chemical transport of components from sedimentary wall rocks into the pluton (forming endoskarn), and more efficient cooling of hydrothermal solutions that produce hydrolytic alteration styles.

Finally, the calcic nature of the vein endoskarn in the porphyry suggests that vertical and/or E-W lateral fluid flow interacting with calcic limestones characteristic of the upper part of the carbonate section may have dominated, rather than N-S lateral fluid flow from the nearby dolomitic carbonate wall rocks to the north where the highly magnesian forsterite-monticellite skarns of the GBT/IOZ/DOZ deposits (EESS) occur. An investigation into the relationship between igneous- and sedimentary-hosted ores of the Ertsberg complex is underway in which we are focusing on documenting fluid flow paths between the porphyry-hosted ores and the circum-Ertsberg skarns and how those flow paths might have affected skarn mineralogy in the EESS, Original Ertsberg, Dom, and other skarns.

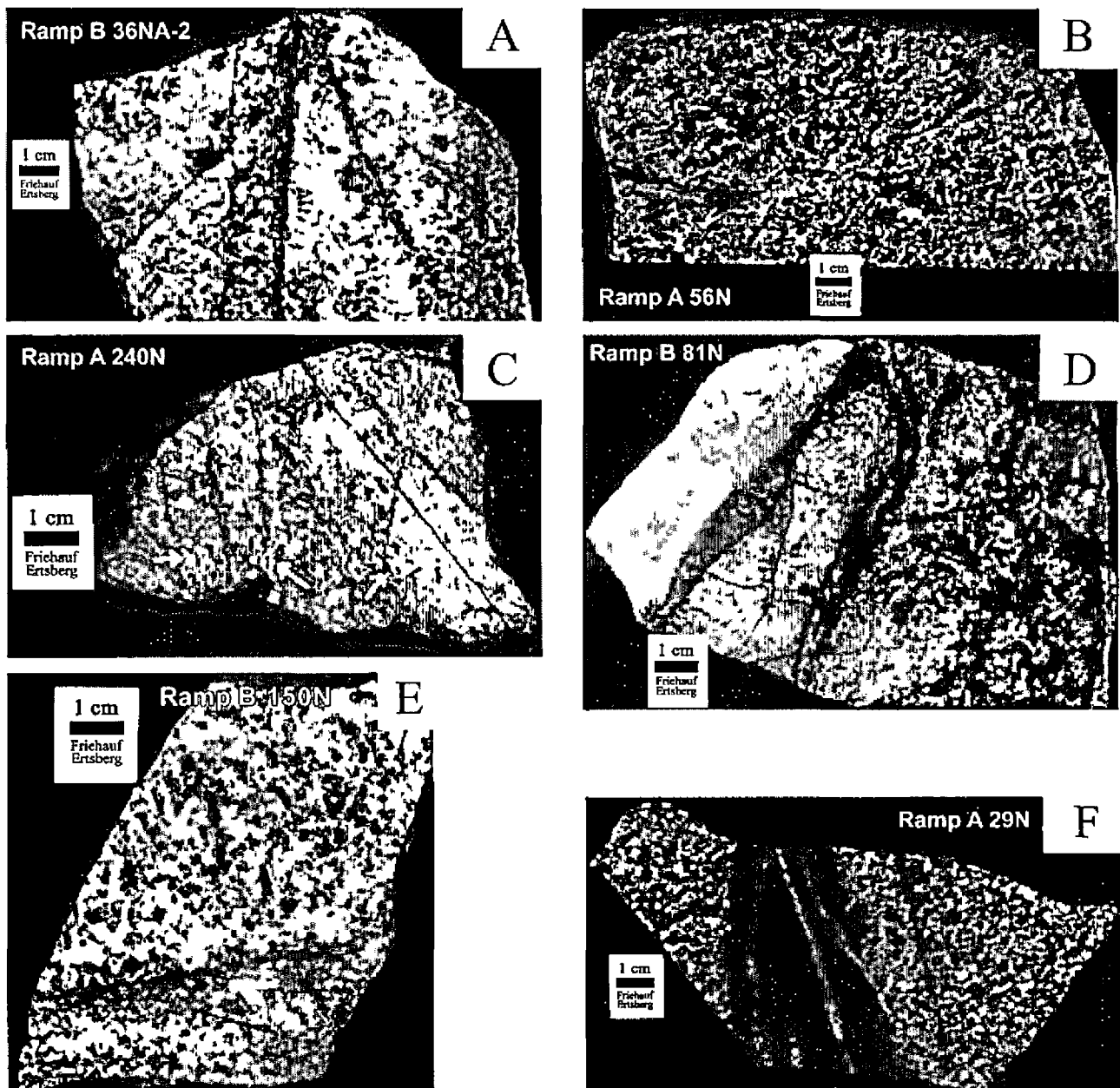
Although world-class when one considers the combined diorite- and skarn-hosted ores of the Ertsberg Stockwork Zone porphyry deposit, the Ertsberg Stockwork Zone is none-the-less smaller than the adjacent Grasberg deposit. The reasons for this disparity in size and the styles of mineralisation remain unproven.

Compared with porphyritic rocks from the nearby Grasberg deposit (Kali dykes), the dykes in the Ertsberg Stockwork Zone have: a) a coarser grained groundmass in the porphyritic phases (Fig. 4), b) a much weaker development of hydrolytic alteration styles, c) an absence of high sulphidation state mineralisation / advanced argillic alteration, and d) an absence of breccias. These differences would seem to suggest that the Ertsberg porphyry deposit might have formed at a greater depth than the Grasberg ores. This certainly would have affected the physio-chemical factors that control exsolution of hydrothermal fluids from the magma, the cooling rates of hydrothermal fluids, and the extents of fluid flow and may be the root cause of some of the differences in mineralisation style between the Ertsberg and Grasberg deposits.

Geochronological evidence suggests, however, that the Ertsberg intrusion is actually slightly younger than the Grasberg intrusions. Given the currently similar elevations of the Grasberg and Ertsberg deposits, and the occurrence of volcanic rocks in the tuff ring at the Grasberg deposit that suggest Grasberg mineralisation occurred very near the surface, any model calling on depth of emplacement as the key difference in mineralising styles would need to somehow submerge the district in the few tens of thousands of years following the formation of the Grasberg deposit and then exhume the district while preserving the Grasberg volcanic rocks. There are no known major faults separating the two deposits.



Figure 5: A) *Early-stage magnetite-albite-actinolite veins*, B) *early-stage potassic alteration veins with secondary biotite selvages*, C) *texture-preserving garnet endoskarn veins* (arrows indicate edge of garnet, ballod arrow indicates edge of texture-destructive alteration), D) *retrograde magnetite alteration of garnet endoskarn veins* (arrow indicates magnetite selvage), E) *late-stage, magnetite-destructive, white sericite veins with pyrite  $\pm$  chalcocopyrite filling*, and F) *transitional-stage magnetite-stable green sericite veins with bornite vein filling*.



Finally, mineralisation within the Ertsberg intrusion appears to lack the multiple, overprinting and repeating stages characteristic of Grasberg and many other large, high-grade porphyry deposits. This simplicity could reflect a one cycle-only hydrothermal system. Alternatively, in view of the size of the skarn orebodies to the north, multiple cycles may have mineralised the deposit, but focused on slightly different centres.

### Acknowledgments

We would like to thank Steve Van Nort, Chuck Brannon, Dave Potter, Wayu Sunyoto, Al Edwards, Chuck Brannon, and Larry Segerstrom for granting us access to the deposit. We thank Noris Belluz, Ben Coutts, Lasito Soebari, Clyde

Leys, Sugeng Widodo, and Paul Warren for assistance during fieldwork. Jay Pennington, George MacDonald, David Flint, and Bambang Irawan provided valuable conversation and advice during many stages of this study. Finally, we would like to thank Emily Cook for her participation in the reconnaissance study of gold mineralogy of the Ertsberg Stockwork Zone.

### References

Clarke, G.W., 2002 - Structural controls on skarn formation at the Big Gossan Cu-Au deposit, Ertsberg District, Irian Jaya: in McLellan, John G., and Brown, Matthew C., (Eds.), Deformation, fluid flow and mineralisation; Rick Sibson symposium;

- extended abstracts; *James Cook University of North Queensland*, Townsville, Australia, pp. 11-18.
- Cook, E., Friehauf, K., Gibbins, S. and Titley, S., 2003 - Gold Occurrences in the Stockwork Mineralization in the Ertsberg Diorite, West Papua, Indonesia; *Geological Society of America 2003, Abstracts with Programs*.
- Coutts, B.P., Susanto, H., Belluz, N., Flint, D. and Edwards, A.C., 1999 - Geology of the Deep Ore Zone, Ertsberg East Skarn System, Irian Jaya; PACRIM '99 congress proceedings, *AusIMM, Melbourne*, pp. 539-547.
- Friehauf, K.C., Soebari, L. and Titley, S.R., 2000 - Porphyry-Style Mineralization in the Ertsberg Diorite, Gunung Bijih (Ertsberg/Grasberg) District, Irian Jaya, Indonesia; *Special Field Conference on Advances in the Geology of the Ertsberg/Grasberg District, Irian Jaya, Indonesia, Institut Teknologi Bandung, Bandung, Java, Indonesia*, September 26-30, 2000.
- Gibbins, S.L., 2000 - Alteration in the southwest wall rocks of the Grasberg Cu-Au porphyry deposit; M.Sc. thesis, *University of Arizona*, 153p.
- Gibbins, S.L., Titley, S.R., Mathur, R., Eastoe, C. and Friehauf, K.C., 2000 - Unusual advanced argillic alteration of the SW rim of the Grasberg Cu-Au porphyry deposit, Irian Jaya, Indonesia [abs.]; *Geological Society of America 2000 Abstracts with Programs*, v. 32, p. 137.
- Glover, J.K., 2001 - Evaluation of the Structural and Lithological Setting and Controls of Mineralization at the Guru Copper-Gold Deposit Ertsberg (Gunung Bijih) Mining District C.O.W. Block A, Irian Jaya; *Internal P.T. Freeport Indonesia report*.
- Harrison, J.S., 1999 - Hydrothermal alteration and fluid evolution of the Grasberg porphyry Cu-Au deposit, Irian Jaya, Indonesia; M.Sc. thesis, *University of Texas, Austin*, 205 p.
- MacDonald, G.D. and Arnold, L.C., 1994 - Geological and geochemical zoning of the Grasberg Igneous Complex, Irian Jaya, Indonesia; *Journal of Geochemical Exploration*, v. 50, pp. 143-178.
- McDowell, Fred W., McMahon, Timothy P., Warren, Paul O., and Cloos, Mark, 1996 - Pliocene Cu-Au-bearing igneous intrusions of the Gunung Bijih (Ertsberg) District, Irian Jaya, Indonesia; K-Ar geochronology; *Journal of Geology*, v. 104, pp. 327-340.
- McMahon, Timothy P., 1994a - Pliocene intrusions in the Gunung Bijih (Ertsberg) Mining District, Irian Jaya, Indonesia; petrography and mineral chemistry; *International Geology Review*, v. 36, pp. 820-849.
- McMahon, T.P., 1994b - Pliocene intrusions in the Gunung Bijih (Ertsberg) Mining District, Irian Jaya, Indonesia; major- and trace-element chemistry; *International Geology Review*, v. 36, pp. 925-946.
- Meinert, L.D., Hefton, K.K., Mayes, D. and Tasiran, I., 1997 - Geology, zonation, and fluid evolution of the Big Gossan Cu-Au skarn deposit, Ertsberg District, Irian Jaya; *Economic Geology*, v. 92, pp. 509-534.
- Mertig, Heidi J., Rubin, Jeffrey N., and Kyle, J. Richard, 1994 - Skarn Cu-Au orebodies of the Gunung Bijih (Ertsberg) District, Irian Jaya, Indonesia; *Journal of Geochemical Exploration*, v. 50, pp. 179-202.
- Mertig, H.J., 1995 - Geology and origin of the Dom copper skarn deposit, Ertsberg (Gunung Bijih) District, Irian Jaya, Indonesia; M.Sc. thesis, *University of Texas, Austin*, 169p.
- New, B., Widodo, S., Wiwoho, N., and Edwards, A., 1999 - Kucing Liar, Irian Jaya; a sedimentary-hosted Cu-Au deposit; *Proceedings of the Fifth biennial SGA meeting and the Tenth quadrennial IAGOD symposium*, v. 5, pp. 1055-1058.
- Pennington, J.B., 1993 - Exploration of the Ertsberg Intrusion - Ertsberg mining district, Irian Jaya; *Freeport Internal Report*, December 20, 1993, 29p.
- Penniston-Dorland, S.C., 2001 - Illumination of vein quartz textures in a porphyry copper ore deposit using scanned cathodoluminescence; Grasberg Igneous Complex, Irian Jaya, Indonesia; *American Mineralogist*, v. 86, pp. 652-666.
- Penniston-Dorland, S., 1997 - Veins and alteration envelopes in the Grasberg Igneous Complex, Gunung Bijih (Ertsberg) District, Irian Jaya, Indonesia; M.Sc. thesis, *University of Texas, Austin*, 402p.
- Pollard, P.J. and Taylor, R.G., 2002 - Paragenesis of the Grasberg Cu-Au deposit, Irian Jaya, Indonesia; results from logging section 13; *Mineralium Deposita*, v. 37, pp. 117-136.
- Prendergast, K., 2002 - Similarities between porphyry-related hydrothermal systems of Wanagon Gold and Big Gossan, Papua, Indonesia; in McLellan, John G., and Brown, Matthew C., (Eds.), Deformation, fluid flow and mineralisation; Rick Sibson symposium; extended abstracts; *James Cook University of North Queensland, Townsville, Australia*, pp. 110-117.
- Rubin, J.N. and Kyle, J.R., 1997 - Precious metal mineralogy in porphyry-, skarn-, and replacement-type ore deposits of the Ertsberg (Gunung Bijih) District, Irian Jaya, Indonesia; *Economic Geology*, 92, Issue 5, pp 535-550.
- Rubin, J.N. and Kyle, J.R., 1998 - The Gunung Bijih Timur (Ertsberg East) skarn complex, Irian Jaya, Indonesia; geology and genesis of a large, magnesian, Cu-Au skarn; in Lentz, D. R., (Ed.), Mineralized intrusion-related skarn systems - *Mineralogical Association of Canada, Short Course Handbook no. 26*, pp. 245-288.
- Sapie, B. and Cloos, M., 1995 - Strike-slip faulting and related veining in the Grasberg porphyry Cu-Au ore system, Gunung Bijih (Ertsberg) Mining District, Irian Jaya, Indonesia (West New Guinea) [abs.]; *Geological Society of America 1995 Abstracts with Programs*, v. 27, p. 377.
- Widodo, S., Manning, P., Wiwoho, N., Johnson, L., Belluz,

N., Kusnanto, B., Macdonald, G. and Edwards, A.C., 1999 - Progress in understanding and developing the Kucing Liar orebody, Irian Jaya, Indonesia; PACRIM '99 congress; proceedings, *AusIMM, Melbourne*, pp. 499-507.

Widodo, S., Belluz, N., Wiwoho, N., Kusnanto, B., Manning, P., Macdonald, G., and Edwards, A., 1998 - Geology of the Kucing Liar ore body, Irian Jaya, Indonesia; *in* Porter, T.M., (Ed.), *Porphyry and Hydrothermal Copper and Gold Deposits - A Global Perspective*, *PGC Publishing*, Adelaide, pp. 49-60.

# ***Eurasia***

---



## MULTI-MILLION-YEAR CYCLIC RAMP-UP OF VOLATILES IN A LOWER CRUSTAL MAGMA RESERVOIR TRAPPED BELOW THE TAMPAKAN COPPER-GOLD DEPOSIT BY MIO-PLIOCENE CRUSTAL COMPRESSION IN THE SOUTHERN PHILIPPINES

<sup>1,2</sup>Bruce D. Rohrlach and <sup>1,3</sup>Robert R. Loucks

<sup>1</sup>*Research School of Earth Sciences, Australian National University, Canberra, Australia.*

<sup>2</sup>*Consultant, Legaspi City, Philippines.*

<sup>3</sup>*Geoscience Research, Lakewood, Colorado, USA*

**Abstract** - Magmatic-related porphyry copper and high-sulphidation epithermal copper-gold ore deposits are spatially and temporally clustered in arc segments that underwent crustal shortening during magmatic differentiation. In the ductile lower crust or uppermost mantle, geodynamically induced horizontal compression inhibits propagation of subvertical dykes and can keep buoyant magmas trapped in sheet-like, subhorizontal chambers. Layered ultramafic-mafic cumulates crystallise within these chambers until the regional stress regime relaxes or until further magmatic differentiation generates the buoyancy needed to overpower the stress field and permit magma ascent. In the hot lower crust or uppermost mantle, magma chambers tend to last long enough to experience multiple episodes of replenishment by primitive magma, partial mixing of arriving mafic and resident evolved melts, and fractional crystallisation of those hybrids. Over a succession of replenishment and partial-crystallisation cycles, the melt's concentration of incompatible chemical components (H<sub>2</sub>O, Cl, SO<sub>3</sub>, etc.) follows a "sawtooth ramp-up" time series. Multi-cycle magma chambers thereby become exceptionally fertile for magmatic-hydrothermal Cu metallogeny. In this case study of the late Miocene to Recent magmatism in the Tampakan ore district of southern Mindanao, Philippines, we integrate the regional tectonic history with local geological, geochronological, petrochemical and crustal stress data, and with magma chamber thermal modelling, formulate a model for arc-scale porphyry Cu-Au metallogenesis in compressional arc segments. Porphyry copper and high-sulphidation epithermal mineralisation within the giant Tampakan Cu-Au deposit (2500 Mt @ 0.48% Cu and 0.2 g/t Au) is hosted by a cluster of four overlapping stratovolcanoes constructed over the past 7 M.y. by intermittent emissions from a lower-crustal magma chamber having the same lifespan. This time interval spans the pre-, syn- and late-collision stages of the Sangihe arc in southern Mindanao where crustal compression commenced at ~7 Ma and peaked at ~4 to 3 Ma. The Tampakan porphyry Cu ore (4.24 to 4.26 Ma) and high-sulphidation Cu-Au ore (3.24 to 3.28 Ma) formed during peak crustal compression. Geochronologic and geochemical studies of the Tampakan volcanic complex identify five mafic-to-felsic differentiation cycles, punctuated by major mafic-magma replenishments into the basal chamber between the late Miocene and present, as the arc underwent a transition from relatively non-compressive subduction to collision. <sup>238</sup>U-<sup>206</sup>Pb geochronology on 471 zircon samples parameterise time series in chemical compositions of volcanic rocks and phenocrysts, and time-series in magmatic temperature, oxygen fugacity and wt % H<sub>2</sub>O in the pre-eruptive melt over the past 7 M.y. The time series of U/Ti, U/Ge and Th/Ti ratios in hundreds of dated detrital zircon grains resolve multiple, million-year-scale magma recharge-mixing-and-crystallisation cycles within a long-lived, lower-crustal magma reservoir near the arc Moho at 18 to 22 km depth (~5 to 6 kbars, by Al-in-hornblende geobarometry). The "sawtooth" cyclic ramp-up of these element ratios in zircons and their parent melts coincides with a 7 M.y. long sawtooth cyclic ramp-up in concentrations of volatiles and crystal-incompatible trace elements in erupted melts of basaltic andesite to dacite composition. At ~6.3 Ma, silicic andesite (62% SiO<sub>2</sub>) of the early mafic-to-felsic differentiation cycle had only ~3 wt% H<sub>2</sub>O in the melt and U/Ti = 20 in zircon, whereas by ~1.3 Ma the late-cycle silicic andesite (62% SiO<sub>2</sub>) had ~7.5 wt% H<sub>2</sub>O in the melt and U/Ti = 80 in zircon, due to inheritance of H<sub>2</sub>O and U and other incompatible components from prior cycles. Porphyry-Cu-ore-related volcanics and epizonal plutons display trace-element evidence that the melts segregated from high pressure (lower-crustal) cumulates consisting largely of olivine, Al-rich augite and hornblende, but little or no plagioclase. Higher Sr/Y ratios in later cycles of the Tampakan igneous complex represent differentiation of increasingly hydrous hybrid melts in the lower crust. Retardation and suppression of plagioclase crystallisation by high magmatic water activities and by high load pressure allowed residual

melt fractions to avoid depletion of Sr and Eu during fractionation crystallisation. Higher pressure and H<sub>2</sub>O activities in melts foster prolific crystallisation of hornblende earlier in the crystallisation sequence of later cycles, thereby depleting the melt in Y and heavy REE, and driving up its Sr/Y and Eu/Yb ratios to produce the distinctive chemical signatures characteristic of porphyry-copper ore-forming magmas worldwide throughout Phanerozoic time

## Introduction

The Tampakan copper-gold deposit in southern Mindanao, Philippines, is a giant high-sulphidation epithermal (Cu-Au) deposit that is developed on older, erosionally exhumed, deeper-level porphyry-Cu mineralisation. The deposit is located within the municipality of Tampakan, Province of South Cotabato in southern Mindanao, Philippines, at approximately 06°28'30"N latitude and 125°03'00"E longitude, 40 km NNW of General Santos City. It lies at 600 to 1200 metres elevation along the southern portion of the Central Mindanao Cordillera. Mineralisation is hosted by altered diorite intrusions and andesitic lava flows that form a late Miocene volcanic basement sequence and an erosionally dissected, late Miocene to Pleistocene stratovolcanic complex. The Tampakan district lies at the northern end of the Miocene-to-Holocene-age Sangihe volcanic arc which extends from northern Sulawesi to southern Mindanao. The district lies between strands of the Cotabato strike-slip fault zone (Fig. 1).

The Tampakan deposit was discovered by WMC Resources Ltd in 1992 and is currently owned by Indophil Resources Ltd and its Philippine partner Sagittarius Mines Ltd. It has a preliminary inferred resource of 2500 million tonnes (Mt) grading 0.48% copper, and includes a higher-grade core with an indicated and inferred resource of 1100 Mt grading

0.7% copper and 0.3 g/t gold (Subang *et al.*, 2004). The total estimated *in-situ* metal content is 12.5 Mt of copper (Cu) and 500 tonnes (16 Moz) of gold (Au). It is the second largest known Cu-Au resource within the western Pacific, after the giant, diatreme-hosted, Grasberg Cu-Au deposit in Irian Jaya. The Tampakan deposit is the first exploration discovery within a newly defined metallogenic province in the southern portion of the Central Mindanao Cordillera, and lies within a syn- to post-collisional tectonic setting related to terrane accretion and arc-arc collision. This collision is associated with widespread thrust faulting and folding within the arc, and subduction polarity reversal. Intense intra-arc compressional deformation penecontemporaneous with mineralisation is observed in all well investigated Cenozoic Cu-dominant Cu ± Au metallogenic provinces around the rim of the Pacific basin.

A poorly understood feature of oceanic-island-arc and continental-arc metallogeny is the highly variable endowment of Cu and Au mineralisation in different arcs and arc segments. A second poorly understood feature of arc metallogeny is its usual development as province-scale metallogenic pulses lasting a few million years that punctuate much longer periods of metallogenically infertile magmatism in the same regions. Many of the major mineralised porphyry and epithermal provinces that contain multiple deposits display a long history of subduction-related magmatism (15 to >60 M.y.). Magmatic

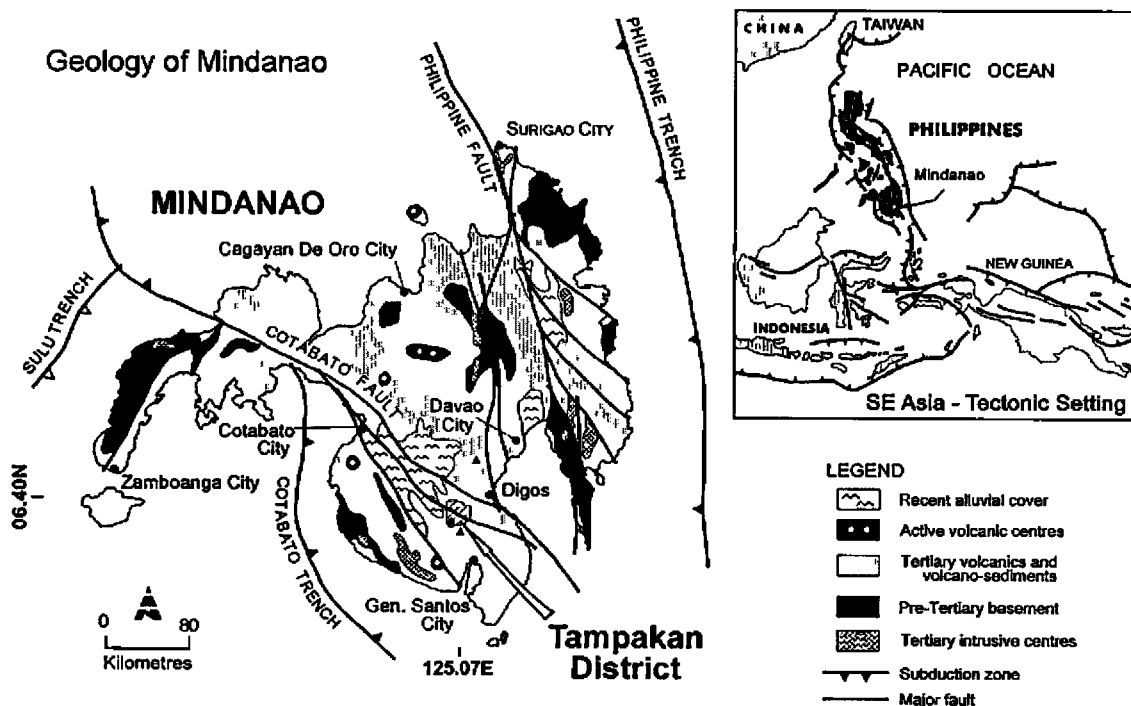


Figure 1: *Geology of Mindanao, southern Philippines, and location of the Tampakan deposit within the transpressional Cotabato Fault Zone.*

differentiation, enrichment of incompatible elements and volatile exsolution are processes that occur in nearly all intra-arc intrusives. However, the emplacement of ore-forming magmas within mineral districts and provinces typically spans a brief time interval (~3 to 10 M.y.). Examples of these short-lived pulses of mineralisation include the various mineral belts of the Andean cordillera [4 to 12 Ma, 20 to 22 Ma, 33 to 41 Ma, 55 to 60 Ma in different segments – Titley and Beane (1981)]; the southwest continental US [39 to 40 Ma, 52 to 59 Ma, 62 to 67 Ma in different regions – Titley and Beane (1981)]; the Philippines [1 to 5 Ma]; New Guinea [1 to 6 Ma] and the New Ireland/Solomon Islands/Fiji region [0 to 4 Ma].

The regional tectonic factors that accompany and contribute to these brief, migratory pulses of metallogenically fertile magmatism are often poorly understood and poorly characterised in district-scale ore-genesis studies. An understanding of the fundamental tectonic controls on province-scale metallogenesis is required in any holistic model for magmatic-related Cu-Au mineralisation. The most appropriate regions to study this problem are those where mineralisation is sufficiently young that the pre-, syn- and post-mineralisation variations in tectonic setting can be tightly constrained. The late Neogene to Recent volcanic island arcs of southeast Asia and the southwest Pacific are suitable localities for this type of study. The Pliocene age of the Tampakan deposit enables interpretation of the petrology, petrochemistry and geochronology of the ore-bearing and barren magmatic suites in the context of the reasonably well constrained tectonic framework for Mindanao in the late Cenozoic. In this paper, we identify the relevant tectonic-plate-scale cause-and-effect relationships responsible for magmatic metallogenic fertility in the Tampakan district, and we determine the diagnostic petrochemical characteristics of ore-forming magmas in the Tampakan district; these characteristics are representative of the broader spectrum of magmas that produce large porphyry and high-sulphidation Cu ± Au ore deposits of Phanerozoic age globally.

## Regional Tectonic Setting

The Philippine archipelago is the site of recent small-scale collisions between extinct early Cenozoic arc systems on the Philippine Sea Plate and continental fragments or island-arc fragments that were rifted from the southeast margin of the Eurasian Plate during Tertiary opening of marginal basins. The principal tectonic element of the archipelago is the elongate Philippine Mobile Belt (PMB; Rangin, 1991) that is bounded to the east by the Philippine subduction system and to the west by the Manila-Negros-Sulu and Cotabato subduction systems. The crustal "raft" that comprises the Philippine archipelago is bisected along its north-south axis by the ~2000-km-long sinistral Philippine Fault (inset to Fig. 1). Taiwan and several segments of the western seaboard of the Philippines that include Zambales, Mindoro, Palawan, western Panay and southern Mindanao, represent collision zones caused by convergent interaction between the Eurasian Plate and the Philippine Sea Plate along the multi-strand boundary zone that comprises the PMB (Pubellier *et al.*, 1991).

According to Hall (1996, 2002) and sources cited therein, a major reorganisation of tectonic plates in the Southwest Pacific and Sundaland region accompanied the late Oligocene (30 to 25 Ma) arrival of the "horn" promontory of northwestern continental Australia (now the Birds Head of Irian Jaya, Seram, Buru, and east arm of Sulawesi) at the north-dipping trench along which the Mesozoic oceanic crust of the Indo-Australian Plate had been subducting under the Sundaland-Philippine Sea Plate. The continental promontory's arrival at the trench divided the Indo-Australian oceanic lithosphere north of Australia into two segments lying west and east of the promontory. The eastern segment was continuous from the Molucca Sea to the Solomon Sea, but that continuity was soon destroyed at ~25 Ma, isolating the Molucca Sea portion, when northern New Guinea arrived at the Philippine-Halmahera-South Caroline Trench situated on the southern edge of the Philippine Sea Plate.

The Molucca Sea oceanic lithosphere fragment lay between southern Mindanao and northern Sulawesi during the Miocene. Clockwise rotation of the Philippine Sea Plate at 25 Ma initiated the Sangihe subduction system along the western margin of the attached Molucca Sea Plate fragment, and by 20 Ma the Molucca Sea Plate was subducting westward at the Sangihe Trench. This subduction zone generated volcanism between 15 and 5 Ma in southern Mindanao. Hall (1996) suggests that at 20 Ma, the proto-Cotabato Fault Zone propagated along the northern edge of the Zamboanga Peninsula as a sinistral strike-slip fault that partly accommodated the clockwise rotation of the Philippine Sea Plate. The Cotabato Fault became a transfer zone along which the southern Mindanao (Zamboanga Peninsula, Daguma Range and the Sarangani Peninsula) portion of the ancestral Zamboanga-Negros-Panay-Luzon arc was translated southeastward to dock with the northern half of Mindanao at the Miocene-Pliocene transition (Rangin 1991; Pubellier *et al.*, 1991; Hall 1996).

The Molucca Sea Plate began to subduct eastward along the Halmahera Trench at around 15 Ma. The Molucca Sea Plate was doubly subducting eastward and westward at 15 Ma, and by 10 Ma the plate was bounded by sinistral strike-slip systems on the north (Cotabato Fault Zone) and on the south (Sorong Fault Zone) (Hall, 1996). At the Miocene-Pliocene transition (6 to 4 Ma), immediately preceding and during porphyry mineralisation at Tampakan (4.24 to 4.26 Ma), the southern portion of Mindanao (Sarangani Peninsula, Zamboanga Peninsula and Daguma Range) was moving southeastward along the Cotabato Transfer Fault Zone which separated basement of Eurasian affinity in the south from basement of oceanic affinity – Philippine Sea Plate – in the north (Fig. 2).

The 5 to 3 Ma period was a dynamic one in the southern Philippines as continental crust of southern Mindanao docked with arc-thickened oceanic crust of northern Mindanao. The 5 Ma date marks the commencement of a prolonged and continuing period of compression throughout southeast Mindanao and was synchronous with porphyry Cu and high-sulphidation epithermal Cu-Au mineralisation in the Tampakan district. Compressional structures related



to this oblique collision include NW-trending sinistral strike-slip faults that define pressure ridges and horst blocks along the Cotabato transfer fault, widespread thrust faults which are east-verging in the southern Mindanao terrane and west-verging in the northern Mindanao terrane (Fig. 3) (Quebral *et al.*, 1996; Domingo *et al.*, 1995), thrust-related ramp anticlines which display dual vergence (Fig. 3), and regional folding (Figs. 6 and 7). Compression during the 5 to 3 Ma period in southeastern Mindanao was compounded by final closure of the northern Molucca Sea as the Sangihe and Halmahera arcs came into frontal collision.

As the central Philippines collided with the continental Palawan block in the late Miocene, jamming the Manila Trench there, the Philippine Trench was initiated along the opposite, eastern margin of the central Philippines at around 8 Ma and propagated southward to the latitude of Mindanao by about 5 Ma (Ozawa *et al.*, 2004). The compressional stress associated with establishment of the new subduction-thrust system was transmitted westward through the interior of Mindanao, contributing to the accumulation of compressional stress within the collision terrane of central and southern Mindanao. Furthermore, a segment of the

Halmahera arc (southern Pacific Cordillera) accreted onto east Mindanao by collision between 5 and 4 Ma (Lallemant *et al.*, 1998).

During this Pliocene compressional period, the Philippine Fault was initiated as a sinistral strike-slip fault within the Philippine Mobile Belt to partly accommodate the oblique component of convergence between the Philippine Sea Plate and the Philippine Mobile Belt (Aurelio *et al.*, 1991; Barrier *et al.* 1991). However, compressional stress was generated faster than it was accommodated by the proto-Philippine Trench and Philippine Fault Zone, so distributed compressional deformation became increasingly focused into a developing subduction thrust zone that became the Cotabato Trench along the southwestern margin of Mindanao (Figs. 3, 4 and 5).

A new geodynamic setting for the southern Philippines was ushered in at ~3 Ma. The Zamboanga Peninsula, Daguma Range and Sarangani Peninsula were tectonically incorporated into the Philippine Mobile Belt. Establishment of the Philippine Trench constitutes an eastward jump of the western margin of the Philippine Sea Plate, thereby tectonically isolating the Philippine Mobile Belt as a crustal "raft" that was trapped between the east-dipping Manila-

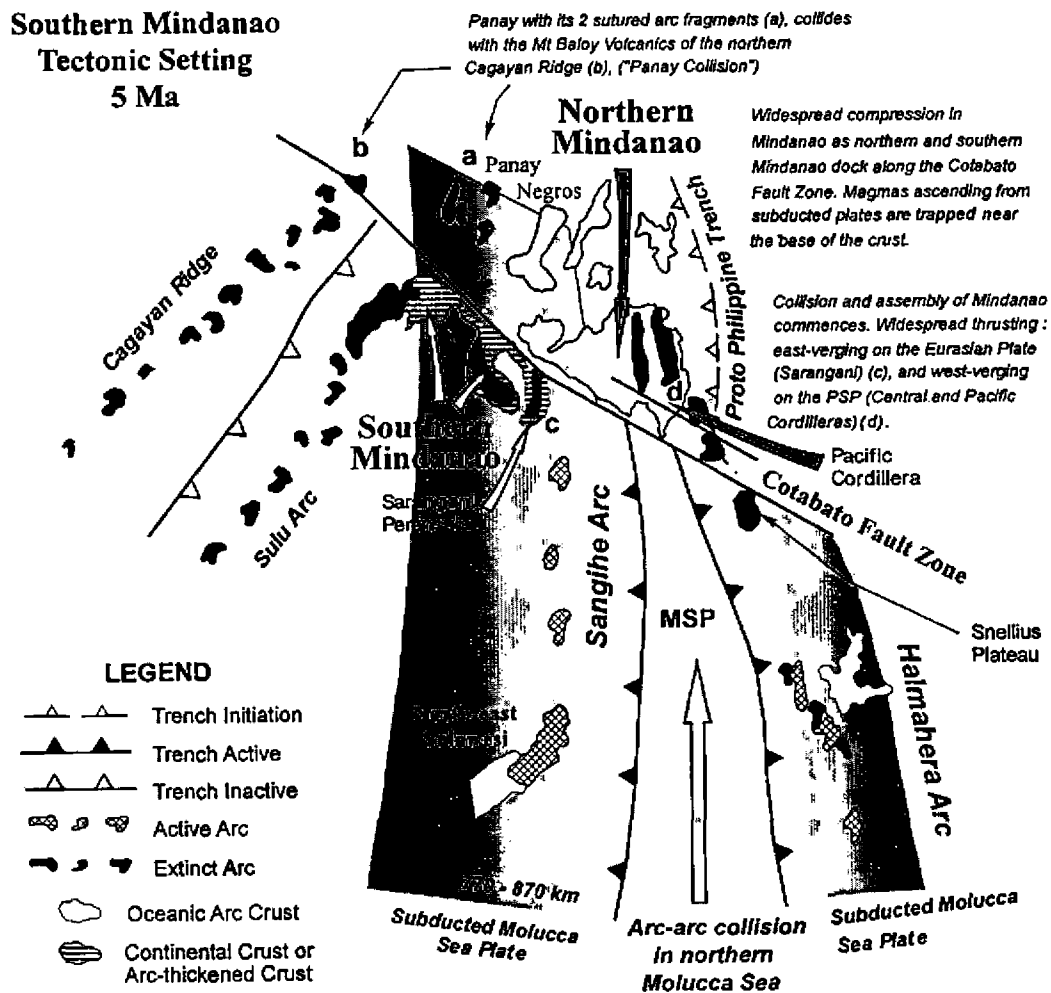


Figure 2: Schematic tectonic reconstruction of southern Mindanao during the Mio-Pliocene collision event at 5 Ma. The docking of northern and southern Mindanao along the Cotabato Fault Zone occurred synchronously with arc-arc collision between the northern end of the Sangihe and Halmahera arcs.

Negros-Cotabato subduction system and the west-dipping Philippine Trench subduction zone. During the late Pliocene and Pleistocene through to the present, the docking of the two terranes along the Cotabato Fault was completed and the Molucca Sea Plate's two outward facing subduction zones (Sangihe and Halmahera) were replaced by the Philippine Trench and Cotabato Trench subduction zones that now dip under the Philippine archipelago. This period of subduction polarity reversal was marked by extensive and rapid uplift of significant portions of Mindanao. Collision is currently ongoing south of the Pujada Peninsula, off the southeast coast of Mindanao (Fig. 4), where segments of the Halmahera arc that have been dislocated by strike-slip faulting are partly under-thrust beneath the Sangihe Trench (Lallemand *et al.*, 1998; Pubellier *et al.*, 1999).

The history of convergence between the Philippine Sea Plate and the Sunda Block of the Eurasian margin, and the partitioning of this convergence into subduction systems, is illustrated in Fig. 5. By integrating the area above the curve that defines the deficit in total convergence, after accounting for convergence at active subduction zones (Fig. 5, shaded black area), we derive a first-order estimate of the portion of the plate convergence that is partitioned into intra-plate compressive deformation. Southern Mindanao has been under significant crustal compression since 7 Ma, with compression peaking between 4 and 2 Ma

(Fig. 5). There is widespread thrusting of Pliocene age throughout southeastern Mindanao and in the Tampakan district. This shortening is implicated in rapid uplift between 3.92 and 4.32 Ma which unroofed the Tampakan porphyry system by ~2 km within a time frame of ~350 K.y. (See 'Geochronology' below). The progressive slowing in subduction rate of the Molucca Sea Plate at the Halmahera and Sangihe trenches, due to the Cotabato suture collision that commenced at ~5 Ma, coincides with the convergence between the Philippine Sea Plate and the Sunda Block becoming increasingly accommodated by intra-plate thrusting and folding in southern Mindanao. It is also synchronous with initiation of thrusting at the nascent Philippine Trench. At present there is a small component of convergence (A-Su on Fig. 5; 8.4 mm y<sup>-1</sup>) which is not accommodated by subduction. This suggests that crustal shortening is still ongoing in southern Mindanao, albeit waning in intensity. Quaternary to Recent uplift of limestone terraces along the western shoreline of Sarangani Bay (pers. observ.) indicate ongoing uplift. The component of convergence available for partitioning into crustal compression is diminishing as current subduction systems become established and as the sinistral Philippine Fault Zone propagates farther south and absorbs some convergence in this region.

The Molucca Sea Plate has submerged into the upper mantle below the over-riding and colliding Eurasian and Philippine

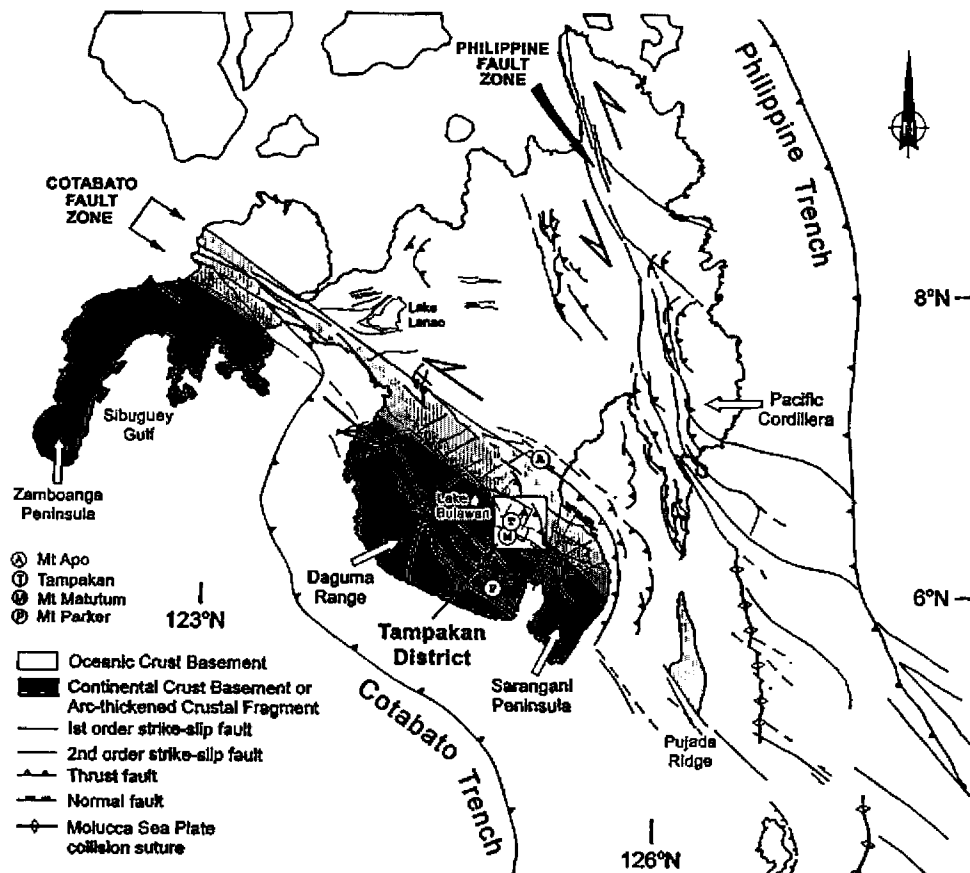


Figure 3: Principal strike-slip and thrust faults in Mindanao. The Tampakan district lies within a ~100-km-wide corridor of sinistral wrench faulting along the Cotabato Fault Zone. Widespread thrust faulting that occurs in proximity to the Tampakan district developed during the Mio-Pliocene collision event in southeast Mindanao. These thrust faults verge to the east in the Tampakan district and Sarangani Peninsula, and verge to the west on the southern portion of the Pacific Cordillera.

lithospheric plates in southern Mindanao; however, arc-arc collision is ongoing in the southern Molucca Sea. The Sangihe and Halmahera volcanic arcs face each other and are underlain by opposite-dipping Benioff zones. The west-dipping portion of the Molucca slab beneath the Sangihe Arc and the Celebes Sea can be traced to at least 650 km depth by earthquake foci (Seno and Kurita, 1978; Cardwell *et al.*, 1980), whereas the east-dipping portion of the doubly subducted A-shaped Molucca slab can only be traced

seismically to around 250 km depth beneath the Halmahera Arc (Hatherton and Dickinson, 1969; Silver and Moore, 1978; Hamilton, 1979; Hall, 1996). The Tampakan district lies along the trace of the suture between northern and southern Mindanao defined by the Cotabato Fault Zone, and falls within a zone of compressional structures defined by thrusting and folding that developed during subduction reversal associated with the transition from the Sangihe-Halmahera to the Cotabato-Philippine subduction pairs.

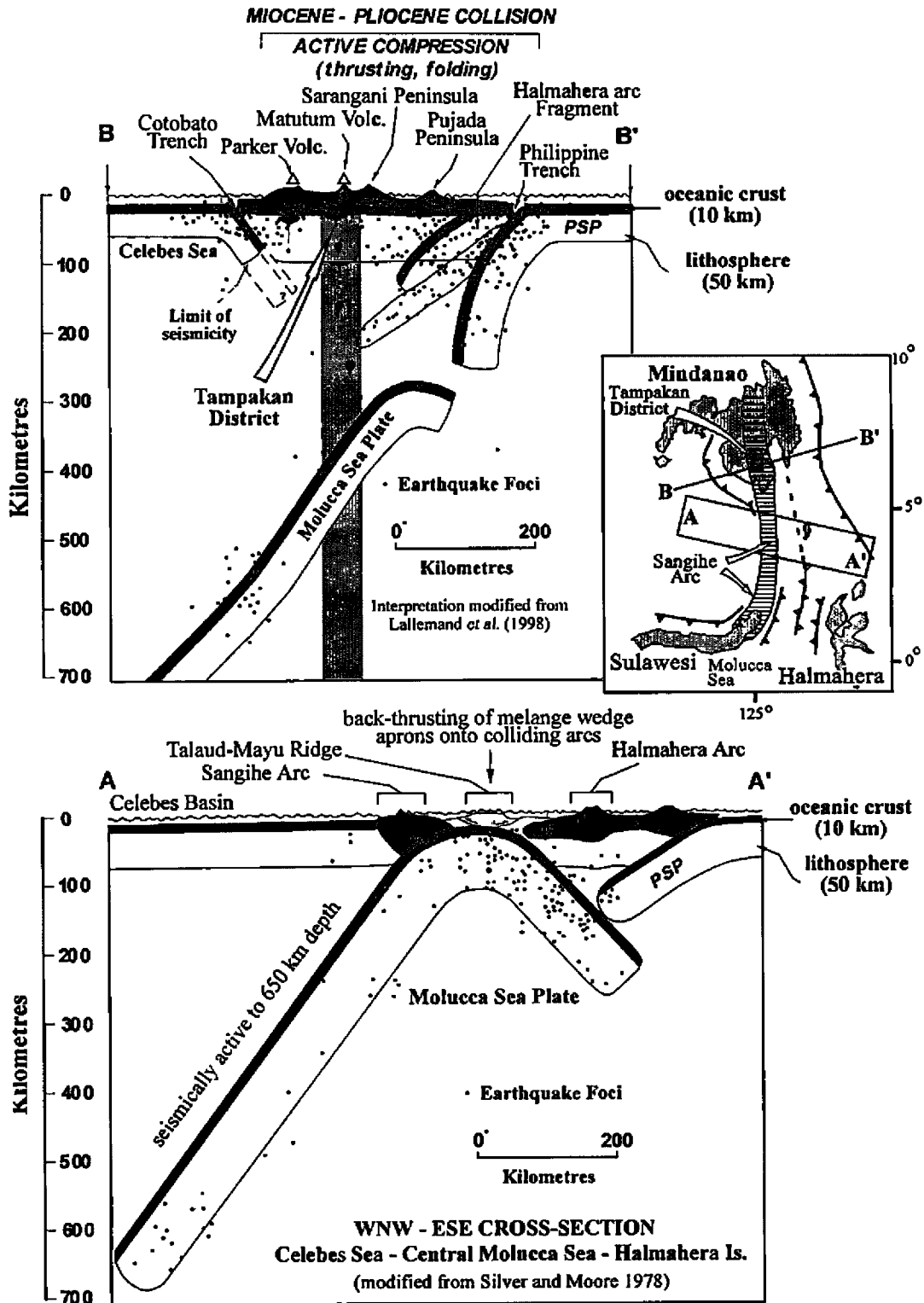


Figure 4: Geometry of subducted ocean floor beneath the collision zone that contains the Tampakan district in southern Mindanao (top), and in the Molucca Sea between Mindanao and Sulawesi where arc-arc collision is presently occurring. Stacking of arc fragments occurs below southeast Mindanao. The Molucca Sea Plate is subsiding into the mantle below the collision zone.

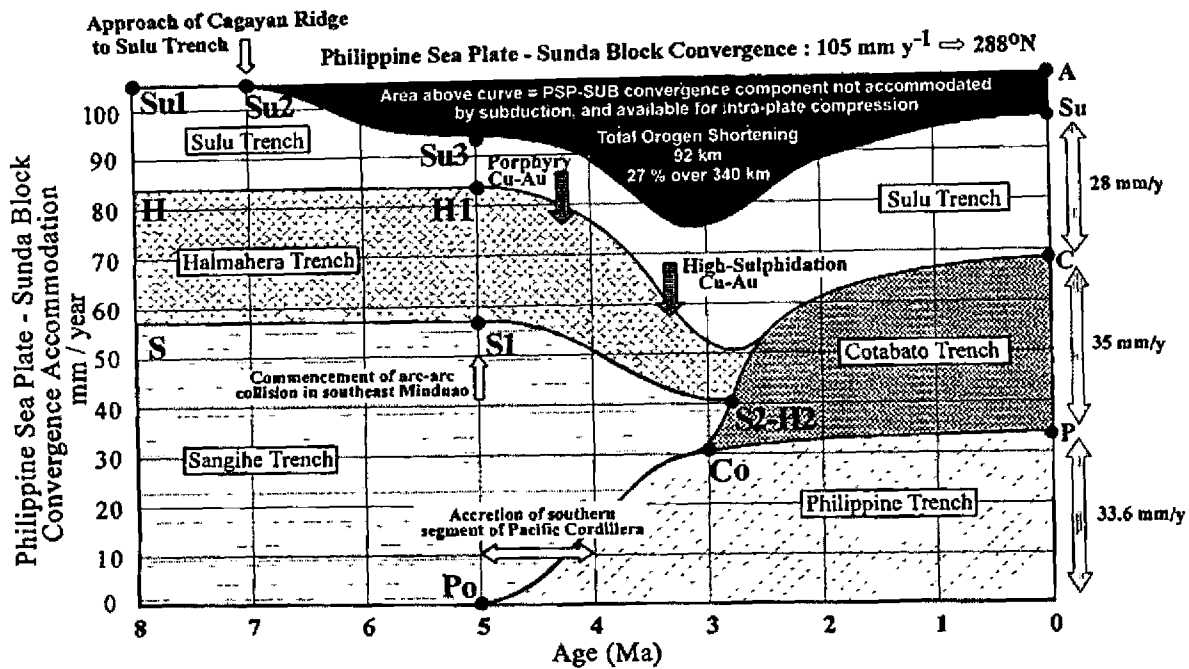


Figure 5: Temporal history of convergence-parallel accommodation of the Philippine Sea Plate motion, relative to the Sunda Block, that is accommodated at subduction zones in southern Mindanao. Residual convergence that is not accommodated by subduction is represented as distributed intra-plate compression (black shading). The geological controls for the tie-points (labelled dots) are discussed by Rohrlach (2002).

## District Geology

The geology of southern central Mindanao is dominated by three segments of the Sangihe volcanic arc; i). the Daguma Range (magmatically active from ~17 to 18 Ma; Pubellier *et al.*, 1993, Sajona 1994); ii). the Sarangani Peninsula (~10 to 12 Ma; Pubellier *et al.*, 1993, Sajona *et al.*, 1994); and iii). the southern Central Mindanao Cordillera which was volcanically active from ~8.5 Ma to the present in the Tampakan district. The Tampakan district is flanked to the west by the Cotabato Basin and to the east by the Sarangani Basin (Fig. 6). The Cotabato Basin separates the Daguma and southern Central Mindanao Cordillera arc segments. It has a long history, initially as a fore-arc basin developed between early Miocene arc volcanism in the Daguma Range and the Sangihe Trench, and more recently, as a developing back-arc basin behind the Daguma Range (Pubellier *et al.*, 1991) as a result of new subduction along the Cotabato Trench. The basin comprises an extensive alluvial plain with several NW-trending ridges (e.g., the Roxas Range) that define *en echelon* folds developed over buried splays of the Cotabato Fault Zone (Fig. 7). Middle Miocene to Pleistocene basin sediments within the Roxas Range comprise bathyal marine mudstone and conglomerate, progressively shallower marine limestone, sandstone, and recent non-marine alluvium. The shallowing palaeo-sedimentary environment reflects prolonged uplift of the region. Coarsely bedded Pleistocene conglomerate beds along the eastern margin of the basin onlap the cordillera west of the Tampakan deposit, and are intruded by Pleistocene-age volcanic plugs in the Tampakan district. The beds are tilted towards the west at 30 to 40° by basin-margin thrust faults. The Sarangani Basin separates the Central Mindanao Cordillera from the Sarangani Peninsula arc segment and is an intra-arc basin that developed within an active synclinal flexure

on the western limb of the Sarangani ramp anticline (Fig. 6). This north-south trending topographic depression is filled by Pliocene-age volcanoclastic sediments and limestones. The volcanoclastic sediments were eroded from the adjacent, actively uplifting arc segments to the east and west. The presence of water-lain tuff interbedded with conglomerate and limestone along the western margin of the basin indicate active volcanism in the hinterland during folding and basin development. Much of the volcanoclastic component was probably sourced from the early to middle Pliocene Tampakan volcano which was the nearest volcanic centre during the Pliocene.

Southern Mindanao has been affected by two styles of deformation. The earliest and most persistent deformation took the form of lithospheric-scale wrench faulting along a Miocene plate boundary that coincides with the ~100-km-wide zone of sinistral faulting that comprises the suturing Cotabato Fault system (Pubellier *et al.*, 1991). The second style of deformation comprises folding and thrusting that developed during collision of the Sangihe and Halmahera arcs in southeastern Mindanao, and during subsequent subduction polarity reversal that formed the Philippine and Cotabato trenches. The thrust faults and ramp-anticlines that dominate east-west geological cross-sections of the southern Pacific Cordillera and Sarangani Peninsula (Quebral *et al.*, 1996; Domingo *et al.*, 1995) are also present within the southern Central Mindanao Cordillera segment of the Sangihe Arc and the Tampakan district (Fig. 3). The Tampakan district is fault-bounded against the western margin of the Sarangani Basin by an east-verging thrust fault which dips westward under the district – the Central Cordilleran Thrust Fault (Fig. 6). The district lies on a ramp anticline that developed in the hanging wall of this thrust fault and which folds the early Miocene volcanic basement (Fig. 7).

The Tampakan district is centred on a deeply eroded polygenetic volcanic complex which was active episodically from the Late Miocene to late Quaternary period. The volcanics and intrusives are dominated by mafic to silicic andesite flows and intrusives of Late Miocene to Middle Pliocene age, with lesser basaltic andesite flows of Late Miocene age and dacitic flow domes and plugs of Pleistocene age. The Tampakan porphyry mineralisation is hosted by Late Miocene and early Pliocene volcanics whereas the Tampakan high-sulphidation deposit is hosted also by younger, middle Pliocene volcanic and intrusive rocks. Digital terrain model (DTM) images of the Tampakan district that have been enhanced using algorithms that simulate solar illumination, clearly identify a deeply dissected, central-vent stratocone that forms the core of the district (Fig. 8). This eroded volcanic centre is overlapped to the south by the juvenile and dormant Mt Matutum stratocone. The digitally enhanced topographic images reveal the preserved basal third of an andesitic stratocone that is erosionally truncated at an elevation of ~1200 to 1300 metres above sea level. The Tampakan deposit lies below the western lip of the truncated surface (Fig. 8). The Tampakan volcanic centre comprises a series of sequentially rebuilt and eroded volcanic centres that have accumulated the Tampakan Andesite Sequence over a 4.5 M.y. interval extending from ~7 to ~2.5 Ma. The eroded topographic stratocone remnant identified in the DTM dataset is a middle Pliocene age stratocone that dominated the volcanic landscape at the time of Tampakan high-sulphidation Cu-Au mineralisation.

The Tampakan Andesite Sequence has a grossly circular distribution, and on a regional-scale unconformably overlies a northwest-trending basement antiform (Fig. 7). The 10 to 15° radial dip angle of andesite lava flows on the flanks of the volcanic structure, and the diameter of the base of the inferred volcanic cone (~18 km) suggest that the original middle Pliocene volcanic summit may have had an elevation of ~3000 metres above sea level, similar in scale

to the 2950 metre-high Quaternary Mt Apo volcanic centre that lies ~60 km to the north in the Davao district. Strands of the Cotabato wrench fault zone that transect the district are the Alip River Fault and the Buayan Fault (Fig. 7). Prominent northeast-trending photo-lineaments lie parallel to mineralised zones within the deposit and cross-cut a district-wide zone of advanced argillic to intermediate argillic and silicic alteration (Fig. 7).

## Deposit Geology

The spatially coupled high-sulphidation-epithermal Cu-Au and porphyry Cu deposits at Tampakan are located on the western rim of an eroded middle Pliocene volcanic centre (Fig. 8), and on the western margin of a series of annular to elliptical topographic anomalies in the core of the eroded volcanic edifice (Fig. 7). High-sulphidation mineralisation and acid alteration form a manto-like zone of mineralisation extending along an erosion surface that exhumed a low-grade porphyry Cu system. Epithermal mineralisation post-dates porphyry mineralisation by ~1 M.y. (See 'Geochronology' below).

### High-Sulphidation Mineralisation

High-sulphidation mineralisation at Tampakan accounts for most of the resource that has been defined to date. Mineralisation covers a lateral area of ~1.6 by 2.0 km (Fig. 9) and forms a generally stratabound and gently-dipping zone between 200 and 500 metres thick on the western flank of the volcanic centre. The zone of high-sulphidation mineralisation and advanced-argillic/silicic alteration crops out at ~1200 metres above sea-level (ASL) in the northern part of the deposit and extends to ~600 metres ASL at the southern end. The stratabound zone of partial to massive silicification displays multi-phase brecciation, acid leaching and vuggy porosity, and is developed within a district-scale advanced-argillic lithocap that exceeds 90 km<sup>2</sup> in area (Fig. 7). The principal host rocks are the Tampakan Andesite Sequence of Late Miocene to

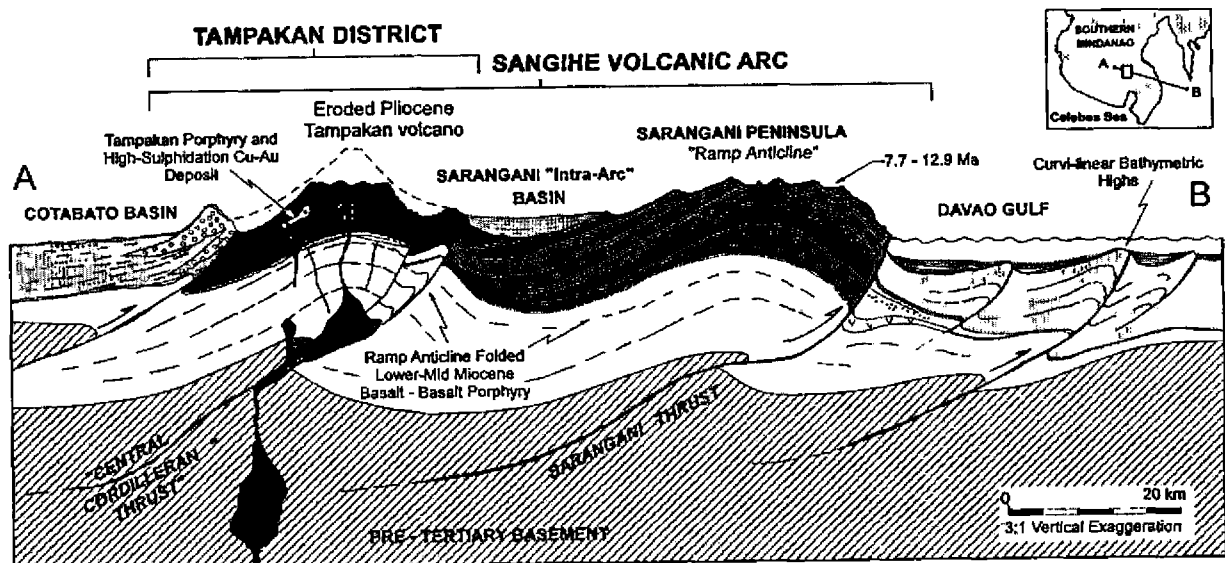


Figure 6: Geological cross-section through south-central Mindanao, showing location of the Tampakan district on a ramp-anticline developed over a Pliocene collision-stage thrust fault. Major folds and thrusts affect latest-Miocene rocks. Thrust faults are east-verging throughout the southern Central Mindanao Cordillera, Sarangani Peninsula and in seafloor sediments of the Davao Gulf (Quebral *et al.* 1996). The convex-to-east geometry of Sarangani Peninsula reflects the largest of the collision-stage thrust faults observed in southeast Mindanao.

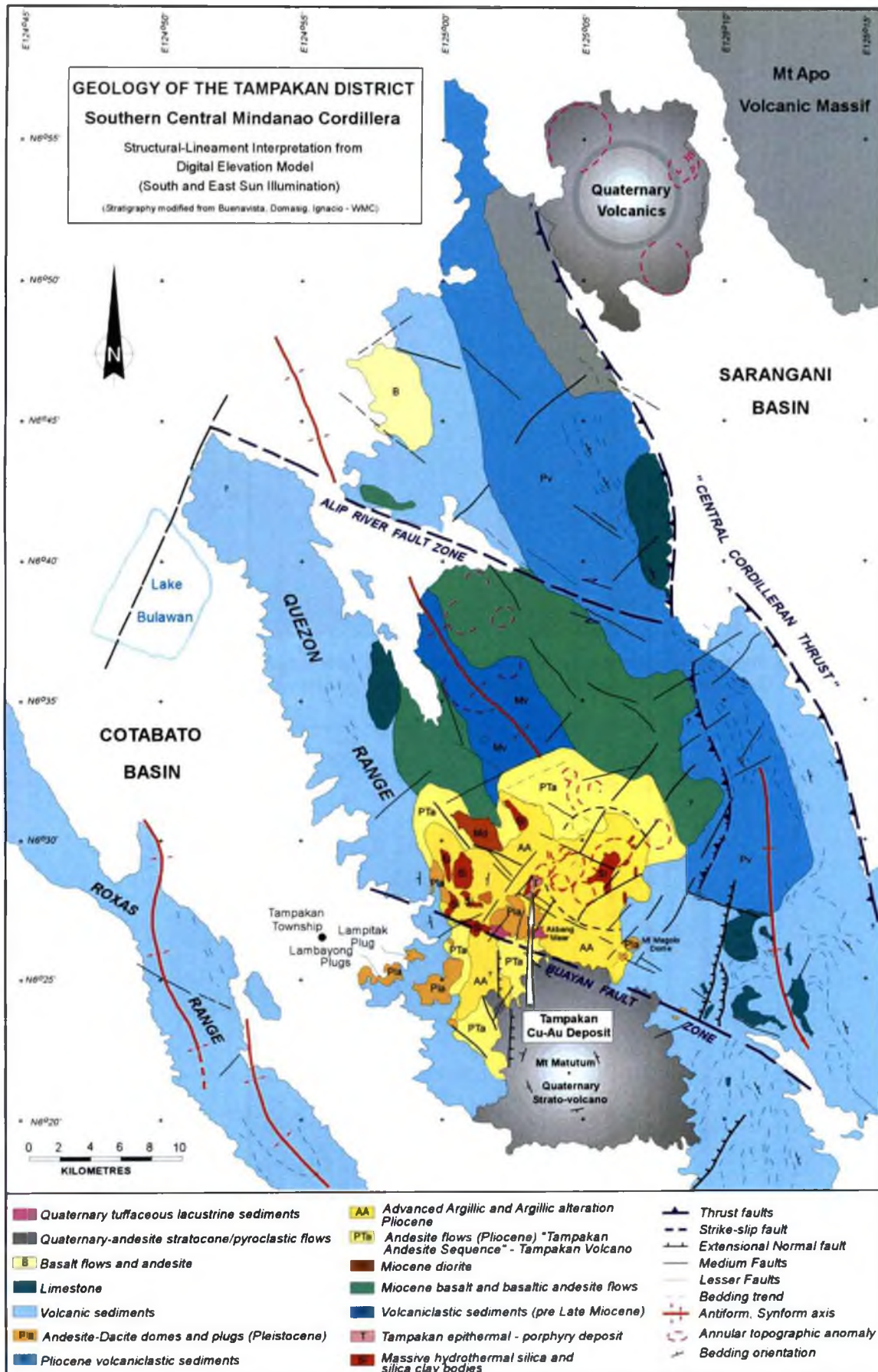


Figure 7: Geology of the Tampakan district, southern Mindanao.

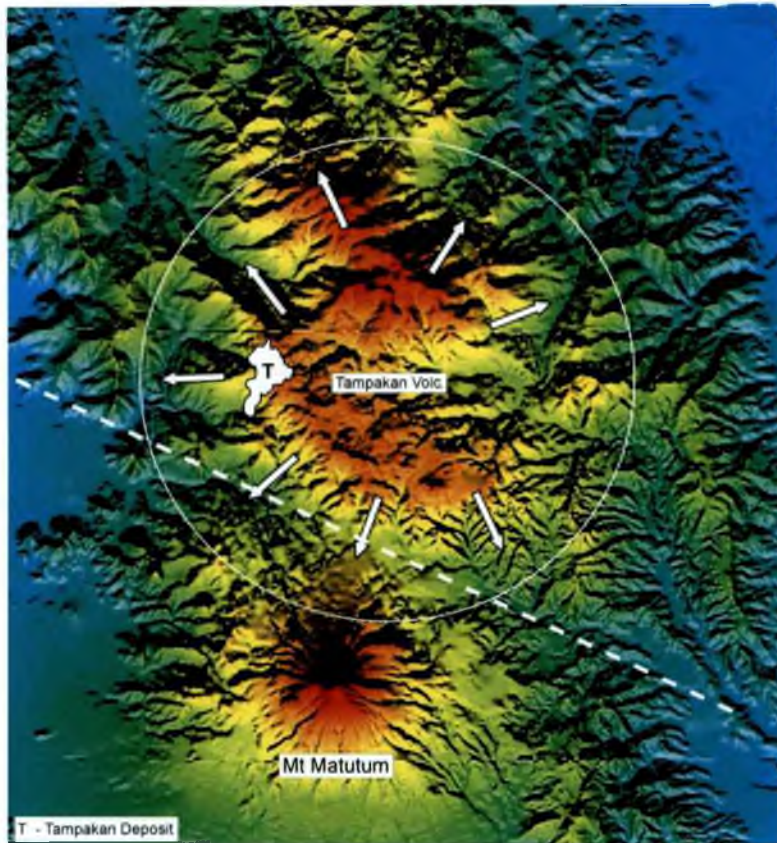


Figure 8: Digital terrain model of the Tampakan district enhanced by a digital illumination from the south. The Tampakan deposit (T) is located on the western rim of a deeply eroded mid-Pliocene-age andesitic stratovolcano.

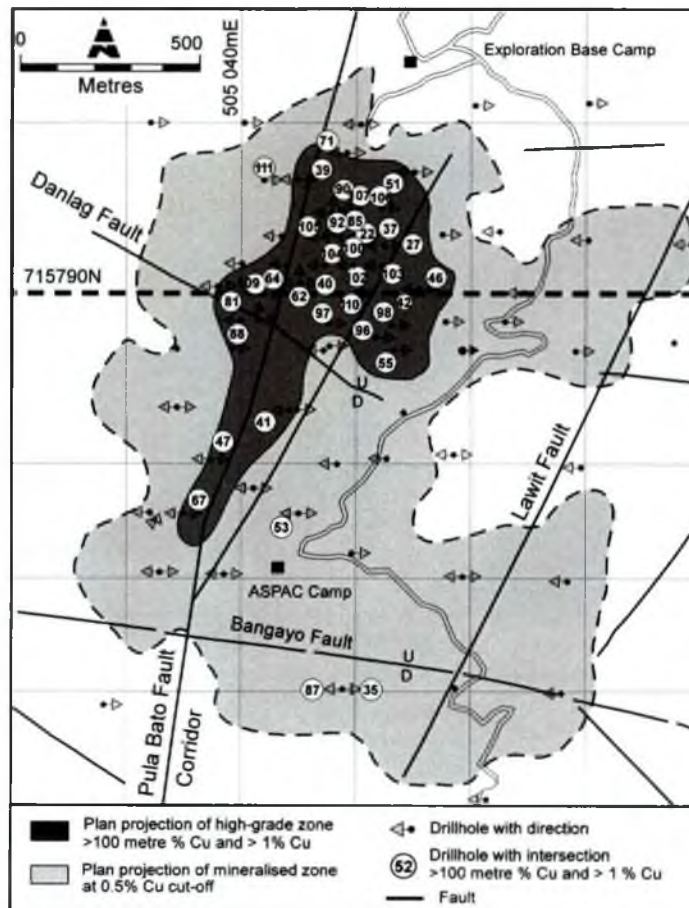


Figure 9. Plan of the projected outline of mineralisation above a cut-off of 100 metres at 1.0% Cu. The location of cross-section 715790 mN (Figs. 10a, b and 11) is shown. Diagram is modified from Middleton *et al.*, (2004).

mid-Pliocene age. They comprise porphyritic hornblende-pyroxene andesite and silicic andesite flows that dip at 10 to 20° towards the WSW, sub-parallel to the mineralised lithocap in the deposit. Hornblende-diorite porphyry stocks intrude the Tampakan Andesite Sequence in the deposit environs. They vary from holocrystalline and equigranular to crowded-porphry-textured intrusives with 70 to 80% phenocrysts. The intrusives form apophysis-like dykes and stocks, and tend to be altered but weakly mineralised.

High-sulphidation mineralisation displays both structural and stratigraphic controls. The Pula Bato Fault Zone comprises a NNE-trending series of faults that transect the Pliocene volcanic edifice and lie along the long-dimension of the Tampakan orebody. High-sulphidation mineralisation pinches downward along the NNE-trending Pula Bato Fault Zone, and mushrooms upward into a broad, manto-like, stratabound zone of advanced-argillic alteration that encapsulates the central zones of high-sulphidation ore. Detailed mapping of alteration assemblages using mineral infra-red spectra collected using a portable spectrometer (PIMA II; Rohrlach 2002) locally defines upward-flaring zones of advanced-argillic alteration that 'flower' into semi-concordance with stratigraphy at shallow levels. This geometry suggests the existence of structurally-rooted feeder faults with steep marginal alteration zones that flare at shallow levels where the faults intersect high-level zones of stratigraphic permeability. A detailed review of alteration textures within the deposit is presented in Rohrlach *et al.*, (1999).

The uppermost zone of hydrothermal alteration at Tampakan comprises argillic-altered porphyritic andesites (Fig. 10b) that overlie patchy zones of massive hydrothermal silica in the upper portions of the manto (Fig. 10a). The textures of the silica bodies include massive hydrothermal silica, multi-cycle silicified hydrothermal breccias, phenocrystic vuggy silica and clotted vuggy silica (Rohrlach *et al.*, 1999). Mineralisation within the silica bodies is typically fracture-controlled and comprises vug-filling sulphides, plus sulphides in hydrofractures, stringer veins and breccia veins. Common sulphide assemblages include i). bornite + digenite + enargite ± pyrite/tetrahedrite/molybdenite, ii). bornite + chalcopyrite + pyrite, and iii). late-stage pyrite + covellite. The silica bodies lie along the upper portion of the manto and are underlain by extensive domains of 'silica-clay' (50 to 90% free silica; Fig. 10a) and 'clay-silica' (10 to 50% free silica; Fig. 10a) that correspond to pyrophyllite + dickite and pyrophyllite + dickite + diaspore alteration assemblages (Fig. 10b). The close proximity of diaspore-bearing alteration zones immediately below zones of massive silica (Fig. 10b) reflect their high degree of acid leaching at shallower levels in the hydrologic system.

The massive silica bodies and the diaspore-bearing alteration zones 'collectively' define a nearly flat-lying blanket on section 715790 mN (Fig. 10b), although this zone of most intense acid-leaching has an overall gentle dip to the southwest across the orebody. Alunite is present in the advanced-argillic alteration zone, although it is rare due to the relatively low potassium content of the andesitic

precursor lithologies. Mineralisation becomes increasingly disseminated at deeper levels in the clay-silica alteration zones. The textures that are present in the pyrophyllite-, dickite- and diaspore-bearing zones of silica-clay alteration include massive silica-clay, porphyritic silica-clay and clotted silica-clay. These are described in detail by Rohrlach *et al.*, (1999) and are depicted in photographic plates in Rohrlach (2002) and Middleton *et al.*, (2004). The zone of higher-grade high-sulphidation mineralisation on section 715790 mN (>1.0% Cu) forms a blanket that is approximately 50 to 150 metres thick (Fig. 11) and coincides with the broad zone of silica-clay alteration. It overlies lower-grade mineralisation at depth that is associated with porphyry Cu ore that formed during a prior mineralising event. Sericitic alteration becomes increasingly prominent at deeper levels in the deposit. Shallow areas of pyrophyllite-dickite-sericite alteration are transitional to deeper zones of sericitic alteration that in turn are transitional downward to sericite-chlorite alteration.

The alteration textures within the advanced-argillic lithocap reflect upward-intensifying degrees of acid-leaching and silicification. The vertical increase in acidity of hydrothermal fluids progressively transformed pre-existing potassic and propylitic alteration assemblages to sericite-chlorite- and phyllic-altered andesite with good textural preservation. At shallower levels, increased intensity and duration of acidic alteration resulted in complete cation leaching to produce massive homogeneous silicified rock above several fluid conduits (Rohrlach *et al.*, 1999). The vertical zonation in alteration textures and mineralogy through the lithocap is produced by progressively increasing hydrolysis of magmatic SO<sub>2</sub> to H<sub>2</sub>S and H<sub>2</sub>SO<sub>4</sub> and subsequent, lower-temperature dissociation of H<sub>2</sub>SO<sub>4</sub> to yield H<sup>+</sup> ions in solution. These reactions progress to greater degrees at lower temperatures (Rye *et al.*, 1992). Mixing with oxidising meteoric ground water at shallower levels oxidised some H<sub>2</sub>S to H<sub>2</sub>SO<sub>4</sub>, further acidifying the fluids. Together, these sources of sulphuric acid account for the increasing degree of acid-leaching and residual silica enrichment at high levels.

High-sulphidation mineralisation is characterised by pyrite, bornite, enargite and digenite, with lesser chalcocite, chalcopyrite, covellite and molybdenite. Although the high-sulphidation-stage veins display variable mineralogy, there are several common sulphide associations that define broad stages of evolution from high-temperature hypogene assemblages to increasingly oxidised, low-temperature hypogene assemblages.

#### *Stage 1: Pyrite+Bornite+Enargite ± Chalcopyrite ± Molybdenite*

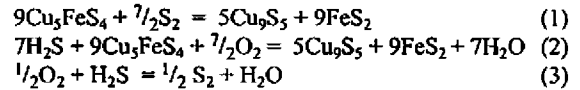
The earliest recognised stage of mineralisation comprises pyrite+bornite+enargite ± chalcopyrite ± molybdenite. An accessory sulphide assemblage occurs as microscopic blebs within bornite, and is characterised by a volatile element suite of Sn, V, Te and Sb. Colusite is a Cu-Sn-V-As-Fe sulphide that occurs with mawsonite (Cu-Fe-Sn sulphide) and goldfieldite (Te-bearing tetrahedrite) as fine anhedral inclusions within bornite.



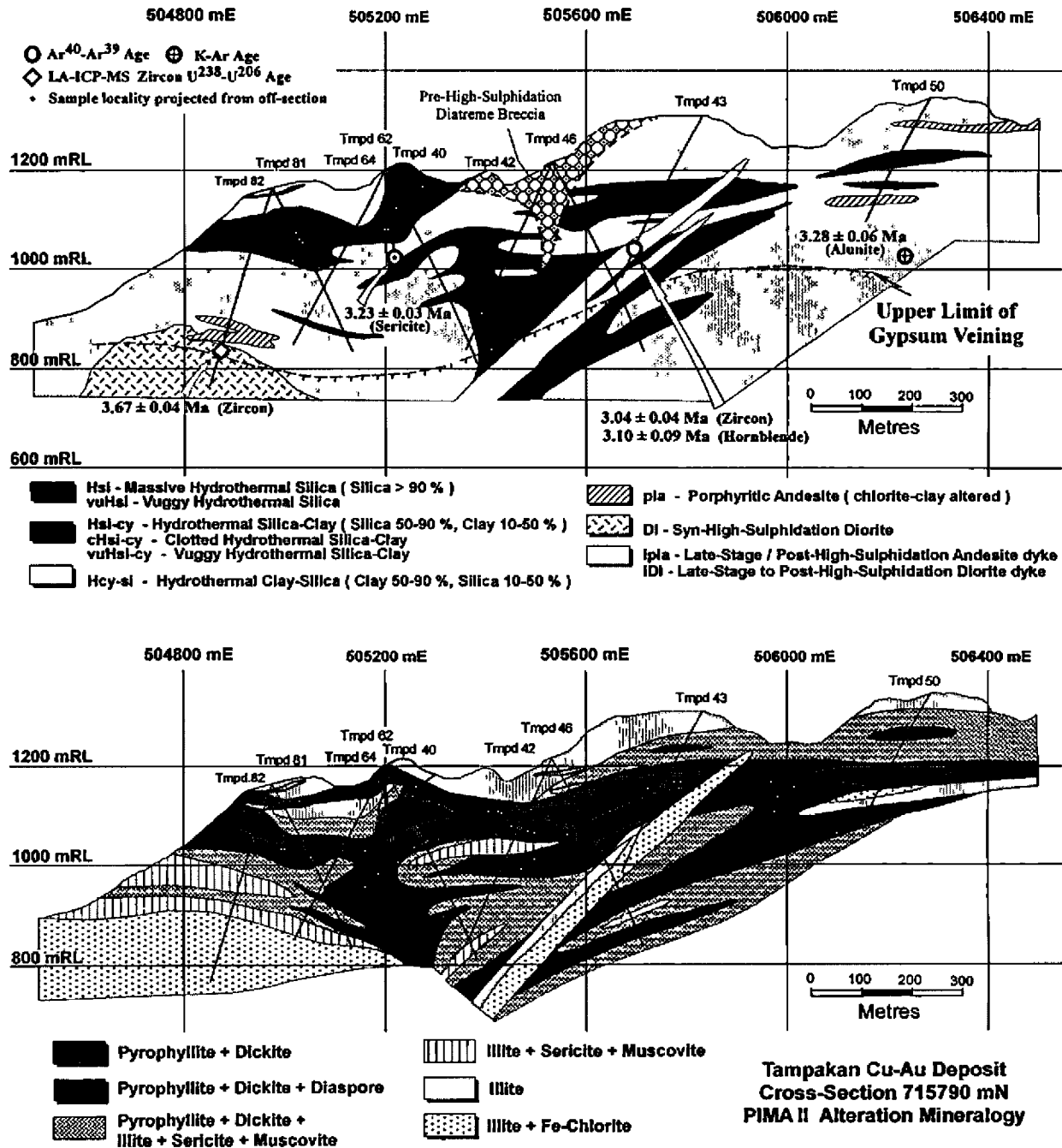
**Stage 2: Digenite+Chalcocite - High Temperature Oxidation.**

Digenite is abundant within the high-sulphidation deposit and occurs as an alteration product of precursor Stage 1 bornite. Digenite forms replacement masses that marginally replace and envelop Stage 1 sulphides. Light grey paramorphic or lamellar chalcocite is ubiquitous as an exsolution product from digenite. Both bornite and locally pyrite are unstable during the conversion of bornite to digenite; however the other sulphide phases of Stage 1 (chalcopyrite, enargite, colusite, mawsonite and goldfieldite) are texturally stable during the transformation. The alteration of

bornite to digenite may involve the sulphidation reaction (1) and/or the oxidation reaction (2).



Increasing oxidation of an early high-sulphidation assemblage (Stage 1) by the downward encroachment of the mixing interface between cool oxidised surface waters and dense ascending magmatic vapours, as the hydrothermal system wanes, may result in increasing  $f_{\text{O}_2}$  and production of  $\text{S}_2$  (3) in the  $\text{H}_2\text{S}$  stability field, both of which drive reactions (2) and (1) towards conversion of bornite to digenite.



**Figure 10:** (a, top) Representative geological cross-section 715790 mN through the Tampakan deposit, and (b, bottom) alteration zonation on section 715790 mN defined from 1160 mineral infra-red spectra acquired by a PIMA II portable spectrometer. Additional alteration cross-sections generated from acquisition of PIMA II infra-red data are sourced in Rohrlach (2002). Alteration assemblages on both diagrams above show an upward mushrooming morphology that is centered on the Pula Bato Fault corridor shown in Fig. 9.

### Stage 3: Pyrite+Covellite Veins

Late-stage pyrite+covellite veins are widespread within the upper portions of the lithocap, and overprint earlier sulphide assemblages. Paragenetically late alunite 'crackle veins' are commonly covellite-bearing. The alunite-covellite-pyrite assemblage reflects an increase in the oxidation state of the fluids as they cooled by mixing with shallow ground water, and reflects the transition to increasingly sulphate-dominated fluids as H<sub>2</sub>S within the hydrothermal fluid was progressively oxidised.

### Stage 4: Covellite+Idaite - Low Temperature Supergene Oxidation

Both covellite and idaite are widespread in the uppermost and oxidised portions of the lithocap, and in areas where further oxidation of pyrite and chalcocopyrite produce low temperature Fe-oxide assemblages. Idaite commonly forms as an alteration product of chalcocopyrite while digenite and chalcocite alter to covellite.

### Stage 5: Supergene Gypsum ± Covellite Veins

Late-stage fibrous gypsum veins consistently overprint all high-sulphidation-related clay veins. They are pervasive in the sericite-chlorite alteration zone and in the underlying relict potassic alteration zones, but are absent in the upper portions of the advanced-argillic zone. Their distribution at depth is restricted to below a sharp sub-horizontal transition zone, typically less than a metre wide, above which the advanced-argillic sequence is highly friable and lacks gypsum, and below which the rock is compact and heavily impregnated by gypsum (Fig. 10a). We interpret this boundary to have formed as a downward-migrating sulphate-saturation

front, whereby cool descending meteoric waters dissolved sulphate from the advanced-argillic alteration blanket at shallow levels and re-precipitated sulphate as low-temperature gypsum veins at depth. A subset of gypsum veins contain minute flecks of covellite, suggesting that they precipitated from low-temperature oxidised fluids.

The transition in sulphide assemblages from Stage 1 through to Stage 5 records a continuum from high-temperature hypogene mineralisation, to high- and medium-temperature hypogene oxidation and finally to lower temperature oxidation and supergene weathering. The primary high-sulphidation assemblage of bornite + enargite + pyrite + chalcocopyrite underwent continuous compositional adjustment as the hydrothermal system waned.

Isotopic and fluid inclusion evidence for fluid mixing between a vapour-rich two-phase magmatic fluid and meteoric waters at the base of the hydrostatically-pressured rock column within the volcanic edifice, and subsequent radial outflow of the hybrid fluids along a palaeo-aquifer on the western flank of the Tampakan volcanic complex, is discussed in the palaeohydrological study of Rohrlach (2002). The P-T-enthalpy-salinity-density coordinates for the high-sulphidation-stage magmatic fluids were calculated by Rohrlach (2002) for the site of two-phase magmatic fluid exsolution (~900°C, ~800 bars, >99% vapour with ~4.4 wt.% NaCl equiv.); immediately below the lithostatic-hydrostatic interface (two-phase fluid, ~500°C, P<sub>Lith</sub> ≅ 550 b, 96.9% vapour that holds 85% of the systems Cl); immediately above the lithostatic-hydrostatic interface (two-phase fluid, ~375°C, P<sub>Hyd</sub> ≅ 200 b, 61.7% vapour that holds 4% of the systems Cl after decompression); and at points along the mixing path in the

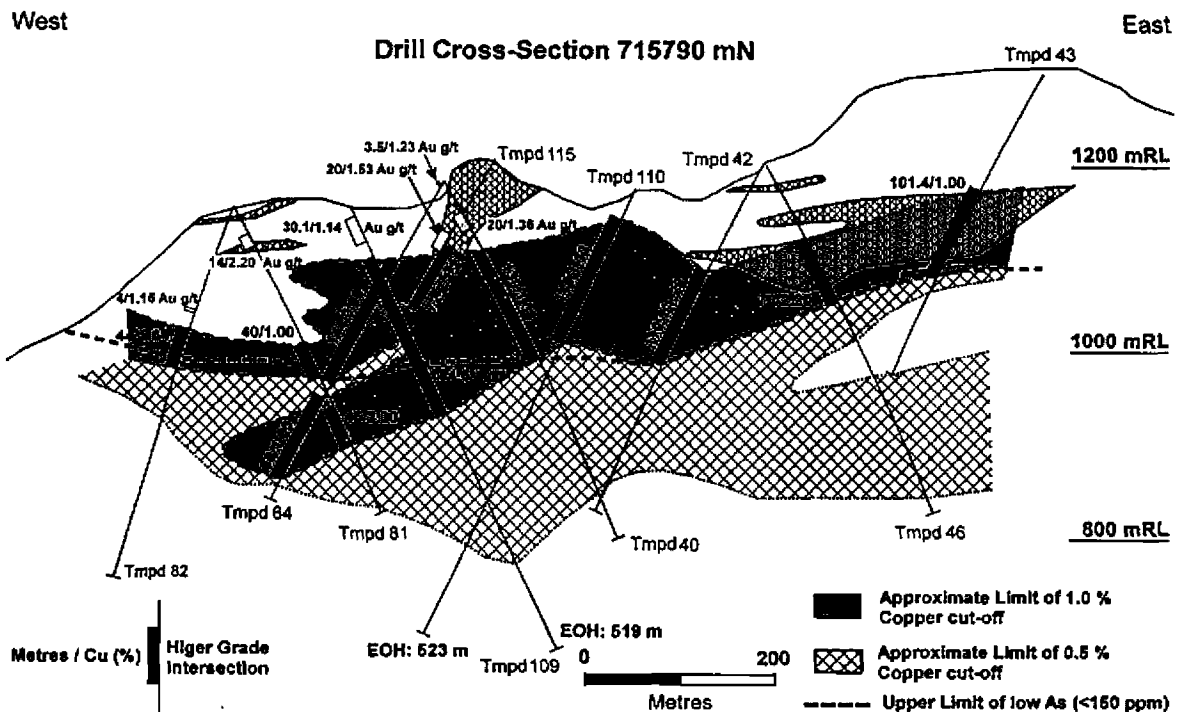


Figure 11: Significant assay intersections on section 715790 mN (modified from Middleton *et al.*, 2004). The zones of massive silica alteration are depicted by the tight cross-hachure pattern at shallow levels across the manto. Additional assay cross-sections through the deposit are presented in Middleton *et al.*, (2004).

hydrostatic domain (375–100°C,  $P_{\text{Sat}}$ ) (Rohrlach *et al.*, 2003). The high-sulphidation-stage magmatic vapour rapidly condensed during isoenthalpic decompression at the lithostatic-hydrostatic interface and cooled instantaneously from ~500 to 375°C. The condensed vapour was modestly saline (~5 wt.% NaCl) and mixed with meteoric water at a constrained depth of ~2 km. Most of the exsolved magmatic chloride (~81 to 85%, and metal) was transported through the ductile rock column to the site of ore deposition by a dense vapour phase.

### Porphyry-Cu Mineralisation

Porphyry Cu-Au mineralisation is widespread in the lower part of most drill-holes that penetrate below the high-sulphidation mineralisation into the zone of sericite-chlorite alteration. The principal sulphide and oxide minerals in equilibrium with porphyry-stage anhydrite-biotite-alteration are chalcopyrite, bornite, pyrite, magnetite (up to 8%), subordinate specular hematite and molybdenite. Porphyry-Cu mineralisation is dominated by pink-grey coloured, multi-directional, crudely laminated veins with medial crack-seal textures that contain traces of bornite and/or chalcopyrite and/or pyrite. Anhydrite-bearing veins are less prevalent. Chalcopyrite is the dominant sulphide and occurs as disseminated grains, as anhedral inclusions within and along the margins of hydrothermal magnetite grains, and as elongate laths that extend along cleavage planes of hydrothermal biotite grains. Bornite is subordinate to chalcopyrite, and both these sulphides are always in textural equilibrium, often forming composite sulphide grains. Molybdenite and hematite are minor phases in the potassic alteration zone. Porphyry-stage sulphides also occur as fracture-controlled disseminations within the wallrock to quartz-dominated and lesser anhydrite-bearing veins.

The porphyry sulphide assemblage lacks the association of enargite/digenite/chalcocite/covellite that is typical of the overprinting high-sulphidation epithermal mineralisation. The chalcopyrite+bornite+pyrite mineral association occurs within the sericite+chlorite alteration zone and areas of relict potassic alteration in the deepest drill tested portions of the deposit. At higher levels within the phyllic and lower advanced-argillic facies, the porphyry quartz veins are grey-coloured and bleached as they become over-printed by acidic conditions of the significantly younger advanced-argillic lithocap. Porphyry quartz veins are *only* observed in the lower portion of the lithocap below an unconformity between magmatic cycles 3 and 4a that unroofed the porphyry system prior to high-sulphidation mineralisation (see 'Geochronology' below). Specular hematite is more abundant within the outer sericite+chlorite alteration facies than in the inner potassic biotite-anhydrite-magnetite zone. The presence of hypogene hematite – locally replaced by chalcopyrite – may reflect more oxidised conditions at shallower levels where Cp+Py+Hem ( $\pm$  Mt  $\pm$  Bn) occurs in preference to Cp+Py+Mt ( $\pm$  Bn) in the porphyry-stage ore.

### Geochronology

Forty-four radiometric ages from 28 representative lavas, intrusive plugs and dykes from the Tampakan volcanic complex, and limestones from the surrounding district, were dated by either  $^{40}\text{Ar}$ - $^{39}\text{Ar}$  step-heating, K-Ar total fusion, zircon  $^{238}\text{U}$ - $^{206}\text{Pb}$  by excimer laser-ablation ICP-MS, or by correlation of limestone  $^{87}\text{Sr}$ / $^{86}\text{Sr}$  with the secular variation of  $^{87}\text{Sr}$ / $^{86}\text{Sr}$  in Neogene seawater as given by Hodell *et al.*, (1990). Only a brief summary of dating results can be presented here; see Rohrlach (2002) for a detailed account of methods and results.  $^{238}\text{U}$ - $^{206}\text{Pb}$  ages were also obtained

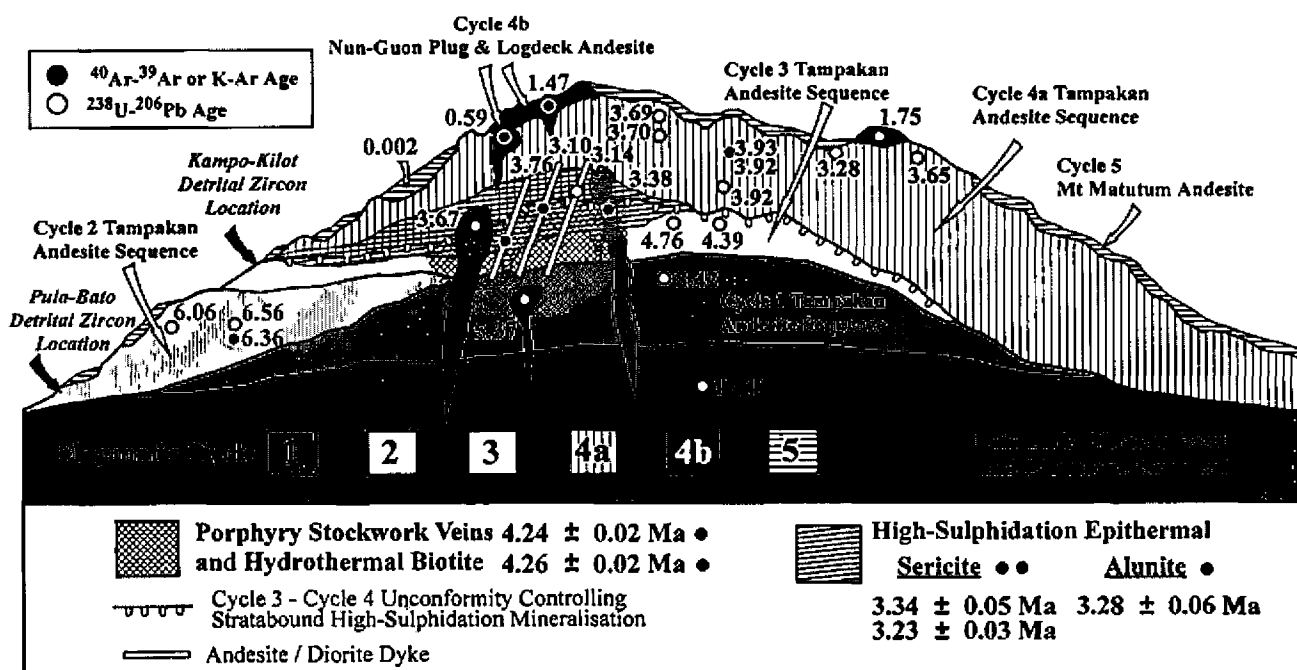


Figure 12: Schematic east-west profile looking north through the Tampakan igneous complex and showing the age relationship of magmatic and hydrothermal events. Ages obtained for magmatic sequences are shown on the diagram, whereas ages obtained for the alteration minerals are shown in the legend. Porphyry mineralisation was exposed at the surface during the early Pliocene by an erosional unconformity that separates Cycle 3 from Cycle 4a magmatism. High-sulphidation mineralisation was localised along this unconformity during the latter part of Cycle 4a magmatism and stratocone rebuilding.

by laser ablation ICP-MS for two suites of detrital zircons that were eroded from the western flank of the Tampakan volcanic complex. The age dating constrains stages of uplift, erosion, sedimentation, folding and faulting, and tightly constrains the duration and the timing of petrochemical evolution of the Tampakan magmatic system and the timing of porphyry Cu and high-sulphidation Cu-Au mineralisation. Two sets of detrital zircons from streams that drain the western flank of the volcanic centre at Pula Bato and Camp Kilot (Fig. 12) yielded 144 representative detrital zircon ages by ELA-ICP-MS. The frequency of detrital zircon ages reveals a long history of zircon crystallisation, and hence magmatic activity that extended from 7.29 Ma to the Holocene. Four episodes of profuse magmatic/volcanic activity (Fig. 13) are defined by peaks in age frequency that extend from ~7 to 6 Ma (late Miocene cluster), 5.3 to 4.1 Ma (Early Pliocene cluster), 3.6 to 2.5 Ma (Middle Pliocene cluster) and 0.3 Ma to the present (Late Quaternary cluster) (Fig. 13). The whole-rock igneous and volcanic rock ages from the Tampakan district coincide with the three early peaks in detrital zircon ages, and corroborate three principal episodes of volcanism that erupted during the Late Miocene, Early Pliocene, and Middle Pliocene.

#### Volcanic History

Geochronologic studies reveal that the Tampakan district has experienced frequent and extensive magmatic activity over the past 8.5 M.y. An episodic and long-lived succession of andesitic stratovolcano-building events extended from the late Miocene to present, and are separated by erosional unconformities. These episodes of volcanism and magmatism are here termed magmatic Cycles 1 to 5. Cycles 2, 3, 4a and 5 were major stratocone-building events.

The oldest dated rocks in the Tampakan district are limestones that are intercalated with porphyritic augite-phyric basaltic andesites that underlie the Tampakan volcanic complex. The  $^{87}\text{Sr}/^{86}\text{Sr}$  of a reefal limestone unit sampled from the southeast side of Mt Matutum indicates an upper early Miocene age of 17 Ma (Fig. 12). The intercalated basement basalts are folded about a broad NNW-trending anticline, so the limestone age places a lower age limit on folding within the district. The oldest dated andesite that erupted onto this basement has an age of  $8.34 \pm 0.32$  Ma obtained by  $^{238}\text{U}$ - $^{206}\text{Pb}$  on zircons from an andesite unit near the base of drill-hole Tmpd 8, deep in the Tampakan porphyry deposit. This event is not represented in the detrital zircon dates, which suggests that the sequence is not exposed on the western flank of the volcanic centre. A 7 to 6 Ma basaltic-andesite to andesite sequence is well represented in detrital zircon populations (Figs. 12 and 13). This age cluster is also represented by two  $^{238}\text{U}$ - $^{206}\text{Pb}$  zircon ages of  $6.06 \pm 0.04$  Ma and  $6.56 \pm 0.05$  Ma, and a  $^{40}\text{Ar}$ - $^{39}\text{Ar}$  age of  $6.36 \pm 0.05$  Ma, which were taken from outcrops of lavas at low elevations along the northwest and southwest flank of the volcanic centre. They lie deep in the Tampakan volcanic pile and belong to Cycle 2 magmatism (Fig. 12). They form part of an underlying and deeply eroded volcanic centre that developed in the late Miocene. Andesites of this age have not been identified in dated samples from drill-holes in the

Tampakan orebody, despite the occurrence of older and younger cycles in the deposit. Cycle 2 volcanics may have been completely eroded down to the Cycle 1 substrate below the Tampakan deposit, where they occurred at higher elevations of the volcanic complex.

The Cycle 1 sequence in the lowermost part of drill-hole Tmpd 8 is intruded by a diorite stock dated by  $^{238}\text{U}$ - $^{206}\text{Pb}$  (zircon) at  $5.3 \pm 0.3$  Ma (Figs. 12 and 13). The stock is overprinted by porphyry-ore-stage quartz veins associated with disseminated biotite-chlorite-anhydrite alteration. This age correlates with the onset of a second, albeit subdued, rise in age frequency of detrital zircons (Fig. 13), which extends from ~5.3 to 4.1 Ma. Two  $^{238}\text{U}$ - $^{206}\text{Pb}$  (zircon) ages of  $4.39 \pm 0.08$  Ma and  $4.76 \pm 0.06$  Ma were obtained from andesites collected from the deeper portions of drill-holes Tmpd 34 and 87. These pre-mineralisation lavas host porphyry-Cu-stage quartz veins, and belong to an early Pliocene, Cycle 3 magmatic event that erupted during a third phase of volcanic edifice construction extending from ~5.3 to 4.1 Ma (Fig. 13), following substantial erosion of the underlying Cycle 2 volcanic edifice (Fig. 12).

Cycle 4 units of the Tampakan Andesite Sequence are extensively dated. They define a middle Pliocene stage of stratocone construction (Cycle 4a) and a late Pliocene to Pleistocene stage of evolved andesitic to dacitic intrusives and volcanic plugs (Cycle 4b). Cycle 4a andesite lavas occur in the upper portion of the drill-holes in the deposit and host high-sulphidation mineralisation and associated advanced-argillic alteration but *lack porphyry-stage quartz veins*. The andesite lavas in drill-holes Tmpd 13 and 33, surface exposures of andesite on the Tampakan drill grid, and numerous high-elevation outcrops in the district are dated as middle Pliocene age and belong to the Cycle 4a andesitic stratocone that is recognisable in the DTM image (Fig. 8). These flows are intruded by dykes and stocks of pre-, syn- and post-high-sulphidation age. The age distribution of rocks dated from the Cycle 4a sequence is broadly coeval with the third peak in frequency of detrital zircons (Fig. 13). Cycle 4b magmatism is represented in the detrital zircon dataset by a minor cluster of 3 detrital zircon ages between 1.8 and 1.3 Ma (Fig. 13). The paucity in ages is consistent with their isolated and scattered outcrop distribution, comprising small, evolved andesitic to dacitic intrusive plugs and extrusive flow-dome complexes located around the southern and southwestern quadrant of the volcanic centre. The Logdeck Andesite, which overlies the southern part of the Tampakan orebody, yielded an age of  $1.47 \pm 0.05$  Ma by  $^{40}\text{Ar}$ - $^{39}\text{Ar}$ . A hornblende-bearing andesite in the southeast quadrant of the Cycle 4a Tampakan volcanic edifice contained zircons dated at  $1.75 \pm 0.16$  Ma. A K-Ar age of 1.47 Ma was obtained for the Lote Plug, and a K-Ar age of 0.86 Ma was determined for the Lambayong volcanic plug (Sajona, 1994). The Nun-Guon plug was dated as  $0.59 \pm 0.03$  Ma by  $^{40}\text{Ar}$ - $^{39}\text{Ar}$  and as  $0.59 \pm 0.02$  Ma by K-Ar. Cycle 4b dacites of Pleistocene age mark a transition to dacitic magmatism. They are widely distributed and do not form a major stratovolcanic edifice in the manner of magmatic Cycle 4a. The youngest magmatic event recorded by the detrital zircon  $^{238}\text{U}$ - $^{206}\text{Pb}$  data is the pyroclastic cover sequence that erupted onto the

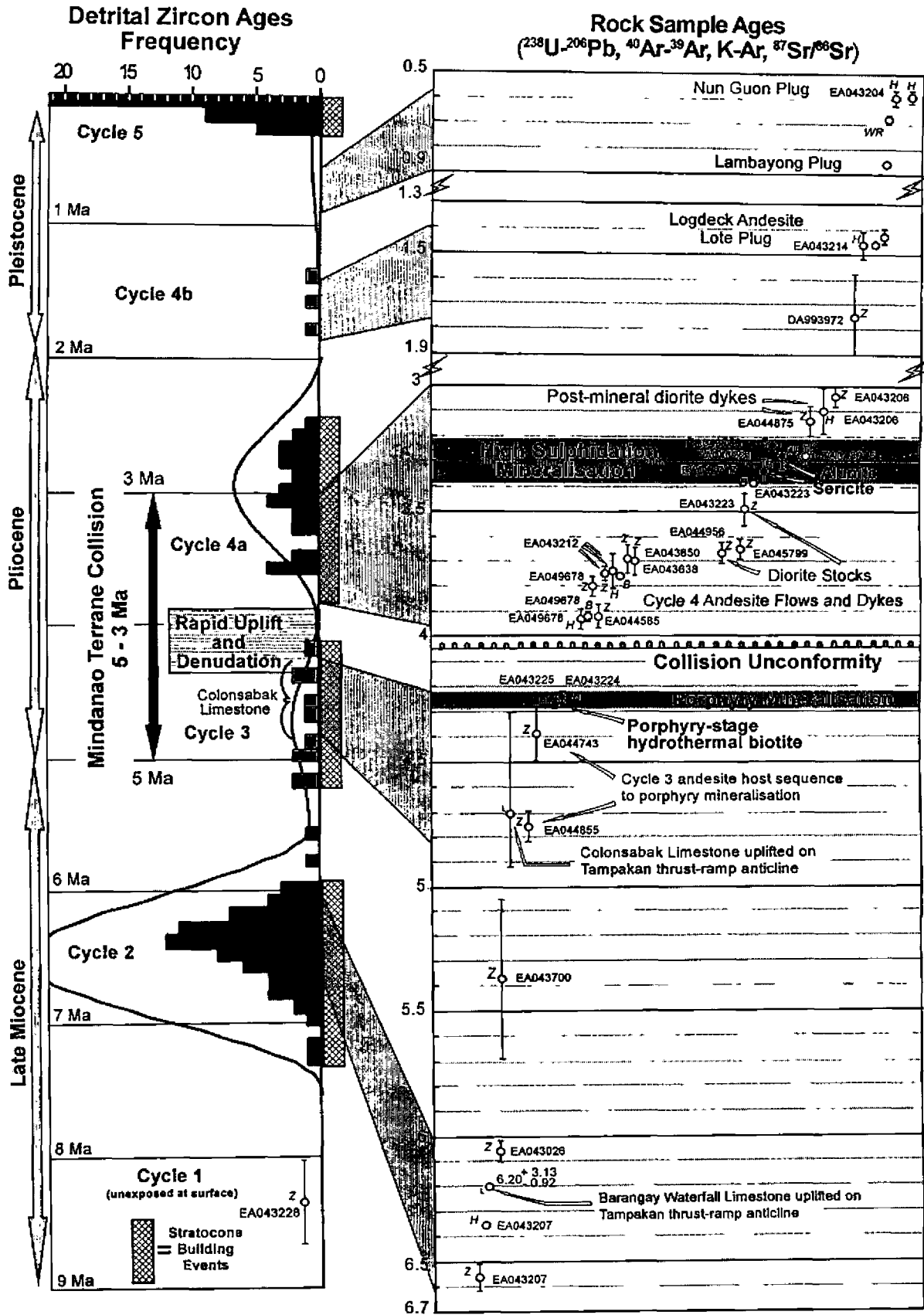


Figure 13: Time sequence of volcanic and intrusive magmatic rocks in the Tampakan district, illustrating the principal stratocone-building events and erosional unconformities. Ages of detrital zircon grains collected from the west flank of the volcanic complex are shown on the left panel and define four peaks of magmatic activity. Corresponding rock ages are shown on the right-hand side. Abbreviations: Z = zircon <sup>238</sup>U-<sup>206</sup>Pb age; H, B, S = hornblende, biotite and sericite <sup>40</sup>Ar-<sup>39</sup>Ar age; L = limestone <sup>87</sup>Sr/<sup>66</sup>Sr age; Al = alunite K-Ar age, and WR = whole-rock K-Ar age.

incised Tampakan volcanic edifice from the overlapping Mt Matutum stratocone, the youngest volcano in the complex, which was constructed during the last 300 Ka.

### *Ages of Mineralisation*

Porphyry mineralisation is dated by  $^{40}\text{Ar}$ - $^{39}\text{Ar}$  ages on two samples of hydrothermal biotite from a relict potassic alteration facies near the base of drill-hole Tmpd 8. Two concordant ages of  $4.24 \pm 0.02$  Ma and  $4.26 \pm 0.02$  Ma indicate that porphyry mineralisation occurred near the end of magmatic Cycle 3. These ages post-date Cycles 1 and 3 dates for rocks that host the lower portions of the porphyry Cu deposit. The hydrothermal biotite dates are minimum ages, as they record the time at which biotite cooled below its closure temperature for argon loss. Nevertheless, the true age of porphyry mineralisation must lie between the 4.25 Ma average date of the biotite samples and the 4.39 Ma date for the youngest Cycle 3 andesite sample that hosts porphyry veins.

The high-sulphidation mineralisation event is constrained by three concordant K-Ar and  $^{40}\text{Ar}$ - $^{39}\text{Ar}$  ages obtained from hydrothermal alunite and sericite. The alunite was extracted from covellite+pyrite-bearing veins and has an age of  $3.28 \pm 0.06$  Ma. This is concordant with two  $^{40}\text{Ar}$ - $^{39}\text{Ar}$  ages of  $3.34 \pm 0.05$  and  $3.23 \pm 0.03$  Ma obtained from hydrothermal sericite within the advanced-argillic lithocap. Thus the age of high-sulphidation mineralisation is constrained to lie between 3.39 and 3.20 Ma at the level of one standard-deviation uncertainty of the ages. These ages are consistent with the  $3.93 \pm 0.04$  Ma to  $3.69 \pm 0.06$  Ma age range of Cycle 4a andesite flow units in the upper portions of the Tampakan deposit that are altered by the high-sulphidation event, and with the  $3.14 \pm 0.06$  Ma and  $3.04 \pm 0.04$  Ma age of two weakly altered, post-mineralisation andesite and diorite dykes that post-date acid-sulphate alteration (Fig. 13).

The difference between the mean age of the two porphyry-stage biotite samples ( $4.25 \pm 0.01$  Ma) and the mean age of the three high-sulphidation-stage sericite and alunite ages ( $3.26 \pm 0.02$  Ma) is a million years. This interval is significantly greater than the possible lifespan of a major porphyry system (Cathles *et al.*, 1997). The Lepanto high-sulphidation epithermal and Far Southeast porphyry deposit "pair" are associated with a hydrothermal system of ~300 000 years duration (Arribas *et al.*, 1995), and the Ladolam deposit evolved from a porphyry to epithermal environment over a similar duration of ~300 000 years (Moyle *et al.*, 1990). The Tampakan porphyry and high-sulphidation epithermal deposits formed from separate magmatic-hydrothermal systems, and although they are not products of the same high-level volcano-scale hydrothermal system, they are related in the context of a consanguineous succession of igneous intrusions from the same deep lower-crustal magmatic reservoir (see the 'Petrochemistry, Magma Mixing and Volatile Ramping' and 'Magmatic Physico-Chemical Properties' sections below).

### *Constraints on Uplift and Unroofing*

Cycle 4a eruptive units dated at between 3.93 and 3.69 Ma lack porphyry-stage quartz veins but host high-sulphidation

mineralisation and alteration, and lie directly on Cycle 3 and Cycle 1 andesites which host porphyry-stage quartz veins associated with hydrothermal biotite of 4.26 to 4.24 Ma in age. These geochronological data and the contrasting depth regimes of the two mineralisation types reveal the presence of a major unconformity representing kilometre-scale erosional loss between preserved units of eruptive Cycles 3 and 4a. The unconformity has not been identified texturally in drill-core due to the extensive acid-sulphate alteration, silicification and hydrothermal brecciation, suggesting the unconformity may have served as an aquifer for palaeo-ground-water flow, which ascending magmatic volatiles condensed to form the stratabound high-sulphidation system. This unconformity is responsible for unroofing the porphyry system to depths near the outer edges of its potassically-altered core in the time frame between hydrothermal biotite alteration at 4.24 to 4.26 Ma (or ~50 K.y. prior, to allow for cooling of hydrothermal biotite through its closure temperature) and the commencement of eruption of Cycle 4a andesites at 3.93 Ma. Some 2 km or more of overburden must have been eroded from above the Tampakan porphyry system within a time-frame of ~370 K.y. An anomalously high erosion rate of 5.4 mm/year over a 370 K.y. time frame is required to remove ~2 km of overburden from above the lithostatically-pressured porphyry veins. The long-term average erosion rate for the Tampakan volcanic centre between 3 Ma and the present, based on reconstruction of volcanic topography, is 0.75 mm/year – identical to the estimate by Ruxton and McDougall (1967) for long-term erosion of a similar stratovolcano in nearly identical climatic conditions in New Guinea. The geochronologically constrained rate of erosion for the Tampakan Cycle 3 sequence between 4.30 Ma and 3.93 Ma (assuming ~2 km of unroofing), prior to eruption of the Cycle 4a sequence on the unroofed porphyry system, implies catastrophic landslides and/or volcanic sector collapse during the pulse of rapid uplift associated with thrust-and-fold deformation of early Pliocene age. Crustal compression, collision-stage thrust faulting and attendant uplift were in maximum effect in the time interval during porphyry and younger high sulphidation mineralisation at Tampakan. The erosional unconformity between Cycles 3 and 4a magmatism became an important control on the distribution of younger high-sulphidation mineralisation within the deposit.

## **Petrochemistry**

In the Tampakan district, volcanic and hypabyssal intrusive rocks comprise porphyritic basaltic andesites, andesites, silicic andesites and dacites that record magmatic evolution processes during an arc-arc-collision event that generated the world-class Cu-Au ore system. The time series of chemical variations from basaltic andesite to dacite define multiple cycles of magmatic differentiation in lower-crustal and sub-volcanic magma chambers that fed a succession of overlapping volcanic centres that developed during the late Miocene to Recent epochs. They are highly oxidised calc-alkaline magmas having petrochemical features typical of subduction-generated arc magmas, such as relative enrichment in the large-ion-lithophile elements Cs, Rb, Ba,

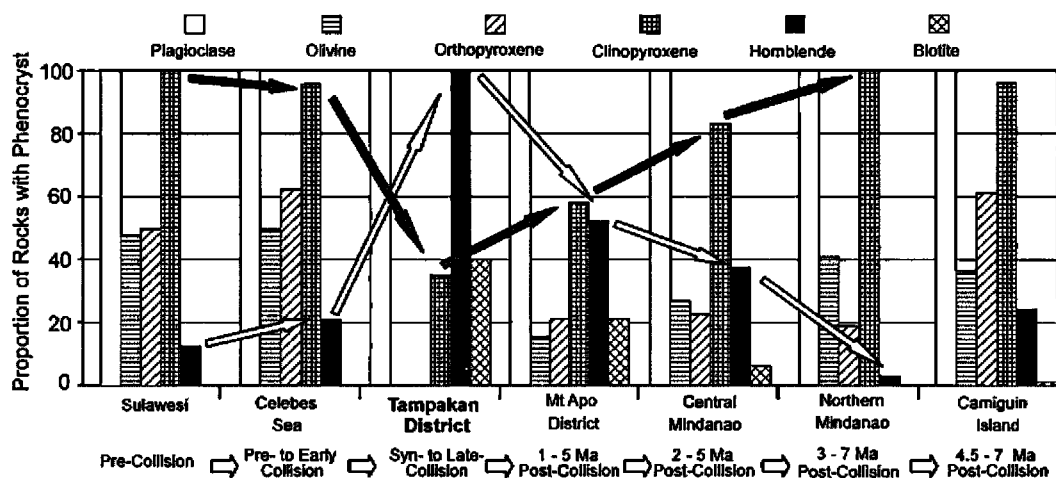
U, K, Pb and Sr due to transport of these fluid-mobile elements from the slab into the source region of the melts. They also exhibit typical arc-type relative depletions in the high-field-strength elements Nb, Ta and Ti. Pliocene-Pleistocene members of the suite display petrochemical signatures atypical of felsic arc magmas, such as high abundances of Sr and Eu and exceptional depletions of Y and heavy REE's that are explicable by protracted fractionation of magmas in the lower crust under high pressure and high magmatic water activity. The principal petrographic distinction of the Tampakan igneous suite is the high abundance of hydrous minerals such as hornblende and biotite in basaltic andesites as well as in more evolved andesites, silicic andesites and dacites. The hydrous mineral phases become modally more abundant over time. The post-middle-Miocene magmatic rocks evolved from ordinary augite-bearing basaltic andesites that lack hydrous phenocryst phases in the latest Miocene, to augite-hornblende andesites in the early Pliocene, to a predominance of pyroxene-free, hornblende- and biotite-bearing silicic andesites in the middle Pliocene and Pleistocene. During the tectonic collision that affected the Tampakan district, there was a progressive increase in the modal abundance of hydrous mineral phases in erupted magmas, a decrease in the modal abundance of anhydrous mineral phases, and an appearance of the hydrous mineral phases, hornblende and biotite, at successively earlier (less silicic) stages of the crystallisation sequence.

#### Along-Arc Variations in Mineralogy

Analyses of magmatic rocks from the succession of igneous complexes along the Sangihe arc allow investigation of the petrologic and petrochemical variations, from south to north, in the context of their pre-, syn- and post-collision tectonic settings. The increase in modal abundance of hydrous mineral species that are observed in the Tampakan segment of the Sangihe arc during the ~0-6 Ma period of arc compression is also reflected in along-arc variations of

the proportion of rocks with hydrous phenocryst phases. Pre-collision magmatism associated with active subduction currently occurs off the northern portion of Sulawesi in the southern Molucca Sea between 0 and 4°N. A presently active collision zone occurs in the northern Molucca Sea between 4 and 6°N where magmatism is sparse compared to the pre-collisional areas farther south. Late Neogene magmatism associated with early- to syn-collision and slab stalling occurs in southeastern and central Mindanao (6 to 9°N) in the Tampakan and Mt Apo districts, whereas Plio-Pleistocene post-collisional magmatism occurs in northern Mindanao and further northward to Camiguin Island (~9.2°N). Igneous petrochemical data were compiled from this extensive section of the Sangihe arc along which the southward-propagating collision zone has migrated during the Late Neogene and Quaternary. Data compiled from Corpuz, (1992), Castillo *et al.*, (1999), Elburg and Foden, (1998), Morrice *et al.*, (1983), Polve *et al.*, (1997), Prouteau *et al.*, (2000), Sajona *et al.*, (1994, 1997, 2000) and Tatsumi *et al.*, (1991) span ~8.3 degrees of latitude (0.9 to 9.2°N; ~960 km) along the arc. There is a latitude-dependant variation in the degree of differentiation of young (<5 Ma) igneous rock types. The Tampakan district contains the highest proportion of evolved magmatic rocks, with  $\geq 60\%$  SiO<sub>2</sub>, compared to arc segments farther north and south. Rocks from the neighbouring Mt Apo district north of Tampakan also have a high proportion of evolved andesites and dacites, reflecting advanced magmatic differentiation. These districts are the only two that contain syn-collisional to recent post-collisional magmatism. The northern Molucca Sea (4 to 6°N) is currently undergoing collision, but the paucity of subaerial magmatism in this latitude interval precludes statistically reliable petrological comparison with the Tampakan and Mt Apo districts.

Fig. 14 illustrates regional systematic trends in the proportion of rocks containing olivine, orthopyroxene, clinopyroxene, hornblende and biotite as phenocrysts, from



**Figure 14:** Along-Sangihe-arc trends in the proportion of magmatic rocks that contain anhydrous phenocrysts (plagioclase, olivine, orthopyroxene, clinopyroxene) and hydrous phenocrysts (hornblende, biotite). Systematic trends are observed northward along the Sangihe arc that reflect a rise in magmatic water activity as the arc becomes increasingly compressional in the Sulawesi to Tampakan interval, with a corresponding increase in the proportion of hydrous mineral phases that are stabilised by the high water activities. Northward from Tampakan, there is a gradual decrease in the proportion of hydrous mineral phases, and increase in anhydrous phases, as the horizontal compressive stress is relieved increasingly by subduction along the Cotobato Trench to the west and by the Philippine Trench to the east. The Late Neogene and Quaternary (<5 Ma) syn-collisional rocks from the Tampakan district lie at the peak of the spatial trends in rising magmatic water activity and proportional abundance of hydrous mineral phases.

south-to-north between the six southernmost districts within the Sangihe arc. These volcanic rocks erupted in varying stress fields associated with their pre-, syn- or post-collision setting during the Late Neogene and Quaternary. The Tampakan district is unique relative to the adjacent non-mineralised districts in that magmatic rocks of <5 Ma lack olivine and orthopyroxene. These smooth trends indicate that hornblende progressively becomes more dominant as the arc is traversed from actively subducting regions in a pre-collision setting (northeastern Sulawesi), to marginal areas undergoing early collision (Celebes Sea), and then to syn-collision and late-collision segments of the arc (Tampakan district). Hornblende progressively, and eventually totally, usurps clinopyroxene and orthopyroxene as the principal mafic phenocryst phase in rocks with >54 wt % SiO<sub>2</sub>. Likewise, a traverse northward along the arc from areas of active collision (Tampakan district) to areas of increasingly post-collision magmatism (Mt Apo district, central Mindanao and northern Mindanao) is associated with trends in which hornblende-bearing rocks decrease in their proportional abundance, and an antithetic trend in which the proportion of rocks with clinopyroxene as a phenocryst phase increases.

The net effect of crustal stress on magmatic differentiation along the Sangihe arc is that volcanism becomes increasingly silicic and hydrous (hornblende ± biotite-bearing) as horizontal compressive stress within the lithosphere increases from that of normal subduction to collision. The reverse trend occurs as the stress within the lithosphere is progressively relieved after collision by initiation of new subduction zones, the Cotobato and Philippine Trenches west and east of the central Mindanao orogen. That is, erupted magmas become less evolved, less hydrous and progressively more clinopyroxene-bearing (at the expense of hornblende) as collisional stress is relieved along new subduction zones.

### Rare Earth Element Chemistry

The lanthanide elements and yttrium are useful as indicators of the identities and approximate proportions of cumulus minerals involved in differentiation processes that produced samples of evolved melts from normal arc-basaltic parents. Seven selected N-MORB-normalised REE profiles for the Tampakan igneous suite are presented in Fig. 15. The middle Miocene Sulop basaltic andesite sequence (sample EA045800) displays a REE pattern of relatively flat middle (MREE) to heavy (HREE) rare earth elements that reflects a combination of pyroxene and plagioclase fractionation, similar to the MORB pattern and consistent with the lack of hornblende in petrographic samples. It exhibits a strong negative Eu anomaly due to a predominance of plagioclase fractionation. The sample is a plagioclase-olivine-pyroxene basalt and represents volcanism in the Tampakan sector of the Sangihe arc during normal subduction, prior to the late Miocene onset of compression.

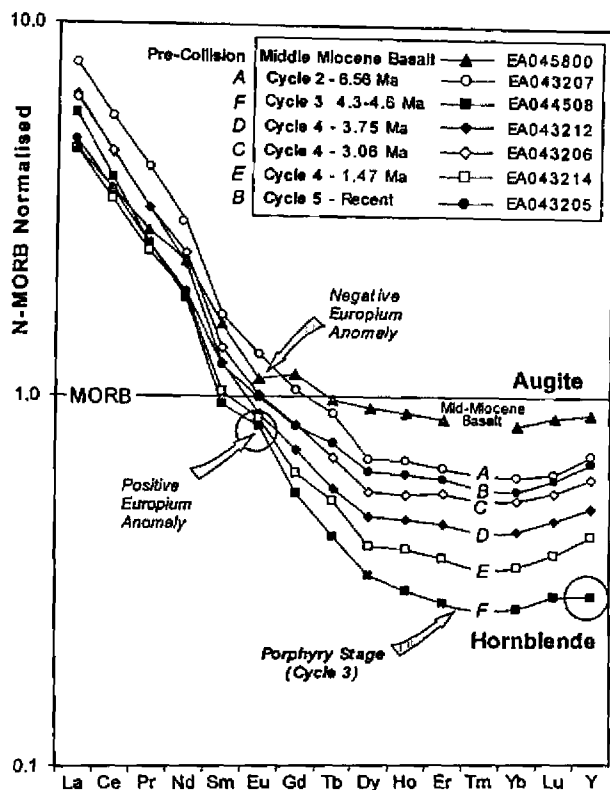
The Cycle 2 magmatic sequence represented by sample EA043207 (6.56 Ma; Figs. 12 and 15) shows a slight concavity in the shape of the HREE patterns that reflects the effect of prior augite and hornblende fractionation which removes the MREE's and HREE's from the melt. The REE profile shows increasing LREE concentrations relative to the middle Miocene sequence, whereas the HREE values decrease modestly. The steepening of the LREE to MREE segment and the diminishment of the Eu anomaly suggests that plagioclase fractionation is decreasing, and hornblende plus augite fractionation collectively produce a steeper LREE to MREE segment of the normalised REE trend. However, the REE profile for this sample shows the least 'hornblende fractionation effect' relative to younger cycles of magmatism. This is corroborated by the relatively low calculated magmatic water contents relative to younger samples (Table 1).

Table 1: Samples selected for determination of magmatic physico-chemical parameters, and resulting values.

Sample	Age	Cycle	Rock-type	Physico-Chemical Variables								
				Temp	fO <sub>2</sub>	H <sub>2</sub> O	P <sub>sat</sub>	P	MD	D <sub>ex</sub>	HD	S <sub>m</sub>
	Ma			(°C)	ΔNNO	(%)	Bar	Kbar	g/cc	Km	g/cc	ppm
EA043228	8.34	1	Cpx-Hbl? BA (flow)									311
EA043207	6.36	2	Cpx-Hbl Ia (flow)	T <sub>Q</sub> = 872	+2.5	4.7	1352			5	0.278	
DA993948	~ 6.0	2	Cpx>>Hbl Ia (flow)	T <sub>SI</sub> = 860		4.1	1094			4.1	0.230	
EA049678	3.80	4a	Hbl-Cpx-Bt Ia	T <sub>Q</sub> = 805	+2.4	5.6	1750			6.5	0.385	
EA043212	3.75	4a	Hbl-Cpx SA (dyke)	T <sub>HP</sub> = 800		6.0	1987			7.4	0.427	188
EA044956	3.67	4a	Hbl Granodiorite	T <sub>HP</sub> = 806		5.8	1901			7.0	0.410	
EA045799	3.65	4a	Hbl-Cpx Ia (flow)	T <sub>Q</sub> = 909	+1.7	4.4	1248			4.6	0.244	
EA043206	3.04	4a	Hbl-Cpx Ia (dyke)	T <sub>Q</sub> = 865	+1.5	5.1	1725			6.4	0.349	312
DA993972	1.75	4b	Hbl-Cpx Ia (flow)	T <sub>HP</sub> = 875		5.4	1961			7.3	0.381	
EA043214	1.47	4b	Hbl-Bt SA Dome	T <sub>HP</sub> = 765	+2.0	8.2	3335	5.1	2.34	12.4	0.605	
EA045009	0.86	4b	Hbl Dacite Plug	T <sub>SI</sub> = 785		7.2	2747	5.0	2.33	10.2	0.535	
EA043204	0.59	4b	Hbl-Bt Dacite Plug	T <sub>Q</sub> = 807	+2.4	6.7	2404	6.0	2.36	8.9	0.481	57
EA045002	-0.1	5	Hbl-Bt Ia	T <sub>Q</sub> = 866	+2.2	4.9	1450			5.4	0.299	
EA046389	-0.1	5	Hbl-Bt Ia	T <sub>Q</sub> = 829	+2.5	5.5	1752			6.5	0.372	

Cycle = magmatic cycle; BA = Basaltic andesite; Ia = Intermediate andesite; SA = Silicic andesite; T<sub>Q</sub> = temperature by QUILF; T<sub>HP</sub> = temperature by hornblende-plagioclase geothermometry; T<sub>SI</sub> = temperature inferred from temperature vs SiO<sub>2</sub> correlation of 11 data points; fO<sub>2</sub> = oxygen fugacity, given as log units fO<sub>2</sub> above the nickel metal-nickel oxide reference buffer; P = total pressure (lithostatic load); P<sub>sat</sub> = H<sub>2</sub>O partial pressure = minimum bound on confining pressure; H<sub>2</sub>O = dissolved water in melt; MD = melt density at calculated pressure (P); D<sub>ex</sub> = minimum depth of hydrothermal fluid exsolution at lithostatic pressure; HD = hydrothermal fluid density during initiation of exsolution (excluding solutes); S<sub>m</sub> = sulphate concentration in melt.





In Cycle 3 – which culminates in the formation of porphyry Cu ore from a dacitic melt – the *entire* NMORB-normalised REE pattern moves to substantially lower values (Fig. 15) relative to Cycle 2, with a severe depletion in the MREE to HREE's. This downward shift is produced by decreasing plagioclase fractionation and a progressive switch from augite to hornblende fractionation. A decrease in plagioclase fractionation is also indicated by a shift from no Eu anomaly (A – EA043207) in Cycle 2 to a positive Eu anomaly in Cycle 3.

The REE profiles for rocks from the first part of Cycle 4 (D and C; Fig. 15) occur at the transition of Cycle 3 to 4 (3.75 Ma; Fig. 19) and at the early stage of Cycle 4 (3.06 Ma; Fig. 19). They show an increase in MREE and HREE normalized values back to levels intermediate between Cycles 2 and 3. They lack the positive Eu anomaly typical of evolved Cycle 3 silicic andesites. These samples at the start of Cycle 4 coincide with the mid-Pliocene recharge of a parental, lower-crustal magma reservoir (Fig. 19), during which resident dacitic magmas of Cycle 3 mixed with primitive magmas from the mantle. During this recharge and mixing event, the predominance of hornblende fractionation at the end of Cycle 3 (Profile F in Fig. 15) decreased relative to augite fractionation during the transition from profiles F to D to C, resulting in shallowing and flattening of the MREE to HREE segment. During the latter part of Cycle 4, the N-MORB-normalised Er-Lu values decrease systematically in Cycle 4 rocks during magmatic differentiation. The progressive deepening trough in the MREE to HREE trends reflects progressive increase in hornblende fractionation throughout Cycle 4 magmatism. The increase in hornblende fractionation continues through the latter part of Cycle 4 until hornblende totally replaces augite as the principal mafic fractionating phase. Sample EA043214 is a hornblende-dacite which

Figure 15: N-MORB-normalised profiles of rare earth elements from selected rocks from the Tampakan district. The entire suite of Late Miocene to Recent magmatic rocks displays moderate to high degrees of hornblende fractionation, evident as a strong depletion of heavy REE, with a minimum around Er and in some cases by a weak positive Eu anomaly (Nagasawa and Schnetzler, 1971). Plagioclase and augite fractionation is dominant in the early part of successive magmatic cycles with minor hornblende fractionation, however hornblende becomes increasingly dominant through the course of each cycle and becomes the principal, or sole, mafic fractionating phase at the dacitic end of the later magmatic cycles. The porphyry Cu-Au mineralisation at Tampakan is associated with the rocks that show the greatest degree of hornblende fractionation at the end of Cycle 3.

lacks augite. Several units within the later part of Cycle 4 exhibit a positive Eu-anomaly (e.g. EA043214; Fig. 15), suggesting  $\text{Eu}^{2+}$  accumulation in residual silicate melt due to substantial delay in onset of plagioclase saturation. REE trends for Cycle 5 magmas from the Quaternary Mt Matutum stratovolcano show a regression to less depleted MREE and LREE values, consistent with decreasing hornblende fractionation and increasing augite fractionation. This regression is also associated with a renewed phase of magma chamber recharge and mixing in the lower crust to form more mafic hybrids (Fig. 19).

The REE data for the Tampakan series reveal successively evolving magmatic cycles (Cycles 1 to 5). During the commencement of each cycle, augite fractionation is either dominant (Cycles 1 and 2) or significant (Cycles 4 and 5). During progressive differentiation of Cycles 2, 3 and 4, both augite and plagioclase become progressively less important while hornblende becomes progressively more important as a fractionating phase. The evolution in the REE patterns described above is consistent with the element ratios in detrital zircons (Fig. 19) that show a corresponding, time-dependant, cyclic evolution in chemistry.

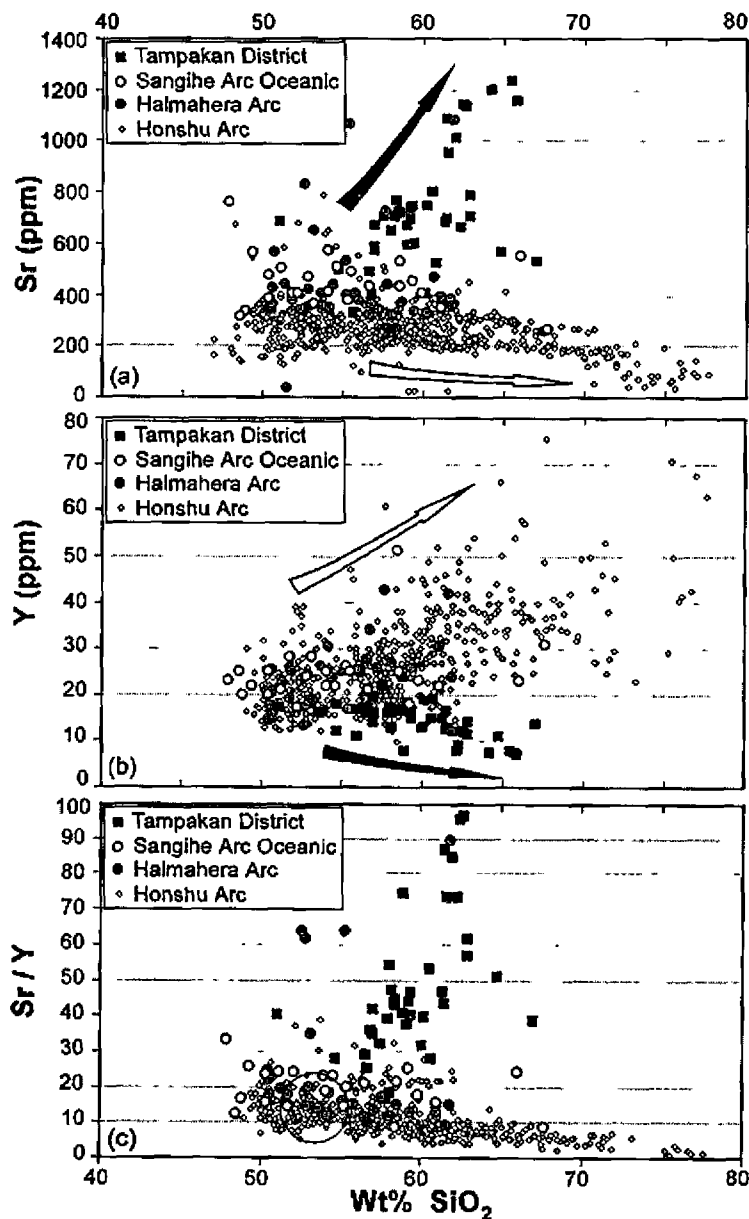
#### Sr and Y Systematics

Anomalous trends in several major and trace elements that partition into plagioclase (Sr,  $\text{Al}_2\text{O}_3$ ) and hornblende (Y, HREE, FeO) are observed in the Tampakan suite relative to other representative arc segments in the western Pacific. Although Sr is enriched in most arc sequences relative to back arc and MORB basalts, due to fluid transfer of Sr from the subducting slab to the mantle wedge source region of melts, the behaviour of Sr during magmatic differentiation is typically that of a compatible element that decreases in abundance during magmatic differentiation. Plagioclase is the major sink for Sr because of the high  $D^{\text{Plagioclase/Melt}}$  for Sr ( $D^{\text{Sr/Plagioclase/Melt}} \approx 3$ ;  $D^{\text{Sr/Andesine/Melt}} \approx 6$ ; Blundy & Wood, 1991) and high modal abundance of plagioclase (>50%) in the crystallising mineral assemblage of evolved basalts, basaltic andesites and augite andesites at upper-crustal pressures. The data for representative arcs in Fig. 16a all show Sr behaving as a compatible element, with the exception of the Tampakan district where Sr increases markedly during magmatic differentiation. The rise in Sr with  $\text{SiO}_2$  is a feature of evolving melt compositions, inasmuch as the Tampakan volcanics are not plagioclase cumulates to a significant degree, and contamination of the melt by Sr-bearing limestone

sequences can be excluded because  $^{87}\text{Sr}/^{86}\text{Sr}$  ratios in representative rocks of the district have typical mantle signatures (Rohrlach 2002). The high Sr values are attributed to retardation of plagioclase saturation due to high contents of dissolved  $\text{H}_2\text{O}$  in the melts, and to diminished modal abundance of plagioclase, because hornblende crystallisation consumes the melt's plagioclase-forming components, allowing Sr to accumulate within the melt to advanced stages of magmatic differentiation.

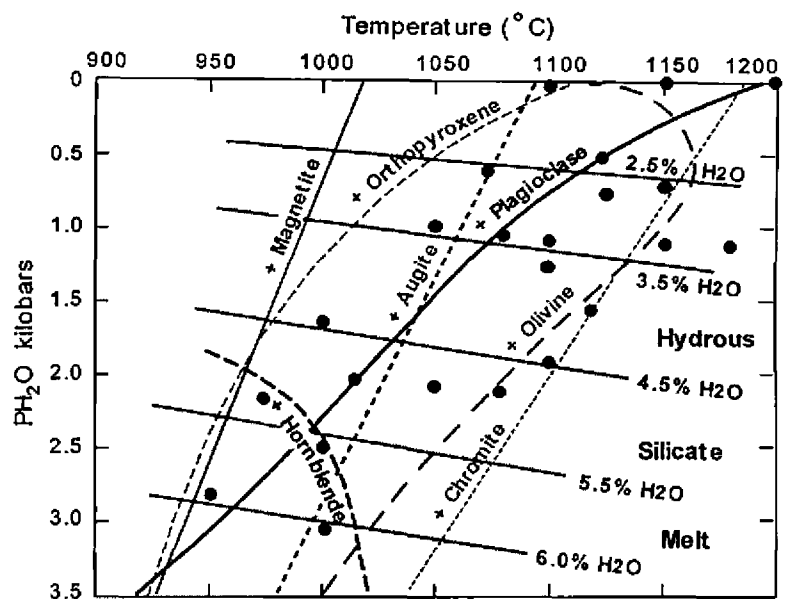
In most arc sequences, Y is residually enriched in the melt during magmatic differentiation because  $Y D^{\text{Plagioclase/Melt}}$  and  $Y D^{\text{Olivine/Melt}}$  are typically  $< 0.2$  for basalts, andesites and dacites (Drake and Weill, 1975; Dunn and Sen, 1994; Ewart

and Griffin, 1994; Bindeman *et al.*, 1998; Beattie, 1994; Nielson *et al.*, 1992 and Kennedy *et al.* 1993), and  $Y D^{\text{Pyroxene/Melt}}$  is  $< 1.0$  for basalts and andesites having  $< 60$  wt %  $\text{SiO}_2$  and  $< 1.0$  for cotectic pyroxene + plagioclase assemblages (Jenner *et al.*, 1994; Hack *et al.* 1994; Hart and Dunn, 1993; Larsen, 1979). Thus Y typically behaves as an incompatible element (accumulating in increasingly silicic residual melt fractions) as observed in the comparative Sangihe-Celebes, Halmahera and north Honshu arcs (Fig. 16b). In contrast, Y at Tampakan behaves as a compatible element, decreasing in abundance during differentiation. Hornblende is the major sink for Y because of high  $D^{\text{Plagioclase/Melt}}$  for Y,  $Y D^{\text{Olivine/Melt}} = 1.5$  for basaltic to andesitic melts, increasing to  $Y D^{\text{Hornblende/Melt}} \geq 2.5$  for dacitic



**Figure 16:** Sr, Y and Sr/Y versus  $\text{SiO}_2$  for the Tampakan district, for the Celebes Sea segment of the Sangihe arc, for the Halmahera arc, and for the north Honshu arc. The data plotted include late Miocene and younger rocks from the Tampakan district ( $n = 49$ ), the Sangihe arc segment in the eastern Celebes Sea ( $n = 24$ ), the Halmahera Arc ( $n = 43$ ) and the North Honshu arc ( $n = 480$ ). The Sangihe-Celebes and Halmahera arcs are built on oceanic crust while the Tampakan district and the north Honshu arc are built on continental crust. The data for the comparative districts were compiled from Morris *et al.*, (1983); Ikeda, (1991); Kimura *et al.*, (2001); Yoshida and Aoki, (1984); Hayashi, (1985); Aoko and Fujimaki, (1982); Kanisawa *et al.*, (1994); Miyajima, (1990); Tamura, (1994); Ujike and Stix, (2000); Togashi *et al.*, (1992); Aoki *et al.*, (1989); Sakuyama and Nesbitt, (1986); Shuto and Yashima, (1990); Fujinawa, (1992); Suzuki, (2000); Tamura and Shuto, (1989) and Kobayashi and Nakamura, (2001).

**Figure 17: Varying the wt %  $H_2O$  dissolved in the silicate melt strongly affects the order of mineral crystallisation from the melt** (and consequently affects the relative rates of depletion or accumulation of various trace elements in the melt), as illustrated by this map of phase assemblages in a series of crystallisation experiments by Moore and Carmichael (1998) on a basaltic andesite composition from the Trans Mexican magmatic arc. Each grey dot represents an experiment in which the crystallising mineral assemblage was identified, and the melt's content of dissolved water (grey contours labelled with wt %  $H_2O$ ) was determined from the composition of the quenched glass according to the method of Moore *et al.*, (1998). At  $P_{H_2O} = 0$  (dry), the crystallisation order of silicates from the cooling melt is plagioclase first, followed by olivine, orthopyroxene, and then augite. At  $P_{H_2O} > 3.5$  kbar and  $> 6.5$  wt %  $H_2O$  dissolved in the melt, plagioclase is the last of those silicates to crystallise, and hornblende is first. (Saturation curves for magnetite and orthopyroxene in the hydrous melts are based on lower-temperature andesite experiments by Blatter & Carmichael, 1998). Because dissolution of  $H_2O$  in the melt depolymerises aluminosilicate polymer units in the melt (Burnham, 1979), minerals such as pyroxenes and especially feldspars that consume higher-order aluminosilicate polymer units of the melt are most severely depressed in saturation temperature as more  $H_2O$  dissolves in the melt. Increase in the supply of silica monomers allows the saturation temperature of orthosilicates, such as olivine to rise initially, but further additions of dissolved  $H_2O$  dilutes the concentrations of all other chemical components of the melt, which depresses the saturation temperatures of all anhydrous minerals. The thermal stability of hydrous minerals, such as hornblende (and biotite and epidote) is increased by  $H_2O$  addition at constant temperature, up to rather high concentrations (beyond the range of this diagram), beyond which the dilution effect takes over and saturation temperatures of hydrous minerals fall with further additions of dissolved  $H_2O$  in the melt. Increasing the lithostatic pressure at constant content of dissolved  $H_2O$  has much the same effect on crystallisation order of plagioclase and hornblende as the  $P_{H_2O}$  effect shown here, because increasing lithostatic pressure also depolymerises aluminosilicate melts, retarding plagioclase saturation to lower temperatures, relative to orthosilicates such as olivine, zircon and garnet, and relative to minerals that use silica dimers and other low-order polymer species in the melt. At any given value of dissolved  $H_2O > 5$  wt%, hornblende reaches its maximum thermal stability and rank in the crystallisation sequence at lower-crustal/uppermost-mantle pressures in the 10-20 kbar range (Ulmer, 1988).



melts (Sisson, 1994; Ewart and Griffin, 1994). In the Tampakan district, hornblende fractionation from basaltic andesitic, andesitic and dacitic melts caused depletion of Y in the melts during magmatic differentiation.

Extrapolation of the trends for Sr and Y (Fig. 16) to more primitive,  $SiO_2$ -poor compositions for the strongly hydrous Tampakan series reveals a convergence with parental basalts of the relatively anhydrous magmatic differentiation series in the Sangihe and Halmahera arc segments farther south. The convergence of differentiation trends at the mafic end implies that all could have been derived from the same type of parent magma under different pressure-depth conditions of magmatic differentiation.

Phase-stability relationships defined from crystallisation experiments by Baker and Eggler, (1983) for a high alumina basalt from Atka Island, Aleutian arc, under water-saturated conditions at 2 kbars, reveal that at low magmatic water contents (2 to 3 wt.%  $H_2O$ ), plagioclase crystallises at high-temperature, well before hornblende enters the crystallisation sequence at lower temperatures. However, there is a reversal in this crystallisation sequence at high magmatic water contents of around 6 wt.%  $H_2O$ . Additional phase relationships defined by Moore and Carmichael, (1998) from crystallisation experiments conducted on a primitive andesite at water-saturated conditions and varying pressure reveal that there is also a pressure dependence on the relative crystallisation sequence of plagioclase and hornblende (Fig. 17). Additional representations are shown in Rohlach (2002) for experimental data compiled for

olivine tholeiite melts, or evolved equivalents that lie close to the liquid line of ascent of an olivine tholeiite. In the case of the olivine tholeiite, at a pressure of 5 to 6 kbars that equals the calculated crystallisation pressure of the Tampakan suite (see the Magmatic Physico-Chemical Properties sections below), hornblende starts to crystallise at  $1050^\circ C$  whereas plagioclase starts to crystallise at  $\sim 920^\circ C$ . The combination of extremely hydrous magmas (Table 1) at Tampakan, combined with their crystallisation in an extremely slow-cooling lower crustal reservoir at  $\sim 20$  km depth below the Tampakan district, and their maintenance at high temperature for prolonged periods of time by episodic recharge (Fig. 19), are responsible for the reversal of the normal plagioclase-hornblende crystallisation sequence which in turn produced the reversed evolutionary trends in Sr and Y that record the lower crustal evolution of hydrous magmas at Tampakan.

Fig. 18 shows the Sr/Y ratios plotted against Y. Hydrous and/or high-pressure magmas, in which plagioclase crystallisation is retarded and hornblende saturation is brought forward in the crystallisation sequence, evolve to high Sr/Y ratios and low Y values as the melt's  $SiO_2$  content increases, because the suppression of plagioclase crystallisation allows Sr to build up in the melt during early stages of differentiation while hornblende fractionation depletes the melt in Y. High Sr/Y ratios ( $> 20$ ) are one of several chemical characteristics of "adakites", a rock-type defined by Defant and Drummond (1990) to be the product of melting of eclogitic portions of the subducted slab.

Melting of subducting Molucca Sea Plate under Tampakan is exceedingly implausible, inasmuch as it is of Mesozoic age (Hall, 1996) and has been subducting throughout much of the Cenozoic and now extends to >600 km depth in the mantle (Silver & Moore, 1978; Lallemand *et al.*, 1998), whereas thermal modeling of subducting slabs by Peacock, (1990a,b) and Peacock *et al.*, (1994) indicate that the conditions that permit melting of the slab are restricted to; i). subduction of young (<10 M.y.) and hence warm oceanic crust; ii). initial stages of subduction wherein the leading edge of the subducting plate intrudes thermally undisturbed and hence hot mantle; and/or iii). high rates of shear heating.

### Magma Mixing

The series of detrital zircon ages from the Tampakan district (see Geochronology section above) record semi-continuous volcanism from the late Miocene to Recent. This detailed chronological record allows the temporal framework of magmatism to be coupled with aspects of the evolving chemistry of the Tampakan magmatic system as recorded by the trace element composition of dated detrital zircon grains. Trends in the elemental compositions of the zircons provide insights into the chemical evolution of their parent melts and corroborate and illuminate the magmatic "cycles" discussed in the Geochronology section. Fig. 19 shows U/Ti ratios of suites of detrital zircons that were collected from two streams in the radial drainage system on the Tampakan edifice. The element ratio U/Ti was determined by excimer laser ablation ICP-MS on zircon grains whose  $^{238}\text{U}$ - $^{206}\text{Pb}$  ages were determined by the same instrument.

The oscillations in the time series of the U/Ti ratio in the zircons mirror oscillatory trends in the differentiation indices (such as wt. %  $\text{SiO}_2$ ) of magmas that built the Tampakan volcanic complex. The U/Ti ratio was selected for examination because the Ti content of residual melts decreases over the course of differentiation from basaltic

andesitic to rhyolitic stages, whereas U behaves as an incompatible element that accumulates in residual melts over the same differentiation interval. We anticipated that zircon crystallising from melts in the 58–68 wt %  $\text{SiO}_2$  range would inherit a biased representation of the parent melt's evolving U/Ti ratio, and thereby could serve as a differentiation index of the zircon's parent melt. The high density of data points in Fig. 19 provides a high-resolution depiction of the evolving magmatic system in the Tampakan district prior to and during generation of the giant porphyry and high-sulphidation ore systems and the unusual petrochemical signatures discussed above. A succession of "ramps" is resolved whereby the magmatic system builds to more evolved compositions (higher U/Ti) in a series of cycles that are separated by abrupt downward steps wherein the magmatic system was re-set to more primitive compositions. Each of these ramps, which collectively extend from the latest Miocene to the present, correlates with the succession of magmatic cycles defined in the Geochronology section and illustrated in the bottom panel of Fig. 19 by the oscillatory trend in wt %  $\text{SiO}_2$  in a smaller number of least-altered drill core samples from which zircons were also separated and dated by the same ELA-ICPMS method. The first ramp in U/Ti, from ~7.3 Ma to ~6 Ma, is equivalent to the first major period of stratocone construction in the Tampakan district (Geochronology section; Figs. 12 and 13) and is labelled Cycle 2. Cycle 1 is not resolved here, as it is represented by only one age date from an andesite sample from deep levels of the Tampakan porphyry deposit. Between ~6 and ~5.4 Ma the U/Ti ratios decrease, reflecting replenishment of the magma chamber by mafic magma having a low U/Ti ratio and blending of the silicic resident and replenishing mafic melt fractions, after which the U/Ti ratio begins to climb steeply again between ~5.4 and ~4.2 Ma. The development of this second ramp coincides with increasing compression within the district (Fig. 5) during docking of northern and southern

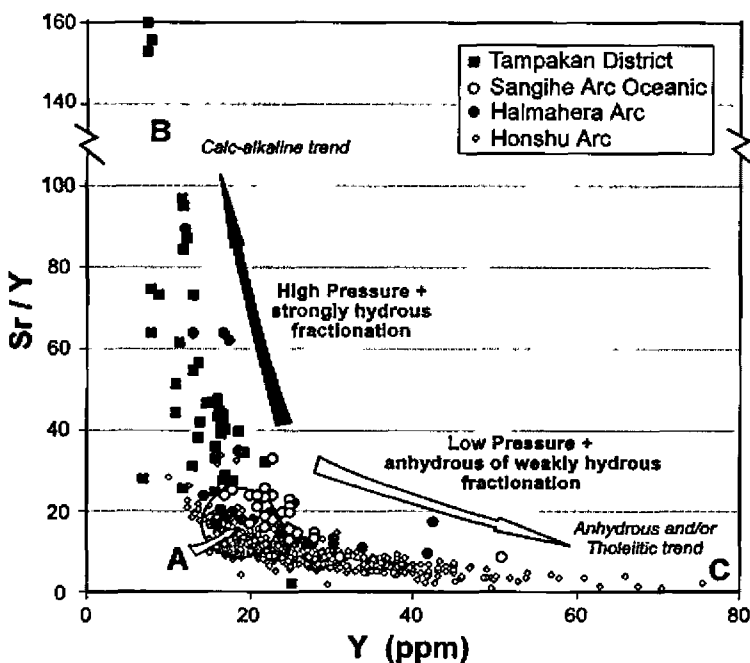
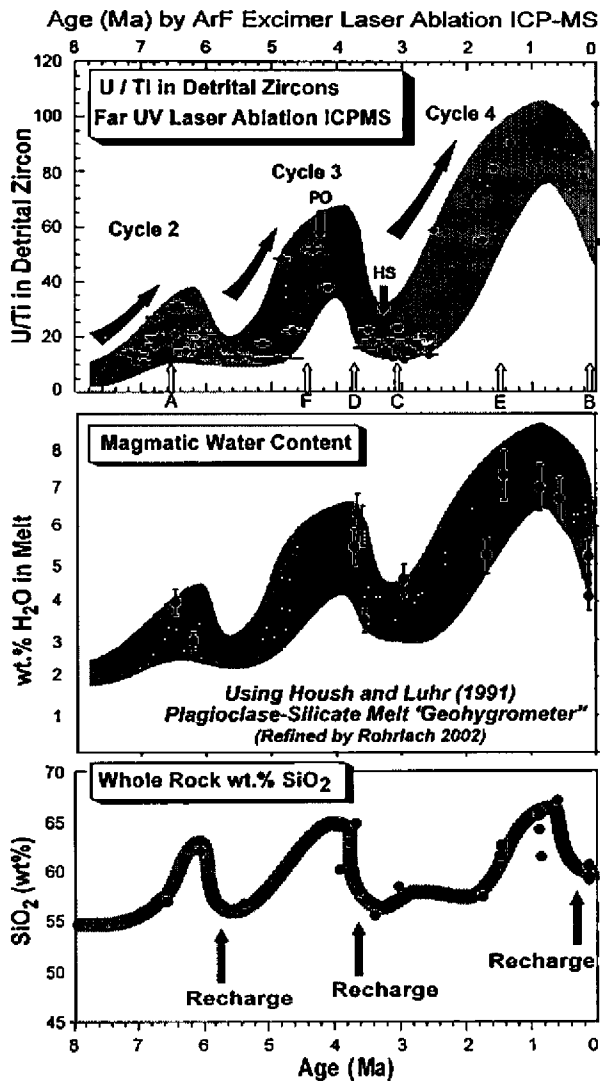


Figure 18: Plot of Sr/Y versus Y for the Tampakan district and several comparative arcs. The Tampakan suite displays an atypical trend wherein Sr/Y increases with increasing magmatic differentiation, opposite to the trend of decreasing Sr/Y with increasing magmatic differentiation that is observed in the Celebes Sea segment of the Sangihe arc, the Halmahera arc and the north Honshu arc. None of the last three arc segments is known to have significant magmatic-hydrothermal copper mineralisation in the time intervals represented by the datasets. High magmatic water contents (up to 8.2 wt.%  $\text{H}_2\text{O}$ ; Section 7) and high crystallisation pressures (6 kbars; Section 7) delay plagioclase saturation in the melt to substantially lower temperatures and advanced stages of differentiation, and advance hornblende saturation in the melt to earlier, more primitive stages of differentiation and at higher temperatures, relative to magmatic series which develop under water-poor conditions and/or low pressures. At Tampakan, the reversal of the usual order of appearance of plagioclase and hornblende in the crystallisation sequence produces the atypical trends in Sr/Y versus Y. Hydrous and high-pressure sequences evolve from A to B during magmatic differentiation whereas water-poor and low-pressure sequences evolve from A to C.



Mindanao along the Cotabato Fault Zone (Fig. 2). The formation of *porphyry copper mineralisation* at 4.26 to 4.24 Ma (Figs. 12 and 13) occurs at the dacitic end of the Cycle 3 ramp. The phase of stratocone construction associated with this magmatic ramp was eroded during unroofing of the porphyry system between 4.25 and 3.93 Ma (Geochronology section) due to high or catastrophic erosion rates as the collision event peaked during the middle Pliocene.

The magmatic system then underwent a replenishment and mixing event resulting in regression to more primitive compositions between ~3.8 and ~3.4 Ma, during the peak of the collision (Fig. 5) and following the evolved magmatism which produced porphyry copper mineralisation at the peak of the preceding ramp. The high-sulphidation epithermal Cu-Au mineralisation at Tampakan (3.39 to 3.20 Ma) is associable with a magma batch emitted from the lower-crustal chamber during the replenishment/mixing event. The third U/Ti ramp that is resolved by the zircon data extends from ~3.7 to ~0.6 Ma (Fig. 19) wherein U/Ti and other incompatible-on-compatible element ratios build to *greater values than in the preceding ramps, albeit within about the same SiO<sub>2</sub> range as preceding cycles*. This last ramp coincides with magmatic Cycle 4. The early part of Cycle 4 (~3.7 to ~2.5 Ma) was the principal stratocone building event during the middle Pliocene (Fig. 13), of

**Figure 19: Upper panel** - Detrital zircons were collected from streams on the western side of the Tampakan volcanic edifice and were dated by <sup>238</sup>U/<sup>206</sup>Pb using a far-ultraviolet argon-fluoride excimer laser microprobe to ablate 25 to 200 μm spots in single crystals for isotopic and trace-element analysis of the ablated material by ICP-MS. As zircon crystallises, it inherits a biased version of the melt's U/Ti ratio, which is a magmatic differentiation index that rises as the melt's SiO<sub>2</sub> content rises. (Both U<sup>4+</sup> and Ti<sup>4+</sup> substitute in Zr<sup>4+</sup> lattice sites). In the 8 to 0.06 Ma time series of ages of eruptive and intrusive units in the continuously evolving Tampakan igneous complex, the oscillations in the zircon's and the melt's U/Ti ratio represent cycles of magmatic differentiation by fractional crystallisation, punctuated by magma-chamber replenishments (labelled "recharge" in the lower panel) by mantle-derived mafic magma that mixed with residual andesitic or dacitic magma already in the lower-crustal chamber. PO and HS show the timing of porphyry and high sulphidation mineralisation.

**The central and lower panels** represent time series of variations in the dissolved H<sub>2</sub>O content or SiO<sub>2</sub> content of magma batches that were erupted or intruded into the volcanic edifice. The age determinations in the central and lower panels are from U-Pb analyses of zircons separated from least-altered whole-rock samples collected from surface outcrops and drill core. Those samples were subjects of whole-rock XRF and ICP-MS analysis. The wt. % H<sub>2</sub>O dissolved in the melt at various stages is calculated from our electron-microprobe measurements of the Ca/Na partition coefficient between plagioclase phenocryst rims and surrounding groundmass (quenched melt), and from the experimentally calibrated effect of dissolved H<sub>2</sub>O (and temperature and pressure) on  $Ca/Na \text{ D}_{\text{plagioclase/melt}}$ .

**The bottom panel** shows the SiO<sub>2</sub> content of least-altered whole-rock samples from which datable zircons were extracted. The maximum SiO<sub>2</sub> content attained at the ends (tops) of differentiation cycles varies little among Cycles 2, 3, and 4, but the maximum U/Ti ratio ramps up by about 3-fold over the same time period, and the maximum H<sub>2</sub>O content in successive cycles approximately doubles over the same time interval.

which the remnant landform is observed in topographic data (Fig. 8). Igneous rocks of the younger part of Cycle 4 comprise widely scattered and evolved hornblende-andesites and -dacites in the southern portion of the district. A minor regression in the U/Ti ratio and whole-rock SiO<sub>2</sub> occurred at the end of Cycle 4 (~0.6 Ma), prior to eruption of the Quaternary Mt Matutum Andesite (Cycle 5) which built a new stratocone that overlaps the southern flank of the older volcanic complex. The important aspect of the trends defined in Fig. 19 is that in each cycle the maximum height of the crest, at the top of each "ramp", is successively higher, and hence more evolved, than in each preceding ramp. This effect arises because i). U and H<sub>2</sub>O are more highly incompatible components of the melt than is SiO<sub>2</sub> and hence climb relative to it, and because ii). hybrid melts at the start of new cycles inherited the accumulated U and H<sub>2</sub>O (and Cl and SO<sub>3</sub>, and other incompatible components) from evolved residual melts of the preceding cycle, and then added to the inherited accumulation by fractional crystallisation of U- and H<sub>2</sub>O-poor cumulates in the current differentiation cycle. The half-wavelength, or evolving portions, of the three resolved differentiation ramps are between ~1 and 3 M.y. duration. This length of time is substantially longer than the life span of magma chambers in the upper crust (typically <400 K.y.) that are broadly equivalent to the construction period of individual stratovolcanoes. If each ramp, or mega-fractional crystallisation cycle were isolated magmatic systems related to independent and evolving chambers, with each being

replenished from the mantle with minimal melt storage in the lower-crust, then chemical inheritance between cycles would not be observed. The relatively long time intervals spanned by the major differentiation cycles implies that they occurred in a slow-cooling lower-crustal/upper-mantle magma chamber, as is also indicated by pressures of 5 to 6 kbar from Al-in-hornblende geobarometry on phenocrysts in silicic dacites (see Magmatic Physico-Chemical Properties section); these pressures correspond to lower-crustal depths under southern Mindanao.

The process of intermittent magma recharge and mixing in a continuously crystallising magma reservoir over a time interval of >7 M.y. is also reflected by evolutionary trends of compatible components such as wt %  $\text{TiO}_2$  in whole-rock samples. Because  $\text{TiO}_2$  is a relatively immobile component during hydrothermal alteration, we have selected it to illustrate the evolutionary process in complex multi-cycle melt fractionation events. Fig. 20 shows a representative plot of mixing relationships between evolved melt at the end of several magmatic cycles and a hypothetical mafic parental melt. The replenishing mafic end of the mixing series is not necessarily a primary, mantle derived melt, but simply a plausible, somewhat evolved end member for the mixing array.  $\text{TiO}_2$  displays compatible behavior throughout the crystallisation interval of the sampled Tampakan series because of early crystallisation of titanomagnetite and ilmenite from the basaltic andesite stage onward. In this example, wherein the component of interest always displays compatible behavior, magmatic differentiation produces concave-upward depletion curves (Fig. 20). Linear mixing between  $\text{TiO}_2$ -poor, silicic residual melt fractions and recharging mafic melts always produces hybrid melts that are more enriched in the compatible component at a given  $\text{SiO}_2$  content. (Mg#, Ni and Cr contents ramp up in essentially the same way during generation of "adakites" by multi-cycle magmatic differentiation, without the commonly inferred implication that silicic melts of subducting eclogite were contaminated by peridotitic mantle wedge during ascent). The  $\text{TiO}_2$  content of hybrid melts parental to successive cycles 1 to 5 climbs due to back mixing of successive silicic residual melts with a common parental melt. The inheritance implicit in this climb in  $\text{TiO}_2$  content among successive

cycles corroborates previously described evidence that the petrochemical evolution toward copper metallogenic fertility was a multi-cycle recharge-and-differentiation process in a magma chamber that was exceptionally long-lived (late Miocene to Recent) because relatively evolved *buoyant* melts remained trapped near the Moho by the sustained compressive stress regime (see Mechanics of Lower Crustal Entrapment by Tectonic Stress section). Multi-cycle inheritance of incompatible components, most notably  $\text{H}_2\text{O}$ , eventually led to development of unusual andesitic and dacitic melts having no negative Eu anomalies, and exceptionally high Sr/Y and  $\text{Fe}^{3+}/\text{Fe}^{2+}$  ratios (oxidation state).

Several textural features of the phenocrysts in the Tampakan suite also provide evidence of repeated magma injection and chemical disequilibrium between resident phenocrysts and the hybridising melts throughout the late Miocene to Recent epochs. Plagioclase phenocrysts commonly display sieve-like textures within the cores of large phenocrysts, along intermediate growth bands or along the exterior portion of phenocrysts. The sieve texture consists of interconnected lacy filaments of melt inclusions that comprise 10-30 % of the sieve-textured zones, and were trapped along resorbed surfaces of phenocrysts. In other examples of chemical disequilibrium within the hybrid magmas, "late-stage" biotite is replaced and mantled by hornblende. This reflects a temporary regression in the crystallisation sequence and is further evidence of crystal-liquid disequilibrium within the crystallising magma. Whereas plagioclase and hornblende phenocrysts display textural evidence of resorption during magma mixing and during shallow-level emplacement, uncorroded augite phenocrysts have remained in textural equilibrium with the melt, which indicates that the disequilibrium perturbations are toward more primitive melt compositions and mineral assemblages. Fe-Ti-oxide and hornblende-plagioclase temperature estimates for sample EA043214 (Magmatic Physico-chemical Properties section) reveal that it had been heated from  $\sim 765^\circ\text{C}$  (hornblende-plagioclase temperature) to  $\sim 906^\circ\text{C}$  (two-oxide temperature), corroborating the textural evidence for magma mixing during input of hotter, more primitive melt into the chamber.

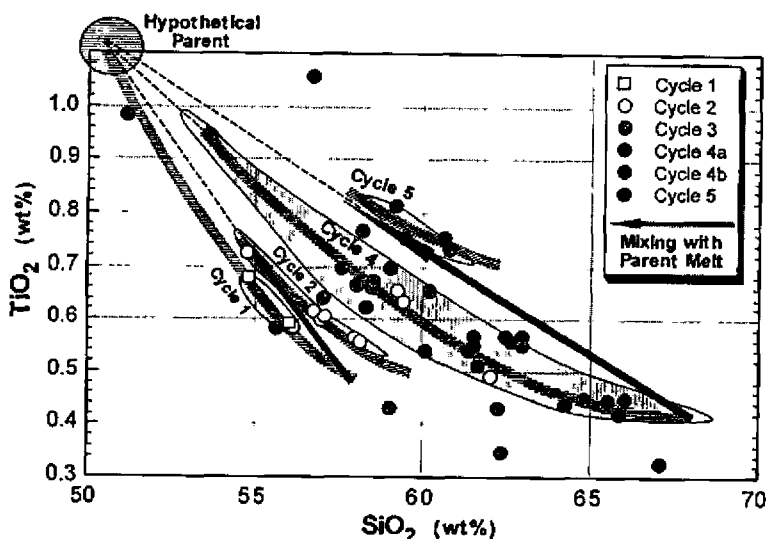


Figure 20: A plot of  $\text{TiO}_2$  versus  $\text{SiO}_2$  for the Tampakan igneous suite. The concentration of  $\text{TiO}_2$ , and by corollary other melt-incompatible elements, decreases monotonically (pale grey curved trend lines of fractional crystallisation) within any single differentiation cycle, but increases in successive cycles 1 to 5 at intermediate to high silica contents, due to linear back mixing (heavy grey arrows) of evolved melts with a primitive parental melt. The effect is a product of the upward concave depletion curve that is characteristic of melt-incompatible elements.

## Magmatic Physico-Chemical Properties

Magmatic physico-chemical parameters are calculated for 13 rocks from successive stages of the differentiation history of the Tampakan volcanic complex in order to constrain the magmatic temperature, oxygen fugacity, pressure of hornblende crystallisation, water content, H<sub>2</sub>O partial pressure, depth at which water would begin to exsolve from the magma at lithostatic pressure, density of the exsolved supercritical brines, magmatic sulphur content, sulphur speciation and melt density. Physico-chemical parameters such as oxygen fugacity, magmatic water activity and sulphur speciation are important factors in controlling the metallogenic ore-forming capability of calc-alkaline melts.

Magmatic temperatures and oxidation states were calculated using the QUILF algorithms of Andersen *et al.*, (1993) (Fig. 21). The Fe-Ti-exchange geothermometer and oxygen barometer is not adequately calibrated at the low-temperature and high oxidation state of magmas that are commonly parental to porphyry-type copper-gold ore deposits, so we recalibrated the output of QUILF using data from five later, precise experimental studies to derive an empirical linear correction term for application to temperature estimates derived for rocks at oxygen fugacities greater than NNO+2 (Rohrlach and Loucks, 2000a). A correction term for magmatic  $fO_2$  was also derived by comparison of QUILF output with the experimentally measured  $fO_2$  and temperature that reproduce the mineral assemblage and compositions of Fe-Ti-oxides and other phenocrysts in the 1991 Pinatubo dacite. Temperatures of the Tampakan suite were also calculated by hornblende-plagioclase geothermometry (Holland and Blundy, 1994).

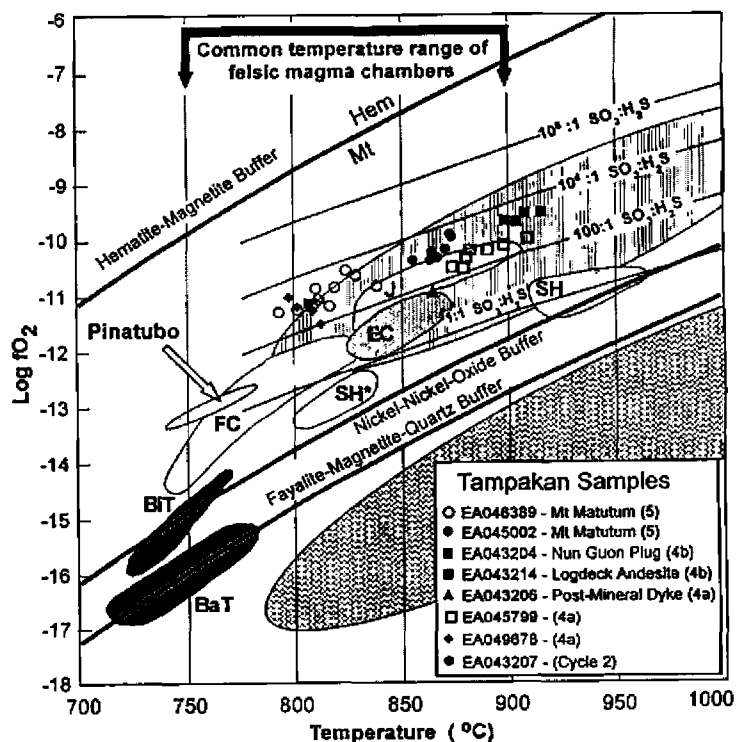
The calculated magmatic temperatures for the Tampakan suite vary from 765°C (hornblende-plagioclase

thermometer) to 909°C (two-oxide thermometer). The wide temperature range of the magmas is a function of the extensive composition range plotted. The disparity between the Fe-Ti-exchange geothermometer and the hornblende-plagioclase geothermometer for temperature estimates of sample EA043214 (909°C vs 765°C), in conjunction with disequilibrium corrosion and replacement textures in plagioclase, biotite and hornblende, indicate that magma mixing between cool resident magmas (765°C) and hot recharging magmas (> 909°C) occurred in a lower-crustal magma chamber.

The  $fO_2$  range of the Tampakan suite varies from NNO+1.5 to NNO+2.5 and lies near the upper limit of the  $fO_2$  range for typical Cu-Au ore-forming, oxidised I-type magmas. The magmas lie in the field where sulphur-as-sulphate (SO<sub>3</sub>) predominates over sulphur-as-sulphide (H<sub>2</sub>S) dissolved in the melt, with SO<sub>3</sub>:H<sub>2</sub>S ratios between ~200:1 and 6000:1. High sulphur concentrations in fresh magmatic apatite from the Tampakan district reveal that many of the melts were anhydrite-saturated (Rohrlach 2002), and that anhydrite saturation was a persistent feature of the dacitic stage of evolution. The series crystallised igneous anhydrite at ~67 wt.% SiO<sub>2</sub> in the melt over a significant portion of the late Miocene to Recent magmatic history, consistent with the SO<sub>3</sub>:H<sub>2</sub>S ratios determined above.

The aluminium-in-hornblende barometer of Anderson and Smith, (1995) was used to calculate crystallisation pressures of magmatic phenocrysts in three Cycle 4b dacite-porphyry units having rhyolitic groundmass (interstitial melt) compositions. This version of the barometer takes into account not only the  $fO_2$  dependence, but also the temperature dependence of the partitioning of aluminium into the tetrahedral site of hornblende, which other calibrations of the barometer fail to consider. The three samples from the Tampakan suite for which the barometer

**Figure 21: Titanomagnetite-hemoilmenite temperatures and oxygen fugacities of Tampakan magmas, plotted with comparison data fields abbreviated as follows: BaT - Bandelier Tuff; BiT - Bishop Tuff; EC - El Chichón; FC - Fish Canyon Tuff; J - Julcani; SH - Mt St Helens; and SH\* - Mt St Helens pumice (after Imai *et al.*, 1993). The field for the Mt Pinatubo dacite is plotted using the  $fO_2$  and temperature constraints from Scaillet and Evans (1999). The fields of FC, SH, EC and J are displaced by 0.57 log units to lower values than represented in Imai *et al.*, (1993) to correct for the error in calibration of the Fe-Ti-oxide model at high  $fO_2$  and  $T < 900^\circ\text{C}$ . The Pinatubo and the El Chichón fields plot at plausible SO<sub>3</sub>:H<sub>2</sub>S ratios for these series (~10:1) in which pyrrhotite coexisted with anhydrite. The plotted mineral buffers and SO<sub>3</sub>:H<sub>2</sub>S concentration ratios in the melt are calculated at 2 kbars. SO<sub>3</sub>:H<sub>2</sub>S contours are derived thermodynamically from Carroll & Rutherford's (1988) experimental finding that a sulphide/sulphate ratio 1:1 occurs in dacitic melt at  $fO_2$  ~1.35 log units above FMQ at 950°C and 2 Kbar PH<sub>2</sub>O. Poulson & Ohmoto (1990) showed that in felsic melts having wt% H<sub>2</sub>O > wt% FeO, sulphide in the melt is bonded mainly to H, not Fe. The field of reduced S-type magmas (cross-hatched region) and oxidised I-type magmas (vertical hatched region) are plotted from Burnham and Ohmoto (1980). The Tampakan suite has similar, or slightly higher,  $fO_2$  (relative to NNO) to the anhydrite-bearing Mt Pinatubo dacite, and are as oxidised as the high- $fO_2$  end-members of the high-sulphidation ore-forming magmas at Julcani, Peru.**



was applied are the most highly differentiated units that have the lowest-variance phase assemblage (six phenocryst minerals + quartz-saturated melt + aqueous fluid), and which satisfy Gibbs Phase Rule requirements for successful application of the barometer (Rohrlach 2002). The pressure estimates are: Nun-Guon Plug ( $6.0 \pm 0.6$  kbars); Logdeck Andesite ( $5.1 \pm 0.6$  kbars); and Lambayong Plug ( $5.0 \pm 0.6$  kbars). These pressure estimates correspond to hornblende crystallisation depths of 17.6 to 21.1 km for mafic crust ( $\rho = 2.90$  g/cc), or 18.6 to 22.3 km for granitic crust ( $\rho = 2.75$  g/cc). The depth estimates obtained from both hornblende rims and cores from the Nun Guon Plug and Logdeck Andesite are indistinguishable within the calibration uncertainty of the barometer. These two units underwent most of their fractionation history in the lower-crust, and were emplaced at the surface directly from a deep, lower-crustal reservoir. The crustal thickness of southern Mindanao is  $\sim 31$  km (Scripps Institute of Oceanography Global Crust Model - CRUST 2.0). These lower-crustal pressure estimates are consistent with the high-pressure mineral assemblages associated with the long-lived magmatic system at Tampakan (as outlined in the Petrochemistry section above).

Water contents dissolved in the melt were calculated for the Tampakan magmatic series using the method of Housh and Luhr, (1991), which experimentally calibrated the effects of dissolved  $H_2O$  and temperature and pressure on Na/Ca partitioning between plagioclase and melt. The program TWATER1™ was used to calculate the dissolved water content of the melt, given input data representing proportions of other chemical components in the melt, the chemical composition of the feldspar, and the pressure and temperature of crystallisation. Rohrlach and Loucks, (2000b) added data for 48 experiments to the experimental database of Housh and Luhr, (1991), and derived a refined empirical algorithm that better accounts for the effect of dissolved  $H_2O$  in depressing the activities of the melt's silica and albite components. Our calibration of the output of TWATER1™ using recently published experimental data yield a much improved standard precision of  $\pm 8.85\%$  in retrieving water contents for experiments with  $H_2O > 4$  wt. % that were less precisely retrieved ( $\pm 14.4\%$ ) by the Housh and Luhr calibration. The dissolved water contents calculated for the Tampakan suite range from 4.1 wt. %  $H_2O$  up to 8.2 wt. %  $H_2O$ . The series has variable to generally high water contents, and a subset of the suite is extremely hydrous. The magmatic water contents display a time-dependent evolution that mimics cyclic trends in the chemistry of whole-rocks and of detrital zircons (see the Petrochemistry section).

The pressures and depths at which silicate-saturated aqueous fluid exsolved from ascending water-saturated melts below the Tampakan orebody were calculated using Moore *et al.*, (1998). The depth (km) of initial magmatic-hydrothermal fluid exsolution from 13 selected melts during their ascent (ignoring pressure effects of dissolved gases and salts) was calculated from the calculated fluid saturation pressures ( $P_{sat}$ ) by assuming a density of 2.70 g/cc and  $dP/dz = 265$  bars/km for the upper crust. The estimated depths for onset of fluid saturation within the Tampakan

melts vary from 4.1 to 12.4 km. Experimental data from Baker and Rutherford, (1992) indicate that  $SO_2$  concentrations in  $H_2O$ -rich fluids co-existing with anhydrite have  $P_{SO_2} \sim 110$  bars at  $P_{sat} = 2200$  bars of pressure fluid. These are thus minimum depth estimates (for a pure  $H_2O$  system), because dissolved  $CO_2$  and  $SO_2$  within the melt will force fluid exsolution at deeper levels.

The density of the silicate melt was calculated for 3 samples using magmatic temperatures, crystallisation pressures and magmatic water contents. The melt densities (Table 1) were calculated using the tabulated temperatures and pressures together with mole fractions of oxide components ( $Al_2O_3$ ,  $K_2O$  etc) and their partial molar volumes as reported by Lange and Carmichael, (1990), Kress and Carmichael, (1991) and the partial molar volume of dissolved water published by Ochs and Lange, (1999). For the Logdeck Andesite, Lambayong Plug and Nun-Guon Plug, which are considered to have the most reliable pressure estimates from Al-in-hornblende barometry, the hydrous melt densities average 2.34 g/cc (Table 1). These melts are highly buoyant relative to mafic lower crust that has densities on the order of 2.90 g/cc.

Table 1 lists estimates of the total sulphur concentration dissolved in the silicate melt for 4 samples. These values are based on the analysed sulphate concentration in apatite phenocrysts in those samples, and on the apatite/melt partition coefficient of sulphate calibrated as a function of temperature by Rohrlach (2002), using data compiled from Peng *et al.*, (1997), Baker & Rutherford, (1996), and Streck and Dilles, (1998). Fig. 21 shows that the Tampakan melts had sulphate/sulphide ratios averaging around 1000:1, so the indicated values for sulphate in the melt are equivalent to total dissolved sulphur. Samples having  $\leq 188$  ppm sulphur plot along the anhydrite saturation curve at their respective temperatures, which implies that evolved magmas of Cycle 4 were generally anhydrite-saturated.

In summary, the calculated physico-chemical properties of the long-lived Tampakan magmatic suite reveal that the magmas are highly oxidised, display substantial temperature fluctuations, and evolved at lower-crustal depths of  $\sim 18$  to 22 km. They underwent progressive enrichment in magmatic water, and attained  $> 8$  wt. %  $H_2O$ , in a manner that mimics the high-resolution pattern of detrital zircon chemistry (see the Petrochemistry section). The magmas were highly buoyant relative to lower crustal country rocks, so some mechanism is required to keep these magmas entrapped for sufficient periods of time in the lower crust so as to generate the multi-million year trends of magmatic evolution that are presented in the Petrochemistry section.

## Mechanics of Lower Crustal Entrapment by Tectonic Stress

Primitive magmas generated by melting of spinel or garnet lherzolite within the mantle are very buoyant relative to ambient peridotitic mantle (density  $\sim 2.8$  g/cc for a hydrous picritic or tholeiitic melt at 20 kb, compared to  $\sim 3.2$  g/cc for peridotite near its solidus at 20 kb). After segregation from the source region, the basaltic melts migrate up to the

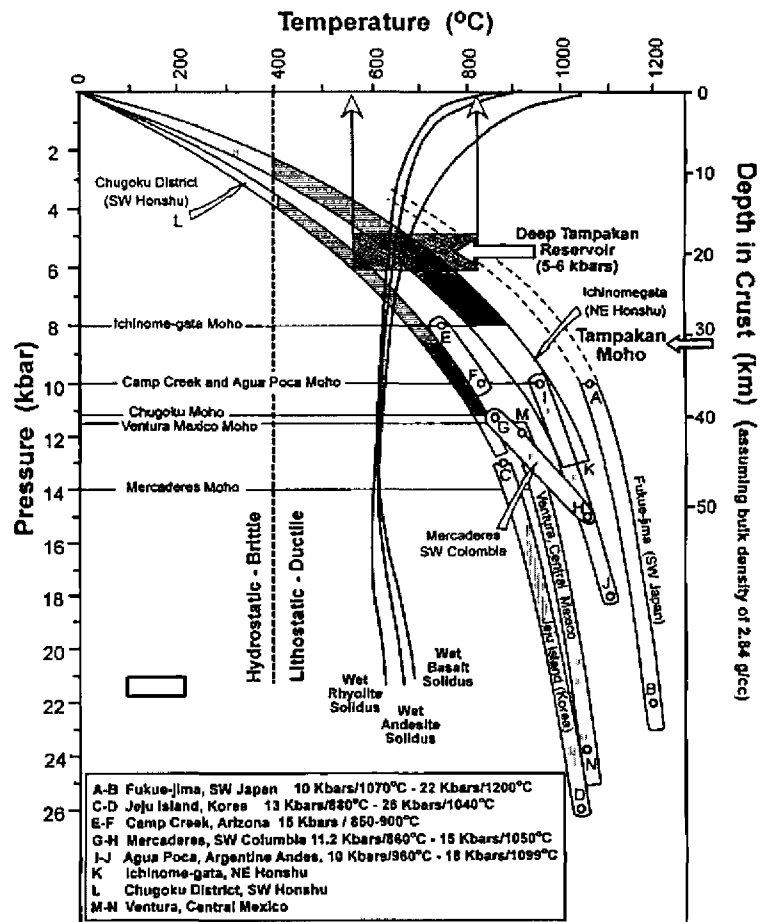


base of the crust or into the lower crust, where the density of mafic granulites and amphibolites is  $\sim 2.9$  to  $3.0$  g/cc, so mafic magmas lose much of their buoyancy at the Moho. The stress regime in the vicinity of the mantle-crust boundary and at rheologic boundaries within the crust strongly influences whether picritic or basaltic melts continue to ascend by dyke propagation, or whether they stall as vertically prolate lenses, or propagate along subhorizontal hydraulic fractures and underplate the crust (or intra-plate the mid-crust) as laterally extensive magma chambers in which ultramafic and mafic layered cumulates develop. In stress regimes where the horizontal tectonic stresses are extensional or hydrostatic, dykes propagate as hydraulic fractures that open at the top and pinch shut at the tail until the magma lozenge reaches neutral buoyancy in a density-stratified crust, whereupon the magma body stalls and crystallises until segregated residual melt fractions have acquired enough compositional buoyancy to resume ascent. In contrast, when the lithospheric stress regime has the minimum stress axis ( $\sigma_3$ ) oriented vertically (e.g. during tectonic collision events), and the horizontal

compressive stresses ( $\sigma_1$  and  $\sigma_2$ ) are of sufficient magnitude to inhibit subvertical propagation of dykes, buoyant magmas that are much more fluid than the country rock (making diapiric ascent unfeasible) can be trapped by the stress regime in subhorizontally propagating magma sheets.

The fluid pressure,  $P_f$ , at the upper tip of a dyke that is available to propagate the hydraulic fracture is  $P_f = (\rho_{rx} - \rho_{melt}) Gz$ , wherein  $\rho_{rx}$  is the density of the country rock,  $\rho_{melt}$  is the density of the magma,  $G$  is gravitational acceleration, and  $z$  is the height of the magma column. Table 1 showed that dacitic melts from eruptive Cycle 4b, having 6.7 to 8.2 wt%  $H_2O$ , contained a phenocryst assemblage that recorded a pressure of  $5.5 \pm 0.5$  kb, which corresponds to  $\sim 20.4 \pm 1.9$  km depth. These were overlain by a rock column with an average composition of andesite having an average density of  $\sim 2.75$  g/cc and a lithostatic pressure gradient of  $\sim 0.2695$  kb/km. At the indicated pressure, the dacitic melts have a density of  $2.34 \pm 0.02$  g/cc (Table 1), so  $dP_f/dz \approx 40$  bars/km of melt column. In the rheologically plastic lower crust, the horizontal deviatoric

**Figure 22: Regional geothermal gradients in a representative suite of active magmatic arcs** are defined by geothermobarometry on suites of lower-crustal and upper-mantle xenoliths in monogenetic volcanoes that sampled rock columns along new magma conduits through the lithosphere. In several regions, xenoliths are derived only from the uppermost lithospheric mantle, while in other regions the xenolith suite spans the local crust-mantle boundary. The crustal and upper-mantle geotherms for the Ichinome-gata (K) and Chugoku (L) districts, of NE and SW Honshu respectively, are reproduced from Kushiro (1987). The remaining data are from: Fukue-jima [(A-B) Umino and Yoshizawa, 1996]; Jeju Island [(C-D) Choi *et al.*, 2001]; Mercaderes, SW Colombia [(G-H) Weber *et al.*, 2002; Conceição *et al.*, 2005; Rodriguez-Vargas *et al.*, 2005]; Camp Creek, Arizona [(E-F) Esperanca and Holloway, 1984; Esperanca *et al.*, 1988] and Ventura, Central Mexico [(O-P) Luhr and Aranda-Gómez, 1997]. The depth scale in km is calculated assuming an average arc-crust density of 2.84 g/cc (Kay and Kay, 1985). The mismatch between this scale and the Moho depth estimate for the Mercaderes district (14 kbars - 42 km, Weber *et al.*, 2001) is due to their assignment of a crustal density of 3.0 g/cc for a basaltic crust. The wet solidus for basalt/gabbro, andesite/tonalite and granite/rhyolite are from Stern *et al.*, (1975). Depth to Moho estimates are available from six of the localities based on petrology of the xenolith suites and/or independent seismic data. For the two localities where Moho depth estimates were not available (Fukue-jima and Jeju Island), the Moho depth is assumed to be equivalent to the nearby Chugoku District (11.1 kbars). All eight districts show temperatures at the Moho of around 760 to 860°C or higher, and all districts have Moho temperatures which are hotter than the wet solidus for basalt, andesite and rhyolite. The estimated depth at which the deep magmatic reservoir resides in the lower crust below the Tampakan district (5 to 6 kbars, 18 to 22 km; A) in hornblende geobarometry) is shown by the light grey band. The band encapsulates the range of ambient temperatures for lower-crustal rocks surrounding the deep chamber, prior to chamber emplacement, as inferred from the illustrated geotherms in other arcs. The dashed vertical line at 400°C represents the brittle-ductile transition. The geothermal gradient in the Tampakan district is likely to be similar to that of other island arc settings such as Ichinome-gata, Chugoku and Fukue-jima in Japan and Jeju Island in Korea, where crustal thicknesses are broadly comparable to the crustal thickness in the Tampakan district ( $\sim 31$  km). These data yield lower-crustal temperature estimates, at 18 to 22 km below Tampakan, in the range of 560 to 810°C. These temperatures straddle the temperature range of the wet-basalt to wet-rhyolite solidi ( $\sim 620$  to  $680^\circ\text{C}$ ). The conclusion to be drawn from these data is that large, hydrous, calc-alkaline magma chambers entrapped at depths of 18 to 22 km would conductively cool extremely slowly, and, if country rock temperatures are above  $\sim 650^\circ\text{C}$ , then low volume, residual fractionated melts could be preserved indefinitely, until relaxation of the tectonic compressive stress permits their buoyant ascent. These data, together with detailed thermal modelling by Rohrlach (2002), show that a large and deep lower crustal chamber may survive between successive recharge events throughout the period of compressive deformation.



stress,  $\sigma_h$ , that is responsible for crustal shortening and for inhibiting propagation of subvertical dykes is well approximated by the relation  $\sigma_h \approx V \cdot \eta / W$ , wherein  $V$  is the fractional shortening rate,  $\eta$  is the average viscosity of the deforming medium, and  $W$  is the distance over which the deformation occurs (England and McKenzie, 1982; Liu *et al.*, 2000).

In the Thermal Modelling of Magma Chamber Longevity section on chamber lifespan and cooling rate, we present a compilation of geotherms in six arcs, derived from geothermobarometry on xenoliths of upper-mantle and lower-crustal country rock sampled by new magma conduits that fed *monogenetic* volcanoes. Along these six geotherms, undisturbed by passage of prior batches of magma, the temperatures at  $5.5 \pm 0.5$  kb (corresponding to the top of the Tampakan magma chamber) lie in the range of 560–810°C and average  $\sim 685^\circ\text{C}$ . At these temperatures, country rock having an average composition of diorite has a viscosity on the order of  $10^{23}$  to  $10^{21}$  Pa-sec (Talbot, 1999). Viscosities in this range also typify gabbroic compositions at 700–800°C in the vicinity of the Moho.

The data in Fig. 5 and the relation  $\sigma_h \approx V \cdot \eta / W$  permit a rough estimate of the magnitude of the regional average  $\sigma_h$  as subduction convergence in south-central Mindanao ground to a halt while new subduction-thrust systems were being established along the Philippine Trench and the Sulu Trench to accommodate the continuing convergence between the Philippine Sea Plate and Eurasia. The diffuse deformation zone spans the interval from the Philippine Trench to the Sulu Trench, a distance of  $\sim 631$  km in the direction of plate convergence.

According to the vertical width of the black band at the top of Fig. 5, the amount of plate convergence not accommodated by subduction at the Sulu, Cotobato, and Philippine trenches was 13.5 mm/yr at the time of Tampakan porphyry copper mineralisation, and 30 mm/yr during high-sulphidation mineralisation. Taking these rates as estimates of  $V$ , 631 km for  $W$ , and  $10^{22}$  Pa-sec for  $\eta$ , we obtain  $\sigma_h \approx 68$  bars during porphyry-copper mineralisation and  $\sigma_h \approx 151$  bars during high-sulphidation mineralisation.

The result calculated in the earlier paragraph,  $(\rho_{rx} - \rho_{melt}) G \approx 40$  bars/km, implies that these values of  $\sigma_h$  would be capable of entrapping a dacitic melt column as thick as 1.7 km around the time of the porphyry copper mineralisation event, or a melt column  $\sim 3.8$  km thick around the time of the high-sulphidation mineralisation event. We note that the large uncertainties in rheology of the lower-crustal rocks make these estimates very rough, but they serve to illustrate the feasibility of entrapping buoyant magmas in the lower crust in regimes of strong horizontal compressive stress. Magmas entrapped by the stress regime can resume ascent when either i). they evolve to greater compositional buoyancy by continued magmatic differentiation, or ii). far-field tectonic stress relaxes. The latter cause may account for the commonly reported approximate synchronicity of mineralisation in several districts along a mineral belt.

## Thermal Modelling of Magma Chamber Longevity

A long-lived calc-alkaline magma reservoir is postulated to have evolved in the lower crust below the Tampakan district, trapped by the ambient stress regime during the early Pliocene collision in Mindanao. A reservoir life-span of  $\sim 7$  M.y. is indicated by prolonged magmatism in multiple over-printing volcanic cycles (see the Geochronology and Petrochemistry sections), and is implied by long-term ramping trends in incompatible and volatile components of the melt that are observed in successive magmatic cycles which erupted in the district. Thermal constraints are discussed below to show that magma can be stored in the lower crust over time frames of 3 to 10 million years, typical of the duration of arc orogenic events, thus allowing inheritance of volatiles through multiple cycles of chamber recharge and fractional crystallisation.

Petrological, temperature and pressure profiles of the lithosphere have been defined in several volcanically active regions, based on the study of xenolith suites, which allow the determination of geothermal gradients (Fig. 22). Regional geothermal gradients derived from studies of xenolith suites need to be interpreted carefully because, in some studies, unusually high geotherms have been attributed to local warming of the lower crust or upper mantle by the prior passage of melt. For reliable geotherm estimation using geobarometry and geothermometry, mafic and ultramafic xenoliths must have equilibrated along the geotherm prior to intrusion of the ascending host magma (Takahashi, 1980). Consequently the temperature in the lower crust is best constrained from geotherms that are calculated from xenolith suites which were entrained into the first eruptions of monogenetic volcanic fields. In these fields, the thermal structure of the upper mantle and lower crust has not been perturbed by prior magmatism. Geothermal gradients tend to be steeper in volcanic island arcs than in passive continental settings because the crust is thinner, and has been thermally heated by subduction-related magmatism. The temperature in the vicinity of the crust-mantle boundary in the Ichinome-gata, Chugoku, Jeju Island, Mercaderes, Camp Creek and Ventura regions (Fig. 22) are all between  $\sim 150$  and  $\sim 250^\circ\text{C}$  hotter than the solidus of differentiation products of mantle-derived arc-basaltic melt having a normal initial content of dissolved  $\text{H}_2\text{O}$  ( $\geq 0.8$  wt. %). These data indicate that if a large, evolving, hydrous calc-alkaline magmatic reservoir is trapped in the lower crust or at the Mohorovicic disconformity, the temperatures of the surrounding rocks are sufficiently high to allow the reservoir to exist for several million years, or indefinitely, if compression in the lower crust prevents ascent of the residual melt. Consequently magma that has ponded at the crust-mantle boundary or at some other horizon of rheological contrast in the lower crust can undergo long-term evolution through multiple fractionation and replenishment cycles over the duration of a typical compressional deformation event and/or orogeny in the overlying crust (3 to 10 M.y.). Upper crustal sub-volcanic chambers have life-spans that are typically less than the 400 K.y., and which match the

lifespan of convergent margin stratovolcanoes that they build. Cooling of these shallow-level chambers is facilitated by the cooler country rocks in the upper crust and by convective groundwater systems. In contrast, the hot thermal regime surrounding lower-crustal magma reservoirs facilitates extremely slow cooling over several million years, and in some thermal regimes guarantees their indefinite longevity during periods of compression in the overlying crust.

Using the finite-element software program KWare HEAT Version 4.03.0131\* (<http://www.ees1.lanl.gov/Wohletz/Heat.htm>; Wohletz and Heiken, 1992), and a range of appropriate geothermal gradients and thermal conductivities of country rocks, and varied thicknesses of horizontal sheet-like magma chambers, Rohrlach (2002) conducted single-stage cooling models and showed that deep-seated magma chambers emplaced into the lower crust could retain magma above the wet solidus on time-scales of 0.4 to over 8 M.y. for chamber thicknesses of 1 to 4 km and emplacement depths of 18 to 30 km.

In arc segments that are under tectonic compression, magmas are trapped in the lower crust by tectonic stress at depths where the normal, ambient thermal regime allows calc-alkaline magma reservoirs to reside at temperatures higher than the wet solidus for several million years, and in some circumstances, indefinitely. Given such long lifespans, there is a very high likelihood that deep magma chambers would experience intermittent replenishment of mantle-derived magma, and partial mixing of evolved resident and primitive replenishing batches. The evolution of fractionally crystallising, intermittently replenished, intermittently tapped chambers entails cyclic ramp-up in the residual melt's concentrations of volatile and other incompatible components, as described previously.

## Model and Metallogenic Implications

Prior to the late Miocene collision in the northern Sangihe arc, relatively primitive, clinopyroxene  $\pm$  olivine-dominated, H<sub>2</sub>O poor, basaltic andesites and basalts erupted along the Sangihe arc. Mantle-derived basaltic arc magmas

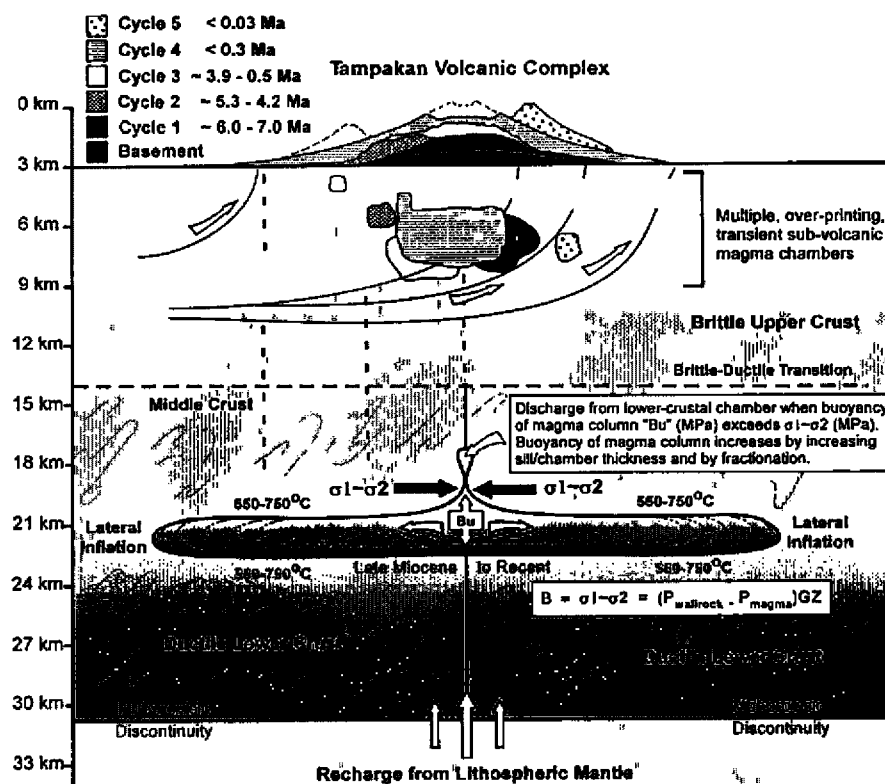


Figure 23: *Dimensionally undistorted representation of the long-lived polygenetic Tampakkan volcanic complex*, with multiple short-lived (0.4 to 1.0 M.y.) upper-crustal magma chambers and volcanic cycles, each of which sequentially tapped a large and long-lived (7 M.y.), sill-like magma chamber near the Moho. During the late Miocene to Recent period of crustal compression, the deep melt reservoir experienced multiple cycles of replenishment and residual accumulation of volatiles and other incompatible components, and evolved by fractionation of ultramafic cumulates that were increasingly hornblende-dominated in later cycles. Tectonic compression entrapped the chamber at or near the Moho, although crustal shortening and magmatic underplating since the late Miocene have since lowered the Moho to present depths of 25 to 30 km. Magmas escaped periodically when the buoyancy of residual melt fractions overpowered the inhibiting stress, or when the horizontal stress relaxed intermittently. Water and chlorine concentrations were ramped by inheritance through successive million-year-scale recharge and differentiation cycles. Porphyry ore formed from water-rich melts that exsolved a magmatic-hydrothermal fluid phase *deep* in the upper crust, where chlorine was efficiently partitioned from the melt to a *high-density* fluid. High-sulphidation mineralisation formed from melts which had lower magmatic water contents and which therefore exsolved a magmatic-hydrothermal fluid at lower pressures where exsolution of two-phase 'dense' vapor + liquid favoured volatile transport of the high-sulphidation metal suite (Cu, Au, As, Tc, V). Although the porphyry and high-sulphidation deposits formed from separate upper crustal hydrothermal systems at Tampakkan, they are intimately related to the same long-lived lower crustal magmatic reservoir which was instrumental in imparting fertile characteristics to the magmatic system. Hydrothermal remobilisation of the older porphyry ore was probably important to generation of the giant accumulation of Cu in the high-sulphidation deposit.

had relatively unimpeded access to the upper crust. Crustal compression in the Tampakan district commenced in the Late Miocene (~6 Ma) and peaked in the middle Pliocene when subduction slowed and then stopped at the outward dipping northern Sangihe and Halmahera trenches, and convergence between the Philippine Sea and Eurasian Plates was partitioned into intraplate deformation and development of new Cotabato and Philippine Trench subduction thrusts. During early collision in the Tampakan district, ascending magmas that were derived from the wedge above the subsiding Molucca slab encountered increasing intensities of compressive stress within the crust. Magmas became entrapped at progressively deeper levels in the lower crust beneath the Tampakan district through the Pliocene and Pleistocene epochs. Pressure-depth estimates using Al-in-hornblende geobarometry record crystal fractionation to rhyolitic residual melt compositions at 5 to 6 kbars pressure and at mean depths of  $20 \pm 2.2$  km depth within the lower crust of southeast Mindanao.

Detailed  $^{238}\text{U}$ - $^{206}\text{Pb}$ ,  $^{40}\text{Ar}/^{39}\text{Ar}$ , K/Ar and  $^{87}\text{Sr}/^{86}\text{Sr}$  geochronological studies reveal that the Tampakan district contains a series of overlapping stratovolcanic centres that developed from the Late Miocene (at the onset of collision) to the present (during the waning stages of collision). Petrological and petrochemical trends reveal that magmatism in successive volcanomagmatic cycles became slightly more siliceous and much more hydrous over a time frame of 6 to 7 M.y. Hornblende and biotite become modally more important over time and appear at more mafic stages of the crystallisation sequence in successive magmatic cycles. U/Ti ratios in detrital zircon grains from the district, and other petrochemical indicators, track the progress of magmatic differentiation and cooling of magmas during the ~6-M.y. collision event, and provide a high-resolution record of magma chamber replenishment and crystallisation cycles in the long-lived magmatic series. The cyclic ramp-up of those element ratios coincides with a 7 M.y.-long "sawtooth" cyclic ramp-up in concentrations of volatiles and incompatible trace-elements relative to whole-rock  $\text{SiO}_2$  in erupted andesites and dacites. Dissolved water contents climbed from 4.1 wt. % to 8.2 wt. % as  $\text{SiO}_2$  in erupted magmas evolved from 57 to 67 wt. %. The deep magmatic reservoir was periodically tapped to form transient sub-volcanic chambers and four overprinting stratovolcanoes (Fig. 23).

In addition to the Tampakan district, some notable examples of long-lived and fertile centres include the Potrerillos district (Cobre, Norte and El Hueso deposits; Marsh *et al.*, 1997) and the Nevados de Payachata region (Choquelimpie high-sulphidation deposit; Wörner *et al.*, 1988). Within deeply exhumed districts, magmatic intrusive complexes also record a similar spatial focus of long-lived magmatism (e.g., the Fortuna and El Abra complexes associated with the Chuquicamata and El Abra porphyry copper deposits (Ballard, 2001).

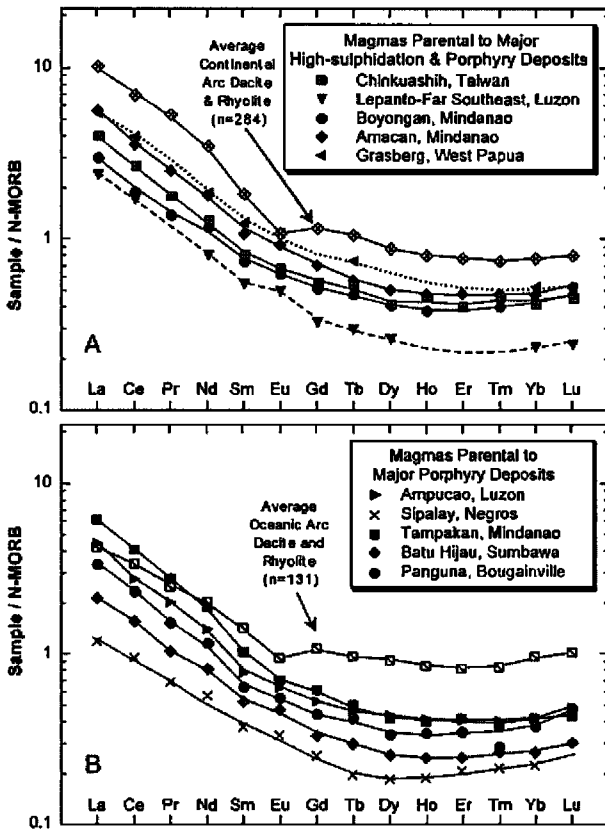
Modelling of crustal stress in the southeast Mindanao collision zone reveals that entrapment of magmas by compressive stress within the crust is easily achieved at typical strain rates of collisional orogens, and is consistent

with the development of volcanic gaps in several other arc segments now undergoing collision with oceanic plateaux or other subduction-resistant features. Numerical thermal modelling of the syn-collisional Tampakan magmatic system, supported by compilation of arc-geotherm data from P-T studies of crust- and mantle-derived xenolith suites elsewhere, reveals that the longevity of a 1 to 4 km thick and 15 to 30 km wide, pancake-shaped, conductively cooling sill in the lower-crust is several million years. This chamber longevity allows its repeated replenishment from the mantle and can sustain multiple upper-crustal volcanic cycles.

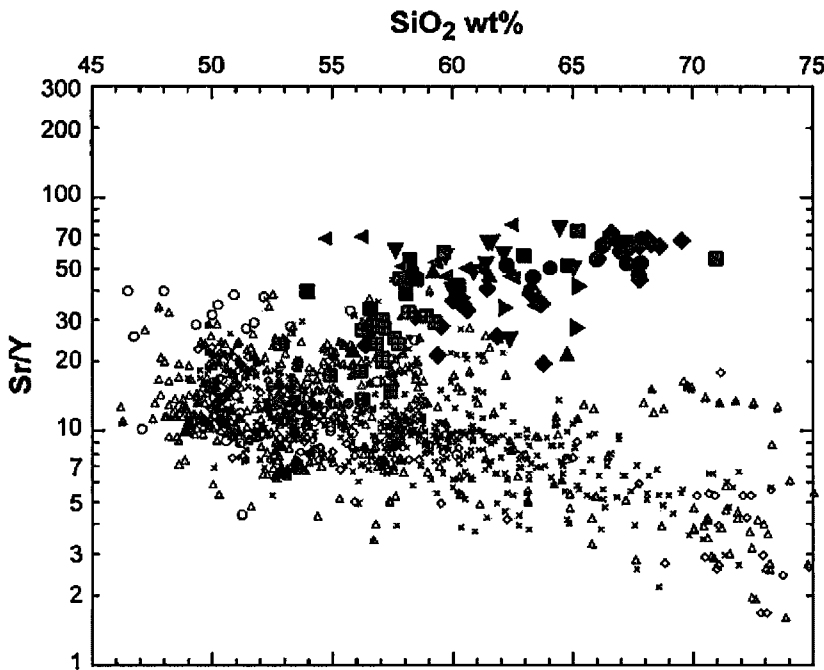
During and following porphyry Cu-Au mineralisation, thrust faulting occurred within the Tampakan district, and was widespread in southeastern Mindanao. The Cycle 3 volcanic centre and its contained porphyry Cu deposit were uplifted by a district-scale ramp anticline that developed on a collision-stage thrust fault. The Cycle 3 stratovolcano underwent rapid, and perhaps catastrophic (?) denudation between 4.25 and 3.93 Ma, when two to three kilometres of overburden were removed, unroofing the Tampakan porphyry system and exposing lithostatically-pressured porphyry-stage veins at the palaeosurface.

The Tampakan high-sulphidation epithermal mineralisation formed between 3.39 and 3.20 Ma, during the latter part of Cycle 4a stratocone construction, at a palaeodepth of ~2 km (Rohrlach, 2002). Parental melts to high-sulphidation ore were less siliceous and had lower water contents than those that formed the preceding porphyry Cu mineralisation, allowing intrusion of high-sulphidation-stage melts to shallow crustal levels where more sulphur- and arsenic- and gold-rich fluids exsolved as a *vapor-dominated* two-phase fluid that may be typical of this deposit style (Hedenquist *et al.*, 1998).

Copper-ore-forming arc magmas of Phanerozoic age worldwide have a distinctive, shared set of lithophile trace-element characteristics that are well accounted for by general aspects of the genetic model above that we have described for the Tampakan ore-forming igneous suite - viz., magmatic differentiation of ordinary mantle-derived basaltic magmas mainly at relatively high pressure in long-lived magma chambers that undergo intermittent replenishment, tapping, and mixing during continuous fractional crystallisation. This process leads eventually to  $n^{\text{th}}$ -cycle residual melts having unusually high contents of dissolved  $\text{H}_2\text{O}$  (and probably of Cl and  $\text{SO}_3$  and other relatively incompatible chemical components), relative to normal contents of major-oxide components that are buffered by the crystallising assemblage of common rock-forming minerals. The build-up of dissolved  $\text{H}_2\text{O}$  causes hornblende to advance in the mineral saturation sequence of successive cyclic units. Hornblende is a relatively strong sink for Y and heavier REEs (especially from Tb to Tm), leaving residual melts depleted in those components. High pressure (~5 to 10 kbar) increases the thermal stability (saturation temperature) of hornblende and markedly retards plagioclase in the saturation sequence of major minerals, for any given composition of the starting melt (e.g., Ulmer, 1988). A high content of dissolved  $\text{H}_2\text{O}$  further



**Figure 24: Abundances of REE in fresh or least-altered whole-rock samples of Pliocene and Pleistocene ore-forming porphyritic intrusives** in compressive segments of the eastern Sunda and western Pacific arcs are compared with REE abundances in ordinary arc dacites and rhyolites from relatively non-compressive segments of 11 active epi-continental arcs (Andean Southern Volcanic Zone, northern Central America, Trans Mexico, Cascade, Alaska Peninsula, Kamchatka, North Honshu, Southwest Honshu, Ryukyu, western Sunda, New Guinea Highlands) and 12 intra-oceanic arcs (Alcuthian, Kurile, Mariana, Izu-Bonin, North Luzon, Sangihe, Halmahera, Banda, Bismarck, Solomon, New Hebrides, Tonga). REE abundances in samples arc related to abundances of those elements in average Normal Mid-Ocean-Ridge Basalts (N-MORB; values of Sun and McDonough, 1989). The average felsic arc magmas in mostly unmineralised arc segments have a conspicuous negative Eu anomaly due to prior fractionation of a large proportion of intermediate-composition plagioclase (labradoritic and andesine, mainly). The barren felsic suites, especially in oceanic arcs, also have a relatively flat pattern of middle to heavy REE's (Gd to Lu), due to fractionation of a large proportion of augite and little or no hornblende. In contrast, the Cu-ore-productive felsic arc magmas are more depleted in REEs of the Gd to Lu interval, and generally have a minimum at around Ho or Er, a shape caused by protracted fractionation of a large proportion of cumulus hornblende from exceptionally hydrous magmas. Data compiled by R.R. Loucks from >200 literature sources.



**Figure 25: Rock suites temporally and spatially associated with major magmatic-hydrothermal Cu-Au deposits of Pliocene and Pleistocene age** in Taiwan, Philippines, Sumbawa, New Guinea, and the Solomon Islands (black and grey solid symbols) are plotted for comparison with barren arc segments (smaller grey open symbols) in the northwest Pacific (Kurile, North Honshu, Ryukyu, and Izu-Bonin arcs) that contain no known significant Cu or Au deposits in the time and space range of the suites plotted. Unaltered or least-altered (to weak propylitic) samples of ore-related igneous suites are from the same volcanic-intrusive centre as hosts the deposit, and all arc < 1 M.y. older than the mineralisation age at each locality, as determined from radiometric dates and structural relations to ore. All these deposits formed in regimes of strong horizontal compressive stress, so parental basaltic magmas were trapped at depth and are poorly represented in the eruptive and epizentral intrusive igneous suites penecontemporaneous with mineralisation. Basalts erupted in these regions before and after the metallogenic epoch plot in the Sr/Y range 7 to 30 typical of tholeiitic to calc-alkalic arc basalts. Data compiled by R.R. Loucks from >100 literature sources.

**Ore-Forming Igneous Suites in Western Pacific Arcs:**

- Chinkuashih, Northern Taiwan
- ▼ Lepanto / Far Southeast, NW Luzon
- ▲ Black Mountain/Thanksgiving, NW Luzon
- ▶ Ampucao Au(-Cu) Porphyry, NW Luzon
- ◆ Santo Tomas II, NW Luzon
- Boyongan, East Mindanao
- Tampakan, Central Mindanao
- ◆ Batu Hijau, Sumbawa, Indonesia
- ▲ Grasberg, West Papua, Indonesia
- Ok-Tedi, Papua New Guinea
- Panguna, Bougainville, Solomon Arc

**Unmineralised Reference Suites:**

- Kurile Arc 43.8-50.9° N, <6 M.y.
- × N. Honshu Arc 35° -41° N, >138° E, <6 M.y. Old
- ◇ Central Ryukyu Arc 25-31° N, <5 M.y. Old
- ▲ Izu-Bonin Arc 27.1-34.9° N, <5 M.y. Old

delays the onset of feldspar saturation, and diminishes the modal proportion of plagioclase in hornblende-bearing assemblages (because hornblende consumes plagioclase-forming chemical components of the melt) and makes the crystallising plagioclase poorer in Na, Eu and Sr at any specified ratio of Na/(Na+Ca) in the melt (Panjasawatwong *et al.*, 1995; Blundy and Wood, 1991), so Cu-ore-forming magmas avoid plagioclase-induced depletion of Sr and Eu and hence lack a conspicuous negative Eu anomaly in their normalised REE patterns. Relatively sensitive discriminants of copper-fertile arc magmas may be formulated by ratioing relatively enriched elements to relatively depleted elements, such as the ratios Eu/Er or Sr/Y.

Fig. 24 illustrates the degree to which copper-ore-forming batches of subduction-generated calc-alkalic magma differ in REE abundances from ordinary metallogenically infertile calc-alkalic arc magmas of similar major-element chemical composition. Lang and Titley, (1998) showed very similar REE distinctions between copper-ore-productive and

unproductive granitoid porphyry intrusives in Arizona. The plotted samples from ore-productive intrusives (from drill core beneath mineralised depths, or from satellite dykes emanating from the mineralised intrusive, or late syn-mineral intrusives in a composite complex, etc.) retain most plagioclase and hornblende in a petrographically fresh condition; advanced propylitic, sericitic and potassic alteration are associated with loss of most uni- and di-valent elements and cannot be used reliably. Spoon-shaped profiles of REE abundances, without significant Eu depletion, are distinctive of arc magmas that are chemically specialised for copper metallogeny. In a global survey (not shown), there is no significant chemical difference between magmas that produce major porphyry Cu(±Au) ore deposits and magmas that produce major high-sulphidation vein- and manto-type Cu-Au deposits.

In Fig. 25, the Sr/Y ratio in mafic-to-felsic differentiation series in arc segments that contain no known significant magmatic-hydrothermal Cu mineralisation is compared

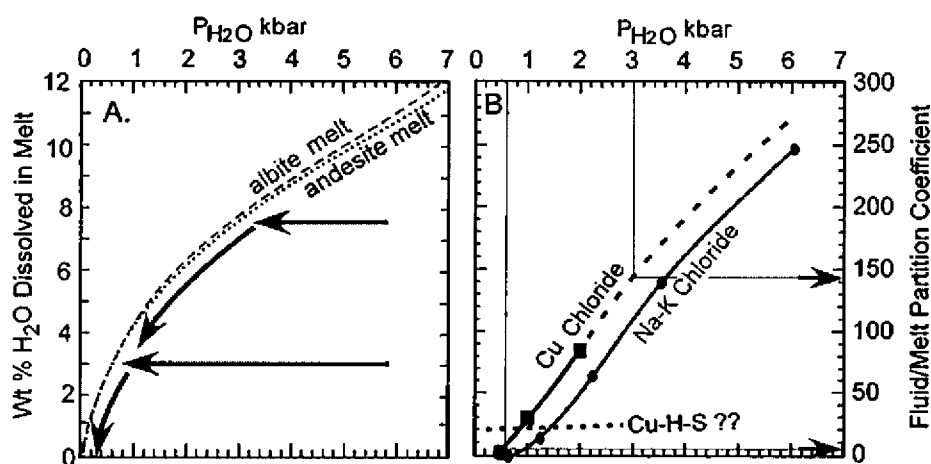


Figure 26: A. Dotted and dashed curves show the solubility of H<sub>2</sub>O in silicate melts of andesitic and "alkali rhyolitic" (albite) composition as a function of confining pressure (Burnham, 1979b). If a water-undersaturated andesitic melt containing 3 wt % dissolved H<sub>2</sub>O (typical of augite andesites) departed a lower-crustal magma chamber at 6 kbar (~22 km depth), its trajectory on this plot (lower horizontal arrow) would intercept the water saturation curve at ~0.6 kbar, and during further ascent of the melt+fluid mixture, the melt's content of dissolved H<sub>2</sub>O would decrease along a trajectory like the arrow in the lower left. One- or two-phase aqueous fluid exsolved at  $P \leq 0.6$  kb is entirely or almost entirely a low-density gas that is a poor solvent of dissolved solids. Alternatively, if a water-undersaturated andesitic melt containing 7.5 wt % dissolved H<sub>2</sub>O departed a lower-crustal magma chamber at 6 kbar (cf. Tampakan pressures and dissolved H<sub>2</sub>O contents in Table 1), its ascent trajectory (upper horizontal arrow) would intercept the water saturation curve at ~3 kbar or ~11 km depth, and during continued ascent the melt's content of dissolved H<sub>2</sub>O would decline along the saturation curve as indicated by sloping arrows. Aqueous fluid exsolved at 3 kbar is a single-phase supercritical fluid of liquid-like density that is an effective solvent of dissolved solids.

B. The partition coefficient of alkali chloride between aqueous fluid and haplogranitic melt varies sensitively with  $P_{H_2O}$  or partial molar density of H<sub>2</sub>O in the aqueous fluid, according to experiments at 810°C and 0.6 to 6.0 kbar by Shinohara *et al.*, (1989). In these experiments, the melt contains ~700 to 2000 ppm Cl, in the typical range of felsic arc magmas (Wallace, 2005). Also plotted are values of fluid/haplogranitic melt partition coefficients of Cu<sup>II</sup> as chloride complexes in the fluid (Williams *et al.*, 1995, mean of 2 relatively low-Cl experiments at 0.5 kbar and 850°C, having ~3500 ppm Cl in the melt and in the fluid; and mean of 6 relatively low-Cl experiments at 1 kbar and 800°C averaging ~1300 ppm Cl in the melt and ~14,500 ppm Cl in the fluid; and 1 experiment by Keppler and Wyllie, 1991, at 2 kbar and 750°C, having ~49 000 ppm Cl in the fluid and ~1000 ppm Cl in the melt, which is their only experiment that closely approximates Cl contents typical of natural felsic melts). The selected Cu partitioning experiments are all those having melt Cl contents like typical pre-eruptive arc dacites and rhyolites, as indicated by fluid salinities reported by Williams *et al.* and by Keppler and Wyllie, in combination with the

$D_{Cl}^{fluid/melt}$  values of Shinohara *et al.*, (1989) at the relevant pressures. The experiments on Cu partitioning only span a  $P_{H_2O}$  range of 0.5 to 2 kbar, so we have estimated the values at higher pressure by extrapolation parallel to the well-constrained curve for alkali chlorides, inasmuch as aqueous CuCl<sup>+</sup> has the same molecular structure as aqueous NaCl<sup>+</sup> and KCl<sup>+</sup>, and Cu is not expected to undergo significant configurational changes in these sulphur-free haplogranitic melts in the 2 to 6 kbar interval. Heinrich *et al.*, (1999) have reported analyses of natural fluid inclusions in sub-volcanic magmatic-hydrothermal systems which show that Cu, Au, and As are concentrated in fluid inclusions that trapped a low-salinity vapour phase, whereas inclusions that trapped a coexisting high-salinity brine have low contents of Cu, Au and As. They infer that Cu, Au, and As were probably partitioned from melt into vapour as metal-hydrosulphide (not chloride) complexes. Equilibrium values of  $D_{Cu}^{fluid/melt}$  as Cu hydrosulphide complexes have not been experimentally determined, but the hypothetical dashed line labelled "Cu-H-S???" considers the possibility that CuCl exsolved at higher pressure may undergo a change of speciation to volatile Cu-H<sub>2</sub>S complexes in sulphur-rich low-density aqueous fluids at magmatic temperatures and low pressures.

with the Sr/Y ratio in volcanic and hypabyssal intrusive rocks spatially and temporally associable with major Cu( $\pm$ Au) ore deposits of porphyry and high-sulphidation types. Chinkuashih, Grasberg and Ok Tedi overlie Palaeozoic to Precambrian continental basement; other deposits are on Mesozoic-Cenozoic arc basement. The Kurile and Izu Bonin arcs are built upon oceanic lithosphere, whereas the Ryukyu and North Honshu arcs overlie mature continental basement of Palaeozoic or greater age. The age of the subducting oceanic lithosphere under some ore deposits is Mesozoic (Chinkuashih, Tampakan, Batu Hijau, Panguna) and Paleogene under the remainder of deposits, making partial melting of the subducting eclogitic slabs an implausible explanation for the high Sr/Y values of the ore-forming igneous suites (Peacock *et al.*, 1994). Compressive-stress entrapment of mantle-derived basaltic magmas in intermittently replenished, continuously crystallising uppermost-mantle or lower-crustal magma chambers can account for a differentiation trend from predominantly ordinary parental arc basaltic melts toward residual felsic melt fractions having high Sr/Y, as described in the Petrochemistry section above.

The reason that lithophile-trace-element indicators of unusually high hydration state of the melt are also indicators of exceptional copper metallogenic fertility seems to be that exceptionally hydrous melts are likely to begin exsolving a hydrothermal fluid at unusually great depth during their ascent from circum-Moho magma chambers. The higher the pressure at which the fluid exsolves, the denser it tends to be, and the more effective as a solvent of dissolved solids, so the more efficient it is in extracting relatively non-volatile copper chloride and other salts and silica from the parental melt. Fig. 26A illustrates the degree to which the pressure (depth) of onset of fluid saturation is sensitive to the dissolved H<sub>2</sub>O content of the ascending, decompressing melt. Fluid that exsolves at shallow subvolcanic depths at which porphyry ore deposits form, is chiefly or entirely a low-density gas (with or without a very subordinate mass of conjugate hypersaline brine), whereas aqueous fluid that exsolves from the melt at mid-crustal pressures  $\geq 3$  kbar is a single-phase supercritical fluid of liquid-like density (Sourirajan and Kennedy, 1962). Figure 26B presents experimental evidence that the partition coefficient of NaCl and KCl from granitoid melt into exsolving fluid increases very sensitively with increasing density (pressure) of the exsolving fluid. In these 810°C experiments by Shinohara *et al.*, (1989), the granitoid melts have Cl contents in the range 700 to 2000 ppm that are typical of felsic arc magmas (Wallace, 2005). Experimental measurements of the partition coefficient of CuCl between granitoid melt and hydrothermal fluid at 800 to 850°C, selected on the basis of having Cl contents in the fluid and melt in same natural range as the experiments by Shinohara *et al.*, (1989) show a sensitivity of  $D_{\text{CuCl}}^{\text{fluid/melt}}$  to fluid pressure and bulk fluid density that parallels the trend of  $D_{\text{(Na,K)Cl}}^{\text{fluid/melt}}$  in the 0.5 to 2 kbar range of the available Cu data. On that basis, we have extrapolated the CuCl trend to higher pressures, parallel to the alkali chloride trend.

A very hydrous silicate melt containing 7.5 wt % dissolved H<sub>2</sub>O (left panel) that began to exsolve a saline (~1.5 to 3.0 molal Cl) hydrothermal fluid at 3.0 kbar would initially have  $D_{\text{Cu}}^{\text{fluid/melt}} \approx 140$ , whereas the ascending melt having only 3 wt. % H<sub>2</sub>O that began to exsolve low-salinity (~0.02 to 0.06 molal Cl) H<sub>2</sub>O gas at 0.6 kbar would initially have only a  $D_{\text{Cu}}^{\text{fluid/melt}} \approx 4$ , as indicated by the arrow pointers in the right panel. If the Cu-rich, dense fluid that exsolves from a H<sub>2</sub>O-rich melt at high pressure segregates buoyantly to the top of an ascending intrusion, the fluid can avoid having to give back its high Cu content to the melt as the ascending magma decompresses and  $D_{\text{Cu}}^{\text{fluid/melt}}$  decreases to low values, and thereby preserve that fluid's advantage as an ore-forming fluid at subvolcanic depths. By the time the magma has ascended by dyke propagation to shallow subvolcanic depths, the accumulated fluid at the top of the intrusion would be a composite of fractions that exsolved earlier at higher pressure and fractions that exsolved later at lower pressure. Later fractions of lower-density fluid exsolving at lower pressure are increasingly efficient at extracting gaseous components (HCl, SO<sub>2</sub>, H<sub>2</sub>S etc.) from the silicate melt (enhancing the fluid's capacity to make high-sulphidation-type mineralisation), but they are much poorer at extracting relatively non-volatile components (chloride salts, silica, etc.) from the melt. Heinrich *et al.*, (1999) have presented empirical evidence that fluid inclusion populations which trapped conjugate magmatic aqueous gas and hypersaline brine have marked enrichments of Cu (as well as Au and As) in the low-density gas phase, relative to the brine. They suggest that partitioning of Cu into the gas phase as sulphide complexes is likely. Such low-pressure re-speciation of Cu from chloride complexes to sulphide complexes as the bulk fluid evolves in density and sulphur content need not affect our interpretations that porphyry- and many coeval high-sulphidation-type Cu deposits developed from unusually H<sub>2</sub>O-rich magmas that must have begun to exsolve dense ore-forming fluid at mid-crustal depths.

Based on our case study of the Tampakan deposit and the chemistry of barren and fertile arc rocks globally, we conclude that the characteristic occurrence of major porphyry copper(-gold-molybdenum) and high-sulphidation gold-copper(-silver) deposits in focussed metallogenic districts and epochs framed by barren arc magmatism is governed and ultimately modulated by the transient stress state in the arc lithosphere, which in turn is mediated by changes in global geodynamics and arrival of buoyant, subduction-resistant features in the subducting plate.

## References

- Anderson, D.J., Lindsley, D.H., and Davidson, P.M., 1993 - QUILF: A PASCAL program to assess equilibria among Fe-Mg-Mn-Ti oxides, pyroxenes, olivine, and quartz, *Computers and Geosciences* v. 19, pp. 1333-1350.
- Anderson, J.L. and Smith, D.R., 1995 - The effects of temperature and  $f_{\text{O}_2}$  on the Al-in-hornblende

- barometer, *American Mineralogist* v. 80, pp. 549-559.
- Aoki, K.-I., Yoshida, T. and Zhe, J.Y., 1989 - Petrology and geochemistry of Pleistocene dacitic and rhyolitic pyroclastic flows from southern part of northeast Honshu Japan, *Journal of Mineralogy, Petrology and Economic Geology*, v. 84, pp. 1-14.
- Arribas, A. Jr, Hedenquist, J.W., Itaya, T., Okada, T., Concepción, R.A. and Garcia, J.S. Jr., 1995 - Contemporaneous formation of adjacent porphyry and epithermal Cu-Au deposits over 300 ka in northern Luzon, Philippines, *Geology*, v. 23, pp. 337-340.
- Aurelio, M.A., Barrier, E., Rangin, C. and Muller, C., 1991 - The Philippine Fault in the late Cenozoic tectonic evolution of the Bondoc-Masbate-N.Leyte area, central Philippines, *Journal of Southeast Asian Earth Sciences* v. 6 (3/4), pp. 221-238.
- Baker, D.R. and Eggler, D.H., 1983 - Fractionation paths of Atka (Aleutians) high-alumina basalts: constraints from phase relations, *Volcanology and Geothermal Research* v. 18, pp. 387-404.
- Baker, L. and Rutherford M.J., 1992 - Anhydrite breakdown as a possible source of excess sulfur in the 1991 Mount Pinatubo eruption, *EOS, Transactions AGU* v. 73, p625.
- Baker, L. and Rutherford M.J., 1996 - Crystallisation of anhydrite-bearing magmas, *Transactions of the Royal Society of Edinburgh, Earth Sciences* v. 87, pp. 33-41.
- Ballard, J., 2001 - A comparative study between the geochemistry of ore-bearing and barren calc-alkaline intrusions, *Unpublished PhD thesis, Australian National University, Canberra*.
- Barrier, E., Huchon, P. and Aurelio, M.A., 1991 - Philippine Fault: a key for Philippine kinematics, *Geology*, v. 19, pp. 32-35.
- Beattie, P., 1994 - Systematics and energetics of trace-element partitioning between olivine and silicate melts: implications for the nature of mineral/melt partitioning, *Chemical Geology*, v. 117, pp. 57-71.
- Bindeman, I.N., Davis, A.M. and Drake, M.J., 1998 - Ion microprobe study of plagioclase-basalt partition experiments at natural concentration levels of trace elements, *Geochimica et Cosmochimica Acta* v. 62, pp. 1175-1193.
- Blatter, D.L. and Carmichael, I.S.E., 1998 - Plagioclase-free andesites from Zitácuaro (Michoacán), Mexico: petrology and experimental constraints, *Contributions to Mineralogy and Petrology*, v. 132, pp. 121-138.
- Blundy, J. and Wood, B.J., 1991 - Crystal-chemical controls on the partitioning of Sr and Ba between plagioclase feldspar, silicate melts, and hydrothermal solutions, *Geochimica et Cosmochimica Acta*, v. 55, pp. 193-209.
- Burnham, C.W., 1979a - The importance of volatile constituents; in Yoder, H.S. Jr. (Ed.), *The Evolution of the Igneous Rocks: Fiftieth Anniversary Perspectives, Princeton University Press, Princeton, N.J.*, pp. 439-482.
- Burnham, C.W. 1979b - Magmas and hydrothermal fluids; in Barnes, H.L. (Ed.), *Geochemistry of Hydrothermal Ore Deposits, New York, John Wiley and Sons*, pp. 71-136.
- Burnham, C.W. and Ohmoto, H., 1980 - Late-stage processes of felsic magmatism, *Mining Geology Special Issue*, v. 8, pp. 1-11.
- Cardwell, R.K., Isacks, B.L. and Karig, D.E., 1980 - The spatial distribution of earthquakes, focal mechanism solutions and subducted lithosphere in the Philippine and northeastern Indonesian islands; in Hayes, D.E., (Ed.), *The Tectonic and Geologic Evolution of Southeast Asian Seas and Islands, American Geophysical Union Monograph* v. 23, pp. 1-35.
- Carroll, M.R. and Rutherford, M.J., 1988. Sulfur speciation in hydrous experimental glasses of varying oxidation state: results from measured wavelength shifts of sulfur X-rays, *American Mineralogist*, v. 73, pp. 845-849.
- Castillo, P.R., Janney, P.E. and Solidum, R.U., 1999 - Petrology and geochemistry of Camiguin Island, southern Philippines: insights to the source of adakites and other lavas in a complex arc setting, *Contributions to Mineralogy and Petrology*, v. 134, pp. 33-51.
- Cathles, L.M., Erendi, A.H.J. and Barrie, T., 1997 - How long can a hydrothermal system be sustained by a single intrusive event, *Economic Geology*, v. 92, pp. 766-771.
- Choi, S.H., Jwa, Y-J. and Lee, H.Y., 2001 - Geothermal gradient of the upper mantle beneath Jeju Island, Korea: evidence from mantle xenoliths, *The Island Arc*, v. 10, pp. 175-193.
- Conceição, R.V., Mallmann, G., Koester, E., Schilling, M., Bertotto, G.W. and Rodriguez-Vargas, A., 2005 - Andean subduction-related mantle xenoliths: isotopic evidence of Sr-Nd decoupling during metasomatism, *Lithos* v. 82, pp. 273-287.
- Corpuz, E.S.G., 1992 - Petrology and geochemistry of the Central Mindanao arc, southern Philippines, *PhD Thesis, University of Canterbury, New Zealand*.
- Defant, M.J. and Drummond, M.S., 1990 - Derivation of some modern arc magmas by melting of young subducted lithosphere. *Nature*, v. 347, pp. 662-665.
- Domingo, E.G., Sevillo, D.J., Ferrer, N., Apostol, A., Aurelio, M., Quebral, R., Pubellier, M., Almeda, R., Ferrer, H., Cadawan, B., Comsti, E., Pena, R., Baluda, R., Yumul, G., Villamor, R., Rillon, E., Umbal, J., Diegor, W., Evangelista, D. and Pascual, M., 1995 - Guidebook for field trips GEOSEA '95 eighth regional conference on geology, minerals and energy resources of Southeast Asia, 19-23 February 1995, Philippines, pp. 61-72.
- Drake, M.J. and Weill, D.F., 1975 - The partition of Sr, Ba, Ca, Y, Eu<sup>2+</sup>, Eu<sup>3+</sup> and other REE between plagioclase feldspar and magmatic silicate liquid, *Geochimica et Cosmochimica Acta* 39, 689-712.



- Dunn, T. and Sen, C., 1994 - Mineral/matrix partition coefficients for orthopyroxene, plagioclase, and olivine in basaltic to andesitic systems: a combined analytical and experimental study, *Geochimica et Cosmochimica Acta*, v. 58, 717-733.
- Elburg, M.A. and Foden, J.D., 1998 - Temporal changes in arc magma geochemistry, northern Sulawesi, Indonesia, *Earth and Planetary Science Letters*, v. 163, pp. 381-398.
- Esperanca, S. and Holloway, J.R., 1984 - Lower crustal nodules from the Camp Creek Latite, Carefree, Arizona; in Kornprobst, J., (Ed.), *Kimberlites II: The mantle and crust-mantle relationships. Proceedings of the Third International Kimberlite Conference- Volume 2*, Elsevier, 1984.
- Esperanca, S., Carlson, R.W. and Shirey, S.B., 1988 - Lower crustal evolution under central Arizona: Sr, Nd and Pb isotopic and geochemical evidence from the mafic xenoliths of Camp Creek, *Earth and Planetary Science Letters*, v. 90, pp. 26-40.
- Ewart, A., 1982 - The mineralogy and petrology of Tertiary-Recent orogenic volcanic rocks: with special reference to the andesitic-basaltic compositional range; in *Andesites: orogenic andesites and related rocks*, Thorpe, R.S., (Ed.), Chichester: Wiley, pp. 26-87.
- Ewart, A. and Griffin, W.L., 1994 - Application of proton-microprobe data to trace-element partitioning in volcanic rocks, *Chemical Geology*, v. 117, pp. 251-284.
- Fujinawa, A., 1992 - Distinctive REE patterns for tholeiitic and calc-alkaline magma series co-occurring at Adatara volcano, northeast Japan, *Geochemical Journal*, v. 26, pp. 395-409.
- Hack, P.J., Nielsen, R.L. and Johnston, A.D., 1994 - Experimentally determined rare-earth element and Y partitioning behavior between clinopyroxene and basaltic liquids at pressures up to 20 kbar, *Chemical Geology*, v. 117, pp. 89-105.
- Hall, R., 1996 - Reconstructing Cenozoic SE Asia; in Hall, R. and Blundell, D., (Eds.), *Tectonic Evolution of Southeast Asia*, *Geological Society*, Special Publication No. 106, pp. 153-184.
- Hall, R., 2002 - Cenozoic geological and plate tectonic evolution of SE Asia and the SW Pacific: computer-based reconstructions, model and animations, *Journal of Asian Earth Sciences*, v. 20, pp. 353-431.
- Hamilton, W., 1979 - Tectonics of the Indonesian region, *US Geological Survey Professional Paper* 1078.
- Hart, S.R. and Dunn, T., 1993 - Experimental cpx/melt partitioning of 24 trace elements, *Contributions to Mineralogical Petrology*, v. 113, pp. 1-8.
- Hatherton, T. and Dickinson, W.R., 1969 - The relationship between andesitic volcanism and seismicity in Indonesia, the Lesser Antilles, and other island arcs, *Journal of Geophysical Research*, v. 74 (22), pp. 5301-5310.
- Hedenquist, J.W., Arribas, A. Jr. and Reynolds, T.J., 1998 - Evolution of an intrusion-centred hydrothermal system: Far Southeast-Lepanto porphyry and epithermal Cu-Au deposits, Philippines, *Economic Geology*, v. 93, pp. 373-404.
- Heinrich, C.A., Günther, D., Audétat, A., Ulrich, T. and Frischknecht, R., 1999 - Metal fractionation between magmatic brine and vapor, determined by microanalysis of fluid inclusions, *Geology*, v. 27, pp. 755-758.
- Hodell, D.A., Mead, G.A. and Mueller, P.A., 1990 - Variation in the strontium isotopic composition of seawater (8 Ma to present): implications for chemical weathering rates and dissolved fluxes to the oceans, *Chemical Geology*, v. 80, pp. 291-307.
- Holland, T. and Blundy, J., 1994 - Non-ideal interactions in calcic amphiboles and their bearing on amphibole-plagioclase thermometry, *Contributions to Mineralogy and Petrology*, v. 116, pp. 433-447.
- Housh, T.B. and Luhr, J.F., 1991 - Plagioclase-melt equilibria in hydrous systems, *American Mineralogist*, v. 76, pp. 477-492.
- Ikeda, Y., 1991 - Geochemistry and magmatic evolution of Pliocene-early Pleistocene pyroclastic flow deposits in central Hokkaido, Japan, *Journal of the Geological Society of Japan*, v. 97 (8), pp. 645-666.
- Imai, A., Listanco, E.L. and Fujii, T., 1993 - Petrologic and sulfur isotopic significance of highly oxidised and sulfur-rich magma of Mt Pinatubo, Philippines, *Geology*, v. 21, pp. 699-702.
- Jenner, G.A., Foley, S.F., Jackson, S.E., Green, T.H., Fryer, B.J. and Longerich, H.P., 1994 - Determination of partition coefficients for trace elements in high pressure-temperature experimental run products by laser ablation microprobe-inductively coupled plasma-mass spectrometry (LAM-ICP-MS), *Geochimica et Cosmochimica Acta*, v. 58, pp. 5099-5103.
- Kay, S.M. and Kay, R.W., 1985 - Role of crystal cumulates and the oceanic crust in the formation of the lower crust of the Aleutian arc, *Geology*, v. 13, pp. 461-464.
- Kennedy, A.K., Lofgren, G.E. and Wasserburg, G.J., 1993 - An experimental study of trace element partitioning between olivine, orthopyroxene and melt in chondrules: equilibrium values and kinetic effects, *Earth and Planetary Science Letters*, v. 115, pp. 177-195.
- Keppler, H. and Wyllie, P.J., 1991 - Partitioning of Cu, Sn, Mo, W, U, and Th between melt and aqueous fluid in the systems haplogranite-H<sub>2</sub>O-HCl and haplogranite-H<sub>2</sub>O-HF, *Contributions to Mineralogy and Petrology*, v. 109, pp. 139-150.
- Kimura, J.-I., Tanji, T., Yoshida, T. and Iizumi, S., 2001 - Geology and geochemistry of lavas at Nekoma volcano: implications for origin of Quaternary low-K andesite in the north-eastern Honshu arc, Japan, *The Island Arc*, v. 10, pp. 116-134.
- Kobayashi, K. and Nakamura, E., 2001 - Geochemical evolution of Akagi Volcano, NE Japan: implications for interaction between island-arc magma and lower crust, and generation of

- isotopically various magmas, *Journal of Petrology*, v. 42 (12), pp. 2303-2331.
- Kress, V.C. and Carmichael, I.S.E., 1991 - The compressibility of silicate liquids containing  $\text{Fe}_2\text{O}_3$  and the effect of composition, temperature and oxygen fugacity and pressure on their redox states, *Contributions to Mineralogy and Petrology*, v. 108, pp. 82-92.
- Kushiro, I., 1987 - A petrological model of the mantle wedge and lower crust in the Japanese island arcs; in Mysen, B.O., (Ed.), *Magmatic processes: Physicochemical principles*, *The Geochemical Society, Special Publication No. 1. Lancaster Press Inc.* 1987.
- Lallemand, S.E., Popoff, M., Cadet, J.P., Bader, A.G., Pubellier, M., Rangin, C. and Deffontaines, B., 1998 - Genetic relations between the central and southern Philippine Trench and the Sangihe Trench, *Journal of Geophysical Research*, v. 103 (B1), pp. 933-950.
- Lang, J.R. and Titley, S.R., 1998 - Isotopic and geochemical characteristics of Laramide magmatic systems in Arizona and implications for the genesis of porphyry copper deposits, *Economic Geology*, v. 93, pp. 138-170.
- Lange R.L. and Carmichael I.S.E., 1990 - Thermodynamic properties of silicate liquids with emphasis on density, thermal expansion and compressibility; in Nicholls, J. and Russell, J.K., (Eds.), *Modern Methods of Igneous Petrology: understanding Magmatic Processes. Mineralogical Society of America, Bookcrafters Inc., Michigan.*
- Larsen, L.M., 1979 - Distribution of REE and other trace elements between phenocrysts and peralkaline undersaturated magmas, exemplified by rocks from the Gardar igneous province, south Greenland, *Lithos*, v. 12, pp. 303-315.
- Luhr, J.F. and Aranda-Gómez, J.J., 1997 - Mexican peridotite xenoliths and tectonic terranes: correlations among vent location, texture, temperature, pressure, and oxygen fugacity, *Journal of Petrology*, v. 38, pp. 1075-1112.
- Marsh, T.M., Einaudi, M.T. and McWilliams, M., 1997 -  $^{40}\text{Ar}/^{39}\text{Ar}$  geochronology of Cu-Au and Au-Ag mineralisation in the Potrerillos district, Chile, *Economic Geology*, v. 92, pp. 784-806.
- Middleton, C., Buenavista, A., Rohrlach, B., Gonzalez, J., Subang, L. and Moreno, G., 2004 - A geological review of the Tampakan copper-gold deposit, southern Mindanao, Philippines; in *Hi Tech and World Competitive Mineral Success Stories Around the Pacific Rim*, Proc. Pacrim 2004 Conference, Adelaide, 19-22 September, 2004, *AusIMM, Melbourne*, pp 273-187.
- Miyajima, H., 1990 - Petrology of Higashi-Izu monogenetic volcano group, implication of xenocrysts, time and spatial variation of ejecta, *Journal of Mineralogy, Petrology and Economic Geology*, v. 85, pp. 315-336.
- Moore, G. and Carmichael, I.S.E., 1998 - The hydrous phase equilibria (to 3 kbar) of an andesite and basaltic andesite from western Mexico: constraints on water content and conditions of phenocryst growth, *Contributions to Mineralogy and Petrology*, v. 130, pp. 304-319.
- Moore, G., Vennemann, T. and Carmichael, I.S.E., 1998 - An empirical model for the solubility of  $\text{H}_2\text{O}$  in magmas to 3 kilobars, *American Mineralogist*, v. 83, pp. 365-42.
- Morrice, M.G., Jezek, P.A., Gill, J.B., Whitford, D.J. and Monoarfa, M., 1983 - An introduction to the Sangihe Arc: volcanism accompanying arc-arc collision in the Molucca Sea, Indonesia, *Journal of Volcanology and Geothermal Research*, v. 19, pp. 135-165.
- Moyle, A.J., Doyle, B.J., Hoogvliet, H. and Ware, A.R., 1990 - Ladolam gold deposit, Lihir island; in Hughes, E., (Ed.), *Geology of the Mineral Deposits of Australia and Papua New Guinea, AusIMM, Melbourne*, pp. 1793-1805.
- Nicholls, I.A. and Harris, K.L., 1980 - Experimental rare-earth-element partition coefficients for garnet, clinopyroxene and amphibole coexisting with andesitic and basaltic liquids, *Geochimica et Cosmochimica Acta*, v. 44, pp. 287-308.
- Nagasawa, H. and Schnetzler, C.C., 1971 - Partitioning of rare earth, alkali and alkaline earth elements between phenocrysts and acidic igneous magma, *Geochimica et Cosmochimica Acta*, v. 42, pp. 1253-1263.
- Nielsen, R.L., Gallahan, W.E. and Newberger, F., 1992 - Experimentally determined mineral-melt partition coefficients for Sc, Y and REE for olivine, orthopyroxene, pigeonite, magnetite and ilmenite, *Contributions to Mineralogical Petrology*, v. 110, pp. 488-499.
- Ochs, A. and Lange, R.A., 1999 - The density of hydrous magmatic liquids, *Science*, v. 283, pp. 1314-1317.
- Ozawa, A., Tagami, T., Listanco, E.L., Arpa, C.B. and Sudo, M., 2004 - Initiation and propagation of subduction along the Philippine Trench: evidence from the temporal and spatial distribution of volcanoes, *Journal of Asian Earth Sciences*, v. 23, pp. 105-111.
- Panjasawatwong, Y., Danyushevsky, L.V., Crawford, A.J. and Harris, K.L., 1995 - An experimental study of the effects of melt composition on plagioclase-melt equilibria at 5 and 10 kbar: implications for the origin of magmatic high-An plagioclase, *Contributions to Mineralogy and Petrology*, v. 118, pp. 420-432.
- Peacock, S.M., 1990a - Numerical simulation of metamorphic pressure-temperature-time paths and fluid production in subducting slabs, *Tectonics*, v. 9 (5), pp. 1197-1211.
- Peacock, S.M., 1990b - Fluid processes in subduction zones, *Science*, v. 248, pp. 329-337.
- Peacock, S.M., Rushmer, T. and Thompson, A.B., 1994 - Partial melting of subducting oceanic crust, *Earth and Planetary Science Letters*, v. 121, pp. 277-244.
- Peng, G., Luhr, J.F. and McGee, J.J., 1997 - Factors

- controlling sulfur concentrations in volcanic apatite, *American Mineralogist*, v. 82, pp. 1210-1224.
- Polvé, M., Maury, R.C., Bellon, H., Rangin, C., Priadi, B., Yuwono, S., Joron, J.L. and Soeria-Atmajda, R., 1997 - Space- and time- controlled magmatic evolution of Sulawesi (Indonesia): constraints on the Cenozoic geodynamic history of the Sundaland active margin, *Tectonophysics*, v. 272, pp. 69-92.
- Poulson, S.R. and Ohmoto, H., 1990 - An evaluation of the solubility of sulfide sulfur in silicate melts from experimental data and natural samples, *Chemical Geology*, v. 85, pp. 57-75.
- Prouteau, G., Maury, R.C., Sajona, F.G., Cotton, J. and Joron, J.-L., 2000 - Behaviour of Nb, Ta and other HFSE in adakites and related lavas from the Philippines, *Island Arc*, v. 9, pp. 487-498.
- Pubellier, M., Quebral, R., Rangin, C., Deffontaines, B., Muller, C., Butterlin, J. and Manzano, J. 1991. The Mindanao collision zone, a soft collision event within a continuous strike-slip setting; *Journal of Southeast Asian Earth Sciences*, v. 6, pp. 239-248.
- Pubellier, M., Quebral, R., Deffontaines, R. and Rangin, C., 1993 - Neotectonic map of Mindanao island, Philippines, *Explanatory Note*.
- Pubellier, M., Gaelle Bader, A., Rangin, C., Deffontaines, B. and Quebral, R., 1999 - Upper plate deformation induced by subduction of a volcanic arc: the Snellius Plateau (Molucca Sea, Indonesia and Mindanao, Philippines), *Tectonophysics*, v. 304, pp. 345-368.
- Quebral, R.D., Pubellier, M. and Rangin, C., 1996 - The onset of movement on the Philippine Fault in Eastern Mindanao: A transition from a collision to a strike-slip environment, *Tectonics*, v. 15(4), pp. 713-726.
- Rangin, C., 1991 - The Philippine Mobile Belt: A complex plate boundary, *Journal of Southeast Asian Earth Sciences*, v. 6 (3/4), pp. 209-220.
- Rodriguez-Vargas, A., Koester, E., Mallmann, G., Conceição, R.V., Kawashita, K. and Weber, M.B.L., 2005 - Mantle diversity beneath the Colombian Andes, Northern Volcanic Zone: constraints from Sr and Nd isotopes, *Lithos* v. 82, pp. 471-484.
- Rohrlach, B., Madera, A. and Watt, R., 1999 - Geology, alteration and mineralisation of the Tampakan copper deposit, in Proc. Pacrim 99, Conference, Bali, Indonesia, *AusIMM, Melbourne* pp 517-525
- Rohrlach, B.D. and Loucks, R.R., 2000a - An extended calibration range for the magnetite-ilmenite Fe-Ti-exchange geothermometer and oxygen barometer, 2000 Annual Report, Research School of Earth Sciences, *Australian National University*, Canberra, ACT.
- Rohrlach, B.D. and Loucks, R.R., 2000b - Refinement of a silicate melt "geohygrometer" based on the depression of feldspar crystallisation temperature by water dissolved in the silicate melt, 2000 Annual Report, Research School of Earth Sciences, *Australian National University*, Canberra, ACT.
- Rohrlach, B.D., 2002 - Tectonic evolution, petrochemistry, geochronology and palaeohydrology of the Tampakan porphyry and high sulphidation epithermal Cu-Au deposit Mindanao, Philippines, *Unpublished PhD thesis, Australian National University*, Canberra, Australia, November 2002.
- Rohrlach, B.D., Loucks, R.R. and Palin, J.M., 2003 - Isochoric ascent of lithostatically-pressured, dense magmatic vapor during gold-enargite ore formation, *13th V.M. Goldschmidt Conference 2003: Frontiers in Geochemistry, 7-12th September 2003, Kurashiki, Japan*. Abstracts Volume.
- Ruxton, B.P. and McDougall, I., 1967 - Denudation rates in northeast Papua from potassium-argon dating of lavas, *American Journal of Science*, v. 265, pp. 545-561.
- Rye, R. O., Bethke, P. M. and Wasserman, M. D., 1992 - The stable isotope geochemistry of acid sulphate alteration, *Economic Geology*, v. 87, pp. 225-262.
- Sajona, F.G., 1994 - Petrographic and geochemical analyses of four igneous rock samples of the Western Mining Corporation from the northwestern flanks of Mt Matutum, Mindanao, Philippines, *Unpublished Report to WMC*, Makati, Metro-Manila.
- Sajona, F.G., Bellon, H., Maury, R.C., Pubellier, M., Cotton, J. and Rangin, C., 1994 - Magmatic response to abrupt changes in geodynamic settings: Pliocene-Quaternary calc-alkaline and Nb-enriched lavas from Mindanao (Philippines), *Tectonophysics*, v. 237 (1-2), pp. 47-72.
- Sajona, F.G., Bellon, H., Maury, R.C., Pubellier, M., Quebral, R.D., Cotton, J., Bayon, F.E., Pagado, E. and Pamatians, P., 1997 - Tertiary and Quaternary magmatism in Mindanao and Leyte (Philippines): geochronology, geochemistry and tectonic setting, *Journal of Asian Earth Sciences*, v. 15, pp. 121-153.
- Sajona, F.G., Maury, R.C., Pubellier, M., Leterrier, J., Bellon, H. and Cotton, J., 2000 - Magmatic source enrichment by slab-derived melts in a young post-collision setting, central Mindanao (Philippines), *Lithos*, v. 54 (3/4), pp. 173-206.
- Sakuyama, M. and Nesbitt, R.W., 1986 - Geochemistry of the Quaternary volcanic rocks of the northwest Japan arc, *Journal of Volcanology and Geothermal Research*, v. 29, pp. 413-450.
- Scaillet, B. and Evans, B.W., 1999 - The 15 June 1991 eruption of Mount Pinatubo. I. phase equilibria and pre-eruption P-T-fO<sub>2</sub>-fH<sub>2</sub>O conditions of the dacite magma, *Journal of Petrology*, v. 40 (3), pp. 381-411.
- Seno, T. and Kurita, K., 1978 - Focal mechanisms and tectonics in the Taiwan-Philippine region; in Uyeda, S., Murphy, R.W. and Kobayashi, K., (Eds.), *Geodynamics of the Western Pacific*, Proceedings of the International Conference on Geodynamics of the Western Pacific-Indonesian

- Region, March 1978, Tokyo. Supplementary Issue of *Journal of Physics of the Earth*. Tokyo.
- Shinohara, H., Iiyama, J.T. and Matsuo, S., 1989 - Partition of chlorine compounds between silicate melt and hydrothermal solutions: I. Partition of NaCl-KCl, *Geochimica et Cosmochimica Acta*, v. 53, pp. 2617-2630.
- Shuto, K. and Yashima, R., 1990 - Lateral variation of major and trace elements in the Pliocene volcanic rocks of the Northeast Japan arc, *Journal of Mineralogy, Petrology and Economic Geology*, v. 85, pp. 364-389.
- Silver, E.A. and Moore, J.C., 1978 - The Molucca Sea collision zone, Indonesia, *Journal of Geophysical Research*, v. 83 (B4), pp. 1681-1691.
- Sisson, T.W., 1994 - Hornblende-melt trace-element partitioning measured by ion microprobe, *Chemical Geology*, v. 117, pp. 331-344.
- Sourirajan, S. and Kennedy, G.C., 1962 - The system H<sub>2</sub>O-NaCl at elevated temperatures and pressures, *American Journal of Science*, v. 260, pp. 115-141.
- Stern, C.R., Huang, W.-L. and Wyllie, P.J., 1975 - Basalt-andesite-rhyolite-H<sub>2</sub>O: Crystallization intervals with excess H<sub>2</sub>O and H<sub>2</sub>O-undersaturated liquidus surfaces to 35 kilobars, with implications for magma genesis, *Earth and Planetary Science Letters*, v. 28, pp. 189-196.
- Streck, M.J. and Dillies, J.H., 1998 - Sulfur evolution of oxidised arc magmas as recorded in apatite from a porphyry copper batholith, *Geology*, v. 26, pp. 523-526.
- Subang, L.L., Buenavista, A.G., Gonzales, J.M., Moreno, G.P., Baratang, V.T.B. Jr., Sebua, M.C. and Santos, N.A., 2004 - Geology and Mineralisation of the Porphyry-High-Sulphidation Epithermal Cu-Au Deposit at Tampakan, Southern Mindanao, Philippines, *Geological Society of the Philippines GeoCon 2004 Modern Technology and Advancement in Geosciences, Dec 8-10, Sulo Hotel, Quezon City, Philippines*, 72p.
- Sun, S.-S. and McDonough, W.F., 1989 - Chemical and isotopic systematics of oceanic basalts: implications for mantle composition and processes, in Saunders, A.D. and Norry, M.J., eds., *Magmatism in the Ocean Basins*, *Geological Society of London*, Special Publication 42, pp. 313-345.
- Suzuki, Y., 2000 - Petrogenesis of felsic magma in the Higashi-Izu monogenetic volcano group, *Bulletin of the Volcanological Society of Japan*, v. 45, pp. 149-17.
- Takahashi, E., 1980 - Thermal history of lherzolite xenoliths-1. Petrology of lherzolite xenoliths from the Ichinomegata crater, Oga Peninsula, Northeast Japan, *Geochimica et Cosmochimica Acta*, v. 44, pp. 1643-1658.
- Talbot, C.J., 1999 - Can field data constrain rock viscosities?, *Journal of Structural Geology*, v. 21, pp. 949-957.
- Tamura, S.-I. and Shuto, K., 1989 - Lateral variation of major and trace elements in the late Miocene volcanic rocks from central part of northeast Japan, *Journal of Mineralogy, Petrology and Economic Geology*, v. 84, pp. 444-459.
- Tamura, Y., 1994 - Genesis of island arc magmas by mantle-derived bimodal magmatism: evidence from the Shirahama group, Japan, *Journal of Petrology*, v. 35, pp. 619-645.
- Tatsumi, Y., Murasaki, M., Arsadi, E. M. and Nohda, S., 1991 - Geochemistry of Quaternary lavas from NE Sulawesi: transfer of subduction components into the mantle wedge, *Contributions to Mineralogy and Petrology*, v. 107, pp. 137-149.
- Titley, S.R. and Beane, R.E., 1981 - Porphyry copper deposits - Part I. Geologic settings, petrology and tectogenesis, *Economic Geology - 75th Anniversary Volume*, pp. 216-269.
- Togashi, S., Tanaka, T., Yoshida, T., Ishikawa, K., Fujimaki, H. and Kurasawa, H., 1992 - Trace elements and Nd-Sr isotopes of island arc tholeiites from frontal arc of northeast Japan, *Geochemical Journal*, v. 26, pp. 261-277.
- Ujike, O. and Stix, J., 2000 - Geochemistry and origins of Ueno and On-take basaltic to andesitic rocks (<3 Ma) produced by distinct contributions of subduction components, central Japan, *Journal of Volcanology and Geothermal Research*, v. 95, pp. 49-64.
- Ulmer, P., 1988 - High-pressure phase equilibria of a calc-alkaline micro-basalt: implications for the genesis of calc-alkaline magmas, *Carnegie Institution of Washington Geophysical Laboratory Annual Report 1987-1988*, pp. 28-35.
- Umino, S. and Yoshizawa, E., 1996 - Petrology of ultramafic xenoliths from Kishyuku Lava, Fukuejima, Southwest Japan, *Contributions to Mineralogy and Petrology*, v. 124, pp. 154-166.
- Wallace, P.J., 2005 - Volatiles in subduction zone magmas: concentrations and fluxes based on melt inclusion and volcanic gas data, *Journal of Volcanology and Geothermal Research*, v. 140, pp. 217-240.
- Weber, W.B.I., Tarne, J., Kempton, P.D. and Kent, R.W., 2002 - Crustal make-up of the northern Andes: evidence based on deep crustal xenolith suites, Mercaderes, SW Colombia, *Tectonophysics*, v. 345, pp. 49-82.
- Williams, T.J., Candela, P.A. and Piccoli, P.M., 1995 - The partitioning of copper between silicate melts and two-phase aqueous fluids: an experimental investigation at 1 kbar, 800°C and 0.5 kbar, 850°C, *Contributions to Mineralogy and Petrology*, v. 121, pp. 388-399.
- Wörner, G., Harmon, R.S., Davidson, J., Moor bath, S., Turner, D.L., McMillan, N., Nye, C., Lopez-Escobar, L. and Moreno, H. 1988 - The Nevados de Payachata volcanic region (18°S/69°W, N.Chile) I. Geological, geochemical, and isotopic observations, *Bulletin of Volcanology*, v. 50, pp. 287-303.
- Wohletz, K. and Heiken, G., 1992 - Volcanology and geothermal energy, *University of California Press*, Berkeley and Los Angeles, California. 432 p.



## DEXING PORPHYRY COPPER DEPOSITS IN JIANGXI, CHINA

<sup>1</sup>Rui Zongyao, <sup>2</sup>Zhang Lisheng, <sup>3</sup>Wu Chengyu, <sup>1</sup>Wang Longsheng and <sup>4</sup>Sun Xinya

<sup>1</sup>*Institute of Mineral Resources, Chinese Academy of Geological Sciences, Beijing, P. R. China*

<sup>2</sup>*Chengdu Institute of Geology and Mineral Resources, Chengdu, Sichuan Province, P. R. China*

<sup>3</sup>*Rio Tinto Mining and Exploration Limited, Beijing, P. R. China*

<sup>4</sup>*Dexing Copper Mine, Dexing, Jiangxi Province, P. R. China*

**Abstract** - The Dexing porphyry copper field in Jiangxi, China, is defined by three porphyry copper deposits which are, from southeast to northwest, Fujiawu, Tongchang and Zhushahong respectively, and by the Guanmaoshan gold deposit which lies between Fujiawu and Tongchang. Tectonically, the field lies on the southeastern edge of the Jiangnan Anticline, and is controlled by the NE-trending, deep-seated, Gandongbei fracture zone. The emplacement of the ore-bearing Fujiawu, Tongchang and Zhushahong granodiorite porphyry intrusions, dated at 184-172 Ma (Zhu *et al.*, 1983; Zhu *et al.*, 1990), was also controlled by NW-trending structures. Mineralisation and alteration continued from 172 Ma to 100 Ma, and are characterised by symmetric zoning centred on the contacts between granodiorite porphyries and the enclosing country rocks of the Mesoproterozoic Shuangqiaoshan Group phyllites.

Alteration weakens gradually away from the contact through the following stages: - (1) quartz-sericite zone (strong alteration); (2) quartz-sericite-chlorite-(epidote)-carbonate-anhydrite zone (intermediate alteration); and (3) chlorite-epidote-illite-albite-anhydrite zone (weak alteration). At Tongchang, approximately two-thirds of the ore is hosted by phyllites and one-third by granodiorite porphyry. The orebody forms a cylinder 2 500 m across with a barren core in the centre extending down plunge for over 1000 m. Chalcopyrite and molybdenite are the main ore minerals, with minor associated tennantite, tetrahedrite, bornite, chalcocite and electrum. The ore reserves at Tongchang are 1 168 Mt @ 0.446% Cu (5.2 Mt of contained Cu), 0.01% Mo and 0.19g/t Au (215 t of contained Au) supporting China's largest open-cut copper mine. Production at the Tongchang mine in 2003 amounted to about 120 000 t Cu, 5 t Au and 20 t Ag, plus by-products of Mo, Re and S. The northeast striking regional structures related to the Gandongbei deep-seated fault zone played a very important role in the generation and emplacement of granitic magma at Dexing, whereas fractures along contact zones between granodiorite porphyries and phyllite country rocks provided crucial conduits and loci for hydrothermal alteration and mineralisation. Various geochemical and isotopic data indicate that ore-forming fluids were primarily derived from volatiles fractionated from secondary boiling of magmatic hydrothermal fluids. These fluids carried metals and caused both symmetric alteration and mineral zoning along the contact zones. Circulation of heated ground water and perhaps deep-seated formation water was involved in later stages, resulting in further water-rock interactions.

### Introduction

The Dexing porphyry copper field is located at 117° 44'E, 29° 01'N, in Dexing County, Jiangxi Province, and, from southeast to northwest, comprises the Fujiawu, Tongchang and Zhushahong porphyry copper deposits (Fig. 2). Fujiawu is about 4 km southeast of Tongchang, while Zhushahong is around 2 km northwest of Tongchang. The Guanmaoshan gold deposit lies between Fujiawu and Tongchang.

According to historic records, copper mining activity in the Tongchang area boomed as early as the Tang (618-907 AD) and Song Dynasties (960-1279 AD), was reactivated between 1465 and 1488 during the Ming Dynasty, then abandoned until 1862-1874 when pyrite ores were mined by local people (Geological Publishing House, 1996).

In the autumn of 1939, Xia Xiangrong and Liu Huisi completed a geological and mineral resources survey at Dexing entitled "Mineral Resources in Dexing County" which described pyrite ores at the Tongchang and Zhushahong copper occurrences.

Malachite, chalcopyrite and pyrite were found outcropping at Tongchang during a reconnaissance survey of old workings by the No. 409 Geological Brigade in 1955 and exploration of the Tongchang deposit was carried out by the No. 420 Geological Brigade and the Copper Exploration Team of the Jiangxi Geological Bureau from 1956 to 1959. The Fujiawu and Zhushahong deposits were found by the Copper Exploration Team during field reconnaissance and mapping in December 1957. In 1972, the Jiangxi Metallurgical Geological Exploration Company initiated an additional exploration program at the Fujiawu deposit

and in 1975, the Jiangxi Geological Bureau carried out further exploration involving over one thousand geological workers at the Tongchang and Zhushahong deposits. These programs, which continued until 1978, delineated ore reserves as follows:

	Mt	Cu%	Mo%	Au g/t	Cu Mt	Au t
Tongchang	1168	0.446	0.01	0.19	5.20	215
Fujiawu	514	0.500	0.03		2.57	
Zhushahong	143	0.423	0.01		0.60	

These reserves make the Dexing porphyry copper field a world-class district with a total of 8.4 million tonnes of contained copper metal, plus recoverable gold, silver, molybdenum, rhenium and sulphur (Geological Publishing House, 1996).

The Tongchang Mine (Fig. 1) is owned by the Jiangxi Copper Company and has been mined since 1965 by open-cut, initially at a rate of 2500 tpd. The mining capacity was expanded to 20 000 tpd in 1990 and to 90 000 tpd in 1995 with an annual capacity of about 1 000 000 t of copper concentrates. A total of 370 000 tonnes of copper in concentrate were produced from 1965 to 1990. Production at the Tongchang mine in 2003 amounted to approximately 120 000 t copper, 5 t gold and 20 t silver, plus by products of molybdenum, rhenium and sulphur. The Fujiawu Mine is owned by Dexing County and has been in production since 1971 with a mining and processing capacity of 1250 tpd.

## Regional Geological Setting

The Dexing porphyry copper field in Dexing County, Jiangxi Province, Southeastern China lies within the outer zone of the Circum-Pacific metallogenic belt (Fig. 2).

Geotectonically, it is located on the southeastern edge of the Jiangnan Antecline of the Yangtze Para-platform, associated with the Qiantang Depression of the South China Fold System and bordered by the Gandongbei deep-seated fracture zone (Fig. 2).

The Jiangnan Antecline is composed mainly of lower greenschist facies metamorphosed, flyschoid volcanic-sedimentary formations of Mesoproterozoic age known as the Shuangqiaoshan Group. This group is divided from the base upwards into the Banqiao, Jiudu and Zhujia Formations. The main lithologies include phyllites, slates, meta-tuffs and meta-sandstones with a total thickness of over 4300 m forming a widely exposed basement in the region. The Jiangnan Antecline was uplifted and subjected to denudation for a long period following the Mesoproterozoic before being overlain by thin marine sediments during the Carboniferous and Permian. Some northeast-trending fault controlled volcanic-clastic filled basins were subsequently developed during the Jurassic and Cretaceous. Wall rocks of the Dexing porphyry copper deposits consist mainly of phyllites, slates and meta-tuffs of the Jiudu Formation with an isotopic age of 1401 Ma. Lithogeochemistry of 1514 rock samples from the Jiudu Formation reveal relatively high Cu background (with maxima from 76 to 203 ppm) averaging 65 ppm Cu, indicating a regional, high background copper province (Rui et al, 1984).

In striking contrast to the Jiangnan Antecline, the Qiantang Depression underwent a long period of subsidence from the Neoproterozoic, through the Paleozoic era. Sinian to Silurian Systems are composed of marine volcanic-clastic-carbonate rocks with a thickness of about 10 000 m, while Devonian to Triassic Systems comprise marine clastic-carbonate rocks with a thickness of around 3500 m. The Jurassic-Cretaceous is similar to the Jiangnan Antecline



Figure 1: *Open pit workings at the Tongchang porphyry copper mine (by Sun Xinya)*

comprising continental fault controlled basins of volcanic and clastic rocks with a thickness of 9 000 m.

Based on the differing thicknesses of sedimentary sequences, the long term subsidence of the Qiantang Depression and rise of the Jiangnan Antecline created an amplitude of up to 18 km. These features are separated by the Gandongbei deep-seated fracture zone which is 200 km long, strikes NE (35° to 60°) and is up to 15 km wide. It is characterised by multiple stages of associated tectonic movement and magmatic activity. Strong tectonic compression resulted in schistosity and local mylonitisation of the Shuangqiaoshan Group, whereas multi-episode magmatic activity created a mineral rich province at Dexing. The area incorporates a cluster of ore deposits. The Jinshan gold deposit (Liao, 1995), lies about 5 km south of the Dexing copper field, while the Yinshan volcanic-hosted lead-zinc-silver deposit (Ye, 1987) is located 20 km southwest of Dexing.

Westward movement of the Izanqi-Pacific Plate during the Yanshanian (Jurassic-Cretaceous) period resulted in subduction of the Qiantang Depression below the Jiangnan Antecline and triggered strong magmatic activity that formed a tectonic background for the formation of the Dexing porphyry copper deposits.

## Regional Magmatic Activity

The Proterozoic Jiudu Formation in the Dexing ore field contains a large amount of dacitic pyroclastic rocks dated

at 1400 Ma (Rb-Sr) and a small amount of dacite, andesite and hornblende gabbro representing intrusive activity of the Jinning Period. These rocks are metamorphosed into phyllites and meta-tuffs and serve as the main host rocks to the Dexing porphyry copper ores.

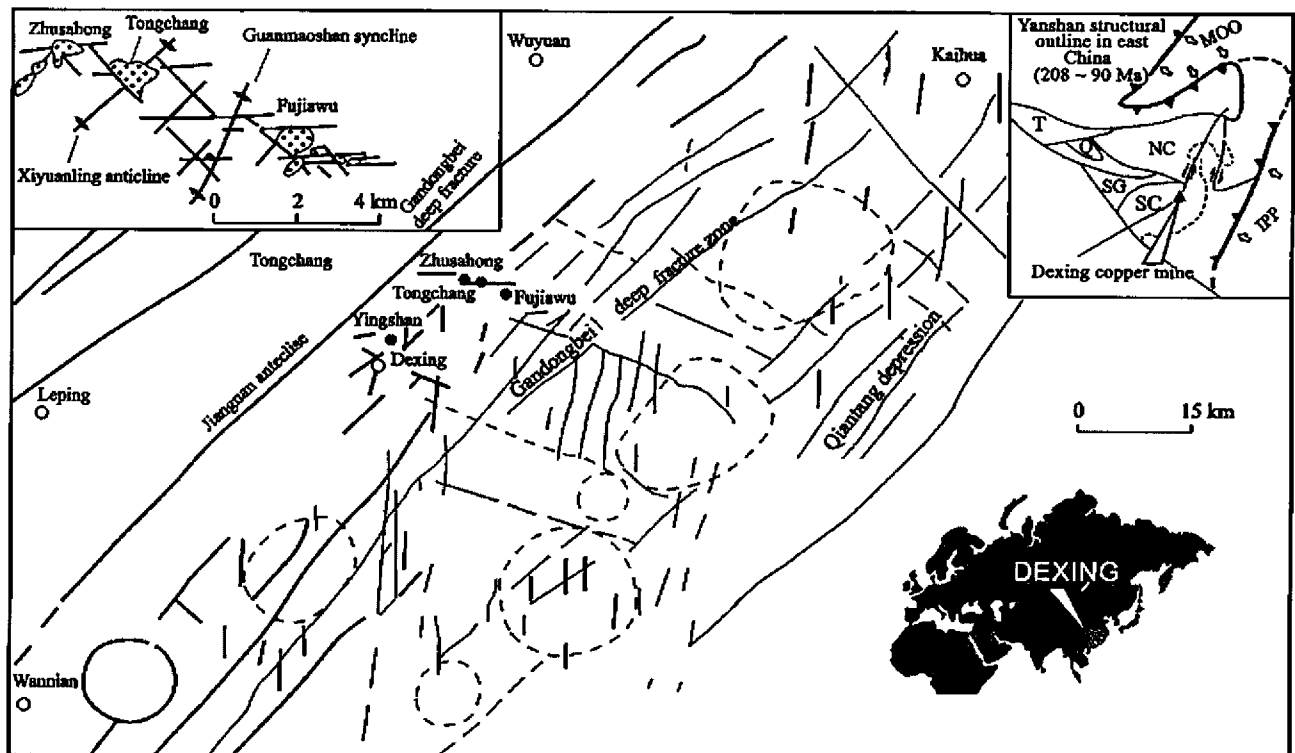
A spilite-keratophyre sequence, including lavas, volcanic breccias, tuffs and tuffaceous sandstones, associated with albite porphyry is believed to have formed in the Xuefeng Period (about 630-680 Ma) and crops out in the southwestern part of the Dexing copper field.

Pyroxene diorite dated at 503-509 Ma (K-Ar) from the Caledonian Period are found in the Jinjia area, while gabbroic dykes with a K-Ar age of 269-328 Ma occur at Huading Hill in the north of the Dexing porphyry copper field and Hercynian gabbro-dolerite (diabase) to diorite porphyry dykes are exposed at Guanmao Hill between Tongchang and Fujiawu.

Strong folding during the Indo-Sinian period was accompanied by emplacement of granitoids with a K-Ar age of 217-234 Ma.

The most important magmatic activity in the Dexing porphyry copper field is of Yanshanian age, divided into five stages as follows:

*Stage 1 - Phase I of the early Yanshanian (190-193 Ma) consists of ultrabasic and basic intrusions including gabbro, pyroxenite, serpentinised peridotite and serpentinite occurring along the Gandongbei deep-seated fracture zone.*



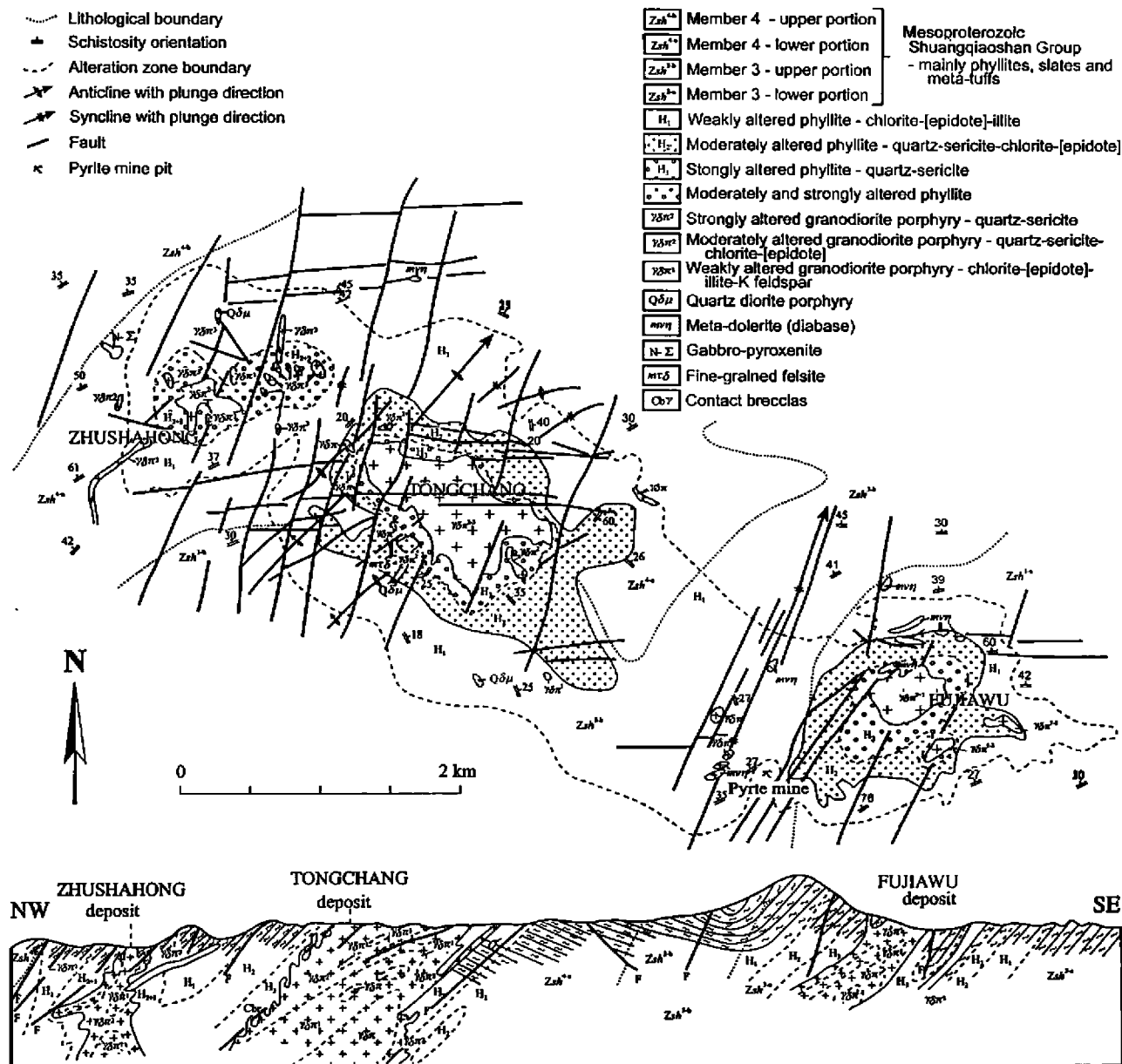
**Figure 2: Regional geological setting of the Dexing porphyry copper field compiled from satellite image interpretation (Modified after Zhu et al., 1983).**

The upper left inset shows the tectonic setting of the three ore-bearing granodiorite porphyries in the Dexing ore field. The upper right inset is after Zhou et al., (2002). IPP = Izanqi-Pacific Plate; NC = North China platform; SC = Yangtze Para platform; MOO = Mongolia-Ohotsk Oceanic basin; SG = Songpan-Garzê basin; Q = Qaidam basin; T = Tarim basin; Black triangle = Dexing porphyry copper field; Dashed line = coast of China and Korea.



**Table 1: Shape and occurrence of the granodiorite porphyry intrusions of Fujiawu, Tongchang and Zhushahong**

Intrusions	Fujiawu	Tongchang	Zhushahong
Shape on surface	Irregular polygon	Rounded triangle	Several apophyses
Length (m)	650	1300	n - 450
Width (m)	300	300 - 800	0.n - 80
Area (km <sup>2</sup> )	0.2	0.7	0.06
Plunge direction	310°	320°	340°
Dip angle	40°	45° - 50°	60° - 70°



**Figure 3: Geological sketch map and longitudinal section of the Dexing porphyry copper field.**  
(After Yan Meizhong et al, 1980)

**Table 2: Petrographic characteristics of granodiorite porphyries from Fujiawu, Tongchang and Zhushahong**

Intrusions	Fujiawu	Tongchang	Zhushahong
Colour	Pinkish grey	Pale grey	Grey
Phenocryst content (%)	50 - 60	35 - 60	20 - 45
Phenocryst grain size (mm)	2 - 5	0.5 - 40	0.5 - 3
Groundmass grain size (mm)	0.1 - 0.3	0.05 - 0.3	0.05 - 0.1

**Stage 2** - Phase II of the early Yanshanian (172-186 Ma) was characterised by Cu-Mo mineralisation related to granodiorite porphyries, diorite porphyry, quartz diorite porphyry and granite porphyry. The granodiorite porphyries were emplaced into Proterozoic phyllites and slates and serve as the major source of copper mineralisation.

**Stage 3** - Phase III of the early Yanshanian (125-145 Ma) was the peak of magmatic activity in the region. Dacitic volcanic and pyroclastic rocks form a sequence with a thickness of 400-1600 m, associated with a variety of subvolcanic rocks including hornblende-andesite porphyry, dacite porphyry, quartz diorite porphyry, trachy-andesite porphyry, quartz porphyry, granite porphyry and quartz syenite porphyry. This sequence was well developed within the Yinshan area. The dacite porphyry is the main host of Pb-Zn-Ag-Cu-Au mineralisation at the Yinshan deposit.

**Stage 4** - Phase I of the late Yanshanian (103-127 Ma) was marked by intermediate to acid volcanics, locally with basalt and associated olivine pyroxenite, gabbro, diorite porphyry and quartz diorite porphyry. These rocks occur in areas neighbouring the Dexing porphyry copper field.

**Stage 5** - Phase II of the late Yanshanian (96-100 Ma) as represented in the Dexing porphyry copper field included post-mineralisation granite, granite porphyry, quartz porphyry and quartz diorite porphyry.

Granodiorite porphyries of Stage 2 served as the main mineralising intrusive of the Dexing porphyry copper deposits.

## Mineralised Granodiorite Porphyries

### Occurrences

Three mineralised, pipe-like bodies of granodiorite porphyry of varying size, each plunging north-westwards at 40° to 70° (Table 1 and Fig. 3), host the Fujiawu, Tongchang and Zhushahong deposits respectively. Drilling and geophysical data indicate that these porphyries are large, near-surface apophyses of a more extensive intrusion at depth.

Potassic aplite and quartz diorite porphyry are present as two common dyke sets intersecting the granodiorite porphyries. Potassic aplite dykes are mainly confined to the granodiorite porphyry bodies and vary in width from several centimetres to tens of centimetres, either as sheeted dykes with sharp contacts or as stockworks which have

obscure boundaries with the host. In the latter case, K feldspar rich aplite grades into pervasive potassic (K feldspar) alteration indicating its pre-ore nature and a close genetic affinity between stockwork veining and potassic alteration. Dykes of quartz diorite porphyry (or diorite porphyry with less quartz) are generally several metres in width, occurring both within mineralised granodiorite porphyry intrusions and extending into the country rocks as post-ore dykes.

### Petrology and Mineralogy

The three mineralised granodiorite porphyries of Fujiawu, Tongchang and Zhushahong share very similar petrographic features. They are porphyritic in texture and massive in structure with varied colour, grain size and phenocryst/ground mass ratio (Table 2).

Phenocrysts are mainly euhedral tabular andesine, with lesser amounts of euhedral and subhedral bladed hornblende, biotite, tabular K feldspar and a small amount of corroded quartz. The groundmass is composed of fine-grained to micro-grained, rounded to granular oligoclase, quartz, K feldspar and minor hornblende and biotite. Accessory minerals include magnetite, apatite, sphene, ilmenite and zircon. A comparison of the mineral compositions of the three granodiorite porphyries and associated potassic aplite and quartz diorite dykes are shown in Table 3.

### Petrochemistry

Chemical compositions of granodiorite porphyries and associated dykes are listed in Table 4. Although the effects of alteration cannot be fully precluded from the analysed samples, they are characterised by relatively high silica: 64.21-66.13% for Fujiawu, 62.32-63.70% for Tongchang and 62.82% for Zhushahong. They also have relatively high (Na<sub>2</sub>O + K<sub>2</sub>O) contents. The K<sub>2</sub>O content is about 1% higher than the average value of similar rocks elsewhere in the world. These granodiorites are calc-alkalic in nature with a calc-alkaline index of 57.4.

### Isotopic ages

Isotopic dating data have been published by several workers. The Tongchang granodiorite porphyry yields a K-Ar age of 186 Ma (Institute of Geology and Mineral Resources, MMI, 1984) and an Rb-Sr isochron age of 172 Ma with an initial Sr<sup>86</sup>/Sr<sup>87</sup> isotopic ratio of 0.7043 (Zhu *et al.*, 1983). Zhu *et al.* reported a Sm-Nd age of 184 Ma for the Dexing granodiorite porphyries (Zhu *et al.*, 1990), and a Rb-Sr isochron age of 165 Ma for Tongchang granodiorite porphyry (Zhu *et al.*, 2002).

Table 3: Mineral compositions of granodiorite porphyries, potassic aplite and quartz diorite porphyrite of the Dexing porphyry copper field

Ore district	Lithology	Quartz	Plagioclase	K feldspar	Hornblende	Biotite	Others
Fujiawu	Granodiorite (4)	21	49	15	8	5	2
Tongchang	Granodiorite (5)	20	49	15	9	5	1
Zhushahong	Granodiorite (1)	20	49	14	9	6	2
Tongchang	Potassic aplite (1)	34	21	43		1	1
Dawutou	Potassic aplite (1)	36	18	44		1	1
Tongchang	Quartz diorite porphyry	8	64	6	11	8	3

All minerals in % by area/lithology. Numbers in brackets are numbers of samples studied under microscope.

Table 4: Chemical compositions of the ore-bearing granodiorite porphyries from Fujiawu, Tongchang and Zhushahong ore districts (wt %)

Intrusion	Number	Lithology	Si <sub>2</sub> O	TiO <sub>2</sub>	Al <sub>2</sub> O <sub>3</sub>	Fe <sub>2</sub> O <sub>3</sub>	FeO	MnO	MgO	CaO	Na <sub>2</sub> O	K <sub>2</sub> O	P <sub>2</sub> O <sub>5</sub>	H <sub>2</sub> O <sup>+</sup>	CO <sub>2</sub>	LOI	Total	
Fujiawu	Fu-1	Granodiorite porphyry	64.64	0.40	15.34	1.44	2.91	0.08	1.88	3.38	3.93	3.00	0.25	1.34		1.38	99.97	
	Fu-2	Granodiorite porphyry	64.76	0.42	15.38	1.88	3.10	0.75	1.83	3.86	4.00	3.00	0.21			1.02	100.21	
	Fu-3	Granodiorite porphyry	65.80	0.42	15.56	1.71	2.04	0.09	1.37	2.99	3.91	3.45	0.20			1.90	99.44	
	Fu-4	Granodiorite porphyry	64.74	0.45	15.90	1.85	2.87	0.11	2.09	4.66	3.22	3.15	0.28	1.40				100.72
	Fu-5	Granodiorite porphyry	64.21	0.41	16.67	1.45	2.10	0.06	1.36	3.63	4.30	3.35	0.15	1.12				98.81
	Fu-6	Granodiorite porphyry	66.13	0.36	15.60	1.83	2.05	0.06	1.62	2.89	3.84	3.28	0.16	1.72			1.50	101.04
	Average	Granodiorite porphyry	65.05	0.41	15.74	1.69	2.51	0.11	1.69	3.57	3.87	3.21	0.21	1.40	0.58			100.04
Tongchang	Tong-1	Adamellite-diorite porphyrite	62.32	0.45	15.79	2.52	2.88	0.08	2.55	4.10	4.23	2.90	0.25	1.82	0.50			100.39
	Tong-2	Granodiorite porphyry	63.70	0.40	14.88	1.77	2.84	0.05	2.07	4.32	3.71	3.19	0.25			3.41	100.39	
	Tong-3	Granodiorite porphyry	63.54	0.45	15.46	2.93	1.97	0.05	2.52	3.84	3.39	3.24	0.23	1.29	0.61			99.52
	Tong-4	Granodiorite porphyry	63.22	0.45	15.07	2.55	2.89	0.05	2.55	3.83	3.78	3.38	0.25	1.12	0.21	1.09		100.44
	Tong-5	Granodiorite porphyry	63.25	0.43	15.65	3.21	1.56	0.04	2.77	4.42	3.68	3.63	0.23	1.17	0.41			100.45
	Tong-6	Granodiorite porphyry	62.60	0.45	15.58	2.73	2.59	0.08	2.55	4.50	4.00	3.33	0.25	1.64	0.12			100.42
	Tong-7	Granodiorite porphyry	62.82	0.45	15.11	2.06	2.80	0.08	2.31	4.33	3.89	3.20	0.30	1.04	0.87	1.75		101.01
	Tong-8	Granodiorite porphyry	62.81	0.44	15.29	3.00	1.98	0.08	2.83	3.80	3.37	3.55	0.24	1.34	1.06			99.79
	Tong-9	Granodiorite porphyry	62.88	0.41	15.60	1.26	4.34	0.31	2.04	4.08	3.63	2.88	0.24	1.69				99.36
	Average	Granodiorite porphyry	63.00	0.43	15.39	2.36	2.69	0.06	2.43	4.15	3.73	3.20	0.25	1.49	0.49			99.67
Zhushahong	Zhu-1	Granodiorite porphyry	62.82	0.40	15.24	0.72	2.52	0.03	2.41	3.17	3.84	3.34	0.25	2.46	0.75	3.58		101.53
Tongchang	Tong-11	Potassic aplite	73.18	0.10	11.43	0.74	2.40	0.02	0.50	1.26	2.88	5.25	0.03	0.82	0.61			99.22
	Tong-12	Quartz diorite porphyry	59.90	0.45	15.02	2.06	3.70	0.03	3.45	4.70	3.30	2.95	0.33	1.68				97.57
	Tong-13	Quartz diorite porphyry	60.66	0.50	15.64	2.02	3.51	0.08	3.60	4.72	3.50	3.15	0.30	1.48				99.16
Dawutou	Da-1	Potassic aplite	76.04	0.10	12.02	0.47	0.74	0.01	0.20	0.80	3.09	5.50	0.03	0.44	0.05			99.49

**Table 5: Mineral compositions of granodiorite porphyry, phyllite and their altered varieties from Fujiawu and Tongchang (%)**

Alteration intensity	Tongchang							Fujiawu								
	Granodiorite porphyry _ Contact zone _ Phyllite							Granodiorite porphyry _ Contact zone _ Phyllite								
	Fresh rock	Weakly	Moderately	Strongly	Strongly	Moderately	Weakly	Fresh rock	Fresh rock	Weakly	Moderately	Strongly	Strongly	Moderately	Weakly	Fresh rock
Rock type	$\gamma\delta\pi$	$\gamma\delta\pi^1$	$\gamma\delta\pi^2$	$\gamma\delta\pi^3$	H <sup>1</sup>	H <sup>2</sup>	H <sup>1</sup>	H	$\gamma\delta\pi$	$\gamma\delta\pi^1$	$\gamma\delta\pi^2$	$\gamma\delta\pi^3$	H <sup>3</sup>	H <sup>2</sup>	H <sup>1</sup>	H
Plagioclase	49.4	18							48.8	14						
K-feldspar	15.1	7							15.5	8						
Hornblende	0.5								8.3							
Biotite	5	1							4.8	2						
Quartz	19.5	22	28	33	28	17	7	1	20.5	23	32	36	31	23	9	1
Illite (Hydro-muscovite)		28	36	58	63	59	15	86		28	34	56	61	52	70	81
Chlorites		15	24			15	13	12		14	21			17	15	14
Epidote		2								4	5				1	
Albite		1								1						
Carbonates		3	4	5	6	6	3			2	3	3	4	5	3	
Anhydrite		2	2	1	1	1	1	1		2	2	2	1	1	1	
Magnetite*	8,763	3,742	5	35	n	n	n	N/A	5,261	2,950	125	73	150	291	112	24
Apatite*	2,546	1,730	969	147				N/A	351	87	13	5				
Zircon*	124	131	49	106	n	n		N/A	194	100	130	153	Trace	Minor	Minor	Minor
Sphene*	1,192	192		1	n	n		N/A	145	19	13					
Ilmenite*	198	14						N/A								

After: Zhu Xianjia (1980, unpublished) and Rui, et al. (1984). Minerals in % studied under microscope except for those marked with \* in g/t in mineral separates; N/A- No data available; n-Several grains.

## Alteration Zonation

Zonation of alteration and mineralisation within the Dexing porphyry copper deposits is well documented by Zhu *et al.*, (1983) and Rui *et al.*, (1984). The country rocks underwent heating during the emplacement of the granodiorites, converting phyllites and slates into biotite and andalusite-biotite hornfels in a 100-400 m wide hornfelsed halo surrounding the intrusions.

Early stage high-temperature potassic alteration was not well developed. Secondary K feldspar and biotite are observable in the Fujiawu granodiorite porphyry, but are rarely recognised at Tongchang and Zhushahong. Subsequent hydrothermal alteration was then focused along the contact zones between the granodiorite porphyries and hornfelsed country rocks, resulting in a symmetric alteration zoning from the contact zone, both inwards and outwards (Fig. 3 and Table 5) as follows:

**Quartz-sericite zone** (strong alteration zone,  $\gamma\delta\pi^3$  and  $H^3$ ) - composed of 80% secondary quartz and sericite which replaced primary feldspars and mafic minerals and destroyed the original textures of phyllites and granodiorite porphyries.

**Chlorite-(epidote)-sericite zone** (intermediate alteration zone,  $\gamma\delta\pi^2$  and  $H^2$ ) - consists of 60-80% alteration minerals of chlorite, sericite, quartz, epidote, carbonate and anhydrite. The original texture was partially destroyed and secondary minerals grew around the edges and along cleavages of primary feldspars. This zone may extend for hundreds of metres into granodiorite ( $\gamma\delta\pi^2$ ) and outwards into country rocks ( $H^2$ ).

**Chlorite-epidote-illite zone** (weak alteration zone,  $\gamma\delta\pi^1$  and  $H^1$ ) - has variable amounts of (10-60%) illite, chlorite, epidote, albite, carbonate and anhydrite replacing primary feldspars and mafic minerals. The original textures are generally preserved.

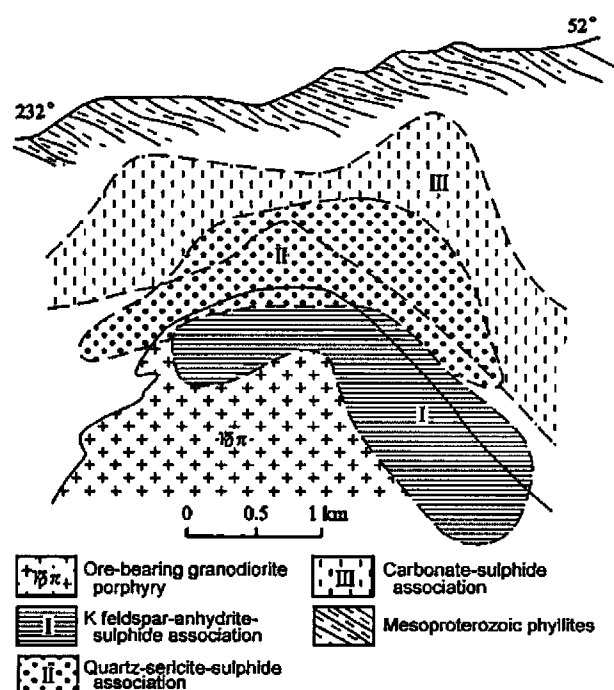


Figure 4: Mineral zoning of the Tongchang deposit

Vertical alteration zoning is also described at Tongchang. A K-feldspar-anhydrite-sulphide association is recognised in the upper portion of the granodiorite porphyry, while a quartz-sericite (illite)-sulphide assemblage occurs in the contact zone and a sulphate-sulphide association in the outer contact zone (Fig. 4).

Within the Dexing porphyry copper deposits hydrothermal micas (sericite and illite) are distributed over a 2 km belt and are related to the contact zones between granodiorite porphyries and wall-rocks (Fig. 3). They were also mentioned as hydromuscovite and hydromica in earlier publications (Zhu *et al.*, 1983; Rui *et al.*, 1984). They occur as fine-grained, muscovite-like clay minerals with variable contents of potassium and  $H_2O$ , and are difficult to distinguish by naked eye in the field from each other and from those of metamorphic origin. X-ray diffraction analyses (Zhu *et al.*, 2002) indicate that the Kübler indices of illites from altered granodiorite porphyry and altered phyllite are  $0.45^\circ$ - $1.37^\circ\Delta ZQ$  and  $0.40^\circ$ - $0.84^\circ\Delta ZQ$  respectively, with an average values of  $0.79^\circ\Delta ZQ$  and  $0.55^\circ\Delta ZQ$ , respectively. For a comparison, Kübler indices measured for illites from phyllite two km away from the contact zone, representing non- or less-altered rocks, are apparently much lower, varying from  $0.11^\circ$  to  $0.18^\circ\Delta ZQ$  with an average value of  $0.16^\circ\Delta ZQ$ . X-ray diffraction spectral comparison also indicated that illites from altered rocks are 1M type with  $I_r$  values  $>1$ , suggesting the presence of an expansion layer and of alteration genesis, while illites from non-altered phyllites are 2M1 type with  $I_r$  values of 1 indicating absence of an expansion layer and a metamorphic genesis.

## Mineralisation

### Orebodies

In general, orebodies are confined to contact zones between granodiorite porphyries and wall-rocks. Shells of 0.4% Cu broadly coincide with the strong alteration zone forming ring-shaped orebodies in plan and, in three dimensions, north-westerly plunging cylinders with barren central cores (Fig. 5). Two-thirds of the ores are hosted by altered phyllites, and one-third by altered granodiorite porphyries. The Tongchang orebody is the largest of the three deposits. It is oval-shaped at surface, with a northwest-southeast trending long axis of 2.54 km and an inner barren core measuring 400 by 700 m. The Fujiawu orebody is a rounded square with a diameter of 1000 m and inner barren core diameter of 800 m. The down plunge extent of both the Tongchang and Fujiawu orebodies is more than 1000 m. In profile, Zhushahong comprises several smaller *en echelon* orebodies (Fig. 5).

Ores from the Fujiawu, Tongchang and Zhushahong deposits are very similar and of typical porphyry copper style. Orebodies are characterised by stockwork and disseminated mineralisation, varying from predominantly disseminated at Fujiawu, to stockwork-dominated at Tongchang and Zhushahong. Millimetre to centimetre wide cross-cutting quartz veins and veinlets form a framework in a strongly quartz-sericite altered background. Disseminated pyrite, chalcopyrite, specularite and

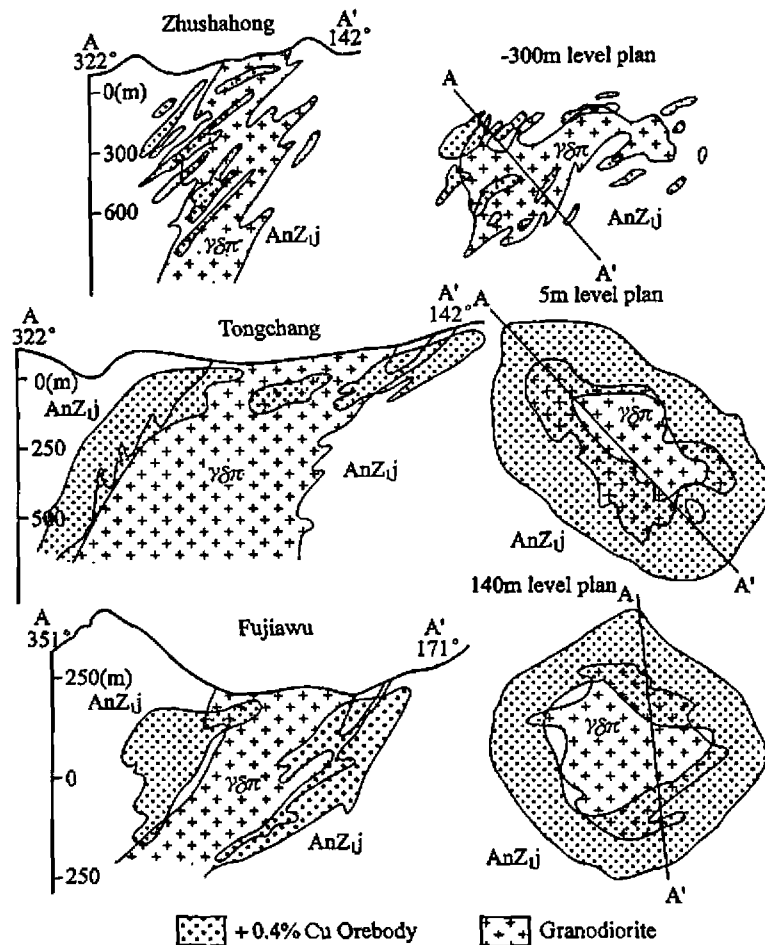


Figure 5: Shape and occurrence of orebodies in profile (left) and in plan (right) of the Fujiawu, Tongchang and Zhushahong deposits

molybdenite are found either in veins or in the altered host rock. Ore grade and metal ratios are controlled by both the density of veining and the abundance of ore-forming minerals. Average Cu:Mo ratios are 15:1 for Fujiawu, 45:1 for Tongchang and 43:1 for Zhushahong. Other associated metals include Au, Ag, S, Re, Te, Se, Co and Os.

Primary sulphide ores account for between 85 and 90% of the total ore reserves at all three deposits, whereas secondary copper sulphides account for about 5 to 12% and oxide ores make up less than 5%. Oxidation and leaching are very weak in this region of mountainous relief and no supergene enrichment zone was developed.

#### Mineralogy

As detailed previously, pyrite, chalcopyrite and molybdenite are the main ore minerals. According to Hu Zongsheng (1981, unpublished), molybdenite:chalcopyrite:pyrite ratios in the Tongchang deposit vary from 1:30:57 in the lower part, through 1:85:205 in the middle part to 1:150:879 in the upper part.

Chalcopyrite contributes about 90% of the copper grade in primary ores, while minor tennantite, bornite, tetrahedrite and chalcocite account for the remainder. Molybdenite contains 244 ppm Re at Fujiawu and 1419 ppm Re at Tongchang (Rui, *et al.*, 1984), and rhenium is recoverable

from molybdenite concentrates. Other minor metallic minerals include galena, sphalerite, magnetite, digenite, covellite, goethite, lepidocrocite, maghemite, tenorite, pyrolusite, malachite and azurite. A complicated ore mineral paragenesis was observed (Rui *et al.*, 1984).

Trace amounts of native gold and electrum are the main gold minerals, producing an average grade of 0.19g/t Au at Tongchang. Other trace metallic minerals are bismuthinite, cubanite, pyrrhotite, arsenopyrite, aikinite, emplectite, carrollite, millerite, gersdorffite, tetradymite, hessite, petzite, calaverite, melanite, merenskyite, ilmenite, anatase, wolframite, cassiterite, manganosiderite, siderite, musketovite, chromite, native copper, native silver, marcasite, wulfenite, cerussite and anglesite.

Quartz is the dominant gangue mineral, and as a result, ores contain generally high silica. Other gangue minerals include sericite, illite, chlorite, epidote, K feldspar, ankerite, dolomite and anhydrite.

Minor gangue minerals are biotite, muscovite, albite, andesine, oligoclase, hornblende, laumontite, zoisite, clinozoisite, tourmaline, gypsum, apatite, barite, rutile, fluorite, kaolinite, montmorillonite, hydrobiotite and chalcantite. Trace amounts of andalusite, sphene, zircon, pyroxene, allanite, garnet, monazite, xenotime and spinel are recorded (Rui *et al.*, 1984).

### Age of Mineralisation

As detailed above, the granodiorite porphyry at Tongchang was isotopically dated by different methods at 172–186 Ma (Zhu *et al.*, 1983; Institute of Geology and Mineral Resources, MMI, 1984; Zhu *et al.*, 1990). Re-Os isotopic dating on two molybdenite concentrate samples from Tongchang yielded  $173 \pm 9$  Ma (Wu Chengyu, Huang Dianhao and Du Andao, 1997, unpublished). Ye (1987) indicated a range of isotopic ages of 157 Ma to 170 Ma for a variety of rocks from Tongchang. Zhu *et al.*, (1983) reported K-Ar ages of 157 Ma and 152 Ma for quartz-K feldspar veins from the Fujiawu granodiorite porphyry and from country rocks, respectively. K-Ar ages for sericite from the Tongchang granodiorite porphyry and for biotite from the Tongchang post-ore quartz diorite porphyry dyke are 112 Ma and 100 Ma, respectively. It is concluded that the Dexing granodiorite intrusions were emplaced at 186–172 Ma, immediately followed the early molybdenum mineralisation at 173 Ma. The subsequent alteration and mineralisation continued from 157 to 112 Ma, followed by emplacement of post-ore quartz diorite porphyry dykes at 100 Ma.

## Ore Genesis and Discussion

### Hydrothermal Fluids

Fluid inclusions from the Fujiawu porphyry copper deposit have three homogenisation temperature ranges, 540–595°C, 255–471°C and 151–218°C, corresponding to magmatic pneumatolytic, hypo-mesothermal and meso-epithermal stages, respectively (Institute of Geology and Mineral Resources, MMI, 1984). Zhu Xun *et al.*, (1983) reported similar homogenisation temperature ranges for fluid inclusions from the Tongchang porphyry copper deposit, namely:

- 425–745°C high volatile and high salinity inclusions related to biotite-K feldspar alteration,
- 275–425°C gaseous-liquid and high salinity inclusions associated with quartz-sericite and quartz-chlorite-anhydrite alteration, closely related to chalcopyrite, molybdenite, bornite and pyrite mineralisation,
- 100–275°C low salinity fluid inclusions associated with quartz-illite alteration.

Recent studies by Zhu Jinchu *et al.*, (2002) indicated that fluid inclusions with a temperature of 570–520°C are high salinity (31.0–63.3 wt% NaCl), representing an immiscible phase, exsolved from granitic magma in equilibrium with residual silicate melt. Decreasing temperature and pressure during ascent resulted in boiling at 480–360°C, forming three immiscible phases, as follows:

- a highly saline (43.0–52.2 wt % NaCl) phase,
- a low salinity (0.05–3.9 wt% NaCl) and gas-rich phase,
- a moderate salinity (11.6–17.5 wt % NaCl) and CO<sub>2</sub>-rich phase, respectively.

Based on geological evidence and fluid inclusion studies, Zhu Jinchu *et al.*, (2002) concluded that the Tongchang granodiorite porphyry was emplaced under pressures of 65 to 15 Mpa, corresponding to a depth of about 1.5 to 2.5 km depth below the surface.

### Source of Ore Metals

$\delta^{34}\text{S}$  values for 136 pyrite and chalcopyrite samples from the Tongchang deposit vary from  $-2.8\text{‰}$  to  $+3.1\text{‰}$  (Zhu *et al.*, 1983). This suggests that sulphide sulphur at Tongchang originated from a mantle-derived magma. This is supported by the low initial  $^{87}\text{Sr}/^{86}\text{Sr}$  ratio (0.7043) of the Tongchang granodiorite (Zhu *et al.*, 1983). According to Zhu *et al.*, (1990),  $\epsilon_{\text{Nd}(t)}$  and  $\epsilon_{\text{Sr}(t)}$  values for the Tongchang granodiorite porphyry are  $-1.9$  and  $0.1$ , respectively and calculated component weight ratios between average mantle-derived end-member and average crustal end-member are 0.719 and 0.281, respectively. From this it could be deduced that granitic magma generated by partial melting of the underplate during subduction of the Izanqi-Pacific plate below the China continental crust was dominated by mantle-derived materials (72%) and contaminated by crustal materials (21%).

Zhu *et al.*, (2002) demonstrated that water-rock interaction and isotopic exchange reaction resulted in increases in  $\epsilon_{\text{Sr}}$  from 10.7 to 79.1 and  $(^{87}\text{Sr}/^{86}\text{Sr})_i$  from 0.70508 to 0.71092 from the central part to the margin of the Tongchang intrusion respectively. This suggests that input of high  $^{87}\text{Sr}/^{86}\text{Sr}$  values (0.71123 to 0.71151) from wall-rock phyllites played an important role. Similarly  $\epsilon_{\text{Nd}}$  values of Tongchang granodiorite porphyry decrease from  $-0.76$  to  $-3.6$  from its centre to the margin.

Oxygen isotopes of primary quartz from the Tongchang granodiorite yield  $\delta^{18}\text{O}_{\text{H}_2\text{O}}$  values of  $+8.0$  to  $+6.2\text{‰}$  for water in equilibrium with the mineral. These typically magmatic signature values decrease to  $+6.0$  to  $+1.4\text{‰}$  for early stage quartz-K feldspar veins and down to  $+4.6$  to  $-2.6\text{‰}$  for later stage quartz-sulphide and chlorite-sericite veins, indicating involvement of meteoric water in the progress of alteration and mineralisation (Rui, *et al.*, 1984). Hydrogen isotopes provide similar support as  $\delta\text{D}$  varies from  $-79$  to  $-82\text{‰}$  for magmatic water in equilibrium with biotite phenocrysts and early stage alteration rocks, to  $-54$  to  $-62\text{‰}$  for fluid inclusions from copper sulphide-quartz veining and post-ore quartz veins (Zhang *et al.*, 1996; Zhu *et al.*, 2002).

Experimental studies (Candela *et al.*, 1984 and Williams *et al.*, 1995) indicated that in a granitic magma-water system, Cu in fluid/melt preferentially enters into a fluid phase with a Cu partition coefficient of more than 10 to 50. In the presence of Cl<sup>-</sup> in the fluid phase in particular, Cu will more readily enter the fluid phase and migrate as complexes.

Granitic magmatic systems generally possess high oxygen fugacities with  $f\text{O}_2$  varying from  $10^{14}$  to  $10^8$ . The  $f\text{O}_2$  values of Cu-Mo-Au mineralisation systems observed in China range from  $10^{24}$  to  $10^{11}$  (Rui *et al.*, 2002). This prevents Cu, Mo and Au from entering into Fe-bearing mineral phases during crystallisation of magma and favours these elements entering into a hydrothermal phase with abundant SO<sub>2</sub>. This process will be enhanced by the hydrolysis of SO<sub>2</sub> and precipitation of anhydrite and gypsum. A reducing environment will further concentrate Cu, Mo and Au in a

hydrothermal system by forming complexes with H<sub>2</sub>S. With a further decrease in temperature, pressure, pH values and degassing of CO<sub>2</sub>, mineralisation occurs by precipitating molybdenite, chalcopyrite and pyrite.

**Ore Forming Controls and Models**

Studies of porphyry copper deposits throughout the world has resulted in the establishment of various models and theories (Lowell and Guilbert, 1970; Sillitoe, 1990; Sillitoe, 1997). A porphyry model has been widely accepted for the Dexing copper deposits, although opinions differ on the interpretation of details relating to the source of ore forming materials and the nature of hydrothermal fluids. As shown above, Zhu Xun *et al.*, (1983) believed on the one hand that primary volatiles resulting from fractionation of the second boiling of magmatic fluids were responsible for alteration and copper-molybdenum mineralisation and that ore-forming materials were primarily derived from magmatic hydrothermal solution, although a mixture of heated meteoric water played a role in the later stage. Ji Kejian *et al.*, (1989) on the other hand emphasised the importance of heated ground water circulating throughout the surrounding country rocks resulting in wall-rock alteration and mineralisation. Their interpretation favoured the main ore-forming materials being derived from country rocks as evidenced by a depletion halo of copper and other metals around the Dexing copper deposits. Based on recent studies, Zhu Jinchu *et al.*, (2002) supported a magmatic source of hydrothermal fluids which brought dominant ore-forming materials and indicated a contribution from meteoric water and deeply-buried formation water through a water-rock interaction process.

Fig. 6 illustrates a generalised zonation pattern of geology, alteration mineral assemblages, ore mineralogy, ore- and rock-forming element geochemistry, mineralisation styles, temperature and sulphur isotopes of the Dexing porphyry copper deposits. From the inner core to outer zone of the deposit, mineral components change from molybdenite, through chalcopyrite to sphalerite and galena; element associations change from W-Bi through Mo-Cu, Ni-Co, Pb-Zn to Mn; while ore textures evolve from disseminated through veinlet-stockwork to veins. It may serve as a comparison to help porphyry copper-gold exploration in the region.

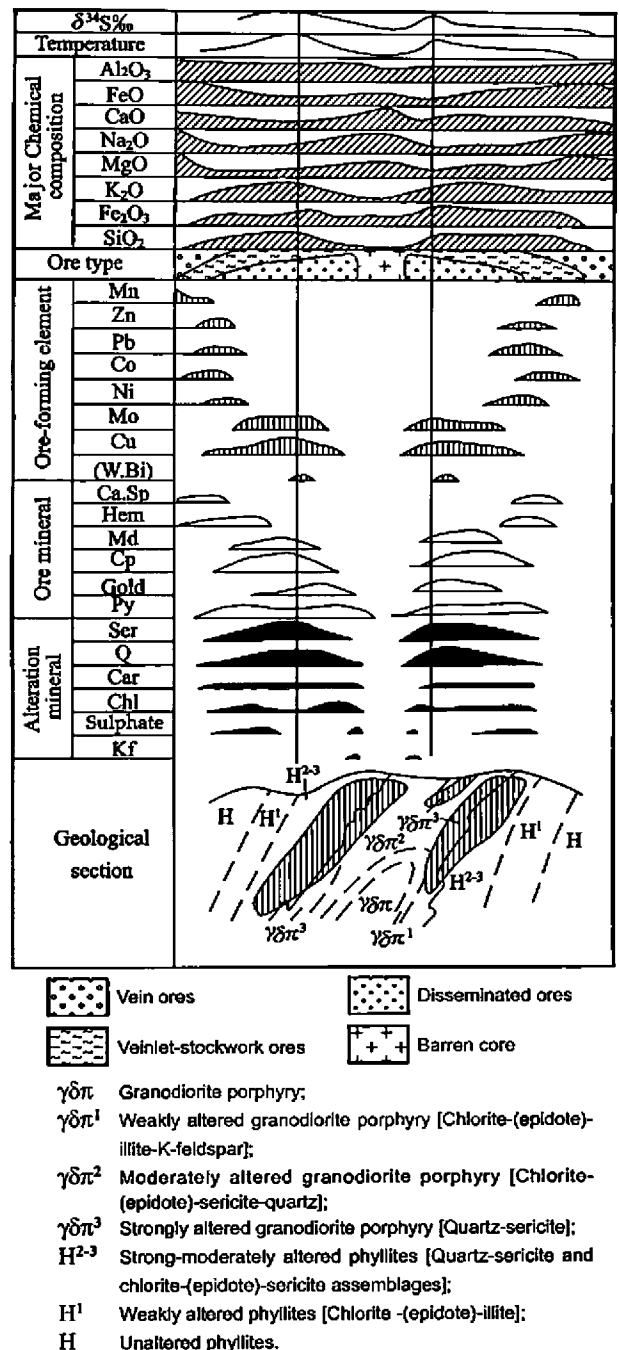


Figure 6: A generalised zonation pattern for the Dexing porphyry copper deposits

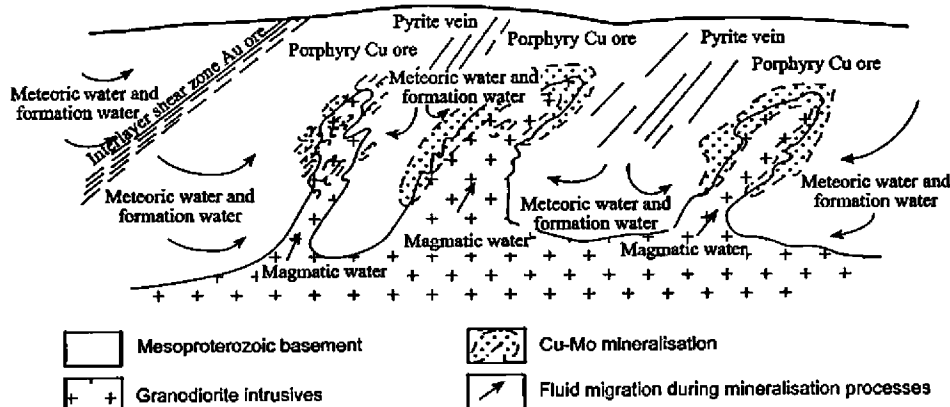


Figure 7: A genetic model for the Dexing porphyry copper deposits, Jiangxi, China.



To conclude, a genetic model for the Dexing porphyry copper deposits is illustrated in Fig. 7. Cross structures, in the form of northwest striking regional faults related to the Gandongbei deep-seated fault zone played a very important role in the generation and emplacement of granitic magma, while fractures along contact zones between granodiorite porphyries and phyllite country rocks provided crucial conduits and loci for hydrothermal alteration and mineralisation. Ore-forming fluids were primarily derived from volatiles fractionated from a second boiling of magmatic hydrothermal fluids which brought metals and caused symmetric zoning of alteration and mineralisation along the contact zones. Circulation of heated ground water and possibly deep-seated formation water, were involved in the process at a later stage, resulting in further water-rock interactions.

## Acknowledgement

Sincere thanks to Dr Ross Andrew who thoroughly reviewed the paper and improved both content and English language.

## References

- Candela, P.A. and Holland, H.D., 1984 - The partitioning of copper and molybdenum between silicate melts and aqueous fluids; *Geochem. Cosmochem. Acta*, v. 48, pp. 373-386.
- Geological Publishing House, 1996 - The discovery history of mineral deposits of China, Jiangxi Volume; *Geological Publishing House*, pp. 62-66 (in Chinese).
- Ji, K.J., Wu, X.H. and Zhang, G.B., 1992 - Ore source, water source and heat source for hydrothermal deposits and regularity of their distribution; *Geological Publishing House*, Beijing, pp. 1-197 (in Chinese with English abstract).
- Institute of Geology and Mineral Resources, MMI. 1984 - Porphyry copper deposits of China. Beijing; *Science Press*, pp. 1-240 (in Chinese).
- Liao, S.Q., 1995 - Geological characteristics of Jinshan gold deposit, Jiangxi; in Cun, G. and Chen, J.M., (Eds.), *The Typical Gold Deposits of China (2)*, pp. 304-312 (in Chinese).
- Lowell, J.D. and Guilbert, J.M., 1970 - Lateral and vertical alteration-mineralization zoning in porphyry ore districts; *Economic Geology*, v. 65, pp. 373-408.
- Ning, Q.S., Li, Y.S. and Liu, L.S., et al., 1979 - Some major metallogenetic characteristics of porphyry copper deposits in China and regularities of their distribution; *Geological Review*, v. 25(2): pp 36-46 (in Chinese with English abstract).
- Porphyry Copper Ore Group, GIGMR, MMI. 1976 - Muscovites in porphyry Cu-Mo deposits; v. 6, pp. 35-45 (in Chinese).
- Porphyry Copper Ore Group, Geochem. Explor. Room, GIGMR, MMI. 1979 - Geochemical Features of the Fujiawu porphyry copper deposit and its geochemical criteria for ore prospecting; *Geology and Prospecting*, v. 6, pp. 29-36 (in Chinese).
- Rock-forming and Ore-forming Laboratory, GIGMR., 1978 - A preliminary experimental study of conditions of K-feldspathization for the Fujiawu porphyry copper deposit; *Geology and Prospecting*, v. 3, pp. 18-23 (in Chinese).
- Rui, Z.Y., Huang, C.K. Qi, G.M., et al., 1984 - Porphyry copper (molybdenum) deposits of China; *Geological Publishing House*, Beijing, pp. 1-350, (in Chinese with English abstract).
- Rui, Z.Y., Li, Y.Q., Wang, L.S., et al., 2002 - Preliminary discussion on ore-forming fluids and enrichment systems of metallic minerals; *Mineral Deposits*, v. 21 (1), pp. 83-90 (in Chinese with English abstract).
- Shao, K.Z., Zhu, X.J. and Feng, Y.C., 1959 - Granodiorite-porphyry of certain districts in China; *Acta Geologica Sinica*, v. 39 (3), pp. 248-278 (in Chinese with English abstract).
- Sillitoe, R.H., 1990 - Gold-rich porphyry copper deposits of the Circum-Pacific region, an updated overview; in Fooks, J. and Brennan, T., (Eds.), *Proceedings of the 1990 Pacific Rim Congress*, Parkville, Australia. *AusIMM*, Melbourne. pp. 119-126.
- Sillitoe, R.H., 1997 - Characteristics and controls of the largest porphyry copper-gold and epithermal gold deposits in the Circum-Pacific region; *Australian Journal of Earth Sciences*, v 44, pp. 373-388.
- Williams, J.J., Candela, P.A. and Piccoli, P.M., 1995 - The partitioning of copper between silicate melt and two phase aqueous fluids: An experimental investigation at 1 kbar, 800°C and 0.5kbar, 850°C; *Contributions to Mineralogy and Petrology*, v. 121, pp. 388-399.
- Yan, M.Z. and Hu, K., 1980 - Geological characteristics of the Dexing porphyry copper deposits, Jiangxi, China; *Mining Geology Special Issue*, v 8, pp. 197-203 (in Chinese with English abstract).
- Ye, Q.T., 1987 - Metallogenic series and mechanism of lead and zinc deposits in the northeast Jiangxi. Beijing; *Beijing Science & Technological Press*. pp. 1-114.
- Zhang, L.G., et al., 1995 - Block Geology of eastern Asia lithosphere - Isotope geochemistry and dynamics of upper mantle, basement and granite; *Science Press*, Beijing, pp. 1-252.
- Zhang, L.G., Liu, J.X. and Chen, Z.S., 1996 - Hydrogen and oxygen evolution for water-rock system in super-huge Tongchang copper deposit, Jiangxi Province; *Scientifica Geologica Sinica* v. 31, pp. 250-263 (in Chinese with English abstract).
- Zhou, T., Goldfarb, R.J. and Phillips, G.N., 2002 - Tectonics and Distribution of gold deposits in China - an overview; *Mineral Deposits*, v. 37, pp. 249-282 (in Chinese with English abstract).
- Zhu, X., Huang, C.K., Rui, Z.Y., et al., 1983 - The geology of Dexing porphyry copper ore field; *Geological Publishing House*, Beijing, pp. 1-336 (in Chinese with English abstract).
- Zhu, J.C., Shen, W.Z. and Liu, C.S., et al., 1990 - Nd-Sr isotopic characteristics and genetic discussion of

Mesozoic granitoids of syntaxis series in south China; *Acta Petrologica et Mineralogica*, v. 9 (2), pp. 97-105 (in Chinese with English abstract).

Zhu, J.C., Jin, Z.D., Rao, B., et al., 2002 - Ore-forming fluid process in the Dexing porphyry copper deposits, Jiangxi Province: Evidence from clay mineralogy, fluid inclusion and isotope tracing: *Journal of Nanjing University (Natural Sciences)*, v. 38 (3), pp. 418-434 (in Chinese with English abstract).



## A TECTONIC MODEL FOR PORPHYRY COPPER-MOLYBDENUM-GOLD DEPOSITS IN THE EASTERN INDO-ASIAN COLLISION ZONE

<sup>1</sup>Hou Zengqian, <sup>2</sup>Zhong Dalai, <sup>2</sup>Deng Wanming and <sup>3</sup>Khin Zaw

<sup>1</sup>*Institute of Mineral Resources, Chinese Academy of Geological Sciences, Beijing, P.R. China*

<sup>2</sup>*Institute of Geology and Geophysics, Chinese Academy of Sciences, Beijing, P.R. China*

<sup>3</sup>*Centre for Ore Deposit Research, University of Tasmania, Private Bag 79, Hobart., Australia 7001*

**Abstract:** Two Himalayan porphyry copper-molybdenum-gold belts have been developed in the eastern part of the Himalayan-Tibet orogenic zone related to the collision between the Indian and Asian Plates. Both were accompanied by the emplacement of high-level intracontinental, alkali-rich, potassic felsic magmas which produced a huge Cenozoic belt of potassic igneous rock. The emplacement of these magmas was controlled by large-scale strike-slip fault systems, orientated roughly orthogonal to the of the Indo-Asian continental convergence, which adjusted the collisional strain. The Jomda-Markam-Xiangyun copper-molybdenum belt is the western of the two, developed along a narrow zone following the Nanqian thrust, the Jinshajiang fault system, and the Red River shear zone, whereas the eastern, the Zhongdian-Yanyuan-Yao'an porphyry copper-gold-silver belt, was developed along the western margin of the Yangtze Craton. The ore-bearing porphyries have compositions which include granite, monzogranite, and monzonite, with a small amount of quartz-syenite porphyry. They are distinguished from barren porphyries by their higher SiO<sub>2</sub> (>63 wt %), lower Y (<20 ppm) and their adakitic magma affinity. All alkali-rich porphyries are relatively enriched in large-ion lithophile elements (K, Rb and Ba) and depleted in high-field strength elements (Nb, Ta, Ti and P) with a wide range of Nb/Y ratios. These porphyries also show strong REE fractionation but no obvious negative Eu anomaly, suggesting that possible magma sources underwent metasomatism by fluids derived from an ancient subducted oceanic slab, and the input of small-volumes of melts derived from the asthenosphere. Adakite-like porphyries might originate from the basaltic lower crust, which probably underwent high-pressure (>40 km), low amphibolite-eclogite facies metamorphism during the Indo-Asian continent collision and metasomatism of slab-derived fluids. Amphibolite and garnet-amphibolite xenoliths in alkali-rich porphyries have been interpreted to be samples of such lower-crustal materials. Barren syenite porphyries might have originated from an enriched mantle characterised by the phlogopite peridotite. Trace element and Sr-Nd-Pb isotope systematics of these barren porphyries indicate that their source was subjected to much strong metasomatism by slab-derived fluid and dissemination of the underlying asthenospheric material. Available geophysical data in eastern Tibet suggest that the Yangtze continental slab was subducted westwards since 50 Ma and collided with the subducted Indian continental slab, thus inducing upwelling, thermal erosion and underplating of asthenospheric melts and giving rise to partial melting of the crust-mantle transition zone to produce adakite-like, potassic, felsic magmas. Such magmatic systems are characteristically rich in water and sulphur with high oxygen fugacity ( $fO_2$ ), which could largely result in the potential for magmatic process to better carry and transport metal and sulphur. The intersection of the large-scale strike-slip faults with basement lineaments controlled the temporal-spatial localisation of porphyry Cu-Mo-Au systems.

### Introduction

Sillitoe (1972) and Mitchell (1973) published their pioneering tectonic models for the setting of porphyry copper deposits i.e., porphyry copper deposits occur in island arcs and continental margin arcs along convergent plate boundaries. The model incorporates magma which originated in a mantle wedge, was metasomatised by fluids from the subducted slab and was then subjected to crystallisation differentiation and/or contamination with crustal material in a relatively closed system, resulting in the formation of ore-bearing porphyries and development

of a magmatic-hydrothermal Cu system. This model has also been strongly supported by studies of a number of large and super-large porphyry copper-gold deposits discovered in the Circum-Pacific metallogenic belts in the last few decades (Griffiths and Godwin, 1983; Sillitoe and Camus, 1991; Camus and Dilles, 2001). However, porphyry copper deposits not only occur in island and continental margin arcs but also in collisional orogenic belts. Typical examples include the Yulong porphyry copper belt in eastern Tibet (Rui *et al.*, 1984; Ma, 1994; Tang *et al.*, 1995) and the Gangdese porphyry copper belt in southern Tibet (Qu *et al.*, 2001). Preliminary studies have

revealed that the Yulong belt Cu deposits formed in a syn-collisional transpressional environment during the collision. The ore-bearing porphyries of these deposits exhibit features of the shoshonite series (Zhang *et al.*, 1988a, 1988b) and were controlled by a large-scale strike-slip fault system (Hou *et al.*, 2003c). The Gangdese belt Cu deposits formed in a post-collisional extensional environment (Hou *et al.*, 2003a, 2004a). Its ore-bearing porphyries have an adakite magma affinity (Gao *et al.*, 2003; Hou *et al.*, 2003b) and were controlled by a normal fault system intersecting the collision belt (Hou *et al.*, 2004b). Nevertheless, a tectonic model for the formation of porphyry copper deposits in collisional orogenic environments has not yet been constructed.

The key to the construction of such a model must involve understanding: i) the temporal and spatial distribution, and environment of formation of the regional porphyry mineralisation event, ii) mechanisms for the formation of ore-bearing and barren porphyries, and iii) the lithospheric

structures in which the porphyry Cu-Mo-Au system originated. Long-term mineral exploration and recent extensive studies have accumulated voluminous information about general framework, spatial-temporal distribution, and features of the porphyry Cu-Mo-Au mineralisation in eastern Tibet, the eastern Indo-Asian collision zone (Rui *et al.*, 1984; Ma, 1994; Bi *et al.*, 1997; Xu *et al.*, 1997; Lo *et al.*, 1998; Hou *et al.*, 2004b). Systematic studies of the >1000 km long alkali-rich porphyry belt in eastern Tibet over many years have greatly increased our understanding of their genetic process and geodynamic setting (Zhang and Xie, 1997; Chung *et al.*, 1998; Deng Wanming *et al.*, 1998a, 1998b; Zhang *et al.*, 2000; J. H. Wang *et al.*, 2001; Wang Jian *et al.*, 2003). Intensive tectonic studies on the Sanjiang Tethys and the eastern collisional zone provide a relatively distinct tectonic framework for the formation of the porphyry Cu-Mo-Au belt (Wang and Buechfiel, 1997; Li *et al.*, 1998; Zhong, 1998). A large amount of geophysical data about this tectonic belt (Lin *et al.*, 1993; Liu *et al.*, 2000; Jiang *et al.*,

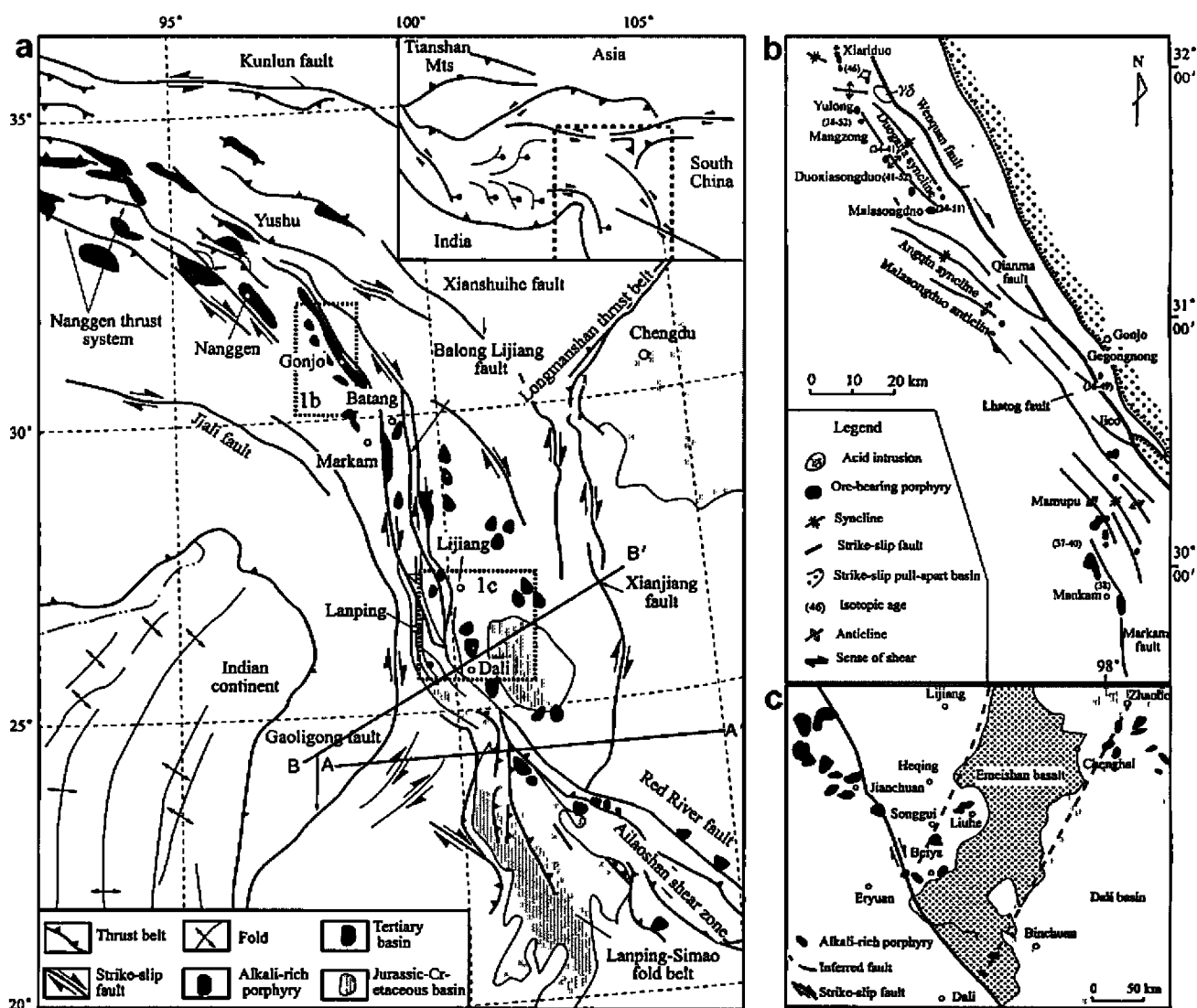


Figure 1: Distribution of Cenozoic structure and porphyries in east Tibet from the eastern Indo-Asian collision zone.

- The tectonic framework of the eastern Indo-Asian collision zone, east Tibet (modified from Deng *et al.*, 1998a; J-H Wang *et al.*, 2001; Hou *et al.*, 2003c);
- Structural features and porphyry distribution in the Yulong porphyry copper belt, east Tibet (after Liu *et al.*, 1993 and Hou *et al.*, 2003e);
- The distribution of porphyry intrusions in the Dali area.

2000; Zhong *et al.*, 2001; Wang Chunyong *et al.*, 2002) provide abundant information for understanding the deep geodynamic processes of the magma genesis, and make it possible for us to discuss and construct a tectonic model for intracontinental porphyry copper deposits.

On the basis of our recent research work, together with data from previous studies, this paper summarises the characteristics of the temporal-spatial distribution of the porphyry copper-molybdenum-gold metallogenic belts, determines the magma affinity and types of ore-bearing and barren porphyries, and discusses the deep processes of their magmatic origin. An attempt is also made to construct a tectonic model for porphyry copper-molybdenum-gold deposits in the eastern Indo-Asian collision zone.

### Regional Geological Setting

The study area is located on the eastern margin of the Tibetan Plateau that was formed by the Indo-Asian collision, i.e., the eastern Indo-Asian collision zone. Tectonically, the area is a tectonic transition belt that accommodated the stress-strains produced by that collision. The area underwent a complex tectonic evolution from the Palaeo-Tethys Orogeny in the Palaeozoic-Mesozoic to Himalayan large-scale intracontinental deformation during

the Cenozoic (Fig. 1). The Palaeozoic Orogeny was mainly marked by subduction of the Jinshajiang oceanic basin since the late Permian (JS) and development of the Jomda-Weixi arc on the Qiangtang terrane (Mo *et al.*, 1993). Cenozoic deformation was chiefly manifested by Eocene-Oligocene (40-24 Ma) transpressional deformation, early-middle Miocene (24-17 Ma) transtensional deformation, and E-W extension since the Neogene (J-H Wang *et al.*, 2001), forming a number of strike-slip fault systems with various strike directions. Of these fault systems, the western includes the Jiali and Gaoligong strike-slip faults, developed around the eastern Himalayan tectonic syntaxis, while the central consists of the Batang-Lijiang fault in the northern segment and the Ailaoshan-Red River fault on the southern segment. The former of the central system is characterised by N-S trending and right-lateral strike-slip movement, and the latter by NW trending and left-lateral strike-slip movement. Both fault systems constitute a significant boundary between the Yangtze Craton (continental block) on the eastern side, and the Qiangtang terrane on the western side. The eastern system consists of the Longmenshan thrust belt and the Xianshuihe and Xiaojiang strike-slip faults (Fig. 1). Both Cenozoic potassic igneous rocks and a series of early-middle Cenozoic pull-apart basins, such as the Gonju, Jianchuan and Dali basins (Fig. 1), developed

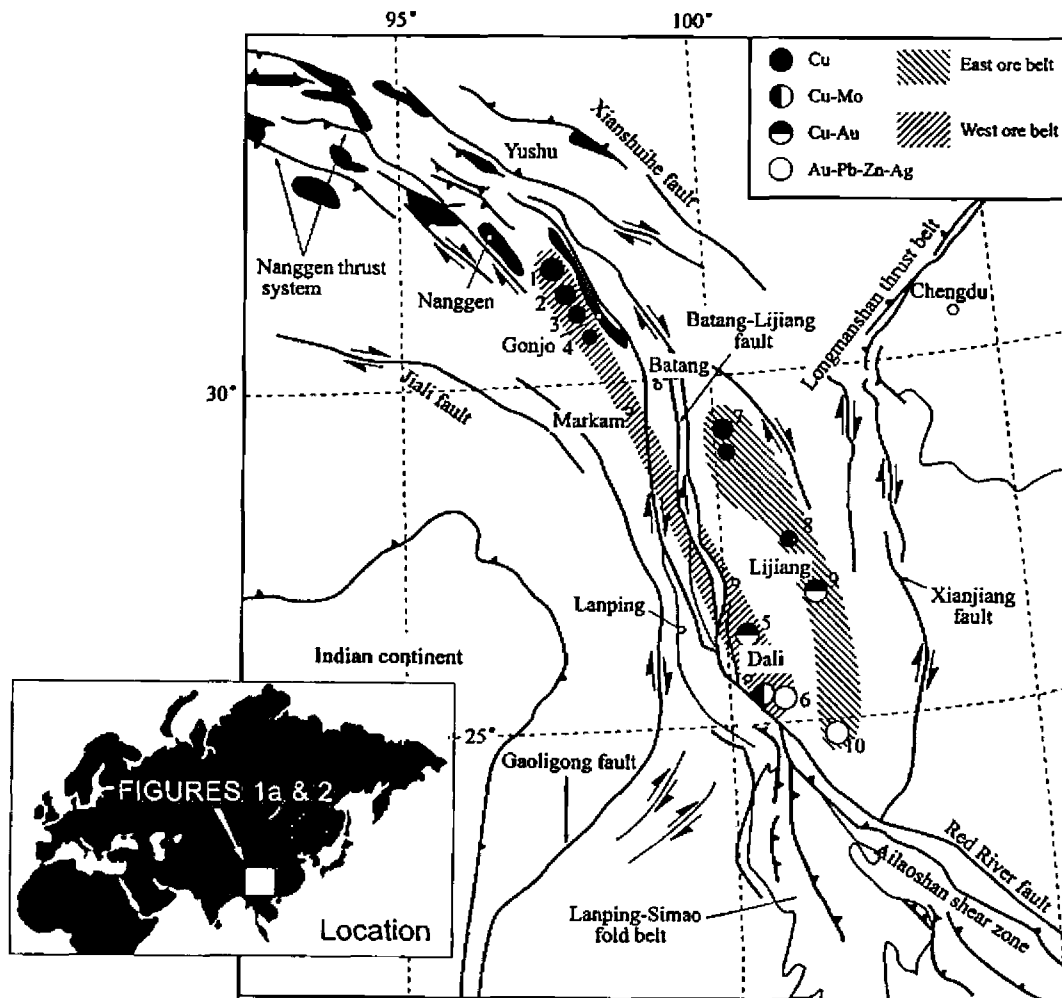


Figure 2: A simplified geological map showing the distribution of various porphyry-type deposits in the eastern Indo-Asian collision zone. 1. Yulong Cu deposit; 2. Malasongduo Cu deposit; 3. Duoxiasongduo Cu deposit; 4. Mangzong Cu deposit; 5. Beiya Au-Cu deposit; 6. Machangqing Cu-Mo and Au deposit; 7. Pulang Cu deposits; 8. Xiaolongtan Cu deposit; 9. Xifanping Cu-Au deposit; 10. Yao'an Au-Pb-Zn-Ag deposit.

along a narrow belt following the Nanqian thrust, the Jinshajiang fault system, and the Red River shear zone, forming the huge, >1000 km long, Jinshajiang-Honghe alkali-rich igneous rock belt (Zhang *et al.*, 1998a, 1998b). In this huge magmatic belt, two ore-bearing potassic porphyry belts exist: one (west) is the Jomda-Heqing-Dali alkali-rich potassic porphyry belt, which is distributed along the junction boundary between the Yangtze Craton and Qiangtang terrane and the other (east) is the Zhongdian-Yanyuan-Yao'an alkali-rich potassic porphyry belt, which occurs on the western margin of the Yangtze Craton. Available dating data indicate that the igneous rocks in the western belt yielded ages ranging between 48 and 27 Ma (Lo *et al.*, 1998; Zhang *et al.*, 1998a) and one in the eastern belt has an age range varying from 48 Ma to 31 Ma (Luo *et al.*, 1998).

## Porphyry Copper-Molybdenum-Gold Mineralisation

Fig. 2 shows the spatial distribution of major porphyry deposits in the eastern Indo-Asian collision zone. The porphyry deposits may be divided into two metallogenic belts, separated by the Jinshajiang suture (JS). The west belt extends for more than 500 km, from the Jomda in eastern Tibet, southward to the Xiangyun in west Yunnan, including the Yulong porphyry Cu sub-belt in the northern segment, the Beiya porphyry Au-Cu Orefield in the south-central segment and the Machangqing Cu-Mo-Au deposit in the southern segment (Fig. 2). The east belt stretches for more than 300 km from the Zhongdian southward to Yao'an in west Yunnan. Its northern segment is the Pulang (Zhongdian) porphyry Cu mineralisation sub-belt that was found recently, while the central segment is the Xifanping porphyry Cu-Au deposit and the southern segment is the Yao'an porphyry Au-Ag-Pb-Zn deposit (Fig. 2). Generally, the western belt is found in the junction zone of the Yangtze Craton and Qiangtang terrane, controlled by large-scale strike-slip faulting systems. The eastern belt occurs on the western margin the Yangtze Craton, with its northern segment controlled by strike-slip faults and the southern segment constrained by faults inherited from those in the Panxi rift phase. These belts appear to extend southward into Myanmar and mainland SE Asia (Khin Zaw *et al.*, 1999). Both porphyry metallogenic belts have the following similarities:

### *Similarity in Mineralising Age*

The ages of porphyry deposits may be either determined by using accurate molybdenite Re-Os dating or indirectly estimated applying crystallisation age of ore-bearing porphyries. Generally, the formation of porphyry deposits occurred 1-3 Ma before the latest-phase of the intrusion of ore-bearing porphyry bodies (Hou *et al.*, 2003c). In the west belt, the Yulong porphyry Cu sub-belt has molybdenite Re-Os ages of 35.6-35.8 Ma (Du *et al.*, 1994). The age of the Machangqing porphyry Cu-Mo deposit has not yet been directly determined; although, according to the Rb-Sr isochron ages of ore-bearing porphyries, this deposit is estimated to have a mineralisation age of ~36.0 Ma (Luo *et al.*, 1998). The mineralisation types of the Beiya

porphyry deposit are rather complex. It is estimated, according to the K-Ar age (48 Ma) of the Beiya quartz-syenite porphyry, that the main mineralisation age should be  $45 \pm 2$  Ma. In the east belt, the Xifanping copper-bearing monzonite porphyry has an amphibole  $^{40}\text{Ar}/^{39}\text{Ar}$  plateau age of 47.52 Ma and an isochron age of 46.8 Ma (Luo *et al.*, 1998); hence the mineralising age is estimated at  $44 \pm 2$  Ma. The K-Ar age for the Yao'an syenite porphyry varies from 31 to 50 Ma; on this basis the age of the deposit is estimated to be between 34 Ma and 47 Ma. Though the above data are somewhat speculative, there is a considerable consistency between the mineralising ages of the two-metallogenic belts.

### *Similarity in Ore-Bearing Porphyry*

The similarity is manifested as follows: i) the ore-bearing porphyry associations of the east and west belts are both monzogranite porphyry and monzonite porphyry with a small amount of quartz-syenite porphyry, and spatially, monzogranite porphyry in the north grades southward to monzonite porphyry along both belts; ii) ore-bearing porphyry bodies mostly occur as small stocks and are generally composite rock bodies, resulting from two or more magmatic intrusions; and iii) in a composite intrusion mineralisation is mostly closely related to the more felsic porphyries intruded in the middle and late stages.

### *Similarity in Wall-Rock Alteration*

Wall-rock alteration is mostly centred on an intrusion and developed as rings. Mineralised intrusions normally have a silicified core, which successively passes outward into the K-silicate zone, then to sericite-quartz and finally to a propylitic alteration zone. In the exocontact, marble, hornfels and skarn zones are mostly developed.

### *Similarity in Mineralisation Features*

The similarity is displayed in the following respects: i) their mineralisation features are consistent; ii) Although they occur in an environment which is different from that for porphyry deposits in the circum-Pacific belts, similar mineralisation assemblages appear in the eastern and western belts, i.e. the Cu, Cu-Mo, and Au-Pb-Zn assemblages in the west ore belt and the Cu, Cu-Au, and Au-Pb-Ag assemblages in the east ore belt; and iii) mineralisation types are similar; for example, in most cases veinlet-disseminated mineralisation occurs inside porphyry intrusions, sulphide-rich tabular orebodies in contact zones, and bed-like, lenticular, and veined orebodies in country rocks.

## Ore-Bearing & Barren Porphyries

There are over 10 Cenozoic alkali-rich porphyry swarms in the eastern Indo-Asian collision zone, including as many as 1000 separate porphyry bodies. Major element, trace elements and Sr-Nd-Pb isotopic systematics for representative samples from several porphyry bodies have been analysed by many authors (Tables 1 & 2; Ma, 1994; Deng *et al.*, 1998, 1999; Chung *et al.*, 1999; Zhang *et al.*, 1997, 1998a, 1998b, 2000; Wang *et al.*, 2003). To correctly distinguish between ore-bearing and barren porphyries and

to establish corresponding geochemical criteria, we have made a preliminary attempt using our previously published geochemical data on alkali-rich porphyries along the eastern Indo-Asian collision zone.

Fig. 3a compares potassic magmatic rocks developed in different areas of the Tibetan Plateau since the Indo-Asian collision at 60 Ma. Three important facts have been observed: i) most alkali-rich porphyries in eastern Tibet are shoshonitic, although some of them are potassic calc-alkaline, which are characterised by higher  $\text{SiO}_2$  contents as compared with the post-collisional potassic-ultrapotassic volcanic rocks in the interior of the Plateau (Turner *et al.*, 1993; Miller *et al.*, 1999); ii) ore-bearing porphyries in eastern Tibet are very similar to those of the Gangdese porphyry belt in southern Tibet, but notably different from those in island arcs, which suggests that the ore-bearing porphyries in the collisional orogenic environment are characterised by high potassium contents; and iii) on the basis of their  $\text{SiO}_2$  content, alkali-rich porphyries in eastern Tibet may broadly fall into two groups: a) barren, alkali-rich porphyries with  $\text{SiO}_2$  of <63 wt %, predominantly syenite porphyries; and b) mineralised, alkali-rich porphyries with  $\text{SiO}_2$  contents of >63 wt %, mainly consisting of granite-, monzogranite-, and monzonite-porphyry, with a small amount of syenite porphyry. In group b), granite porphyry is associated with copper-molybdenum, monzogranite porphyry with copper, monzonite porphyry with copper-gold, and syenite porphyry with gold (-lead-zinc) mineralisation.

Y and Yb are two trace elements that do not participate in mantle inhomogeneity (e.g., mantle metasomatism) and also display incompatible behaviours, remaining stable during alteration (Gill, 1981; Tatsumi, 1986). Unlike both Y and Yb, the high field strength elements (HFSE) (e.g., Nb), show high incompatibility in their geochemical behaviours during magmatic processes, and also remain stable during fluid metasomatism. Therefore, the Nb/Y ratio is free from the influence of fluid metasomatism and may sensitively reflect the enrichment process in a source related to a magmatic melt. In contrast, large ion incompatible elements (LILE) (e.g., Ba) are very active and may be considered key elements indicating fluid metamorphism and enrichment in trace elements. Accordingly, we divide alkali-rich porphyries in the eastern Tibet into these three categories:

#### Low-Y and low-Ba porphyries

Represented by Cu-bearing porphyries in the Yulong belt, the dominant rocks of this category are monzogranite- and syenogranite-porphyry, generally with <20 ppm Y and <1000 ppm Ba, while Nb/Y varies from 0.35 to 1.25. These Cu-bearing porphyries form a horizontal trend parallel to the Nb/Y axis on Fig. 3a, suggesting that magmatic processes controlled the geochemical variations among different porphyry intrusions or among different porphyry phases.

#### High-Y and high-Ba porphyries

These are usually barren syenite-porphyries which are widely developed throughout the alkali-rich porphyry belt

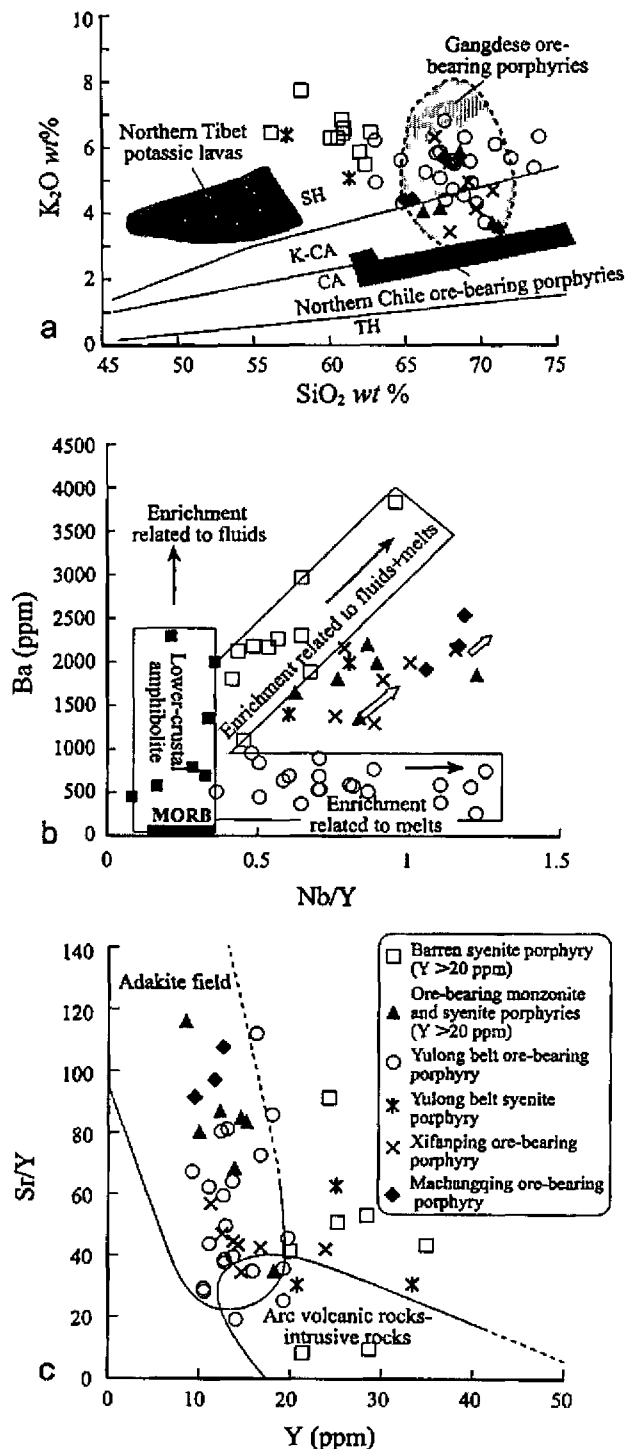


Figure 3: Discrimination diagrams for alkali-rich porphyries in east Tibet, the eastern Indo-Asian collision zone.

- $\text{SiO}_2$ - $\text{K}_2\text{O}$  diagram of alkali-rich porphyries showing that they are characterised by higher  $\text{SiO}_2$  (>63 wt %) and higher potassium, similar to those at Gangdese but different from the Plateau.
- Y-Sr/Y diagram of alkali-rich porphyries illustrating their adakitic affinity (Defant and Drummond, 1990).
- Ba-Nb/Y diagram of alkali-rich porphyries illustrating that ore-bearing and barren porphyries have different variation trends.



**Table 1: Major and trace element geochemical data of the representative porphyries from the eastern Indo-Asian collision zone.**

Low-Y and low-Ba porphyries																	
	1	2	3	4	5	6	7	8	9	10	11	12	13	14	15	16	17
SiO <sub>2</sub>	64.8	67.6	68.9	71	63.1	69.42	67.04	68.94	68.21	68.16	69.3	71.9	73.5	66.4	68.31	67.4	67.29
TiO <sub>2</sub>	0.52	0.39	0.35	0.31	0.34	9	0.3	0.27	0.27	0.28	0.28	0.23	0.21	0.22	0.33	0.33	0.42
Al <sub>2</sub> O <sub>3</sub>	16.4	15.2	15	14.2	18	14.12	14.14	14.26	13.04	14.3	14	13.1	13.3	14.8	15.15	15	14.58
Fe <sub>2</sub> O <sub>3</sub>	1.23	1.37	1.16	0.54	1.87	1.09	0.94	1.59	1.01	1.02	1.49	1.43	0.66	1.46	1.5	1.22	1.68
FeO	1.76	1.67	1.44	1.5	1.03	1.51	1.1	1.23	2.71	0.43	0.74	1.36	1.38	1	0.82	1.33	1.68
MnO	0.06	0.06	0.07	0.05	0.05	0.15	0.06	0.08	0.12	0.06	0.07	0.12	0.13	0.09	0.1	0.11	0.07
MgO	2.47	1.42	0.79	1.23	1.45	0.83	1.22	1.01	0.99	0.96	1.27	0.63	0.59	1.38	0.99	1.19	1.47
CaO	2.94	2.34	2.83	1.27	2.76	1.86	1.48	1.3	1.67	2.29	0.76	0.65	0.62	0.7	0.99	1.81	2.82
Na <sub>2</sub> O	3.77	3.67	3.32	2.87	4.39	3.67	3.27	3.12	2.01	2.82	2.84	2.44	2.95	3.11	3.8	3.31	3.72
K <sub>2</sub> O	4.27	4.33	4.52	6.04	4.89	4.85	5.79	6.25	5.57	4.76	5.52	5.6	5.32	5.23	5.45	5.8	5.01
P <sub>2</sub> O <sub>5</sub>	0.03	0.07	0.11	0.05	0.4	0.1	0.11	0.1	0.11	0.13	0.12	0.13	0.14	0.19	0.12	0.14	0.23
H <sub>2</sub> O*	0.6	0.67	0.54	0.53	1.21	0.5	0.76	1.04	1.32	1.27	1.08	0.78	0.73		0.7	0.97	0.71
Total	98.9	98.9	99	99.5	99.5	98.38	96.21	99.19	97.03	96.48	97.5	98.4	99.6	94.6	98.26	98.6	99.68
La	82.2	67	63	51.9	97.4	45.3	82.11	48.85	32.5	72.76	77.3	60.3	86.3	60.5	57.45	68.7	62.01
Ce	162	123	119	96.4	175	87.09	158.7	86.59	55.5	136.9	143	112	149	108	99.14	122	120.1
Nd	65.9	45.8	45.9	34.4	72.4	33.51	55.28	29.7	20	47.03	50.5	38.2	43.4	43.3	33.05	43.1	45.68
Sm	10.4	7.08	7.36	5.25	10.7	5.56	8.26	4.77	3.6	6.97	7.53	5.51	5.35	6.21	5.32	6.58	7.24
Eu	1.9	1.49	1.52	1.06	2.28	0.97	0.94	0.88	0.78	1.32	1.46	0.88	0.66	1.36	0.95	1.36	1.53
Gd	7.44	5.19	5.45	3.81	6.36	4.41	6.2	3.76	4.2	4.87	5.15	3.98	3.83	3.74	4.21	4.81	5.33
Tb	0.54	0.49	0.4	0.16	0.85	0.39	0.65	0.45	0.78	0.34	0.57	0.31	0.31	0.51	0.43	0.53	0.5
Dy	3.9	2.82	2.99	2.11	3.85	2.98	3.89	2.54	1.9	2.74	2.83	2.27	2.3	2.42	2.5	2.73	2.93
Ho	0.69	0.51	0.59	0.39	0.68	0.58	0.77	0.54	0.62	0.5	0.52	0.4	0.41	0.44	0.43	0.49	0.56
Er	1.89	1.37	1.46	1.07	1.87	1.61	2.07	1.42	0.74	1.45	1.43	1.2	1.27	0.32	1.21	1.37	1.44
Tm	0.29	0.22	0.22	0.14	0.24	0.26	0.35	0.26	0.24	0.24	0.19	0.18	0.19	0.18	0.2	0.25	0.25
Yb	1.52	1.18	1.31	0.94	1.5	1.62	1.92	1.5	1.1	1.3	1.31	1.16	1.17	1.26	1.11	1.2	1.24
Lu	0.28	0.29	0.3	0.19	0.23	0.3	0.36	0.36	0.54	0.26	0.24	0.28	0.2	0.2	0.19	0.32	0.21
Y	16.8	12.4	13.7	9.33	19.7	15.94	19.31	13.88	12.8	12.73	12.9	11.1	10.6	14.2	10.56	12.7	13.15
Sc	8.02	5.12	5.51	4.2		4.84	5	3.53	3.84	3.16	3.65	2.91	1.97		4.12	3.94	5.09
Rb	237	217	225	246	224	229	268	236	240	257	315	203	287	178	269	287	227
Sr	1220	995	878	631	899	559	491	550	480	493	638	486	298	276	306	735	1068
Ba	440	939	636	362	760	571	754	580	740	498	682	379	255	562	678	583	835
Nb	9	6	8	6	72	13	17	15	16	11	9	12	13	17	6	10	7
Ta					0.95									1.37			
Zr	159	113	124	115	288	114	148	101	138	109	101	104	119	242	146	114	94
Hf	19	8	8	9	7	6	15	8	6	4	4	6	5	6	6	6	9
Th	27	29	27	28	20	38	37	36	28	47	48	48	54	32	34	45	38
U																	
Cr																	
Ni																	

1-17: Low-Y and low-Ba porphyries, predominantly monzogranite porphyries; samples 1-5 from the Yulong bodies; 6-9 from the Malasongduo bodies; 10-14 from the Duoxiasongduo bodies; 15-16 from the Zhanaga bodies; 17 from the Mangzong bodies.

18-27: Low-Y and medium-Ba porphyries. - Sample 18-19 from the Xifanping district (quartz monozite porphyries); 20-21 from the Machangqing district (20: granitic porphyry; 21: quartz-syenitic porphyry); 22-25: from the Beiya district (quartz-syenitic porphyries); 26: syenitic porphyry in the Jianchuan; 27: syenitic porphyry in the Liuhe

Table 1: *Continued*

	Low-Y and medium-Ba porphyries										High-Y and high-Ba syenitic porphyries											
	18	19	20	21	22	23	24	25	26	27	28	29	30	31	32	33	34	35	36	37	38	39
SiO <sub>2</sub>	65.47	65.04	69.72	66.94	68.63	62.73	66.24	70.74	67.32	68.64	60.95	60.56	62	60.07	57.36	71.23	73.9	67.7	45.54	46.38	51.55	39.08
TiO <sub>2</sub>	0.42	0.39	0.32	0.29	0.19	0.71	0.34	0.3	0.39	0.27	0.77	0.65	0.62	0.47	0.59	0.27	0.22	0.22	0.72	0.54	0.97	3.13
Al <sub>2</sub> O <sub>3</sub>	15.3	15.57	15.18	14.94	16.16	14.04	15.5	14.8	15.71	14.94	14.24	14.26	14.53	14.18	14.31	13.54	13	15.6	13.93	13.81	17.89	16.15
Fe <sub>2</sub> O <sub>3</sub>	1.89	1.88	1.12	1.22	1.37	2.72	1.68	1.36	2.11	1.15	2.1	1.92	1.84	2.34	2.38	1.18	0.63	1.71	4.3	4.06	4.36	3.61
FeO	1.69	1.44	1.18	1.18	0.35	4.81	1.6	0.98	0.88	0.47	2.7	2.59	2.32	1.77	2.82	1.03	1.06	1.13	7.13	7.77	4.33	10.58
MnO	0.17	0.07	0.05	0.07	0.03	1.09	0.07	0.04	0.06	0.04	0.09	0.1	0.09	0.1	0.11	0.47	0.07	0.07	0.24	0.32	0.29	0.11
MgO	1.52	1.59	0.8	1	0.18	0.23	1.67	0.54	1.08	0.36	2.51	2.65	2.46	2.3	2.77	1.32	0.07	1.77	11.26	10.32	3.96	12.9
CaO	2.19	2.29	1.6	2.9	1.14	0.48	2.8	1.93	2.43	1.94	4.76	4.77	4.01	3.69	4.41	1.98	0.97	0.65	10.6	11.02	6.54	1.83
Na <sub>2</sub> O	5.16	4.85	4.03	3.08	4.95	0.26	4.56	4.58	4.89	4.96	3.33	3.91	4.19	3.67	3.34	4.22	2.36	2.68	2.24	2.06	4.36	0.95
K <sub>2</sub> O	4.37	4.36	4.1	6.3	5.81	6.45	4.02	3.69	4.13	5.6	6.39	6.34	5.84	6.28	6.56	3.57	6.29	6.75	1.56	1.23	3.64	8.21
P <sub>2</sub> O <sub>5</sub>	0.28	0.21	0.13	0.11	0.07	0.24	0.19	0.14	0.18	0.09	0.42	0.39	0.39	0.3	0.39	0.18	0.1	0.22	0.12	0.14	0.27	1.06
H <sub>2</sub> O*	1.22	1.61	0.9	0.76		1.23	0.59	0.04			1.27					0.46	1.09					
Total	99.68	99.3	99.13	99.31	99.69	99.52	99.46	99.52	99.96	99.27	99.55	99.51	99.46	99.75	99.5	99.49	99.13	99.6	99.98	99.48	99.47	99.69
La	70.66	81.76	47.85	53.3	16.28	30.68	27.28	16.16	42.06	45.69	33.44	35.81	32.83	51.75	49.43	53.03	79.75	61	11.91	11.5	26.5	73
Ce	126.9	127.5	84.88	73.7	26.79	52.88	50.37	35.49	78.59	83.12	61.94	66.88	61.97	94.91	97.37	94.3	152.1	117	16.74	12.02	69.48	182.8
Nd	46.8	51.31	29.79	33.4	11.35	19.84	22.37	14.42	29.95	30.72	26.52	26.95	25.47	36.97	41.36	34.71	64.93	47.4	9.68	8.46	48.58	82.72
Sm	8.18	7.2	4.9	5.2	2.37	3.66	4.31	2.75	5.9	5.47	5.1	5.41	4.82	7.34	8.87	5.72	10.32	7.36	2.58	2.03	13.79	16.28
Eu	1.75	1.63	1.03	1.04	0.93	1.24	1.22	0.86	1.61	1.79	1.5	1.75	1.71	2.21	2.63	1.89	2.32	1.84	0.92	0.83	2.79	3.2
Gd	4.84	4.48	3.48	3.44	2.49	3.14	3.55	2.23	5.26	4.84	4.4	4.59	5.2	6.36	8.93	5.11	6.76	5.26	2.56	2.52	12.26	15.08
Tb	0.58	0.59	0.46	0.44	0.29	0.46	0.46	0.28	0.62	0.52	0.61	0.71	0.71	0.85	1.12	0.64	0.93	0.71	0.4	0.45	2.21	2.04
Dy	2.73	2.43	2.07	1.94	1.57	2.44	2.33	1.36	2.97	2.65	3.19	3.69	3.55	4.8	5.9	2.92	4.41	3.53	2.33	3.09	12.7	9.19
Ho	0.51	0.46	0.41	0.47	0.32	0.48	0.45	0.25	0.5	0.53	0.63	0.64	0.75	0.87	1.08	0.48	0.79	0.67	0.49	0.68	2.53	1.5
Er	1.21	1.12	1	1.02	0.76	1.23	1.18	0.65	1.32	1.32	1.666	1.86	2.05	1.54	2.79	1.26	2.26	1.91	1.33	1.56	7.68	3.58
Tm	0.18	0.17	0.15	0.26	0.13	0.18	0.18	0.1	0.16	0.17	0.26	0.23	0.27	0.34	0.4	0.15	0.3	0.26	0.17	0.18	1.11	0.41
Yb	1.11	1.08	0.94	0.85	0.83	1.11	1.18	0.65	1.18	0.98	1.64	1.56	1.88	2.31	2.59	0.94	1.93	1.72	1.21	1.38	6.14	1.82
Lu	0.16	0.17	0.14	0.29		0.16	0.19	0.11			0.25		0.25			0.19	0.29	0.27	0.19	0.21	0.97	0.27
Y	12.61	11.36	14.2	12.5	10	13.21	14.52	8.48	15.18	13.82	19.96	18.23	20.35	25.15	28.45	12.16	23.85	20.8	12.58	15.78	63.09	32.35
Sc			4	3.3		2.13	5.23	1.81			10.6											
Rb	134	137	158	218	241.4	325.4	105.7	89.71	134.8	253.6	211.4	220.5	211.3	270.8	231.8	131.2	124.6	293	49.43	34.64	70.14	302
Sr	708	1332	616	590	805.6	70.51	1231	983.8	1266	943.8	831.4	641.6	646.7	1285	1517	1059	1002	628	346.1	311.1	124	224.7
Ba	1787	2148	1368	2130	1848	592.6	1637	1353	1980	1796	2303	2969	2069	1884	2267	2194	524	893	568	444.6	2294	2006
Nb			10.7	14.4	12.21	24.63	8.93	7	13.54	10.57	12.8	11.71	15	16.78	15.99	10.5	17	15	2.01	1.28	13.47	12.06
Ta		0.56			0.71	1.41	0.63	0.5	1.04	0.56	0.7	0.48	0.74	1.08	1.08	0.67	1.33	1.22	0.11	0.08	0.71	7.92
Zr	306	349	40.8	70.2	310.9	222.2	148	131.1	398.8	200.4	207.1	229.1	233.9	515.8	415.2	253.2	265	267	79.95	72.13	234.6	456.4
Hf	5.3	6.5			4.19	6.48	4.35	4.12	5.05	5.11	5.5	5.86	5.42	5.68	4.76	5.72	7	7	1.28	1.14	5.6	9.77
Th	28.17	28.41	26.3	26.9	12.31	10.71	10.83	6.13	16.49	14.04	2.87	9.29	10.21	28.62	19.99	22.86	34	33	3.11	1.71	2.01	18.41
U	2.6	3.4	13.3	9.3	2.15	3.61	3.55	5.6	4.29	2.37	2.87	2.47	3.52	8.93	6.37	4.87			0.41	0.35	1.47	3.02
Cr	111	150	39.8	16.8	11.43	99.13	273.7	222.3	14.54	120.4	235	72.62	68.03	85.54	80.08	42.39			148.2	156.1	49.24	220.2
Ni	36	30	21.6	15.6	0.81	39.65	132.6	114.2	5.9	38.76	133.1	37.02	31.9	37.35	36.22	22.3			87.19	70.1	17.14	139.7

28-35: High-Y and high-Ba syenitic porphyries. - Sample 28-30 from the Liuhe; 31-32 from the Jianchuan; 33 from the Zhanhe; 34-35 from the Mangzong.

36-39: Amphibolite xenoliths. - Sample 36-38 from the Liuhe, 39 from the Dali. Samples 36-37 are no-plagioclase amphibolites, 38 and 39 are plagioclase-bearing amphibolites plagioclase-bearing amphibolites.

in the eastern Indo-Asian collision zone. Their Y content is commonly >20 ppm, while Ba is usually > 1000 ppm, varying from 1000 to 4000 ppm. Although the Nb/Y ratios of these porphyries also vary from 0.35 to 1.25, these ratios form a Nb/Y-Ba positive correlation trend (Fig. 3b), implying the combined control of both subducted-slab fluid metasomatism and magmatic processes.

#### *Low-Y and medium-Ba porphyries*

The Y content of this group is generally similar to that of the low-Y and low-Ba porphyries, varying from 10 to 20 ppm, while Ba is usually >1000 ppm. The representative intrusives are granite-, monzonite- and quartz-syenite-porphyries. Of these, granite porphyry occurs in the Machangqing Cu-Mo ore district; monzonite porphyry is developed in the Xifanping Cu-Au ore district; and quartz-syenite porphyry is mainly developed in the Beiya and Yao'an Au or Au-Ag ore districts. Compared with the low-Y and low-Ba porphyries, their mineralisation potential is slightly poorer. In Fig. 3b this group usually lies between the variation trends for low-Y, low-Ba porphyries and those with high-Y, and high-Ba. However, a positive Nb/Y-Ba correlation trend is also observed, suggesting that their sources experienced similar fluid metasomatism, but that the degree of fluid metasomatism and trace element enrichment is higher than those of low-Y, low-Ba porphyries.

In Fig. 3c the magmatic affinities of ore-bearing porphyries and barren porphyries are further distinguished. The great majority of ore-bearing porphyries lie in the adakite field (Defant and Drummond, 1990), whereas barren syenite porphyry is located outside the adakite field. A typical example is the Yulong porphyry Cu sub-belt, where mineralised monzogranite (syenogranite) porphyry and a small amount of quartz-syenite porphyry with lower Y and higher Sr/Y lie in the adakite field, while the barren syenite porphyry with higher Y content plots outside the adakite field. In addition, such features as higher SiO<sub>2</sub> (>63 wt %) and higher Al<sub>2</sub>O<sub>3</sub> (>15 wt % with SiO<sub>2</sub> = 65 wt %), strong fractionation between LREE and HREE, and no negative Eu anomaly for the ore-bearing porphyries also suggest that they have an adakitic affinity (Defant and Drummond, 1993). However, compared with typical adakite, the ore-bearing porphyries in the study area are high in potassium and enriched in LILE. We call these ore-bearing porphyries "adakite-like" rocks.

Similar "adakite-like" rocks have been reported in the Andean arc orogenic belt, the largest porphyry Cu belt in the world (Oyarzun *et al.*, 2001). Two metallogenic belts have been recognised in northern Chile (Sillitoe, 1982). One is the arc-related calc-alkaline porphyry Au-Cu belt, dominated by epithermal Au-Cu deposits, and the other is the adakitic porphyry Cu belt, in which a considerable number of large and super-large porphyry Cu deposits occur (Sillitoe, 1982; Oyarzun *et al.*, 2001). The reserves of copper metal in adakitic porphyry Cu belts are ten times larger than those in normal calc-alkaline belts (Oyarzun *et al.*, 2001). In the Gangdese porphyry Cu belt of southern Tibet, the ore-bearing porphyries are also adakitic, but show

high-K characteristics (Hou *et al.*, 2003b). The ore-bearing porphyries in eastern Tibet are generally similar to the Gangdese porphyries, except for relatively high abundances of LILE and Y. The geochemical similarities of porphyries hosting Cu deposits in arc and collisional zones indicate that "adakite-like" rocks have a significant ore potential (Hou *et al.*, 2003b).

## Genesis of Alkali-Rich Porphyries

Many models have been proposed for the genesis of alkali-rich porphyries in eastern Tibet, including partial melting of an enriched mantle (Zhang *et al.*, 2000), or the melting of the crust-mantle transition zone (Deng Wanming *et al.*, 1998a, 1998b; Zhong *et al.*, 2001) related to eastward subduction of the continental slab along the Red River fault (J-H Wang, *et al.*, 2001), or the partial melting of an "island arc-type" mantle induced by large-scale strike-slip movement (Hou *et al.*, 2003c; Wang Jian *et al.*, 2003). However, any model must explain the following four important facts: i) the temporal-spatial association between alkali-rich porphyry intrusions and lamprophyres and between ore-bearing adakitic porphyry and barren syenite porphyry; ii) geochemical characteristics such as LILE enrichment, HFSE depletion, and Nd-Sr homogenisation of alkali-rich porphyries and their associated rocks; iii) the control of lithosphere-scale strike-slip fault systems on temporal-spatial localisation of alkali-rich porphyries; and iv) the geodynamic setting characterised by subduction of the Yangtze block at about 50 Ma and upwelling of asthenospheric material beneath eastern Tibet (Liu *et al.*, 2000; Zhong *et al.*, 2001). The porphyry genesis is further constrained by the xenoliths hosted by the porphyry intrusions, and the trace element geochemistry and Sr-Nd-Pb isotopic systematics of alkali-rich porphyries.

#### *Constraint from Deep-Seated Xenoliths*

In the alkali-rich porphyries and their associated lamprophyres, two different kinds of xenoliths have been found, i.e., upper-mantle xenoliths and lower-crustal xenoliths. The major upper-mantle xenoliths are phlogopite harzburgite, found in potassic lamprophyres at Muli, Yanyuan, and Dali (Lu and Zheng, 1998), which suggests that the lamprophyres are derived from the hydrous upper mantle. The lower-crustal xenoliths dominantly comprise amphibolite, garnet amphibolite, and eclogite which are recognised in syenite- and monzonite-porphyry at Jianchuan, Liuhe, and Dali (Cai, 1992; Deng *et al.*, 1998a, 1998b; Wang Jian *et al.*, 2003). These xenoliths demonstrate that the lower crust in eastern Tibet underwent shortening and thickening (>40 km) during the Indo-Asia collision. The primary rocks were probably basaltic in composition (Deng *et al.*, 1998a), which had been metamorphosed during the collision to garnet amphibolite and/or eclogite, which are usually considered an ideal source for adakitic melts (Defant and Drummond, 1990; Drummond *et al.*, 1996). Of course, the fact that they are hosted in alkali-rich porphyries might also imply that monzonite- and syenite-porphyries may have originated at the top of the upper mantle and were brought up during magmatic segregation, uplift and emplacement.

Based on the mineral assemblages in the xenoliths, there are two types of lower crust amphibolites, i.e., those containing, and those without, plagioclase, with the former being relatively enriched in LILE and HFSE and the latter being relatively depleted in these elements (Deng *et al.*, 1998a). On the Ba-Nb/Y diagram (Fig. 3b), the Nb/Y ratios of both amphibolites are equivalent, but the former is characterised by higher Ba, while the latter is closer to MORB. These features suggest that the lower crust in eastern Tibet is chemically heterogeneous, possibly reflecting a difference in the degree of fluid metasomatism. Plagioclase-bearing amphibolite shows a higher degree of fluid metasomatism and enrichment, whereas plagioclase-free amphibolite indicates a slightly lower degree of metasomatism and enrichment. Assuming the fluids participating in the metasomatism originated from the ancient subducted slab (Hou *et al.*, 2003c; Wang Jian *et al.*, 2003), then plagioclase-bearing amphibolites should lie vertically below plagioclase-free amphibolites. This suggestion is obviously contrary to the metamorphic facies transformation for lower-crustal rock at >400 km depth. The simultaneous occurrence of two types of xenoliths in the same porphyry swarm possibly implies that the variation in chemical composition of the lower crust is mainly lateral, i.e., the slab fluid metasomatism led to the geochemical inhomogeneity at the base of the lower crust, which is also manifested in the Sr, Nd and Pb isotopic compositions (Fig. 5a).

#### Constraint from Trace Elements

Although divergent views exist as to the genesis of alkali-rich porphyries, it has been generally accepted that alkali-rich porphyries have the following geochemical characteristics: i) alkali-rich porphyries are relatively enriched in LILE, such as K, Rb, Ba, and Sr, and relatively depleted in HFSE, such as Nb, Ta, P, and Ti, showing geochemical characteristics similar to those of the island arc-type magma source (Fig. 4a); ii) the REE pattern is LREE-enriched, and LREE and HREE exhibit strong fractionation but no pronounced negative Eu anomalies (Fig. 4b); and iii) the less evolved alkali-rich porphyries have a slightly intermediate composition but are relatively enriched in transition elements (Cr, Ni, Co) that are usually enriched in basic magmas. These characteristics have an important constraint on their genesis.

It is more reasonable to suggest that subducted slab fluid metasomatism and enrichment has occurred in the source rather than to consider that the source of the alkali-rich porphyries has had "island arc-type" geochemical characteristics. This is because: i) the fluids produced by the dehydration of a subducted slab will carry large quantities of mobile elements (e.g., LILE), metasomatising the overlying mantle wedge and making it highly enriched in LILE (Tastumi, 1996); ii) partial melting under hydrous conditions tends to cause the Nb-, Ta-, Ti-, and P-bearing mineral phases such as rutile to remain stable in the source (Tastumi, 1996) so that their melts are relatively enriched in LILE but strongly depleted in HFSE; and iii) the dehydrated subducted slab may be either an oceanic slab rich in seawater (ODP Leg 110 Scientific Party, 1987) or a

continental slab rich in formation water (Oliver, 1992; Johnston, 1999). In eastern Tibet, both slab-types appeared in different periods of time. The Jinshajiang oceanic slab was subducted westward during the Permian, forming the Jomda-Weixi volcanic arc (Mo *et al.*, 1993) and the Yangtze continental slab was subducted westward in the Cenozoic and induced the upwelling of asthenospheric material (Liu Futian *et al.*, 2000; Zhong *et al.*, 2001). The question of which type of slab caused the fluid metasomatism remains to be further constrained by isotope data.

Alkali-rich porphyries usually exhibit no pronounced negative Eu anomalies, but are relatively enriched in Sr. Conversely, this suggests that the porphyry magma is not a residual melt evolved after the segregation and crystallisation of plagioclase from mantle-derived primitive basaltic magma, i.e., the porphyry itself should represent an independent magma with an intermediate composition. However, this also indicates that the magma source contains either minimal amounts of plagioclase or no plagioclase at all. In other words, the possible source for alkali-rich porphyries is either amphibolite and/or garnet amphibolite or hydrous upper mantle.

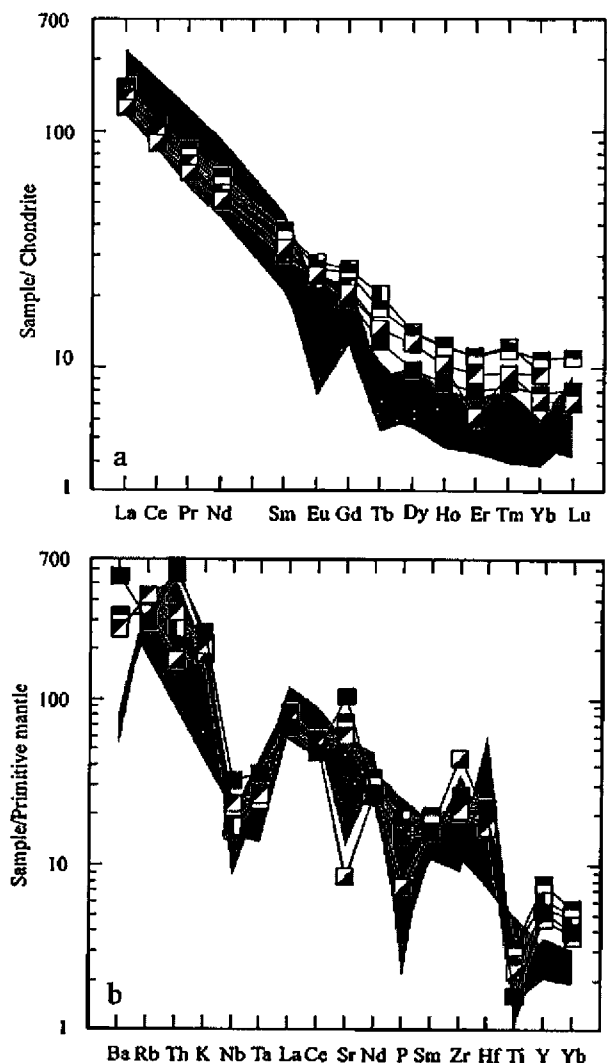


Figure 4: a) REE patterns, and b) trace element abundance patterns, for alkali-rich porphyries in east Tibet, the eastern Indo-Asian collision zone. Shadow fields are ore-bearing, others are barren alkali-rich porphyries.

The Y content of porphyries is an important criterion for determining whether a garnet mineral phase existed. The reason why adakite with low Y and an intermediate-acid composition is generally considered to have been derived from partial melting of eclogite caused by the metamorphism of basaltic rocks, is that the Y-rich garnet mineral phase is preserved in a stable form in the source during the partial melting process (Defant and Drummond, 1990). The "adakite-like" rocks represented by the Yulong ore-bearing porphyries has <20 ppm Y, suggesting that their

source should be amphibolite or garnet amphibolite. The lower-crustal xenoliths are typical representatives of such source rock. Although the LILE-enriched and HFSE-depleted characteristics of these porphyries reveal important information on metasomatism of the magma source by subducted slab fluids, the geochemical modification of the magma is little affected by the slab fluids, possibly due to the control by the enrichment process related to melts (Fig. 3b). High-Y syenite porphyry is high in Ba, Rb, and K and low in Ti and Nb. These features suggest that the

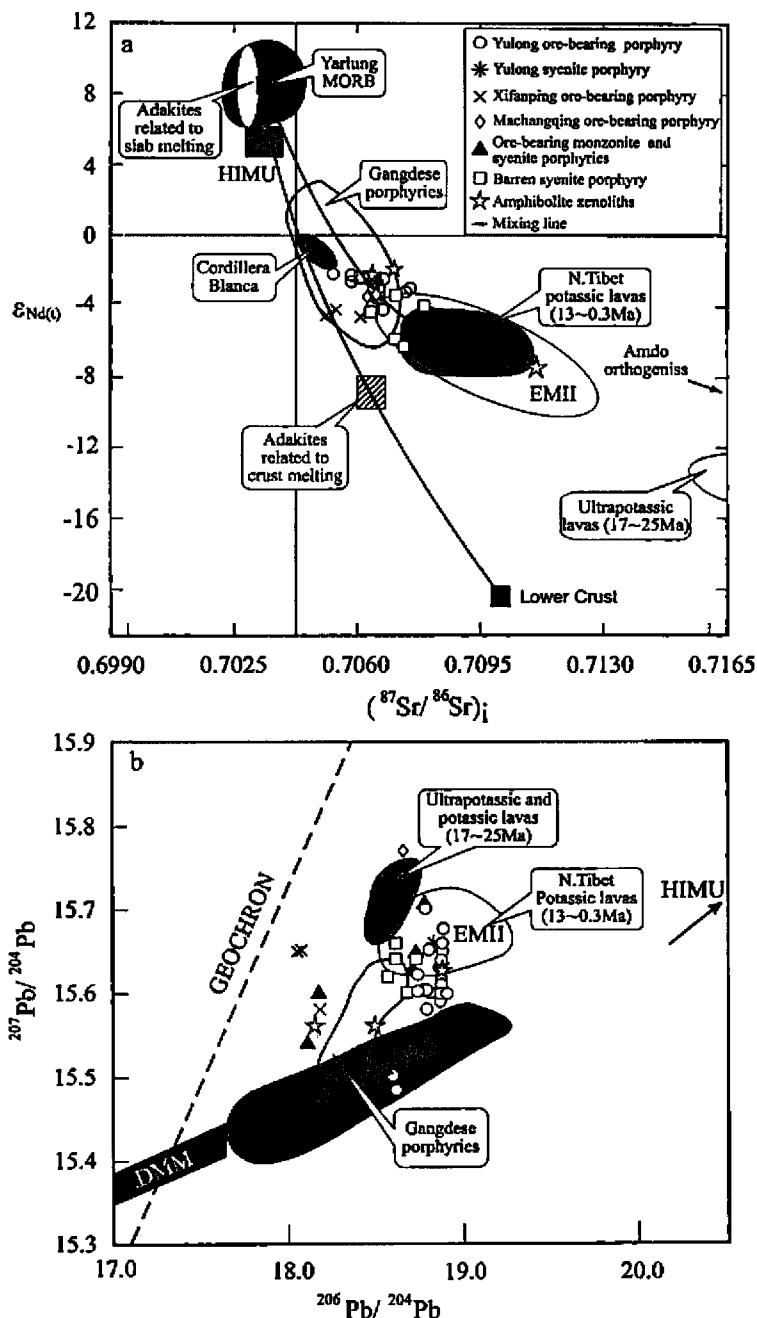


Figure 5: Sr-Nb-Pb isotopic systematics of alkali-rich porphyries in the eastern Indo-Asian collision zone.

- Nd and Sr isotopic compositions of alkali-rich porphyries and lower-crustal xenoliths. Data sources: adakite related to slab melting from Defant and Drummond (1993), Kay *et al.*, (1993), and Stern *et al.*, (1996); adakite related to crust melting from Xu *et al.*, (2001). Gangdese ore-bearing porphyries from Hou *et al.*, (2004a); potassic and ultra-potassic lavas in north Tibet from Turner *et al.*, (1993); Cordillera Blanca adakite from Petford and Atherton (1996).
- Pb isotopic composition of alkali-rich porphyries and lower-crustal xenoliths. The east and west porphyry metallogenic belts show two different variation trends. Data source: potassic and ultra-potassic lavas in north Tibet from Turner *et al.*, (1996); Gangdese ore-bearing porphyries from Hou *et al.*, (2004b).

garnet mineral phase possibly did not exist in its source, which should therefore be hydrous upper-mantle. The mantle-derived xenoliths of "phlogopite harzburgite" in lamprophyres are possibly its typical representatives of such a source. It is especially noteworthy that the positive Ba-Nb/Y correlation trend formed by these high-Y porphyries (Fig. 3b) implies that the geochemical changes to syenite-porphyry are possibly controlled by two kinds of enrichment processes: one is enrichment associated with melts (the Nb/Y ratio increase), while the other is the process of fluid metasomatism. The former process might be related to discontinuous upward infiltration of melts from the asthenosphere (McKenzie, 1989) (see the next section); whereas the latter process is related to the dehydration of the ancient subducted slab (Wang Jian *et al.*, 2003). However, it is not yet clear whether the source was metasomatised again by fluids derived from the subducted Yangtze continental slab.

#### Constraint from Sr-Nd-Pb Isotopes

The interpretation arising from studies of deep-seated xenoliths and trace element geochemistry are strongly supported by the Sr-Nd-Pb isotope systematics of the porphyries (Table 2). Fig. 5 shows that the initial Nd, Sr, and Pb isotopic compositions of both alkali-rich porphyries and potassic lamprophyres are different, not only from the isotope-depleted asthenospheric mantle (MORB) but also from the normal crust. Based on these isotopic signatures, Deng Wanming *et al.*, (1998a, 1998b) proposed that the type II enriched mantle (EM II), formed by mixing of subducted oceanic crust and upper mantle, is probably an ideal source melt for the production of alkali-rich porphyries. Wang Jian, *et al.*, (2003) suggested that a mantle wedge, subjected to metasomatism by fluids derived from the ancient Jinshajiang subduction slab, became an "island arc-type" mantle to produce the alkali-rich porphyry magma. In comparison, we consider that the crust-mantle transition zone, metasomatised by subducted slab fluids and mixed with asthenospheric material, is a likely source for alkali-rich porphyries in eastern Tibet.

This crust-mantle transition zone shows lateral and vertical inhomogeneity in trace element and isotopic geochemistry. Vertically, in the lower part of the transition zone, it comprises hydrous mantle peridotite with EM II characteristics due to strong metasomatism by subducted slab fluids. The partial melting of the lower part of the transition zone, triggered by the input of asthenospheric material, might have produced high-Y syenite magma, which fall in between EM II and MORB on the ( $^{87}\text{Sr}/^{86}\text{Sr}$ ), - Nd diagram (Fig. 5a). In the upper part of the transition zone, the basaltic lower-crust is metamorphosed to amphibolite and garnet-amphibolite as a result of crustal shortening and thickening during the Himalayan collisional orogeny. Moreover, the lower-crust in the transition zone also experienced slab-derived fluid metasomatism and the input of small volumes of asthenospheric melts. The lower-crustal samples brought up by magmas display appreciable variations in Sr, Nd, and Pb isotopic compositions, which never the less plot between EM II and MORB and coincide

with the isotopic compositions of low-Y porphyries (Fig. 5). Laterally, the crust-mantle transition zone also shows geochemical inhomogeneity, manifested most obviously by the Pb isotopic composition (Fig. 5b). The  $^{260}\text{Pb}/^{204}\text{Pb}$  ratios of ore-bearing and barren alkali-rich porphyries vary between 18.078 and 18.205 in the east belt and between 18.576 and 18.908 in the west belt. In Fig. 5b they form two separate, sub-vertical arrays, with one end approaching MORB and the other tending towards EM II. These variation features imply that the magmatic sources for the east belt had undergone much larger-scale contamination by asthenospheric material, compared with those from the west belt.

Deng Wanming *et al.*, (1998b) inferred that the source of alkali-rich porphyries in eastern Tibet formed at ~220-250 Ma, based on the lead isotope study of alkali-rich porphyries in western Yunnan. Wang Zeng *et al.*, (1995) also reached a similar conclusion for the Yulong copper-bearing porphyries, based on the estimation of the Nd model ages of 200-240 Ma. This suggests that large-scale regional fluid metasomatism in the source is possibly related to the westward subduction of the Late Palaeozoic Jinshajiang oceanic slab, which gave rise to an embryonic source for alkali-rich porphyry magmas (Fig. 6a). On the other hand, the input of asthenospheric material into the source, and its consequent contamination, are possibly related to the upwelling of the asthenosphere, triggered by the subduction of the Indian and Yangtze continents toward each other (Fig. 6b). This has been also supported by deep geophysical exploration data.

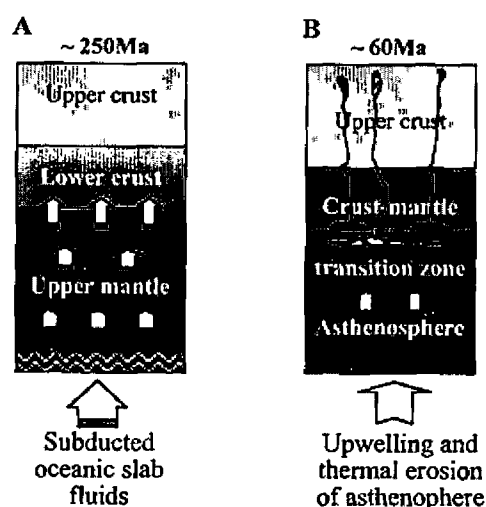


Figure 6: Diagrams illustrating the evolutionary processes of the alkali-rich porphyry source in the eastern Indo-Asian collision zone.

- Metasomatism of the lithosphere by the underlying Jinshajiang subducted oceanic slab fluids since ~250 Ma.
- A complex crust-mantle transition zone was formed by upwelling and thermal erosion of the lithosphere induced by the subduction of the Yangtze continental block and input of a small stream of melts. This zone is a possible source region of alkali-rich porphyries.

Table 2: Sr-Nd-Pb isotopic systematics of the representative porphyries from the eastern Indo-Asian collision zone.

Location	Rocks	$^{206}\text{Pb}/^{204}\text{Pb}$	$^{207}\text{Pb}/^{204}\text{Pb}$	$^{208}\text{Pb}/^{204}\text{Pb}$	$^{143}\text{Nd}/^{144}\text{Nd}$	$\epsilon\text{Nd}_t$	$^{87}\text{Sr}/^{86}\text{Sr}$	$\delta\text{Sr}$
<b>Porphyries in the West Ore Belt</b>								
Yulong <sup>b</sup>	Monzogranite porphyry	18.757	15.642	38.903	0.512427±19	-4.2	0.706765±8	32.2
		18.779	15.642	38.924	0.512525±11	-2.2	0.706576±11	29.5
		18.733	15.626	38.890				
		18.890	15.682	39.119				
		18.608	15.488	38.528				
		18.805	15.648	38.866				
Malasongduo <sup>b</sup>	Monzogranite porphyry	18.826	15.608	38.872	0.512473±9	-3.2	0.706832±10	33.1
		18.888	15.643	38.955				
		18.864	15.615	38.869				
Duoxiasongduo <sup>b</sup>	Monzogranite porphyry				0.512492±14	-2.8	0.706576±8	29.5
		18.852	15.634	38.915	0.512532±11	-2.1	0.705453±20	13.5
		18.871	15.622	38.920				
		18.867	15.586	38.799				
		18.788	15.583	38.801				
		18.869	15.627	38.911				
Zhanaga <sup>b</sup>	Monzogranite porphyry	18.867	15.661	38.963	0.512509±9	-2.5	0.705817±21	18.7
	Syenitic-granite porphyry	18.870	15.648	38.955	0.512485±8	-3.0	0.705997±9	21.2
Mangzong <sup>b</sup>	Monzogranite porphyry	18.883	15.629	38.921	0.512522±9	-2.3	0.706329±14	26.0
Mamupu <sup>b</sup>	Syenitic porphyry	18.825	15.659	38.958	0.512496±10	-2.5	0.706191±6	24.0
					0.512464±8	-3.4	0.706212±8	24.3
Beiya <sup>a</sup>	Quartz-syenitic porphyry	18.652±1	15.586±3	38.646±5	0.512380±15	-4.6	0.707455±21	0.70719
		18.791±2	15.706±4	38.992±1	0.512409±16	-4.0	0.707614±18	0.70737
		18.702±2	15.634±6	38.781±13	0.512440±8	-3.4	0.707361±30	0.70655
		18.714±1	15.649±4	38.824±14	0.512395±17	-3.3	0.708070±36	0.70752
		18.605±2	15.637±6	38.899±1	0.512296±26	-6.3	0.707968±25	0.70756
		18.583±2	15.618±3	38.787±8	0.512319±21	-5.8	0.707799±39	0.70729
Machangqing <sup>a</sup>	Syenitic porphyry	18.670	15.773	39.754	0.512460±8	-3.5	0.706499±5	29.8
					0.512464±9	-3.4	0.706871±12	35.1

Table 2: Continued from previous page.

Location	Rocks	<sup>206</sup> Pb/ <sup>204</sup> Pb	<sup>207</sup> Pb/ <sup>204</sup> Pb	<sup>208</sup> Pb/ <sup>204</sup> Pb	<sup>143</sup> Nd/ <sup>144</sup> Nd	εNd <sub>t</sub>	<sup>87</sup> Sr/ <sup>86</sup> Sr	δSr
<b>Porphyries in the East Ore Belt</b>								
Yao'an <sup>d</sup>	Syenitic granite porphyry	18.094	15.537	38.682				
		18.205	15.478	38.834				
		18.177	15.609	38.951				
		18.177	15.609	38.951				
Xifanping <sup>c</sup>	Quartz monozite porphyry	18.082	15.645	38.401	0.512409±24	-4.1	0.705703±25	
		18.078	15.644	38.467	0.512384±24	-4.5	0.705467±26	
Zhanhe <sup>a</sup>	Monozite porphyry	18.174±21	15.579±19	38.342±8	0.512376±13	-4.6	0.706488±20	26.4
<b>Barren alkali-rich rocks</b>								
Nanqen <sup>b</sup>	Trachyte	18.908±17	15.608±14	38.996±35	0.512597±11	-0.84	0.705739±	17.6
Zongguo <sup>b</sup>	Trachyte	18.861±9	15.659±11	38.965±17	0.512552±16	-1.7	0.705187±9	9.8
Midu <sup>b</sup>	Trachyte	18.730±6	15.599±5	38.776±14	0.512630±10	-0.2	0.706759±6	32.1
Xiaoguancun <sup>b</sup>	Trachyte	18.564±6	15.552±13	38.408±16	0.512403±25	-0.2	0.706759±6	32.1
Lijiang <sup>b</sup>	Pyroxene syenite	18.678	15.601	38.664	0.512517±8	-2.4	0.706519±11	30.1
					0.512463±16	-3.4	0.706244±8	26.2
Binchuan <sup>b</sup>	Pyroxene syenite	18.576	15.514	38.664	0.512544±39	-1.8	0.706360±14	27.8
Dali <sup>b</sup>	Alkali syenite				0.512536±13	-2.0	0.705677±7	18.1
					0.512487±50	-2.9	0.705488±9	15.0
<b>Lower-crust xenoliths</b>								
Liuhe <sup>a</sup>	Amphibolite	18.846 ±1	15.631±3	39.191±7	0.512240±18	-7.4	0.711559±25	68.8
		18.136±1	15.557±1	37.839±3	0.512540±13	-1.9	0.707356±25	37.8
Dayingjie <sup>a</sup>	Amphibolite	18.480±5	15.562±8	38.431±9	0.512511±6	-2.4	0.706759±25	29.4

Data source: a. Deng et al.(1998); b. Zhang et al. (1997) and Zhang et al. (2000); c. Xu et al. (1997); d. Luo et al. (1998)



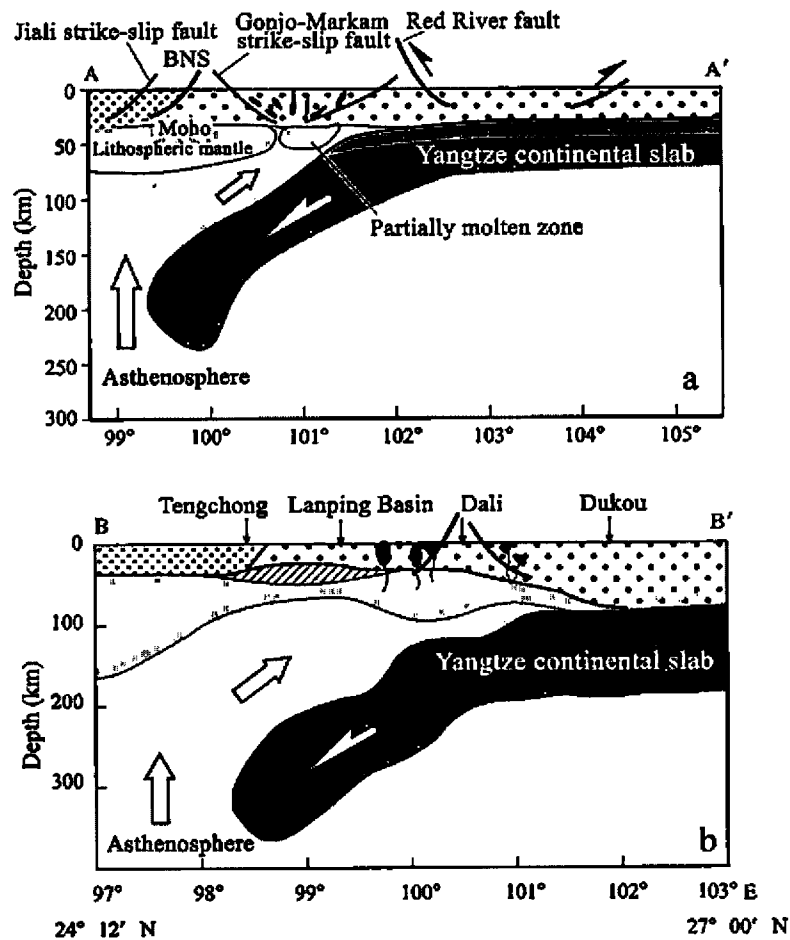
## Deep Crust-Mantle Structure and Magmatic Processes

Using deep geophysical data, Zhong *et al.*, (2001) have considered that the spatial distribution of Cenozoic magmatic rocks in eastern Tibet was constrained by mantle upwelling, whereas alkali-rich, potassic magma originated from partial melting of the crust-mantle transition zone. Here we will further discuss the relationship of formation of alkali-rich porphyry magmas with subduction of the Yangtze block and upwelling of the asthenosphere, mainly on the basis of the tomographic data.

Fig. 7 presents two composite interpretative cross-sections deduced from seismic tomographic data, combined with regional tectonics. Though the two sections have different azimuths, they transect similar tectonic units and reveal very consistent information of the deep lithospheric structure. The nearly E-W section at 23.5°N shows that the Indian and the Yangtze continental slabs are subducted toward each other (Zhong *et al.*, 2001). The Indian continental slab, which appears west of the Jiali-Gaoligong strike-slip fault (94°-97° E), is subducted at a gentle angle beneath the Tethys-Himalaya; the subducted front reaching 96°-97° E, then suddenly plunging down and extending sub-vertically to a depth of 180 km (Jiang *et al.*, 2000; Wang Chunyong *et al.*, 2002). The Yangtze continental slab

appears east of the Jiali-Gaoligong strike-slip faults (99°-102° E). This slab is subducted westward at a gentle angle along the Red River strike-slip fault, and at around 100°-E the angle of the subducted slab becomes steep and plunges down, reaching a depth of 250 km (Fig. 7a; Liu *et al.*, 2000). At the NE-directed velocity perturbation section, the image of the subducted Yangtze continental slab is still clearly visible, and the slab also steepens suddenly at 100°-99° E, with its front reaching a depth of almost 300 km (Fig. 7b; Zhong *et al.*, 2001).

The subduction of the Yangtze and Indian continental slabs toward each other, and successive oblique collision between the Indian and Asian continents since 60 Ma, may have induced the upwelling of asthenospheric material in eastern Tibet. Seismic tomographic imaging has verified that in the area (97°-99° E) between the fronts of the two subducted slabs there is an occurrence of a notably low-velocity upwelling of the asthenosphere derived from 450 km depth and its continuation took place at a depth of 200-250 km. From 200 km upward, the upwelling led to a significant thinning of the overlying continental lithosphere to 70-80 km and was underplated laterally eastward, causing a decrease in the seismic velocities of the upper mantle and lower crust (Liu *et al.*, 2000). Underneath the modern Tengchong volcanic area, the underplated basaltic magmas derived from asthenosphere thermally corroded away most of the overlying lithospheric mantle (Zhong *et al.*, 2001).



**Figure 7:** Lithospheric structure beneath the eastern margin of the Plateau inferred from the tomographic image data and surface geological structure. For the locations of sections A-A' and B-B', see Fig. 1. For the tomographic image data of section A-A', see Liu *et al.*, (2000). For the data of the velocity perturbation section (section B-B'), see Zhong *et al.*, (2001).

It seems that upwelling and underplating of hot asthenosphere provided the necessary heat energy for partial melting of the source to form the alkali-rich magmas. Furthermore, the infiltration and input of asthenospheric melts into the overlying lithosphere supplied a "brand" of MORB components at the crust-mantle transition zone and in its magmatic products.

## A Possible Tectonic Model for Porphyry Cu-Mo-Au Deposits

Two different tectonic models have been proposed for the formation of the Cenozoic igneous rocks and associated porphyry Cu-Mo-Au deposits in the Indo-Asian collision zone, based on the study of tectono-magmatic processes of the alkali-rich porphyry belt (Chung *et al.*, 1998; Zhong *et al.*, 2001; Wang J-H. *et al.*, 2001). Chung's model emphasises that the formation of the alkali-rich magmas in eastern Tibet were attributed to the convection and thinning of lithospheric mantle, triggered by the post-collisional crustal extension and partial melting of subcontinental enriched mantle in eastern Tibet (Chung *et al.*, 1998). Based on the peak age of alkali-rich magmas, Chung *et al.*, (1998) inferred that the uplift of the eastern margin of the Plateau reached a maximum height before 40 Ma. The transpressional tectonic model proposed by Zhong *et al.*, (2001) suggested that the alkali-rich magmas originated from small-scale upwellings of the asthenosphere and partial melting of the crust-mantle transition zone in an intra-continental transpressional environment. They consider that, at least before 40 Ma, the eastern margin of the Plateau was in a long-term transpressional regime, which was replaced by regional extension at ~20 Ma (J-H Wang *et al.*, 2001). Our new observations and interpretation on the regional structure and magmatism, along with the above-mentioned geophysical data, support the second model.

The key to the construction of a tectonic model for porphyry Cu-Mo-Au deposits in the Indo-Asian collision zone is to understand the origin of the ore-bearing adakite-like rocks. Several genetic models for the formation of adakite have been proposed, including, i) partial melting of subducted oceanic crust (Peacock and Rusher, 1994; Sajona *et al.*, 2000), ii) partial melting of the mafic lower-crust (Petford and Atherton, 1996; Xu *et al.*, 2002), and iii) assimilation and fractional crystallisation (AFC) of basaltic magmas (Castillo *et al.*, 1994). The ore-bearing porphyries in eastern Tibet reveal information about metasomatic fluids from the Jinshajiang subducted oceanic slab, although deep geophysical data has not detected such a subducted slab in the depth range (48-60 km) within which the porphyry magma originated. Even though the westerly-subducted Jinshajiang oceanic slab may act as a possible source for the ore-bearing porphyries in eastern Tibet, this cannot explain the genesis of the ore-bearing porphyries in the east metallogenic belt that occurs in the interior of the Yangtze block. Multiple intrusions of the ore-bearing porphyries in eastern Tibet suggest that their parent magma underwent crystallisation, differentiation and even crustal contamination; however, the small compositional variation and no pronounced Eu anomaly within the ore-bearing

porphyries indicate that the AFC process is not the leading mechanism for generation of adakitic porphyries; on the contrary, deep-seated xenolith, trace element, and isotope geochemical evidence all indicate that the ore-bearing porphyries were derived from mafic lower-crust that underwent metasomatism of the components from the subducted slab and input of asthenospheric material at depth. As a result of thickening (to >40 km) caused by the Indo-Asian continent collision after 60 Ma, the mafic lower-crust had probably been transformed into amphibolite and/or garnet-amphibolite and their partial melting may have given rise to adakitic melts.

The heat energy inducing partial melting of the mafic lower-crust was either derived from underplating of the basaltic magma at depth (Petford and Atherton, 1996), or upwelling of the hot asthenosphere generated by delamination of the lithosphere (Xu *et al.*, 2002). Upward injection of asthenospheric melts and the thermal erosion of the upwelling asthenosphere, as indicated by the tomographic imaging in eastern Tibet, might have resulted in melting of the lower crust. However, upwelling of the asthenosphere was not induced by the large-scale delamination of the lithosphere, but by the subduction of the Indian continent and Yangtze block toward each other. The top of the upwelling asthenosphere does not have an extensive "mushroom" shape, but takes the form of a zonal upright "tile sheet" (Zhong *et al.*, 2001). This spatial shape of the upwelling asthenosphere fundamentally constrains the huge belt-shaped distribution of alkali-rich porphyries and their associated volcanic lavas. Melts from the top of the asthenosphere might have occurred as small streams of magma injecting into the lower crust and mixing with the lower-crustal material. Such a process resulted in relative enrichment in Mg and the transition elements such as Cr, Ni, and Co of the ore-bearing porphyries.

The adakitic magma produced by partial melting of the lower crust that had been metasomatised by slab fluids and injected by asthenospheric material is a possible carrier of some metals (Cu, Au, Mo etc.) and sulphur for porphyry Cu-Mo-Au deposits (Hou *et al.*, 2003b). This is because: i) the adakitic magma produced by the hydrous source region exhibits the features of a "wet magma" and has strong potential for segregation and production of magmatic ore fluids; ii) the adakitic magma is relatively enriched in sulphur (Oyarzun *et al.*, 2001), with higher oxygen fugacity ( $fO_2$ ) buffered by the nickel/nickel oxide and hematite/magnetite buffers (Imai *et al.*, 1993), which would have caused an increase in the  $SO_2/H_2S$  ratio in the magmatic system, thus completely removing sulphur from the adakitic melts (Burnham, 1979); and iii) the input of asthenospheric material into the adakitic magma source also causes the melts to obtain large amounts of metals and sulphur effectively from more mafic melts (Hattori and Keith, 2001).

Based on the integration of the above analyses, we propose a tectonic model for porphyry Cu-Mo-Au deposits in collisional orogenic belts (Fig. 8). Our model emphasises that subduction of a continental slab during a collisional orogeny results in crustal shortening and thickening, and

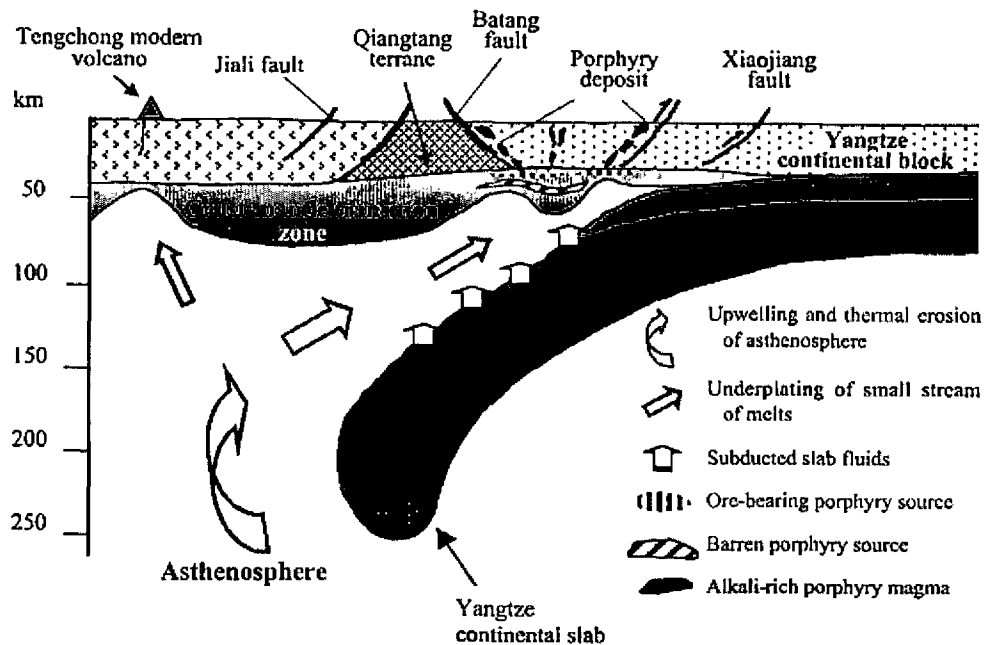


Figure 8: A possible tectonic model for porphyry Cu-Mo-Au deposits in the eastern Indo-Asian collision zone.

triggers upwelling of the asthenosphere. The crust-mantle transition zone that underwent strong metasomatism by ancient oceanic slab fluids was subjected to partial melting under the effects of the tectono-thermal erosion of the asthenosphere and input of a small stream of melts and continental crustal slab fluids. Melting of hydrous phlogopite peridotite in the lower part of the transition zone produced barren syenite-porphyry magmas, whereas melting of hydrous garnet amphibolite in the lower crust gave rise to the ore-bearing adakitic magmas. These porphyry magmas were emplaced at a shallow level along strike-slip faults at their intersections with basement faults, while the ore-bearing magmatic fluids were segregated in a local extensional and stress release regime, which finally

evolved into a porphyry magmatic-hydrothermal ore-forming system. Copper-rich fluids might have been segregated from more felsic monzogranite porphyry magmas, forming porphyry copper deposits; whereas gold (and lead-zinc) rich fluids might have been segregated from more intermediate quartz monzonite porphyry magmas, generating porphyry gold deposits.

## Acknowledgments

This study was supported by the project "Metallogeny of Collisional Orogeny in Tibet" (No. 2002CB412600) to implement the State Plan for Development of Basic Research.

## References

- Burnham, C.W., 1979 - Magma and hydrothermal fluids. *in* Barnes, H.L., (Ed.), *Geochemistry of Hydrothermal Ore Deposits*, 2<sup>nd</sup> ed.: Wiley, New York, pp. 71-136.
- Camus, F. and Dilles, J.H., 2001 - A special issue devoted to porphyry copper deposits of northern Chile. Preface: *Economic Geology*, v. 96, pp. 233-238.
- Castillo, R.P., Pringle, M.S. and Carlson, R.W., 1994 - East Mariana basin tholeiites: Cretaceous intraplate basalts or rift basalts related to the Ontong Java plume?: *Earth and Planetary Science Letter*, v. 123, pp. 139-154.
- Chung Sun-Lin, Lo Ching Hua, Tung-Yi Lee, *et al.*, 1998 - Disynchronous uplift of the Tibetan plateau starting from 40 My ago: *Nature*, v. 349, pp. 769-773.
- Defant, M.J. and Drummond, M.S. 1990 - Derivation of some modern arc magmas by melting of young subducted lithosphere: *Nature*, v. 347, pp. 662-665.
- Defant, M.J., 1993 - Mount St. Helens: potential example of partial melting of subducted lithosphere in a volcanic arc. *Geology*, v. 21, pp. 547-550.
- Deng Wanming, Huang Xuan, Zhong Dalai, 1998a - Petrological characteristics and genesis of Cenozoic alkali-rich porphyries in eastern Yunnan. *Scientia Geologica Sinica*, v. 33, pp. 412-425 (*in Chinese with English abstract*).
- Deng Wanming, 1998b - Alkali-rich porphyries in the northern segment of the Jinshajiang belt, western Yunnan, and their relations to intraplate deformation: *Science in China (Series D)*, v. 28, pp. 111-117 (*in Chinese*).
- Deng Jinfu, Zhao Hailing, Mo Xuanxue, *et al.*, 1996 - Root-Column Structure of the Continent of China - a Key to Continental Geodynamics: *Geological Publishing House*, Beijing (*in Chinese*).
- Ding Jianchao, Wang Zeng and Shentu Baoyong, 1990 - Nd-Sr isotope features of major ore-forming intrusions in the Yulong porphyry Cu (Mo) belt, eastern Tibet: *in* CGQXT Editorial Committee, Ministry of Geology and Mineral Resources (Ed.), *Contributions to the Geology of the Qinghai-Xizang (Tibet) Plateau*, No. 20: *Geological Publishing House*, Beijing, pp. 160-167 (*in Chinese with English abstract*).
- Drummond, M.J., Defant, P.K. and Kepezhinskas, 1996 -

- Petrogenesis of slab-derived trondhjemite-tonalite-dacite/adakite magmas: *Transactions of the Royal Society of Edinburgh, Earth Sciences*, v. 87, pp. 205–215.
- Du Andao, He Hongliao and Yin Wanning, 1994 - The study on the analytical methods of Re-Os age for molybdenites: *Acta Geologica Sinica*, v. 68, pp. 339–346 (in Chinese with English abstract).
- Gao Yongfeng, Hou Zengqian, Wei Ruihua, 2003 - Petrology and geochemistry of Neogene Gangdese porphyries and their geodynamic significance: *Acta Petrologica Sinica*, v. 19 (3), pp. 418–428 (in Chinese with English abstract).
- Griffiths, J.R. and Godwin, C.I., 1983 - Metallogeny and tectonics of porphyry copper-molybdenum deposits in British Columbia: *Canadian Journal of Earth Science*, v. 20, pp. 1000–1018.
- Hattori, K.H. and Keith, J.D., 2001 - Contribution of mafic melt to porphyry copper mineralization: evidence from Mount Pinatubo, Philippines, and Bingham Canyon, Utah, USA: *Mineralium Deposita*, v. 36, pp. 799–806.
- Hou, Z-Q., Qu, X-M., Wang, S-X., et al., 2003a - Re-Os ages of molybdenite in the Gangdese porphyry copper belt, Qinghai-Tibet Plateau: timing of mineralization and application of the dynamic background: *Science in China*, v. 32, pp. 509–618 (in Chinese).
- Hou, Z-Q., Mo, X-X., Gao, Y-F, Qu, X-M. and Meng, X-J., 2003b - Adakite, a possible host rock for porphyry copper deposits: A case study of porphyry copper belts in Tibetan Plateau and in northern Chile: *Mineral Deposits*, v. 22 (1), pp. 1–12 (in Chinese with English abstract).
- Hou, Z-Q., Ma, H-W., Khin Zaw and Zhang, Y-Q., 2003c - The Himalayan Yulong porphyry copper belt: product of large-scale strike-slip faulting in eastern Tibet: *Economic Geology*, v. 98, pp. 125–145.
- Hou, Z-Q., Meng, X-J., Qu, X-M., et al., 2004a - Gangdese adakitic porphyry copper belt in Tibet: *Acta Petrologica Sinica*, v. 20, pp. 239–248 (in Chinese with English abstract).
- Hou, Z-Q., Gao, Y-F., Qu, X-M., Rui, Z-Y. and Mo, X-X., 2004b - The mid-Miocene adakitic rocks generated during the east-west extension in south Tibet: *Earth and Planetary Science Letter*, v. 220, pp. 139–155.
- Imai, A., Listanco, E.L. and Fujii, T., 1993 - Petrologic and sulfur isotopic significance of highly oxidized and sulfur-rich magma of Mount Pinatubo, Philippines: *Geology*, v. 21, pp. 699–702.
- Jiang Chaosong, Wang Shaojin, Zhou Ruiqi, et al., 2000 - Dynamic study of the Tengchong volcanic active structure: *Seismological Research*, v. 23, pp. 179–187 (in Chinese with English abstract).
- Johnston, J.D., 1999 - Regional fluid flow and the genesis of Irish Carboniferous base metal deposits: *Mineralium Deposita*, v. 34, pp. 571–598.
- Kay, S.M., Ramos V.A. and Marquez M., 1993 - Evidence in Cerro Pampa volcanic rocks for slab-melting prior to ridge-trench collision in Southern South America: *Journal of Geology*, v. 101, pp. 703–714.
- Li, X-Z., Liu, W-J., Wang, Y-Z. and Zhu, Q-W., 1999 - The tectonic evolution of the Tethys and mineralisation in the Sanjiang, southwestern China: *Geological Publishing House*, Beijing, 258p. (in Chinese with English abstract).
- Lin Zhongyang, Hu Hongxiang, Zhang Wenbin, et al., 1993 - Study of the characteristics of the velocity structures of the crust and upper mantle in western Yunnan: *Acta Seismologica Sinica*, v. 15, pp. 427–440 (in Chinese).
- Liu Futian, Liu Jianhua, He Jiankun and You Q-Y, 2000 - The subducted slab of the Yangtze continental block beneath the Tethyan orogen in western Yunnan: *China Science Bulletin*, v. 45, pp. 466–469.
- Lo Yaonan, et al., 1998 - Longmanshan-Jinpingshan intracontinental orogenic belt. *Science and Technology Publishing House*, Chengdu, Sichuan, 171p. (in Chinese).
- Lu Fengxiang and Zheng Jianping, 1998 - Mantle petrology of China since the 1990s: retrospect and prospect: in Ouyang Ziyuan (Ed.), *Retrospect and Prospect of Mineralogy, Petrology and Geochemistry at the Turn of the Century*. Atomic Energy Publishing House, Beijing, pp. 118–122 (in Chinese).
- Ma, H-W., 1990 - Granitoids and mineralization of the Yulong porphyry copper belt in eastern Tibet. *China University of Geosciences Press*, Beijing, 157p. (in Chinese with English abstract).
- Miller, C., Schuster, R., Klotzli, U., Frank, W. and Purtscher, F., 1999 - Post-collisional potassic and ultrapotassic magmatism in SW Tibet: geochemical and Sr-Nd-Pb-O isotopic constraints for mantle source characteristics and petrogenesis: *Journal of Petrology*, v. 40, pp. 1399–1424.
- Mitchell, A.H.G., 1973 - Metallogenic belts and angle of dip of Benioff zones: *Nature*, v. 245, pp. 49–52.
- Mo, X-X., Lu, F-X., Shen, S-Y., Zhu, Q-W. and Hou, Z-Q., 1993 - The Tethyan volcanism and mineralization in the Sanjiang region: *Geological Publishing House*, Beijing, 250 p. (in Chinese with English abstract).
- ODP Leg 110 Scientific Party, 1987 - Expulsion of fluids from depth along a subduction zone decollement horizon: *Nature*, v. 326, pp. 785–788.
- Oliver, J., 1992 - The spots and stains of plate tectonic: *Earth Science Reviews*, v. 32, pp. 77–106.
- Oyarzun, R., Marquez, A., Lillo, J., Lopez, I. and Rivera, S., 2001 - Giant versus small porphyry copper deposits of Cenozoic age in northern Chile: adakitic versus normal calc-alkaline magmatism: *Mineralium Deposita*, v. 36, pp. 794–798.
- Peacock, S.M., Rusher, T. and Thompson, A.B., 1994 - Partial melting of subducting oceanic crust: *Earth and Planetary Science Letter*, 121: pp 224–227.
- Petford, N. and Atherton, M., 1996 - Na-rich partial melts from newly underplated basaltic crust: the Cordillera Blanca batholith, Peru: *Journal of Petrology*, v. 37, pp. 1491–1521.
- Qu Xiaoming, Hou Zengqi, Gao Yongfeng, et al., 2001 -

- Gangdese porphyry copper belt: the second "Yulong porphyry copper belt in Tibet?: *Mineral Deposits*, v. 20 (3), pp. 355–366 (in Chinese with English abstract).
- Rui, Z.-Y., Huang, C.-K., Qi, G.-M., Xu, J. and Zhang, M.-T., 1984 - The porphyry Cu (-Mo) deposits in China: *Geological Publishing House*, Beijing, 350p. (in Chinese with English abstract).
- Sajona, F.G., Maury, R.C. and Pubellier, M., 2000. Magmatic source enrichment by slab-derived melts in a young post-collision setting, central Mindanao (Philippines): *Lithos*, v. 54, pp. 173–206.
- Sillitoe, R.H., 1972 - A plate tectonic model for the origin of porphyry copper deposits: *Economic Geology*, v. 67, pp. 184–197.
- Sillitoe, R.H., Camus, F., (Eds.), 1991 - A special issue devoted to gold deposits in the Chilean Andes: *Economic Geology*, v. 86, pp. 1153–1345.
- Stern, C.R. and Kilian, R., 1996 - Role of the subducted slab, mantle wedge and continental crust in the generation of adakites from the Andean Austral Volcanic Zone: *Contributions to Mineral Petrology*, v. 123, pp. 263–281.
- Tang, R.-L. and Luo, H.-S., 1995 - The geology of Yulong porphyry copper (molybdenum) ore belt, Xizang (Tibet): *Geological Publishing House*, Beijing, 320p. (in Chinese with English abstract).
- Tapponnier, P., Lacassin, R., Leloup, P.H., et al., 1990 - The Ailao Shan/Red River metamorphic belt: Tertiary left-lateral shear between Indochina and South China: *Nature*, v. 343, pp. 431–437.
- Tatsumi, Y., 1986 - Chemical characteristics of fluid phase released from a subduction lithosphere and origin of arc magma: evidence from high-pressure experiments and natural rocks: *Journal of Volcanology and Geothermal Research*, v. 29, pp. 293–309.
- Turner, S., Hawkesworth, G., Liu, J., Rogers, N., Kelley, S. and Calsteren, P.V., 1993 - Timing of Tibetan uplift constrained by analysis of volcanic rocks: *Nature*, v. 364, pp. 50–54.
- Wang Chunyong, Lou Hai, Wu Jianping, Bai Xhiming, Huangfu Gang and Qin Jiazheng, 2002 - Seismological study on the crustal structure of the Tengchong volcano-geothermal area: *Acta Seismologica Sinica*, v. 24 (3), pp. 230–240 (in Chinese with English abstract).
- Wang, E. and Buechfiel, B.C., 1997 - Interpretation of Cenozoic tectonics in the right-lateral accommodation zone between the Ailao Shan shear zone and the eastern Himalayan syntaxis. *International Geology Review*, v. 39, pp. 191–219.
- Wang, J., Li, J.-P. and Wang, J.-H., 2003 - Shoshonitic magmatism in Dali-Jianchuan area, western Yunnan: a geochemical study of arc magmatism in a post-collisional strike-slip extensional setting: *Acta Petrologica Sinica*, v. 19 (1), pp. 61–71 (in Chinese with English abstract).
- Wang, J.-H., Yin, A., Harrison, T.M., et al., 2001 - A tectonic model for Cenozoic igneous activities in the eastern Indo-Asian collision zone: *Earth and Planetary Science Letter*, v. 88, pp. 123–133.
- Wang, Z., Shentu, B.-Y., Ding, J.-C., Yao, P., and Geng, Q.-R., 1995. Granitoid and its mineralization in the eastern Tibet, China: *Southwestern University of Communication Press*, Chengdu, 150p. (in Chinese with English abstract).
- Xu, J.F., Shinjo, R., Defant, M.J., Wang, Q. and Rapp, R.P., 2002 - Origin of Mesozoic adakitic intrusive rocks in the Ningzhen area of east China: partial melting of delaminated lower continental crust?: *Geology*, v. 30, pp. 1111–1114.
- Xu Shijing, Shen Weizhou, Wang Rucheng, Lu Jianjun, Lin Jinping, Ni Pei, Luo Yaonan and Li Lizhu, 1997 - Characteristics and origin of the Xifanping porphyry copper deposit, Yanyuan County, Sichuan Province: *Acta Mineralogica Sinica*, v. 17, pp. 56–62 (in Chinese with English abstract).
- Zhang, Y.-Q. and Xie, Y.-W., 1997 - Chronology and Nd-Sr isotopes of the Ailaoshan-Jinshajiang alkali-rich intrusions: *Science in China*, v. 27, pp. 289–293 (in Chinese).
- Zhang, Y.-Q., Xie, Y.-W. and Li, X.-H., 2000 - Isotope features of magmatic rocks of the shoshonitic series in the eastern Qinghai-Tibet Plateau: origin of the rocks and their tectonic significance: *Science in China (Series D)*, v. 30, pp. 493–498 (in Chinese).
- Zhang, Y.-Q., Xie, Y.-W., Qiu, H.-N., Li, X.-H. and Zhong, S.-L., 1998a - Petrogenesis series and the ore-bearing porphyries of the Yulong copper ore belt in eastern Tibet: *Geochimica*, v. 27, pp. 236–243 (in Chinese with English abstract).
- Zhang, Y.-Q., 1998b - Shoshonitic series: Sr, Nd, and Pb isotopic compositions of ore-bearing porphyry for the Yulong copper ore belt in eastern Tibet: *Scientia Geologica Sinica*, v. 33, pp. 359–366 (in Chinese with English abstract).
- Zhong Dalai (Ed.), 1998 - Paleotethyan Orogenic Belt in Yunnan-Western Sichuan: *Science Press, Beijing*, 232p. (in Chinese).
- Zhong, D.-L., Ding, L., Liu, F.-T., Liu, J.-H., Zhang, J.-J., Ji, J.-Q. and Chen, H., 2001 - The poly-layered architecture of lithosphere in the orogen and its constraint on Cenozoic magmatism: *Science in China*, v. 30, pp. 1–8 (in Chinese).

## **PORPHYRY COPPER DEPOSITS OF THE URUMIEH-DOKHTAR MAGMATIC ARC, IRAN**

<sup>1</sup>Alireza Zarasvandi, <sup>2</sup>Sassan Liaghat and <sup>3</sup>Marcos Zentilli

<sup>1</sup>*Department of Geology, Shahid Chamran University, Ahwaz, Iran*

<sup>2</sup>*Department of Earth Sciences, Shiraz University, Shiraz, Iran*

<sup>3</sup>*Department of Earth Sciences, Dalhousie University, Halifax, Canada*

**Abstract** - Three of the major copper provinces of the Tethyan metallogenic belt lie within Iran. Two of these, the southeastern and north western provinces, contain the major Sar-Cheshmeh (1.2 Gt @ 0.7% Cu, 0.03% Mo) and Sungun (500 Mt @ 0.75% Cu, 0.01% Mo) porphyry copper deposits respectively. The copper mineralisation of these provinces bears a direct relationship to the evolution and closure of the Neo-Tethys Ocean and the collision of the Iranian and Afro-Arabian plates. All of the significant porphyry type copper deposits in Iran are associated with granitoids of the subduction-related, Eocene to Miocene age, volcanism and plutonism in the northwest-southeast oriented Central Iranian Volcano-Plutonic Belt (better known as the Urumieh-Dokhtar Magmatic Arc). The peak of mineralisation was during the Miocene. The Urumieh-Dokhtar Magmatic Arc developed in parallel with the collisional Zagros Fold and Thrust Belt to the southwest, and the intervening Sanandaj-Sirjan Metamorphic Zone. Although many examples of porphyry copper mineralisation are known within these provinces, potential still remains for large discoveries in several prospective districts through further studies and systematic exploration.

### **Introduction**

Iran is a one of the major copper provinces in the Tethyan metallogenic belt. Ancient mine workings and records indicate that copper mining was an important industry in Iran, and that its peoples have had exploration, mining and metallurgical knowledge of this metal for a long time. Exploration has been undertaken by the Geological Survey of Iran (GSI), Yugoslavian, Australian, Canadian and French mining companies, and the National Iranian Copper Industries Company (NICICO) between 1966 and 2003. This work has identified many copper deposits and occurrences in various parts of Iran, especially along the Central Iranian Volcanic-Plutonic Belt, better known as the Urumieh-Dokhtar Magmatic Arc (hereforth referred to as the UDMA). About 250 copper deposit and occurrences associated with vein type, porphyry, skarn, skarn-porphyry, or massive sulphide genesis have been described in reports (e.g., Bazin and Hubner, 1969; Forster et al., 1972). The most important mining districts and the significant currently mined copper resources in Iran are porphyry copper style deposits located within the UDMA. Almost all known porphyry type copper deposits in Iran are associated with Cenozoic granitoids within the UDMA (e.g. Bazin and Hubner, 1969; Jankovic, 1984). The volcanism, plutonism and associated mineralisation in the UDMA are considered to be the result of subduction (e.g. Berberian and King, 1981) within the collisional Zagros belt. The main known porphyry copper deposits and porphyry occurrences of Iran are located in the north western and central-south eastern sections of the UDMA, respectively (Fig. 1).

### **Regional Geologic Setting of Iran**

The geotectonic setting of Iran with respect to the Scytho-Turanian plate in the north and the Arabian plate (Gondwana) in the south is still a matter of controversy (e.g. Soffel *et al.*, 1996). Subduction between the Iranian and Afro-Arabian plates during the Mesozoic defined three main parallel tectonic zones: i) the Zagros fold and thrust belt, ii) the Sanandaj-Sirjan metamorphic zone, and iii) the UDMA (Fig. 1). Most Iranian igneous rocks associated with copper mineralisation are in the UDMA. This magmatic belt is considered to be an integral part of the Zagros orogenic belt (e.g., Stocklin, 1968; Alavi, 1994), which is in turn part of the Alpine-Himalayan orogenic/metallogenic belt. The Zagros orogenic belt extends from the Eastern Anatolian Fault in eastern Turkey, to the Oman line in southern Iran, a distance of over 2000 km. Early studies suggested either a subduction model (e.g., Takin, 1972; Forster, 1978; Niazi and Asoudeh, 1978, Alavi, 1980; Berberian, *et al.*, 1982) or a continental rifting model (e.g., Sabzehie, 1974; Amidi, 1975) for the tectonic setting and formation of the Zagros orogenic belt. According to the subduction model, a small continental block (the Central Iranian Block, CIRB) separated from Gondwana in the early Mesozoic and formed the Iranian plate and the intervening Neo-Tethys basin, floored by oceanic crust (Alavi, 1980; Sengör, 1990). In the early Cretaceous, movement of the Iranian plate and expansion of the Neo-Tethys oceanic crust ceased and was then reversed. This resulted first, in the subduction of the Neo-Tethian oceanic lithosphere below the CIRB, and subsequently, in collision between the Afro-

Arabian and Iranian plates. In contrast, the continental rifting model assumed that magmatism in the Central Iranian block was the result of episodic opening of a continental rift zone during the Eocene. Most recent work however, fully supports the subduction model (e.g. Alavi, 1994), and also emphasises the tectonic effects of oblique subduction (Sokoutis *et al.*, 2000) in the generation of parallel strike-slip and reactivated structures in the UDMA.

## Geological Framework of the Urumieh-Dokhtar Magmatic Arc

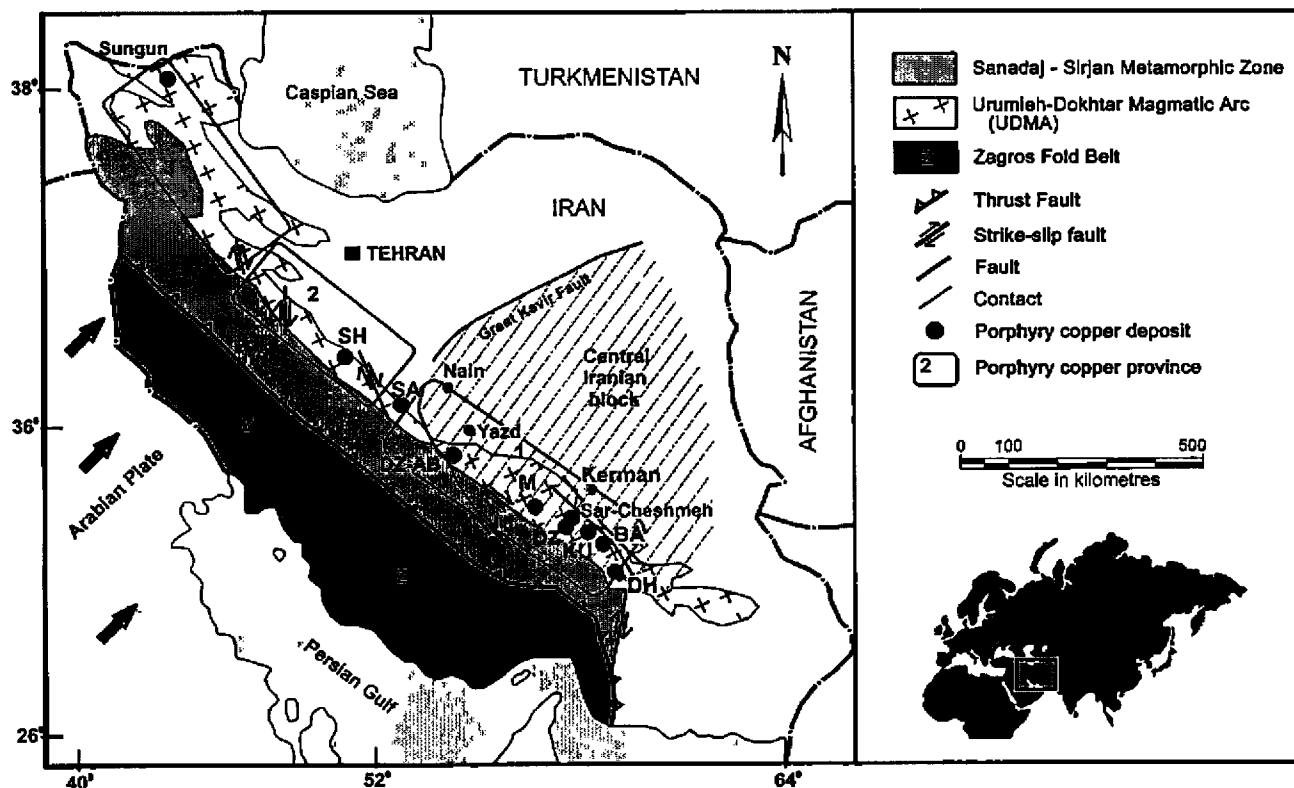
Early studies of the UDMA generally suggested that it represents an Andean type magmatic arc formed by subduction along the active continental margin of the Central Iranian Block during the Alpine orogeny (Takin, 1972; Berberian *et al.*, 1982; Sengör, 1990; Alavi, 1994). However, other workers proposed that the belt was formed by post-collision magmatism related to orogenic collapse (e.g. Stocklin, 1974; Berberian and King, 1981). Within the UDMA, Late Mesozoic and Palaeogene plutons intruded sedimentary rocks of Cretaceous age (Nabavi, 1976; Alavi, 1980). Magmatic activity peaked during the Eocene, leading to widespread extrusion of volcanic rocks consisting of trachy-basalt, andesite and dacite lavas, domes, ignimbrites and tuffs (Alavi, 1980). These rocks were in turn intruded by granitoids of Oligocene-Miocene age, which in many parts of the UDMA are spatially associated with copper mineralisation (Jankovic, 1984). Based on geochemical investigations (e.g., Forster *et al.*, 1972; Berberian *et al.*, 1982; Shahabpour, 2004) volcanic

and plutonic rocks in this belt are mainly calc-alkaline and related to subduction between the Arabian and Iranian plates. Young alkaline volcanic rocks in some parts of this belt may be the result of melting of the broken oceanic crust slab after collision and the cessation of subduction (Berberian and Berberian, 1981).

The metallogenic characteristics and copper occurrences of the UDMA have been described by many authors (e.g., Bazin and Hubner; 1969; Forster, 1972; Jankovic, 1984; Shahabpour, 1999, 2004; Yaghubpur, 2003; Richards, 2003). These studies indicate Cenozoic granitoid and volcanic bodies related to subduction played a key role in the formation of different types of copper-mineralisation in the UDMA, particularly porphyry style occurrences. Porphyry style mineralisation accompanied the final phases of arc magmatism in the Middle Miocene, following the peak of arc magmatism in the Eocene (Richards, 2003). Development and evolution of the UDMA is coeval with magmatic up-welling and crustal thickening, and in several parts of the belt, was accompanied by Miocene age reactivation of older structures and tectono-magmatic zones parallel to the Zagros orogenic belt (Zarasvandi, 2004).

## Urumieh-Dokhtar Magmatic Arc and Porphyry Copper Deposits

The UDMA is subdivided into a number of separate copper provinces by a series of structural features, including major strike-slip faults and long lived structural lineaments. Remote sensing studies (e.g., Ranjbar *et al.*, 2004;



**Figure 1:** Index map showing the geographical position and main tectonic zones of Iran. Dashed area is Central Iranian Block (CIRB). Porphyry Copper Provinces are: 1. The Ardestan-Sarcheshmeh-Kharestan region; 2 The Savch-Ardestan district; 3 The Takab-Mianeh-Qarahdagh-Sabalan region. Porphyry copper deposits are: M = Meiduk; SA = South Ardestan; SH = Sharifabad; DZ-AB = Darreh-Zerreshk and Ali-Abad; DZ = Darreh-Zar; KU = Kuh-Panj; BA = Bahr-Aseman; DH = Darreh-Hamzeh. Black arrows indicate relative plate motion from Sokoutis *et al.* (2000).

Tangestani and Moore, 2002), field mapping by the Geological Survey of Iran and NICICO, and geochemical, petrological and geochronological studies by many authors (e.g., Aftabi, 1999; Shahbpour, 2004; Zarasvandi *et al.*, 2005; Hezarkhani and Williams Jones, 1998; Calagari, 2004; Karimzadeh, 2004) indicate that most of the copper deposits (skarn, porphyry, skarn-porphyry and vein-type) in the copper provinces of the UDMA share direct, or parental genetic relationships.

The copper deposits in this belt are related to a common calc-alkaline magmatism, and are developed in a similar crustal thickness and structural regime. They also share a common, time of emplacement and the same range of mineralisation styles. These relationships may be the result of their common subduction history, including the time of collision, and the trend and angle of subduction subduction between the Arabian and Iranian plates (Berberian and King, 1981; Shahabpour, 1999; Richards, 2003; Yaghubpur, 2003; Zarasvandi *et al.*, 2005; Richards, 2003; Shahabpour, 2004).

Geological studies undertaken by numerous authors and companies between 1969 and 2003 indicate that the bulk of the exposed porphyry copper deposits are concentrated in three major copper provinces within the UDMA (Fig. 1). Erosion and good exposure of the lithostratigraphy and magmatic sequences in these provinces has assisted in the discovery of most of the porphyry copper mineralisation. Although many deposits have been outlined, there are still prospective districts that may be considered promising for further studies, systematic exploration and discoveries.

The three main porphyry copper bearing provinces within the UDMA (Fig. 1) are:

- 1) The Ardestan-Sarcheshmeh-Kharestan region in the centre and southeast, which includes the major Sar-Cheshmeh and Meiduk porphyry copper deposits. Both are currently being mined by separate companies under the supervision of NICICO. Many of the other deposits in this district, such as those at Darreh-Zerreshk, Ali-Abad, Abdar, Darreh-Zar, Saridoon and Kharestan are

either being explored or developed by Iranian and foreign companies.

- 2) The Saveh-Ardestan district in the central sections of the UDMA does not contain any known major copper deposits.
- 3) The Takab-Mianeh-Qarahdagh-Sabalan region in the northwest of Iran is the second most important copper province in the UDMA, containing both porphyry and other styles of copper deposit, including the Sungun porphyry copper orebody, the second largest in Iran. This deposit is currently being developed by a subsidiary of NICICO. No detail is available of exploration or development programs at the other porphyry copper deposits in this province, although some could be targets for future mining operations.

Most of the important porphyry copper deposits and occurrences in the major copper province of the central Iranian volcano-plutonic belt and their characteristics are listed in Table. 1. A summary of the geology of the major porphyry copper deposits in the UDMA follows.

### Sar-Cheshmeh Porphyry Copper Deposit

Sar-Cheshmeh is the largest porphyry copper deposit in Iran, and one of the largest in the world, containing 1200 Mt of sulphide ore at an average grade of 1.2 % Cu, 0.03 % Mo, 0.27g/t Au, and 3.9 g/t Ag (Ellis, 1991). The deposit is located 60 km south of the city of Rafsanjan in southwest Kerman Province, at an altitude of approximately 2500 m above sea level. It is elongate in shape, with dimensions of around 2000 m in length by 1000 m in width and trends northeast-southwest. There are two low grade porphyry copper deposits to the south and north of the Sar-Cheshmeh mine which NICICO plans to develop in the future by extending the current open pit.

Waterman and Hamilton (1975), and Shahabpour and Kramers (1987) classified Sar-Cheshmeh as a porphyry copper-molybdenum-gold deposit. Rapid erosion has exposed the magmatic sequence both at the deposit and in

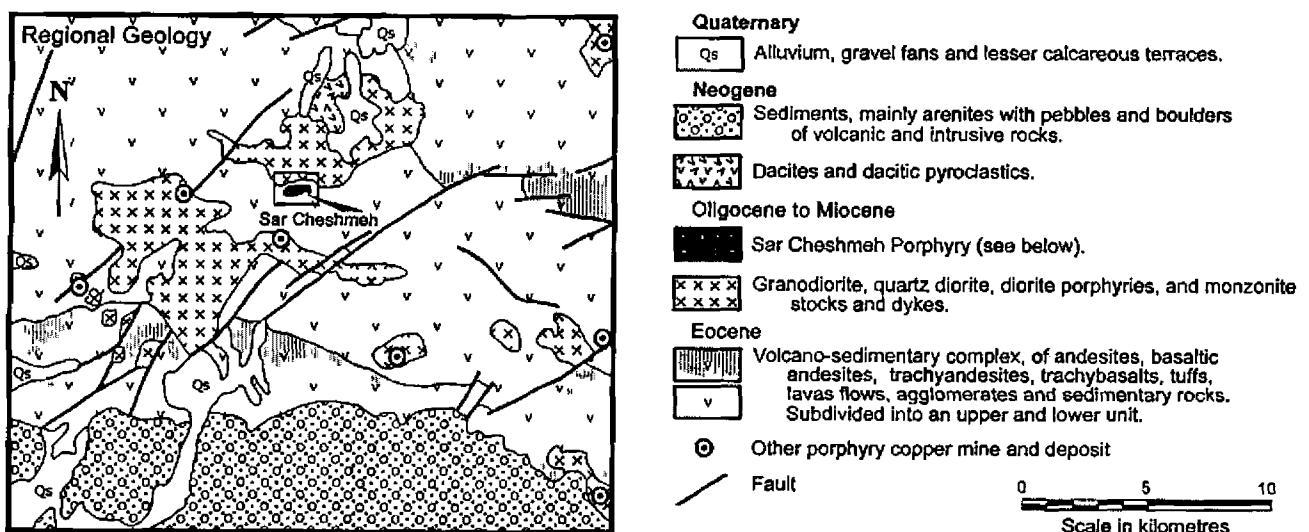


Figure 2: The regional scale geological setting of the Sar Cheshmeh porphyry copper deposit, southeastern Iran. After Honarmand *et al.*, (2002) and Ranjbar *et al.*, (2004). The rectangle surrounding the Sar Cheshmeh deposit is the area of Figs.3 and 4.

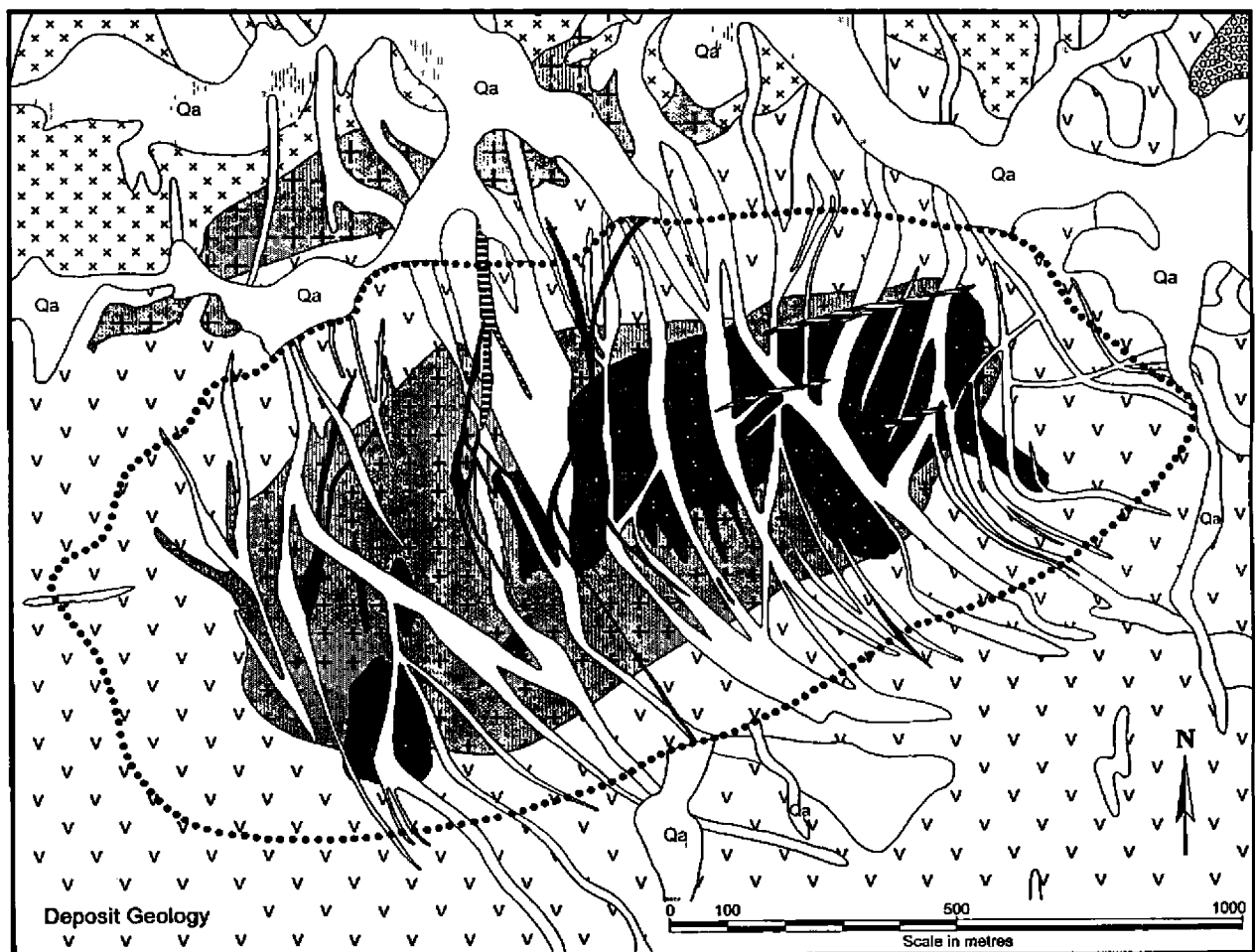


the surrounding area, where the Miocene Sar-Cheshmeh granodioritic porphyry has intruded Eocene andesites (Waterman and Hamilton, 1975; Ellis, 1991 Shahabpour and Kramers, 1987). This granodiorite stock and biotite altered andesites are the main hosts to mineralisation (Waterman and Hamilton, 1975).

Waterman and Hamilton (1975) and Shahabpour and Kramers (1987) have reported six magmatic units in the Sar-Cheshmeh deposit, namely: i) Sar-Cheshmeh granodiorite porphyry stock; ii) Late feldspar porphyry; iii) Early hornblende porphyry; iv) Late hornblende porphyry; v) feldspar porphyry dykes; and vi) Biotite porphyry dykes (Fig 2).

Intrusion of the Sar-Cheshmeh porphyry stock into the Eocene andesitic wall rock created four alteration zones associated with the deposit. These consist of a core of strong biotite alteration, grading out to weak biotite, followed by a strong phyllic zone and an outer peripheral halo of pyrophyllite.

The intense biotitisation and overprinting, abundant phyllic zone are the most important features in the alteration pattern at Sar-Cheshmeh. Different zones of mineralisation include hypogene chalcocite, molybdenite and magnetite, with minor bornite, which have been replaced in the supergene blanket by chalcocite. These sulphides occur both as disseminations and in veinlets.



#### Quaternary

Qa Alluvium (only shown outside mineralised area).

#### Neogene

Dacites, dacitic pyroclastics and arenites with pebbles and cobbles of volcanic and intrusive rocks.

#### Oligocene to Miocene

Post-mineral biotite porphyry dykes - biotite books in fine grained, generally flow banded feldspathic groundmass.

Intra-mineral feldspar porphyry dykes - large plagioclase widely dispersed in a feldspathic groundmass.

Intra-mineral hornblende porphyry dykes - large euhedral plagioclase, biotite and hornblende phenocrysts set in a dense, fine grained groundmass.

"Late"-mineral porphyry and breccia - irregular shaped masses, dykes and breccias with fragments of older rock types. Sparse plagioclase laths, thin biotite and quartz eyes in a fine grained feldspathic groundmass.

#### Oligocene to Miocene (continued)

Sar Cheshmeh Porphyry - variable in composition, but generally euhedral to subhedral plagioclase phenocrysts and a few quartz eyes, thin biotite books and minor hornblende in a medium grained aplitic groundmass of mainly quartz and K feldspar.

Quartz-eye porphyry - near contemporaneous with Sar Cheshmeh Porphyry. Intrudes granodiorite. Phenocrysts of euhedral plagioclase, K feldspar, biotite and erratic quartz-eyes in an aplitic groundmass.

xx Granodiorite - pre-mineral, near batholith sized mass, variable in composition, from extremes of gabbro to aplite.

#### Eocene

v Andesitic volcanics - mainly fine grained andesitic porphyries.

..... Outer 0.4% Cu cut-off contour.

**Figure 3: The deposit scale geological setting of the Sar Cheshmeh porphyry copper deposit, southeastern Iran.** The detail within the 0.4% Cu contour on the deposit scale plan is the interpreted geology on the 2400 m elevation level. After Waterman and Hamilton (1975) and Ghorashi-Zadch (1979).

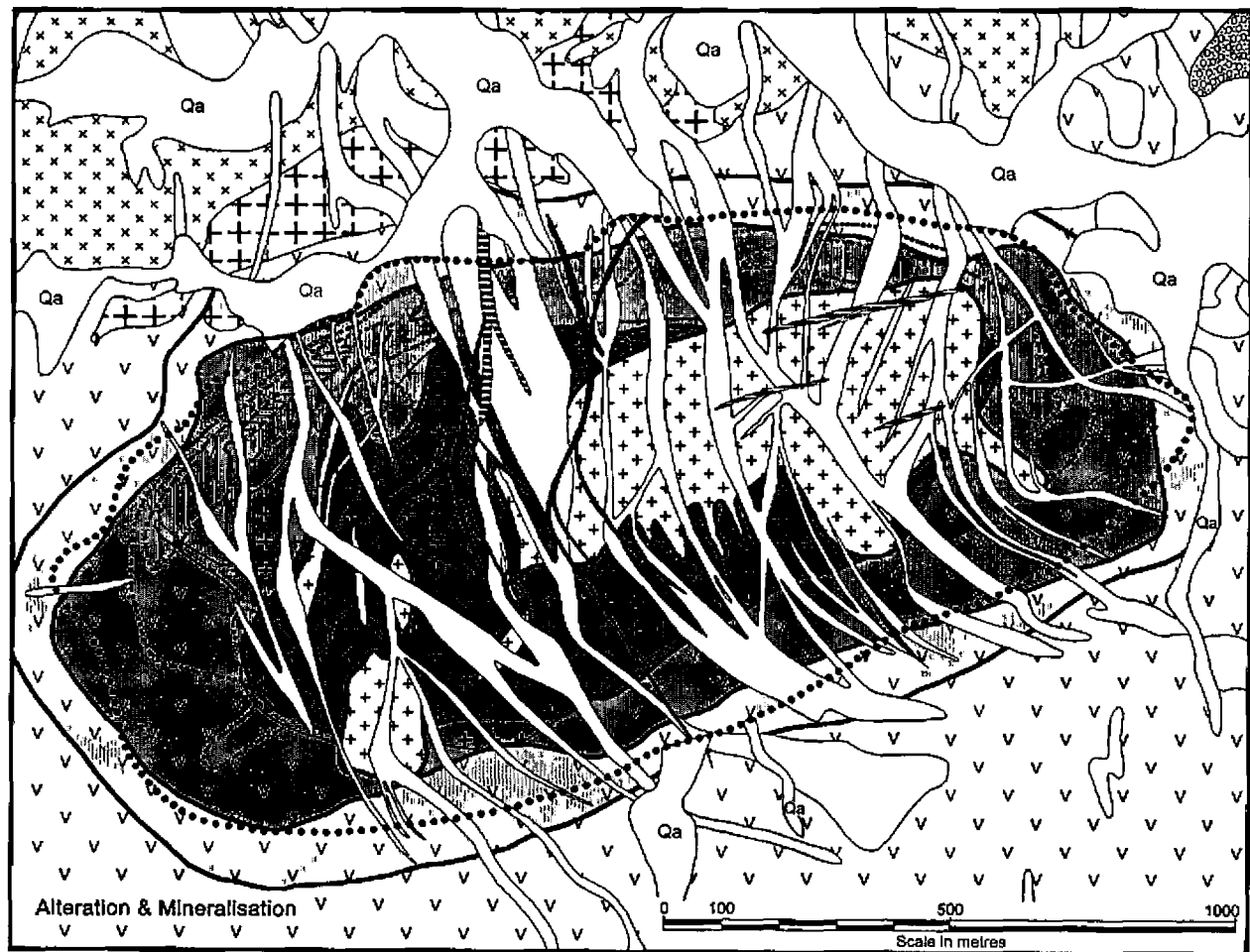
The first geochronological study of the deposit was undertaken by Shahabpour and Kramers (1987).  $^{206}\text{Pb}/^{204}\text{Pb}$  and  $^{207}\text{Pb}/^{204}\text{Pb}$  isotope ratios yielded ages of  $18.580 \pm 0.005$  and  $15.581 \pm 0.004$  Ma respectively for the Sar-Cheshmeh porphyry.

### Sungun Porphyry Copper Deposit

The Sungun porphyry copper deposit is located 75 km northwest of Ahar in Azarbaijan Province of northwestern Iran. It is currently being developed by NICICO and it will commence production in the near future. The host porphyry stocks are Oligocene-Miocene in age and were intruded into Cretaceous carbonate and Eocene volcano-sedimentary rocks (Figs. 5 and 6) (Hezarkhani and

Williams-Jones, 1998). Sungun contains more than 500 Mt of hypogene sulphide ore at 0.75 % Cu and 0.01% Mo (unpublished data, NICICO).

Bazin and Hubner (1969) classified the Sungun deposit as skarn-type mineralisation at the contact between a granodioritic stock and Cretaceous carbonate rocks. More recent studies (Etminan, 1977; Hezarkhani and Williams Jones, 1998; Calagari, 2004; Hezarkhani, 2004) have, on the basis of alteration and mineralisation patterns and magmatic petrogenesis, concluded that it is a porphyry-related copper deposit. The Sungun Oligocene-Miocene porphyries occur as stocks and dykes, and were derived from a calc-alkaline, syn-collisional magma that was generated in a continental arc (Hezarkhani and Williams



**Geological Legend - symbols as for Fig. 2, but without shading.**

— Boundary of alteration zone. Mostly gradational, except at contacts with the predominantly unaltered Intra-mineral dykes and Late-mineral porphyry and breccias.

**Alteration Zones**

- Weak to un-altered rocks with only low grade copper mineralisation in the Intra-mineral dykes and Late-mineral porphyry.
- Propylitic zone - altered andesitic volcanic rocks peripheral to the phyllic (sericitic) zone. Contains pyrite and rare chalcopyrite.
- Sericitic (phyllic) zone - strong sericitisation with abundant pyrite and minor chalcopyrite.
- Biotite zone - with decreased sericite content and a marked increase in copper grade. Nearer the andesite - Sar Cheshmeh Porphyry contact, biotite is replaced by sericite and a quartz stringer zone with good Cu & Mo mineralisation.
- K-silicate zone - erratic K-silicate alteration within the Sar Cheshmeh Porphyry, grading to sericite on the outer margin.

**Mineralisation**

Grade contours - hypogene mineralisation

- 2.0% Cu
  - 1.4% Cu
  - 1.0% Cu
  - 0.4% Cu
  - >2% Cu
  - 1.4-2% Cu
- Copper mineralisation occurs as fine (a significant percentage of <50 micron) chalcopyrite, pyrite and only minor bornite, as disseminations within the andesite and porphyry hosts. A higher percentage of fine grained sulphide accompanies low grade ore. Sulphides are finer grained in the andesites compared to the porphyry.
- Molybdenite occurs as disseminated blebs and streaks, generally following the better Cu grades.

A leached capping, which averages 26 m in thickness and generally follows the current topography overlies a supergene enriched sulphide blanket across a sharp boundary. An erratic oxide orebody overlies the sulphide zone. The supergene sulphide zone averages 37 m in thickness. It contains disseminated chalcocite overprinting chalcopyrite. Grades are controlled by the hypogene grade and structure, including dyke contacts.

**Figure 4: The distribution of alteration and mineralisation on the 2400 m elevation level at the Sar Cheshmeh porphyry copper deposit, southeastern Iran. After Waterman and Hamilton (1975), Ghorashi-Zadch (1979).**

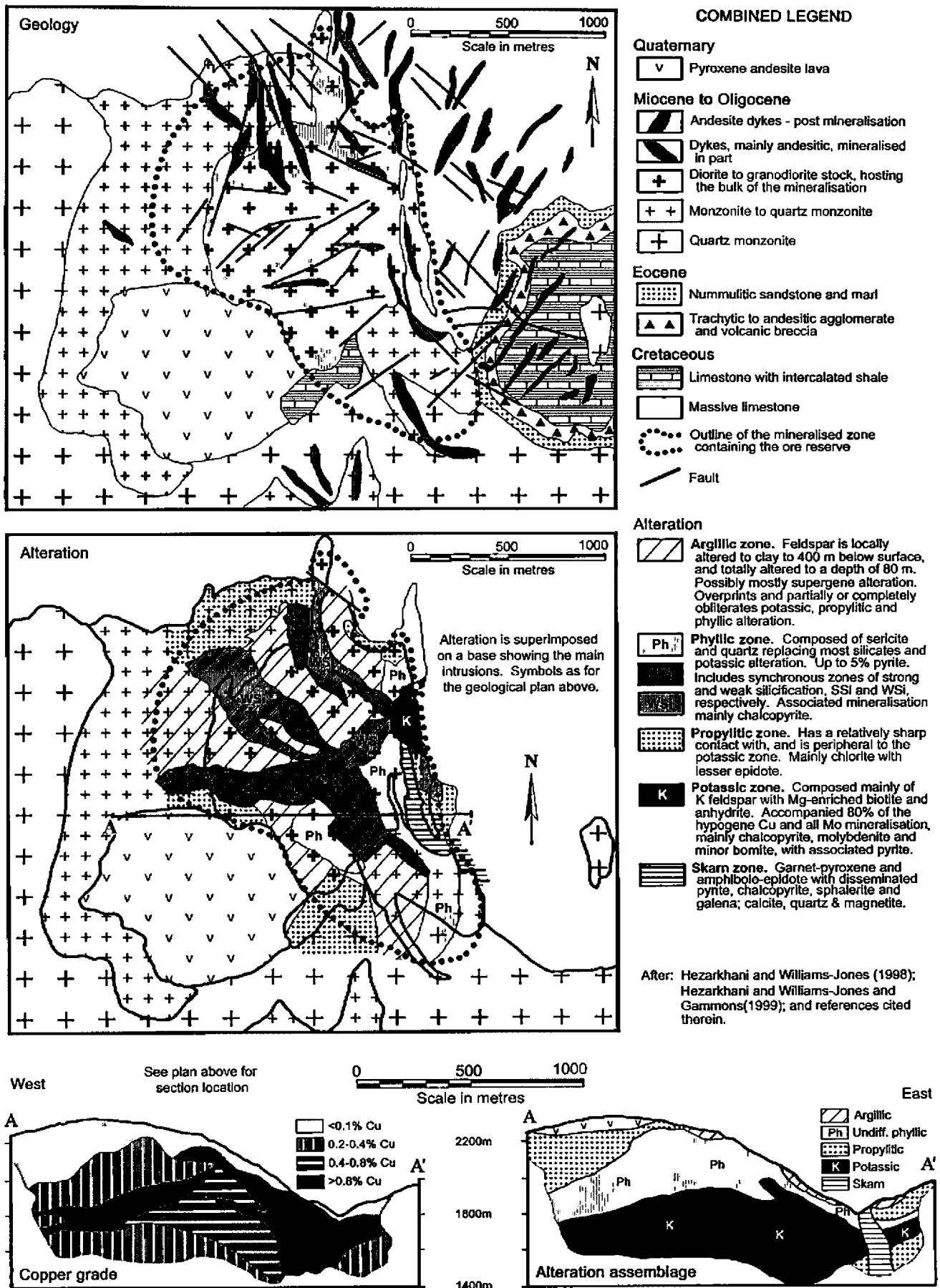


Figure 5: The geological setting and distribution of alteration and mineralisation at the Sungun porphyry copper deposit, north western Iran. After Hezarkhani and Williams-Jones (1998) and Hezarkhani et al., (1999).

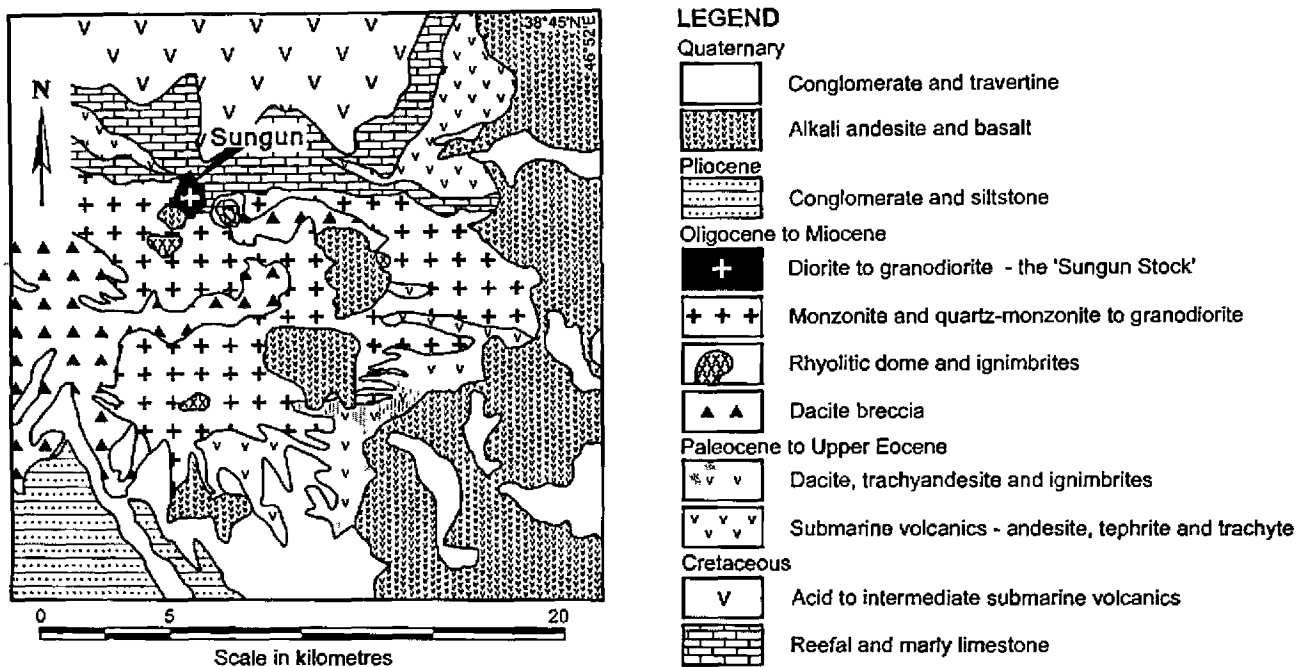


Figure 6: The district scale geological setting of the Sungun porphyry copper deposit, northwestern Iran. After Hezarkhani et al., (1999) and references quoted therein.

Jones, 1998). The rock composition ranges from early diorite/granodiorite to a later monzonite/quartz-monzonite rock. Calagari (2004) believed that porphyry stocks in the Sungun deposit can be classified in two porphyry groups: Porphyry Stock I (quartz-monzodioritic rocks) and Porphyry Stock II (quartz-monzonite to granitic rocks). These intrusions are situated in the northwestern part of the northwest-southeast trending Cenozoic UDMA.

Fig. 5 summarises the geology, alteration and distribution of mineralisation at the Sungun deposit.

Detailed stable isotope and fluid inclusion studies were provided by Hezarkhani and Williams Jones (1998) and Calagari (2003, 2004). Based on these investigations, typical alteration and mineralisation patterns of porphyry copper deposits were formed by the intrusion of Oligocene-

Miocene porphyries in the Sungun porphyry copper deposit. Calagari (2003) suggests that the isotopic data is similar to that reported at El Salvador, Chile and Ajo, Arizona, U.S.A. These stable isotope studies reveal that the alteration and mineralisation at Sungun formed under the influence of magmatic and meteoric waters similar to those reported at other porphyry copper deposits around the world (Calagari, 2004).

Fluid inclusion studies indicate that the temperature and salinity of fluids in the Sungun deposit varies from 160 to 600°C and 2 to 50 wt. % NaCl (Hezarkhani and Williams Jones, 1998; Calagari, 2004). Three types of mineralisation are recognised at Sungun, namely: i) hypogene, ii) supergene, and iii) skarn. Chalcopyrite, molybdenite and pyrite are the most important ore minerals in these zones.

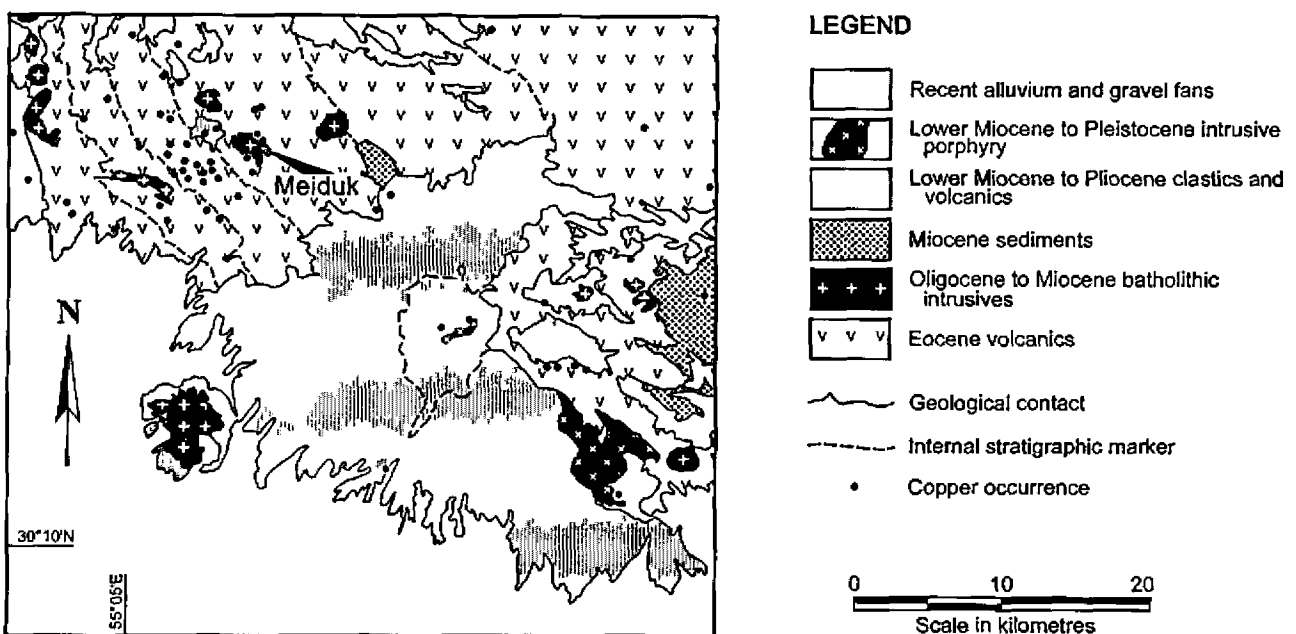


Figure 7: The district scale geological setting of the Meiduk porphyry copper deposit, southeastern Iran

Porphyry	Mineralisation	Tonnage	Grade	Wall rock	Age	Rock type	Alteration	Ore structure	Main minerals	Metallic type	Mining
Sar-Cheshmeh	2 Km <sup>2</sup>	1200 Mt	0.7% Cu 0.03% Mo	Eocene andesite	Miocene	Granodiorite	Outward from centre: potassic, phyllic, argillic, propylitic	Veinlet Disseminated	Cpy, mag, chl, bor, py, cov, cup, moly, gal, sph,	Cu+Mo+ Au+Ag	Active
Melduk	2 Km <sup>2</sup>	180 Mt	0.83% Cu	Eocene andesite alkali-basalt, pyroclastic rocks	Mid-Miocene	Diorite	Outward from centre: potassic, phyllic, argillic, propylitic	Veinlet Disseminated	Py, cpy, cov, chl, ma, azu, chr	Cu	Active
Sungun	1.5 Km <sup>2</sup>	500 Mt	0.75% Cu 0.01% Mo	Cretaceous Limestone, Eocene dacite to trachy-andesites	Upper Oligocene to Mid-Miocene	Diorite to quartz- monzonite, granodiorite	Outward from centre: potassic, phyllic, argillic, propylitic, skarn	Veinlet Disseminated skarn	Cpy, mag, moly, chl, bor, cov, gal, tet, py, sph	Cu+Mo± Au±Ag	Under development for mining
Darreh-Zar	2 Km <sup>2</sup>	80 Mt	0.64% Cu 0.004% Mo	Eocene andesite trachy-andesite	Miocene	Diorite to granodiorite	Outward from centre: potassic, phyllic, argillic, propylitic	Veinlet Disseminated	Cpy, mag, chl, bor, py, cov, cup, gal, sph	Cu+Mo	Active
Sara	1.5 Km <sup>2</sup>	Unknown	0.15% Cu	Eocene andesite alkali-basalt, pyroclastic rocks	Mid-Miocene	Diorite	Outward from centre: potassic, phyllic, argillic, propylitic	Veinlet Disseminated	Cpy, py, mal, azu	Cu+Mo	Non-active, under exploration
Kuh Panj	3 Km <sup>2</sup>	Unknown	0.3% Cu 0.001% Mo	Eocene tuffs	Oligocene- Miocene	Granodiorite to tonalite	Outward from centre: potassic, phyllic, argillic, propylitic	Veinlet Disseminated	Cpy, mag, moly, chl, cov, tet, py	Cu+Mo	Non-active
Darreh-Alu	4 Km <sup>2</sup>	Up to 25 Mt	0.4% Cu 0.003% Mo	Eocene andesite	Oligocene- Miocene	Quartz- diorite	Outward from centre: potassic, phyllic, argillic, propylitic	Veinlet Disseminated	Cpy, mag, chl, py	Cu+Mo	Non-active
Darreh-Hamzeh	0.4 Km <sup>2</sup>	Unknown	0.3%Cu	Eocene andesite, trachyte, pyroclastic rocks	Oligocene- Miocene	Diorite to granodiorite	Outward from centre: potassic, phyllic, argillic, propylitic	Veinlet Disseminated	Cpy, py	Cu+Mo+Au+Ag	Non-active
Darreh-Zerreshk	1.2 Km <sup>2</sup>	23 Mt	0.8-0.97% Cu 0.004% Mo	Cretaceous carbonates, Eocene tuffs	Miocene	Diorite to granodiorite	Outward from centre: potassic, phyllic, argillic, propylitic	Veinlet Disseminated skarn	Cpy, mag, chl, py, cov, bor	Cu+Mo+Au+Ag	Under exploration
Ali-Abad	1.6 Km <sup>2</sup>	40 Mt	0.7% Cu 0.005% Mo	Cretaceous sediments, Eocene tuffs	Oligocene- Miocene	Quartz- monzodiorite granodiorite granite	Outward from centre: potassic, phyllic, argillic, propylitic	Veinlet Disseminated	Cpy, mag, chl, py, cov, bor	Cu+Mo+Ag	Under exploration

Table 1: Summary of the geology and mineralisation of the main porphyry copper deposits in Iran.

### Meiduk Porphyry Copper Deposit

The Meiduk porphyry copper deposit is located in Kerman province, approximately 35 km north of Shahr-e-Babak and 86 km south-southwest of Sar Cheshmeh. It was discovered in 1966 by geochemical and follow-up drilling programs. The ore deposit was formed by the intrusion of a Mid-Miocene dioritic stock into Eocene andesitic and alkali-basaltic volcanics and volcano-sedimentary rocks (Bazin and Hubner, 1969; Geological Survey of Iran, 1973; Hassanzadeh, 1993). All of these lithologies have also been intruded by numerous diorite porphyry dykes (Fig. 7).

Hassanzadeh, (1993) considered that the tectonic setting and magmatic series associated with the Meiduk deposit are consistent with those of diorite related porphyry copper deposits. <sup>40</sup>Ar/<sup>39</sup>Ar geochronology of five biotite samples collected from the ore deposit indicate an age of 11.3 ± 0.5 Ma for the emplacement of the Meiduk porphyry (Hassanzadeh, 1993). Studies of Sr isotope ratios (<sup>87</sup>Sr/<sup>86</sup>Sr = 0.40455; Hassanzadeh, 1993) and the tectonic evolution of the region (e.g., Shahabpour, 2004) indicate that the deposit was formed in the transition between an island-arc and continental margin-arc setting.

Copper mineralisation is hosted by both volcanic and intrusive rocks (Fig. 8), although the bulk is within the main intrusive body (Geological Survey of Iran, 1973). The ore

grade in the hypogene zone is between 0.5 and 1% Cu and in the supergene blanket is from 1 to 3% Cu, with an average grade of 1.52% Cu (Geological Survey of Iran, 1973). The supergene zone averages over 50 m in thickness and is characterised by a mineralogy dominated by chalcocite, covellite and chalcopyrite (Geological Survey of Iran, 1973). The total combined supergene and hypogene reserve in 1973 amounted to around 20 million tonnes of ore which was mined and explored on a small scale. Subsequent detailed exploration and development programs undertaken by NICICO in the past seven years have enlarged the reserve to 180 million tonnes with an average grade of 0.83% Cu. This deposit is now the core asset of a new copper complex (the Meiduk mine and Khatoon-Abad copper plant) which commenced operations in December, 2004.

### Darreh-Zerreshk and Ali-Abad Porphyry Copper Deposits

Darreh-Zerreshk and Ali-Abad are two relatively small porphyry copper deposits located 60 km southwest of Yazd city in central Iran. Both were discovered in 1972 as the result of geophysical surveys and drilling by the French company COFIMINS. They lie within the central part of the UDMA and are located where the UDMA intersects the Central Iranian block (Fig. 1). In addition to Cu mineralisation, in historical times, several Cu-Fe skarns

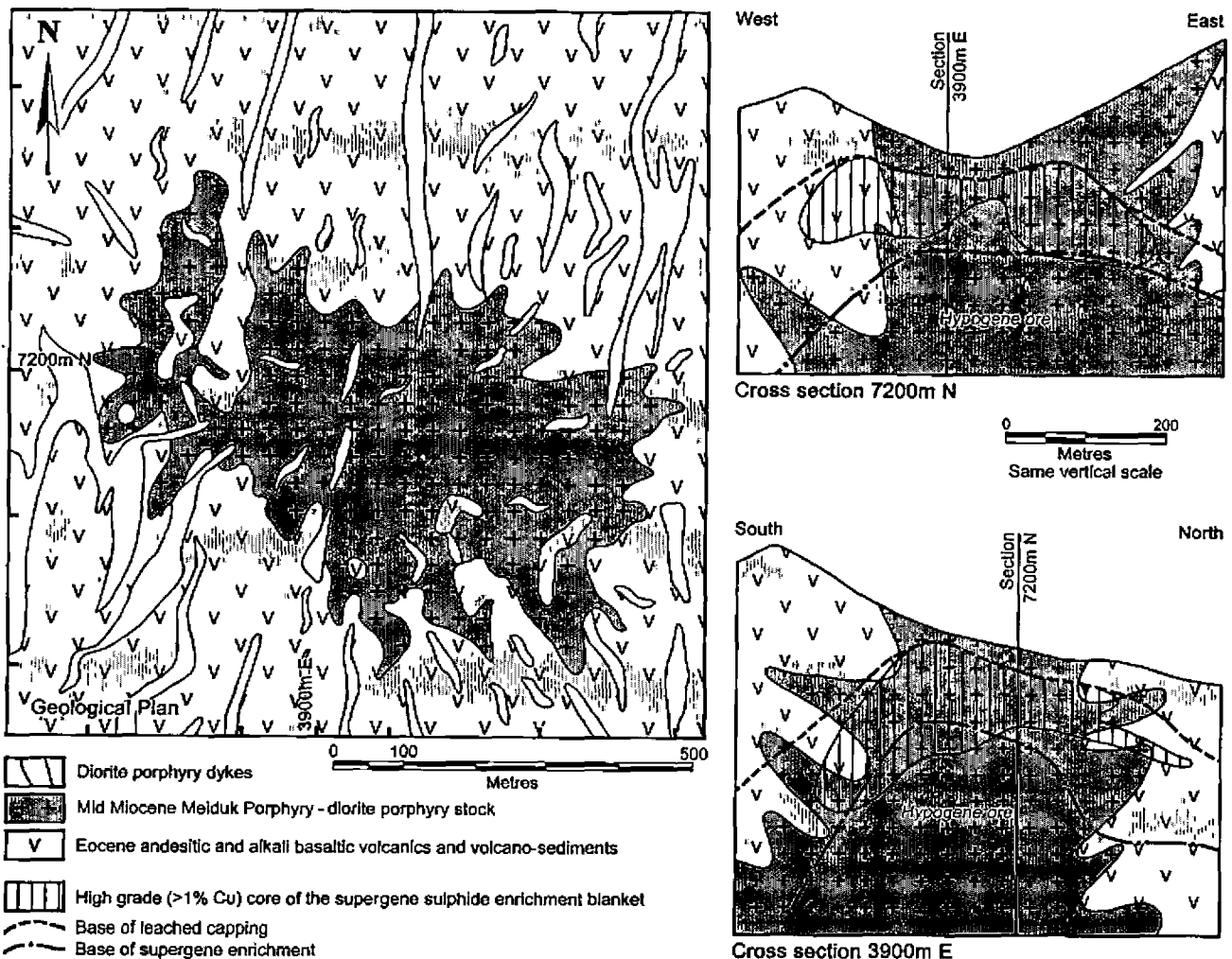


Figure 8: Geological sketch plan and generalised cross sections through the Meiduk porphyry copper deposit, southeastern Iran.

were mined on a small scale, as were minor polymetallic veins, stratabound Pb-Zn (Mississippi Valley Type) mineralisation, kaolin and travertine.

Exploration and assessment of Cu-mineralisation in this area is actively being carried out by NICICO. Drillhole data and surface outcrops were used to produce the first geological reports, which recognised these deposits as porphyry style mineralisation (COFIMINS, 1972; NICICO, 2001). Assessment drilling defined indicated resources of 40 Mt at 0.73% Cu, 0.0059% Mo and 19 g/t Ag at Ali-Abad (NICICO, 2001), and 23 Mt at 0.8 to 0.97% Cu, 0.0040% Mo and 1 g/t Ag at Darreh-Zerreshk (COFIMINS, 1972). Copper ore minerals in the Ali-Abad and Darreh-Zerreshk deposits occur in three main assemblages namely: hypogene sulphides, supergene sulphides, and copper oxides. The total resource at Darreh-Zerreshk is 8.9 Mt of oxide ore at 0.8% Cu and 14.6 Mt of sulphide at 0.95% Cu. At Ali-Abad the total resource consists of sulphide ore averaging 0.9% Cu (NICICO, 2001). The petrology, mineralogy, alteration, structural characteristics, geochronology and geological evolution of the Darreh-Zerreshk and the Ali-Abad copper deposits was discussed by Zarasvandi *et al.*, (2003, 2005). Zarasvandi *et al.*, (2005) concluded from the studies reported that the Cu-Mo mineralisation at both Darreh-Zerreshk and Ali-Abad qualifies the two mineralised systems as probable porphyry Cu (Mo) deposits. Intrusions in the area, a result of subduction related magmatism, range in composition from quartz monzo-diorite to granite, although the porphyry style copper-molybdenum mineralisation is restricted to the quartz monzo-dioritic to granodioritic plutons. These Miocene (16 Ma; Zarasvandi, 2004) mineralising intrusions cut Cretaceous sedimentary and Eocene volcano-sedimentary rocks.

## Conclusions

Most of the porphyry copper style mineralisation in Iran has been identified within the Central Iranian Volcano-Plutonic Belt or Urumieh-Dokhtar Magmatic Arc (UDMA), which is part of the Tethyan-Eurasian metallogenic belt. The southeast, central and northwest segments of the UDMA are remarkably rich in Cu mineralisation which is associated with granitoid igneous activity. This activity is believed to be the result of steep northeastward subduction of Tethyan oceanic lithosphere, followed by the collision of the Afro-Arabian and Iranian (Eurasian) plates. The most important porphyry copper deposits are in the southeast of Iran (e.g. Sar-Cheshmeh, Meiduk and several clustered deposits; Waterman and Hamilton, 1975; Shahabpour, 2004) and the northwest of the country (e.g. the Sungun deposit; Jankovic, 1984), while several smaller deposits are found in the intervening central sections of the porphyry belt (e.g., Darreh-Zerreshk and Ali-Abad; Zarasvandi *et al.*, 2004). The peak granitoid magmatism responsible for porphyry copper mineralisation in Iran occurred during the Miocene, although granitoid rocks in the area span a range from Oligocene to Miocene. While many different studies have been carried out on the porphyry copper provinces of the UDMA, the geology of these regions is not well known. However, the current understanding of the tectono-

magmatic framework of this magmatic arc indicates potential for further porphyry copper discoveries.

## Acknowledgments

The first author thanks all the Iranian authors and National Iranian Copper Industries Company for permission to publish the data. Andrea Mosher helped edit the manuscript.

## References

- Alavi, M., 1994 - Tectonics of the Zagros Orogenic Belt of Iran: new data and interpretations; *Tectonophysics*, v. 229, pp. 211-238.
- Alavi, M., 1980 - Tectonostratigraphic evolution of the Zagros of Iran; *Geology*, v. 8, pp. 144-149.
- Aftabi, A., 1999 - Geochemical aspects of sheared zones as an indication of porphyry Cu-Mo-Au-Ag mineralization at Derehamzeh, Kerman, Iran; *Exploration and Mining Geology*, v. 6, pp. 261-267.
- Amidi, S.M., 1975 - Contribution al etude biostratigraphique, petrologique et petrographique des roches magmatiques de la region Natanz-Nain-Surk (Iran Central); PhD thesis, *University of Grenoble, France*, 250p.
- Bazin, D. H. and Hubner, H., 1969 - Copper deposits in Iran; Ministry of Economy, *Geological Survey of Iran*, Report No. 13, 232p.
- Berberian, F. and Berberian, M., 1981 - Tectono-plutonic episodes in Iran; in Gupta, H.K. and Delany, F.M., (Eds.), *Zagros Hindukush, Himalaya Geodynamic Evolution*; *American Geophysical Union*, Washington, DC, pp. 5-32.
- Berberian, M. and King G.C.P., 1981 - Towards a paleogeography and tectonic evolution of Iran; *Canadian Journal of Earth Sciences*, v. 18, pp. 210-265.
- Berberian, F., Muir, I.D., Pankhurst, R.J. and Berberian, M., 1982 - Late Cretaceous and Early Miocene Andean-type plutonic activity in northern Makran and central Iran; *Journal of the Geological Society of London*, v. 139, pp. 605-614.
- Calagari, A.S., 2003 - Stable isotope (S, O, H and C) studies of the phyllic and potassic-phyllic alteration zones of the porphyry copper deposit at Sungun, East Azarbaijan, Iran; *Journal of Asian Earth Sciences*, v. 21, pp. 267-280.
- Calagari, A.S., 2004 - Fluid inclusion studies in quartz veinlets in the porphyry copper deposit at Sungun, East-Azarbaijan, Iran; *Journal of Asian Earth Sciences*, v. 23, pp. 179-189.
- COFIMINS. Co, 1972 - Geology and feasibility study of the Darreh-Zerreshk and the Ali-Abad deposits; Unpublished report, Library NICICO, Tehran, Iran.
- Ellis, R., 1991 - Sar-Cheshmeh: Mining Magazine, October, pp. 192-196.
- Etninan, H., 1977 - The discovery of porphyry copper-molybdenum mineralization adjacent to Sungun village in the northwest of Ahar and a proposed program for its detailed exploration; Confidential

- Geological Report, *Geological Survey of Iran*, p. 26.
- Forster, H., 1978 - Mesozoic-Cenozoic metallogenesis in Iran; *Journal of the Geological Society*, v. 135, pp. 443-455.
- Forster, H., Fesefeldt, K. and Kursten, M., 1972 - Magmatic and orogenic evolution of the central Iranian volcanic belt; *24<sup>th</sup> International Geology Congress*, Section 2, pp. 198-210.
- Geological Survey of Iran, 1973 - Exploration for ore deposits in Kerman Region; Report no. Yu/53.
- Ghorashi-Zadeh, M., 1979 - Development of hypogene and supergene alteration and copper mineralisation patterns, Sar Cheshmeh porphyry copper deposit, Iran; Unpublished M.Sc. Thesis, *Brock University*, 223p.
- Hassanzadeh, J., 1993 - Metallogenic and tectonomagmatic events in the SE sector of the Cenozoic active continental margin of Iran (Shahre Babak area, Kerman Province); Unpublished PhD thesis, *University of California*, Los Angeles, 204p.
- Hezarkhani, A. and Williams-Jones, J.A., 1998 - Controls of alteration and mineralization in the Sungun porphyry copper deposits, Iran: evidence from fluid inclusions and stable isotopes; *Economic Geology*, v. 93, pp. 651-670.
- Hezarkhani, A., Williams-Jones, A.E. and Gammons, C.H., 1999 - Factors controlling copper solubility and chalcopyrite deposition in the Sungun porphyry copper deposit, Iran; *Mineralium Deposita*, v. 34, pp. 770-783.
- Hezarkhani, A., 2004 - Mass changes during hydrothermal alteration/mineralization in a porphyry copper deposit, eastern Sungun, northwestern Iran; *Journal of Asian Earth Sciences (in Press)*.
- Honarmand, M., Ranjbar, H. and Meozifar, Z., 2002 - Integration and Analysis of Airborne Geophysics and Remote Sensing Data of Sar Cheshmeh Area, Using Directed Principal Component Analysis; *Exploration and Mining Geology*, v.11, pp. 43-48.
- Jankovic, S., 1984 - Metallogeny of the Alpine granitoids in the Tethyan-Eurasian Metallogenic Belt: Proceeding of the 27<sup>th</sup> International Geological Congress, Moscow, August 4-14. v. 12, *VNU Science Press*, the Netherlands, pp. 247-273.
- Karimzadeh, S.A., 2004 - Garnet composition as an indicator of Cu mineralization: evidence from skarn deposits of NW Iran; *Journal of Geochemical Exploration*, v. 81, pp. 47-57.
- Niazi, M. and Asoudeh, I., 1978 - The depth of seismicity in the Kermanshah region of Zagros Mountains (Iran); *Earth and Planetary Science Letters*, v. 40, pp. 270-274.
- Nabavi, M.H., 1976 - An Introduction to the geology of Iran; *Geological Survey of Iran*, 110p. (in Persian).
- NICICO., 2001 - Geology of Ali-Abad area; Unpublished company reports, Library NICICO, Tehran, Iran, (in Persian).
- Ranjbar, H., Shahriaria, H. and Honarmandb, M., 2004 - Integration of Aster and Airborne Geophysical Data for exploration of Copper Mineralization. A Case Study of Sar cheshmeh Area; *Proceedings Volume, Geo-Imagery Bridging Continents, XXth ISPRS Congress*, 12-23 July 2004 Istanbul, Turkey, pp. 701-706.
- Ranjbar, H., Honarmand, M. and Moezifar, Z., 2004 - Application of the Crosta technique for porphyry copper alteration mapping, using <sup>+</sup>ETM' data in the southern part of the Iranian volcanic sedimentary belt; *Journal of Asian Earth Sciences*, v. 24, pp. 237-243.
- Richards, J.P., 2003 - Metallogeny of the Neo-Tethys Arc in central Iran; in Eliopoulos et al., (Eds.), *Mineral Exploration and Sustainable Development*, Millpress, Rotterdam, pp. 1237-1239.
- Sabzehei, M., 1974 - Les mélanges ophiolitique de la region de Sphandagheh (Iran Meridional). Etude petrolique et structurale, interpretation dans le carde Iranian: PhD thesis, *University of Grenoble*, France, 205p.
- Sengör, A.M.C., 1990 - A new model for the Late Paleozoic-Mesozoic tectonic evolution of Iran and implication for Oman Region; *Geological Society of London*, Special Publication 49, pp. 797-831.
- Shahabpour, J., 1999 - The role of deep structures in the distribution of some major ore deposits in Iran, NE of Zagros Thrust Zone; *Journal of Geodynamics*, v. 28, pp. 237-250.
- Shahabpour, J., 2004 - Tectonic evolution of the orogenic belt in the region located between Kerman and Neyriz; *Journal of Asian Earth Sciences*, v. 24, pp. 405-417.
- Shahabpour, J. and Kramers, J.D., 1987 - Lead isotop data from the Sar-Cheshmeh porphyry copper deposit, Kerman, Iran; *Mineralium Deposita*, v. 22, pp. 278-281.
- Soffel, H.C., Davoudzadeh, M., Rolf, C. and Schmidt, S., 1996 - New palcomagnetic data from Central Iran and a Triassic palaeoreconstruction; *Geol. Rundsch*, v. 85, pp. 293-302.
- Sokoutis, D., Bonini, M., Medvedev, S., Boccaletti, M., Talbot, C.J. and Koyi, H., 2000 - Indentation of a continent with a built-in thickness change: experiment and nature; *Tectonophysics*, v. 320, pp. 243-270.
- Stocklin, J., 1968 - Structural history and tectonics of Iran: a review; *American Association of Petroleum Geologists (AAPG) Bulletin*, v. 52, pp 1229-1258.
- Stocklin, J., 1974 - Possible ancient continental margins in Iran; in Burke, C.A. and Drake C.A., (Eds.), *The Geology of Continental Margins*, Springer, New York, pp. 837-887.
- Takin, M., 1972 - Iranian geology and continental drift in the Middle East; *Nature*, v. 235, pp. 147-150.
- Tangestani, H.M. and Moore, F., 2002 - The use of Dempster-Shafer model and GIS in integration of geoscientific data for porphyry copper potential mapping, north of Shahr-e-Babak, Iran; *International Journal of Applied Earth Observation and Geoinformation*, v. 4, pp. 65-74.
- Waterman, G.C. and Hamilton, R.L., 1975 -The Sar-



Cheshmeh porphyry copper deposit; *Economic Geology*, v. 70, pp 568-576.

Yaghubpur, A., 2003 - Mineral deposits in metallogenic belt east of Zagros Thrust fault; in Eliopoulos *et al.*, (Eds.), *Mineral Exploration and Sustainable Development*, Millpress, Rotterdam.

Zarasvandi, A., 2004 - Magmatic and structural controls on localization of the Darreh-Zerreshk and Ali-Abad porphyry copper deposits, Yazd Province, Central Iran, PhD thesis, *Shiraz University*, Shiraz, Iran, 280p.

Zarasvandi, A. and Liaghat, S., 2003 - The role of strike-slip faults in emplacement of Darreh-Zerreshk and Ali-Abad porphyry copper deposits, SW of Yazd (In Persian with English abstract)., 7<sup>th</sup> Geological Society of Iran, Esfahan, Iran, p. 102-112.

Zarasvandi, A., Liaghat, S. and Zentilli, M., 2005 - Geology of the Darreh-Zerreshk and Ali-Abad porphyry copper deposit, central Iran, *International Geology Reviews*, v. 47 (6), pp. 620-646.

## THE MAJDANPEK PORPHYRY Cu-Au DEPOSIT OF EASTERN SERBIA A REVIEW

<sup>1</sup>Robin Armstrong, <sup>2</sup>Dejan Kozelj and <sup>1</sup>Richard Herrington

<sup>1</sup> *The Natural History Museum, London, UK.*

<sup>2</sup> *Formerly RTB Bor, Bor, Serbia.*

**Abstract** - The approximately 1000 Mt @ 0.6% Cu, 0.3-0.4 g/t Au Majdanpek porphyry copper is the most northerly deposit within the Timok Magmatic Complex (TMC) which also hosts the exploited Bor and producing Veliki Krivelj deposits. Slightly older, but similar magmatic rocks southeast of the region host the significant porphyry-high sulphidation mineralisation at Elatsite and Chelopech in neighbouring Bulgaria. Similar porphyry deposits are also known in Romania, across the Danube river to the north of Majdanpek. The TMC igneous rocks show clear evidence of crustal contamination and thus likely relate to an eastward dipping subduction zone beneath a continental margin located to the west. Mineralisation is related to sparse and narrow north-south trending andesitic dykes dated at 83 Ma. These dykes intrude along a north-south trending fracture zone cutting Proterozoic and Palaeozoic metamorphic rocks, and Jurassic limestones. Extrusive facies of the TMC are rare at Majdanpek, although they are common farther to the south of the region. Mineralisation is typically developed as stockworks, the bulk of which are actually within the metamorphic aureole of the andesitic dykes. There are also numerous skarns and replacement bodies flanking the intrusives, while more distal replacement bodies are found in the Jurassic limestones. The highest copper grades relate to K-silicate alteration and zones of strong silicification. Mo grades are very low throughout the deposit, while the Cu%:Au g/t ratio is approximately 2:1. PGEs occur as minor phases accompanying the copper mineralisation and are recovered at the smelter. Significant supergene upgrading is recorded in an oxidation blanket that was 25 m thick in the north and covered the deposit.

### Introduction

The giant Majdanpek porphyry copper deposit, which had an estimated total pre-mining resource of ca. 1000 million tonnes (Mt) @ 0.6% Cu, 0.3-0.4g/t Au, is located in the Timok Mountains of eastern Serbia, approximately 120 km SE of the capital, Beograd (Belgrade). The deposit shares its name with the town that is situated close to the eastern side of the main open pit (Plate 1). Majdanpek is served by a good transport infrastructure with road links to the Danube and to the Bor mining centre to the south. A railway line was used to transport ore and concentrate to the Bor metallurgical plant. The mine site is currently under licence to RTB Bor, the Serbian State owned mining company. Porphyry copper style mineralisation was first discovered at Majdanpek in 1961, with production commencing in 1962.

Modern mining started prior to 1962 with the exploitation of massive pyrite-limonite bodies within Jurassic limestone marginal to the porphyry system, although archaeological evidence indicates that mining activity has taken place in the local region for approximately 3000 years (Jankovic, 1990). The limestone hosted massive pyrite-limonite mineralisation originally contained 3 to 15 g/t Au in a total resource of approximately 15 Mt of ore. Production at Majdanpek reached its peak in the period 1962-1990 when 12 to 14 Mt of ore were mined per annum from two open pits, North and South Revir. The initial porphyry operation in the 1960s commenced with grades of 0.82% Cu and close to 0.8 g/t Au. Historic production has amounted to

1.55 Mt of Cu and 100 t of Au from approximately 500 Mt of ore with an average recovered grade of 0.31% Cu, 0.2 g/t Au. After 1999, Majdanpek has encountered a number of production problems as a result of the NATO bombing, diminishing grade and geotechnical problems. Current feasibility studies indicate a remaining resource of 108 Mt @ 0.424 wt% Cu, 0.273 g/t Au and 1.49 g/t Ag in the South Revir (open pit), which is currently not in production. Sporadic operations have continued up to the present from North Revir.

### Setting and Geology of the Timok Magmatic Complex

Majdanpek is the most northerly of the porphyry copper deposits associated with the Timok Magmatic Complex (TMC). The TMC is part of the greater geological framework that comprises the Alpine-Balkan-Carpathian-Dinaride metallogenic-geodynamic province (Heinrich and Neubauer, 2002), also elsewhere referred to as the Carpatho-Balkan Magmatic Belt (see Herrington *et al.*, 2003 and references therein).

The Alpine-Balkan-Carpathian-Dinaride (ABCD) Province (Fig. 1) is in turn, part of the Alpine-Himalayan (or Tethyan) orogenic system that extends from western Europe to southeast Asia and resulted from the convergence and collision of the Indian, Arabian and African plates with Eurasia. This on-going collision was for the greater part initiated during the Cretaceous. The complex geometry of the collision interface and the presence of several micro-

plates within the orogenic collage resulted in a variety of collision products, notably some segments characterised by extensive regional metamorphism and others by calc-alkaline igneous activity (Heinrich and Neubauer, 2002). This segmentation has resulted in discontinuous distribution of mineral deposits within the ABCD province (Mitchell, 1996 and Jankovic, 1997) and the limited lateral extent of the various metallogenic belts along the trace of the orogen.

While magmatic activity is evident within the ABCD from the Cretaceous to the present, two overlapping, arcuate segments have been delineated representing the bulk of the magmatism, one to the south in which the majority of the intrusion and volcanism is Late Cretaceous and a second to the north, where Late Miocene activity predominates (Fig. 1). These and adjacent segments of the ABCD host a series of significant porphyry Cu-Au deposits and related

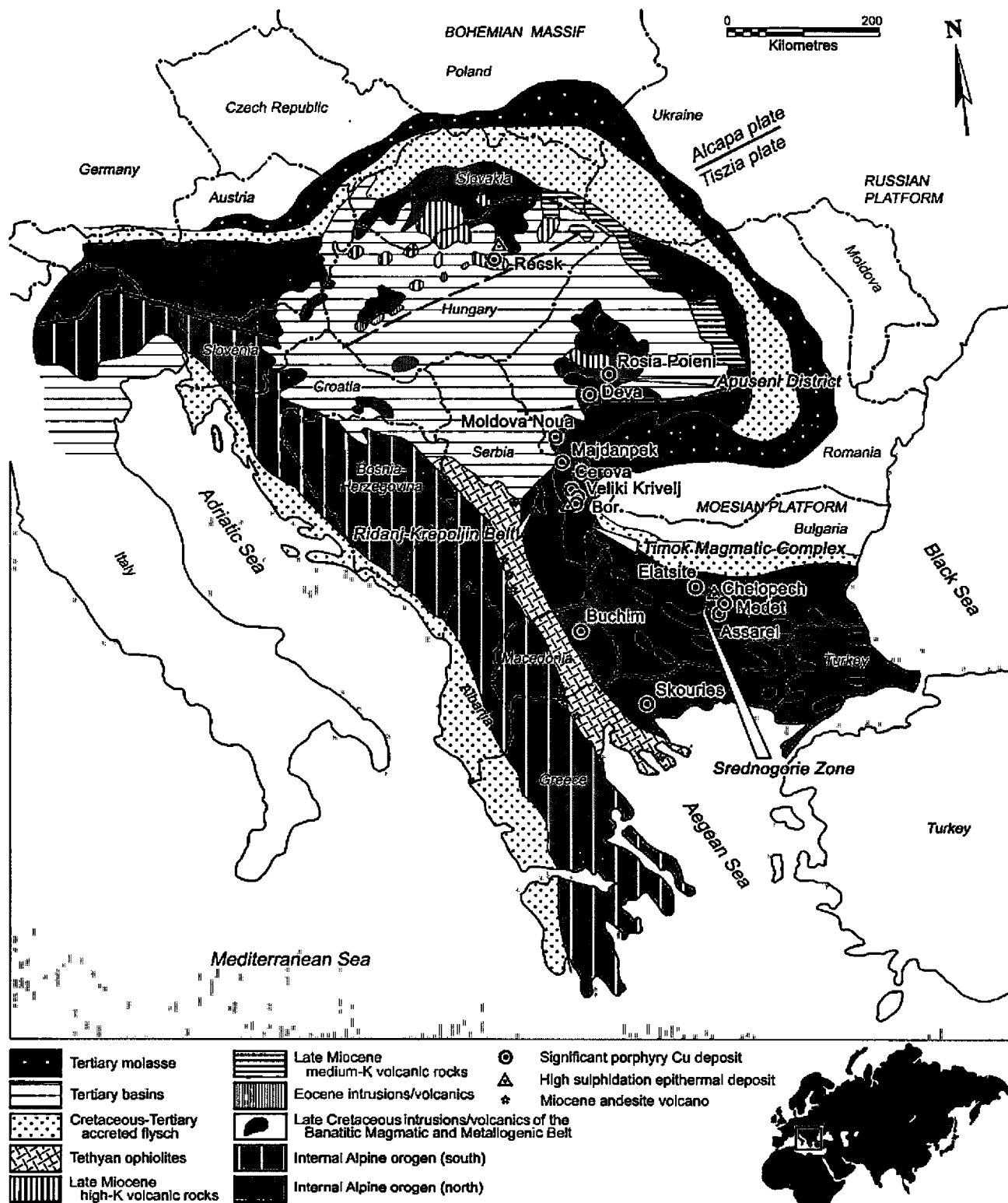


Figure 1: The tectonic and geologic setting, and principal magmatic arc rocks hosting porphyry copper deposits in the Alpine-Balkan-Carpathian-Dinaride (ABCD) Province (modified from Herrington et al., 2003).

**Table 1: Tonnage (production + resources), grade and age details of a representative selection of the porphyry Cu-Au/Mo deposits of the Alpine-Balkan-Carpathian-Dinaride metallogenic-geodynamic province.** See Fig. 1 for locations.

Deposit	Country	Tonnage @ Grade	Age
Recsk (porphyry/skarn)	Hungary	109.4 Mt at 0.96 % Cu / 36 Mt at 2.19 % Cu (historic production); 700 Mt @ 0.66% Cu, 0.006% Mo (potential resource) (a,e)	Late Eocene
Rosia Poieni	Romania	350 Mt @ 0.36% Cu, 0.5 g/t Au (a)	Late Miocene
Deva	Romania	Not known (e)	Late Miocene
Moldova Noua	Romania	500 Mt @ 0.35% Cu (e)	Late Cretaceous
Majdanpek	Serbia	~1000 Mt @ 0.4 to 0.8% Cu, 0.25-1.0 g/t Au	Late Cretaceous
Veliki and Mali Krivelj	Serbia	>840 Mt @ 0.4% Cu, 0.1 g/t Au	Late Cretaceous
Bor - Borska Reka porphyry - High sulphidation	Serbia	600 Mt @ 0.6% Cu, 0.25 g/t Au (f) 200 Mt @ 1.5% Cu, 0.8 g/t Au (f)	Late Cretaceous
Elatsite	Bulgaria	320 Mt @ 0.36% Cu, 0.21g/t Au (Au historic grade) (b)	Late Cretaceous
Medet	Bulgaria	163 Mt @ 0.32% Cu, 0.1 g/t Au (b)	Late Cretaceous
Assarel	Bulgaria	354 Mt @ 0.44% Cu (b)	Late Cretaceous
Chelopach (high sulphidation)	Bulgaria	61.5 Mt @ 1.32% Cu, 3.24 g/t Au (b,c)	Late Cretaceous
Buchim	Macedonia	85 Mt @ 0.3%Cu, 0.3g/tAu (a)	Early Miocene
Skouries	Greece	500 Mt @ 0.37% Cu, 0.47 g/t Au (d)	Early Miocene

a – GEODE Database, <http://www.gl.rhnc.ac.uk/geode/ABCD.html>; b – Strashimirov *et al.*, 2002; c – Bonev, *et al.*, 2002; d – Tobey *et al.*, 1998; e – Herington *et al.*, 1998; f – Monthel *et al.*, 2002.

high sulphidation Cu-Au mineralisation, as shown on Fig. 1 and listed in Table 1.

Within the ABCD province the most economically significant segment comprises the Upper Cretaceous subduction-related magmatic rocks and mineral deposits referred to by various authors as the Banatitic Magmatic and Metallogenic Belt, BMMB, or the Apuseni-Banat-Timok-Srednogorie belt (Berza *et al.*, 1998; Strashimirov and Popov, 2000). This belt forms an L-shape extending from Romania through Serbia and into Bulgaria (see Fig. 1). The BMMB intrusive and extrusive rocks were emplaced during a 30 M.y. period from ~90 Ma to 60 Ma and may have been the result of several different subduction zones of varying polarity (Ciobanu *et al.*, 2002). Lips (2002) suggests that the subduction regime that produced the BMMB commenced with the convergence between Africa and Eurasia at c.110 Ma. Due to the relatively slow rate of this convergence, there was a lag of 10 to 20 M.y. before the initiation of the melting that led to the emplacement of the BMMB magmatic rocks.

Temporal variations in the ages of mineral deposits within the belt are attributed to variations in convergence direction relative to the geometry of the active margin (Lips 2002). Specifically the deposits in south-western Romania, eastern Serbia and in central Bulgaria have been dated at 77, 85 and 91 to 80 Ma respectively (Lips, *et al.*, 2004). The distribution of related igneous rocks along this belt is nearly continuous, although in eastern Serbia they appear to be restricted to the TMC and a narrower, sub-parallel belt which is some 30 to 40 km to the west of the TMC (see Fig. 1), known as the Ridanj-Krepoljin Belt (RKJ) (Karamata *et al.*, 1997). Only minor bodies of andesite are exposed northwards from the TMC towards the Danube (which forms the Serbian-Romanian frontier north of Majdanpek – Fig. 1) (Karamata *et al.*, 1997). These two magmatic belts have petrological and geochemical characteristics similar to the West and East Banatite zones defined to the north of the Danube in Romania (Karamata

*et al.*, 1997). The RKJ is an extension of the West Banatite belt that includes the Moldova Noua porphyry Cu deposit (Fig. 1) (Cioflica and Vlad, 1984; Vlad 1984; Karamata *et al.*, 1997), while the TMC is thought to be the southerly extension of the eastern belt (not sufficiently significant to appear on Fig. 1) that contains some porphyry and related skarn mineralisation in Romania.

The RKJ lies to the west of the TMC and is predominantly composed of dacite with subordinate andesite, that have been dated at 70-74 Ma by K/Ar methods (Pecskay *et al.*, cited in Karamata *et al.*, 1997). The rocks of the TMC are predominantly intermediate to felsic (subordinate) in composition with medium to high K-series calc-alkaline affinities (Jankovic *et al.*, 2002; Karamata *et al.*, 1997; Banjesevic *et al.*, 2002). Magmatic activity is dated at between 82.73±0.03 and 86.29±0.32 Ma by U/Pb methods (von Quadt *et al.*, 2002), and 84 ± 1.5 Ma using Ar-Ar methods (Lips *et al.*, 2004). The westerly younging direction of these magmatic complexes suggests that they formed as a result of westerly migrating subduction of the oceanic lithosphere of the Vadar Sea during the late Cretaceous north-south convergence between Africa and Eurasia that resulted in the closure of the Neotethys Ocean (Ciobanu *et al.*, 2002; Lips, 2002; Banjesevic *et al.*, Karamata *et al.*, 1997).

The TMC is an approximately north-south, lozenge shaped belt of extrusive and intrusive units emplaced during the late Cretaceous (see Figs. 1 and 2). The complex is approximately 100 km in length north-south, up to 25 km at it's widest, and has a total area of around 1130 square kilometres (Cocic *et al.*, 2002).

The country rocks of the TMC comprise a basement of Proterozoic metamorphics overlain by Palaeozoic metamorphic and sedimentary formations intruded by Hercynian granitoids (Cocic *et al.*, 2002). Xenoliths of these units have been observed within the TMC volcanic succession. For the most part, the Mesozoic of the region is dominated by carbonate units of Triassic, Jurassic and

lower Cretaceous ages. These units are folded with a broad regional NW-SE strike.

To the west, the TMC is bounded by the approximately north-south trending Zlot fault zone and by the Belorecko-Bucje fault zone in the east (Jankovic *et al.*, 2002). Both are interpreted from geophysical data as being deep-seated

structures that converge at depth contributing to the graben-like character of the TMC (Andric *et al.*, 1972; Karamata *et al.*, 2002). This graben-like structure is often referred to in the Serbian literature as a 'rift-dyke complex' or 'dyke syncline' (Jankovic *et al.*, 2002; Cocic *et al.*, 2002; Andric *et al.*, 1972). Other large scale NNW-SSE striking longitudinal faults are also reported within the TMC, cut by numerous WNW-ESE to NW-SE and ENE-WSW to NE-SW striking transverse faults (Fig. 2), described by Kozelj (2002) as a result of subsidence within the 'rift-dyke complex'. The observed spatial distribution of these faults may be interpreted as evidence of the TMC graben being a pull-apart basin (Richards, 2003), consistent with the observed discontinuity in mineralisation and magmatism trends along the length of the BMMB.

The igneous rocks of the TMC have historically been the subject of extensive study, in part due to the occurrence of Timocite, an andesite containing large phenocrysts of hornblende and biotite in an idiomorphic matrix (Historic reference Breithaupt, 1861, cited by Jankovic, 2002). Later studies by Drovenik (1960) and Drovenik *et al.* (1962) were the first to describe three phases of volcanism in the late Cretaceous. For a number of years the view persisted that the TMC consisted of three distinct phases of volcanism, with the intrusion of plutonic bodies following the cessation of eruptive activity. Karamata *et al.*'s review (2002) reinterpreted the magmatic history to comprise four main phases, the first two characterised by volcanic activity, followed by two dominated by intrusion, all related to several large stratovolcanic edifices (See Table 2). Volcanic facies analysis of the TMC volcanic successions describe the presence of andesitic crypto-domes with hyaloclastic margins, autobrecciated andesitic flows, epiclastics and tuffs. The wide range of facies and their variation with time suggests periods of both sub-aerial explosive, and relatively quiescent sub-aqueous volcanism, which lasted from the Turonian to the Campanian. Absolute ages of the TMC igneous suite indicate a tight range from 86 to 83 Ma. Quartz diorite close to the Majdanpek Dolovi-1 orebody (Fig. 3) was dated at 83 Ma while sub-volcanic andesite from the Veliki Krivelj deposit yielded an age of 86 Ma, both from U-Pb dating of zircons (Von Quadt *et al.*, 2002). In addition, fresh andesite from Bor was dated at  $84 \pm 1.5$  Ma using Ar-Ar methods (Lips *et al.*, 2004). Earlier studies indicated much younger dates using less reliable K-Ar methods. Strontium isotope data from various TMC rocks range from 0.7039 to 0.7060, inferring that the magmas show significant modification by continental crust material, either through subduction fluids or via high-level chamber processes (Von Quadt *et al.*, 2002).

For detailed descriptions of the TMC volcanic succession the reader is referred to Djordjevic and Banjesevic (1997, 1998) and Banjesevic (1998).

On a more regional scale, preliminary U-Pb zircon dates of the arc volcanic rocks in the Ridanj-Krepoljin (RKJ) zone suggest an age of about 70 Ma for the andesite-dacite at Krepoljin (M. Banjesevic pers comm.). These data support the proposal for a trenchward migration of Late Cretaceous magmatism westwards from the TMC, possibly

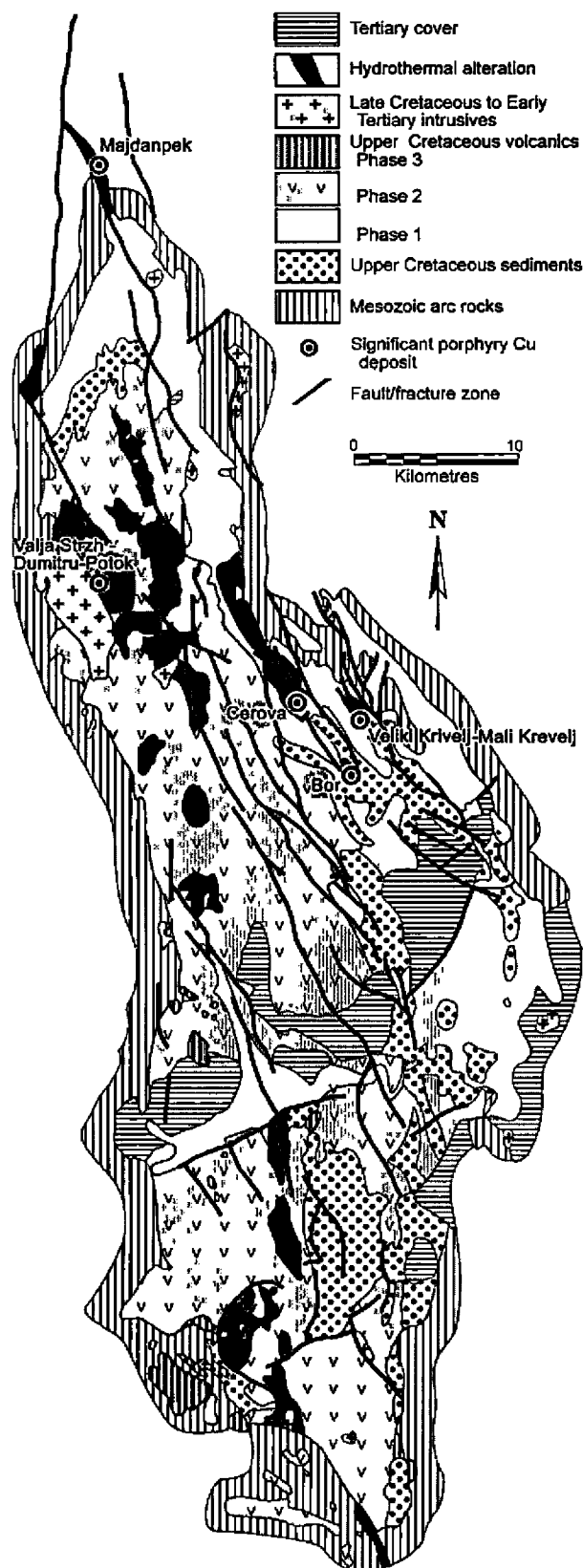


Figure 2: Geology, structure and porphyry Cu deposits of the Timok Magmatic Complex (after Kozelj 2002).

Table 2: Summary of main periods of magmatism in the Timok Magmatic Complex (Karamata et al., 2002).

Magmatic phase	Rock types and lithologies	Age
1 <sup>st</sup> phase volcanics	Hornblende ± biotite ± pyroxene andesites with subordinate dacite lavas, volcanoclastics and pyroclastics	Turonian – Coniacian
1 <sup>st</sup> phase intrusives	Hornblende ± biotite ± pyroxene andesite and dacite porphyries, and porphyritic diorites and quartz diorites. These rock types mostly form N-S striking dykes which are tens of metres wide and subvolcanic intrusions of dimensions ~1 km <sup>2</sup> .	Turonian - Coniacian
2 <sup>nd</sup> phase volcanics	Basaltic-andesites and minor andesites. Abundant volcanoclastic material, lava flows and tuffs.	Senonian
2 <sup>nd</sup> phase intrusives	Monzonites, monzodiorites, diorites, granodiorites, quartz diorites and their porphyritic facies. These rocks are mostly found in dykes and subvolcanic intrusions. The only intrusive body of any size is the Valja Strz monzonite that which has an exposed surface area of ~20 km <sup>2</sup> .	Campanian

in response to steepening of the subduction angle (Von Quadt *et al.*, 2002). This steepening may have been the initiator of the extension resulting in eruption of the TMC.

## Mineralisation in the Timok Magmatic Complex

The TMC contains some of the largest examples of porphyry style mineralisation in Europe, including Veliki Krivelj, Majdanpek and the gold-rich Bor deposit. Total tonnage and grade figures for these deposits and others are listed in Table 3. Despite porphyry copper style mineralisation being restricted to a relatively small geographical area in the northern part of the TMC, there are a variety of mineralisation morphologies and significant variations in Cu and Au grade (Jelenkovic and Kozelj, 2002; Herrington *et al.*, 1998). The TMC also contains high sulphidation epithermal Cu-Au deposits, none of which are currently being mined, with the exception of care and maintenance work at Bor. A detailed review of epithermal gold mineralisation is given by (Kozelj, 2002a, 2002b).

The following are summaries of other key porphyry style deposits within the TMC, after Herrington *et al.*, (1998).

### Bor Porphyry and High Sulphidation Cu-Au

Sub-cropping massive, high sulphidation mineralisation was discovered at Bor at the turn of the 20th century with mining commencing in 1903. Subsequent mining and

exploration drilling has shown that the massive sulphide orebodies are spatially related to deeper porphyry style mineralisation, the Borska Reka deposit. The two styles are continuous, linked by a transitional stockwork zone (Fig. 3). The length of the altered and mineralised structural zone exceeds 2000 m with a width of around 1000 m, while the mineralised zone, which dips at 50° to the west, has been drill tested to a depth of at least 1500 m below surface. Past production + current reserves of the high sulphidation Cu-Au zone is estimated to total 3 Mt Cu, 160 t Au and 600 t Ag from 200 Mt of ore with an average grade of 1.5% Cu and 0.8 g/t Au (Monthel *et al.*, 2002).

The host sequence at Bor is dominated by porphyritic hornblende-biotite andesites, andesitic tuffs and minor dacites. These volcanic rocks are overlain by pelitic sediments, and are underlain by a series of Late Cretaceous conglomerates and sandstones, which are nowhere mineralised.

High sulphidation mineralisation is characterised by a series of massive, cigar-shaped, or pipe-like bodies, together with mineralisation in fracture zones and in volcanic breccias. The largest of the sulphide bodies is Tilva Rosh with other major bodies such as Choka Dulkan and Tilva Mika (Fig 3). Tilva Rosh, which had maximum plan dimensions of 650 x 300 m and extended vertically for as much as 800 m, comprised both massive and disseminated sulphide mineralisation. The massive sulphide orebody of Choka Dulkan has a strike of some 150 m, thickness of 60-70 m and a vertical extent of around 300 m.

Table 3: Summary of the total resources for differing styles of porphyry copper related mineralisation in the Timok Magmatic Complex (Jelenkovic and Kozelj, 2002; Jankovic, 1990; Herrington *et al.*, 1998).

Deposit	Total Size (Mt) Production+resource	Cu (%)	Au (g/t)	Morphological Type (Jelenkovic and Kozelj, 2002)
Bor - Porphyry - High sulphidation	600 200	0.62 1.5	0.25 0.8	Porphyry copper and high sulphidation massive sulphide.
Veliki Krivelj	>540	0.35	0.068	Porphyry copper related to high-level dyke swarms.
Mali Krivelj	>300	0.5	0.147	Porphyry copper related to high-level dyke swarms.
Valja Strzh	482	0.2	0.04	Porphyry copper hosted by composite pluton.
Dumitru Potok	290	0.21	0.1	Porphyry copper hosted by composite pluton.
Majdanpek	~1000	0.4-0.8	0.25 - 1.0	Porphyry copper related to an initial rift structure.

The massive copper ore at Bor contains 3 to 6% Cu and comprises up to 70% (by volume) fine-grained pyrite, accompanied by up to 2.5 to 3.75 (locally to 18) g/t Au and 10 g/t Ag (Jankovic, 1982; Monthel *et al.*, 2002). The principal copper minerals are chalcocite, covellite and enargite, with associated marcasite, chalcopyrite, tetrahedrite and sylvanite. Spectacularly bladed hypogene covellite is common in the massive sulphide ore. Traces of galena and sphalerite are present in the massive sulphides, although these minerals form a major component of the Choka Marin high-sulphidation body which lies to the north of Bor. Associated gangue minerals are significant amounts of silica, barite, ubiquitous anhydrite and native sulphur. Barite is more common in the upper sections of the system, while the predominant sulphate mineral in the lower levels is anhydrite. Native sulphur accompanies high-grade enargite and covellite veining in one of the orebodies. Very late gypsum veins are also common.

There is a suggestion of a sulphide mineralogy zonation within the massive ore to a pyrite-chalcopyrite-bornite (occasionally pyrrhotite) association in the lower levels, possibly indicating a change in sulphur activity. The massive ores grade laterally and at depth to disseminated mineralisation. A system of thin sub-parallel veins is

developed beneath the large Tilva Rosh body although post-ore faulting has removed the lower sections of bodies such as Choka Dulkan. The disseminated zones also carry significant sulphide mineralisation (>0.6% Cu) and form part of the ore reserves.

Alteration is distinctive around the high-sulphidation deposits with a change at depth towards the porphyry style mineralisation. In the upper parts of the high-sulphidation system, silicification is the common alteration with vuggy silica developed close to the interpreted palaeosurface. Outward zoned advanced argillic alteration, characterised by an inner envelope of kaolinisation and peripheral chlorite surrounds the orebodies, in places accompanied by pyrophyllite, diaspore and alunite, and locally with andalusite, zunyite, sericite and some corundum. Alunite is most abundant in the upper parts of the alteration. Kaolinite is commonly associated with the alunite (Karamata *et al.*, 1983).

The porphyry style disseminated and stockwork mineralisation of Borska Reka is associated with dykes and minor intrusions of diorite which are restricted to its lower sections. The bulk of the mineralisation is hosted by altered andesite which has a distinct porphyritic texture. Alteration

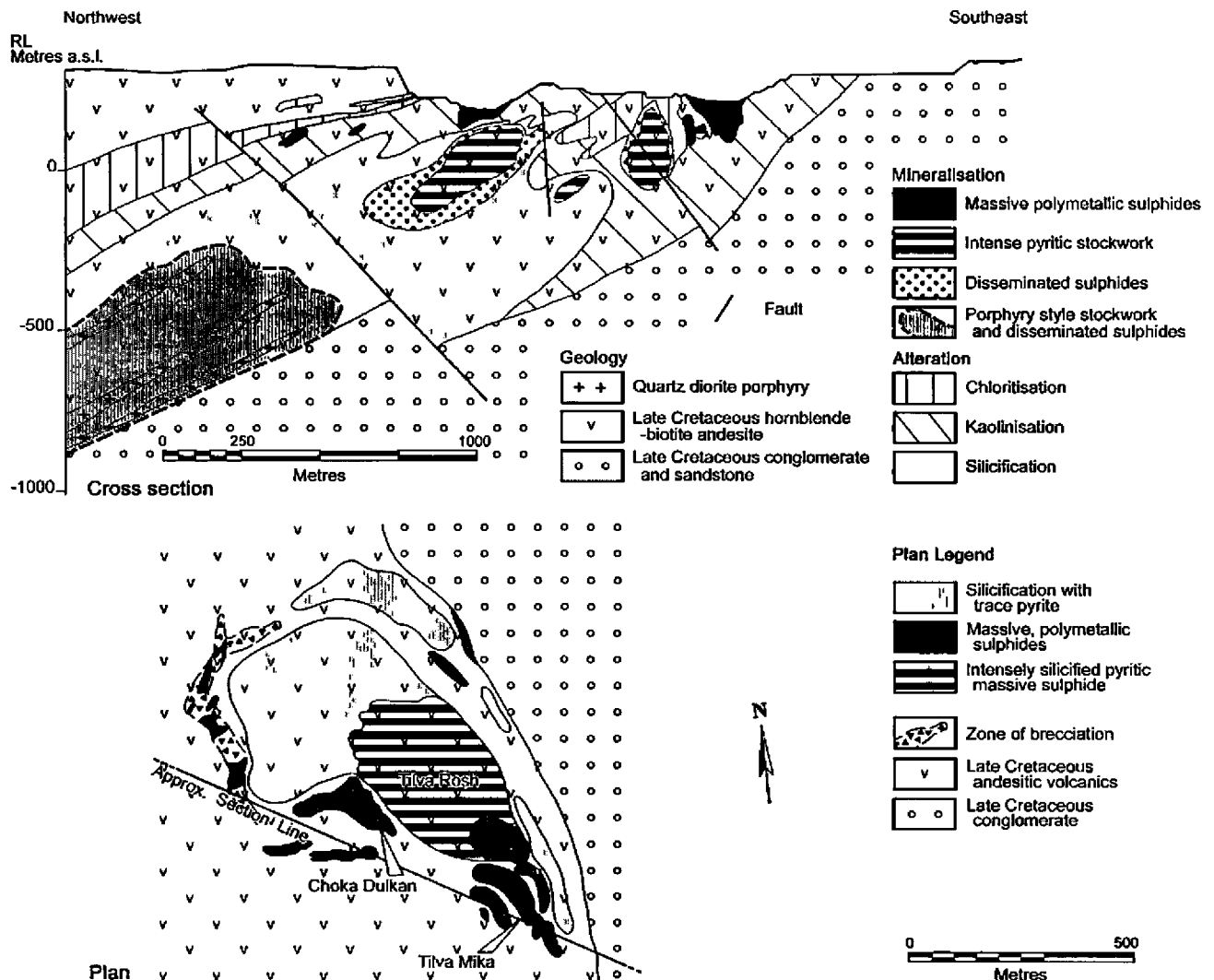


Figure 3: Geological cross section through the Bor high sulphidation and porphyry Cu-Au deposits (top) and sub-crop geological map of the high sulphidation deposits and alteration (bottom).

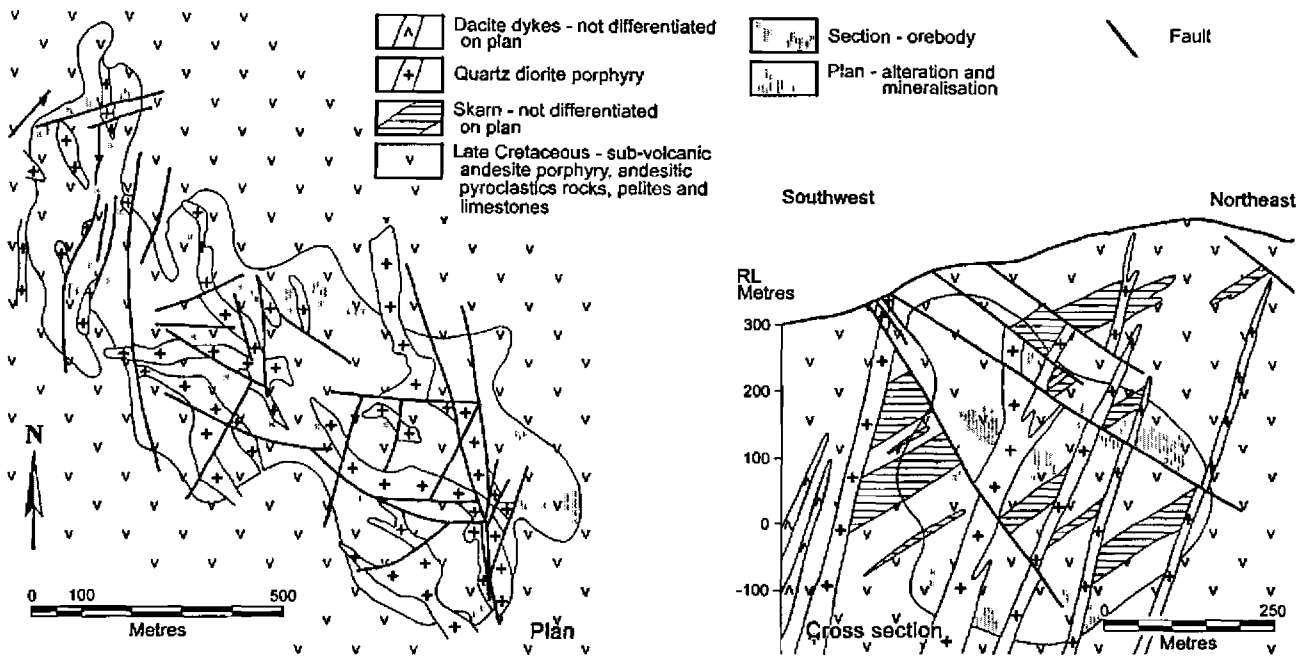


Figure 4: Simplified geological plan (left) and cross section (right) through the Veliki Krivelj porphyry Cu deposit

is characterised by silicification and illite-argillisation, accompanied by chlorite, alunite and carbonates, although alunite is widespread in parts of the deposit. The principal Cu sulphide is chalcopyrite with up to 6% (by volume) pyrite, and in the lower levels, molybdenite. These sulphides are accompanied by magnetite, minor pyrrhotite, enargite and bornite, and are overprinted in parts by chalcocite and covellite. This porphyry deposits contains around 600 Mt @ 0.6% Cu, 0.25 g/t Au.

**Veliki Krivelj Porphyry Cu**

The Veliki Krivelj deposit is approximately 3 km to the northeast of Bor. It has maximum sub-surface plan dimensions of 1500 x 700 m and a vertical extent of more than 800 m as indicated by diamond drilling. Historic production since operations commenced in 1982 has amounted to 0.51 Mt Cu, 120 Kt Mo, 60 t Ag and 10 t Au from ore with a recovered grade of 0.34% Cu, 0.4 g/t Ag and 0.07 g/t Au (Montheil *et al.*, 2002). At a cut-off grade of 0.15% Cu, the deposit is quoted as originally containing a mineable reserve of approximately 2.5 Mt of Cu from ore averaging 0.44% Cu, within a larger geologic resource. The Mo content of the ore is generally only 0.003 to 0.005%, although it may locally reach 0.02 to 0.03%. The deposit has been previously described by Aleksic (1969, 1979); Jankovic *et al.*, (1980); Jankovic (1990, 1990b).

The porphyry style mineralisation at Veliki Krivelj occurs in hydrothermally altered Upper Cretaceous sub-volcanic hornblende andesite and pyroclastic equivalent breccias, tuffs and agglomerates as well as the Upper Cretaceous volcano-sedimentary series of pelites and limestones. This mineralisation, prominent Late Cretaceous to Early Tertiary diorite and quartz diorite porphyry dykes as well as andesite dyke swarms, are all superimposed on earlier skarns formed in the Upper Cretaceous pelites and limestones.

Hydrothermal alteration is mainly developed in the pyroclastic facies of the host hornblende biotite andesite, predominantly as a potassic assemblage characterised by

secondary biotite, accompanied by widespread silicification and by sericite on the margins. Pyrophyllite is found locally. On the periphery of the porphyry copper mineralisation, where silicification is weak, chlorite, epidote and calcite are developed. Late intense zeolite, gypsum and sporadically anhydrite are also apparent. Strong pyritisation is associated with the silicification.

Porphyry style mineralisation is dominated by chalcopyrite, pyrite, minor molybdenite, magnetite, pyrrhotite, hematite, traces of cubanite, enargite, bornite, covellite, chalcocite, galena and sphalerite. The occurrence of up to 50 m thick zones of pyrophyllite, alunite and kaolinisation in parts of the alteration system indicates the presence of advanced argillite alteration, although this has not been studied systematically.

The early skarn assemblage includes garnet, calcite, epidote, quartz, biotite, pyrite and sporadically wollastonite, with disseminated chalcopyrite.

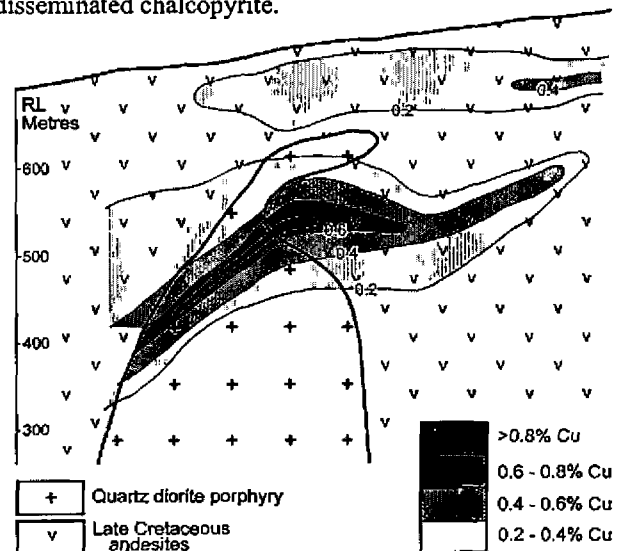
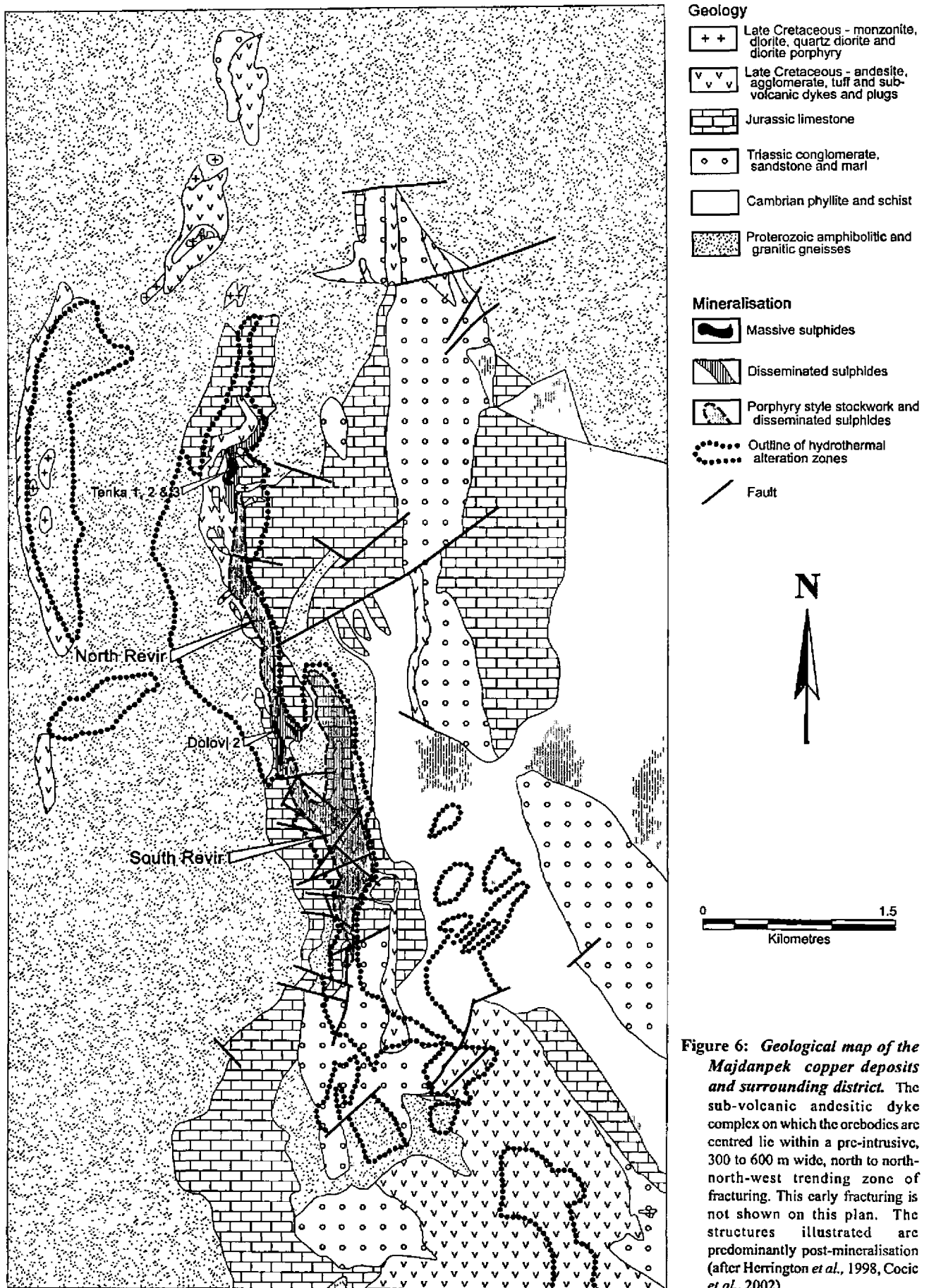


Figure 5: Sketch geological section through the Valja Strž porphyry Cu deposit showing Cu grades. Other data suggest the deposit thickens and widens along trend.





**Figure 6: Geological map of the Majdanpek copper deposits and surrounding district.** The sub-volcanic andesitic dyke complex on which the orebodies are centred lie within a pre-intrusive, 300 to 600 m wide, north to north-north-west trending zone of fracturing. This early fracturing is not shown on this plan. The structures illustrated are predominantly post-mineralisation (after Herrington *et al.*, 1998, Cocic *et al.*, 2002).

**Footnote:** The precise outline of the Dolovi-1 orebody and associated sub-volcanic andesite dykes could not be obtained to plot on this plan. These are believed to be located in the alteration zone to the west of the main North Revir orebody. They are illustrated on the geological cross section (Fig. 7), and are described in the text on page 464.

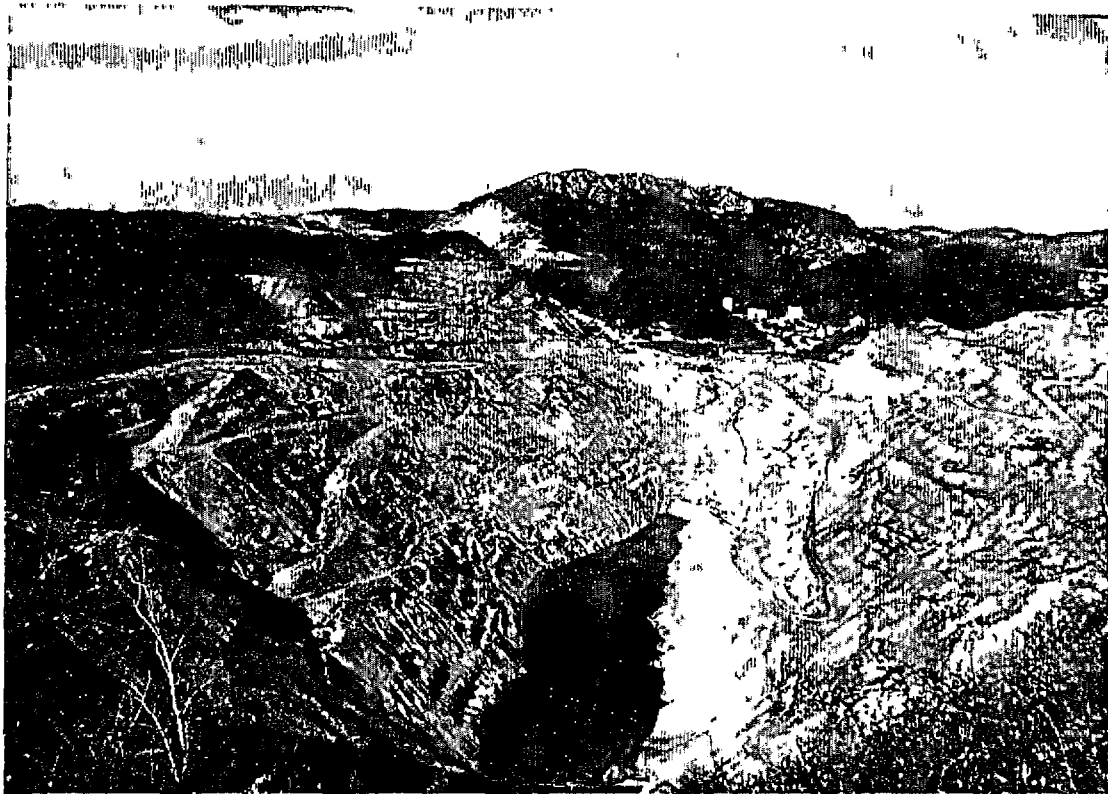


Plate 1: View looking north over Majdanpek South Revir (flooded in foreground – autumn 2002) with North Revir visible in the background behind ridge of trees left of centre. Majdanpek town is visible in the valley centre right. Mesozoic limestones form the background hills.

#### *Valja Strzh and Dumitru Potok*

The Valja Strzh and Dumitru Potok zones of porphyry style mineralisation are developed adjacent to the Late Cretaceous to Early Tertiary Crni Vrh plutonic complex which was emplaced along a regional fracture zone on the western margin of the TMC. This complex intruded Late Cretaceous (Turonian) andesites and in part into clay-rich sediments of similar age. The plutons are composite magmatic complexes represented by a potassic intrusive series. Initial strontium ratios ( $^{87}\text{Sr}/^{86}\text{Sr}$ ) show variations between 0.708 and 0.714, indicating a continental crust contaminated mantle source. In the deeper parts of the complex, monzonite and granodiorite prevail, while syenite, quartz diorite and quartz diorite porphyry are developed along the margin (Terzic, 1966)

Copper mineralisation is related to hydrothermally altered intrusives and to andesitic sub-volcanic and extrusive complexes. Extensive zones of alteration occur at the margins and in the central parts of the plutonic complex in a zone which is over 8 km in length. Alteration facies include propylitic, dominated by chlorite and epidote with silicification and pyritisation (Jovanovic, 1974). Several occurrences of copper mineralisation have been so far identified but only two large, sub-marginal grade deposits of are known, namely Valja Strzh and Dumitru Potok (see Fig. 5 and Table 3). There are some indications of epithermal mineralisation developed at the margins of these bodies (Jovanovic 1974).

#### *Cerova*

Cerova is a small porphyry copper deposit to the north of Bor, worked for its secondary enrichment zone.

### **The Majdanpek Deposit.**

The Majdanpek deposit is located at the most northerly tip of the TMC (Fig. 2). The deposit is approximately 5 km in length with an average width of 300 m. Weak copper mineralisation ( $>0.1\%$  Cu) has been detected to a depth of at least 1000 m (Cocic *et al.*, 2002). The elongate morphology of the mineralised system results from the mineralisation being focused on a Late Cretaceous andesitic dyke complex which was intruded into a 300 to 600 m wide zone of fracturing and pre-existing faulting which cuts Proterozoic to Cambrian metamorphic suites, Triassic clastic rocks and Jurassic limestone (Jelenkovic and Kozelj, 2002; Jankovic *et al.*, 1980).

Jelenkovic and Kozelj (2002) outline three tectonic stages key to the formation and location of the Majdanpek deposit:

- i) *A pre-ore stage* consisting of the folding of the Proterozoic to Early Mesozoic basement, commencing in the Hercynian and involving the initiation of faulting. These faults underwent further reactivation during the Alpine orogeny, cumulating in the intrusion of the TMC along pre-existing north-south faults.
- ii) *An intra-ore stage* saw the further reactivation of the major north-south fault zone that controls the spatial distribution of magmatic bodies and ore mineralisation. Jelenkovic and Kozelj (2002) suggest that during this period extensive localised faulting took place, improving the structural permeability and facilitating the passage of ore forming fluids.
- iii) *A post-ore tectonic stage* resulted in the re-faulting of the newly emplaced orebody and was responsible for the structure observed today.

The country rocks to the deposit consist of Proterozoic amphibolites and gneisses; Cambrian phyllites, schists and subordinate amounts of marble with serpentinised lenses that are assumed to be metamorphosed igneous sheets (Cocic *et al.*, 2002). This metamorphic basement is unconformably overlain by a series of Mesozoic formations comprising Triassic conglomerates and sandstones, Upper Jurassic limestones and Senonian (Upper Cretaceous) Flysh deposits. The TMC is represented in the area by numerous smaller andesite dykes which follow the strike of the main north-south structural trend, and a number of minor diorite and quartz diorite intrusions and dykes. The presence of the diorite and quartz diorite bodies has been inferred to indicate a larger intrusion at depth (Jankovic, 1990). The relationship between the dyke complex and the mineralised stockwork shows that dyke emplacement took place pre-, syn- and post- the major stockwork forming event (Clarke and Ullrich, 2004).

### Porphyry Copper Style Mineralisation at Majdanpek

The Majdanpek deposit is divided into two mining areas, North and South Revir. North Revir is characterised by the presence of polymetallic Pb-Zn-rich limestone replacement ores and smaller porphyry copper style bodies. In contrast, South Revir comprises the large porphyry copper occurrence, the Cu-Au-rich massive sulphide Knez Lazar body, and a number of contact skarns.

A total of 10 orebodies have been recognised at Majdanpek, including porphyry style, massive sulphide-limestone replacement and skarn ores. The locations of a selection of these bodies are shown on Fig. 6. The styles of mineralisation found in the Majdanpek deposit are described in Cocic *et al.*, (2002). The volumetrically most significant mineralisation types are the disseminated-stockwork-veinlet porphyry ores, the most significant of which is the South Revir orebody.

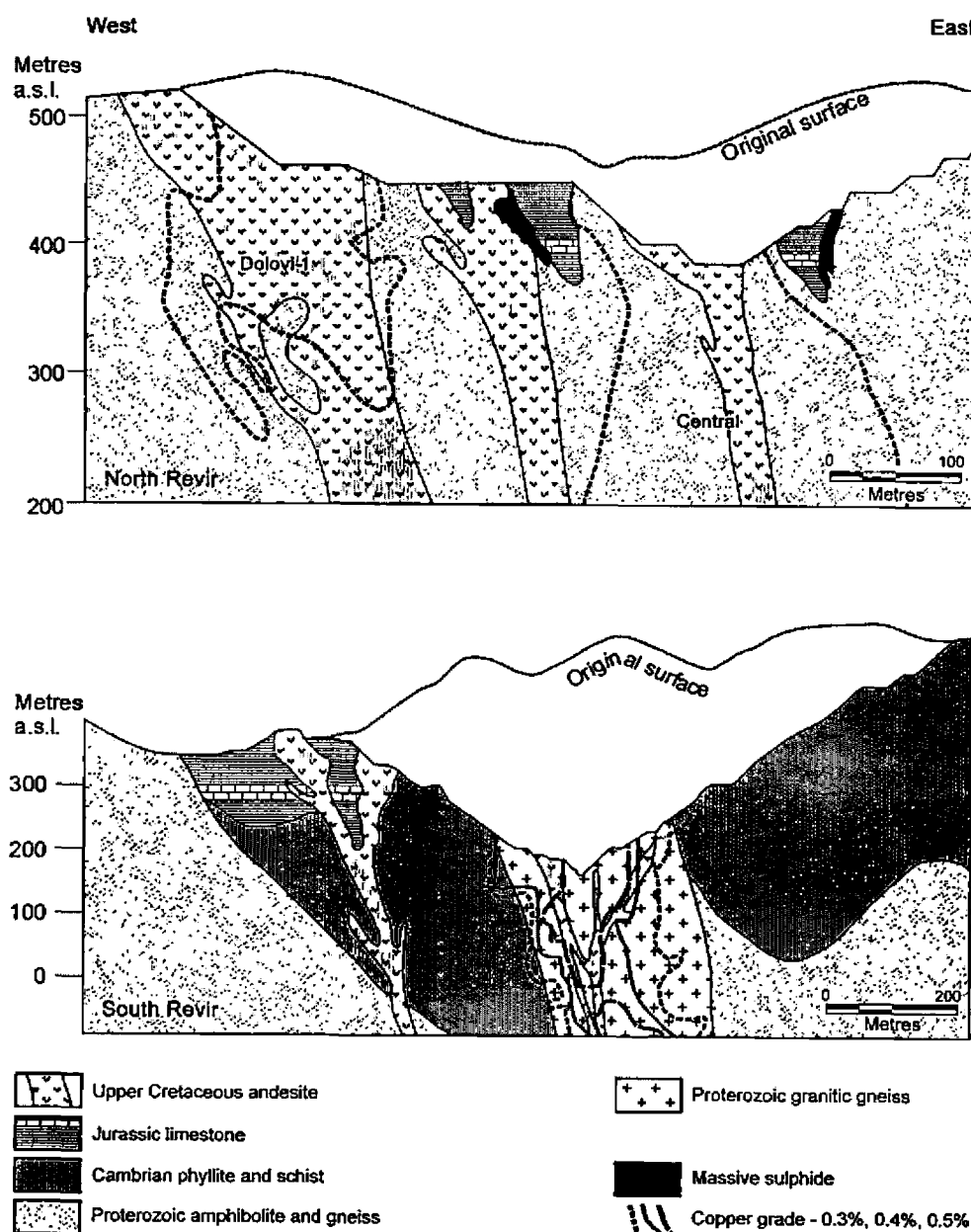


Figure 7: Typical cross sections through North Revir, Central Orebody (Top) and South Revir, Main Orebody (bottom) showing copper grade contours (after Herrington *et al.*, 2003).

### South Revir Porphyry Copper

The main porphyry-copper mineralisation at South Revir has a prismatic form, with a north-south strike length of more than 2 km. The orebody width in a generally east-west direction ranges between 270 m and 350 m at the +110 m level (Cocic *et al.*, 2002). This reduces to a width of between 170 m and 250 m at the -100 m level (the current deepest level of exploration). Data from the Mine Geological Department indicates that there is an observed decrease in Cu grade with depth and it is postulated that overall, the orebody has a funnel shaped cross section (Fig. 7). Historic mine records show that the original vertical extent of the porphyry style mineralisation was approximately 800 m (from the +600 m to the -200 m level). While there is a consensus on the east-west limits of the mineralisation, there currently appears to be little knowledge of its north-south extent, particularly to the south (Cocic *et al.*, 2002; Zivkovic and Momcilovic, 2002).

The morphology of the orebody roughly follows that of the porphyritic dykes that intruded along the main north-south fracture zone. Two styles of porphyry-copper mineralisation are recorded from the South Revir orebody, namely a "stockwork" and an "impregnation-metasomatic" (disseminated) type (Cocic *et al.*, 2002). Reported grades show that the richest parts of the orebody were located in the higher sections of the system (+200 m level) and are associated with stockwork style mineralisation, averaging 1.5% Cu and 0.8 g/t Au. The grade diminishes as the stockwork is replaced by disseminated mineralisation, with grades averaging around 0.4% Cu and 0.25 g/t Au.

The ore mineralogy is dominated by chalcopyrite, accompanied by pyrite, magnetite and molybdenite. The overall Mo content of the deposit is low, averaging 0.003 to 0.008%. Minor minerals recorded include bornite,

galena, sphalerite, marcasite, tetrahedrite, arsenopyrite, enargite, stannite and colusite, along with Ag-tellurides and Ag-selenides. Gold occurs in the native form and/or with sulphides. Of note is that minor amounts of PGE have historically been recovered from the concentrate. Jankovic (1990b) reported the occurrence of Pd-tellurides with traces of silver of the composition Pd(Ag)Te<sub>2</sub> up to PdAgTe<sub>2</sub>.

The highest copper grades are found in the areas of K-silicate alteration close to the central parts of the orebody. This potassic alteration is spatially associated with strong silicification (Herrington *et al.*, 2003; Jelenkovic and Kozelj, 2002). The alteration mineralogy is characterised by an association of quartz, sericite, biotite, hydro-biotite and rare but poorly preserved K-feldspars. <sup>40</sup>Ar/<sup>39</sup>Ar analysis of biotite samples from the potassic alteration yielded an age of 83.6 to 84.0±0.6 Ma, placing the main mineralisation at the Santonian-Campanian boundary in the Upper Cretaceous (Clarke and Ullrich, 2004).

The silicification of the potassic alteration is manifested by fine grained quartz veinlets and disseminations. Sericite is found as thin threads and appears to be closely associated with the silicification. The potassic alteration is surrounded by a zone of sericite-quartz-chlorite-calcite (Cocic *et al.*, 2002). The transition from potassic to sericite (phyllitic) dominated alteration appears to correlate with the change from stockwork- to more disseminated-type pyrite-dominated mineralisation. Further from the core of the orebody alteration is represented by a more distal propylitic facies characterised by a chlorite-calcite ± sericite/epidote assemblage.

Skarn mineralisation is also developed at South Revir, following the contact between the andesite and quartz-diorite intrusives and Jurassic limestone. The skarn bodies, which consists of garnet, epidote, chlorite, calcite, magnetite

Table 4: Summary of the types of mineralisation described at the Majdanpek deposit (Cocic *et al.*, 2002).

Cu ore types	Description	Mineralogy
Impregnation-metasomatic (i.e. disseminated)	A finely disseminated ore consisting of very fine grained aggregates of predominantly pyrite and chalcopyrite with minor concentrations of rutile & magnetite. Sulphide deposition can be strongly correlated with altered former Fe-Mg silicates.	Mt-py-cp
Stockwork	Veinlets of pyrite, chalcopyrite, and magnetite with quartz ± carbonate ± sericite ± chlorite. Some veins show evidence of multiple deposition events. Veinlet thickness rarely exceeds 2 mm.	Py-cp-mt
Vein (stockwork)	Similar mineralisation to that of Stockwork-type, the key difference being vein widths of up to 20 mm. Non-ore minerals include quartz, carbonate, anhydrite and gypsum. It is from these veins that the most native gold has been observed in association with chalcopyrite.	Py-cp-mt
Massive sulphide	Massive pyrite bodies with subordinate chalcopyrite, sphalerite, and galena with quartz and carbonate gangue.	Py-cp-sl-gn
Oxidation zone	An oxidized zone of variable thickness (max 50 m), dominated by limonite with subordinate lazurite, malachite, native copper, cerussite, smithsonite, jarosite and cuprite. No gold has been observed.	Limonite
Supergene	Found in the highest levels of fault zones to a maximum depth of 15 m from surface with widths of up to 15 m. Cu-minerals includes chalcocite, covellite, bornite and idaite.	Co-cc-bn
Skarn	This style of mineralisation is very localised and occurs at contact zones between both andesites and quartz-diorite-porphyrries with Jurassic limestones. Skarn bodies are generally of limited size and are dominated by magnetite with minor chalcopyrite, sphalerite and galena. Bornite is occasionally present.	Mt-(cp-sl-gn)

mt = magnetite; py = pyrite; cp = chalcopyrite; bn = bornite; co = covellite; cc = chalcocite; sl = sphalerite; gn = galena;

and hematite are small, with widths rarely exceeding a few metres before passing into marble and limestone. The metallic mineralisation associated with the skarns is predominantly magnetite with subordinate amounts of hematite, pyrite, chalcopyrite, and minor Pb-Zn sulphides and Pb-Sb sulphosalts (Herrington *et al.*, 2003; Cocic *et al.*, 2002). Grades of the order of 42% Fe, 2.35% Cu, 1.75 g/t Au and 4.2 g/t Ag have been reported from skarn ore (Jankovic, 1990b).

#### **North Revir Porphyry Copper**

The North Revir area is located approximately 1 km north to northwest from the town of Majdanpek and comprises a number of orebodies. Porphyry copper mineralisation at North Revir consists of several small orebodies, none of which have either the tonnage or grade of those at South Revir. As a consequence, the North Revir area has not been as extensively explored or exploited. The two main examples of porphyry-style mineralisation at North Revir are the Central (North Revir) Orebody and Dolovi-1 (Fig. 7).

The Central Orebody has dimensions of approximately 1500 x 150 m and is ellipsoidal in plan. The remaining resource is estimated to have a grade of 0.29% Cu, 0.25 g/t Au at a 0.1% Cu cut-off. Its morphology and orientation is strongly controlled by a NNW-SSE striking fault zone along which a number of amphibole-biotite andesite dykes and quartz-diorite porphyries have intruded into the basement gneisses (Fig. 7). The known mineralisation extends over a vertical interval of approximately 600 m and comprises a stockwork of quartz-pyrite-chalcopyrite veins, with chalcopyrite being the main ore mineral. Other minerals present include minor amounts of magnetite, hematite, pyrite, arsenopyrite, marcasite, bornite, tetrahedrite, molybdenite, sphalerite, galena and native gold (Cocic *et al.*, 2002).

The stockwork is similar to that of the South Revir porphyry-style orebody and is characterised by a potassic K-feldspar-biotite altered core, with marginal silicification and sericite alteration. These alteration types in turn grade outwards to a peripheral propylitic zone, dominated by chlorite-calcite-epidote (Cocic *et al.*, 2002). The hypogene mineralisation is blanketed by an oxidation zone with a mean thickness of 25 m and mean grades of 0.45% Cu and 0.4 g/t Au. A striking feature of the Central Orebody is the development of smaller polymetallic and Cu-rich massive sulphide bodies that have formed at the contact zone between the intrusive andesites and Jurassic limestones (Cocic *et al.*, 2002).

The Dolovi-1 deposit is located approximately 200 m west of the Central Orebody and is another example of porphyry copper style mineralisation. At a 0.2% Cu cut-off, it is estimated to comprise 150 Mt @ 0.313% Cu, 0.109 g/t Au. In plan, the mineralised body is roughly ovoid in shape with a maximum strike length of 430 m and a width of up to 140 m. It is centred on a hornblende-biotite andesite that has been intruded into basement gneisses and amphibolites. All of the observed contacts are tectonic (Momcovic *et al.*, 2002). The host andesite is strongly

silicified and propylitically altered, and is cross cut by quartz veins. In contrast to the Central Orebody and South Revir porphyry copper, no potassic core is observed (Momcovic *et al.*, 2002). The mineralisation comprises both stockwork and disseminated sulphides. Higher grades are associated with a stockwork of chalcopyrite-pyrite-quartz veins at the centre of the mineralised mass, which grades outward into lower grade disseminated sulphides.

Significant massive sulphide developments are hosted by Jurassic limestone units marginal to the porphyry mineralisation at the northeastern end of the North Revir pit. The Tenka polymetallic sulphide bodies (Fig. 6) contain a geological resource of approximately 4 Mt @ 8% Pb+Zn and 3 to 4 g/t Au, with a Zn:Pb ratio of around 5:1. The ore mineralogy comprises major sphalerite and galena, with associated pyrite, chalcopyrite, arsenopyrite and marcasite. Collomorphous sulphide textures are very common. Pb and Sb sulphosalts are present with Ag-rich tetrahedrite, freibergite and native gold. Quartz, calcite and rare barite are the main gangue minerals. These same limestones hosted the historically important Blanchard Fe-Cu-Au deposits, which originally comprised massive auriferous pyrite that was largely weathered to goethite with free gold. These small bodies outcropped and were exploited in the 19<sup>th</sup> Century. The remnant ore has a grade of 1.1% Cu, 3.1 g/t Au. Systematic exploration for further carbonate-hosted deposits has not been carried out (P. Zivkovic, pers. comm.)

#### **Summary**

- The Majdanpek porphyry copper orebody is the largest and the most northerly deposit within the Timok Magmatic Complex (TMC) of eastern Serbia.
- Related magmatic rocks host significant porphyry-high sulphidation mineralisation to the southeast in Bulgaria (e.g., the Elatsite and Chelopech deposits of the Srednogorie district), and across the Danube river to the north of Majdanpek in Romania.
- The 86 to 83 Ma igneous rocks of the TMC show evidence for crustal contamination and are related to an eastward dipping continental subduction zone located to the west.
- Mineralisation, which has been dated at 83 Ma, is associated with sparse, narrow north-south trending, sub-volcanic andesitic dykes intruding a north-south fracture zone cutting Proterozoic and Palaeozoic metamorphic rocks and inliers of Jurassic limestone.
- Mineralisation is developed as stockworks, and disseminations, and as skarns and replacement bodies flanking the intrusives.
- The highest copper grades are found in zones of K silicate and silica alteration.
- The Majdanpek deposit has low Mo, contains PGE and has a Cu%:Au g/t ratio of around 2:1. Significant supergene upgrading is recorded over parts of the deposit.
- Numerous porphyry and high sulphidation prospects define a 20 km-wide corridor within the TMC, running for 40 km from Majdanpek in the north to Bor in the south.

## References

- Aleksic, D., 1969 - Results of two years of exploration at Veliki Krivelj (Rezultati dvogodisnjeg istrazivanja u Velikom Krivelju) *Zb. rad. Rud. met. fak. Inst., Bor*, za bakar IX, pp. 27-40 (in Serbian).
- Aleksic, D., 1979 - The deposit Veliki Krivelj - Guide for Field Excursion, *Int. Conf. of European Copper Deposits*, RTB Bor, Bor, pp. 39-51.
- Andric, B., Antonijevic, I., Grubic, A., Dragasevic, T., Djordjevic, M., and Terzic, M., 1972 - Analiza Geoloska grade Timockog Sinklorijum u svertosti novih geoloskih istrazivnja. III Savetovanje o istrazivnja bakrove mineralizacije na teritriji SFRJ, RTB, Bor.
- Banjesevic, M., Cocic, S. and Radovic, M., 2002 - Petrographic-Geochemical characters and K-Ar ages of late Cretaceous volcanic rocks in the Bor Zone part of the Timok Magmatic Complex (Eastern Serbia). *Rev Roum. Geologie*. v. 46, pp. 47-59.
- Banjesevic, M., Cvetkovic, D., Kozelj, D., Peytcheva, I. and von Quadt, A., 2002 - The Timok magmatic complex and Ridanj-Krepoljin Zone: Geodynamic Evolution; in *Geology and Metallogeny of Copper and Gold Deposits in the Bor Metallogenic Zone*, Conference; Abstracts Bor 100 years, 2002.
- Berza, T., Constantinescu, E. and Vlad, S.N., 1998 - Upper Cretaceous magmatic series and associated mineralisation in the Carpatho-Balkan Orogen. *Resource Geology*, v. 48, pp. 291-306.
- Bonev, I.K., Kerestedjian, T., Atanassova, R. and Andrew, C.J., 2002 - Morphogenesis and composition of native gold in the Chelopech volcanic-hosted Au-Cu epithermal deposit, Srednogie zone, Bulgaria; *Mineralium Deposita*, v. 37, pp 614-629.
- Breithaupt, J.F.A., 1861 - Timazit, eine neue Gesteinart, und Gamsigradit, ein neuer Amphibol. *Berg-und-Hüttenmännische Zeitung*. Freiberg, Leipzig. v. 20, pp. 51-54.
- Ciobanu, C.L., Cook, N.J. and Stein, H., 2002 - Regional setting and geochronology of the Late Cretaceous Banatitic Magmatic and Metallogenetic Belt. *Mineralium Deposita*, v. 37, pp. 541-567.
- Cioflica, G. and Vlad, S., 1984 - Alpine metallogeny in Romania. *An Inst Geol, Geofiz*, Bucharest, v. LXIV, pp. 174-175.
- Clark, A.H. and Ullrich, T.D., 2004 -  $^{40}\text{Ar}$ - $^{39}\text{Ar}$  age data for andesitic magmatism and hydrothermal activity in the Timok Massif, eastern Serbia: Implications for metallogenic relationships in the Bor copper-gold subprovince; *Mineralium Deposita*, v. 39, pp. 256-262.
- Cocic, S., Jelenkovic, R.J. and Zivkovic, P., 2002 - Excursion Guide: Symposia Bor 100 years 24-25 October 2002, Bor, Serbia, ISBN 86-84265-00-9.
- Djordjevic, M. and Banjesevic, M., 1997 - Geology of the southern part of the Timok Magmatic Complex. Booklet and Geological Map 1:50 000, *Federal Ministry of Economy*, Belgrade, (in Serbian).
- Djordjevic, M. and Banjesevic, M., 1998 - Development of the Cretaceous volcanism in the Timok-Srednja Gora belt southwardly from the Bor Mine (Eastern Serbia), *Carpathian-Balkan Geological Association XVI Congress - Abstracts Vienna*, Austria, p. 132.
- Drovenik, M., 1960 - Geolosko-petroloska studija sire okoline rudnika Bor / Istocna Srbija/, Doktorska disertacija, Fond strucnih dokumentacija RTB Bor, Bor.
- Drovenik, M., Antonijevic I. and Mici, I. 1962 - Novi pogledni na magmatiza I geolosku gradju Timocke eruptivne oblasti. *Vesnik Geozavoda*, Ser. A. Knj. XX, Beograd, pp. 67-79.
- Heinrich, C.A. and Neubauer, F. 2002 - Cu-Au-Pb-Zn-Ag metallogeny of the Alpine-Balkan-Carpathian-Dinaride geodynamic province, *Mineralium Deposita*, v. 37, pp. 533-540.
- Herrington, R.J., Jankovic, S.R. and Kozelj, D.I., 1988 - The Bor and Majdanpek copper-gold deposits in the context of the Bor Metallogenic Zone (Serbia, Yugoslavia): in Porter, T.M., (Ed.), *Porphyry and Hydrothermal Copper and Gold Deposits - A Global Perspective*, PGC Publishing, Adelaide, pp. 185-194.
- Herrington, R.J., First, D.M. and Kozelj, D.I., 2003 - Copper porphyry deposits of Hungary, Serbia, Macedonia, Romania and Bulgaria. in *Europe's Major Base Metal Deposits*. *Irish Association for Economic Geology*, Dublin, pp. 303-322.
- Jankovic, S., Terzic, M., Aleksic, D., Karamata, S., Spasov, T., Jovanovic, M., Milicic, M., Miskovic, V., Grubic, A. and Antonijevic, I., 1980 - Metallogenic features of copper deposits in the volcano-intrusive complexes of the Bor district, Yugoslavia; in Jankovic, S. and Sillitoe, R., (Eds.), *European Copper Deposits*, SGA Special Publication 1 and *Department of Economic Geology, Faculty of Mining and Geology*, Belgrade University, pp. 42-49.
- Jankovic, S.R., 1982 - Yugoslavia; in Dunning, F.W., Mykura, W. and Slater, D., 1982 - *Mineral Deposits of Europe*, v. 2 Southeast Europe, *The IMM, and The Mineralogical Society*, London, pp. 143-202.
- Jankovic, S.R., 1990 - Types of ore deposits related to volcanic environments in the Bor district, Yugoslavia. *Geologische Rundschau*, v. 79, pp. 456-478.
- Jankovic, S.R., 1990b - Ore deposits of Serbia: Regional metallogenic settings and types of deposit. *Rud. Geol. Fak.* Beograd, 760p.
- Jankovic, S.R., Jelenkovic, R.J. and Kozelj, D., 2002 - The Bor Copper and Gold Deposit, Mining & Smelting Basin Bor and the Copper Institute Bor, Bor, Serbia ISBN 86-84265-01-7.
- Jelenkovic, R.J. and Kozelj, D.I., 2002 - Morphogenetical types of porphyry copper mineralisation in the Bor Metallogenic Zone; in *Geology and Metallogeny of Copper and Gold Deposits in the Bor Metallogenic Zone*, Conference Abstracts, Bor 100 years, 2002; pp. 29-56.

- Jovanovic, M., 1974 - Porphyry copper deposits of the Dumitru Potok - Valja Strz area (Porofiska rudista bakra u reonu Dumitru Potok - Valja Strz), Mag. Thesis, *Faculty of Mining and Geology, Belgrade University*, pp. 143-202.
- Karamata, S., Knezevic-Djordjevic, V. and Milovanovic, 2002 - A review of the evolution of upper Cretaceous-Paleogene magmatism in the Timok Magmatic Complex and the associated mineralization; in *Geology and Metallogeny of Copper and Gold Deposits in the Bor Metallogenic Zone*, Conference Abstracts, Bor 100 years, 2002; pp. 15-28.
- Karamata, S., Knezevic, V., Pécskay, Z. and Djordjevic, M., 1997 - Magmatism and metallogeny of the Ridanj-Krepoljin belt (eastern Serbia) and their correlation with northern and eastern analogues. *Mineralium Deposita*, v. 32, pp 452-458.
- Kozelj, D., 2002a - Epithermal Gold Mineralization in the Bor Metallogenic Zone. *Pub of The Copper Institute, RTB Bor, Bor*, (in Serbian with English Summary).
- Kozelj, D., 2002b - Morphogenetical types of epithermal gold mineralization in the Bor Metallogenic Zone; in *Geology and Metallogeny of Copper and Gold Deposits in the Bor Metallogenic Zone*, Conference Abstracts, Bor 100 years, 2002; pp. 57-70.
- Lips, A.L.W., 2002 - Correlating magmatic-hydrothermal ore deposit formation over time with geodynamic processes in SE Europe. in Blundel, D.J., Neubauer, F. and von Quadt, (Eds.) - *The Timing and Location of Major Ore Deposits in an Evolving Orogeny. Geological Society of London, Special Publication 204*, pp. 69-79.
- Lips, A., Herrington, R., Stein, G., Kozelj, D., Popov, K. and Wijbrans, J., 2004 - Refined timing of porphyry copper formation in the Serbian and Bulgarian portions of the Cretaceous Carpatho-Balkan Belt, *Economic Geology*, v. 99, pp. 601-609.
- Mitchell, A.H.G., 1996 - Distribution and Genesis of some epizonal Zn-Pb and Au provinces in the Carpathian-Balkan Region. *Trans. Inst. Min. Metall.* B105: pp. 127-138.
- Momcilovic, S., Zivkovic, P. and Krstic, S., 2002 - Geological characteristics of the ore body Dolovi-1 copper deposit Majdenpek; in *Geology and Metallogeny of Copper and Gold Deposits in the Bor Metallogenic Zone*, Conference Abstracts, Bor 100 years, 2002; pp. 181-187.
- Monthel, J., Vadala, P., Leistel, J.M. and Cottard, F., 2002 - Mineral deposits and mining districts of Serbia, compilation map and GIS databases; *Republic of Serbia, Ministry of Mining and Energy*; Publication BRGM/RC-51448-FR. Also available from <http://www.mineralinfo.org/Cartes/Serbie/serbie.htm>.
- Pécskay, Z., Djordjevic, M., Karamata, S. and Knezevic, V., 1992 - First Data on the age of the volcanic rocks from the Ridanj-Krepoljin zone. *Zapiski SGD*, zbor 24.12.1992. Beograd (In Serbian).
- Ralevic, B., Antonijevic, I. and Zivkovic, P., 1997 - Mineral Deposits of the Derdap Region, Serbia. International Symposium - *Geology in the Danube Gorges*, Yugoslavia and Romania. pp. 155-161.
- Richards, J.P., 2003 - Tecton-magmatic precursors for porphyry Cu-(Mo-Au) deposit formation. *Economic Geology*, v. 98, pp. 1515-1533.
- Strashimirov, S., Petrunov, R. and Kanazirski, M., 2002 - Porphyry-copper mineralisation in the central Srednogorie zone, Bulgaria; *Mineralium Deposita*, v. 37, pp. 587-598.
- Strashimirov, S. and Popov, P., (Eds.), 2000 - Geology and metallogeny of the Panagyurishte ore region (Srednogorie Zone, Bulgaria). Geodynamics and ore deposits evolution of the Alpine-Balkan-Carpathian-Dinaride Province. ABCD-GEODE Workshop, Borovets, Bulgaria, Guide to excursions *A and C. Publishing House*, St. Ivan Riliski, Sofia.
- Terzic, M., 1966 - Dimitru Potok - Valja Strz; in *Review of Detailed Exploration of the Timok Volcanic Massif (Dimitru Potok - Valja Strz; u Prikaz detaljnije istarzivanih zona u Timockom eruptivnom masivu) - Conference on the results of exploration of copper mineralisation on the territory of SFRJ; Bor*, pp. 1-29 (in Serbian)
- Tobey, E., Schneider, A., Alegria, A., Olcay, L., Perantonis, G. and Quiroga, J, 1998 - Skouries porphyry copper-gold deposit, Chalkidiki, Greece: Setting, mineralization and resources: in Porter, T.M., (Ed.), *Porphyry and Hydrothermal Copper and Gold Deposits - A Global Perspective, PGC Publishing*, Adelaide, pp. 175-184.
- Vlad, S (1984) Alpine porphyry copper occurrences in Romania. *Bull. Acad. Serbe. Sci. Arts*, LXXXIV, Class Sci Nat Math, v. 25, pp. 111-127.
- Von Quadt, A., Peytcheva, L., Cvetkovic, D. and Banjesevic, M., 2002 - Geochronology, geochemistry, and isotope tracing of the Cretaceous magmatism of East-Serbia and part of the Apuseni-Timok-Srednogorie metallogenic belt. *Geologica Carpathica*, v. 53, pp. 175-177 (Special Issue).
- Zivkovic, P. and Momcilovic, S., 2002 - Vertical distribution of gold and silver in different types of Cu-Au and polymetallic ore bodies of the North Revir Deposit Majdenpek; in *Geology and Metallogeny of Copper and Gold Deposits in the Bor Metallogenic Zone*, Conference Abstracts, Bor 100 years, 2002; pp. 173-180.

# THE PORPHYRY Cu-Au/Mo DEPOSITS OF CENTRAL EURASIA

## 1. TECTONIC, GEOLOGIC AND METALLOGENIC SETTING, AND SIGNIFICANT DEPOSITS

<sup>1</sup>Reimar Seltmann and <sup>2</sup>T. Mike Porter

<sup>1</sup>Centre for Russian and Central EurAsian Mineral Studies, Department of Mineralogy, Natural History Museum, London, UK.

<sup>2</sup>Porter GeoConsultancy Pty Ltd, Adelaide, South Australia

**Abstract** - Major porphyry Cu-Au and Cu-Mo deposits (e.g. *Oyu Tolgoi* in Mongolia - >2.3 Gt @ 1.16% Cu, 0.35 g/t Au and *Kal'makyr-Dalnee* in Uzbekistan - >5 Gt @ 0.5% Cu, 0.4 g/t Au) are distributed over an interval of almost 5000 km across central Eurasia, from the Urals Mountains in Russia in the west, to Inner Mongolia in north-eastern China, to the east. These deposits were formed during a range of magmatic episodes from the Ordovician to the Jurassic. They are associated with magmatic arcs within the extensive subduction-accretion complex of the Altaid and Transbaikal-Mongolian Orogenic Collages that developed from the late Neoproterozoic, through the Palaeozoic to the Jurassic intra-cratonic extension, predominantly on the palaeo-Tethys Ocean margin of the proto-Asian continent, but also associated with the closure of two rifted back-arc basins behind that ocean facing margin. The complex now comprises collages of fragments of sedimentary basins, island arcs, accretionary wedges and tectonically bounded terranes composed of Neoproterozoic to Cenozoic rocks.

The development of these collages commenced when slivers of an earlier Proterozoic subduction complex accreted to the palaeo-Tethys Ocean margin of the combined Eastern Europe and Siberian cratons were rifted from the main cratonic mass. These slivers were the contiguous Karakum and Altai-Tarim micro-continents, which became separated from the main cratonic mass by oceanic spreading that created the Khanty-Mansi back arc basin. Subduction of the palaeo-Tethys Ocean beneath these micro-continents and the adjacent back-arc basin produced the overlapping late Neoproterozoic to early Palaeozoic Tuva-Mongol and Kipchak magmatic arcs. Contemporaneous intra-oceanic subduction within the back-arc basin from the Late Ordovician produced the parallel Urals-Zharma magmatic arc, and separated the main Khanty-Mansi back-arc basin from the inboard Sakmara marginal sea. By the Late Devonian the Tuva-Mongol and Kipchak arcs had amalgamated to form the Kazakh-Mongol arc which extended over the whole palaeo-Tethys Ocean margin of the combined cratonic mass, while magmatic activity continued on the Urals-Zharma arc. During the mid Palaeozoic the two main cratonic components of the proto-Asian continent, the Siberian and Eastern European cratons, began to rotate relative to each other, "drawing-in" the two sets of parallel arcs to form the Kazakh Orocline between the two cratons. During the Late Devonian to Early Carboniferous, the Khanty-Mansi back-arc basin began subducting beneath the oroclinally infolded outer island arc mass to form the Valerianov-Beltau-Kurama arc. At the same time the palaeo-Pacific Ocean began subducting below the Siberian craton to form the Sayan-Transbaikal arc, which expanded by the Permian to become the Selanga-Gobi-Khanka arc which for a period was continuous with the Kazakh-Mongol arc. By the Mid to Late Permian, as the Kazakh Orocline had continued to develop, both the Sakmara and Khanty-Mansi back-arc basins had been closed and the collage of cratons and arcs were sutured by accretionary complexes. During the Permian and Triassic the North China craton approached and docked with the continent, closing the Mongol-Okhotsk sea (an embayment on the palaeo-Pacific margin) to form the Mongolian Orocline. Subduction and arc building activity on the palaeo-Pacific Ocean margin continued to the Mid Mesozoic as the Indo-Sinian and Yanshanian orogenic cycles.

Significant porphyry Cu-Au/Mo and Au-Cu deposits were formed during the: Ordovician in the Kipchak arc (e.g. *Bozshakol* Cu-Au in Kazakhstan and *Taldy Bulak* porphyry Cu-Au in Kyrgyzstan); Silurian to Devonian in the Kazakh-Mongol arc (e.g. *Nurkazgan* Cu-Au in Kazakhstan; *Taldy Bulak-Levoberezhny* Au in Kyrgyzstan); Devonian in the Urals-Zharma arc (e.g. *Yubileinoe* Au-Cu in Russia); Devonian in the Kazakh-Mongol arc (e.g. *Oyu Tolgoi* Cu-Au, and *Tsagaan Suvarga* Cu-Au, both in Mongolia); Carboniferous in the Kazakh-Mongol arc (e.g. *Kharmagtai* Au-Cu in Mongolia, *Tuvu-Yandong* Cu-Au in Xinjiang, China; *Koksai* Cu-Au, *Sayak skarn* Cu-Au, *Kounrad* Cu-Au and the *Aktogai Group* of Cu-Au deposits, all in Kazakhstan); Carboniferous in the Valerianov-Beltau-Kurama arc (e.g. *Kal'makyr-Dalnee* Cu-Au and *Kochbulak* epithermal Au, both in Uzbekistan; *Bengala* Cu-Au in Kazakhstan); Late Carboniferous to Permian in the Selanga-Gobi-Khanka arc (e.g. *Duobaoshan* Cu-Au in Inner Mongolia, China); Triassic in the Selanga-Gobi-Khanka arc (e.g. *Erdenet* Cu-Mo in Mongolia); and Jurassic in the Selanga-Gobi-Khanka arc (e.g. *Wunugetushan* Cu-Mo in Inner Mongolia, China).

In addition to the tectonic, geologic and metallogenic setting and distribution of porphyry Cu-Au/Mo mineralisation within central Eurasia, a description of the setting, geology, alteration and mineralisation recorded at each of the deposits listed above is included within this paper.



## Introduction

The Altaid tectonic collage (Sengör *et al.*, 1993; Sengör and Natalin, 1996; Yakubchuk, 2004), also known as the Central Asian Orogenic Belt (Jahn *et al.*, 2000), combined with the Transbaikali-Mongolian orogenic collage (Yakubchuk, 2002, 2005), stretch across central Eurasia for almost 5000 km. These combined collages are also known from the Russian literature as the Ural-Mongolian belt (*syn.* Central Asian fold belt in its Palaeozoic part) and Baikhalides (Zonenshain *et al.*, 1990; Mossakovskiy *et al.*, 1993). They extend (Fig. 1) from the Urals Mountains in Russia and Kazakhstan in the west (*syn.* Uralides; see Shatov *et al.*, 2003; Herrington *et al.*, 2005) through Kazakhstan, Uzbekistan, Tajikistan, Kyrgyzstan, Xinjiang in northwestern China, and parts of Mongolia (forming the Tien Shan Mineral Belt; see Windley *et al.*, 1990; Allen *et al.*, 1992; Jun *et al.*, 1998; Shayakubov *et al.*, 1999; Shatov *et al.*, 2001; Seltmann *et al.*, 2000, 2001; Mao *et al.*, 2003; and references therein) to Inner Mongolia in northeastern China and the adjacent regions further to the

northeast (Jahn, 2004). They contain major porphyry Cu-Mo (e.g. Erdenet in Mongolia), Cu-Au (e.g. Oyu Tolgoi in Mongolia and Kal'makyr-Dalnee in Uzbekistan) and related epithermal gold ores, as well as some of the world's largest and richest orogenic gold accumulations (e.g. Muruntau in Uzbekistan). The same belt also embraces a variety of other mineralisation styles, including porphyry molybdenum and tungsten deposits, intrusion related tin, and volcanic, carbonate and sediment hosted base metals (Kudrin *et al.*, 1990; White *et al.*, 2001; Yakubchuk *et al.*, 2002, Seltmann *et al.*, 2004).

The porphyry Cu-Au/Mo and epithermal gold deposits are associated with magmatic arcs of the extensive Palaeozoic subduction-accretion complex that has subsequently been tectonically rearranged to form the Altaid and Transbaikali-Mongolian Orogenic Collages. This complex was progressively developed from the late Neoproterozoic, through the Palaeozoic to the early Mesozoic, predominantly on the Palaeo-Tethys Ocean margin of the proto-Asian continent, but also on the adjacent Palaeo-

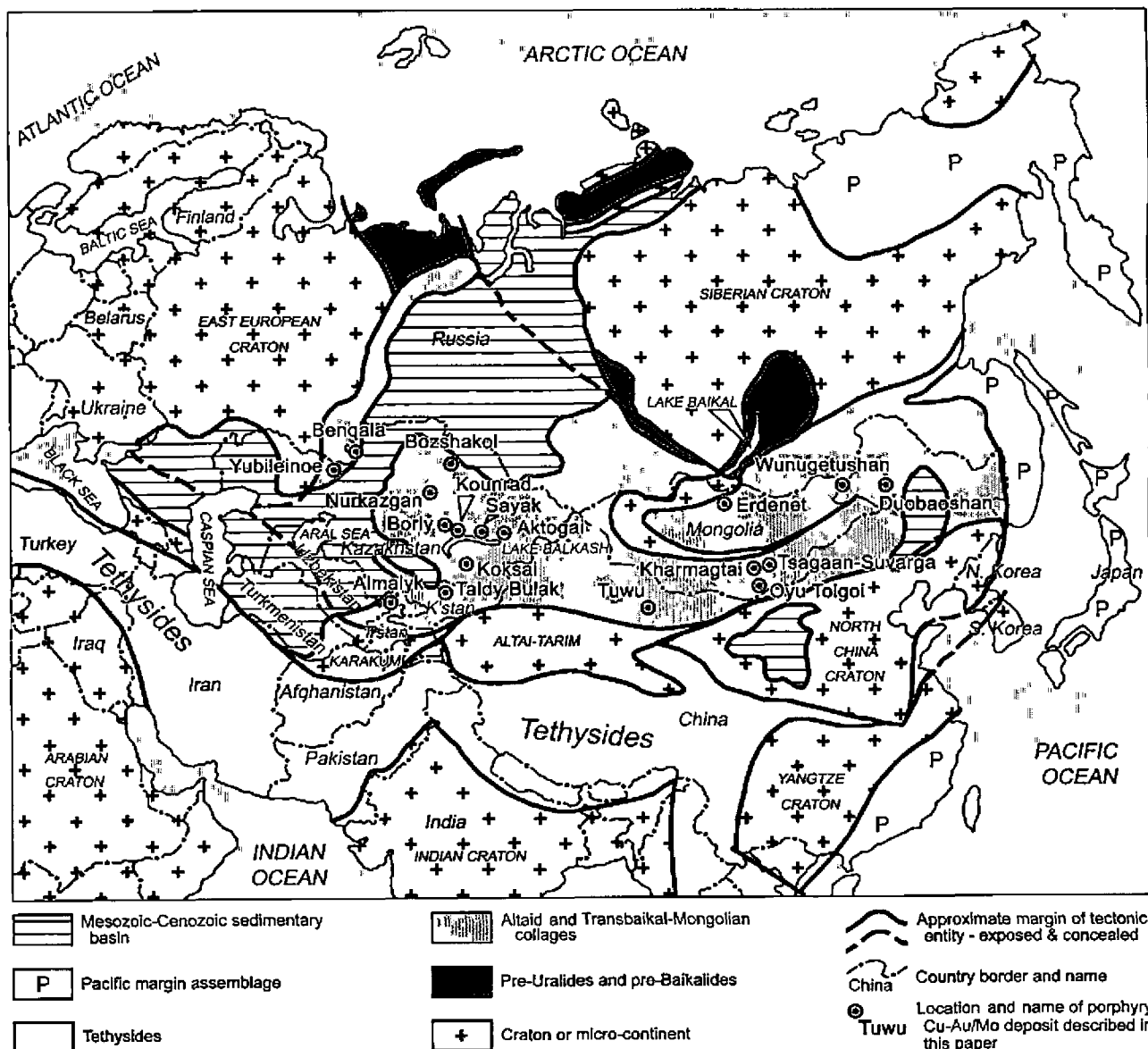


Figure 1: Location plan showing the tectonic elements of Eurasia and the porphyry Cu-Au/Mo deposits described in this paper. Note that T'stan = Tajikistan, K'stan = Kyrgyzstan. Tectonic subdivisions in part after Yakubchuk (2005) and a variety of other sources.

**Table 1: Tonnage, grade and age statistics of a selection of the more significant porphyry Cu-Au/Mo and related epithermal Au deposits of the Altai and Transbaikal-Mongolian Orogenic Collages in central Eurasia.** Refer to Fig. 1 for locations.

Deposit	Location	Tonnage	Grade		Contained Metal		Age
Bozshakol (a,b)	Kazakhstan	1.0 Gt	0.67% Cu		0.05 g/t Au	6.7 Mt Cu, 49 t Au	481 Ma
Andash (a)	Kyrgyzstan	n.a.	0.4% Cu		2.64 g/t Au	60 t Au	Ordovician
Taldy Bulak (a,b)	Kyrgyzstan	540 Mt	0.27% Cu		0.5 g/t Au	1.4 Mt Cu, 270 t Au	Ordovician
Nurkazgan (a)	Kazakhstan	na	1 to 3% Cu		0.4 to 1 g/t Au	1.5 Mt Cu, 65 t Au	410 Ma
TB Lev. <sup>Meso-Porph</sup> (a,f)	Kyrgyzstan	18.7 Mt	0.2-0.3% Cu		6.9 g/t Au	129 t Au	Devonian
Yubileinoe (a)	Kazakhstan	~ 10 Mt	0.42% Cu		4 to 5 g/t Au	<0.05 Mt Cu, 45 t Au	~380 Ma
Oyu Tolgoi (c)	Mongolia	2.3 Gt	1.16% Cu		0.35 g/t Au	>27 Mt Cu, >810 t Au	370 Ma
Tsagaan Suvarga (b,e)	Mongolia	240 Mt	0.53% Cu	0.02% Mo	1.3 Mt Cu		325-365 Ma
Kharmagtai (c)	Mongolia	n.a.	0.5 to 0.8% Cu		0.7 to 1.25 g/t Au	n.a.	~330 Ma
Tuwu-Yandong (g)	China, (Xin)	n.a.	~0.7% Cu		~0.15 g/t Au	7 Mt Cu	330 Ma
Koksai (a,b)	Kazakhstan	320 Mt	0.52% Cu		0.12 g/t Au	1.6 Mt Cu, 37 t Au	Carbonif
Sayak <sup>Sk</sup> (a)	Kazakhstan	55 Mt	1.1-3.2% Cu		0.2-2.1 g/t Au	1 Mt Cu, 30 t Au	330 Ma
Kounrad (a,b)	Kazakhstan	>800 Mt	0.62% Cu		0.1-0.76 g/t Au	5 Mt Cu, 600 t Au	330 Ma
Aktogai Group (a)	Kazakhstan						~320 Ma
Aktogai (a,b)		1.5 Gt	0.39% Cu		0.01% Mo, 0.03 g/t Au	6 Mt Cu, 45 t Au	
Aidarly (a,b)		1.1 Gt	0.38% Cu		0.01% Mo, 0.013 g/t Au	4.2 Mt Cu, 14 t Au	
Benqala (a)	Kazakhstan	~100 Mt	0.42-0.55% Cu		0.3 g/t Au	30 t Au	Carbonif.
Kalmakyr-Dalnee(a)	Uzbekistan	> 5 Gt	0.47-0.51% Cu		0.35 - 0.6 g/t Au	>21 Mt Cu, >2650 t Au	~315 Ma
Kochbulak <sup>Ep<sup>th</sup></sup> (a)	Uzbekistan	~11 Mt	-		12 g/t Au	135 t Au	280-290 Ma
Kyzylalma <sup>Ep<sup>th</sup></sup> (a)	Uzbekistan	~20 Mt	1.62% Cu		8 g/t Au	165 t Au	280-290 Ma
Duobaoshan (b)	China, (I.M.)	508 Mt	0.47% Cu		0.14 g/t Au	2.4 Mt Cu, 70 t Au	292 Ma
Tongshan (b)	China, (I.M.)	180 Mt	0.47% Cu	0.023% Mo	0.8 Mt Cu, 0.04 Mt Mo		~290 Ma ?
Erdenet (d,e)	Mongolia	1.78 Gt	0.62% Cu		0.025% Mo	11 Mt Cu, 0.45 Mt Mo	240 Ma
Wunugetushan (b)	China, (I.M.)	495 Mt	0.45% Cu		0.09% Mo	2.2 Mt Cu, 0.45 Mt Mo	188-182 Ma

Abbreviations: Gt = billion tonnes; Mt = million tonnes; t = tonnes; <sup>Sk</sup> = skarn; <sup>Ep<sup>th</sup></sup> = epithermal; <sup>Meso-Porph</sup> = mesothermal to porphyry Au; Carbonif. = Carboniferous; Xin = Xinjiang; I.M. = Inner Mongolia; TB Lev. = Taldy Bulak Levoberezhny; n.a. = not available.

Source: (a) Seltmann *et al.*, (2004) and references cited therein; (b) Mutschler *et al.*, (2000) and references cited therein; (c) Ivanhoe Mines, (2005); (d) Gerel & Munkhtsengel, (2005); (e) Watanabe & Stein, (2000); (f) Central Asia Gold, (2005); (g) Han, (2003).

Pacific margin and associated with the closure of rifted back-arc basins behind the ocean facing margins. Porphyry style ores were emplaced from Ordovician times to the Jurassic, although the most prolific interval of ore deposition, including the largest deposits, was during the Late Devonian and Early Carboniferous (Yakubchuk *et al.*, 2002).

By the early Mesozoic, subduction on the Palaeo-Pacific Ocean margin had become more significant, accompanied by the collision of the North China and Yangtze cratons, with late Permian and Triassic porphyry deposits being emplaced in what is now eastern China and Mongolia. Following the closure of the Tethys Ocean and the Indo-Asian collision during the Cenozoic, activity within the main Altai Orogenic Collage was restricted to uplift associated with the ongoing Himalayan Orogeny (Yakubchuk *et al.*, 2002).

Table 1 lists tonnage, grade and age details of a selection of representative porphyry and epithermal deposits within the Altai and Transbaikal-Mongolian Orogenic Collages. The emplacement location of each of these deposits is shown on Fig. 1 and the palinspastic reconstruction of central Eurasia on Fig. 3. The geology and mineralisation of most of the porphyry deposits in Table 1 are summarised

later in this paper, while one of the largest, Kal'makyr-Dalnee is the subject of part 2 by Golovanov *et al.*, (2005, this volume).

While this paper is primarily concerned with porphyry style mineralisation, mention is also made of some representative epithermal gold deposits found in proximity, and possibly related to, major porphyry deposits. It is now generally appreciated that in many cases within magmatic arcs, there is a close relationship between the development of porphyry-style Cu/Au and measurably younger epithermal Au deposits. Porphyry-style mineralisation forms at depths of 1 to 2 km under conditions of confinement (Richards, 2005, this volume), while epithermal gold is precipitated at shallower, near surface levels, when the system is subsequently allowed to vent to the surface (Corbett, 2004). As such, the epithermal deposit may be seen as a late phase of the same hydrothermal system that formed porphyry style mineralisation. In many magmatic arcs, epithermal gold deposits are telescoped onto either economic porphyry Cu/Au systems (e.g. Lepanto-Far Southeast in the Philippines; Hedenquest *et al.*, 1998) or incipient porphyry systems (e.g. Lihir in Papua New Guinea; Kidd and Robinson, 2004) which were developed at greater depths and at an earlier stage in the development of an intrusion related hydrothermal system.

The main focus of this review paper is on the tectonic, geologic and metallogenic setting, and the occurrence of porphyry Cu deposits with accompanying gold or molybdenum within central Eurasia. It summarises the palinspastic reconstruction and tectonic history of the Altaid and Transbaikal-Mongolian Orogenic Collages, from eastern Europe to the Pacific coast, and the temporal and spatial distribution of porphyry Cu-Au/Mo both within these collages. There is also a description of the geology, alteration and mineralisation of each of the key deposits in the region.

### Tectonic Architecture

The Altaid and Transbaikal-Mongolian Orogenic Collages, as currently mapped, are made up of fragments of sedimentary basins, island arcs, accretionary wedges and tectonically bounded terranes composed of Neoproterozoic

to Cenozoic rocks (Fig. 2). These collages are the product of a complex sequence of processes resulting from subduction, collision, transcurrent movement and continuing tectonism over the interval from the mid Neoproterozoic to the present. The pattern was further complicated by the late overprint of the Alpine-Himalayan deformation related to Indo-Asian collision between Gondwana and Asia (Yakubchuk *et al.*, 2002).

Fig. 3 is a palinspastic reconstruction of central Eurasia, updated from Yakubchuk *et al.*, (2002) and Seltmann *et al.*, (2004). It illustrates an interpretation of the evolution of the Palaeozoic subduction-accretion complex on the Palaeo-Tethys Ocean margin of the proto-Asian continent from the late Neoproterozoic to the end of the Permian. Yakubchuk *et al.*, (2002) postulate that the collage represents three sub-parallel island arcs, the late Neoproterozoic (Vendian) to early Palaeozoic Tuva-

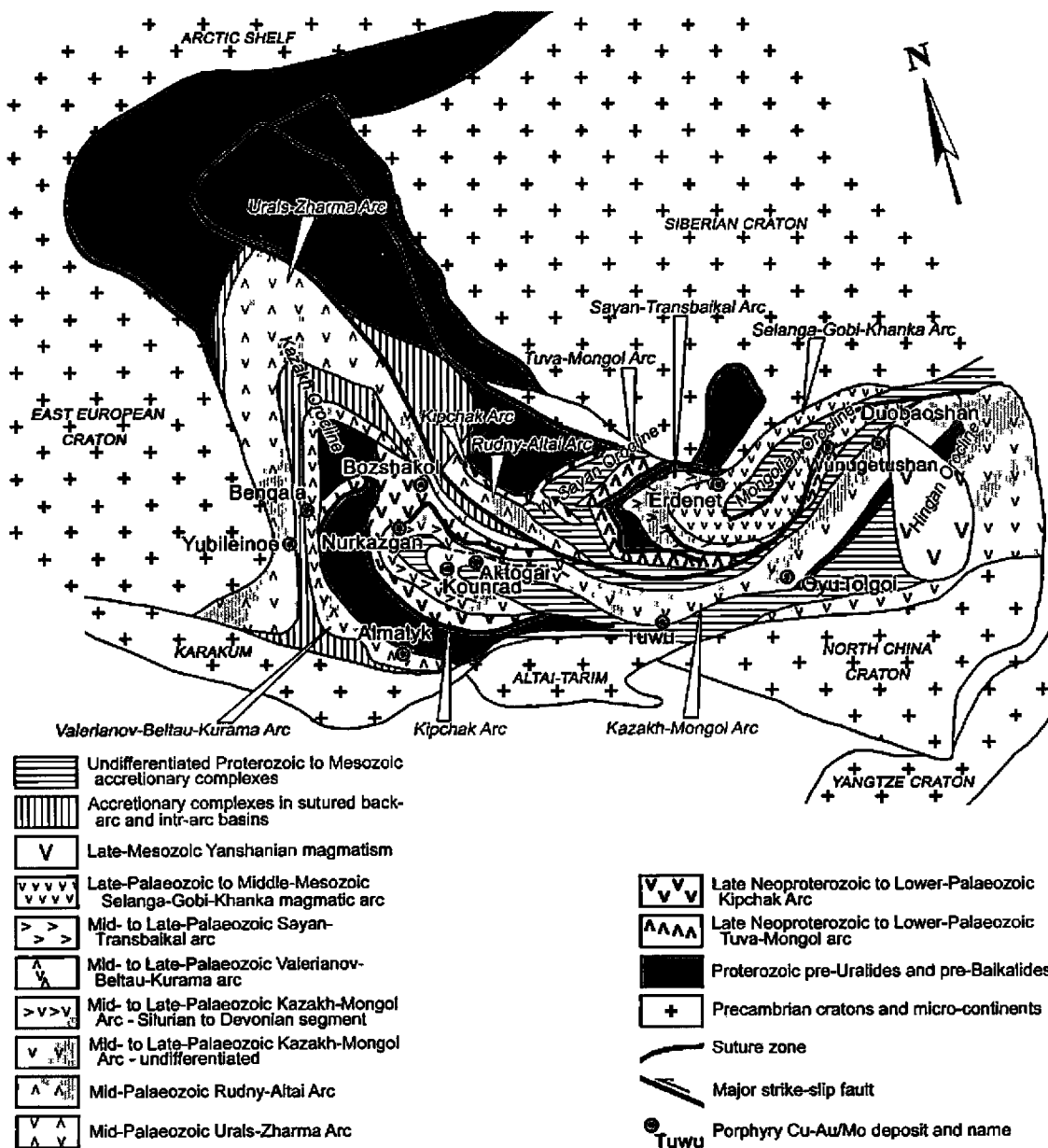


Figure 2: Simplified tectonic map of the Altaid and Transbaikal-Mongolian Orogenic Collages in central Eurasia, showing the location of selected porphyry Cu-Au/Mo deposits, after removal of Mesozoic-Cenozoic basins and superficial cover. See Fig. 1 also for additional deposits and Fig. 3 for a palinspastic reconstruction of the sequence of tectonic events that produced this configuration. Modified after Yakubchuk (2005) and Seltmann *et al.*, (2004).

Mongol, Kipchak and Urals-Zharma (also known as the Mugodzhar-Rudny Altai) arcs. Each is separated by accretionary complexes formed during the subduction of the oceanic crust of the main Palaeo-Tethys Ocean and two principal back-arc basins - the Khanty-Mansi back-arc basin and the Sakmara marginal sea. These elements are followed by continued activity on the Urals-Zharma arc and by the younger Kazakh-Mongol and Valerianov-Beltau-Kurama arcs, developed in the middle Palaeozoic to early Carboniferous and early Carboniferous to Permian respectively. These younger arcs were related to continued subduction of the Palaeo-Tethys Ocean and the oceanic crust of the Khanty-Mansi and Sakmara back-arc basins. By the late Permian, both of the back basins were closed and sutured with the development of substantial accretionary wedges separating the sequences representing those magmatic arcs (Yakubchuk *et al.*, 2002; Seltmann *et al.*, 2004).

The development of the collages was further complicated by the relative rotation of the two main building blocks of the proto-Asian continent, the Siberian and Eastern European cratons. The clockwise rotation of the Siberian craton relative to Eastern Europe produced the oroclinal bending of the tectonic framework evident during the late Palaeozoic on Fig. 3, resulting in the Kazakh Orocline, now located between the two cratonic blocks (Yakubchuk *et al.*, 2002).

The tectonic history of the region may be summarized as follows, mainly after Yakubchuk *et al.*, 2002; Seltmann *et al.*, 2004, and references cited therein, except where otherwise noted.

#### **Archaean to Early Neoproterozoic**

Archaean to Palaeoproterozoic crystalline basement occurs both within the Eastern Europe and Siberian cratons, the Arctic Shelf flooring part of the current Arctic Ocean (but originally connected the two cratons), and in several elongate, tectonically bounded terranes within the Alaid Orogenic Collage, e.g. the Altai-Tarim and Karakum microcontinents (see Fig. 3). The crystalline suites within these latter terranes have been dated at 2800 to 1780 Ma (Pb-Pb and U-Pb) and comprise crystalline gneisses, schists and amphibolites, with rare marble and quartzite. These terranes are believed to represent slivers rifted from the larger cratons and subsequently accreted during the Palaeozoic. They are overlain by poorly age constrained Mesoproterozoic sequences of shallow-marine carbonates and terrigenous rocks which have been variably metamorphosed to sub-greenschist, up to amphibolite facies.

The most extensive Precambrian sequences were deposited during the Neoproterozoic when the Eastern Europe and Siberian cratons were part of the super-continent Rodinia. During the Vendian (650 to 570 Ma) subdivision of the late Neoproterozoic, a single orogen occupied the active flank of Rodinia. This orogen was represented by the post 1100 Ma Baikhalides and 800 to 550 Ma pre-Uralides, subsequently dismembered and dispersed as tectonic slivers throughout the region. This Vendian orogen was the result of collision and suturing of Neoproterozoic back-arc basins,

and was flanked on its ocean-ward margin by the Precambrian Karakum and Altai-Tarim microcontinents and the Precambrian slivers of Kazakhstan. All have subsequently served as basement for Palaeozoic magmatic arcs facing the palaeo-Tethys Ocean. At the same time, the Tuva-Mongol magmatic arc separated the proto-Pacific and proto-Tethys oceans, developed over Precambrian basement slivers (Fig. 3).

#### **Late Neoproterozoic to Middle Ordovician**

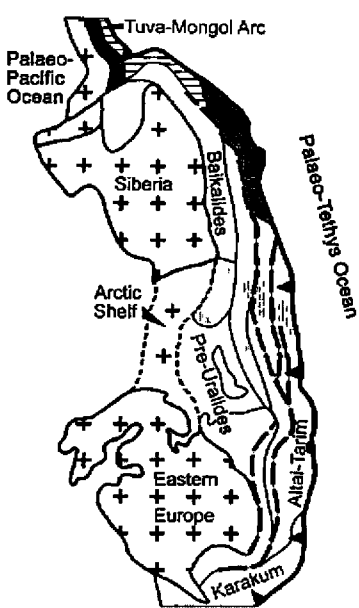
During the latest Neoproterozoic, the orogen flanking the active margin of Rodinia was subjected to subduction related processes which initiated back-arc rifting along a number of incipient spreading centres. The succeeding back-arc spreading led to the formation of the broad Khanty-Mansi back-arc basin, separating the combined Eastern Europe and Siberian cratons from the interpreted contemporaneous subduction on the active margin that was building the Kipchak magmatic arc. This back-arc spreading also resulted in the Karakum and Altai-Tarim microcontinents and other Precambrian slivers being separated from the main Baikhalide and pre-Uralide elements, and becoming the basement for the southern continuation of the Kipchak arc (Yakubchuk *et al.*, 2002; Seltmann *et al.*, 2004). Magmatic activity continued on the Tuva-Mongol arc, contemporaneously with the Kipchak arc, although the latter was developed behind the former at their overlap (Yakubchuk, 2005). However, while Kipchak Arc volcanism is evident, particularly in Kazakhstan, the arc may not have been as extensive as shown on Fig. 3.

During the early Palaeozoic, as a result of spreading between Siberia and Laurentia, the Siberian craton commenced a clockwise rotation relative to the Eastern Europe craton. This in turn led to intra-arc spreading within segments of the Kipchak arc (Fig. 3 - Middle Ordovician) and the development of a strike slip faulting pattern longitudinally compressing the Kipchak arc. Continued rotation (clockwise of Siberia and anti-clockwise of Eastern Europe) caused the closure of the intra-arc basins of the Kipchak arc, and then its segmentation (Fig. 3 - Late Ordovician) (Yakubchuk *et al.*, 2002).

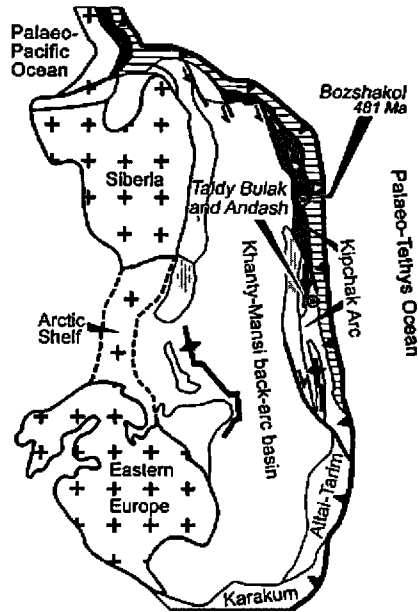
#### **Late Ordovician to Late Devonian**

By the Late Ordovician, continuing spreading of the Khanty-Mansi back-arc basin had produced a wide back-arc sea. At this stage, a new intra-oceanic subduction zone was initiated, forming the new Urals-Zharma (or Mugodzhar-Rudny Altai) magmatic arc which split the broad back arc sea into the Khanty-Mansi and Sakmara basins, both of which had continuing active spreading centres (Fig. 3). The polarity of the magmatic arc is a subject of discussion, although it is currently thought to relate to 'east-directed' subduction of Sakmara basin oceanic crust below the Khanty-Mansi basin (Yakubchuk *et al.*, 2002).

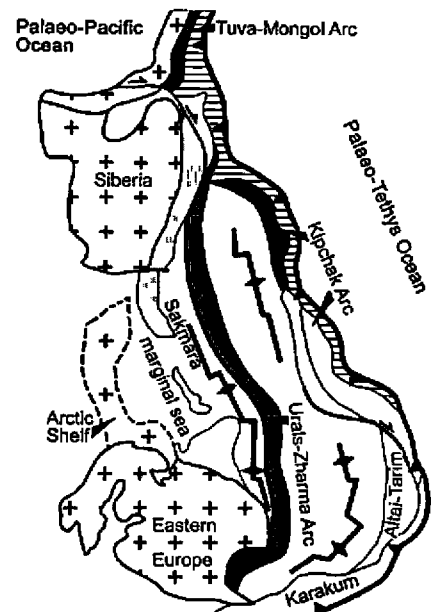
Continued relative rotation of the East Europe and Siberian cratons resulted in the commencement of oroclinal bending of the Kipchak and Urals-Zharma arcs. With oroclinal bending, the subduction zone responsible for the Urals-Zharma arc split, with opposite polarities in the north and



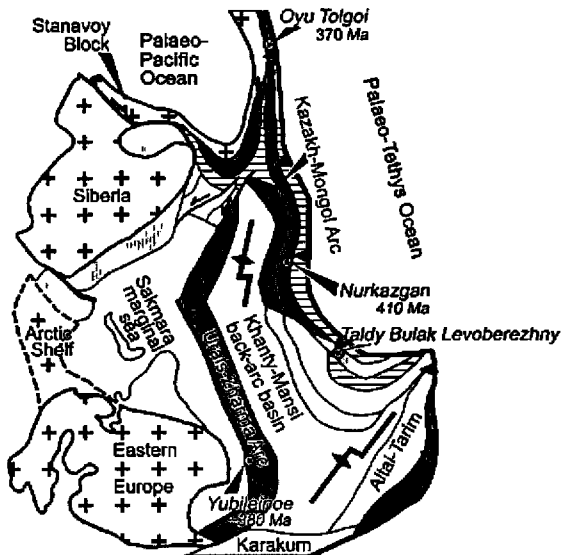
Late Neoproterozoic, 630 to 540 Ma



Middle Ordovician, 460 Ma



Late Ordovician, 450 Ma

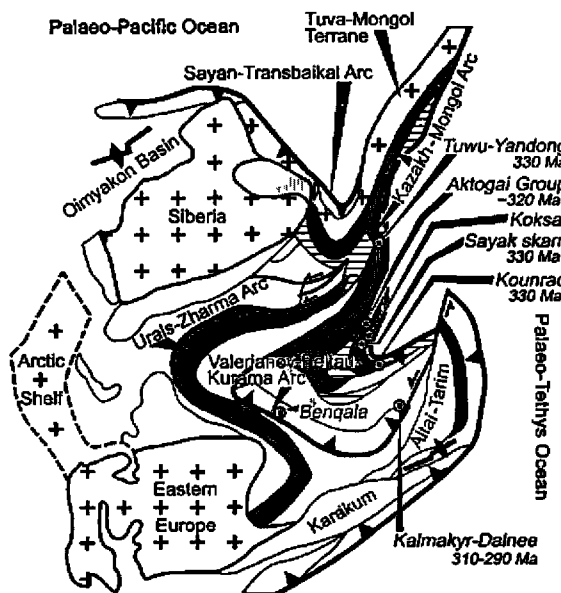


Late Devonian, 360 Ma

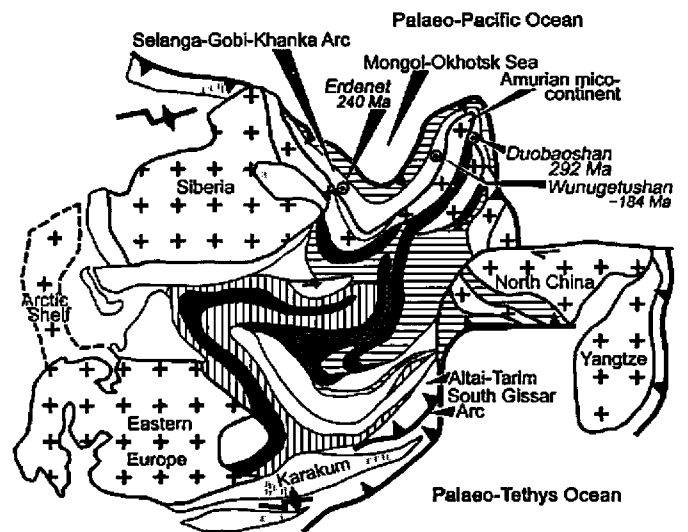
**Kounrad**  
● 330 Ma  
Major porphyry Cu-Au or Cu-Mo deposit  
Location, name and age of emplacement



- Strike-slip faulting
- Focus of future back-arc rifting
- Spreading centre
- Subduction zone
- Accretionary complex - in sutured back-arc and intra-arc basins
- Growing accretionary complex
- Ensialic arc segment
- Ensimatic arc segment
- Precambrian craton



Early Carboniferous, 340 Ma



Late Permian, 225 Ma

south (Fig. 3). At the same time, the Kipchak magmatic arc front was migrating to the southeast (and ocean-ward), into the growing subduction-accretionary complex. The strike slip faulting that accommodated the rotation and oroclinal development and disrupted the arc, also resulted in the amalgamation of the Kipchak and Tuva-Mongol arcs into the single, continuous Kazakh-Mongol arc. By the Late-Devonian, a substantial accretionary complex had formed in front of this new composite arc).

The Rudny-Altai arc, which is juxtaposed across the continental scale Late Permian to Triassic Trans-Eurasian strike-slip fault with the eastern section of the Urals-Zharma arc (Fig. 2) is now regarded as a fault offset of the Kazakh-Mongol Arc (Yakubchuk, 2005).

Towards the end of the Middle Palaeozoic, subduction was initiated on the margin of the palaeo-Pacific Ocean with the Siberian Craton and parts of the adjacent Tuva-Mongol terrane to produce calc-alkaline volcanic rocks of the Sayan-Transbaikal arc (Figs. 2 and 3).

#### *Carboniferous to Mesozoic*

Oroclinal bending persisted into the Early to Middle Carboniferous as the cratons continued to rotate. This activity was accompanied by further southeastward migration of the subduction-related magmatism of the Kazakh-Mongol arc. Subduction continued below the Urals-Zharma arc, closing the Sakmara basin, while a new east-directed subduction zone was activated during the Late Devonian, consuming oceanic crust of the Khanty-Mansi back-arc basin below the extinct Kipchak arc to form the Valerianov-Beltau-Kurama arc. During the Middle- to Late-Carboniferous, subduction had closed both back-arc basins, the Urals-Zharma arc had collided with both of the cratons and with the Kazakh-Mongol arc. These closures resulted in extensive suture zones occupied by the development of substantial accretionary complexes (Yakubchuk *et al.*, 2002).

During the Permian, oroclinal bending and suturing of back-arc basins continued in the west of the Palaeozoic orogenic collage that is known as the Altaids. The main orocline that had developed between the Siberian and East Europe cratons is known as the Kazakh Orocline. Arc development was now concentrated on the Palaeo-Tethyan margin to the east, and on the Palaeo-Pacific margin which had commenced during the Carboniferous (Yakubchuk *et al.*, 2002).

Compression on the Palaeo-Tethys ocean margin led to the obduction of ophiolite complexes over the Precambrian Karakum and Altai-Tarim micro-continents and the accompanying development of nappe structures, north-verging under-thrusting of the Karakum and Altai-Tarim micro-continents below the Valerian-Beltau-Kurama arc, and to closure of the small back-arc basin between the latter two micro-continents via the South Gissar subduction zone (Fig. 3 - Late Permian) (Yakubchuk *et al.*, 2002).

On the Palaeo-Pacific Ocean margin, the subduction that had produced the Sayan-Transbaikal arc had expanded to produce the 3000 km long Selanga-Gobi-Khanka magmatic arc (Figs. 2 and 3). This coincided with remnants of the elongate Tuva-Mongol arc and its basement (the Tuva-Mongol terrane of Fig. 3) being dislocated by strike slip folding and telescoped to form the composite Amurian micro-continent, separated from the Siberian craton by the gulf-like Mongol-Okhotsk sea which was open to the north into the Palaeo-Pacific ocean. The Amurian micro-continent was composed of Lower Palaeozoic back-arc, fore-arc and volcanic rocks of the Tuva-Mongol arc, slivers of Meso- to Neoproterozoic basement metamorphics, separated by intra-arc suture related accretionary wedge sequences which include Late Neoproterozoic (Vendian) to Early Cambrian ophiolites. All of these have been welded by voluminous Late Carboniferous to Permian granites (Yakubchuk, 2005; Zonenshain *et al.*, 1990).

The Selanga-Gobi-Khanka magmatic arc extended from the palaeo-northern margins of the Siberian craton, around the shore of the Mongol-Okhotsk sea to the palaeo-eastern margin of the Amurian micro-continent, to the North China craton. It briefly overlapped with the last stages of the Kazakh-Mongol arc, with which it was subsequently juxtaposed by strike-slip faulting. Magmatic activity on the Selanga-Gobi-Khanka magmatic arc continued to the Middle Jurassic, and although the majority of its volcanic sequences have been eroded, widespread granites of the arc's root zone reflect its extent (Fig. 2) (Yakubchuk, 2005).

From the Carboniferous, and into the Triassic, the Mongol-Okhotsk sea (bordering section of the Selanga-Gobi-Khanka magmatic arc) progressively closed from palaeo-south to north in a scissor like fashion, with the intervening oceanic crust being mainly subducted to the west, below the Siberian craton (Lamb and Cox, 1998; Watanabe and Stein, 2000; Zonenshain *et al.*, 1990). Collision between the Siberian craton and the Amurian micro-continent was not finalised until the late Triassic to early Jurassic (Zonenshain *et al.*, 1990). This closure was accompanied by the approach and collision of the North China craton from the palaeo-east in the Permian, and its rotation and amalgamation with the Amurian micro-continent during the Mesozoic as the latter was sandwiched between the North China and Siberian cratons (Yakubchuk *et al.*, 2002; Zonenshain *et al.*, 1990). The approach and collision of the North China craton corresponded to the Triassic Indo-Sinian orogeny in East Asia. Subduction was subsequently focussed along what is now the east coast of Asia and the transition to the Jurassic to Cretaceous Yanshanian orogeny in the region. The Yanshanian Orogeny resulted in the development of volcanic piles (Fig. 2) over the extinct Kazakh-Mongol and Selanga-Gobi-Khanka magmatic arcs (Yakubchuk, 2005).

A second major oroclinal structure was developed in what is now southeastern Siberia, Mongolia and northeast China,

Figure 3 (on facing page): *Palinspastic reconstruction of the Central Asian Orogenic Belt, showing selected major porphyry Cu-Au/Mo, related epithermal Au, and major orogenic Au deposits of the Tien Shan Mineral Belt.* Modified and updated after Yakubchuk *et al.*, (2002) and in Seltmann *et al.*, (2004).

occurring as a mega- 'S' shaped structure, incorporating the Mongolian and Hingan oroclines shown on Fig. 2. This structure was largely a response to compression during the Triassic to Mid Jurassic Indo-Sinian and Yanshanian orogenic cycles as the North China and Siberian cratons converged, sandwiching the Amurian micro-continent and closing the Mongol-Okhotsk sea (the latter forming the Mongol-Okhotsk Suture Zone - MOSZ), and by sinistral offset of hundreds of kilometres along the Late Permian to Triassic Trans-Eurasian strike-slip fault (Fig. 2) (Yakubchuk, 2005).

#### *Mesozoic to Cenozoic*

Following late Palaeozoic tectonism, the Mesozoic was largely characterised by uplift, particularly in the Kazakh Orocline, and by the development of large dextral strike-slip fault zones with offsets of up to 70 to 100 km (Yakubchuk 2005). This strike-slip faulting may in part represent reactivated Palaeozoic structure, although the bulk of the dislocation was during the late Jurassic and Cretaceous, with some continuing to the present. In Kazakhstan and central Asia, these faults largely strike to the northwest, swinging to east-west in northwestern China, to northeast to northerly in Mongolia and northeastern China where displacements of from 100 to 700 km are estimated. Movement is dextral on the northwest set to the west, and sinistral in the northeast conjugate set in the east. This activity has been largely attributed to the amalgamation of the North China and Yangtze cratons and by continued compression between the rotating and converging Siberian and East Europe cratons and corresponds with the Jurassic to Cretaceous Yanshanian orogeny mentioned previously.

Intra-cratonic basins formed within central Asia during the Mesozoic to Cenozoic extension in three stages, namely the Late Triassic to Middle Jurassic, Late Jurassic to Eocene and Oligocene to Quaternary. The boundaries of these basins were influenced by the strike-slip faulting described in the previous paragraph (Yakubchuk *et al.*, 2002).

In the late Cenozoic the area was affected by the Alpine-Himalayan orogeny associated with the progressive Indo-Eurasian collision as Gondwana approached and the Tethys Ocean was closed (Yakubchuk *et al.*, 2002).

### **Distribution of Porphyry Cu-Au/Mo and Au Deposits**

Within the Altai and Transbaikal-Mongolian Orogenic Collages of central Eurasia, porphyry Cu-Au/Mo and epithermal gold deposits have been emplaced in magmatic arcs ranging in age from Ordovician to early Mesozoic, and from the Urals Mountains in the west to northeast China in the east. The key settings, which except where otherwise cited, are summarised as follows from Seltmann *et al.*, 2004, and references cited therein.

#### *Kipchak and Tuva-Mongol Arcs*

The outboard Kipchak arc was developed marginal to the Palaeo-Tethys Ocean during the early Palaeozoic and is composed of segments with ensialic basement and others built on ensimatic precursors. Porphyry Cu and VHMS mineralisation were emplaced in ensimatic segments of the

arc, localised within intra-arc basins that developed in response to stresses imposed by the rotation of the Siberian craton during the middle Ordovician. The best example is the 481 Ma *Bozshakol* Cu-Au porphyry deposit – see Table 1 for size and grade statistics (Yakubchuk *et al.*, 2002; Mutschler *et al.*, 2000).

Early Palaeozoic (Caledonian - Ordovician to Silurian) porphyry Cu-Mo and Mo-Cu mineralisation is exploited in the Altai-Sayan region of Russia, on the limbs of the West Sayan Orocline, as shown on Fig. 2. The best example is the *Sorsk* Mo-Cu deposit, located 300 km southwest of Krasnoyarsk (Pokalov, 1977), where the head grade in 1992 was 0.051% Mo, 0.06% Cu. Other porphyry Cu-Mo deposits within the Altai Sayan region, and which Zvezdov *et al.*, (1993) attribute to the Tuva-Mongol Arc, include *Aksug* and *Kyzyk-Chadyr*.

#### *Urals-Zharma Arc*

The Urals-Zharma (previously known as the Mugodzhars-Rudny Altai) and Kipchak arcs were initially contemporaneous, although the former continued to develop after the cessation of activity on the Kipchak arc. The remnants of this extensive volcanic belt are exposed in the Urals Mountains on the current eastern flanks of the Eastern Europe craton, and on the western margin of the Siberian craton. The arc overlies subduction zones that consumed oceanic crust of both the Khanty-Mansi and Sakmara back-arc basins and is largely developed on ensimatic basement.

The arc is most notable for the large VHMS deposits it hosts in the Urals, although it also has associated porphyry Au mineralisation as at the ~380 Ma *Yubileinoe* porphyry Au deposit (Table 1) in Kazakhstan Urals, and igneous related orogenic gold deposits.

#### *Kazakh-Mongol Arc*

The middle to late Palaeozoic Kazakh-Mongol arc was developed over, and seaward of, the extinct Kipchak arc, also marginal to the Palaeo-Tethys Ocean. During its development the arc continued to migrate sea-ward, such that in places, as in southern Kazakhstan, there are two belts of volcanics, an earlier 'Devonian' and a younger Upper Palaeozoic 'Balkhash-Ili' zone which is a further 300 km toward the ocean. Both segments host gold rich porphyry and skarn mineralisation, although the former are more gold rich and smaller.

The most significant porphyry style deposit in the 'Devonian' Middle Palaeozoic segment of the arc is the Siluro-Devonian 410 Ma *Nurkazgan* Cu-Au deposit in Kazakhstan – (Table 1). The Middle Palaeozoic segment also hosts granite related gold deposits.

The Upper Palaeozoic 'Balkhash-Ili' zone contains a number of large tonnage porphyry deposits, including *Kounrad* (330 Ma), *Aktogai* (~320 Ma), *Aidarly* (~320 Ma), *Kyzilkia* (~320 Ma), *Koksai*, and the *Sayak skarn* (~320 Ma), all of which are in Kazakhstan (Table 1).

Further to the palaeo-north, still within the Kazakh-Mongol arc is the giant *Oyu Tolgoi* Cu-Au deposit in southern Mongolia, which has been dated at 372 to 370 Ma (Late-

Devonian). The Early-Carboniferous *Tsagaan Suvarga* Cu-Mo and *Kharmagtai* Au-Cu deposits in southern Mongolia, and *Tuwu-Yandong* Cu-Au in eastern Xinjiang, China (dated at 330 Ma), are also within the Kazakh-Mongol arc. The two former deposits are located just to the north of Oyu Tolgoi, while Tuwu-Yandong lies between this Mongolian cluster and the deposits in Kazakhstan described in the previous paragraph.

#### *Valerianov-Beltau-Kurama Arc*

This arc is currently concealed by thick younger cover over much of its length. It was developed above an ensialic basement on the western margin of the earlier and extinct Kipchak arc and was active through several magmatic episodes in the Devonian but predominantly in the Early to Middle Carboniferous. Subduction associated with this arc consumed the oceanic crust of the Khanty-Mansi back-arc basin. Magmatic activity and porphyry-style mineralisation were broadly contemporaneous with the 'Balkhash-Ili' zone of the Kazakh-Mongol arc to the east.

The arc hosts the giant 320 to 290 Ma *Kal'makyr-Dalnee* and the much smaller *Benqala* porphyry Cu-Au systems in Uzbekistan and Kazakhstan respectively (Table 1). In addition to these porphyry deposits, the Almalyk district which includes the *Kal'makyr-Dalnee* porphyry system, also embraces the *Kochbulak* and *Kyzylalma* volcanic associated epithermal/stockwork deposits, both of which have been dated at 290 to 280 Ma.

#### *Accretionary Complexes*

Two styles of accretionary complex have been described within the Altaid Orogenic Collage. The first of these is principally a growing complex, generally ocean facing related to magmatic arc development. The second is found in sutured back-arc and intra-arc basins and marks the final stages after arc-arc and arc-basement block collision.

No significant porphyry style deposits are found within the accretionary complexes of the sutured back-arc and intra-arc basins, although they do host large and giant, non-arc related orogenic gold deposits within fold and thrust belts. The most significant of these are found in Uzbekistan, Kyrgyzstan and Kazakhstan and include the 286 Ma *Muruntau*. Other major orogenic gold deposits in the region (Fig. 20) have been dated at ~270 to 260 Ma. These are believed to be temporally and spatially related to syntectonic granitoid intrusions into metamorphosed Proterozoic and Palaeozoic sediments.

#### *Pacific Margin*

Subduction on the margin of the Palaeo-Pacific ocean commenced during the Carboniferous and became more strongly established in the Permian and into the Mesozoic with the development first of the limited Sayan-Transbaikal and then of the extensive Selanga-Gobi-Khanka magmatic arc. Porphyry style mineralisation was developed along this margin during the Permian and into the Triassic, both on the edge of the Siberian craton as the Mongol-Okhotsk Sea (an embayment of the Palaeo-Pacific coast) progressively closed in a scissors like fashion, and on the Amurian micro-continent which had been constructed from

the telescoped Tuva-Mongol arc and associated terranes (Zonenshain *et al.*, 1990, Nie *et al.*, 2004).

The 292 Ma *Duobaoshan* Cu-Au and adjacent *Tongshan* Cu-Mo porphyry systems in Inner Mongolia, China, were emplaced during the waning stages of the Kazakh-Mongol arc, near its overlap with the Selanga-Gobi-Khanka arc on the Pacific margin. The 240 Ma *Erdenet* Cu-Mo deposit was formed in the Selanga-Gobi-Khanka magmatic arc on the northern limb of the Mongolian Orocline in Mongolia. A few hundred kilometres to the north of Erdenet, in the same arc in southern Siberia, Triassic porphyry stockwork (and related vein-type) Mo-W mineralisation is exploited in the *Dzhida ore field*.

The younger 184 Ma *Wunugetushan* Cu-Mo orebody in Inner Mongolia, China was emplaced during the closing stages of the Selanga-Gobi-Khanka magmatic arc on the southern arm of the Mongolian Orocline (Zonenshain *et al.*, 1990; Gerel *et al.*, 2005; Mutschler *et al.*, 2000; Qin *et al.*, 1997). Jurassic aged porphyry-style Mo mineralisation is mined at the *Zhireken* deposit (head grade 0.083% Mo in 1992) immediately to the north in southern Siberia. This deposit is part of the established Au-Mo district that includes the Baley-Taseyev epithermal gold district (Pokalov, 1977).

## Descriptions of Significant Porphyry Cu-Au/Mo Deposits

The following summaries describe selected examples of the porphyry Cu-Au/Mo deposits of central Eurasia, representing the different ages and styles of mineralisation encountered across the continent from the Urals Mountains in Russia to near the Pacific Ocean coast in northeast China.

#### *Bozshakol, Kazakhstan*

The Bozshakol porphyry Cu-Au deposit is located near the town of Eqibastuz in northeastern Kazakhstan, approximately 1000 km north of Almaty. A resource of >1 Gt @ 0.67% Cu, 0.05g/t Au has been published (Mutschler *et al.*, 2000) while the proven reserves have been quoted as 176.2 Mt @ 0.72% Cu, 0.014% Mo, 0.28 g/t Au (Kudryavtsev, 1996). The deposit was emplaced in an ensimatic segment of the Kipchak magmatic arc during the during the Late Cambrian to Early Ordovician at approximately 481 Ma.

#### *Geology*

The Bozshakol district straddles an east to ENE trending anticline, which is on the limb of a larger regional anticlinorium that deforms a sequence of predominantly Lower to Middle Cambrian volcanogenic rocks of calc-alkaline to sub-alkaline composition, typical of an island arc setting. Some 5 to 15 km to the south of the ore deposit, the core of the anticlinorium exposes underlying late Neoproterozoic (Vendian) to Cambrian rocks of an ophiolite association and Proterozoic metamorphics. The Cambrian volcanogenic rocks are cut by a progression of Cambrian to Ordovician intrusives, ranging from gabbros through tonalite, granite and syenite and finally gabbro again. Mineralisation is associated with Middle Cambrian granitoids of this suite, mainly tonalites, with the bulk of



the ore being hosted by the volcanic wallrocks to the intrusives. The volcanogenic and intrusive rocks are overlain by post-ore Ordovician sediments (Kudryavtsev, 1996).

Locally, the lowest sections of the Cambrian volcanogenic sequence are exposed in the core of the Bozshakol anticline, from the western flank of the orebody, to approximately 4 km to the northeast of the deposit. The sequence commences with 250 to 300 m of greenish-grey sandstone, siliceous siltstone, tuff and dacitic lavas with thin interlayers of pale jasper and andesitic flows. These are overlain by a 500 to 600 m thick unit, noted for the predominance of andesitic lavas and tuffs which host the northern section of the East Bozshakol deposit. The succeeding unit, also of Lower to Middle Cambrian age, comprises a further 1000 m of basaltic rocks that outcrop within the district as folded inliers (Kudryavtsev, 1996).

On the northern limb of the anticline the sequence is dominated by an up to 1500 m thick sedimentary-volcanogenic package that overlies the units described above. The volcanic suite of this package is composed

predominantly of amygdaloidal and massive hornblende-pyroxene basaltic rocks. These are intercalated with compositionally similar layers of litho- and crystallo-clastic tuffs and thin bands of gritstone, sandstone, siltstone and siliceous rocks. The rocks of this limb have been simply folded, with dips averaging 40 to 45° (Kudryavtsev, 1996).

Intrusive rocks are areally less extensive than the volcano-sedimentary intruded sequence and have been subdivided into four groupings, as follows: i). an initial Middle Cambrian complex of gabbro and diorite occurring as small bodies in the central and eastern part of the district; ii). a spatially separated, closely succeeding Middle Cambrian Bozshakol granitic complex, exposed at surface as quartz-diorite and tonalite stocks, including the main Bozshakol intrusion and others east and south of the deposit, as well as apophyses of porphyritic tonalite, dykes of tonalite porphyry and the more deep seated Dalnezapadny tonalite intersected in drilling at depths of 300 to 400 m; iii). a Middle Ordovician syenite complex, which includes the Ashchikol intrusion and a series of associated scattered dykes to its west and east; iv). an Upper Ordovician sub-

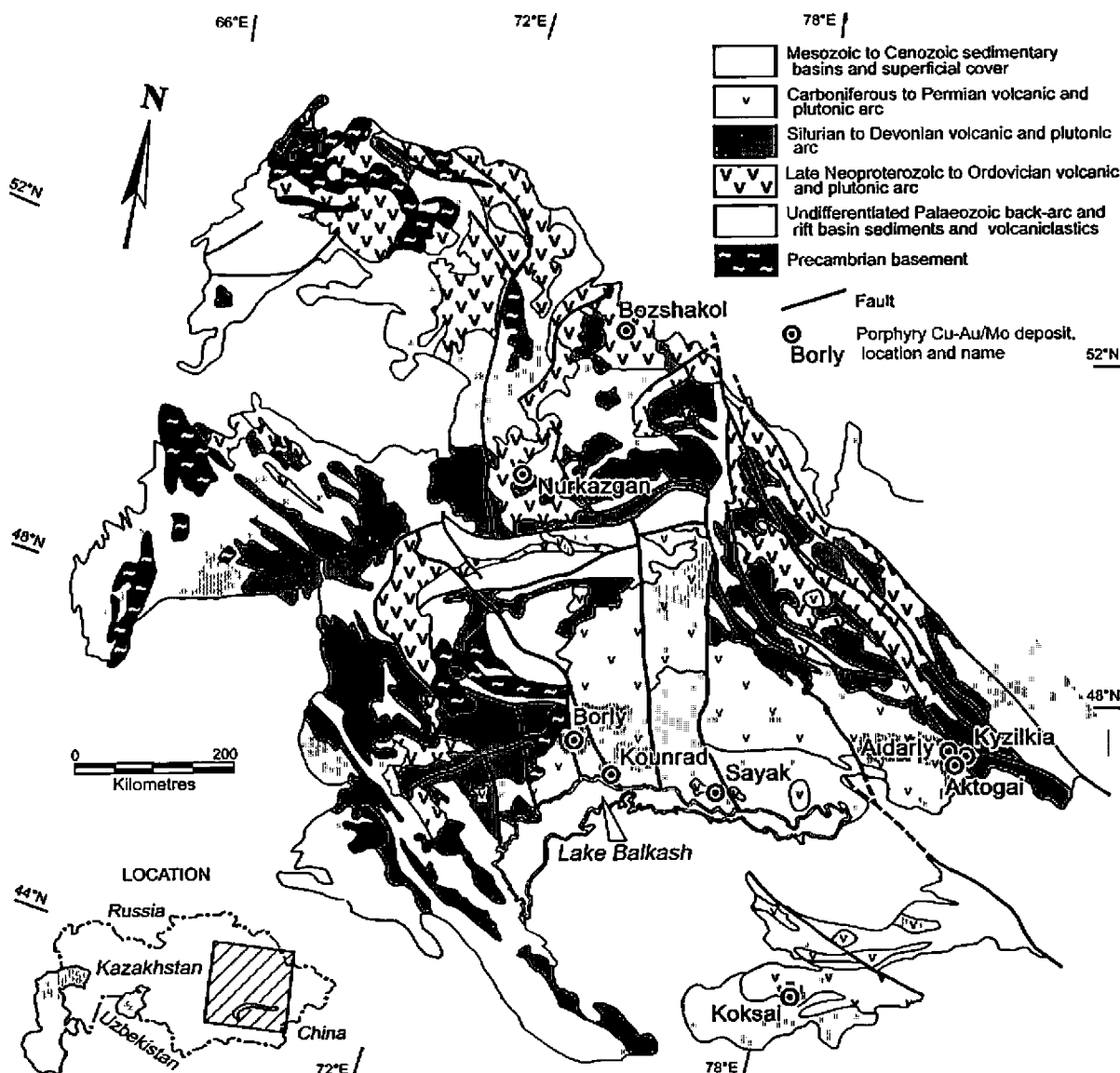
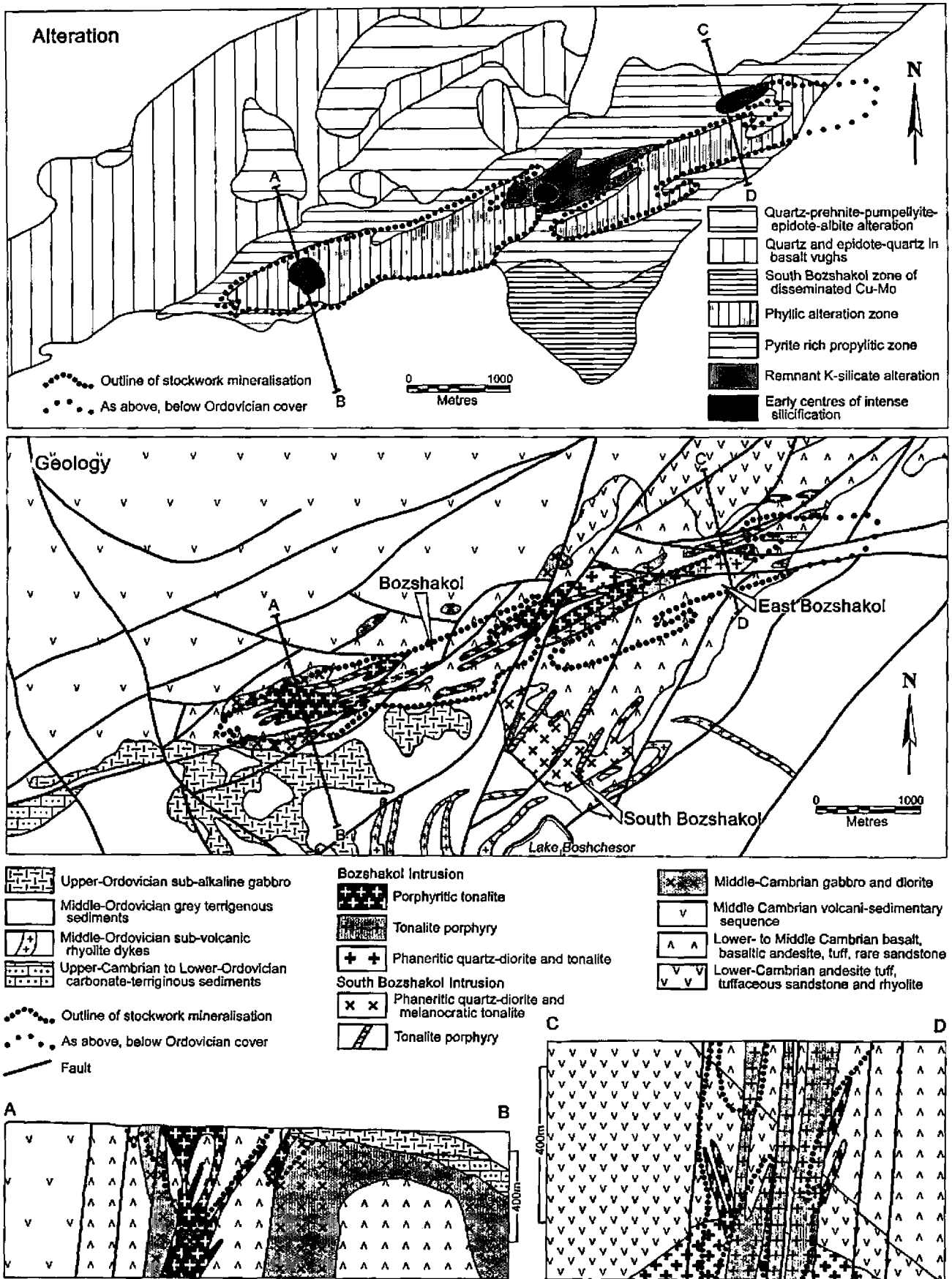


Figure 4: Geological summary of eastern Kazakhstan showing the structure and key porphyry Cu-Au/Mo deposits. After Heinhorst *et al.*, (2000); Kudryavtsev, 1996.



**Figure 5: Geology, alteration and mineralisation at the Bozshakol porphyry Cu-Au deposit in northern Kazakhstan.** The top diagram illustrates the alteration pattern surrounding and overlapping the ore deposit. The middle plan, covering the same area, shows the geology of the deposit and shares a common legend with the two representative cross sections, A-B through the main Bozshakol deposit and C-D through East Bozshakol. The two sections are at different scales and are located on both of the plans. The outline of the "commercial" stockwork zone is shown on both plans and sections as a common reference. Summarised from Kudryavtsev, (1996).

alkaline gabbro complex, known as the Southwestern Intrusive Sheet. The youngest magmatic activity in the district is represented by rhyolite sills within Middle Ordovician sediments (Kudryavtsev, 1996).

The core intrusive within the district is the Bozshakol Intrusion. Gravity data indicates it to be a sheet-like mass that can be traced over a distance of 7 km long by 0.5 to 0.7 km wide, underlying a corridor of outcropping, isolated granitoid stocks, dykes and apophyses, the largest of which separates the main Bozshakol and the East Bozshakol orebodies. The early phases of the Bozshakol Intrusion are represented by fine-grained hornblende diorite and diorite porphyry which cut Lower to Middle Cambrian volcanic rocks in the western part of the Bozshakol deposit. These early phases are cut in turn by medium- to coarse-grained quartz diorite and tonalite, and subsequently by porphyritic tonalite, the first of the ore related porphyry bodies (Kudryavtsev, 1996).

The porphyritic tonalite of the first mineralising phase is composed of up to 80% phenocrysts, most of plagioclase, set within a cryptic groundmass. In the western part of the Bozshakol deposit, it occurs as a steeply plunging stock some 300 m in diameter, with numerous faulted offsets across a northeast trending fracture set. In the East Bozshakol deposit it occurs as several lenticular dyke-like bodies (Kudryavtsev, 1996).

The second phase of ore-related granitic rocks are represented as tonalite porphyry dykes in the eastern part of the deposit. It differs from the earlier phase in that it has lesser phenocrysts - 30 to 40%, of which idiomorphic quartz is particularly prominent - in a fine-grained to crypto-felsic groundmass. This phase intrudes Lower to Middle Cambrian country rocks, but has only rarely been observed cutting Middle Cambrian lithologies. In the southeastern parts of the district, granitic rocks of the Bozshakol Intrusive are overlain by sediments containing Late Cambrian to Early Ordovician fossil fragments. In addition, grit bands within Middle Ordovician terrigenous sediments in the district contain mineralised pebbles of the ore bearing granitoids. Rb-Sr dating of the phaneritic tonalite yielded an age of  $481 \pm 23$  Ma. These observations all suggest a latest Cambrian to Early Ordovician age of intrusion and mineralisation (Kudryavtsev, 1996).

The unconformably overlying Middle Ordovician sequence is largely restricted to the southeast of the deposit and is composed of grey carbonate-terrigenous sediments with lenses and horizons of gritstone, siliceous siltstone, and shale at the base. It partially covers the ore on the southern margin of the deposit and has only been affected by post ore hydrothermal alteration (Kudryavtsev, 1996).

#### *Alteration and Mineralisation*

The emplacement of the mineralised intrusives and the distribution of ore are controlled by a northeast trending fault set. A second, northwest striking set offset the mineralised system and divide it into four blocks - the eastern, central, western and far-western blocks. Ore grade mineralisation is restricted to the central block, which includes the main Bozshakol and South Bozshakol deposits.

The eastern block only contains un-economic mineralisation within Lower Cambrian andesite and andesitic tuff. Minor lenses of ore grade intersected by drilling in the western block are pinched out, fault dislocated extremities of the main orebody in the central block. The far-western block contains disseminated Zn-Cu mineralisation within pyritic, propylitic altered hosts, principally Lower to Middle Cambrian mafic volcanic rocks. Overall, the Cu-Mo mineralisation is localised in altered volcanics adjacent to dyke-like apophyses from deeper intrusions of porphyritic tonalite and tonalite porphyry. It passes outwards into zones characterised by base metal enrichment and siderophile geochemical associations. The tonalite porphyry dykes are mineralised to a much lesser extent, while at depth some ore has also been found within phaneritic granite (Kudryavtsev, 1996).

The mineralisation in both the main Bozshakol orebody and at East Bozshakol represent an elongate stockwork zone with a steep, mostly northerly dip, and a northeast plunge. It lenses out into a series of fingers on the lateral (northeast and southwest) extremities and down dip, related to both faulting and the distribution of dykes (Fig. 5). The maximum length of the main orebody is 3 km, with a thickness of near 285 m at its widest point, and a down-dip extent of over 600 m. Bozshakol South has been traced for 425 m along strike, has a thickness of 33 m and persists down dip for 120 m. The mineralisation at East Bozshakol extends over a length of from 1.2 to 1.5 km, is 400 to 500 m wide and has a grade of 0.3 to 0.35% Cu (Kudryavtsev, 1996; Seltmann *et al.*, 2004 and sources quoted therein).

Ore grade mineralisation is located within the inner sections of the alteration system, largely associated with a phyllic assemblage of quartz-sericite-carbonate-chlorite in the volcanic hosts and by quartz-sericite within granitic rocks. Dykes of tonalite porphyry and adjacent narrow zones near their contacts have been affected by quartz-hydromica argillic alteration. However, while phyllic alteration dominates, all of the stockworks, particularly on their northern margins, show evidence of a biotite (potassic) phase. Potassic alteration is most marked in the central portions of the system, focused on the granitoid intrusions (Fig. 5), where K feldspar pseudomorphically replaces plagioclase within the granitoids, and forms veins and veinlets accompanied by quartz and less frequently by biotite. Fragments of this style of alteration are found within intra-ore hydrothermal breccias (Kudryavtsev, 1996).

These central zones, which form the elongate core of the mineralised system, are surrounded by shells of biotite enrichment and by a pyritised propylitic halo. Weak biotite alteration has been observed in Cambrian volcanics as much as 1 km distant from the orebody. Quartz-chlorite altered volcanics with abundant veinlets and disseminations of pyrite are developed closer to the orebody, while actinolite bearing varieties are localised closest to the intrusive contacts. These manifestation of propylitisation form a halo that is 6.5 km long and ranges from 0.4 to 1 km wide on the western part of the mineralised system, is up to 700 m wide in the east and 2.2 km wide in the central sections (Kudryavtsev, 1996).

The principal hypogene mineral assemblage comprises pyrite and chalcopyrite with accessory magnetite, molybdenite and sphalerite, and rare galena, marcasite, maghemite, mushketovite, martite, bornite, hematite, tetrahedrite, pyrrhotite, pentlandite, cubanite and other metallic minerals. The initial potassic alteration phase resulted in assemblages, listed in order of formation, of hematite-quartz, biotite-magnetite, pyrrhotite-chalcopyrite-pyrite, chalcopyrite with prehnite and molybdenite-chalcopyrite. The subsequent phyllic leaching produced pyrite, pyrite-molybdenite, pyrite-chalcopyrite-molybdenite, chalcopyrite-sphalerite and chalcopyrite-galena. In the western part of the deposit, cobalt, nickel and platinum minerals and early gold are widely associated with the pyrrhotite-chalcopyrite assemblage. In addition, the chalcopyrite-sphalerite and chalcopyrite-galena associations contain electrum, telurides and silver minerals. Post ore alteration minerals comprises quartz, zeolite and quartz-calcite veinlets (Kudryavtsev, 1996, and sources quoted therein).

The lower grade East Bozshakol mineralisation has a simpler suite of minerals, predominantly composed of pyrite, chalcopyrite, magnetite and molybdenite, with accessory hematite, martite, mushketovite, sphalerite, galena, tetrahedrite and pyrrhotite, and rare maghemite, barite, marcasite, and native gold and silver veinlets (Kudryavtsev, 1996, and sources quoted therein).

Fluid inclusion studies indicate temperatures of formation from 380 to 100°C, commencing with the higher temperatures typical of quartz-K feldspar alteration

(380 to 320°C) and quartz-sulphide veining (320 to 180°C). The quartz-polysulphide mineralisation is characterised by temperatures of 220 to 100°C, while post ore veinlets were formed at 200 to 80°C (Kudryavtsev, 1996).

The upper 5 to 54 m of the orebody have been subjected to oxidation producing malachite-kaolinite-atacamite and goethite-malachite-clay assemblages. Over sections of the orebody, the zone of oxidation has been subjected to leaching to depths of as much as 35 m, to produce underlying supergene enrichment with a chalcantite-chalcopyrite-covellite mineralogy over vertical thicknesses of from 5 to 60 m. This supergene enrichment was most intensely developed in the upper sections of the main Bozshakol ore deposit. Palaeo-supergene enrichment from the Cambrian is also recognised, preserved below the Late Cambrian to Ordovician cover on the south of the ore deposit, typified by the presence of barite. The next phase of supergene enrichment, which is only poorly developed, is of Mesozoic age and is characterised by the development of chalcocite and covellite veinlets (Kudryavtsev, 1996, and sources quoted therein).

**Andash and Taldy Bulak, Kyrgyzstan**

A group of gold rich, Ordovician age, porphyry related copper deposits define a 30 km long mineralised corridor in northern Kyrgyzstan (Fig. 6), approximately 120 km to the southwest of the capital, Bishkek. The principal deposits include porphyry style mineralisation at Taldy Bulak, Andash and Tokhtonysai and skarn ores at Aktash (Nikonorov et al., 2000; Jenchuraeva et al., 2005). All are developed within rocks formed in the Lower Palaeozoic

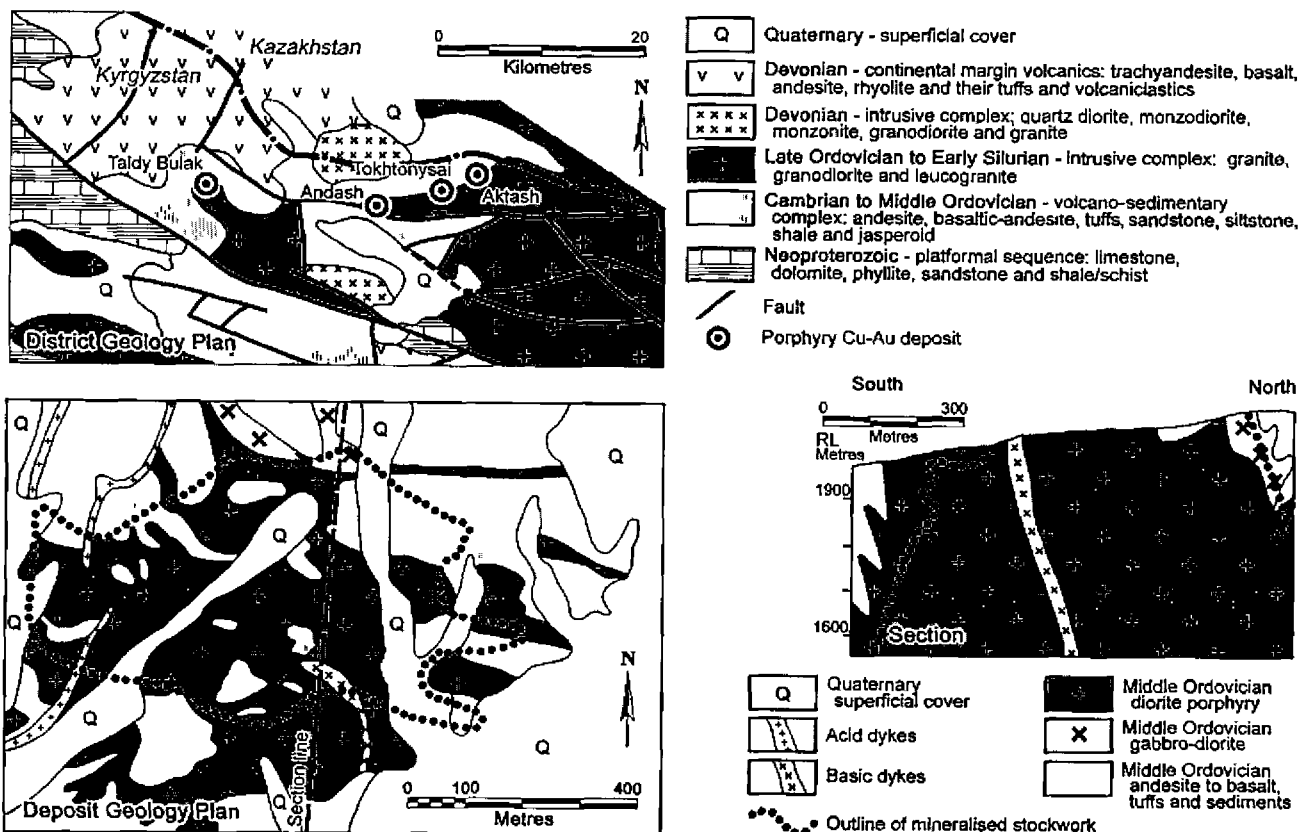


Figure 6: District scale geological plan showing the location of the Taldy Bulak, Andash, Tokhtonysai porphyry Cu-Au and Aktash skarn Cu-Au deposits (top) and a deposit scale geological plan (bottom left) and cross section (bottom right - location on deposit geology plan) through the Taldy Bulak deposit. After Jenchuraeva et al., (2005).

Kipchak magmatic arc (Fig. 3), and are associated with Middle Ordovician diorite to monzodiorite porphyries which intrude Late Cambrian to Middle Ordovician island arc terrigenous volcanogenic sequences (Seltmann *et al.*, 2004; Jenchuraeva, 1997).

*Taldy Bulak*, which is the largest of the group, is often confused with Taldybulak Levoberezhny (described later) in the available literature and on the web. It is quoted by Mutschler *et al.*, (2000) as containing a resource of 540 Mt @ 0.27% Cu, 0.5 g/t Au, 0.008% Mo, based on data sourced from the Metal Mining Agency of Japan (Kamitani and Naito, 1998; Hedenquist and Daneshfar, 2003). Mineralisation is predominantly hosted by a stock of Middle Ordovician diorite porphyry developed on the margin of a more extensive Late-Ordovician to Early-Silurian granite-granodiorite-leucogranite complex which intrudes a Late Cambrian to Middle Ordovician island arc sequence that locally comprises shale, siltstone, sandstone, conglomerates, tuffs and Middle Ordovician porphyritic andesite and basaltic-andesite. This latter sequence overlies a basement of Neoproterozoic platformal carbonate, sandstone, phyllite and shale, and is respectively overlain and intruded by Devonian basalt, andesite, rhyolite, tuffs and volcanics and an intrusive complex of quartz

diorite, monzodiorite, granodiorite and granite of a similar Devonian age.

The mineralised stock covers an area of approximately 1200x800 m at surface and comprises 50 to 70% plagioclase, 15% mafic minerals and 15% quartz. It has a complex shape, with an irregular contact characterised by numerous embayments and large xenoliths of the surrounding country-rock. The dense xenolithic zone near the outer contact resembles a breccia with a diorite porphyry matrix. The diorite becomes finer grained and more porphyritic in the vicinity of the xenolith zone where it also tends to have a higher gold grade. The stock includes an early phase, dark-grey gabbro-diorite and is cut by a series of late acid and basic dykes.

The main mineralisation is almost completely confined to within the diorite porphyry stock, occupying approximately 75% of its surface exposure, and is accompanied by dense fracturing and intense alteration. The fracturing, which reaches a density of as much as 150 to 200 per metre, is healed by grey quartz which forms five main, steeply dipping (70-90°) mineralised veins sets, each with a differing trend direction, namely, 32°, 70°, 90°, 140° and 170°. The best mineralised set trends east-west. The veins vary from 0.5 to 25 mm in thickness.

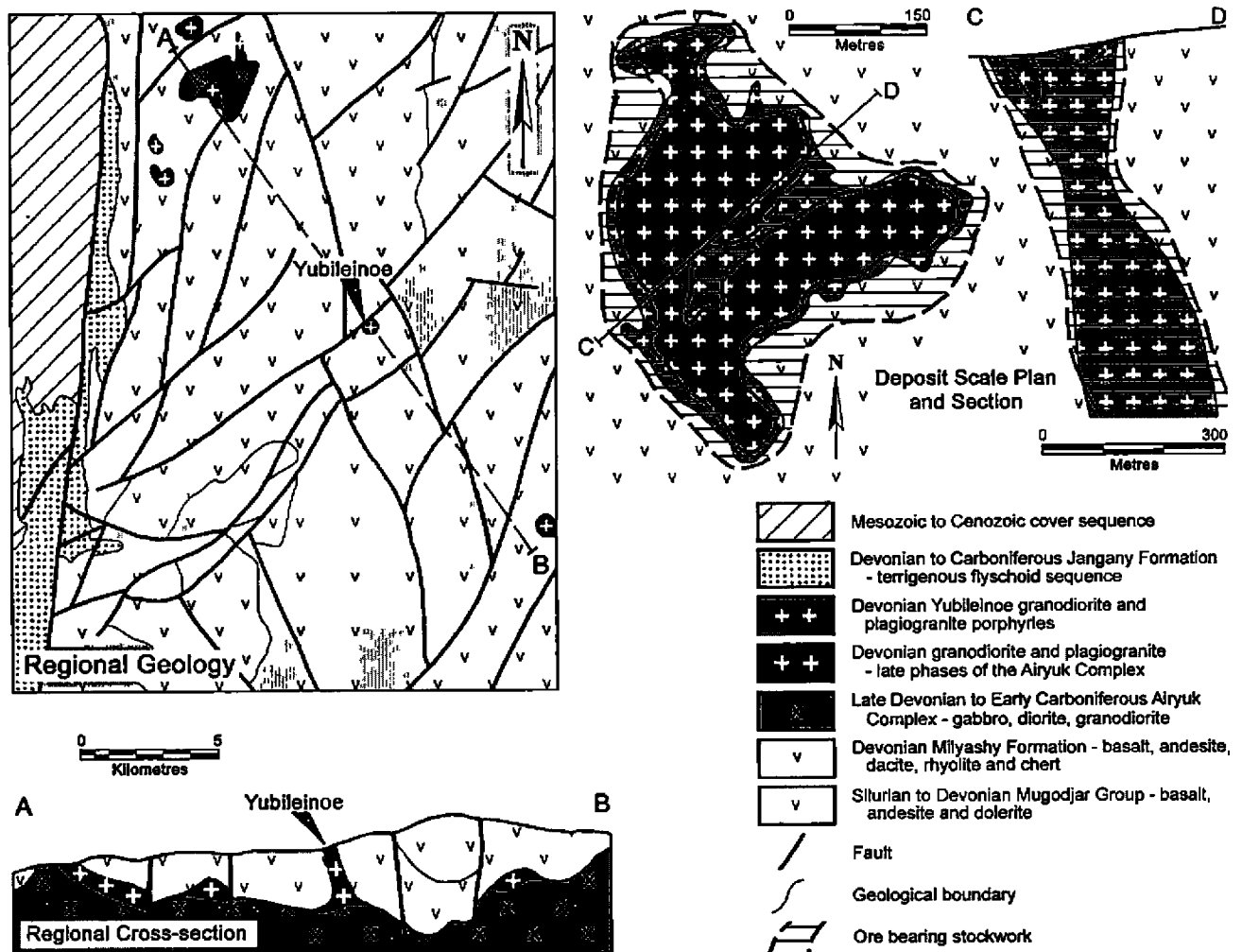


Figure 7: The Yubileinoe porphyry Au (-Cu) deposit in north-western Kazakhstan. The plan on the top left illustrates the regional scale geological setting, and the location of the stylised cross section A-B on the bottom left. The diagrams on the top right shows the outline of the mineralised intrusive at the Yubileinoe deposit, the outline of the ore bearing stockwork and the location of the generalised southwest-northeast cross section C-D through the deposit. After Shatov *et al.*, (2003) and Seltmann *et al.*, (2004).

The orebody has a general elliptical shape, defining an overall mineralised envelope with dimensions of 1100x700 m, enclosing three east-west trending lensoid developments of higher grade ore, comprising a northern 200x60 m, central 1200x25 to 170 m and southern 700x140 m zone. Mineralisation has been traced to a depth of 500 m below the surface.

At *Andash*, 15 km to the east of Taldy Bulak, similar mineralisation is present as a flat dipping, 400 x 200 m stockwork within a granodiorite to diorite porphyry host, associated with pipe- to lens-like explosive breccia zones which have been silicified to form "quartzose metasomatites". The principal alteration types recorded include quartz-feldspar, quartz-tourmaline, propylitic, phyllic and argillic. Copper mineralisation is generally related to zones of quartz-sericite-chlorite alteration, while gold is associated with quartz-tourmaline veining and argillic altered zones. The principal metallic minerals include pyrite, chalcopyrite, magnetite and hematite with minor sphalerite, tetrahedrite, galena and pyrrotite. Gold is closely associated with pyrite, and occurs at grades of around 2.6 g/t Au with 0.4% Cu (Seltmann, et al., 2004).

#### *Nurkazgan (or Samarka), Kazakhstan*

The Nurkazgan porphyry Cu-Au deposit is located in northeastern Kazakhstan, 240 km southwest of Bozshakol. It was emplaced during the Late Silurian to Early Devonian (410 Ma), in the 'Devonian' segment of the Kazakh-Mongol magmatic arc, and has a resource of 65 tonnes of Au and 1.5 Mt of Cu at grades of 1 to 3% (averaging 1.2%) Cu and 0.4 to 1 g/t Au. The ore deposit is hosted by monzonite to granodiorite porphyries of the Turkulamsky Massif intruding wall rocks of the Late Silurian to Devonian Zharsorskaya suite that comprise: i), a lower unit of andesitic to basaltic agglomeratic tuffs, lavas and automagmatic breccias with rare interbeds of andesitic porphyry, tuffs, tuffaceous siltstones and tuffites; ii), an upper sequence of andesitic to dacitic tuffites, tuffaceous conglomerate-breccias, tuffs and lavas with lenses of tuffaceous sandstones and conglomerates (Seltmann et al., 2004).

The mineralised intrusives and country rocks are overlain by units of the terrigenous, post-ore, Middle Devonian Konyrskaya suite, comprising red tuffaceous sandstones with lenses of boulder to pebble conglomerate, grits and siltstones. Mineralisation took place as: i), initial porphyry-style Cu, accompanying an early monzonite and ii), an overprinting, high grade, high sulphidation Cu-Au phase related to the intrusion of a late stage porphyritic diorite and numerous associated breccia pipes. The early porphyry-style mineralisation is predominantly composed of disseminations and stockworks of chalcopyrite, pyrite and molybdenite with grades of 0.3 to 0.5% Cu. It is accompanied by potassic alteration comprising K feldspar and biotite, and is surrounded by a propylitic halo characterised by chlorite and epidote. The overprinting high sulphidation phase, and its associated porphyritic diorite and breccia pipes, are localised in the core of the earlier monzonite intrusive and porphyry mineralisation. This phase is represented by a chalcocite-covellite-

tetrahedrite assemblage with sericite-chlorite-carbonate alteration and has grades of >1 to 1.5%, locally to 3% Cu, and 1 g/t Au. The high grade zone has an areal extent of at least 600 x 600 m and is restricted to depths of more than 200 to 300 m below the surface. At 700 m it has contracted to a steep 20 to 30 m wide band averaging 3% Cu. Mineable high grade ore has been delineated to a depths of 1400 m (Seltmann et al., 2004).

#### *Yubileinoe, Kazakhstan*

The Yubileinoe deposit is located in western Kazakhstan, some 200 km southeast of the city of Aqtobe. It lies within the Magnitogorsk-Mugodzhaz zone of the Urals, just east of the major north-south trending West Mugodzhaz deep regional fault, and was emplaced within the ensimatic Urals-Zharmag magmatic arc at approximately 380 Ma in the Middle Devonian (Fig. 3). The host porphyry was intruded at the intersection of the Aulinskaya and Treshchinnaya faults which strike northeast and northwest respectively. It is a small to medium sized Au rich porphyry-style deposit with accompanying low grade Cu (Table 1).

Mineralisation is associated with a 250 to 300 m diameter stock of plagiogranite porphyry. This stock is assumed to be an apophysis of a local concealed cupola of gabbrodiorite/granodiorite that in turn is part of the larger Late Devonian to Early Carboniferous Airyuk Intrusive Complex (Fig. 7). The mineralised stock was intruded into a sequence of Siluro-Devonian volcanics and sediments that are part of the tholeiitic mafic volcanic dominated Mugodzhaz Group which is overlain by the Mialyshy, Qundyzdy and Janghany Formations that comprise island arc volcanics and sediments (Shatov et al., 2003).

Ore mineralisation accompanies a stockwork developed within both the plagiogranite porphyry and its mafic volcanic wall rocks (Fig. 7), and has been drill tested to more than 600 m below surface where it is still open at depth. Skarn, potassic and phyllic alteration are present within the orebody, although the latter predominates and is directly related to the stockwork and disseminated Au-Cu porphyry mineralisation. The principal metallic minerals are magnetite, pyrite, chalcopyrite, arsenopyrite, tetrahedrite, stibnite and native gold, with minor sphalerite, galena, scheelite, molybdenite, bornite, hematite (martite), rutile, ilmenite, anatase, and cinnabar.

Four ore zones have been delineated within the larger zone of stockwork mineralisation shown on Fig. 7. The Central orebody, located within the core of the stock, is the largest and the richest of the four, with grades of from 5 to 10 g/t Au. The Western orebody lies along section of the western outer margin of the plagiogranite stock. It is 80 to 240 m long and 10 to 25 m thick, with grades ranging from 3.5 to 6.7 g/t Au, and has been traced to a depth of over 110 m. The Northern orebody is hosted by the wallrock volcanics, and follows the northeastern contact of the stock. It has surface dimensions of 80 x 16 to 37 m and has been traced to a depth of 100 m, with from 3.4 to 8 g/t Au. The Southeastern orebody straddles the contact of the plagiogranite porphyry stock, and carries 3.8 to 11 g/t Au. It is 60 to 120 m in length and from 10 to 121 m in thickness. The average grade is 4 to 5 g/t Au, 0.42% Cu

and 65 g/t Ag (Seltmann *et al.*, 2004, and references cited therein).

### Taldy Bulak Levoberezhny, Kyrgyzstan

The Taldy Bulak Levoberezhny deposit is located in northern Kyrgyzstan, approximately 120 km to the southeast of the capital, Bishkek. The deposit is a granitoid-related mesothermal vein/stockwork associated with Devonian diorite porphyry and Carboniferous sub-alkaline diorite-monzonite porphyry dyke swarms. While it has some porphyry style characteristics, it has not been conclusively classified as a porphyry style deposit. It lies within the Boordu-Taldy Bulak zone of the western Aktyuz-Boordu Metallogenic Province. The province is characterised by Baikalian and Caledonian Orogeny structures, while Palaeoproterozoic basement is intruded by Meso- to Neoproterozoic igneous rocks. The Boordu-Taldy Bulak zone comprises a 20 x 30 km diameter volcanic dome-like structure, the central point of which is occupied by the deeply eroded core of a Palaeozoic volcanic edifice. Within and peripheral to this structure, Palaeoproterozoic metamorphics and Lower Palaeozoic volcano-sedimentary rocks are overlain by Devonian, Carboniferous and Lower Permian volcanic and volcano-sedimentary complexes. Throughout the domal structure, there are abundant Middle to Late Palaeozoic mafic to felsic subvolcanic intrusions, occurring as dykes, sills and stocks controlled by deep-rooted faults, representing the root zones of the various overlying volcanic sequences of the Kipchak and Kazakh-Mongol magmatic arcs. Late Tertiary dolerite dykes cut all of the preceding rocks (Chisholm, 2003).

The Taldy Bulak Levoberezhny deposit is located on the margin of a folded and deeply eroded 2 x 4.5 km horst of Palaeoproterozoic basement, cut by sub-volcanic intrusive rocks. The principal lithologies of the basement are a greenschist, amphibolite and mafic migmatite suite overlain by felsic gneiss and mica schist. The mafic and felsic Palaeoproterozoic basement suites are separated by a

tectonic contact and are intruded by a sub-volcanic complex of Devonian to Carboniferous diorite to monzonites, which are considered to be almost synchronous with, and genetically and spatially associated with the Au-Cu mineralisation. The area is structurally complex with at least five generations of faulting and large 'crush zones' of brecciated material that dip at 30 to 40° and have focussed mineralisation. These 'crush zones' are believed to be original thrusts which have been reactivated by shearing and/or by subsequent hydrothermal activity (Chisholm, 2003).

The bulk of the mineralisation occurs within a 200 to 300 m thick tabular 'melange zone' (Fig. 8) which represents one of the 'crush zones'. The 'melange' comprises highly altered rocks that dip at 35 to 40° to the southwest and can be traced for 1.2 to 1.5 km along the southwestern limb of a large antiform, before splitting into a series of horsetails down plunge. It appears to occupy the thrust contact between the Palaeoproterozoic mafic and felsic suites. The 'melange' has been altered to quartz-sericite, quartz-carbonate and quartz-tourmaline assemblages, and intruded by both Devonian diorite porphyry and Carboniferous sub-alkaline diorite-monzonite porphyry (no dating evidence provided). The porphyries have been altered to quartz-sericite. The orebody occurs as a stockwork of sulphide and quartz-tourmaline veining in a zone of sulphide rich, intense multiple brecciation. Lesser mineralisation is associated with faults and tectonic breccias (Chisholm, 2003; pers. comm. John Leishman).

The main gangue minerals within the ore are quartz (45 to 60%), muscovite-sericite (up to 55%), carbonates (up to 30%), tourmaline (up to 40%), fuchsite (1 to 5%) and other chlorites (up to 10%), with lesser barite, fluorite, apatite (0.1 to 1%), feldspar (albite, K feldspar), epidote, pyroxene, amphibole, garnet and traces of topaz. Sulphides comprise 2 to 40% of the mineralised zone, 95% of which is pyrite. Other sulphides present include chalcopyrite, galena, arsenopyrite and sphalerite. Gold is found as small

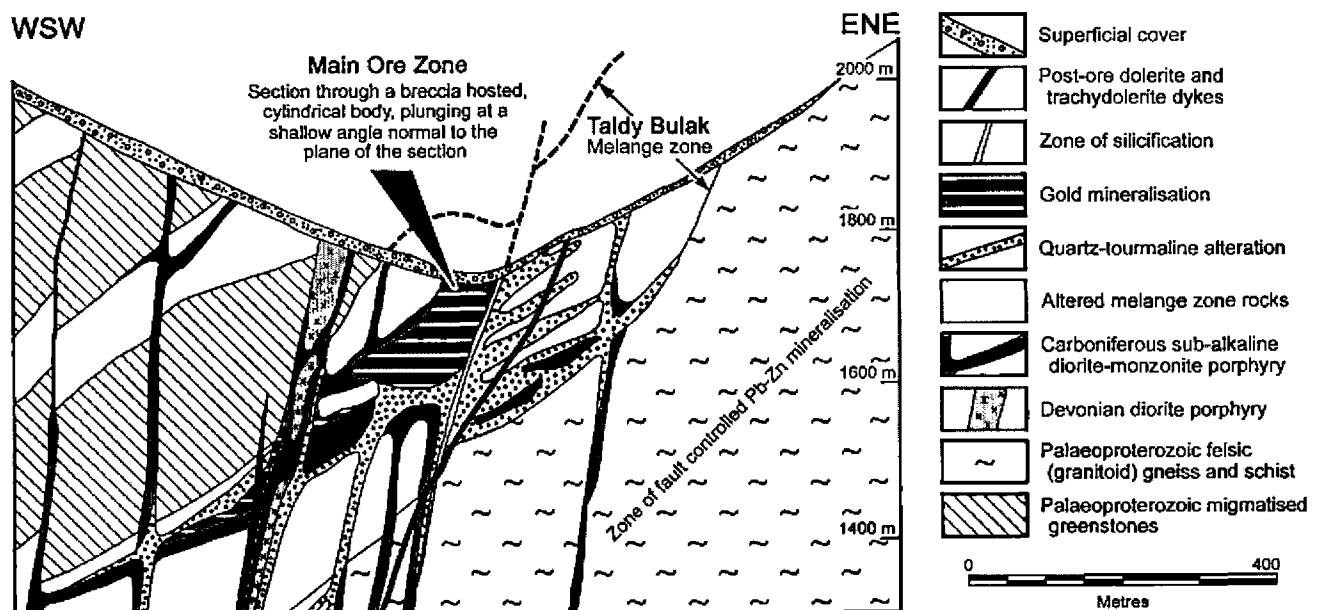


Figure 8: Representative cross section through the Taldy Bulak Levoberezhny porphyry related Au deposit in northern Kyrgyzstan showing geology, alteration and mineralisation. After Chisholm, (2003).

grains of native gold up to 0.4 mm but generally in the 0.01 to 0.1 mm ranges, occurring along grain boundaries, interstitial fractures and to a lesser extent as lamellae within sulphide minerals. Some 46% of the gold is free, 23% occurs as coarser grains with sulphides, 21% as fine inclusions in sulphides, 4% in quartz and 6% in carbonates. At a cutoff of 1 g/t Au, the main deposit contains resources and reserves, in various grade and resource classifications, totalling 18.7 Mt at an average grade of 6.9 g/t Au, for 129 tonnes of gold (Central Asia Gold, 2005) with 4 to 5 g/t Ag and 0.2 to 0.3% Cu (Chisholm, 2003; Seltmann *et al.*, 2004 and sources quoted therein).

The main high grade gold orebody has the form of a tapering pipe which has been disrupted by faulting and becomes less continuous down plunge. It plunges at between 8 and 40°, steepening with depth, at an azimuth of 300°, has a long axis of 570 m and is 30 to 60 m in diameter. Seven zones of mineralisation, both within this and adjacent pipes, have been identified, two of which make up the quoted resource (Chisholm, 2003).

Malyukova (2001) describes the deposit in detail and notes that while it shares some characteristics with mesothermal Au mineralisation, it has similarities with Au-bearing tourmaline breccia pipes in the porphyry copper belt of Chile. Malyukova (2001) concludes that the deposit may be referred to as a gold-sulphide-quartz-tourmaline type of porphyry gold deposit on the basis of specific features, including i). high abundance of pyrite mainly occurring in quartz-tourmaline altered rocks, ii). veined, disseminated and stringer style mineralization, iii). extensively developed phyllic (and potassic) alteration that predates the tourmalinisation, iv). relation of ore to minor intrusions, v). great vertical extent of ore mineralization, and vi). occurrence of basic volcanics as host rocks.

#### *Aktogai Group, Kazakhstan*

The Aktogai (Aqtogai) group of porphyry Cu-Mo-Au deposits, Aktogai, Aidarly and Kyzilkia are located in the 'Balkhash-Ili' zone of the Upper Palaeozoic Kazakh-Mongol magmatic arc, northeast of Lake Balkhash in southeastern Kazakhstan, and some 450 km NNE of Almaty. Together they have resources of more than 2.5 Gt of ore containing over 10 Mt of Cu and near 60 tonnes of Au (Mutschler *et al.*, 2000). See Table 1 for more details.

#### *Geology*

The three main deposits of the Aktogai district are associated with stock-like granodiorite and plagiogranite porphyries intruding the extensive laccolith like Late Carboniferous Koldar Pluton and large rafts of Carboniferous volcano-sedimentary rocks within the pluton. The volcano-sedimentary rafts are composed predominantly of andesites, dacites and rhyolites, and their tuffs (Zvezdov *et al.*, 1993; Bespaev and Miroshnichenko, 2004).

The *Aktogay* deposit is confined to the eastern part of the Central Aktogai raft of volcanics (Fig. 9) and the enclosing pluton. The raft is intruded by a stock like body of porphyritic granodiorite which also cross-cuts diorite,

quartz-diorite and granodiorite of the Koldar pluton. The porphyritic granodiorite is in turn, cut by an elongate stock composed of ore-bearing granodiorite and plagiogranite porphyries, accompanied by a series of pipe-like bodies of explosive breccia with quartz-biotite and sericite-tourmaline matrices. The ore bearing stockwork occurs in the outer contact zone of the porphyry stock, forming a hollow, downward tapering conical body, which pinches out at depth into a series of linear west to northwest trending mineralised zones. At the surface, the orebody has an elliptical annular shape, partially opened to the west, with a maximum diameter of approximately 2500 m, and a radial width of 80 to 530 m (Zvezdov *et al.*, 1993; Seltmann *et al.*, 2004).

#### *Alteration and Mineralisation*

All rocks in the orebody area, with the exception of late mafic dykes, have been altered. The barren core of the cone/annulus is occupied by a siliceous zone, comprising quartz bodies surrounded by a dense stockwork of barren quartz veinlets, and a thin zone of sericite-quartz alteration. Towards its margins, the silicified core passes out into a thick zone of early potassic alteration, comprising K feldspar and biotite, that encompasses the main annular orebody. Included within this potassic zone are several linear intervals which are poorly mineralised, but intensely K feldspar altered, and flanked by a wide halo of biotite. Phyllic alteration, characterised by quartz-(carbonate)-chlorite-sericite, appears as impersistent, thin linear zones, confined to the contacts of granodiorite porphyry apophyses and to zones of fracturing along the flanks of the orebody. The periphery of the porphyry copper system is occupied by a large propylitic halo containing epidote-amphibole and albite-chlorite-prehnite (Zvezdov *et al.*, 1993).

The mineralised system exhibits an outward zonation from bornite-chalcocopyrite at the centre to chalcocopyrite-pyrite to a pyritic halo on the outer margins. Cu and Mo overlap, while Pb-Zn is confined to zones of carbonatisation on the flanks of the orebody. The paragenetic sequence is as follows: i). magnetite; ii) pyrrhotite-cubanite; iii) quartz-pyrite; iv) quartz-(magnetite)-bornite-chalcocopyrite; v) quartz-molybdenite-pyrite-chalcocopyrite; vi) quartz-(pyrite)-bornite-chalcocopyrite-chalcocite; vii) quartz-sericite-pyrite; viii) quartz-galena-sphalerite-chalcocopyrite-pyrite-tennantite; ix) post ore zeolite-carbonate. Quartz is the dominant gangue mineral within the stockwork veins, although K feldspar and biotite are also found in early veins, while late veins carry chlorite, epidote, prehnite and carbonate. Fluid inclusion studies indicate that the early quartz-K feldspar veinlets were formed at between 490 and 320°C, while the late sulphide-quartz veinlets range from 320 to 180°C (Zvezdov *et al.*, 1993, and references cited therein).

The *Aidarly* deposit is located approximately 4 km to the WNW of Aktogai, and falls within the same 8 x 2 km, WNW elongated sulphidic alteration halo. It is centred on a small, north-west trending stock of ore bearing granodiorite porphyry which intrudes diorite, quartz diorite and granite phases of the Koldar pluton. The granodiorite



porphyry stock has steep contacts, characterised by numerous apophyses, and is accompanied by a series of fault controlled dykes of the same composition with northeast and northwest orientations. All of these intrusives are cut by late quartz diorite and dolerite dykes. Small tubular breccia bodies near the granodiorite porphyry are composed of mineralised rock fragments, cemented by rock flour (Zvezdov *et al.*, 1993).

Mineralisation is confined to the outer margins of the stock and the surrounding Koldar pluton, and closely follows the

trend of the stock. At surface, the orebody outcrops as a north-west elongated annulus, surrounding a slightly mineralised granodiorite-porphyry. As at Aktogai, the orebody resembles a downward tapering, hollow, truncated cone, with a barren core occupied by poorly mineralised granodiorite porphyry and a zone of silicification. Alteration and mineral zoning is similar to that described at Aktogai. The outcropping granodiorite porphyry has been subjected to slight silicification and sericitisation. At a depth of 600 m the porphyry has a barren core of intense silicification, with scattered anhydrite in its outer margins.

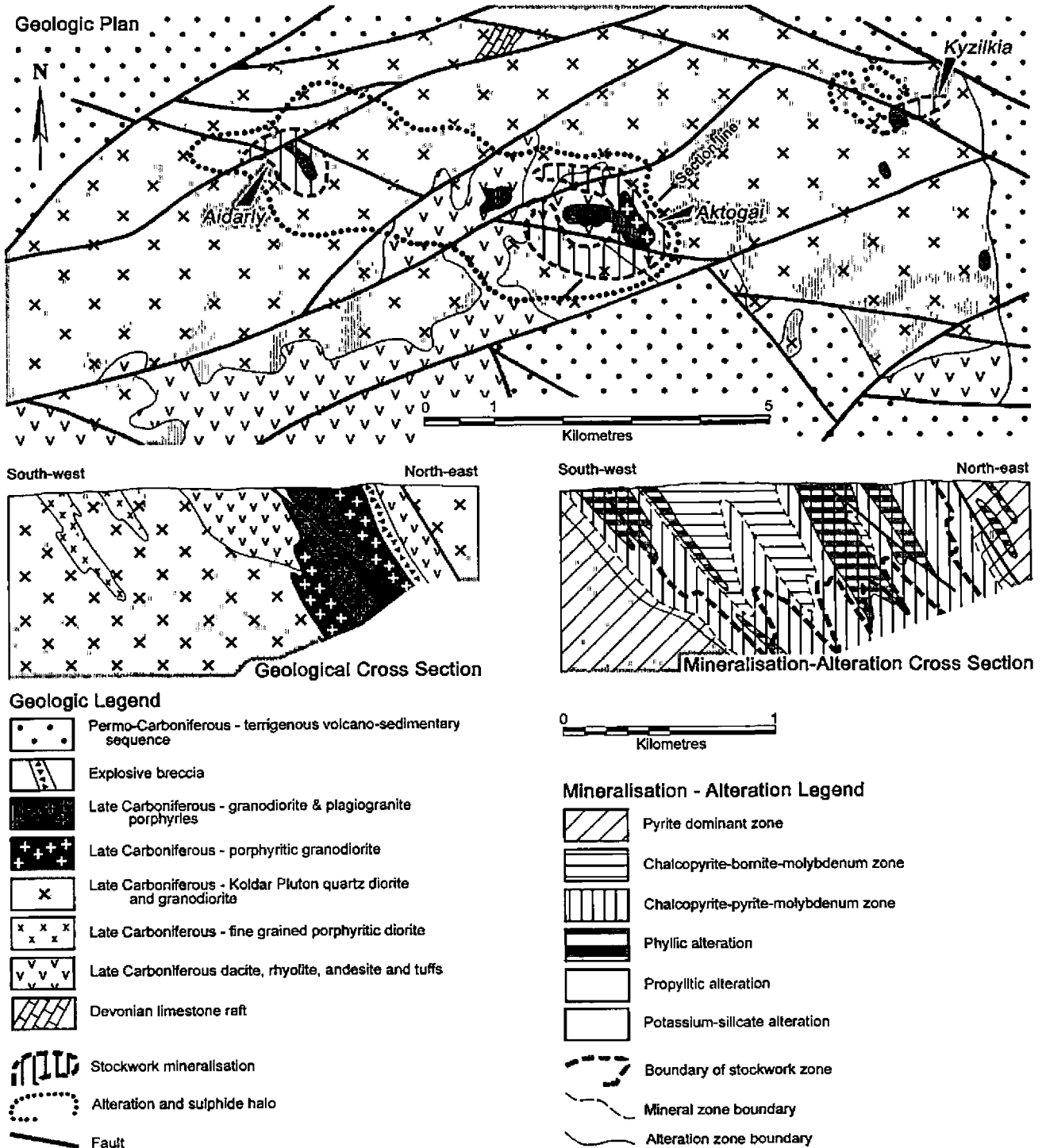


Figure 9: Geology, alteration and mineralisation at the Aktogai Group of porphyry Cu-Au deposit in southeastern Kazakhstan. The geology and lateration-mineralisation are also separately shown on a NE-SW oriented section through the Aktogai deposit. After Zvezdov, *et al.*, (1993).

Towards the periphery of the porphyry system the silicification passes outward into potassic alteration of quartz-K feldspar-biotite. Higher in the system, at intermediate and near surface depths, this pattern is overlain by a zone of phyllic alteration characterised by quartz-sericite-chlorite-carbonate, with occasional tourmalinisation. The potassic zone is in turn surrounded by a wide halo of propylitic alteration (Zvezdov *et al.*, 1993).

The orebody takes the form of a Cu-Mo stockwork concentrated in the early potassic zone and overprinted by the phyllic alteration. Although most aspects of the mineralisation and alteration are similar to that described above for Aktogai, the deposit differs in that it has a more extensive and better developed polymetallic (Pb-Zn) veinlet and vein mineralisation zone on its outer margins. These comparisons suggest that the Aidarly deposit is less deeply eroded than Aktogai (Zvezdov *et al.*, 1993).

The small *Kyzylkia* deposit is 4 km to the east of Aktogai, on the opposite side to Aidarly (Fig. 9). It appears to have been more deeply eroded than either of the other two, supporting the implication of deep erosion in the east, shallowing to the west within the Aktogay district. At *Kyzylkia* Cu-Mo mineralisation is associated with a small granodiorite porphyry stock intruding the granodiorites of the Koldar Pluton. Orebodies are present as a series of *en echelon* like zones of stringer chalcocite-bornite-chalcopyrite ore accompanied by erratic K-silicate and phyllic alteration (Zvezdov *et al.*, 1993).

#### ***Kounrad (or Konyrat, Qonyrat), Kazakhstan***

The Kounrad porphyry Cu-Au deposit (also known as Qonyrat or Konyrat) is located in the 'Balkhash-Ili' zone of the Upper Palaeozoic Kazakh-Mongol magmatic arc (Fig. 3). It is 10 km north of the town of Balqash on the northern shore of Lake Balkhash, in Kazakhstan and 450 km NNW of Almaty (Fig. 4). Kounrad is the largest of a group of deposits, in the district, which also include Kaskyrkazgan and Ken'kuduk. Prior to mining, the Kounrad deposit is believed to have totalled more than 800 Mt of ore averaging 0.62% Cu, and locally up to 0.76 g/t Au. Much of the ore removed from the open pit up until 1996, when it covered an area of 2.2 x 1.8 km and was 330 m deep, was supergene enriched to depths of 54 to 450 m below the surface (generally 150 to 200 m thick), with grades of up to 1% Cu. The remaining reserves in 1996, primarily of hypogene mineralisation, were 220 Mt @ 0.35% Cu, 0.1 g/t Au, 0.005% Mo (Seltmann *et al.*, 2004; Mutschler *et al.*, 2000; Kudryavtsev, 1996; Zvezdov *et al.*, 1993). See Table 1 for additional details.

#### ***Geology***

The Kounrad ore deposit is related to the intrusion of Middle Carboniferous (~330 Ma) granitic bodies into a sequence of Late Devonian (Famennian) to Early Carboniferous (Tournaisian) sedimentary, volcano-sedimentary and volcanic units and coeval pre-orogenic granitic rocks, as well as early orogenic Middle Visean (Early Carboniferous) volcanics and associated intrusives. Late Carboniferous granites of the East Qonyrat pluton that are found to the

northeast of the deposit are post ore and late orogenic. The upper contact of the East Qonyrat pluton dips to the southwest at around 50° to pass below the ore deposit (Kudryavtsev, 1996).

The volcano-sedimentary sequence commenced with a monotonous grey to greenish-grey polymict sandstone of Famennian age, which passes upwards into Lower Tournaisian greenish-grey tuffaceous sandstone and siliceous siltstone, with intercalated dacitic and andesitic volcanics and thin lenses of crinoidal limestone. Andesitic tuffs and lavas increase and predominate in the upper sections of the latter unit. In the western part of the district, the Tournaisian is more than 1000 m thick and is overlain by intensely altered felsic volcanics which define a domal structure, the core of which is occupied by the mineralised porphyritic granodiorite.

The felsic pile is composed of a lower massive rhyolitic tuff, overlain by flow banded, spherulitic and amygdaloidal rhyolitic lava flows and finally by flow banded rhyolitic lava through which the mineralised granodiorite porphyry has been intruded. The upper two units are up to 700 m in thickness (Kudryavtsev, 1996) and have been altered to highly aluminous "secondary quartzite" composed of quartz, quartz-alunite, quartz-sericite and diaspore-pyrophyllite which are the result of syn- and post-volcanic activity (Zvezdov *et al.*, 1993).

The granitoid rocks in the district are subdivided into the following, from oldest to youngest: i). Early Carboniferous (Visean) coarse-grained biotite-hornblende plagiogranite which is found in the southern part of the district where it is part of the large Toqrau pluton. ii). A late Lower Carboniferous (Serpukhovian/Namurian) complex composed of diorite, medium-grained granodiorite and the early porphyritic granodiorite (the main mineralising intrusive dated by the K-Ar method at approximately 335 Ma). iii). Late, porphyritic granodiorite to tonalite (324 Ma) and associated dykes, which in order of emplacement are composed of granodiorite porphyry, quartz-diorite porphyry and dolerite of Middle Carboniferous age. All are intra-ore and are consequently both mineralised and altered. The dykes are a few, to a few tens of metres in thickness and may be up to 1 km in length. iv). Late Carboniferous, coarse-grained, post mineralisation granitic rocks of the 300 to 285 Ma East Qonyrat pluton (Kudryavtsev, 1996).

The main structural elements of the district are northwest and northeast trending faults which control the direction of dykes and intrusive margins (Kudryavtsev, 1996). The main ore deposit is related to the northeast elongated, 1100 x 700 to 800 m northern stock of early porphyritic granodiorite, which intrudes Tournaisian volcano-sedimentary rocks on its eastern margin, and altered felsic volcanics on the remainder of its perimeter. The mineralised stock has undulose steep to vertical contacts and tapers slightly with depth. The contact has numerous dyke like apophyses of granodiorite porphyry extending up to 250 m outward from the main stock margin (Kudryavtsev, 1996).

Breccia pipes and pebble dykes of several stages are widespread, but are best developed in the eastern part of



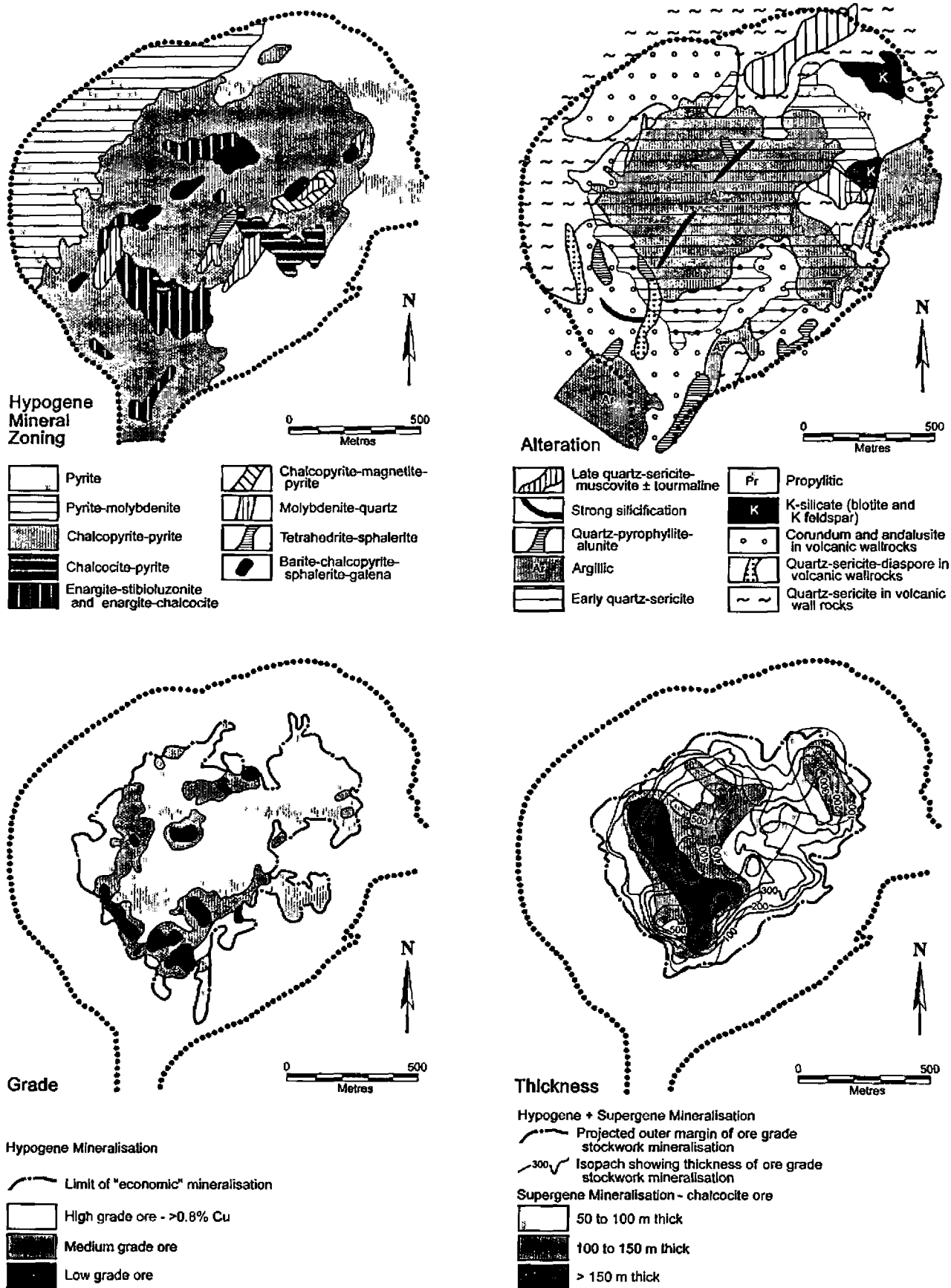


Figure 10b: The pit scale distribution of the ore mineralogy (top left), hydrothermal alteration (top right), Cu grade (bottom left) and the thickness of both the total orebody and the superimposed supergene enrichment blanket (bottom right) at the Kounrad porphyry Cu-Au deposit in south-eastern Kazakhstan. The common point of reference between the four plans and the pit geology shown on Fig. 9a (all of which are at the same scale) is the open pit pit outline. Note that the 'dot and dash' outline shown on most plans relates to the limit of ore and/or the mineralised stockwork, depending on the plan - and as a consequence is a little different on each. After Kudryavtsev, (1996), Zvezdov, et al., (1993) and Samonov and Pozharisky (1977).

silicified rhyolites. It has a generally northwest elongation, reflecting the orientation of the host intrusive, with dimensions of approximately 725 x 1050 m. Higher grade hypogene mineralisation (>0.8% Cu) is concentrated towards the outer margin approximating an annular shape with a lower grade (<0.8% Cu) core (Fig. 10b). This higher-grade annulus coincides with the more heavily fractured outer sections of the host granodiorite porphyry. The bulk of the mineralisation is present as uniformly disseminated sulphide grains which vary from several  $\mu\text{m}$  to several mm, averaging 0.2 to 0.5 mm, and as ore bearing stockwork veinlets of grey, greyish-white and white quartz containing sulphides and ranging from several tenths of a mm to 100 mm in thickness. Individual veins may be as long as several metres, and rarely up to a few tens of metres. At deeper levels stockwork veins are reported to thicken, although their frequency diminishes. The ore stockwork takes the form of a 200 to 400 m thick, sub-horizontal layer with an undulose lower surface, and thicker cores of high grade related to downward protrusions of the base of the zone. This morphology has been interpreted to represent a series of overlapping downward tapering cones (Kudryavtsev, 1996).

Hypogene mineralisation has been overprinted by a pronounced *supergene* profile, comprising an oxidised cap of from 2 to 50 m in thickness, averaging 20 m, underlain by a preserved leached zone of 7 to 56 m, averaging 32 m in thickness. Below the leached zone, a supergene enriched chalcocite blanket extends to depths of 350 to 450 m in the western part of the orebody, to 54 to 144 m below the surface in the eastern part (Kudryavtsev, 1996). The oxide cap contains hematite, jarosite and other limonites, cuprite, melaconite, native copper, brochantite and chrysocolla, while the zone of secondary enrichment is characterised by chalcocite and covellite (Zvezdov *et al.*, 1993).

The primary sulphide assemblage within the disseminated and stockwork ore comprises: pyrite, chalcopyrite, molybdenite, enargite, tetrahedrite and hypogene chalcocite, with accessory sphalerite, galena, bornite and magnetite, and rare covellite, arsenopyrite, marcasite, pyrrotite, idaite, colusite, native silver, native gold, tennantite, famatinite, luzonite, stibio-luzonite, ranerite, altaite, vallerite, cubanite, sternbergite, hematite. Although Cu is dominant Mo is present with a Cu:Mo ratio of close to 110 in the hypogene mineralisation. Within the breccia pipes described above, the quartz-sericite matrix of the early breccia contains pyrite, chalcopyrite, bornite, tetrahedrite and molybdenite. The late breccias carry barite, chalcopyrite, molybdenite and rarely sphalerite and galena in a phyllic altered matrix (Kudryavtsev, 1996).

The sulphide zoning illustrated on Fig. 10b outlines the distribution of nine assemblages, as follows: i) *Pyrite* within the older granitoids surrounding the mineralised porphyritic granodiorite plug on the eastern side of the deposit; ii). *Pyrite-molybdenite* within silicified rhyolites of the felsic volcanic suite on the northwestern margin of the mineralised porphyritic granodiorite plug; iii). *Pyrite-chalcopyrite* within silicified rhyolites of the felsic volcanic suite on the northwestern margin and within the mineralised porphyritic granodiorite plug (i.e. including the main

orebody); iv). *Pyrite-chalcocite* corresponding to part of the higher-grade annular ore zone within the host porphyritic granodiorite; v). *Enargite-stibioluzonite* and *enargite-chalcocite*, also occurring within the higher-grade annular ore zone, hosted by both the silicified rhyolites and porphyritic granodiorite, on either side of their mutual contact on the western side of the orebody; vi). *Chalcopyrite-magnetite-pyrite*, as a localised elongate zone coinciding in part with the northeast oriented string of occurrence of the following three assemblages; vii). *Molybdenite-quartz*, occurring as generally northeast elongated and aligned localised zones within the pyrite-chalcopyrite zone and hosted by both the silicified rhyolites and porphyritic granodiorite; viii). *Tetrahedrite-sphalerite*, as for vi.; ix). *Barite-chalcopyrite-sphalerite-galena*, as for vi. (Kudryavtsev, 1996, and references quoted therein).

Alteration and mineralisation has been subdivided into three stages, as follows: i) *Early syn- to post-volcanic alteration related to fumarolic-sulfataric activity* during the final stages of volcanism, prior to the emplacement of the mineralised early porphyritic granodiorite. This phase affects the rhyolites of the felsic volcanic suite and comprises quartz-sericite, quartz-sericite-diaspore assemblages. It is considered to have possibly continued during the emplacement of the intrusive phase. This phase produced a screen of non-reactive volcanics that were to subsequently partially surround the mineralised intrusive and focus the deposition of ore. ii). *A second stage related to the intrusion of the early porphyritic granodiorite*. This phase modified the altered felsic volcanics adjacent to the intrusive contact to produce an assemblage of corundum-quartz, quartz-andalusite, quartz-sericite and propylitic minerals, with a late quartz-kaolinite argillic suite. Within the intrusive, alteration of the porphyritic granodiorite was characterised by quartz-sericite accompanying the main Cu-Mo mineralisation, with a propylitic pyritic outer zone.

Argillic alteration, related to the final stages of mineralisation is superimposed on quartz-sericite rocks, being most intense in the transition from preceding quartz-sericite to propylitic zones. The early breccia pipes formed during this same interval. This stage of mineralisation and alteration originated at temperatures of from 400 to 240°C, with the early barren veinlet quartz at 400 to 380°C, pyrite at 330°C and tennantite at 240°C. iii). *The final stage related to the late porphyritic granodiorite to tonalite and associated dykes*. This stage is also associated with ore development and is characterised by mica-quartz-tourmaline within the porphyritic granodiorite and associated felsic dykes, while albite, K feldspar and biotite were formed within the dolerite dykes. The muscovite-tourmaline assemblage of this stage was formed at 470 to 440°C, while the late milky-white quartz was precipitated when the system had cooled to around 210 to 160°C (Kudryavtsev, 1996; Zvezdov *et al.*, 1993).

Zvezdov *et al.*, (1993) point out that chalcopyrite ore is largely confined to the zones of phyllic and argillic alteration within the granodiorite porphyry, while molybdenite, enargite and pyrite are restricted to areas of argillic and phyllic alteration (with considerable

accompanying chlorite) at the outer contact of the porphyritic granodiorite. Molybdenite increases with depth. They add that the galena-sphalerite association is a late feature and is controlled by northeast trending fractures across the Cu-Mo orebody.

#### **Koksai and Borly, Kazakhstan**

A number of other small to medium porphyry copper deposits are found around Lake Balkhash in Kazakhstan, both to the northwest and southeast of Kounrad. All lie within the 'Balkhash-Ili' zone of the Upper Palaeozoic Kazakh-Mongol magmatic arc and are associated with intrusives, similar to that described at Kounrad. They include Koksai and Borly, which are approximately 400 km southeast, and 50 km northwest of Kounrad respectively.

**Koksai** comprises approximately 320 Mt @ 0.52% Cu, 0.12 g/t Au (Table 1) and is associated with a porphyry laccolith cutting a sequence of Lower to Middle Carboniferous dacitic and rhyolitic lavas and tuffs, tuffaceous sandstones and sandstones which unconformably overlie Silurian basement. These are unconformably overlain in turn by Middle Carboniferous gritstones and tuffaceous sandstones with sub-volcanic rhyolite and andesite porphyries, and extrusive equivalents. The ore deposit is lens shaped, elongated in a WNW direction. Sulphides have been traced to a depth of 1000 m and comprise pyrite, chalcopyrite, magnetite, bornite and molybdenite. Alteration includes early silica-feldspar with associated chlorite, a subsequent acid quartz-sericite-chlorite stage and a late overprint characterised by calcite and sometimes barite (Seltmann *et al.*, 2004).

**Borly** is centred on the Carboniferous Borlinky intrusive body which is an apophysis of the larger Kyzylzhalsky pluton. The intruded sequence includes Lower Carboniferous rhyolitic to dacitic tuffs, litho-crystalline tuffs, lavas and subvolcanic rocks, overlain by a Middle to Upper Carboniferous suite of dacitic and sometimes trachydacitic or andesitic to dacitic ignimbrites, vitro-tuffs, tuffaceous lavas, lavas and sub-volcanic masses. Two separate elongated ore zones have been delineated, both striking north to northwesterly and dipping steeply to the northeast. The central orebody is 800 m long, 15 to 340 m wide and has been traced to a depth of between 200 and 460 m, while the eastern zone is 260 x 50 to 150 m at surface and persists to a depth of 120 m. The principal alteration style accompanying mineralisation is quartz-sericite with associated chlorite and carbonates. The sulphide assemblage comprises pyrite, chalcopyrite and molybdenite with minor sphalerite, tetrahedrite, tennantite, galena, magnetite, bornite, chalcocite and pyrrotite. The grade quoted averages 0.34% Cu, 0.011% Mo, 0.03 g/t Au (Seltmann *et al.*, 2004).

#### **Sayak, Kazakhstan**

The Sayak group of skarn deposits are located in the 'Balkhash-Ili' zone of the Upper Palaeozoic Kazakh-Mongol magmatic arc in eastern Kazakhstan (Figs. 3 and 4), which also embraces the large Kounrad, Aktogai Group and other porphyry Cu-Au-Mo deposits (Bespaev and Miroshnichenko, 2004). Sayak is approximately 140 km

east of the Kounrad deposit, a few tens of kilometres north of Lake Balkhash, and 450 km NNW of Almaty. The skarns of the district are medium sized Cu-Au-Mo deposits hosted by a Middle Carboniferous carbonate unit, and related to Carboniferous (330 Ma) granodiorite intrusives, similar to those hosting the large porphyry copper deposits of the same magmatic arc. The deposits contain more than 1 Mt of Cu and 30 tonnes of Au (Seltmann *et al.*, 2004; Kudryavtsev, 1996). See Table 1.

#### **Geology**

The Sayak deposits are hosted within the Sayak Group, a sequence of marine volcanogenic-carbonate-terrigenous molasse sediments of Middle Carboniferous age (from middle Viséan to middle Moscovian). The base of this sequence, is separated from the underlying Siluro-Devonian terrigenous sediments and pre-Silurian ophiolites by an angular unconformity, and the intervening Late Devonian (Famennian to the middle Viséan) Alabiin Formation. The *Alabiin Formation* comprises 350 to 500 m of alternating greywacke-sandstone, siltstone, gritstone and tuffite, with thin layers of limestone which pass into calcareous sandstone. The succeeding basal unit of the Sayak Group, the *Buruntas Formation*, is made up of 650 m of intercalated greywacke, polymict and arkosic sandstone, conglomerate, tuffaceous sandstone and tuffite. The conformably overlying Late Carboniferous (Bashkirian to Moscovian age) *Tastyquduk Formation* totals 1300 to 1650 m in thickness and commences with a sequence of clastic sediments which progressively fine upwards from a basal conglomerate. The uppermost 200 m of this formation is a carbonate unit that hosts all of the skarns of economic significance within the district. It commences in the west with 1 to 2 limestone beds, increasing to 5 to 7 in the centre of the basin, coinciding with a proportionate increase in the thickness of the unit. The carbonates of the *Tastyquduk Formation* are conformably followed by the lower Moscovian *Kungheisayak Formation*, composed of a 150 m thick basal conglomerate, overlain by 1000 m of rhythmically intercalated greenish-grey and buff sandstone, siliceous siltstone, thin limestone and tuffite beds (Kudryavtsev, 1996).

The Sayak Group is more than 4000 m thick and is intruded by numerous sub-volcanic bodies of basic, intermediate and felsic composition. The sedimentary basin in which it was deposited, the Sayak Basin, is an asymmetric graben with steep southern and southwestern, and gentle northern slopes. The structure of the basin is complicated by several anticlinal flexures and abundant faulting. All of the known skarn deposits are associated with local anticlinal ore controlling structures (Kudryavtsev, 1996).

Five main composite plutons cut the Sayak Basin sequence, localised in the central axis and the southern and northern margins of the basin, namely, the Aqshoqy, Zhambas, Kungheisayak, Lebai and Umit plutons (Fig. 11). The latter two are accompanied by Cu-Mo mineralisation, both in skarns and as disseminated, low grade porphyry-style. Two extended dyke swarms are evident, a northeast trending swarm associated with the Kungheisayak intrusive, while a northwest aligned set that cuts the northeast faults is

associated with the Umit pluton. The Umit and Lebai plutons are predominantly composed of granodiorite, although quartz diorite represents the initial phase of their intrusion. The other three plutons are tonalitic in composition, cutting initial phases of plagiogranite and hornblende-biotite granite. The tonalites of the Kungheisayak pluton fall within the age range of 347 to 307 Ma, while its plagiogranite is 314 to 310 Ma. In comparison, the granodiorite of the Umit pluton are 335 to 304 Ma (Kudryavtsev, 1996).

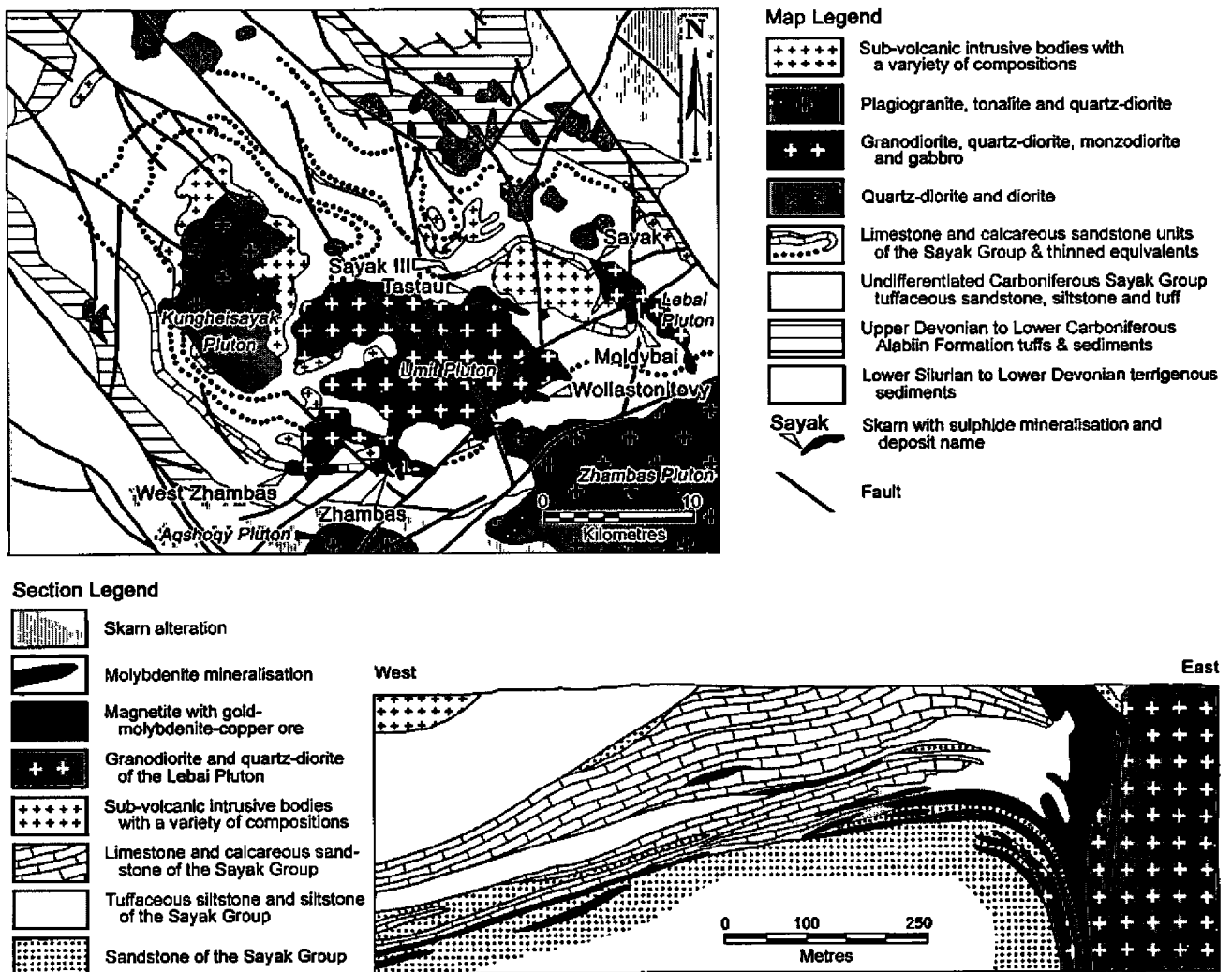
**Alteration and Mineralisation**

Mineralisation within the Sayak district is represented by i). hydrothermal skarn, ii). porphyry Cu and iii). veins. All of the mineralisation of economic significance however, is skarn-type, containing arseniferous Co-Au-Mo-Cu. The most important are in "near intrusion" locations on the northern contact of the Umit and western margin of the Lebai plutons, within a 2 to 3 km wide belt, hosted by Tastyquduk Formation carbonates. All are characterised by the presence of dyke swarms of diverse composition, systems of cross-cutting faults and fracture zones in anticlinal crests capped by impermeable tuffaceous siltstones. Individual orebodies have strike lengths of from

0.5 to 12 km, although the distribution of grade is very patchy, occurring as veins, or as sheet-, ribbon-, pipe- or pocket-like masses, or as irregular shapes (Kudryavtsev, 1996).

The deposits exhibit a zonation outwards from the intrusive contact along the host carbonate bed, as follows: i). An inner zone of magnetite, immediately outboard of the granodiorite contact, with Mo-Cu ores, native gold, and associated late garnet and pyroxene-garnet skarn alteration. Pre-skarn potassic and sodic alteration of aluminosilicate rocks are rare. Poorly mineralised endo-skarn alteration of the granodiorite plutons and dyke rocks was coeval with the skarn development. ii). The "middle part" of the ormetasomatic zonation is represented by Au-Bi-Cu mineralisation associated with epidote- and actinolite-altered carbonates. The actinolite rich segment marks the outer rim of the ore deposit. iii). The "outer" propylitic transition to unaltered marble and limestone is characterised by quartz-calcite-chlorite alteration (Kudryavtsev, 1996).

The largest of the deposits of the Sayak district is Sayak-I (Sayak), developed on the western exo-contact of the Lebai pluton, and concentrated in a north to northwest trending anticlinal axis which plunges to the south. The fold is



**Figure 11: Geological plan showing the distribution of skarn mineralisation in the Sayak district (top) and a representative cross section (bottom) illustrating the geology, alteration and mineralisation at the Sayak skarn Cu-Au deposit in southeastern Kazakhstan. After Kudryavtsev, (1996).**

asymmetric, with a gently dipping (<15°) western limb, opposite the pluton margin. In contrast, the eastern limb dips into the pluton at 25 to 30°, steepening to 60 to 90° at depth. The area also corresponds to the maximum development of the host carbonate of the upper Tastyquduk Formation which at Sayak-I totals 200 m in thickness. The host carbonate is composed of two beds which are 30 to 50 m and 130 to 150 m thick respectively, separated by a thin impersistent layer of tuffaceous siltstone and sandstone, and overlain by a thick bed of tuffaceous siltstone to siltstone. The axis of the mineralised fold is almost parallel to the pluton contact in the centre of the deposit, where the contact is near vertical, although, it shallows to the north. The pluton is composed of granodioritic adjacent to Sayak-I, while the dense array of dykes that cut the ore deposit are predominantly diorite porphyry and dolerite, with lesser granite and plagiogranite. These dykes are generally 3 to 5 m thick and of different relative ages, including pre-, intra- and post-ore (Kudryavtsev, 1996).

Contact metamorphism has hornfelsed the silicate lithologies and produced marbles from the carbonates, while metasomatic processes have formed the skarns over a width of 500 to 1000 m outboard from the intrusive contact, over a length of 3 km parallel to the pluton margin. Skarn alteration has also locally affected dykes of diorite and granodiorite. At the immediate intrusive contact, the limestone host is completely altered to skarn over a 40 to 100 m thickness parallel to the contact, forming a steeply dipping, generally tabular body. On its western margin, this skarn body splits into isolated sheets parallel to the host bedding, which finally give way to marble and recrystallised limestone at the rim of the skarn zone, down dip on the western limb of the fold (Fig. 11) (Kudryavtsev, 1996).

The main skarn is composed of pyroxene-garnet and pyroxene-feldspar. Post-skarn alteration is widespread, with quartz-actinolite-calcite-chlorite and epidote rich propylitic rocks well developed at the transition from skarn to marble and limestone. A major magnetite body formed on the northern part of the deposit almost simultaneously with the epidote- and actinolite-bearing alteration. Au-Mo-Cu mineralisation occurs in both skarn and magnetite hosts, as well as in actinolite and quartz-calcite-chlorite calc-silicate altered rocks, while a steeply dipping 10 to 15 m thick zone of poorly disseminated mineralisation occurs within the granodiorite intrusion. The bulk of the ore is concentrated as a complex "near contact" lode, dipping roughly parallel to the host carbonates and to the intrusive contact to a depth of 500 m. The Cu grades are highest in the centre of the lode, decreasing down dip and towards the margins. Mo mineralisation is best developed on the gently dipping west limb of the fold where it is hosted by the basal sections of the skarn and by altered sandstone in the footwall of the carbonate unit. These bodies extend for 350 to 750 m in a northeast direction, parallel to the fold axis, with widths of 25 to 60 m in the northeast and up to 250 m in the southeast. They average 0.35% Mo with 0.2 to 0.3% Cu (Kudryavtsev, 1996).

There is a well developed zonation within the orebody. Pyroxene-feldspar and pyroxene-garnet skarns contain

magnetite rich ore and limited bornite-chalcocopyrite, while the garnet skarn hosts molybdenite-bornite-chalcocopyrite to the north. Arsenopyrite-cobalt mineralisation predominates in the outer actinolite and quartz-calcite-chlorite altered rocks. The intensity of mineralisation is related to the Fe/(Fe+Mn) ratio of the alteration minerals. The highest grades accompany skarns with 70-80 mol% andradite and 20-30 mol% grossular and high Fe pyroxene (>60 mol% hedenbergite). In contrast, the barren skarn has >60 mol% grossular and 5 to 25% hedenbergite. Similarly, rich Cu mineralisation accompanies Fe-rich epidote and chlorite of the thuringite series. The primary ores contain chalcocopyrite, magnetite, bornite, pyrrhotite, arsenopyrite and cobaltite, with rare pyrite, molybdenite, marcasite, melnikovite-pyrite, native gold, galena, sphalerite, electrum, calaverite, petzite, sylvanite and nessite. Oxidation is only poorly developed, limited to depths of 10 to 15 m, accompanied by the formation of azurite, cuprite, chalcocite and scorodite (Kudryavtsev, 1996).

There is strong evidence to confirm that the metallic mineralisation post dates skarn formation. Fluid inclusion studies indicate a reverse temperature zoning of skarn and ore minerals. The earliest and highest temperature (590 to 540°C) gersdorffite-arsenopyrite-cobalt assemblage is found in the relatively low temperature (430 to 210°C) outer quartz-calcite-chlorite rocks. The medium temperature (540 to 470°C) emplectite-chalcocopyrite-pyrrhotite assemblage is typically found in the middle epidote-actinolite (630 to 440°C) zone, while the relatively cool wittichenite-molybdenite-chalcocopyrite mineralisation occurs in the high temperature (670 to 600°C) proximal skarn (Kudryavtsev, 1996).

In addition to Sayak-I, there are a number of other similar skarns with significant economic mineralisation, including Sayak-III and IV, and Tastau.

#### *Kal'makyr -- Dalnee, Uzbekistan*

The contiguous Kal'makyr-Dalnee Cu-Au deposits of the Almalyk district in Uzbekistan, are located approximately 45 km southeast of the capital, Tashkent. Together, they represent the largest ore tonnage of the known porphyry systems of central Eurasia, containing >21 Mt of Cu and >2650 tonnes of Au in >5 Gt of ore, although they are rivalled by the higher grade Oyu Tolgoi deposits in Mongolia. They were emplaced within the Carboniferous Valerianov-Beltau-Kurama magmatic arc (Fig. 3) at approximately 320 to 290 Ma.

Kal'makyr has been mined on a large scale (up to 27 Mt of ore per annum) since 1954, while Dalnee, the down plunge continuation of the same mineralised system, has not yet been brought into production. Mineralisation at both is predominantly in the form of stockwork veining with lesser disseminations, and is associated with Late Carboniferous quartz monzonite porphyry plugs intruding earlier dioritic and monzonitic intrusive rocks of the same magmatic complex. The orebodies take the form of a cap like shell developed above and draped over the flanks of the related quartz monzonite porphyry stock. Alteration comprises an early K-silicate phase followed by albite-actinolite and peripheral epidote-chlorite-carbonate-pyrite propylites,



overprinted by an abundant phyllic episode which is closely related to the final distribution of the ore. Associated mineralisation commenced with barren quartz-hematite veining, followed by quartz-magnetite, quartz-pyrite-molybdenite-chalcocopyrite with the bulk of the contained gold, quartz-carbonate-polysulphide with lesser gold, then by zeolite-anhydrite, and finally carbonate and barite veining. The geology, mineralisation and alteration at Kal'makyr and Dalnee are described in more detail in part 2 of this pair of papers (Golovanov *et al.*, 2005 - this volume).

At Kal'makyr, the dominant hosts to ore are the monzonite and diorite wall rocks, with the quartz monzonite porphyry only containing ore in its outer margins, surrounding and/or overlying a barren core. The barren core is surrounded by an elongate annulus of high grade (>0.8% Cu, including 'eyes' of >1.4% Cu) hypogene mineralisation and within a broader annular zone with a radial width of 200 to 500 m which is reported (Sokolov, 1995) to average 0.7% Cu. This is in turn flanked by a broad halo of low grade mineralisation with grades of from 0.1 to 0.3% Cu (see Fig. 5 in Golovanov *et al.*, in this volume). The deposit is capped by an up to 70 m thick zone of variably developed oxidation, leaching and supergene sulphide enrichment which laterally varies from high grade oxide ore to leached capping overlying either supergene sulphides of a partially or wholly oxidised supergene blanket.

The historic production and reserves/resources at Kal'makyr, Dalnee and the Sarycheku orebody (18 km to the south) are summarised in Table 2. These figures also incorporate the halo of low grade mineralisation (0.1 to 0.3% Cu) that has not been differentiated from either past production or remaining reserve/resource estimates. Statistics available (e.g. Golovanov *et al.*, 2005, in this volume) are largely based on recovered grades and on tonnages treated at the metallurgical facilities. The figures listed in Table 2 attempt to provide data on the *in situ* ore and are based on discussions with mine staff and back-calculations taking into account metallurgical recoveries, but still incorporating the low grade mineralisation.

**Table 2: Historic production and resource/reserve statistics for the Kal'makyr, Dalnee and Sarycheku porphyry Cu-Au deposits of the Almalyk district, Uzbekistan.** The 'Ore' column represents the millions of tonnes of ore treated, excluding any stockpiled, while the 'recovered' columns are based on the tonnes of metal obtained after losses in the concentrator and smelter. The '*in situ* ore' columns are the grade and tonnes of metal contained in the original ore and assume a metallurgical recovery of between 75 and 80% of the contained Cu. The Sarycheku figures combine both production and resources. Estimates based on information from Kal'makyr mine geologists, pers. comm., and from Golovanov, *et al.*, (2005, this volume).

	Ore Mt	Cu%	Au g/t	Mo%	Recovered				In situ ore	
					Ag g/t	Cu Mt	Au t	Mo Kt	Cu%	Cu Mt
Kalmakyr Mined	775	0.38	0.51	0.006	2.5	2.94	650	38.34	0.49	3.6
	to 700	to 0.42	to 0.6						to 0.54	
Remaining	1750	0.38	0.5	0.006	2.5	6.6	900	104	0.49	8.5
	to 1650	to 0.4	to 0.6						to 0.51	
Oxide dump Low grade	140	0.27	0.65	0.006	2.5	0.378	91			0.38
	1700	0.17				2.8				
Dalnee	2800	0.36	0.35	0.004		10.2	995	105	0.46	13
	to 2500	to 0.4	to 0.5						to 0.51	
Sarycheku	200	0.5	0.09	0.0075		1	18	6.9	0.64	1.25
TOTAL	5665	0.37	0.4	0.006		21	2650		0.47	27
	to 5000	to 0.40	to 0.53						to 0.51	

Note: Total excludes Kal'makyr low grade mineralisation. The range of grades and tonnages are the limits of available estimates.

### Kochbulak, Uzbekistan

The Kochbulak epithermal Au-Ag deposit is located in Uzbekistan, 30 km northeast of the giant Kal'makyr-Dalnee porphyry copper deposits and 55 km southeast of the capital, Tashkent. It was emplaced within the Carboniferous Valerianov-Beltau-Kurama magmatic arc (Fig. 3) at approximately 290 to 280 Ma, and prior to mining contained approximately 135 tonnes of gold at an average grade of 12 g/t Au, 120 g/t Ag. See Table 1.

Kochbulak is not a porphyry Cu/Au deposit. However, it is hosted by the same magmatic arc that has produced the giant Kal'makyr and Dalnee deposits a few tens of kilometres to the southwest in the Almalyk district, and is less than 20 M.y. younger than the 315 to 290 Ma age of mineralisation at Kal'makyr (Seltmann *et al.*, 2004, Golovanov *et al.*, 2005, in this volume). In the light of the comments on the inter-relationship between porphyry Cu-Au and epithermal Au deposits in the Introduction to this paper, it is reasonable to imply that Kochbulak might represent the higher level, late phase of a hydrothermal system, similar to that which produced the giant porphyry deposits of the Almalyk district, and as such provides a broader appreciation of the porphyry systems being discussed in this paper. It is therefore described here as an example of the magmatic arc hosted epithermal deposits of central Eurasia. It must be stressed that it is not representative of all epithermal deposits in the belt. An exploration model currently controversially discussed among local researchers emphasises that the setting of Kochbulak relates to a stratovolcano, having similarities with Mt. Pinatubo or Bingham Canyon, and may host mineralised porphyry systems at depth, thus qualifying for the continuum model addressed by Cole (2000) and further elaborated in Yakubchuk *et al.*, (2002).

### Geology

The Kochbulak gold deposit is located within the Karatash caldera at the intersection of the South Angren and Lashkerek-Dukent fault zones. The caldera is filled by: i). The Middle to Upper Carboniferous Akcha Formation

which comprises more than 1000 m of andesitic and dacitic lavas, and pyroclastic rocks. ii). The unconformably overlying Nadak Formation, which has been divided into ten units and commences with a basal volcani-mictic conglomerate and sandstone, overlain by andesitic and dacitic lavas and tuffs. The relatively thick units of lava and tuff are separated by thin interlayers of tuffite, sandstone and siltstone. iii). The Upper Carboniferous Oyasai and Upper Permian to Lower Triassic Kyzylnura formations which comprise rhyolitic lava and pyroclastics confined to the southern part of the caldera (Islamov *et al.*, 1999).

The volcanic succession of the caldera, which represents a calc-alkaline to sub-alkaline, high potassic latite series, is cut by dykes, sub-volcanic intrusions and associated extrusives. The sequence is also cut by Middle Carboniferous pre-mineral granodiorite and monzodiorite porphyry which are comagmatic with the Akcha Formation at the base of the caldera, and by minor rhyolite intrusions related to the Oyasai Formation. Pre-mineral basic dykes of Early Permian age are widespread, while rhyolite, granosyenite, syenite, monzodiorite porphyry and late basic dykes are post-mineral (Islamov *et al.*, 1999).

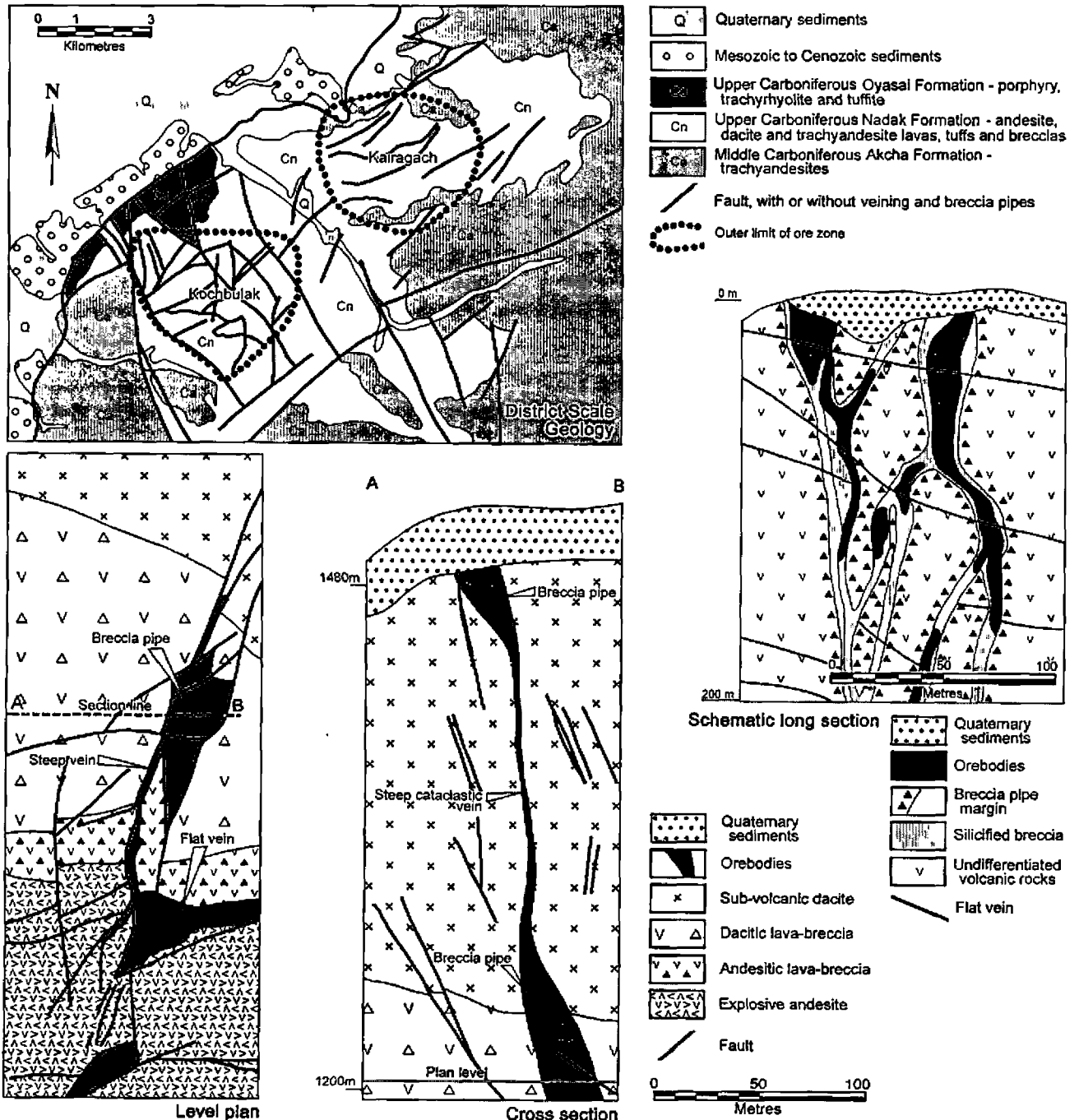


Figure 12: Geology, alteration and mineralisation at the Kochbulak epithermal Au deposit, Uzbekistan. The district scale geology plan (top left) shows the location of both the Kochbulak and neighbouring Kairagach deposits and the structural elements that control the distribution of mineralisation. A representative level plan and coincident cross section (bottom left) illustrate the relationship between structure and the distribution of steep and flat vein, and breccia pipe mineralisation, while a schematic long section (centre right) shows the morphology of the breccia pipe mineralisation and alteration. After Islamov *et al.*, (1999) and references cited therein.

The deposit area is cut by four large, near north-south trending faults which dip steeply to the west and southwest. Further sets of intervening fractures parallel to the main trend are found in the deposit area, as are intra-formational detachments along the contacts between massive lava units (Islamov *et al.*, 1999).

The Kochbulak mineralisation is restricted to volcanics of the Middle to Upper Carboniferous Nadak Formation on the northern flank of the caldera, close to the Shaugaz Fault. The setting corresponds to the near vent facies of a strato-volcano which was rimmed by sub-volcanic intrusives. Approximately 120 orebodies have been tested, controlled by 32 mineralised structures within a volume of some 4500 x 3000 x 550 m (Kovalenker *et al.*, 1997; Islamov *et al.*, 1999; Yakubchuk *et al.*, 2002).

#### *Alteration and Mineralisation*

Three types of orebody are recognised, as follows: i). Steeply dipping, north to northeast aligned veins (40% of the reserve) controlled by the major and intervening faults described above. Some 45 of these steep veins are recognised; ii). Moderately dipping, (20 to 40°) near east-west veins (20% of reserves) which are concentrated where the north-south fault set intersects the intraformational detachments, also mentioned above, and iii). Pipe-like orebodies (40% of the reserves), which are composed of mineralised explosion breccia and which terminate the steeply dipping vein set. There are some 14 pipes, each with a small diameter, but high grade (Islamov *et al.*, 1999).

Mineralisation occurs as massive, banded, brecciated and breccia like textures, with festoon and incrustate structures. Quartz is the dominant gangue mineral, varying from coarse-grained to meta-colloidal to drusy, chalcedonic and amethyst, accompanied by subordinate carbonates and barite. The sulphide content of the two vein types is generally <10%, while in the breccia pipes it may reach 20%. Gold is mainly present as microscopic inclusions, occurring as sheeted, dendritic and cloddy grains in the upper levels and as spongy and drusy gold lower in the deposit. The finest gold is within meta-colloidal quartz, calaverite, sylvanite and altaite, while that in goldfieldite, chalcopryrite and galena is of lower fineness. Electrum accompanies sulphosalts and sulphostannites (Islamov *et al.*, 1999).

The gold mineralisation is present in three associations, namely: i). *Gold-telluride*, which occurs as calaverite, petzite, sylvanite, hessite, stutzite, empressite, goldfieldite and a wide range of other tellurides, and is particularly well developed in the upper level veins and in shallow-formed breccia pipes. ii). *Gold polysulphide* comprises the association of native gold with sulphides of Cu, Pb, Zn, Bi and Sb, and is most frequently found in the upper levels of both the steep and flat veins. iii). *Gold-pyrite*, which is found to varying degrees throughout the system, but is best developed and mineralised with increasing depth. It predominantly occurs as disseminated, uneconomic mineralisation with finely dispersed gold in pyrite, generally only averaging 4 g/t Au (Islamov *et al.*, 1999). In general, the explosive breccia pipes are found in the upper levels of

the deposit, passing through a transition zone to steeply dipping mesothermal veins at depth. Mineralisation is known to extend a depth of more than 2000 m.

The pattern of development of the three gold mineralisation associations is zoned both vertically (as described above), and laterally, with the gold-telluride association being the most proximal, within and immediately adjacent to the veins, flanked by the gold-polysulphides, passing out into the lower grade quartz-sulphide association. The distribution is also complicated by the telescoping and resultant superposition of the three zones from different episodes of mineralisation as the deposit evolved (Islamov *et al.*, 1999).

The host volcanics underwent a mild propylitic alteration forming chlorite-carbonate and epidote prior to mineralisation. Alteration related to mineralisation within both the steeply dipping and shallow veins is evident as a regular zonation, with a progressive outward gradation from the ore vein to i). hydrosericite; ii). adularia-sericite; and iii). chlorite-carbonate, to iv). the 'unaltered' country rock. All of the altered rock contains pyrite, which decreases from around 30% in the hydrosericite to 10% in the chlorite-carbonate zone. Pervasive sericite-hydromica dominates in the exploited parts of the deposit, while the chlorite facies was only penetrated in drilling at depths of >1200 m. The breccia-pipe bodies are accompanied by an intense silicification of the hosts, accompanied by variable amounts of sericite, alunite and diaspore (Islamov *et al.*, 1999).

The Kairagach gold deposit is hosted by similar rocks within the same caldera, some 3.5 km to the northeast of Kochbulak. It has a potential resource of 50 t of Au and 150 t of Ag at a comparable grade to Kochbulak and is similar in many aspects, but with variations in detail (Islamov *et al.*, 1999).

#### *Benqala, Kazakhstan*

Benqala North and South represent a small to medium sized porphyry Cu-Au system in northern Kazakhstan, approximately 450 km north of the Aral Sea, and 300 km southeast of Magnitogorsk in the Russian Urals. They were emplaced within the Carboniferous Valerianov-Beltau-Kurama magmatic arc (Fig. 3) and are believed to contain around 30 tonnes of contained gold at an average grade of 0.3 g/t, which would equate with approximately 100 Mt of ore. The hypogene Cu grade has been quoted at 0.42% Cu, with 0.55% Cu in the oxide zone.

Mineralisation is associated with Lower to Middle Carboniferous intrusions and dykes of the Sokolov-Sarbai diorite-granite complex which intrude a middle to upper Visean (Lower Carboniferous) volcano-sedimentary sequence. In the western part of the district, the latter is predominantly volcanic, comprising dacites, andesites, andesitic-basalt and basalt porphyry, while to the east it is largely tuffs and sediments, including tuffites, tuffaceous sandstones, tuffaceous siltstones, and tuffaceous argillites, with thin interbeds of effusives and other sedimentary rocks. The mineralised intrusive comprises an early porphyritic quartz diorite and later associated granodiorite and plagiogranite porphyries. Pre-ore dykes of granite porphyry

and post ore micro-dolerite, dolerite and lamprophyre are widespread.

Mineralisation is present as a stockwork which is restricted to the northwestern margin of the host porphyry. The main ore zone has dimensions of more than 1200 x 700 m and extends to a depth of 700 m. It has been subjected to oxidation to 110 m below surface, which is thickest over the immediate ore deposit and its altered hosts. Alteration comprises an early alkaline phase characterised by albite, K feldspar, biotite, silica and tourmaline, accompanied by a propylitic halo of chlorite, epidote and prehnite. This was overprinted by an acid quartz-sericite phase and the development of chlorite and carbonate alteration. The principal metallic minerals are pyrite, chalcopyrite and magnetite, with minor molybdenite, bornite, chalcocite, digenite and rutile (Seltnann *et al.*, 2004).

#### *Tuwu-Yandong, Xinjiang - China*

The Tuwu, Yandong (6 km west of Tuwu), Chichu (30 km ENE of Tuwu) and Linglong porphyry Cu-Au deposits are located within eastern Xinjiang in western China, some 500 km ESE of the provincial capital of Urumqi and 80 km directly southwest of the city of Hami. They were deposited at 330 Ma during the Carboniferous, within the Kazakh-Mongol magmatic arc. They occur immediately to the north of the major Kangguer Fault which marks the northern margin of the broad, transitional suture zone between the arc and the Tarim micro-continent to the south. To the south of this fault, a 10 km wide belt is characterised by an ophiolite bearing ductile shear deformed melange. The Carboniferous island arc succession that hosts the deposits is bounded to the north by a Devonian arc assemblage (Wang *et al.*, 2001a; 2001b, Mao *et al.*, 2003).

The Tuwu-Yandong cluster of deposit is quoted as containing 7.5 Mt of Cu metal (Kirkham and Dunne, 2000). Han *et al.*, (2003), quote a resource at the main Tuwu deposit alone of 144.5 Mt @ 0.72% Cu, 0.16 g/t Au at a 0.5% Cu cut-off, or 292 Mt @ 0.49% Cu at a 0.2% Cu cut-off.

#### *Geology*

The arc and overlying sequence north of the Kangguer Fault comprises the Carboniferous (Han *et al.*, 2003; Wang *et al.*, 2001a, 2001b), or Devonian (Qin *et al.*, 2002) Qi'eshan Group, which has been subdivided into the following units, from the base: i). Unit 1 - light grey-brown, grey and grey-green medium to coarse-grained schistose greywacke - >100 m thick; ii). Unit 2 - purple-red andesitic volcanic breccia and grey-green tuff - 100 m thick; iii). Unit 3 - grey-green amygdaloidal basalt - 130 m thick; iv). Unit 4 - grey-green and light grey to grey-white pebbly-lithic sandstone, locally grading into polymictic conglomerate, lithic sandstone and bedded tuff, with intercalated basalt, andesite and dacite flows - 170 m thick; v). Unit 5 - grey-green amygdaloidal spilite-keratophyre lavas and brecciated flows, including intercalated trachy-basalt, basaltic trachy-andesite, trachy-andesite, dacite and rhyolite. This unit is the principal wall rock and host to the mineralised intrusives of the Tuwu porphyry Cu-Au deposit - 200 m thick; vi). Unit 6 - grey-green polymict

conglomerate with granite, basalt and felsic porphyry clasts, with intercalated fine-grained lithic sandstone - 25 m thick.

The Qi'eshan Group is unconformably overlain by Middle Triassic sandstone and conglomerate of the Xishanyao Formation and by Quaternary sand and gravel cover (Han *et al.*, 2003).

Diorite porphyry and at least 23 individual small stocks of plagiogranite porphyry have been intruded into the Qi'eshan Group in the Tuwu district. The plagiogranite intrusives are massive in appearance and have a porphyritic texture with phenocrysts of quartz, plagioclase and biotite in a subhedral matrix and comprise the mineralised porphyries of the district hosting the Tuwu, Yandong, Linglong and Chichu porphyry Cu-Au deposits (Han *et al.*, 2003).

While Han *et al.*, (2003) describe the deposit as lying within a consistent south dipping succession as described above, Wang *et al.*, (2001a; 2001b) concluded that the mineralised diorite and plagiogranite porphyries have intruded the core of an east-west trending anticline of Qi'eshan Group sediments and volcanics, the limbs of which comprise an outward succession of siltstones, to tuffs and then basalt. This would imply a thinner host succession with only four units. Wang *et al.*, (2001a; 2001b) also observe that the intersection of east-west strike slip faulting and cross trending NNW structures control the localisation of mineralisation. The diorite porphyry, which trends ENE and covers an area of 4 km<sup>2</sup>, precedes the less extensive plagiogranite porphyry.

#### *Alteration and Mineralisation*

The main Tuwu porphyry Cu-Au deposit is a steeply dipping, east-west elongated body with a surface length of 1400 m, a maximum width of 175 m (20 m at surface, thickening with depth) and down-dip extent of more than 600 m. Its hangingwall and footwall both dip south at 60 to 65° and 65 to 80° respectively, while the orebody tends to plunge to the east. A lower grade deposit, Tuwu East, which is 1300 m long and varies from 32 to 85 m in width, occurs 200 m to the east of the main Tuwu orebody (Han *et al.*, 2003; Wang *et al.*, 2001a; 2001b).

Mineralisation occurs as veinlet, disseminated and less commonly nodular sulphides, principally chalcopyrite and pyrite, with minor bornite, sphalerite, magnetite and rickardite. Molybdenite is also present at Tuwu East. Chalcocite and digenite are found in the supergene enriched ore, while malachite occurs in the oxide zone. Gangue minerals within, and as selvages to veinlets, are quartz, plagioclase, sericite, chlorite and biotite with minor pyroxene, epidote, zoisite and calcite. Mineralisation is hosted by plagiogranite porphyry which occurs in the deposit area as large dykes, in the adjacent diorite porphyry and in basaltic wall rocks. Within the plagiogranite, sulphides are predominantly disseminated, with the principal copper sulphide being medium- to coarse-grained chalcopyrite (or chalcopyrite aggregates) while in the volcanics and diorite porphyry, mineralisation takes the form of well-developed disseminations, veinlets and aggregates of chalcopyrite with associated disseminated bornite (Han *et al.*, 2003).

A number of hypogene mineralised stages are recognised, as follows: i). Stage 1 is characterised by biotite alteration, accompanied by albite and K feldspar, with disseminated chalcopyrite + bornite mineralisation; ii). Stage 2 comprises phyllic alteration with associated quartz + pyrite + chalcopyrite assemblages occurring as veins; iii). Stage 3 is represented by quartz-molybdenite veining and molybdenite disseminations; iv). Stage 4 is composed of sulphates (gypsum and anhydrite) with some accompanying sulphide veinlets; v). Stage 5, late stage carbonate (calcite), laumontite and minor sulphides. The hypogene mineralisation has been subjected to oxidation at surface with the formation of malachite and limonite with brochantite and black copper-wad, underlain by some supergene enrichment to produce chalcocite and digenite (Han *et al.*, 2003). There is an outward alteration zonation of alteration as follows: i). siliceous core; ii). biotite;

iii). phyllic; iv). argillic; and v). propylitic outer halo (Fig. 13). In practice however, only three alteration styles are recognised. Phyllic alteration (including an intensely siliceous zone) predominates in the plagiogranite porphyry in the core of the deposit, and is associated with the main orebody, comprising quartz-sericite (muscovite and hydro-muscovite), with minor albite and chlorite. The chlorite-biotite zone is found in the more extensive diorite porphyries (and basalts ?) into which the plagiogranite porphyry dykes were intruded, and as such is on either side of the phyllic zone. It accompanies the outer sections of the main orebody and is characterised by mafic biotite with minor accompanying K feldspar. The outer propylitic zone is mainly composed of chlorite, epidote and albite and is only accompanied by low grade mineralisation on the periphery of the orebody (Han *et al.*, 2003; Wang *et al.*, 2001a; 2001b).

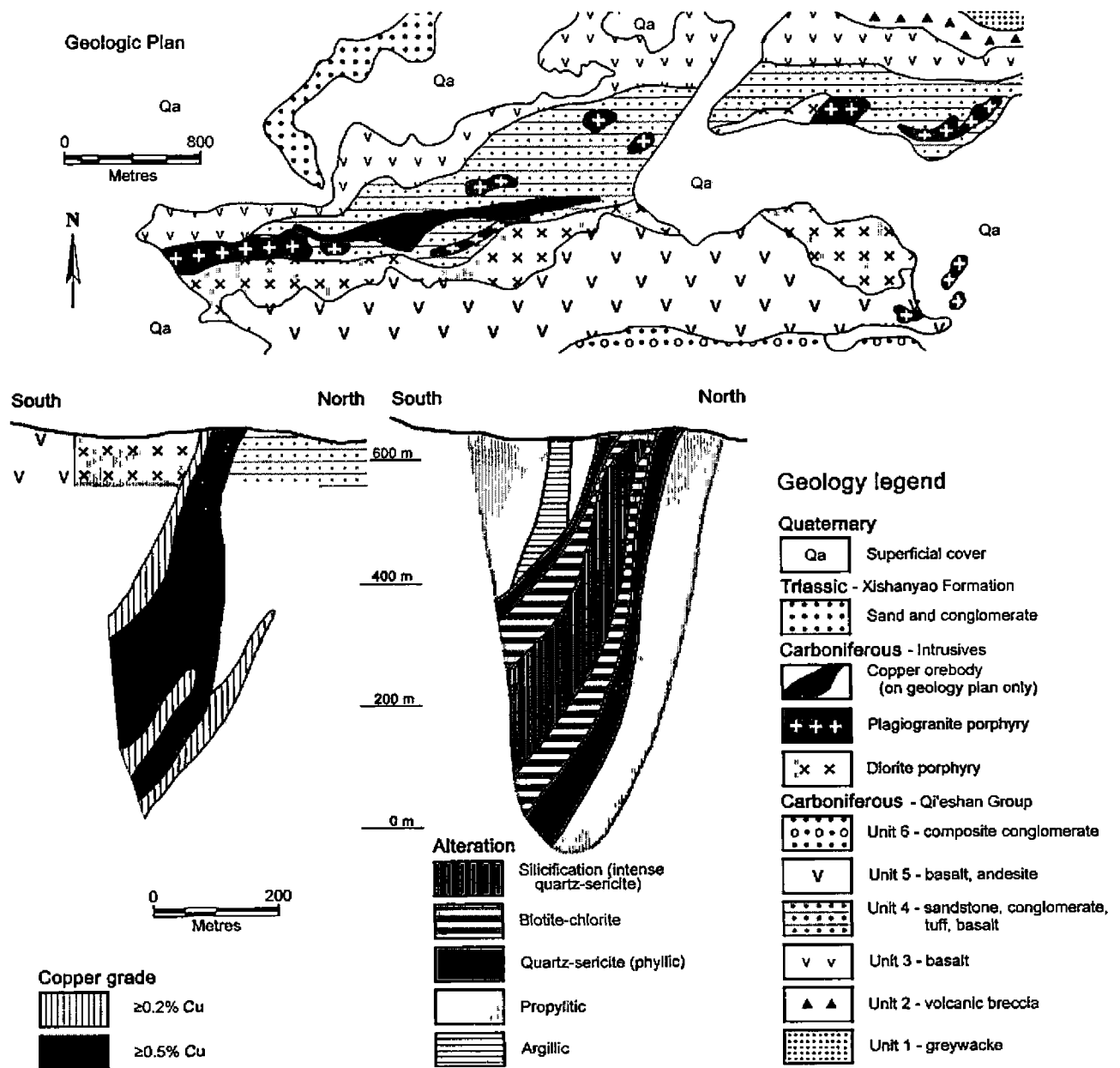


Figure 13: Geologic plan (top), and grade (bottom left) and alteration zoning (bottom centre) cross sections through the Tuwu porphyry Cu-Au deposit, Xinjiang, China. After Han *et al.*, (2003) and Wang *et al.*, (2001a, 2001b).

### Oyu Tolgoi, Mongolia

The Oyu Tolgoi porphyry Cu-Au deposit is located approximately 550 km due south of Ulaanbaatar in southern Mongolia, and 80 km north of the Chinese-Mongolian border. It was formed at 370 Ma (Late Devonian) in the Kazakh-Mongol magmatic arc, and is among the largest and richest known hypogene porphyry Cu-Au deposit in the world.

During the 1980s, a joint Mongolian and Russian regional geochemical survey of the region reported a molybdenum anomaly over what is now the Central Oyu deposit (Fig. 14). Follow-up work noted evidence of copper mineralisation and alteration at South Oyu in the form of sub-cropping malachite, chrysocolla and copper wad. In addition, a number of small, circular pits and minor copper-bearing slag were evident at South Oyu, probably relating to Bronze age activity. A subsequent inspection in 1996 by Magma Copper geologists recognised outcrops of stockwork quartz veining at Central Oyu which were identified as the leached cap of a porphyry copper deposit. Subsequent testing by BHP Minerals after their acquisition of Magma Copper indicated 438 Mt @ 0.52% Cu and 0.25 g/t Au at South and Central Oyu (Perello *et al.*, 2001; Kirwin *et al.*, 2005). The project was farmed out to Ivanhoe Mines in 1999 who have continued exploration to the present. For details of its discovery and delineation see Kirwin *et al.*, (2003).

Declared resources in April 2005 (Ivanhoe Mines press release, May 2005) were:

- At a 0.6% Cu equivalent cut-off, the Measured + Indicated resource = 1.149 Gt @ 1.30% Cu, 0.47 g/t Au, or 1.54% Cu equivalent; plus an Inferred resource = 1.160 Gt @ 1.02% Cu, 0.23 g/t Au, or 1.16% Cu equivalent. The total Measured + Indicated + Inferred resource = 2.309 Gt @ 1.16% Cu, 0.35 g/t Au, or 1.35% Cu equivalent, comprising 26.8 Mt of contained Cu and 810 tonnes (26 Moz) of contained Au.
- At a 1% Cu equivalent cut-off, the Measured + Indicated resource = 0.647 Gt @ 1.82% Cu, 0.58 g/t Au, or 2.13% Cu equivalent; plus an Inferred resource = 0.602 Gt @ 1.35% Cu, 0.28 g/t Au, or 1.54% Cu equivalent. The total Measured + Indicated + Inferred resource = 1.249 Gt @ 1.59% Cu, 0.44 g/t Au, or 1.36% Cu equivalent, comprising 19.8 Mt of contained Cu and 550 tonnes (17.5 Moz) of contained Au.

The extent of economic mineralisation is currently only partially tested, and is open to the north and at depth, with potential for the current drilled resource to be substantially increased. Step-out drilling 200 and 450 m to the north of the 3.5 km long Hugo Dummett deposit intersected 608 m @ 3.24% Cu, 0.82 g/t Au (including 322 m @ 4.59% Cu, 1.07 g/t Au) and 324 m @ 2.45% Cu, 1.23 g/t Au respectively. This drilling is progressively following a 3 km long extension of the induced polarisation anomaly that follows the known mineralisation (Ivanhoe Mines press release, June 2005).

### Regional Setting

The Oyu Tolgoi deposit lies within the Middle Palaeozoic Kazakh-Mongol magmatic arc, represented by a 100 to 250

km wide arcuate swathe of arc-related terranes in southern Mongolia (Fig. 14). This swathe of terranes, which has been variously referred to as the Southern Magmatic Belt (Gerel, 1998), the South Mongolian and South Gobi tectonic units (Perello *et al.*, 2001 and references cited therein), follows the southern border between Mongolia and China, with a trend that curves from northeast in the east of Mongolia, to WNW where it passes into western China. The individual terranes are predominantly composed of island arc volcanic rocks and are extensively intruded by voluminous Permo-Carboniferous granites.

To both the north and south, the magmatic arc is bounded by tectonically complex suites of 'basement' terranes composed of Lower to Middle Palaeozoic back- and fore-arc sequences, volcanic rocks of the late Neoproterozoic to Lower Palaeozoic Tuva-Mongol magmatic arc and slivers of basement Meso- to Neoproterozoic metamorphics, separated by intra-arc suture related accretionary wedge sequences which include Late Neoproterozoic (Vendian) to Early Cambrian ophiolites (Figs. 3 and 14) (Yakubchuk *et al.*, 2002; Yakubchuk, 2005; Zonenshain *et al.*, 1990; Lamb *et al.*, 1999; Wainwright *et al.*, 2004, and references quoted therein).

Oyu Tolgoi is within the Gurvansayhan Terrane of Badarch *et al.*, (2002), which is located in the central-southern section of the magmatic arc where it trends roughly east west. The geology of the 600 x 200 km triangular shaped terrane is predominantly composed of Silurian to Carboniferous terrigenous sediments, carbonates, volcanosediments and intermediate to felsic volcanics, all cut by extensive Devonian granitoids and by Permo-Carboniferous diorite, monzodiorite, granite, granodiorite and syenite bodies, ranging in size from dykes to batholiths that are tens of kilometres across (Perello *et al.*, 2001; Wainwright *et al.*, 2004).

The original architecture of the sequence and the magmatic arc has been masked by alluvium on a mature surface, disrupted by intrusive masses and modified by both mid- to late-Palaeozoic accretion and Mesozoic thrust and sinistral strike-slip faulting. This has resulted in a complex of imbricate thrust sheets, dismembered blocks, mélanges and high strain zones (Badarch *et al.*, 2002). The abundant Permo-Carboniferous intrusive complexes of the terrane appear to be closely related to a major northeast-trending fault zone known as the East Mongolian or Zuunbayan fault zone which cuts obliquely across the arc and forms the southeastern boundary of the Gurvansayhan terrane (Lamb and Badarch, 2001).

The sequence within a 20 km radius surrounding the Oyu Tolgoi deposit (Fig. 14) is predominantly composed of Devonian basaltic to intermediate volcanic and volcanoclastic rocks, overlain by layered pyroclastics and sedimentary rocks with andesitic sills. Layered Carboniferous pyroclastic and sedimentary rocks, cut by andesitic sills overlie and are in fault contact with the Devonian hosts. Several large masses of granitic rocks surround the deposit, the largest being the 287±2 Ma (K-Ar) Hanbogd Mountain peralkaline granite 5 km to the east, while the 308±2 Ma (U-Pb zircon) Javhalant Mountain

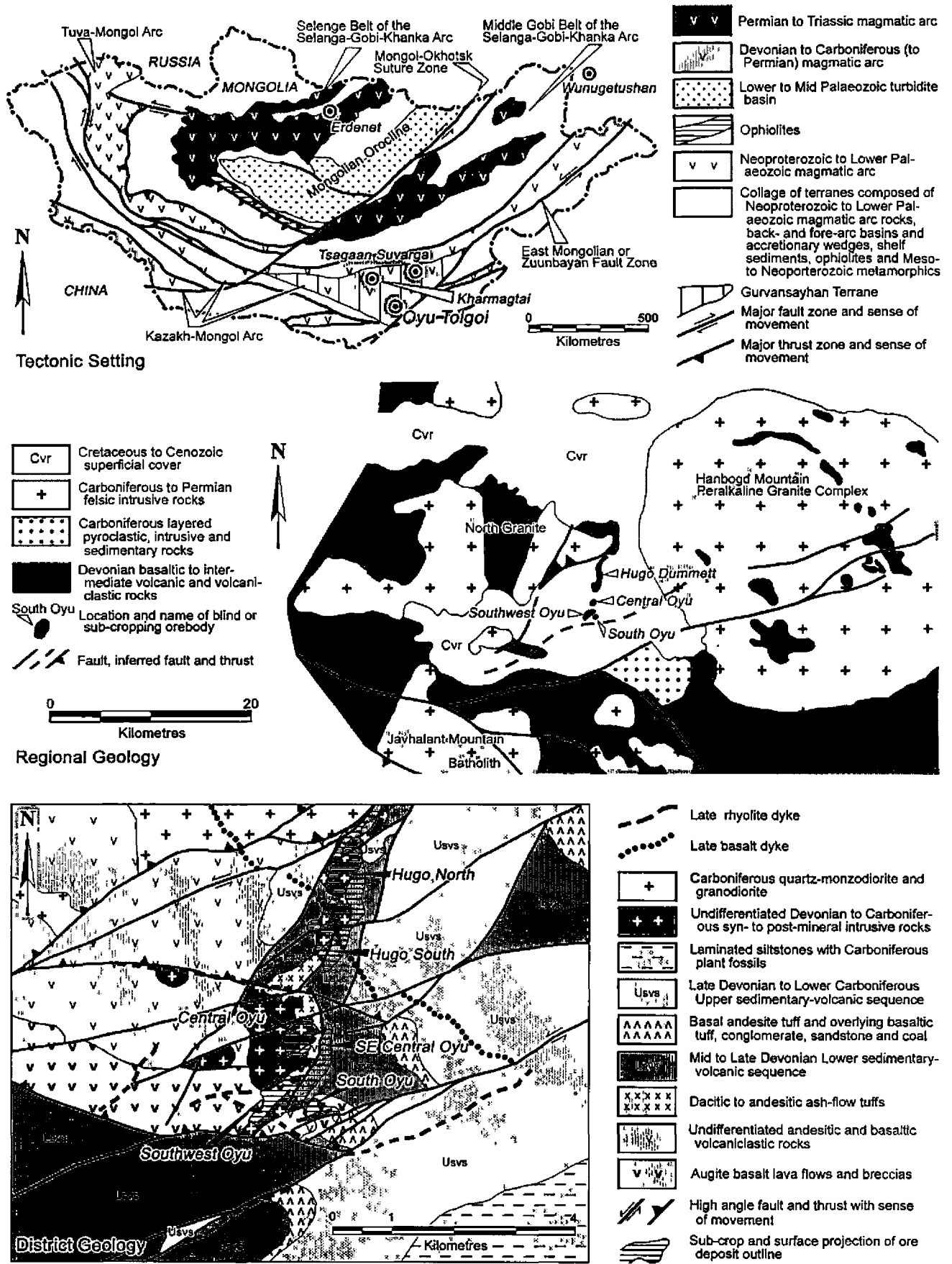


Figure 14: Tectonic, regional and district scale geological setting of the Oyu Tolgoi porphyry Cu-Au deposits, Mongolia. The upper diagram illustrates the location of the Oyu Tolgoi deposit and the Gurvansayhan Terrane within the tectonic framework of Mongolia. The middle figure represents the outcrop geology surrounding the Oyu Tolgoi group of deposits, while the lower plan shows the interpreted solid sub-crop geology in the immediate vicinity of the deposits. After Kirwin *et al.*, (2005); Ivanhoe Mincs, (2005); Wainwright *et al.*, (2004) and references cited therein; Perollo *et al.*, (2001) and references cited therein.

Batholith is a similar distance to the south and the  $348 \pm 2$  Ma (U-Pb zircon) North Granite is closer to the north and west (Wainwright *et al.*, 2004).

At the end of the Palaeozoic, the area was subjected to Basin and Range style rifting, with associated bimodal volcanism. This was followed during the early Mesozoic, by widespread uplift and associated thrusting which unroofed the magmatic arcs. Terrigenous sediments were deposited during both the basin and range and uplift/thrusting episodes in fault controlled basins. By the Late Cretaceous, the region had become increasingly arid, similar to the present day Central Asian basins (Ivanhoe Mines, 2005).

#### Deposit Geology

The Oyu Tolgoi porphyry Cu-Au deposit comprises four discrete zones namely: i). Hugo Dummett (divided into South and North Hugo, previously Far North Oyu); ii). Central Oyu; iii). South-West Oyu; and iv). South Oyu. These zones are hosted at different stratigraphic levels within a sequence of pre-ore tholeiitic basaltic volcanic and dacitic pyroclastic rocks overlain disconformably by clastic sedimentary and volcanoclastic rocks, and by basalt to dacite lava flows that are locally peperitic. The Cu-Au mineralisation is associated with intermediate- to high-K granitoids emplaced as structurally controlled dykes and small plugs (Ivanhoe Mines, 2005; Kirwin *et al.*, 2005).

Outcrop is generally strongly weathered, and is sparse and subdued, amounting to less than 20% of the deposit area. The host sequence and intrusives are largely masked by a flat to gently south dipping, NNW trending terrace of Neogene(?) piedmont outwash deposits, occurring as a 40 m thick layer of red clay and gravel, in the centre of the deposit area. Two major SSE drainages which incise this terrace are filled by Quaternary sands and gravels (Ivanhoe Mines, 2005).

The host succession within the deposit area, from the lowest to highest stratigraphic level, is as follows (Ivanhoe Mines pers. comm.; Ivanhoe Mines, 2005; Kirwin *et al.*, 2005; Wainwright *et al.*, 2004):

- i) *Laminated, andesitic volcanoclastic rocks* are the lowest unit encountered in the deposit area.
- ii) *Augite Basalt* lava flows and related breccias which are altered to chlorite/biotite with augite phenocrysts, and total around 800 m in thickness.
- iii) *Dacitic to Andesitic Tuffs*, comprising an upper thin block-ash tuff and the underlying ash flow tuff, which represents the bulk of the unit. This unit varies from 80 to 400 m in thickness. It disconformably overlies the Augite Basalt.
- iv) *Lower Sedimentary-Volcanic Sequence*, which is approximately 350 m thick, and disconformably overlies the dacitic tuffs. It is composed of red to green-brown siltstone and fine sandstone, with minor conglomerate and carbonaceous shale, and intercalated auto-brecciated basaltic lava and tuff. Some basalt flows in the upper parts of sedimentary sequence are strikingly similar to the lowermost porphyritic augite basalt, and therefore suggest that

all the basaltic volcanics are co-magmatic. The lowest 50 m of this unit is a laminated siltstone with carbonaceous shale and coal.

- v) A 250 m thick unit comprising an upper sequence of coal, conglomerate, sandstone and a thin green tuff, which overlies a slightly thicker andesitic ignimbrite pile. The last four units (v to viii herein) are also referred to as the *Upper Sedimentary-Volcanic Sequence*.
- vi) *Basaltic volcanoclastic unit*, comprising polymictic, subrounded, lapilli-sized clasts in a plagioclase-bearing to silty matrix intercalated with locally peperitic basalt. This unit is up to 400 m thick, and has a thin andesitic lava flow at the base.
- vii) *Basaltic lava flows* with minor intercalated breccia and tuff, up to 200 m thick.
- viii) *Dacite flow*, possibly a flow or dome facies, up to 200 m thick.

A wide variety of felsic to mafic dykes have been encountered in drill holes throughout the deposit area. The orientations of these intrusives are largely controlled by the dominant structural fabric of the area, which from satellite imagery and geophysical interpretation, trend at both  $35^\circ$  and  $70^\circ$ . The mineralisation is apparently genetically associated with a suite of variably altered and mineralised porphyritic quartz monzodiorite dykes that cut the Augite Basalt and Dacitic to Andesitic Tuff units in the lower part of the host sequence. Post mineral dykes include basalt, rhyolite, hornblende-biotite andesite, and biotite granodiorite intrusive rocks. The closest, large outcropping felsic intrusive mass, is approximately 3 km to the northwest of the deposit area (Fig. 14). Gravity data suggests additional large granitoid intrusives to the west of the deposit area (Ivanhoe Mines, 2005; Kirwin *et al.*, 2005; Wainwright *et al.*, 2004).

The intrusive history of the deposit area can be summarised as follows, from oldest to youngest (Wainwright *et al.*, 2004; Ivanhoe Mines, 2005; Kirwin *et al.*, 2005):

- i) Early mineralised and altered quartz monzodiorite, mainly found at South Oyu;
- ii) Late mineralised quartz monzodiorite, which only intrudes to the top of the Dacitic to Andesitic Tuff. This phase varies from moderately- to un-mineralised.
- iii) Biotite Granodiorite which is largely unaltered, and intrudes the Lower Sedimentary-Volcanic Sequence and into the base of the overlying andesite ignimbrites. This phase is locally altered and mineralised in the Hugo Dummett deposit.
- v) Hornblende-biotite andesite dykes which persist into the Basaltic volcanoclastic unit.
- vi) Rhyolite dykes, which are found to the top of the sequence.
- vii) Basalt dykes, occurring throughout the full sequence.
- viii) Dolerite dykes, which were the latest intrusive phase.

#### Mineralisation and Alteration

The Oyu Tolgoi deposit comprises four main mineralised centres, Hugo Dummett, Central Oyu, South-West Oyu and South Oyu, distributed over an interval of approximately 6.5 km in a NNW trending, 1 to 1.5 km wide corridor of



alteration and mineralisation. Each represents a porphyry copper-gold centre with an associated late high sulphidation system, which occurs above, and is partially telescoped onto the underlying porphyry mineralisation. The corridor appears to have been tilted to the north, such that erosion has removed much of the high sulphidation system at South and South-West Oyu, exposing the roots and mid levels of the porphyry system. In contrast, at Hugo Dummett North, the entire high sulphidation system and underlying and overprinted porphyry mineralisation is preserved and plunges north at depth, below poorly mineralised hosts (Ivanhoe Mines, 2005; Kirwin *et al.*, 2005).

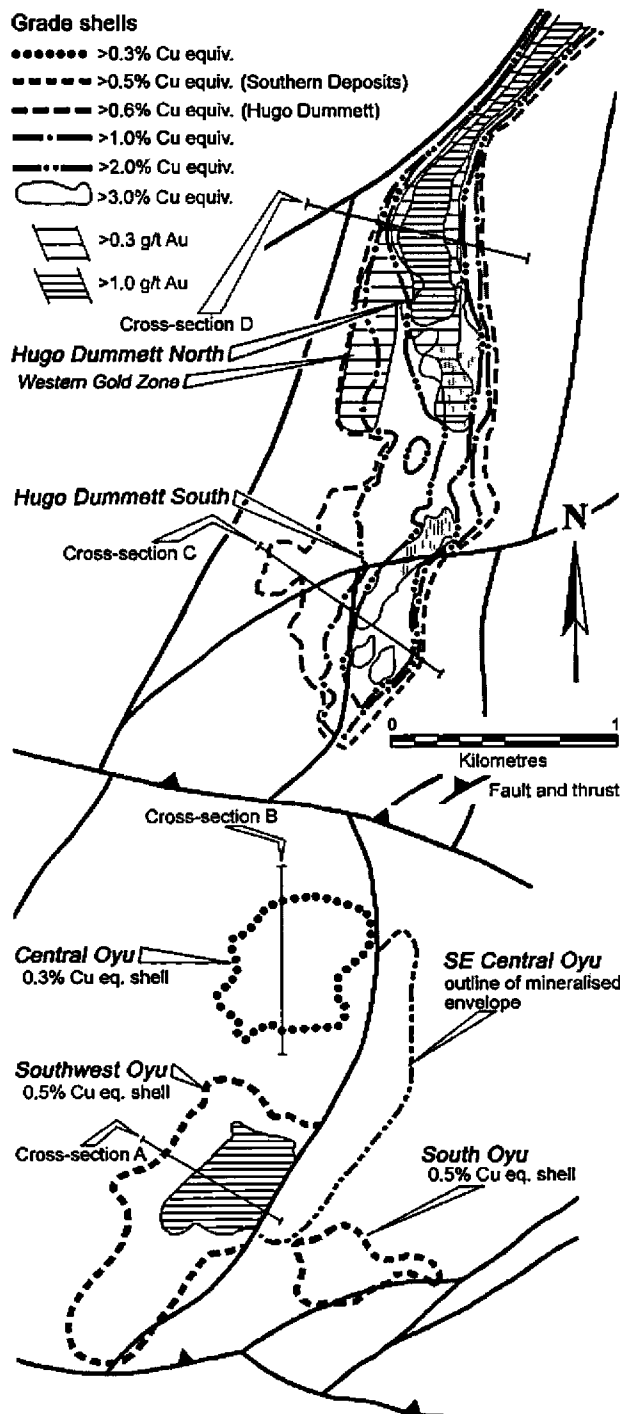


Figure 15: Distribution of mineralisation and grade within the Oyu Tolgoi porphyry Cu-Au deposits, Mongolia. The grade shells illustrated represent widths along the axis of the deposit projected to surface. The location of sections on Figs. 16 and 17 are also indicated. After Ivanhoe Mines, (2005).

*South-West Oyu* is centred on a cluster of small 10 to 30 m wide syn- to late-mineral porphyritic quartz monzodiorite dykes (Fig. 16). Mineralisation extends for more than 100 m into the adjacent basaltic volcanic hosts from each dyke. The higher-grade core of the centre, within a >1 g/t Au zone, has a 250 m diameter and extends down plunge to the southwest over a vertical interval of more than 800 m. The grade of mineralisation within the broader 0.3% Cu equivalent shell at South-West Oyu averages 0.41% Cu, 0.47 g/t Au, while at a 1% Cu equivalent cut-off it increases to 0.77% Cu, 1.44 g/t Au.

The main mineralisation is represented by early, relatively high temperature, milky white quartz veins, which cut both the quartz monzodiorite and in the basaltic wall rocks. These veins occur as contorted, sinuous networks, rather than as planar veinlets. Chalcopyrite and subordinate pyrite and bornite are found as disseminations and as late fracture fillings within both the quartz veins and the adjacent host rocks. Gold is very fine, ranging from 1 to 120  $\mu\text{m}$ , and is intergrown with chalcopyrite as veinlet infill, healing hydrofracturing of pyrite crystals and as inclusions within, or on grain boundaries of chalcopyrite and bornite or gangue minerals. It increases in grade with depth, from an Au (g/t):Cu (%) ratio of 2:1 near surface, to 3:1 at depth, while low grade propylitic basalts surrounding the main high grade core maintain a ratio of 1:1 over an area of 600 x 2000 m (Ivanhoe Mines, 2005; Kirwin *et al.*, 2005).

The dominant alteration in the quartz monzodiorite at South-West Oyu comprises early pervasive albite, overprinted by quartz sericite and minor tourmaline and fluorite, while biotite-magnetite and late chlorite-sericite is the principal alteration facies in the surrounding basalts. Pervasive biotite alteration is found in the core of the deposit, but further outward is only present as selvages to the mineralised veinlets. A quartz monzodiorite dyke which forms the southeastern margin of the South-West Oyu deposit is altered to sericite in its upper levels with weak disseminated pyrite and chalcopyrite. This mineralisation is not characteristic of the porphyry style at South-West Oyu and is believed to represent the root zone of an eroded high sulphidation system (Ivanhoe Mines, 2005; Kirwin *et al.*, 2005).

*Central Oyu* comprises a high sulphidation systems developed above, and partly telescoped onto, an underlying centre of porphyry mineralisation (Fig. 16). Covellite and pyrite are developed within an upwardly flared zone of intense quartz-muscovite alteration with subordinate minamite, dickite and pyrophyllite, while primary apatite has been altered to secondary phosphates (crandellite, svanbergite and woodhouseite). In addition, a supergene-enriched chalcocite blanket several tens of metres thick has been superimposed on the high sulphidation covellite-pyrite mineralisation. This has produced sooty chalcocite coatings on pyrite and as fracture fillings below a 20 to 60 m thick hematite and goethite rich leached cap. Minor exotic copper mineralisation has been encountered in some drill adjacent to the main prospect. The grade of mineralisation at Central Oyu within the 0.3% Cu equivalent shell averages 0.62% Cu, 0.17 g/t Au (Ivanhoe Mines, 2005; Kirwin *et al.*, 2005).

**South Oyu** has similarities to South-West Oyu and at a 0.3% Cu equivalent cut-off has an average grade of 0.46% Cu, 0.11 g/t Au (Ivanhoe Mines, 2005).

The *Southern deposits* at Oyu Tolgoi, namely Central, South-East Central, South and South-West Oyu, were estimated at April 2005, to contain a Measured + Indicated + Inferred resource of 995.4 Mt @ 0.49% Cu, 0.37 g/t Au at a 0.3% Cu equivalent cut-off, or 655.7 Mt @ 0.60% Cu, 0.64 g/t Au at a 0.6% Cu equivalent cut-off, or 176.7 Mt @ 0.80% Cu, 1.08 g/t Au at a 1% Cu equivalent cut-off (Ivanhoe Mines press release, May 2005). Fig. 15 illustrates the location of these segments of the deposit.

**Hugo Dummett** also represents a high sulphidation system that has been telescoped onto porphyry-style mineralisation formed at an earlier stage in the evolution of the hydrothermal centre. High grade copper mineralisation extends over a distance of more than 3.5 km in two connected segments, Hugo Dummett South and North. Mineralisation dominantly occurs as bornite, chalcocite and chalcopyrite, with subordinate amounts of pyrite, enargite

and tetrahedrite-tennantite. The sulphides that are formed relate directly to the associated alteration assemblage, which in turn is partially dependent upon the lithology of the host rock, but also the position in the outward zonation from the core of the high-grade shell ellipse. The outward zonation from high to low grade Cu ore corresponds with the progression from bornite + chalcocite, to chalcopyrite ( $\pm$ tetrahedrite-tennantite) to pyrite ( $\pm$ enargite) (Ivanhoe Mines, 2005; Kirwin *et al.*, 2005).

A large part of the **Hugo Dummett South** deposit is hosted by dacitic to andesitic ash flow tuff, in contrast to Hugo Dummett North which is predominantly within augite basalt and quartz monzodiorite (Fig. 16). This difference in host lithology has a strong influence on both the alteration and sulphide species that are developed. Advanced argillic alteration within the ash flow tuffs is characterised by alunite, pyrophyllite, diaspore, dickite, topaz, zunyite, minor fluorite and rare dumortierite. Enargite, bornite+pyrite, and locally covellite are common sulphide minerals in the ash flow tuff. The observed mineralisation

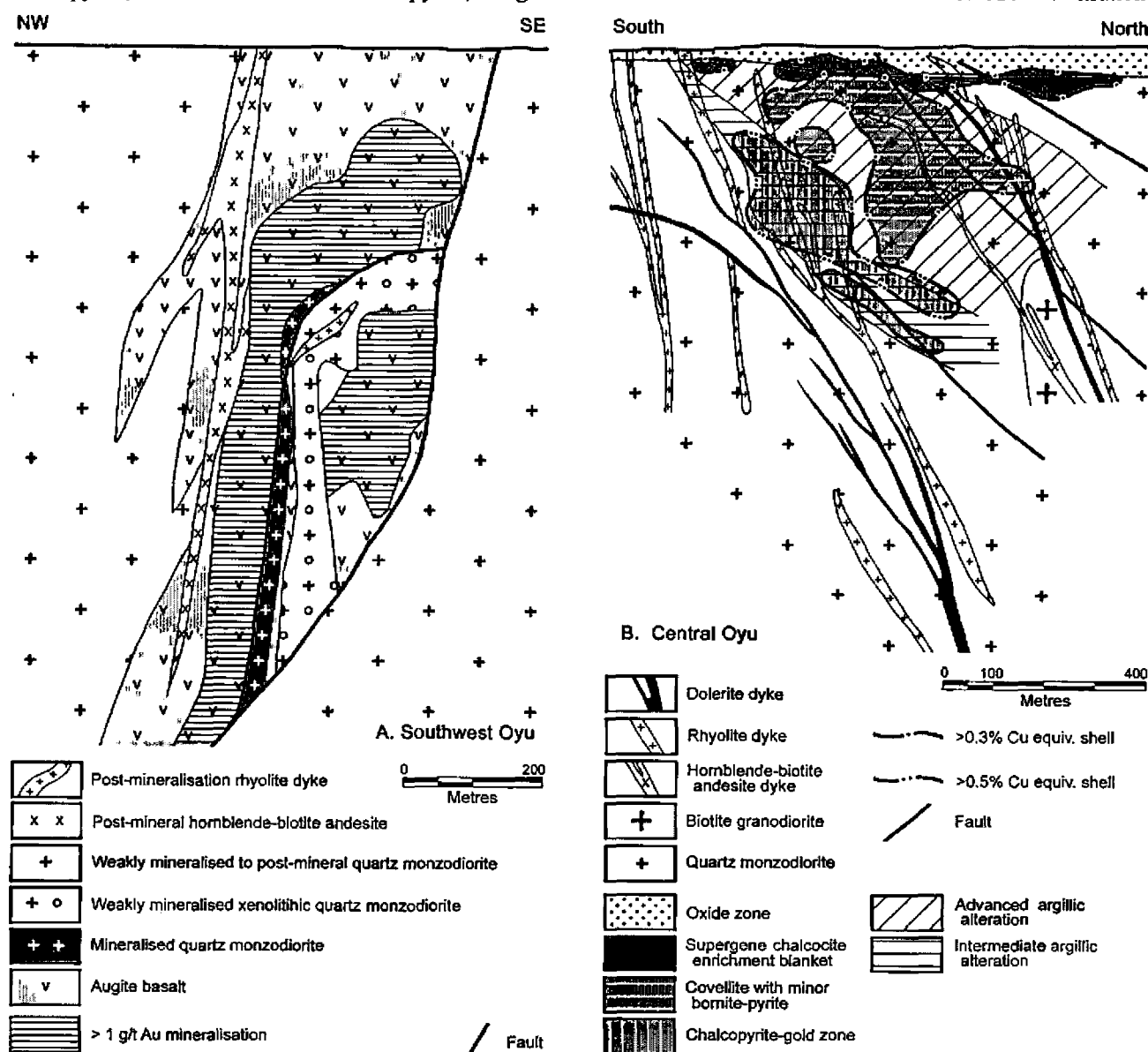
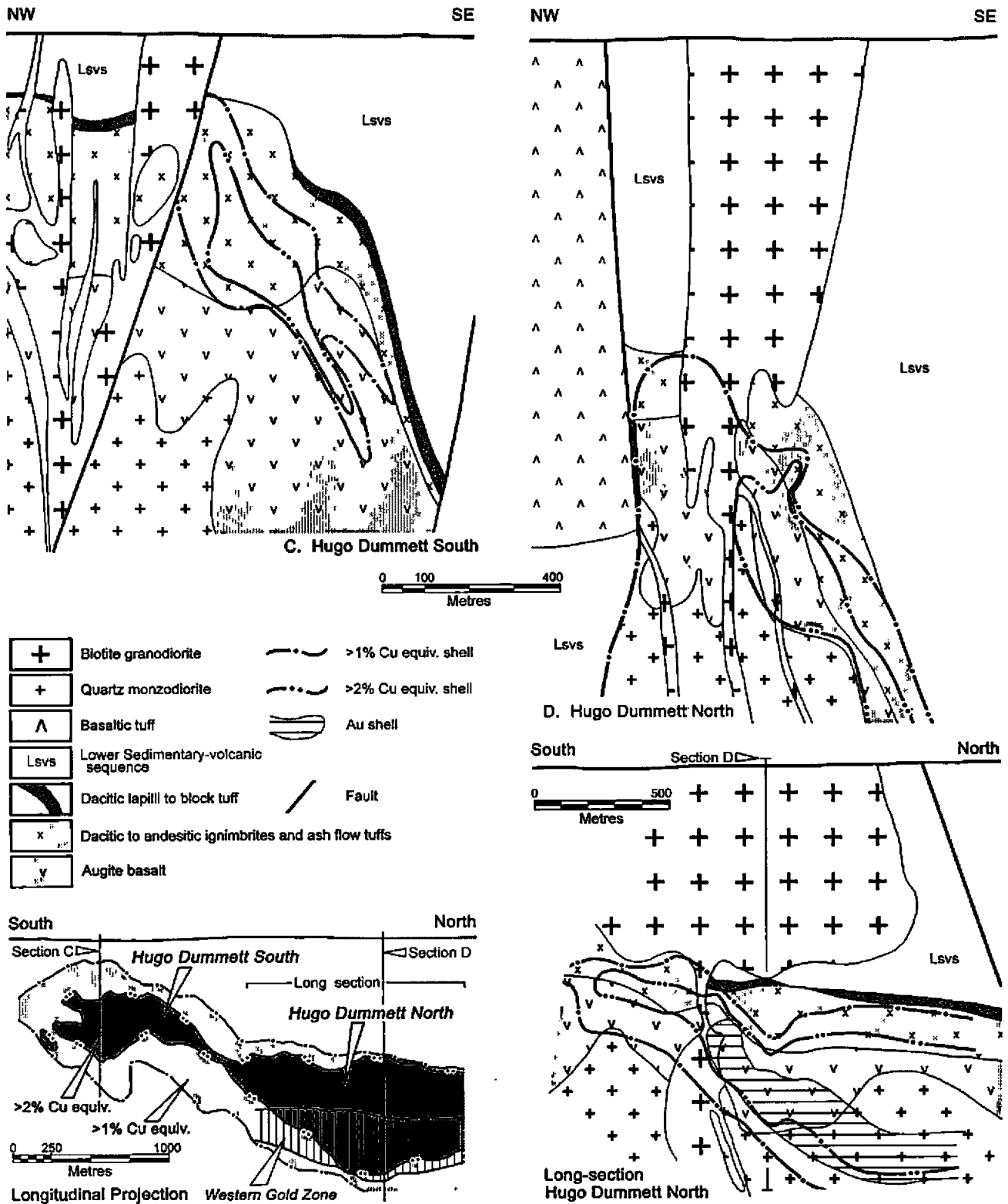


Figure 16: Geological cross sections through two of the Southern deposits, Southwest and Central Oyu, of the Oyu Tolgoi porphyry Cu-Au system, Mongolia. See Fig. 15 for the location of sections. After Ivanhoe Mines, (2005) and Kirwin *et al.*, (2005).

is related, both vertically and laterally to a series of porphyritic monzodiorite apophyses and to a deeper-seated porphyry-style intrusive core. Magnetite and chalcopyrite veining in biotite and chlorite altered porphyritic augite basalt, similar to South-West Oyu, has been encountered

in deep drilling. Exceptional copper grades (locally as high as 10% Cu over 2 m sample intervals) have been intersected at Hugo South, occurring as bornite, chalcopyrite and chalcocite (Ivanhoe Mines, 2005; Kirwin *et al.*, 2005 and references quoted therein).



**Figure 17: Representative geological cross and long sections through the Hugo Dummett deposits of the Oyu Tolgoi porphyry Cu-Au system, Mongolia.** Cross-section C (top left) is the NE6200 section through the Hugo Dummett South deposit ; Cross-section D (top right) is the N4767200 section at Hugo Dummett North. The longitudinal section (bottom right) through part of the Hugo Dummett deposit is a diagrammatic representation of the geology and grade distribution of the ore deposit. The longitudinal projection (bottom left) is a representation of the outline of the ore grade shells at both the Hugo Dummett South and section of the Hugo Dummett North deposit. See Fig. 15 for the location of cross-sections C and D also. After Ivanhoe Mines, (2005) and Kirwin *et al.*, (2005).

**Hugo Dummett North** is predominantly within basalt and quartz monzodiorite (Fig. 17), which are characterised by sulphide assemblages of bornite+chalcocite and chalcopyrite with minor, enargite and tetrahedrite-tennantite. This section of the deposit has a continuous high-grade bornite dominant core which extends for at least 1.6 kilometres to the NNE from South Hugo. This core corresponds to a zone containing around 90% vein quartz. It has a vertical extent that varies from 100 m in the neck connecting Hugo Dummett South and North, but expands to more than 700 m on the northern most section drilled (but unclosed) in 2005. The corresponding horizontal width of the high grade core ranges from 150 to 180 metres up to approximately 200 m in the south and north respectively and is entirely enveloped by the greater than 1% Cu grade shell which reaches a maximum horizontal thickness of 450 m at zero RL (1160 m below surface). Maximum gold grades are associated with bornite with Au g/t:Cu% ratios varying from 1:10 to as high as 1:1 in the northern part of the deposit (Ivanhoe Mines, 2005; Kirwin *et al.*, 2005 and references quoted therein).

The main Hugo Dummett North orebody is limited to the west by a thick dyke of late- to post-ore biotite granodiorite. It redevelops again on the western side of this dyke, hosted by quartz monzodiorite to form the gold and bornite rich Hugo *Western Gold* orebody which is up to 100 m thick, with a vertical extent of 300 m and a strike length in excess of 1 km, open to the north, south. In May 2004 it was estimated to contain a minimum of 57.6 Mt @ 0.96% Cu, 0.85 g/t Au (Ivanhoe Mines press release, May 2004).

Molybdenite occurs locally in all rock types. A Re-Os determination from molybdenite in the orebody gave an age for the ore of  $372 \pm 1.2$  Ma (Kirwin *et al.*, 2005 and references quoted therein; Wainwright *et al.*, 2004).

The Hugo Dummett deposits, were estimated at April 2005, to contain an Indicated + Inferred resource of 1.071 Gt @ 1.07% Cu, 0.21 g/t Au at a 0.6% Cu equivalent cut-off, or 595.7 Mt @ 1.36% Cu, 0.28 g/t Au at a 1% Cu equivalent cut-off. In addition, the same resource classifications for the high-grade core were estimated to contain 335.4 Mt @ 2.84% Cu, 0.49 g/t Au at a 2% cut-off. This resource is still open to the north and at depth (Ivanhoe Mines press release, May 2005) with substantial potential to be expanded. Fig. 15 illustrates the location and geometry of these segments of the deposit.

#### **Tsagaan-Suvarga, Mongolia**

The Tsagaan-Suvarga porphyry copper-molybdenum deposit is located approximately 150 km to the northeast of Oyu Tolgoi in southern Mongolia (Fig. 14) and also lies within the Gurvansayhan Terrane (*see* Oyu Tolgoi description above). Like Oyu Tolgoi, it was formed within the Southern Mongolian Magmatic Belt segment of the Upper Palaeozoic Kazakh-Mongol magmatic arc, and has been dated at approximately 365 Ma (Lamb and Cox, 1998). The published resource at the deposit is 240 Mt @ 0.53% Cu, 0.018% Mo.

Arc magmatism within the Southern Mongolian Magmatic Belt was intermittent through the Late Palaeozoic to the

Permian and was predominantly of calc-alkaline to potassic calc-alkaline composition, with a minor alkaline component. The main activity within the arc persisted to at least 370 Ma before shifting south during the Carboniferous. The deposit lies within the Late Devonian to early Carboniferous Tsagaan-Suvarga intrusive complex, which comprises gabbro, diorite, syenite, syenogranite and subordinate granodiorite, and is fringed by Carboniferous and Jurassic to Cretaceous volcanic and sedimentary rocks. The final stages of the Tsagaan-Suvarga complex are represented by a series of intrusive stocks and dykes in its north and northwest, composed of granite, granite porphyry and syenogranite porphyry. Mineralisation within the complex and at Tsagaan-Suvarga is associated with these late stage intrusives. Both the intrusive complex and the overlying Carboniferous volcano-sedimentary sequence are cut by hornblende syenite and monzonite porphyries (Lamb and Cox, 1998; Watanabe and Stein, 2000).

The Tsagaan-Suvarga deposit comprises quartz-chalcopyrite stockwork mineralisation which is developed over an area of 1000 x 300 m, and has been traced by drilling to a depth of 600m. K silicates (mainly K feldspar) are the dominant alteration, overprinted by sulphide bearing 'bands' of sericite reaching tens of centimetres in width. The major ore minerals are chalcopyrite, bornite, molybdenite and pyrite, which are concentrated in the sericitic bands. A supergene chalcocite blanket has also been developed over the deposit (Lamb and Cox, 1998; Watanabe and Stein, 2000).

#### **Kharmagtai, Mongolia**

The Kharmagtai Au-Cu porphyry district is located in the southern Gobi desert of Mongolia, 120 km north of the Oyu Tolgoi porphyry Cu-Au deposit and 500 km south of the capital Ulaan Baatar. Like Oyu Tolgoi and Tsagaan-Suvarga, described previously, it lies within the Late Palaeozoic Gurvansayhan Terrane which is characterised by calc-alkaline to potassic-calc-alkaline igneous complexes, and comprises section of the Mid- to Late-Palaeozoic Kazakh-Mongol magmatic arc (Fig. 14).

Outcrop throughout the district is sparse, although available exposure indicates large areas are underlain by a Devonian silty clastic sedimentary package which includes arenaceous volcanoclastic rocks with andesitic lava fragments, and plagioclase and hornblende crystals, as well as lesser felsic ash crystal tuffs, reworked tuffaceous sediments and locally, limited exposures of basaltic to andesitic volcanics. All of these lithologies have been intruded by monzodiorite, monzonite and diorite porphyry stocks. The magmatic arc has been eroded and unroofed in the district, with little evidence of comagmatic volcanic equivalents of the intrusive complex, although abundant sediment roof pendants within the stocks imply they are exposed at their upper-most levels. Preliminary Re-Os dates of  $330.2 \pm 1.0$  Ma in the Carboniferous have been determined from samples of these intrusives at Kharmagtai.

While the majority of the intrusive rocks encountered to date have been altered, studies of drill core reveal that the diorite has phenocrysts of plagioclase, hornblende and apatite in a fine grained groundmass of plagioclase,

hornblende, quartz, magnetite and zircon, consistent with a potassic-calc-alkaline magmatic association. Numerous tourmaline breccia pipes are scattered throughout the district, the largest of which has a diameter of 500 m, while local, linear, structurally controlled, silicified zones contain abundant tourmaline. Quaternary to Recent sands and loess form a thin cover over most of the district.

Exploration has identified at least four significant zones of IP anomalism and coincident centres of porphyry related gold-copper mineralisation and alteration within an area of around 7x3 km. Some 10 km to the west, distal gold-base metal-bearing breccia pipes has been recognised and several kilometres to the southwest again, complex, structurally controlled, gold bearing silicified zones occur within the volcano-sedimentary pile.

A representative example (see Fig. 18 for location and cross section) of one of these centres of porphyry related gold-copper mineralisation and alteration is represented by a 200 m diameter sub-cropping zone that was oxidised to depths of approximately 60 metres below surface. The oxide zone contains fracture controlled goethite, malachite, copper-wad, minor chalcocite and occasionally native copper. Drilling of the hypogene zone encountered chalcopyrite and subordinate pyrite associated with up to 10% stockwork quartz veins, mostly hosted in microdiorite, with lesser late chalcopyrite-rich sulphide veins (<5% sulphides) containing minor bornite. Rare molybdenite occurs as fracture coating and within milky quartz veins in the stockwork zone. Native gold is present as small inclusions in chalcopyrite grains and to a lesser extent in pyrite and as minor Au tellurides. In high-grade zones the Au g/t:Cu% ratios frequently exceeds 2:1. Narrow zones (normally less than 10 metres in width) of hydrothermal tourmaline breccias contain quartz-veined microdiorite clasts in a matrix of quartz, tourmaline, sericite, pyrite and minor chalcopyrite. Magnetite is a major accessory mineral in this and all of the Kharmagtai mineralised porphyries, occurring within pre-mineral quartz veins and in sulphide-rich veins. Planar "centre-line" and "railroad textured" quartz - sulphide  $\pm$  magnetite veins are characteristic of the Kharmagtai porphyry mineralisation. Drill intersections across this zone are generally of

80 to 100 m @ 0.5 to 0.8% Cu, 0.7 to 1.25 g/t Au and define a 60° south dipping stockwork zone that has been traced to a depth in excess of 250 m below surface.

Initial potassic alteration affected both intrusives and sediments, represented by an assemblage of variably developed albite + biotite + K-feldspar + minor magnetite + quartz + pyrite with veinlets of quartz, magnetite, chalcopyrite, pyrite, apatite, epidote and chlorite. Propylitic (chlorite  $\pm$  calcite  $\pm$  pyrite) and phyllic (sericite + pyrite + quartz  $\pm$  chlorite  $\pm$  tourmaline  $\pm$  chalcopyrite  $\pm$  gold) alteration commonly overprints the potassic assemblages. Some 1.5 km to the north, within another of the mineralised stockwork zones, the early potassic phase is overprinted by quartz-carbonate-sulphide veins and breccias with quartz, calcite, tourmaline, chlorite, sericite, pyrite, chalcopyrite, sphalerite, galena and tennantite-tetrahedrite enclosed by selvages of high-intensity texture-destructive phyllic type alteration in the form of quartz + sericite + pyrite + Ti-phase (rutile, leucosene and anatase) minerals. Younger tourmaline breccias contain mostly pyrite. Late calcite - zeolite fracture fillings are also recorded, with trace pyrite, hematite, quartz and chalcopyrite.

The individual centres of copper-gold bearing porphyry related quartz stockwork mineralisation identified in the Kharmagtai district are all quite similar. Some occurs as broad planar zones, which in some cases are focused on narrow quartz diorite dykes within the diorite to quartz-diorite hosts, while others are more diffuse and irregular. It is considered possible that the individual stockwork zones may amalgamate at depth to form a single large porphyry deposit. The section on Kharmagtai has been drawn from Kirwin *et al.*, (2005a) and references cited therein

#### Duobaoshan, Inner Mongolia - China

The Duobaoshan Cu-Au-Mo deposit and Tongshan Cu-Mo immediately to the south, both lie within the Xinganling block of Inner Mongolia (Heilongjiang Province) in northeastern China. Duobaoshan is associated with Late Carboniferous to Early Permian granodioritic intrusives of the Kazakh-Mongol magmatic arc, intruding Lower Palaeozoic arc volcanics of the extinct Tuva-Mongol arc. These deposits were emplaced in the waning stages of the

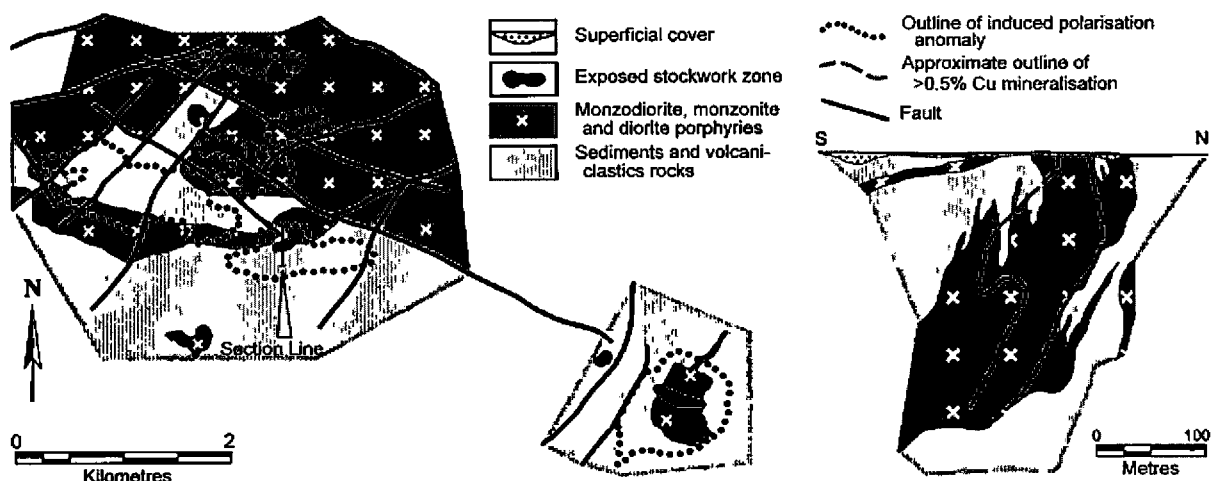


Figure 18: Simplified interpretive geological plan of the Kharmagtai district showing the main centres of porphyry style Au-Cu mineralisation and a representative section through one of those mineralised centres. After Kirwin, *et al.*, (2005a).

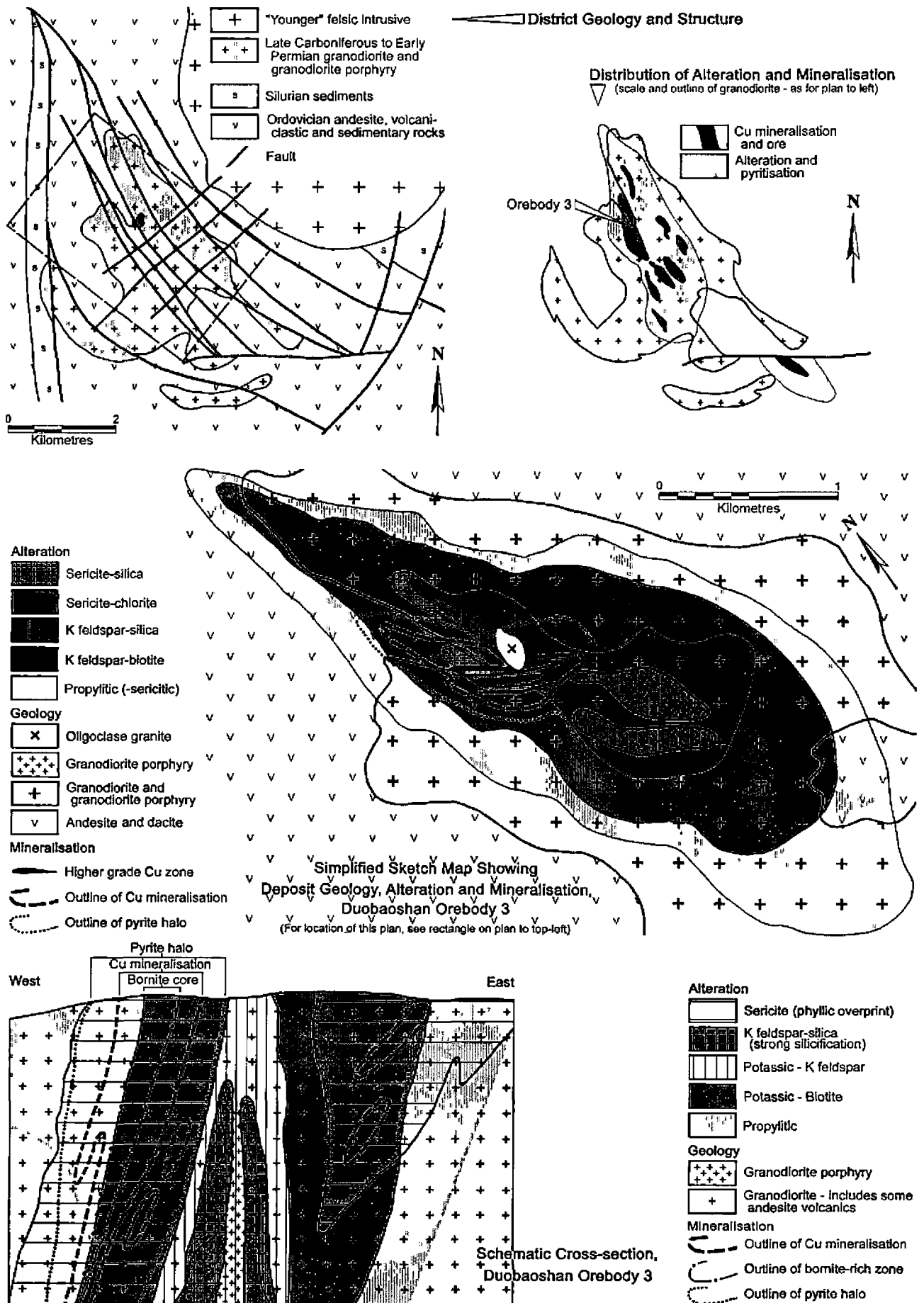


Figure 19: Geology, mineralisation and alteration of the Duobaoshan porphyry Cu deposit in Inner Mongolia, northeastern China. After Zhao, et al., (1995, 2005), Qi (2004).

Kazakh-Mongol arc, near its overlap with the Selanga-Gobi-Khanka arc of the Palaeo-Pacific Ocean margin. Duobaoshan is reported to have a resource of 508 Mt @ 0.47% Cu, 0.2 g/t Au, 2 g/t Ag, 0.02% Mo, while Tongshan is believed to contain 180 Mt @ 0.47% Cu, 0.023% Mo (Zhao *et al.*, 2005, Mutschler *et al.*, 2000).

The country rock at Duobaoshan comprises a Caledonide sequence of andesitic to dacitic arc-related volcanic and volcanoclastic rocks of the Ordovician Duobaoshan Formation, overlain by Silurian sediments. The volcanic rocks of the Duobaoshan Formation show an alkalic to calc-alkalic trend and were intruded by a composite granodioritic complex predominantly composed of granodiorite and granodiorite porphyry. This intrusive mass covers an exposed area of 8 km<sup>2</sup> within an arcuate, northwest-southeast trending structural zone (Fig. 19). Two strongly altered, lens-like, northwest striking and southwest dipping granodiorite porphyry bodies with exposed areas of 0.08 and 0.09 km<sup>2</sup> respectively are located within the centre of the granodiorite. The granodiorite and granodiorite porphyry have been dated by K-Ar isotopes at 292 and 283 Ma respectively (Zhao *et al.*, 2005).

Mineralisation is associated with a northwest-southeast corridor of alteration that extends across the granodiorite mass over a length in excess of 6 km (Fig. 19) and comprise a large number of lenticular mineralised zones that define the orebodies. The largest of these is Orebody No. 3 which occurs in the hangingwall of the granodiorite porphyry and is associated with an episode of phyllic sericite and quartz-sericite alteration that overprints an earlier potassic phase

characterised by intense silicification of the granodiorite porphyry margin, surrounded progressively outwards by K feldspar and then biotite alteration which grades to a periphery that was subjected to propylitic alteration. The phyllic phase overprints the potassic zone near its transition to the propylitic zone. The bulk of the mineralisation was emplaced outside of the granodiorite porphyry, predominantly within the granodiorite mass, but also partially within the Ordovician volcanic wall rock. The core of Orebody No. 3 is occupied by a bornite rich core which passes outwards into chalcopyrite and a pyritic halo. The accompanying ore minerals include pyrite, cuprite and covellite (Zhao *et al.*, 2005; 1995; Yin *et al.*, 1997; Du, 2004).

Fig. 19 summarises the setting, and the distribution of mineralisation and alteration at the Duobaoshan porphyry Cu-Au-Mo system. These diagrams are sketches and comprise the combination of different pieces of information from the range of sources quoted above.

**Erdenet, Mongolia**

The Erdenet porphyry Cu-Mo deposit is located in northern Mongolia, some 240 km northwest of the capital, Ulaanbaatar. It was emplaced within the Late Palaeozoic to Early Mesozoic Selanga-Gobi-Khanka magmatic arc on the margin of the Siberian Craton at 240 Ma in response to the closing of the Mongol-Okhotsk Sea and subduction of the palaeo-Pacific ocean below the Siberian craton. Erdenet is described in detail in Gerel, (2005), in this volume. See Table 1 for details.

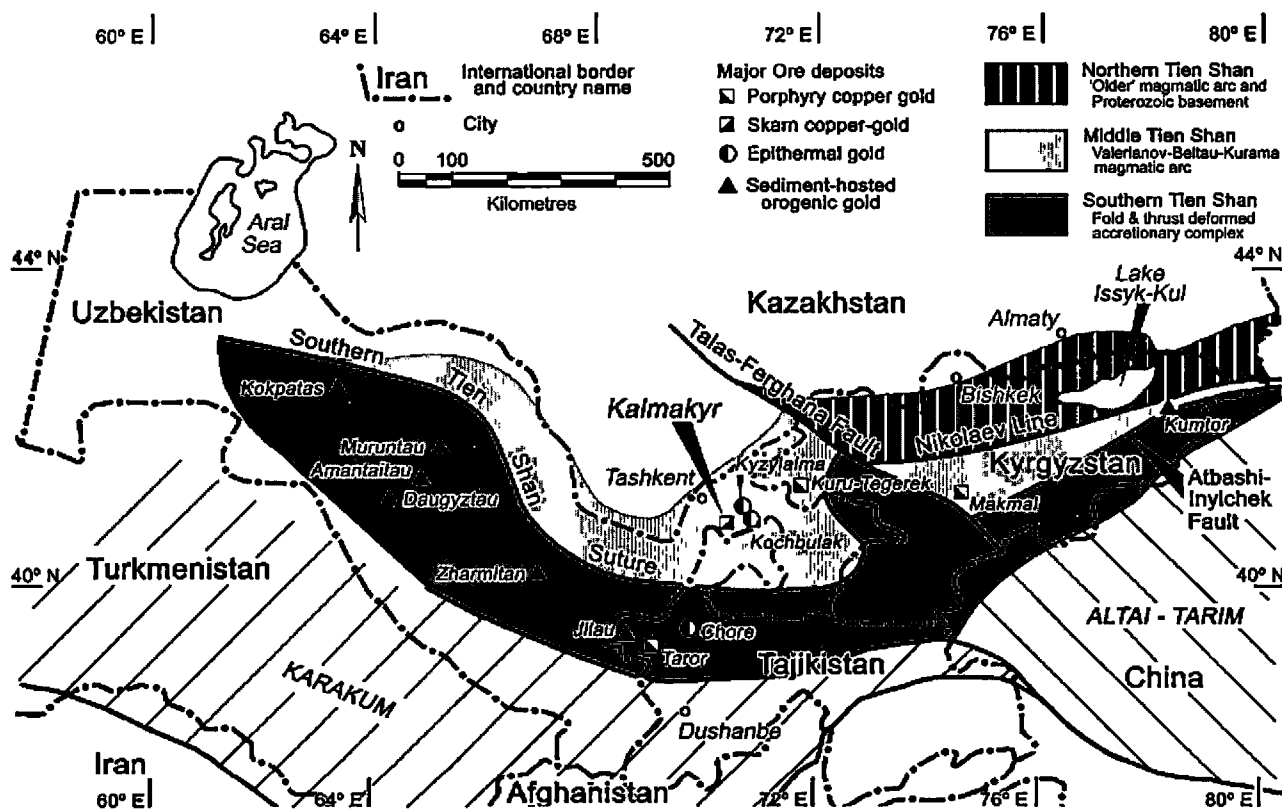


Figure 20: Tectonic framework and distribution of gold ore deposits in the southwestern section of the Tien Shan Mineral Belt. After Yakubchuk, *et al.*, (2002); Mao *et al.*, (2004) and others.

### *Wunugetushan (Wushan), Inner Mongolia - China*

The Wunugetushan (abbreviated to Wushan) porphyry Cu-Mo deposit is located in Inner Mongolia, China within 70 km of the border with northeastern Mongolia and 30 km south of the Russian frontier. It was emplaced at 184 Ma (Early Jurassic) within the late stages of the Selanga-Gobi-Khanka magmatic arc and lies on the southern limb of the Mongolian Orocline (Fig. 2). The deposit is quoted as containing 495 Mt @ 0.45% Cu, 0.09% Mo (Mutschler *et al.*, 2000). The host terrane is predominantly composed of Mesozoic calc-alkaline volcanic rocks of the Selanga-Gobi-Khanka magmatic arc, which are bounded by metamorphosed Permian volcanic rocks and older Palaeozoic sequences of the basement to the magmatic arc. Granitic rocks belonging to the Triassic Indo-Sinian, Jurassic Early Yanshanian and Cretaceous Late Yanshanian orogenic episodes intrude all of the basement rocks (Qin *et al.*, 1997).

The immediate wall rocks to the deposit are biotite monzogranite of a 120 km<sup>2</sup> diameter Indo-Sinian batholith dated at between 177 and 201.6 Ma (K-Ar), and 212.85±6.76 Ma (Rb-Sr). The monzogranite batholith is intruded by a monzogranite porphyry stock (188.3±0.6 Ma by U-Pb in zircon) which is associated with the mineralisation. Three alteration zones are recorded, namely an inner quartz-K feldspar zone, a surrounding quartz-sericite phase and an outer illite-hydromuscovite periphery. The Cu orebody is hosted in the outer sections of quartz-K feldspar zone, while the peak Mo mineralisation is in the inner sections of the quartz-sericite annulus. The sericite alteration associated with mineralisation has been dated at 182.3 to 184.7 Ma (Qin *et al.*, 1997).

## Orogenic Gold Deposits

Gold mineralisation occurs in two principal settings within the central part of the Altaids, the Tien Shan Mineral Belt, namely as i). *porphyry and epithermal* systems developed within magmatic arcs, as described in the bulk of this paper, and ii). *orogenic-type* gold deposits that are structurally controlled, and temporally and spatially associated with late Palaeozoic, syntectonic to early post-collisional, highly evolved, I-type granodioritic to monzonitic intrusives in fore- and back-arc terranes (Cole and Seltmann, 2000; Yakubchuk *et al.*, 2002; Mao *et al.*, 2004).

While these orogenic-type gold deposits are not directly related to porphyry systems, they are a product of the same larger scale metallogenic evolution and set of tectonic processes as the gold rich porphyry and epithermal deposits of the belt, and hence are briefly discussed herein.

Moreover, although belonging to two different terrane settings, the giant Cu-Au porphyries of the Chatkal-Kurama range (Almalyk district, in the Valerianov-Beltau-Kurama magmatic arc, of the Middle Tien Shan) and the giant orogenic Au mineralisation hosted by the black-shale series of the Central Kyzylkum slate belt (Southern Tien Shan, Khanty-Mansi accretionary complex) have some striking similarities. These hint at crust-mantle interaction and dominance of a deep-seated regime during emplacement,

referred to as the "Chatkal-Kurama hot spot" (I.M. Golovanov, pers. comm.; Dalimov *et al.*, 2003). They are temporally close (315 to 285 Ma, Seltmann *et al.*, 2004), their isotope signatures reveal the incorporation of a moderate mantle component (Chiaradia *et al.*, 2005), and geophysical patterns from the middle crust in the region exhibit zones of low reflection indicating the existence of extended mafic bodies just beneath both giant ore-magma systems (S. Cherkasov, pers. comm.). Focused studies are required to provide evidence that may substantiate this controversial discussion.

The orogenic gold deposits of the Tien Shan Mineral Belt include some of the largest economic gold accumulations in the world, e.g. Muruntau in Uzbekistan which contains over 5400 tonnes (175 Moz) of gold at an open pit recovered grade of 3.4 g/t Au. These deposits are spread across the belt in Russia, Uzbekistan, Tajikistan, Kyrgyzstan, Kazakhstan and western China, and span the time scale from Lower to Late Palaeozoic. The greatest concentration of significant orogenic gold deposits however, is in the southwestern part of the belt, in the South and Middle Tien Shan of Uzbekistan and Kyrgyzstan. These deposits are associated with Permian magmatism emplaced during the final- to early post-collisional stages of orogenesis, within a sutured back-arc setting containing carbon-rich sedimentary sequences (Cole and Seltmann, 2000; Yakubchuk *et al.*, 2002; Mao *et al.*, 2004).

The orogenic gold deposits of the South Tien Shan are controlled by structures related to the Southern Tien Shan Suture Zone that separates the Carboniferous Valerianov-Beltau-Kurama magmatic arc to the north, and the Altai-Tarim-Karakum micro-continent to the south. They are hosted by the back arc accretionary complex deposited in the basin that had separated these two tectonic elements (Fig. 20). The suture zone is defined by ophiolites and borders the strongly deformed fold and thrust belt of the Southern Tien Shan that has been extensively intruded by Permian granitoids and hosts most of the significant orogenic-style gold deposits (Mao *et al.*, 2004).

Most of the orogenic-gold deposits within the Tien Shan are located at mesozonal crustal levels, within Late Palaeozoic granitoid intrusives, or their contact metamorphic aureoles, and yield radiometric dates of mineralisation coincident with the magmatism. However, few can be shown to have a direct genetic link with the associated intrusives. Never-the-less, geochemical, isotope and fluid-structural models have implicated highly evolved Late Palaeozoic, syntectonic I-type granitoids as the source of metals and/or fluids for spatially associated orogenic gold deposits within the belt. The gold-quartz vein systems produced appear to represent only part of a larger magmatic-hydrothermal system that often includes earlier scheelite (±Au) skarn mineralisation (e.g. Zharmitan in Uzbekistan and Jilau in Tajikistan, while Muruntau, also in Uzbekistan, exhibits some similarities). In these examples, Au and W occur together with characteristic enrichments of As, Bi, Mo and Te deposited from CO<sub>2</sub>-rich fluids at temperatures of up to 400°C and pressures of approximately 2 Kbar (Cole and Seltmann, 2000).



The distribution of the granitoids and the associated gold deposits are both controlled by the same regional deep seated faults and shear zones that were the primary focus of regional fluid flow and of deformation. Mineralisation appears to have been formed by CO<sub>2</sub>-rich fluids of deep crustal origin that episodically escaped from geopressed reservoirs along major high angle reverse faults and deposited gold in zones of local structurally enhanced permeability (Cole, 1998; 2002).

Cole and Seltmann, (2000) note that a general trend can be recognised in these granitoid related systems, where W, in the form of scheelite, dominates in mesozonal, more reduced settings, whereas Cu substitutes for W in the paragenesis of epizonal, more oxidised systems. They also observe that these same Late Palaeozoic (Variscan-Hercynian) granitoids are temporally, mineralogically, compositionally and isotopically similar, whether related to orogenic-style Au-W veins and associated skarn systems in the South Tien Shan fore-arc accretionary complex, or, related to shallower porphyry Cu-Au systems in the magmatic arc of the Middle Tien Shan. They suggest a continuum which would encompass classic Cu-Mo-Au porphyry, Cu-Au skarn and Au-Ag epithermal deposits in epizonal crustal environments/levels, passing down into W-Mo-Au with associated Bi-As-Te associations in skarn, lode and stockwork deposits (i.e. orogenic-style Au) at mesozonal depths.

## Acknowledgments

This paper merges the professional experience of TMP in mineral exploration and synthesis of information with the results of almost 15 years of collaborative applied research by RS in the framework of a series of international academic network projects. The latter studies were coordinated by RS and funded initially through the INTAS 93-1783 project "Anatomy and magmatic-hydrothermal mechanisms of ore deposition" (1993-1996), followed by the IUGS-UNESCO funded projects IGCP-373 "Ore-bearing granites of Eurasia" (1997-2002) and IGCP-473 "GIS metallogeny of Central Asia" (2002-2006). The resulting output was supplemented and enhanced by advanced mineral deposit case studies combining the development of regional-scale GIS packages and focused petrochemical and geochronological research along selected geodynamic-metallogenic geotraverses. Since 2002, this approach has been initiated and coordinated through NHM's Centre for Russian and Central Asian Mineral Studies (CERCAMS) and has led to new insights and additional information. The long-term research benefited from the scientific contributions of several dozen teams in the countries of the former Soviet Union, Mongolia and China, representing the knowledge input of several hundreds of regional and local specialists of various specialisation. Without their continuous support and stable cooperation over more than a decade, providing access to unpublished data and key samples, inspiring discussions, field support, their papers, maps and reports used for the CERCAMS database, facilitating this compilation would not have been possible. The remarkable input and collaboration of all those friends and colleagues is highly appreciated. Among all those

involved, the cooperation and fruitful discussions especially with Igor Golovanov, Rustam Koneev, Ochir Gerel, Rosalia Jenchuraeva, Olga Plotinskaya, Victor Popov, Andy Cole, Vertrees M. Canby, Dmitry Konopelko, Vjacheslav Serykh, Vladimir Dolgoplov and Alla Dolgoplova are highly appreciated. Special thanks is owed to Vitaly Shatov and Alexander Yakubchuk for their cooperation, specifically for their assistance in developing the CERCAMS mineral deposits maps and databases on Central Asia, Mongolia and the Urals. Deep appreciation is due to Douglas Kirwin for a thorough review of an earlier version of this paper, for his comments and suggestions that improved the paper and the valuable information he provided on ore deposits in Mongolia and China. This CERCAMS publication is simultaneously a contribution to the IGCP-473 project.

## References

- Allen, M.B., Windley, B.F. and Zhang, C., 1992 - Palaeozoic collisional tectonics and magmatism of the Chinese Tien Shan, Central Asia. *Tectonophysics*, v. 220, pp. 89-115.
- Badarch, G., Cunningham, W.D. and Windley, B.F., 2002 - A new terrane subdivision for Mongolia: implications for the Phanerozoic crustal growth of Central Asia; *Journal of Asian Earth Sciences*, v. 21, pp. 87-110.
- Bespaev, Kh.A. and Miroshnichenko, L.A., (Eds.), 2004 - Atlas of Mineral Deposit Models of the Republic of Kazakhstan. Almaty, Kazakhstan; English edition by Halls, C., Seltmann, R., Dolgoplova, A., *CERCAMS NHM*, London, 2004, 142p.
- Central Asia Gold Ltd, 2005 - Web-site at <http://www.cagl.com.au>.
- Chiaradia, M., Konopelko, D., Seltmann, R. and Cliff, R., 2005 - Lead sources in ore deposits and magmatic rocks of the Tien Shan and Chinese Altay; in Mao, J.W., *et al.*, (Eds.), *Mineral Deposit Research: Meeting the Global Challenge, Proceedings of the Eighth Biennial SGA Meeting, Beijing, China, 18-21 August, 2005*; *Springer*, pp. 1301-1304.
- Chisholm, J.M., 2003 - Independent Geologist's Report; Continental Resource Management Pty Ltd, attached to Central Asia Gold Limited Prospectus, submitted to ASX, Australia.
- Cole, A., 1998 - Gold mineralisation in the southern Tien Shan, Central Asia: tectonic setting, characteristics and regional exploration criteria; (Abstract) in *Geological Society of London, Mineral Deposits Studies Group Annual Meeting, Programs and Abstracts*, v. 22. p. 27.
- Cole, A., 2000 - Genesis of granitoid-hosted gold-tungsten mineralization, Jilau, Tajikistan: Unpublished Ph.D. thesis, UK, *University of London*, 240 p.
- Cole, A. 2002 - The Great Silk Road paved with gold. *International Mining and Minerals*, No. 48, pp. 13-15.
- Cole, A. and Seltmann, R., 2000 - The role of granitoids during Variscan orogenic gold mineralization in the Tien Shan and Ural mountain belts of central Eurasia; in Bouchot, V. and Moritz, R. (Eds.),

- Orogenic Gold Deposits in Europe, *Editions BRGM*, v. 297, pp. 110-111.
- Corbett, G., 2004 - Epithermal and Porphyry Gold - Geological Models; in *Hi Tech and World Competitive Mineral Success Stories Around the Pacific Rim*, Proc. PACRIM 2004 Conference, Adelaide, 19-22 September, 2004, *AusIMM*, Melbourne, pp. 115-125.
- Dalimov, T.N., Ganiev, I.N. and Ishbaev, Kh..D., 2003 - The Chatkal-Kurama "hot spot" and history of magmatic evolution.- *Geologiya i Mineral'nyie Resursy* (Geology and Mineral Resources), Tashkent, v. 5 (5), pp. 3-14 (in Russian).
- Du Qi, 2004 - The alteration and mineralization features of the Duobaoshan porphyry copper deposit; *Bulletin of the Geological Survey of Japan*, v. 33, pp. 469-477.
- Gerel, O., 1998 - Phanerozoic felsic magmatism and related mineralization in Mongolia; *Bulletin of the Geological Survey of Japan*, v. 49, pp. 239-248.
- Gerel, O. and Munkhtsengel, B., 2005 - Erdenetiin Ovoo Porphyry Copper-Molybdenum Deposit in Northern Mongolia; in Porter, T.M. (Ed.), *Super Porphyry Copper & Gold Deposits: A Global Perspective*; *PGC Publishing*, Adelaide, v. 2, pp. 525-543.
- Golovanov, I.M., Seltmann, R. and Kremenetsky, A.A., 2005 - The Porphyry Cu-Au/Mo Deposits of Central Eurasia: 2. The Almalyk (Kal'makyr-Dalnee) and Saukbulak Cu-Au Porphyry Systems, Uzbekistan; in Porter, T.M. (Ed.), *Super Porphyry Copper & Gold Deposits: A Global Perspective*; *PGC Publishing*, Adelaide, v. 2, pp. 513-523.
- Han, C., Rui, Z., Mao, J., Yang, J., Wang, Z. and Yuan, W., 2003 - Geological characteristics of the Tuwu copper deposit, Hami, Xianjiang; in Mao, Goldfarb, Seltmann, Wang, Xiao and Hart, (Eds.), 2003 - Tectonic Evolution and Metallogenesis of the Chinese Altay and Tianshan, *Proceedings Volume of the International Symposium of the IGCI - 473 Project in Urumqi and Guidebook of the Field Excursion in Xinjiang, China: August 9-21, 2003. IAGOD Guidebook Series 10: CERCAMS/NHM*, London, pp. 249-260.
- Hedenquist, J.W., Arribas, A. Jr and Reynolds, T.J., 1998 - Evolution of an intrusion-centered hydrothermal system: Far Southeast-Lepanto porphyry and epithermal Cu-Au deposits, Philippines; *Economic Geology*, v. 93, pp. 373-404.
- Hedenquist, J.W. and Daneshfar, B., 2003 - Mineral potential of Central and East Asia. Basis for mining investment in transition economy countries; *The World Bank Group, Mining Department; Mining Journal Books Ltd.*, London. 105p. PDF document on CD-ROM.
- Heinhorst, J., Lehmann, B., Ermolov, P., Serykh, V. and Zhurutin, S., 2000 - Paleozoic crustal growth and metallogeny of Central Asia: evidence from magmatic-hydrothermal ore systems of Central Kazakhstan, *Tectonophysics* v. 328, pp. 69-87.
- Herrington, R.J., Puchkov, V.N. and Yakubchuk, A.S., 2005 - A reassessment of the tectonic zonation of the Uralides: implications for metallogeny; in McDonald, I., Boyce, A.J., Butler, I.B., Herrington, R.J. and Polya, D.A., (Eds.), *Mineral Deposits and Earth Evolution. Geological Society, London, Special Publications*, v. 248, pp. 153-166.
- Islamov, F., Kremenetsky, A., Minzer, E. and Koneev, R., 1999 - The Kochbulak - Kairagach ore field; in Shayakubov, T., Islamov, F., Kremenetsky, A. and Seltmann, R., (Eds.), *Au, Ag, and Cu deposits of Uzbekistan. Excursion guidebook to the International Field Conference of IGCP-373, Excursion B6 of the Joint SGA-IAGOD symposium, London/Tashkent, 27/28 August - 4 September 1999, Chapter 5*, pp. 91-108.
- Ivanhoe Mines, 2004-2005 - Web-site at <http://www.ivanhoe-mines.com/s/OyuTolgoi.asp>.
- Jahn, B.-M., 2004 - The Central Asian Orogenic Belt and growth of the continental crust in the Phanerozoic; in Malpas, J., Fletcher, C.J.N., Ali, J.R. and Aitchison, J.C., (Eds.), *Aspects of the Tectonic Evolution of China*, *Geological Society, London, Special Publications*, v. 226, pp. 73-100.
- Jahn, B.-M., Wu, F. and Chen, B., 2000 - Granitoids of the Central Asian Orogenic Belt and continental growth in the Phanerozoic: *Transactions of the Royal Society of Edinburgh, Earth Sciences*, v. 91, pp. 181-193.
- Jenchuraeva, R.J., 1997 - Tectonic setting of porphyry-type mineralization and hydrothermal alteration in Paleozoic island arcs and active continental margins, Kyrghyz Range, (Tien Shan) Kyrghyzstan, *Mineralium Deposita*, v. 32, pp. 434-440.
- Jenchuraeva, R.D., Nikonorov, V.V. and Karaev, Yu.V., 2005 - Atlas of Economic Types of Ore Deposits in Kyrgyzstan; State Agency on Geology and Mineral Resources under the Government of the Kyrgyz Republic and Institute of Geology, National Academy of Sciences, Kyrgyz Republic, Bishkek. English edition by *CERCAMS, NHM*, London (in press).
- Jun, G., Maosong, L., Xuchang, X., Yaoqing, T. and Guoqi, H., 1998 - Paleozoic tectonic evolution of the Tianshan Orogen, northwestern China, *Tectonophysics*, v. 287, pp. 213-231.
- Kamitani, M. and Naito, K, (Eds.), 1998 - Mineral resources map of Asia, Metal Mining Agency of Japan, Scale 1:10,000,000, accompanied by one booklet of tables and an html CD-ROM; [http://www.mmaj.go.jp/mric\\_web/deposit/index.htm](http://www.mmaj.go.jp/mric_web/deposit/index.htm)
- Kidd, R.P. and Robinson, J.R., 2004 - A Review of the Kapit Orebody, Lihir Island Group, Papua New Guinea; in *Hi Tech and World Competitive Mineral Success Stories Around the Pacific Rim*, Proc. PACRIM 2004 Conference, Adelaide, 19-22 September, 2004, *AusIMM*, Melbourne, pp. 323-331.
- Kirkham, R. V. and Dunne, K.P.E., (compilers), 2000, *World*

- distribution of porphyry, porphyry associated skarn and bulk-tonnage epithermal deposits and occurrences; *Geological Survey of Canada*, Open File 3792, Scale 1:35,000,000, accompanied by one diskette.
- Kirwin, D.J., Forster, C.N. and Garamjav, D., 2003 - The discovery history of the Oyu Tolgoi porphyry copper-gold deposit, South Gobi, Mongolia; *in Proceedings of the NewGenGold 2003 Conference*, Perth, WA, pp. 130-146.
- Kirwin, D.J., Forster, C.N., Kavalieris, I., Crane, D., Orsich, C., Panther, C., Garamjav, D., Munkhbat, T.O. and Niislekhuu, G., 2005 - The Oyu Tolgoi Copper-Gold Porphyry Deposits, South Gobi, Mongolia; *in Seltmann, R., Gerel, O. and Kirwin, D.J., (Eds.), Geodynamics and Metallogeny of Mongolia with a Special Emphasis on Copper and Gold Deposits: SEG-IAGOD Field Trip, 14-16 August 2005, 8th Biennial SGA Meeting. IAGOD Guidebook Series 11: CERCAMS/NHM*, London, pp. 155-168.
- Kirwin, D.J., Wilson, C.C., Turmagnai, D. and Wolfe, R., 2005a - Exploration History, Geology, and Mineralisation of the Kharmagtai Gold-Copper Porphyry District, South Gobi Region, Mongolia; *in Seltmann, R., Gerel, O. and Kirwin, D.J., (Eds.), Geodynamics and Metallogeny of Mongolia with a Special Emphasis on Copper and Gold Deposits: SEG-IAGOD Field Trip, 14-16 August 2005, 8th Biennial SGA Meeting. IAGOD Guidebook Series 11: CERCAMS/NHM*, London, pp. 175-191.
- Kovalenker, V.A., Safonov, Yu.G., Naumov, V.B. and Rusinov, V.L., 1997 - The Epithermal Gold-Telluride Kochbulak Deposit, Uzbekistan. *Geology of Ore Deposits*, v. 39, N2, March-April 1997, pp. 107-128.
- Kudrin, V.S., Solov'yev, V.A., Stavinskiy, V.A. and Karabdin, L.L., 1990 - The gold-copper-molybdenum-tungsten ore belt of the Tien Shan; *International Geology Review*, v. 32, pp. 930-941.
- Kudryavtsev, Yu.K., 1996 - The Cu-Mo deposits of Central Kazakhstan; *in Shatov, Seltmann, Kremenetsky, Lehmann, Popov and Ermolov, (Eds.) - Granite-Related Ore Deposits of Central Kazakhstan and Adjacent Areas; INTAS-93-1783 Project, GLAGOL Publishing House, St. Petersburg*, pp. 119-144.
- Lamb, M.A. and Badarch, G., 2001 - Paleozoic sedimentary basins and volcanic arc systems of southern Mongolia: New geochemical and petrographic constraints; *in Davis, G.A. and Hendrix, M.S., (Eds.), Paleozoic and Mesozoic Tectonic Evolution of Central Asia from Continental Assembly to Intracontinental Deformation, Geological Society of America, Memoir 194*, pp. 117-149.
- Lamb, M.A. and Cox, D., 1998 - New  $^{40}\text{Ar}/^{39}\text{Ar}$  age data and implications for porphyry copper deposits of Mongolia; *Economic Geology*, v.93, pp. 524-529.
- Lamb, M.A., Hanson, A.D., Graham, S.A., Webb, L.E. and Badarch, G., 1999 - Left-lateral sense offset of Upper Proterozoic to Palaeozoic features across the Gobi Onon, Tost and Zuunbayan faults in southern Mongolia and implications for other central Asian faults; *Earth and Planetary Science Letters*, v. 173, pp. 183-194.
- Malyukova, N.N., 2001 - The Taldybulak Levoberezhny gold deposit; *in Seltmann, R. and Jenchuraeva, R., (Eds.), Palaeozoic Geodynamics and Gold Deposits in the Kyrgyz Tien Shan; IGCP-373 Field Conference in Bishkek and the Kyrgyz Tien Shan; 16-25 August, 2001 & Pre-meeting Field Trip A5 of the Joint 6th Biennial SGA Meeting in Krakow, Poland, Excursion Guidebook*, pp. 97-110.
- Mao, J., Goldfarb, R., Seltmann, R., Wang, D., Xiao, W. and Hart, C., (Eds.), 2003 - Tectonic evolution and metallogeny of the Chinese Altay and Tianshan. International Association on the Genesis of Ore Deposits (IAGOD), London, Guidebook Series 10, *CERCAMS NHM*, London, 286p.
- Mao, J., Konopelko, D., Seltmann, R., Lehmann, B., Wen Chen, Yitian Wang, Eklund, O. and Usabaliev, T., 2004 - Postcollisional age of the Kumtor gold deposit and timing of Hercynian events in the Tien Shan, Kyrgyzstan; *Economic Geology*, v. 99, pp. 1771-1780.
- Mossakovskiy, A.A., Ruzhentsev, S.V., Samygin, S.G. and Kheraskova, T.N., 1993 - Central Asian fold belt: geodynamic evolution and history of formation; *Geotektonika*, no. 6, pp. 3-33 (*in Russian*).
- Mutschler, F.E., Ludington, S. and Bookstrom, A.A., 2000 - Giant porphyry-related metal camps of the world - a database; *U.S. Geological Survey Open-File Report 99-556*, Online Version 1.0, [http://geopubs.wr.usgs.gov/open-file/of99-556/world\\_ppy.xls](http://geopubs.wr.usgs.gov/open-file/of99-556/world_ppy.xls)
- Nie Fengjun, Jiang Sihong, Zhang Yi, Liu Yan and Hu Peng, 2004 - Geological features and origin of porphyry copper deposits in China-Mongolian border region and its neighbouring areas; *Mineral Deposits*, v. 23, No. 2, pp. 176-189 (*in Chinese, English abstract*).
- Nikonorov, V.V., Karaev, J.V., Zamaletdinov, T.S., Borisov, F.I., Tolskiy, V.I., Larina, T.V., Gorbaneva, T.V., 2000 - Explanatory Notes and Catalogue of mineral deposits shown on the Map of Mineral Resources of the Kyrgyz Republic, Scale 1 : 1 000 000, Bishkek, 75p.
- Perello, J., Cox, D., Garamjav, D., Sanjdorj, S., Diakov, S., Schissel, D., Munkhbat, T.-O. and Oyun, G., 2001 - Oyu Tolgoi, Mongolia: Siluro-Devonian Porphyry Cu-Au-(Mo) and high-sulfidation Cu mineralization with a Cretaceous chalcocite blanket; *Economic Geology*, v. 96, pp. 1407-1428.
- Pokalov, V.T., 1977 - Deposits of molybdenum, *in Smimov, V.I., (Ed.), 1977 - Ore Deposits of the USSR; Pitman Publishing*, v. 3, pp. 125-179.
- Qin, K., Li, M. and Ishihara, S., 1997 - Intrusive and mineralization ages of the Wunugetushan porphyry Cu-Mo deposit, NE-China: Evidence from single grain zircon U-Pb, Rb-Sr isochron and

- K-Ar ages; *Resource Geology*, v. 47 (6), pp. 293-298.
- Qin, K., Sun, S., Li, M. Fang, T., Wang, S. and Liu W., 2002 - Paleozoic epithermal Au and porphyry Cu deposits in north Xinjiang, China: Epochs, features, tectonic linkage and exploration significance; *Resource Geology*, v. 52 (4), pp. 291-300.
- Richards, J.P., 2005 - Cumulative Factors in the Generation of Giant Calc-alkaline Porphyry Cu Deposits; in Porter, T.M. (Ed.), *Super Porphyry Copper & Gold Deposits: A Global Perspective*; PGC Publishing, Adelaide, v. 1, pp. 7-25.
- Samonov, I.Z. and Pozharisky I.F., 1977 - Deposits of copper, in Smirnov, V.I., (Ed.), 1977 - Ore Deposits of the USSR; *Pitman Publishing*, v. 2, pp. 106-181.
- Seltmann, R. and Jenchuraeva, R., (Eds.), 2001 - Paleozoic geodynamics and gold deposits in the Kyrgyz Tien Shan: IGCP 373 International Field Conference, Bishkek and Kyrgyz Tien Shan, Kyrgyz Republic, 16-25 August 2001, Guidebook Series 9, 183p.
- Seltmann, R., Koroteev, V., Fershtater, G. and Smirnov, V., (Eds.), 2000 - The eroded Uralian Paleozoic ocean to continent transition zone: Granitoids and related ore deposits: IGCP 373 International Field Conference, Urals, Russia, 18-30 July 2001, Excursion Guidebook, 102p.
- Seltmann, R., Shatov, V. and Yakubchuk, A., 2004 - Mineral Deposits Database and Thematic Maps of Central Asia, Scale 1.5 million: ArcView 3.2 and MapInfo 6.0(7.0) GIS Packages, Explanatory Notes, CERCAMS, Natural History Museum, London, UK., 117p.
- Sengör, A.M.C., Natal'in, B.A. and Burtman, V.S., 1993 - Evolution of the Altaid tectonic collage and Paleozoic crustal growth in Eurasia: *Nature*, v. 364, pp. 299-307.
- Sengör, A.M.C. and Natal'in, B.A., 1996 - Palaeotectonics of Asia: Fragments and synthesis; in Yin, A. and Harrison, M., (Eds.), *The Tectonic Evolution of Asia*; Cambridge University Press, pp. 486-640.
- Shatov, V.V., Cole, A., Seltmann, R. and Yakubchuk, A., 2001 - Metallogeny of gold in the Tien Shan and Urals Paleozoic fold belts: A GIS-based approach; in Piestrzynski, A., et al., (Eds.), *Mineral deposits at the beginning of the 21st century*; Lisse, Swets and Zeitlinger, pp. 489-492.
- Shatov V.V., Seltmann R. and Moon C. J., 2003 - The Yubileinoe porphyry Au(-Cu) deposit, the South Urals: Geology and alteration controls of mineralization; in Eliopoulos, D.G., et al., (Eds.), *Mineral Exploration and Sustainable Development, Proceedings 7th Biennial SGA Meeting, Athens, 24-28 August 2003*; Millpress Rotterdam, v. 1, pp. 379-382.
- Shayakubov, T., Islamov, F., Kremensky, A. and Seltmann, R., (Eds.), 1999 - Au, Ag, and Cu deposits of Uzbekistan: IGCP 373 International Field Conference, Excursion B6 of the Joint SGA-IAGOD Symposium, London-Tashkent, 27 August-4 September 1999, Excursion Guidebook, 112p.
- Sokolov, A.L., 1995 - The regional and local controls on giant-scale copper and gold mineralisation, Uzbekistan; in Clark, A.H., (Ed.), *Giant Ore Deposits II. Controls on the scale of orogenic magmatic-hydrothermal mineralisation*; Proceedings of the second giant ore deposits workshop, Kingston, Ontario, Canada, April 25-27, 1995. Department of Geological Sciences, Queens University, Kingston Ontario, pp. 450-474.
- Wainwright, A.J., Tosdal, R.M., Forster, C., Kavalieris, I., Crane, D., Findlay, A. and Kirwin, D., 2004 - Structure and Stratigraphy of the Oyu Tolgoi Cu-Au porphyry, Mongolia; Poster, Cordilleran Roundup 2004; www.mdru.ubc.ca/home/research/tog-ot-roundup\_04\_poster.pdf.
- Wang Futong, Feng Jing, Hu Jianwei, Wang Lei, Jian Lifeng and Zhang Zheng, 2001a - Characteristics and significance of the Tuwu porphyry copper deposit, Xinjian [J]; *Chinese Geology*, v. 28 (1), pp. 36-39 (in Chinese).
- Wang Futong, Zhuang Daoze, Hu Jianwei, Feng Jing, Jian Lifeng, Zhang Zheng and Hu Changan, 2001b - Application of geophysical exploration method in the Tuwu area, Winjiang - On the prospecting model of porphyry copper deposit [J]; *Chinese Geology*, v. 28 (3), pp. 40-46 (in Chinese).
- Watanabe, Y. and Stein, H.J., 2000 - Re-Os ages for the Erdenet and Tsagaan Suvarga porphyry Cu-Mo deposits, Mongolia, and tectonic implications; *Economic Geology*, v. 95, pp. 1537-1542.
- White, N.C., Hedenquist, J.W. and Kirkham, R.V., 2001 - Asia: The waking giant; *Mining Journal* supplement, March 2001, 12p.
- Windley, B.F., Allen, M.B., Zhang, C., Zhao, Z.-Y. and Wang, G.-R., 1990 - Paleozoic accretion and Cenozoic reformation of the Chinese Tien Shan Range, central Asia; *Geology*, v. 18, pp. 128-131.
- Yakubchuk, A., 2002 - The Baikaside-Altaid and North Pacific orogenic collages: similarity and diversity of structural patterns and metallogenic zoning; in Blundell, D., Neubauer, F. and von Quadt, A., (Eds.), *Geological Society*, London, Special Publications, v. 204, pp. 273-297.
- Yakubchuk, A., 2004 - Architecture and mineral deposit settings of the Altaid orogenic collage: a revised model; *Journal of Asian Earth Sciences*, v. 23, pp. 761-779.
- Yakubchuk, A.S., 2005 - Geodynamic evolution of accreted terranes of Mongolia against the background of the Altaids and Transbaikal-Mongolian collages; in, Seltmann, R., Gerel, O. and Kirwin, D.J., (Eds.), *Geodynamics and Metallogeny of Mongolia with a Special Emphasis on Copper and Gold Deposits: SEG-IAGOD Field Trip, 14-16 August 2005, 8th Biennial SGA Meeting*; IAGOD Guidebook Series 11: CERCAMS/NHM, London; pp. 13-24.

- Yakubchuk, A.S., Cole, A., Seltmann, R. and Shatov, V., 2002 - Tectonic setting, characteristics and regional exploration criteria for gold mineralization in central Eurasia: The southern Tien Shan province as a key example; in Goldfarb, R. and Nielsen, R., (Eds.), *Integrated Methods for Discovery: Global Exploration in Twenty-First Century; Economic Geology*, Special Publication No. 9, pp. 177-201.
- Yin Bingchuan and Ran Qingchang, 1997 - The tectonic environments of metallogenesis of Duobaoshan superlarge copper deposit; *Jilin Geology*, v. 17, no. 2. (*in Chinese, English abstract*).
- Zhao Yuanyi and Zhao Guangjiang, 1995 - Geochemical characteristics of the Duobaoshan copper orefield REE and its genetic model in Heilongjiang Province; *Jilin Geology*, v. 14, no. 2 (*in Chinese, English abstract*).
- Zhao Yuanyi, Ma Zhihong and Zhong Chongxue, 2005 - Ore-forming geochemistry of the Duobaoshan copper deposit, Heilongjiang Province, China; The 8th Biennial SGA Meeting, Beijing, China, Extended Abstract Volume, Chapter 9-65, pp. 1119-1121.
- Zonenshain, L.P., Kuzmin, M.I. and Natapov, L.M., 1990 - Mongol-Okhotsk fold belt; in Page, B.M., (Ed.), *Geology of the USSR: a Plate Tectonic Synthesis; American Geophysical Union*, Washington, Geodynamic Series, v. 21, pp. 97-108.
- Zvezdov, V.S., Migachev, I.F. and Girfanov, M.M, 1993 - Porphyry copper deposits of the CIS and the models of their formation; *Ore Geology Reviews*, v. 7, pp. 511-549.

## THE PORPHYRY Cu-Au/Mo DEPOSITS OF CENTRAL EURASIA 2. THE ALMALYK (KAL'MAKYR-DALNEE) AND SAUKBULAK Cu-Au PORPHYRY SYSTEMS, UZBEKISTAN

<sup>1</sup>Igor M. Golovanov, <sup>2</sup>Reimar Seltmann and <sup>3</sup>Alexander A. Kremenetsky

<sup>1</sup> *Scientific Research Institute of Mineral Resources of the State Committee for Geology of the Republic of Uzbekistan, Tashkent, Uzbekistan.*

<sup>2</sup> *Centre for Russian and Central EurAsian Mineral Studies, Department of Mineralogy, Natural History Museum, London, UK.*

<sup>3</sup> *Institute of Mineralogy, Geochemistry and Crystal Chemistry of Rare Elements, Moscow, Russia.*

**Abstract** – The Almalyk porphyry Cu-Au system of eastern Uzbekistan encompasses the giant ore deposits at Kal'makyr (2.5 Gt @ 0.38% Cu, 0.5 g/t Au) and Dalnee (2.8 Gt @ 0.36% Cu, 0.35 g/t Au). The Sarycheku orebody (200 Mt @ 0.5% Cu, 0.1 g/t Au) is part of the Saukbulak porphyry Cu-Au system, some 18 km to the south. Both systems are associated with the second, Middle- to Late-Carboniferous, pulse of magmatic activity within the Devonian-Carboniferous Valerianov-Bel'tau-Kurama volcano-plutonic belt that is the main element of the Middle Tien Shan terrane in Central Asia. Previous K-Ar dating of the ore-related porphyry intrusive and the mineralisation has returned ages in the range of 310 to 290 Ma, whereas recent U-Pb zircon dating reported for the intrusive sequence in the Almalyk district partially overlaps in the range of 320 to 305 Ma, with ore-related porphyries 315 to 319 Ma.

Mineralisation at both Kal'makyr and Dalnee is predominantly in the form of stockworks with lesser disseminations, and is associated with Late Carboniferous quartz monzonite porphyry plugs intruding earlier dioritic and monzonitic intrusive rocks of the same magmatic complex. The orebodies take the form of a cap like shell developed above and draped over the flanks of the related quartz monzonite porphyry stock. The dominant hosts to ore are the monzonite and diorite wall rocks, with the quartz monzonite porphyry only containing ore in its outer margins, surrounding and/or overlying a barren core. The focus of stockwork development is fracturing related to both the intrusive contact of the porphyry stock and to crosscutting faulting. Alteration comprises an early K-silicate phase followed by albite-actinolite and peripheral epidote-chlorite-carbonate-pyrite propylites, overprinted by an abundant phyllic episode which is closely related to the final distribution of the ore. Associated mineralisation commenced with barren quartz-hematite veining, followed by quartz-magnetite, quartz-pyrite-molybdenite-chalcocopyrite with the bulk of the contained gold, quartz-carbonate-polysulphide with lesser gold, then by zeolite-anhydrite, and finally carbonate and barite veining. Subsequent oxidation and uplift developed a layer of oxide ore, a limited leached cap and supergene sulphide enrichment, largely in zones of fault related fracturing.

### Introduction

The Almalyk and Saukbulak ore fields embrace the Kal'makyr-Dalnee and Sarycheku porphyry Cu-Au deposits respectively and define a mineralised district located in the northern foothills of the Kurama Range (heights of 750 to 1350 m A.S.L.), south of the Angren River (Fig. 1) in eastern Uzbekistan. The town of Almalyk is 65 km to the southeast of Tashkent, the capital, while Sarycheku is 18 km to the southeast of Kal'makyr-Dalnee.

This district, with its porphyry copper, base metal-skarn (e.g. Kurgashimkan, Kul'chulak and Kulemes) and epithermal gold-silver (e.g. Sartabutkan, Akturpak and Kaul'dy) deposits, is among the most economically important in central Asia (Grauch, 1996; Kremenetsky *et al.*, 1996; Isakhojaev, 1998; Shayakubov *et al.*, 1998; Shayakubov, 1999). The most significant are the large, low grade porphyry copper deposits with their critical gold

credits, accounting for a recently estimated combined production + resource of >5 Gt @ 0.36% Cu, 0.6 g/t Au.

Green copper oxide mineralisation was discovered at Almalyk in 1926 during a geological mapping program. Exploration was subsequently undertaken from 1931 to 1941 and between 1947 and 1951, and open pit mining commenced at Kal'makyr in 1954. Additional exploration and delineation work between 1961 and 1980, and from 1986 to 1996 culminated in the estimation of reserves/resources of 2 Gt @ 0.38% Cu, 0.6 g/t Au, 0.006% Mo at a 0.2% Cu cut-off, plus 1700 Mt of lower grade 0.15 to 0.19% Cu. The chief contributors to the exploration, evaluation and associated research were T. Shayakubov, E. But'eva, V. Dedy, S. Badalov, I. Golovanov, and A. Rakhubekov.

The Kal'makyr open-pit is located approximately 3 km southeast of the town of Almalyk and has yielded more than 2.94 Mt of Cu and 650 t of Au from 1954 to the

present from treated ore with a recovered grade averaging 0.381% Cu and 0.51 g/t Au. Approximately 1.75 Gt at a recoverable grade of 0.38% Cu, 0.5 g/t Au, 0.004% Mo and 2.5 g/t Ag remain, accounting for a reserve/resource of 6.6 Mt of contained Cu and 900 t of Au. The pit currently covers an area of 3750 x 2000 m and has been excavated to a depth of 660 m on 15.0 and 22.5 m benches. The present annual mine capacity is 27 Mt of ore and 13 Mt of waste, totalling 35 million m<sup>3</sup> of material to yield 100 Kt of recovered Cu metal. In 2003, the mine produced 100 kt of Cu, 14.5 t of Au and 900 t of Mo from ore with a recovered grade of 0.413% Cu, 0.042% Mo. Ore is moved by truck from the lower levels to a rail loading facility on the upper benches of the pit for the 8 km transit to the mill, while waste is railed 5 to 10 km to dumps (Kashirsky and Turesebekov, 1999).

Hypogene sulphide, as well as oxide and supergene enriched ores have been mined at Kal'makyr, with hypogene ore being defined as having <10% oxides and/or supergene sulphides. Virtually all of the oxides and supergene sulphides have now been removed and currently 96 to 99% of extractable Cu, Mo, Au, Re, Se, and Te is contained in primary sulphide ore. While the Cu grade of the remaining resource is low by world standards, by-products significantly enhance the value of the ore. In late 1997 to early 1998, the value of Cu in the Kal'makyr ore was estimated as 52% of the total, Au - 41.69%, Ag - 4.4%, Mo - 0.44%, Re - 0.80%, Te - 0.46%, and Se - 0.12%.

*Dalnee* comprises a string of three interconnected orebodies, Central, Northwestern Balykty and Karabulak, which represent structural offsets of the down plunge continuation of the Kal'makyr deposit at deeper levels. Appreciable intersections of ore were first encountered in drill holes at Dalnee in 1962. The ensuing exploration and delineation commenced in 1963 and was completed in 1978. The total reserves/resources are estimated at 10.22 Mt of contained Cu and 994 t of Au at average

recoverable grades of 0.36% Cu and 0.35 g/t Au, using a cut-off of 0.2% Cu. A 7 km long open-pit with a capacity of 30 Mt of ore per annum is proposed to exploit the resource over a 70 to 80 year period, although the decision has not yet been taken to proceed. Mining would require relocation of much of the transport lines at Kal'makyr and sections of the town of Almalyk. In addition, the establishment of overburden dumps is also problematical (Kashirsky and Turesebekov, 1999).

The *Sarycheku* porphyry copper deposit is located 18 km to the southeast of the Almalyk (Fig. 2). Mineralisation was discovered in 1927, and subsequently explored and proved between 1955 and 1983, and mined by open-pit from 1974 to the present. The pit now covers an area of some 1800 x 1000 m and is 250 m deep with an annual capacity of 4 to 5 Mt of ore. To date, 640 Kt of Cu, 4.84 t of Au and 6890 t of Mo have been extracted from ore with a recovered grade of 0.496% Cu, 0.09 g/t Au and 0.0075% Mo. Ore is transported by truck to a transfer station and loaded onto rail cars for the 20 km transit to the central mill. Production in 2003 yielded 11.6 Kt of Cu, 0.203 t Au and 140 t Mo from ore with a recovered grade of 0.505% Cu, 0.09 g/t Au and 0.0062% Mo. The current reserve/resource is stated at 0.36 Mt of recoverable Cu, 6.7 t Au and 5520 t of Mo at similar grades.

Processing of Kal'makyr and Sarycheku ore is undertaken at the Almalyk concentrator, part of the Almalyk Mining and Metallurgical Integrated Works (AGMK). The current mill capacity is 29 Mt of ore per annum to produce separate Cu and Mo concentrates. Copper recovery averages 75 to 80%. The Cu concentrate is processed at the Almalyk smelter while the Mo concentrate is transported to the Chirchik integrated works for refractory and heat-stable materials. AGMK which controls both the mining and metallurgical operations, produces refined copper, gold, selenium, tellurium, and sulphuric acid which are marketed both in Uzbekistan and abroad.

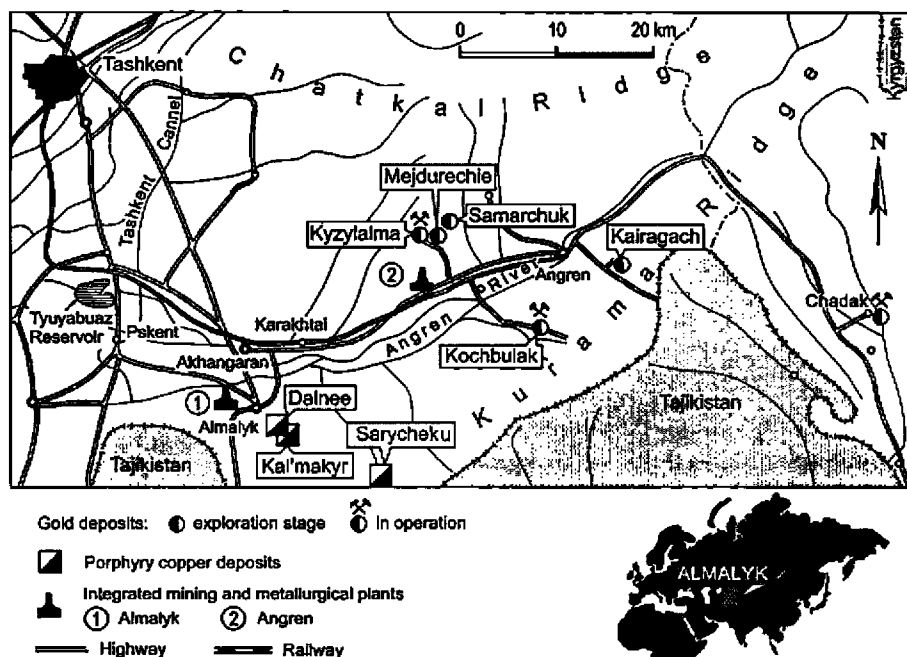


Figure 1: Location map of the Almalyk district.

Reserves/resources delineated in the three porphyry copper deposits: Kal'makyr, Dalnee and Sarycheku total 17.2 Mt of contained Cu; 59.5% in the Dalnee deposit, 38.5% in Kal'makyr and 2% in Sarycheku. In addition to copper, >1800 t of Au, 12.5 Kt of Ag, 229 Kt of Mo, 13.2 Kt of Se, 1000 t of Te, and 566 t of Re are estimated to remain. Other mineralised material that may be amenable to retreatment is piled up in dumps, tailings and waste from metallurgical processing. In particular, approximately 130 Mt of low grade material containing <0.2% Cu remain in stockpiles as well as 13 Mt of oxide ore with 0.5 to 0.6% Cu and 10 to 12 Mt of slag containing 1% Cu. The 450 Mt of tailings occupy an area of 4x2 km and include 165 Mt of which are potentially retreatable.

### Geology

The Almalyk district is located within the southeastern section of the Devonian-Carboniferous Valerianov-Bel'tau-Kurama volcano-plutonic belt (or magmatic arc) which extends for 1500 km in a general east-west direction and forms part of the Middle Tien Shan terrane in Kyrgyzstan, Uzbekistan and southern Kazakhstan. The Southern Tien Shan Suture zone separates this volcanic belt from the Middle- to Late-Palaeozoic back-arc accretionary complex (the Southern Tien Shan terrane) that formed in the Turkestan Basin between the original Valerianov-Bel'tau-

Kurama arc and the Karakum - Altai-Tarim micro-continent to the south (see Fig. 18 in Seltmann and Porter, 2005, in this volume). Un-eroded fragments of the initial pulse of this volcano-plutonic belt remain exposed as outcrops of Siluro-Devonian I and I-A type granitoids and as Devonian terrigenous-volcanogenic rocks (alkaline basalt-andesite-rhyolite units) with an Andean type geochemical signature. The reconstructed volcano-plutonic belt was as much as 120 km wide, averaging, 50 to 70 km (I. Golovanov, pers. comm.).

From the Lower Visian to the Lower Bashkirian in the Carboniferous, the rocks of the magmatic belt floored a flat underwater shelf on the passive southern margin of the Kyrgyz-Kazakh micro-continent, and were overlain by thick carbonate and terrigenous sequences. The second pulse of magmatic activity accompanied the intense subduction of the Turkestan basin beneath the Kyrgyz-Kazakh micro-continent during the Middle- to Late-Carboniferous resulting in basin closure, collision and formation of another Andean type volcano-plutonic belt within the active wedge. Rb-Sr age dating of volcanic rocks from this pulse yielded ages of 320 to 290 Ma.

The mineralised porphyry stocks of the Kal'makyr-Dalnee mineralised system were intruded into this sequence, represented by lower meta-terrigenous Ordovician and Silurian units that are overlain by Lower-Devonian volcanic

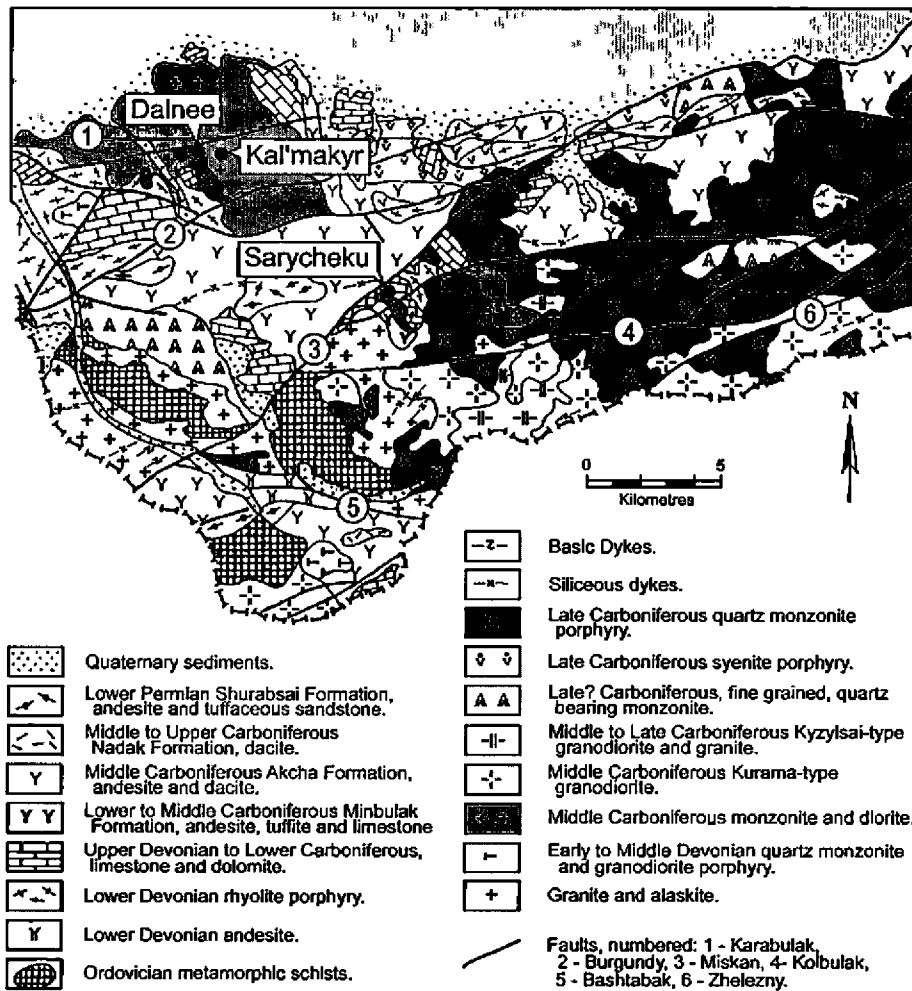


Figure 2: Schematic geological map of the Almalyk district and adjacent areas (after data of the Almalyk Geological Exploration Expedition).



rocks, passing upward, in turn into a Middle-Devonian to Lower-Carboniferous carbonate sequence and then to Upper Palaeozoic sedimentary rocks and a volcanic pile. Mesozoic and Cenozoic sediments occur locally.

Widespread Hercynian intrusive magmatism in the belt is represented by older monzonite, gabbro and diorite, and by younger granitoids of the Kurama batholith, minor porphyry intrusions (predominantly granodiorite porphyry) and numerous and diverse late dykes.

A vast descriptive literature exists representing the past and current knowledge on the geological framework and the exploration history of the Almalyk district, including Dalimov and Ganiev, 1995; Golovanov *et al.*, 1986; Islamov, 1998; Kudrin *et al.*, 1990; Lyashenko *et al.*, 1998; Nikolayeva *et al.*, 1991; Shayakubov *et al.*, 1988; Tulyuganov, 1974; Zav'yalov and Islamov, 1995 and others.

### Structure

Three fault trends are recognised in the Almalyk district, namely northwest, east-west and northeast trending sets. The most fundamental of these is the deep seated northwest trending set which appears to control the distribution of the mineralised stocks, associated alteration and geochemical metal dispersion patterns, defining a 30 km long and 5 to 10 km wide corridor encompassing the known significant mineralisation. However, it is not reflected in the current topographic relief.

The east-west trending set of faults is clearly reflected in the present day erosional surface and include the Karabulak, Kal'makyr and Burgundy Faults (Figs. 2 and 3). These faults have controlled the distribution of mineralisation and alteration, but have also displaced the same mineralisation with late Alpine related sinistral strike-slip dislocations of as much as 2 km and 0.5 km on the Karabulak and Kal'makyr faults respectively.

The northeast trending set, which includes the Central, Southern and Mishkan faults (Fig. 2) are post mineral structures which and displace the mineral belt and are

related to the Alpine orogenic phase. The Mishkan Fault can be traced for 40 km and has horizontal and vertical displacement components of 2 to 2.5 and 0.5 to 0.7 km respectively.

The Burgundy and Miskan faults subdivide the southwestern part of the Almalyk district into three blocks, each with a different geological character (Fig. 2). Ordovician - Silurian rocks intruded by a large granitic pluton are exposed in southern block, which has experienced the greatest uplift and thus is more deeply eroded. The central block is relatively less eroded and is overlain by Carboniferous volcanics, while the northern block is composed of Devonian - Carboniferous carbonate and volcanic rocks intruded by monzonitic plutons. The Kal'makyr and Dalnee deposits are located within the northern block and are predominantly hosted by plutonic rocks related to the large Almalyk monzonitic pluton which extends well beyond the deposits (Fig. 3).

The Kal'makyr-Dalnee copper mineralisation is controlled by both the distribution of the mineralised porphyry stocks and by faulting. The steeply dipping Karabulak, Kal'makyr, and Burgundy faults are clearly expressed as zones of cataclasis and hydrothermal alteration. The Kal'makyr and Burgundy faults both dip southward while the Karabulak Fault dips in the opposite direction near surface, but and curves with depth to parallel to the other two faults.

### Intrusive rocks

The intrusive host rocks of the Almalyk district comprise a gabbrodiorite-diorite-monzonite-quartz monzonite porphyry series. The most widespread intrusive phase is represented by batholithic syenodiorites which are equigranular, composed of feldspar, plagioclase, biotite, hornblende and less commonly, pyroxene, and contain approximately 15% mafic minerals. The next most common intrusive phase is a hypidiomorphic diorite characterised by 60 to 75% plagioclase. Bright pink syenite with up to 70% feldspar is less common. The syn-mineral

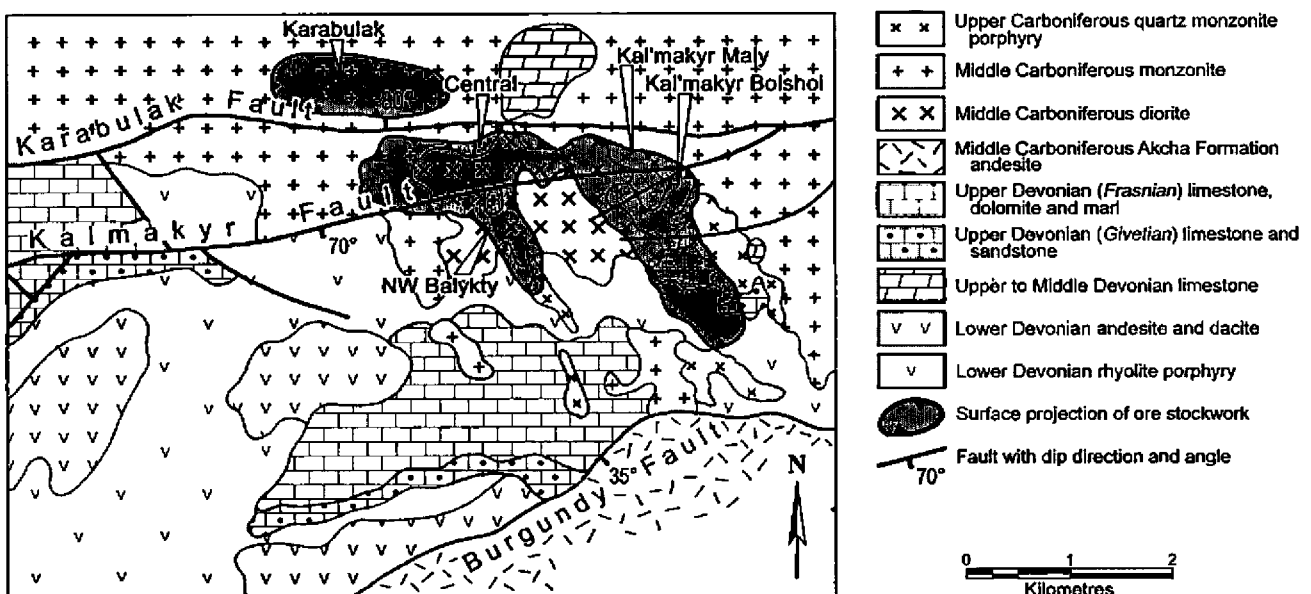


Figure 3: Schematic geological map of the Almalyk district (after Shayakubov *et al.*, 1983).

**Table 1: Average Pb, Zn, Cu, and Au contents (ppm) in monzonite of the Almalyk pluton**

Monzonite	No. of samples	Pb	Zn	Cu	Au
Medium-grained	34	43	78	49	0.0052
Fine-grained	29	41	89	48	0.0041

**Table 2: Distribution of Pb, Zn, Cu, and Au in minerals of monzonite, of the Almalyk pluton**

Mineral	Contribution of mineral, %			
	Pb	Zn	Cu	Au
Quartz	—	—	2.0	1.8
Orthoclase	30.8	10.0	20.4	19.5
Plagioclase	40.3	17.1	32.6	28.7
Biotite	14.1	30.0	10.2	13.3
Hornblende	9.5	22.8	12.2	17.2
Magnetite	2.4	20.0	20.4	—

**Table 3: Average Pb, Zn, Cu, and Au contents (ppm) in monzonite of the Almalyk pluton**

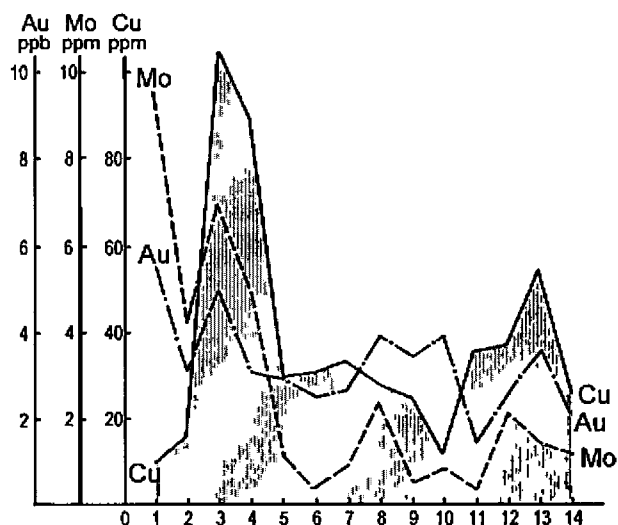
Element (ppm)	Kal'makyr	Dalnee
Cu,	374 (16)	507 (8)
Mo	8.0 (10)	8.0 (10)
Au	0.03 (10)	0.04 (7)
Ag	0.20 (10)	0.24 (7)
Ni	11.3 (12)	15.0 (14)
Co	10.6 (12)	4.8 (14)
Sn	6.3 (7)	3.0 (4)
Pb	34.0 (5)	trace
Bi	1.5 (12)	1.3 (7)
Rb	49.0 (5)	46.9 (7)
REE	180.0 (12)	125.7 (7)
V	72.9 (12)	35.0 (2)
Cr	6.1 (12)	5.5 (6)

Note: Numbers of samples are in parentheses.

quartz monzonite porphyry occurs in stocks has been dated at 290 Ma (K-Ar). It is a pale grey or light pink porphyritic rock with clearly visible phenocrysts of quartz (25%), plagioclase (32%), potassic feldspar (28%), and biotite (15%).

The belt of quartz monzonite porphyry intrusions can be traced from the northwest to southeast along a concealed basement fault of the northwest set. Some of the porphyries are exposed at the surface, while others are only cut by drill holes at a depth, or are reflected in geophysical data. The porphyry stocks commonly have steep contact at upper levels, but gradually flatten with depth accompanied by the development of apophyses. All are considered to be salients of a large deep-seated intrusion. Porphyritic dykes of syenodiorite, syenite, diorite, 'black' granodiorite and dacite as well as dolerite are less common and 2 to 25 m thick, and are considered to be the youngest intrusive phases.

The general variations of Cu, Mo, and Au contents in intrusive rocks within the Almalyk district are illustrated on (Fig. 4). Unaltered monzonite is slightly enriched in Pb, Zn, and Cu and characterised by a virtually Clarke Au content (Table 1). More than 70% of the Pb is contained within feldspars and only 2% is related to sulphides. Zn is incorporated into Fe-bearing minerals (biotite, hornblende, magnetite), while Cu and Au are fairly uniformly distributed in both the leucocratic- and mafic-minerals (Table 2).

**Figure 4: Distribution of Cu, Mo, and Au in intrusive rocks of the Almalyk ore field and adjacent areas (after Golovanov et al., 1988).**

Early Paleozoic rocks: (1) biotite granite, (2) alaskite; Late Paleozoic rocks: (3) diorite, (4) monzonite, (5) granodiorite of Kurama type, (6) granodiorite of Kyzylsai type, (7) granodiorite porphyry of Kuyundy type, (8) quartz monzodiorite porphyry of the Almalyk type, (9) quartz monzodiorite, (10) felsic porphyry, (11) granodiorite porphyry of Gushsai type, (12) granodiorite porphyry (dykes), (13) black granodiorite porphyry, (14) amphibole granodiorite porphyry.

The quartz monzonite porphyry is anomalously rich in Cu, Mo, and Au (Table 3). The contents of these metals increase with alkalinity, i.e. toward the upper contacts of the intrusions. At the same time, porphyry is depleted in Ni, V, Cr. It should be noted that even "fresh" porphyry is commonly affected by a hydrothermal alteration.

## Hydrothermal Alteration and Mineralisation.

Hydrothermal alteration and mineralisation are related to the emplacement of the late quartz monzonite porphyry stocks which have been dated as Late Carboniferous to Early Permian. Except for preliminary U-Pb zircon SHRIMP ages (R. Seltmann & D. Konopelko, pers. comm.) of 315-319 Ma for the various ore-related porphyry intrusives from the Kal'makyr pit, modern age determinations are lacking with only old K-Ar datings of limited accuracy available (Table 4). Nevertheless, these ages are consistent with geological relationships and support the commonly accepted assumption of a Late Carboniferous - Early Permian age of mineralisation (Askarov et al., 1975).

**Table 4: Absolute age of altered rocks and ores at Almalyk.**

Sample	Method	Age (Ma)	Source
Altered rocks, unspecified	K-Ar	280-290 (3)	Golovanov et al., (1988)
		290-300 (1)	
		300-310 (2)	
		310-320 (2)	
Phlogopite Sericite Hydromica	K-Ar	294	Golovanov et al., (1988)
		301-309	
		273-276	
Molybdenite	Re-Os	270	Badalov (1970)

Note: Numbers of determinations are in parentheses.

**Table 5: Chemical compositions of fresh and altered plutonic rocks from the Kal'makyr deposit** (after Korolev, unpubl. report; Zakirov, 1959; Mchshchaninov, 1970)

Component	1	2	3	4	5	6	7	8	9	10	11	12	13
SiO <sub>2</sub>	48.10	54.87	55.02	55.75	55.75	52.74	72.74	65.89	55.08	85.99	61.28	67.64	79.54-87.60
TiO <sub>2</sub>	0.79	0.68	0.52	-	0.41	0.72	0.30	0.19	-	0.18	0.37	-	0.15
Al <sub>2</sub> O <sub>3</sub>	18.25	16.39	16.23	16.42	14.73	19.02	6.18	16.61	13.75	1.14	16.85	12.94	4.78-1.62
Fe <sub>2</sub> O <sub>3</sub>	3.03	3.73	3.12	4.44	10.91	10.73	12.50	4.84	15.00	8.23	3.08	9.06	9.99-7.04
FeO	5.42	3.46	4.38	3.46	5.07	-	0.47	3.42	-	0.40	2.40	-	-
MnO	0.03	0.12	0.14	-	0.09	-	0.01	0.14	-	<0.01	0.07	-	-
MgO	6.11	3.55	3.17	4.86	4.77	4.57	0.50	2.73	4.10	0.36	1.79	0.55	0.30-0.18
CaO	5.27	5.23	3.68	3.62	1.49	0.71	1.60	5.10	0.12	0.90	4.40	<0.01	0.26-0.33
K <sub>2</sub> O	2.51	4.57	4.04	4.15	2.40	5.20	1.90	2.35	3.54	0.62	2.16	3.67	1.66
Na <sub>2</sub> O	2.50	4.00	3.20	1.45	3.31	0.52	1.74	5.02	0.58	1.71	4.72	0.97	0.21
P <sub>2</sub> O <sub>5</sub>	0.08	-	-	-	0.07	-	0.08	0.05	-	0.21	0.04	-	-
SO <sub>3</sub>	2.75	-	-	-	1.08	-	0.47	1.00	0.09	0.31	0.06	0.09	0.1
H <sub>2</sub> O	0.27	LOI= 1.31	LOI= 1.40	-	1.12	-	-	0.38	-	0.25	0.82	-	-
S	0.31	-	-	1.32	1.78	1.42	0.35	0.17	2.02	0.15	0.01	4.13	2.76
CO <sub>2</sub>	-	-	-	-	0.73	-	-	0.05	-	<0.01	0.39	-	-
Cu	0.05	-	-	-	-	0.63	0.69	-	0.57	0.24	-	0.85	0.37-0.13
Total	95.47	97.91	94.9	95.47	103.71	96.26	99.53	97.94	94.85	100.69	98.44	99.90	100.03-101.69
n	1	31	18	1	10	3	8	11	7	11	1	1	2

Note: (1) diorite (propylitized), (2) medium-grained monzonite; (3) fine-grained monzonite; (4) monzonite (propylitized); (5) monzonite affected by quartz-sericite-(biotite)-chlorite alteration; (6) monzonite affected by quartz-sericite alteration; (7) intensely silicified monzonite (quartzite); (8) syenite (slightly propylitized), (9) syenite affected by quartz-sericite-(biotite)-chlorite alteration; (10) intensely silicified syenite (quartzite); (11) quartz monzonite porphyry; (12) quartz monzonite porphyry affected by quartz-sericite-(biotite)-chlorite alteration; (13) intensely silicified quartz monzonite porphyry. n is number of samples. The dash denotes that data are lacking.

According to Golovanov *et al.*, (1988), the earliest hydrothermal alteration was a K-silicate phase which resulting in the replacement of felsic intrusives by amphibole, biotite and potassic feldspar. Subsequently, albite-actinolite and epidote-chlorite-carbonate-pyrite propylites were developed, overprinted by the abundant phyllic episode which is closely related to the final distribution of the ore mineralisation. Three facies of the phyllic stage are recognised, namely: i). quartz-sericite-chlorite, ii). quartz-sericite and iii). quartz.

The margins of the mineralised stockwork are irregular grade boundaries determined by assays. At both Kal'makyr and Dalnee these stockwork zones are present as a cap like shell developed above and draped down the flanks of the related quartz monzonite porphyry (QMP) stock. In both cases the best development of ore is on the fractured contact zone of the QMP, particularly where that contact coincides with fracturing associated with an east-west of northwest trending fault zone. At Dalnee, the bulk of the stockwork takes the form of a flat lying, irregular ellipsoid above the elongate stock, the margins of which are faulted, displacing ore developed on its flanks (Figs. 6 and 7). At the more deeply eroded Kal'makyr deposit, the remaining ore is principally preserved on the flanks of the QMP stock which forms a barren core to the surrounding doughnut shaped deposit (Fig. 5).

In both deposits there is a zoning pattern to the alteration. The upper central, barren part of the QMP stock has been subjected to potassic alteration and strong silicification, representing the silica facies of the phyllic alteration stage overprinting early K silicate alteration. This zone passes outwards and upwards into sub-ore mineralisation accompanied by the quartz-sericite facies alteration with

hematite and magnetite mineralisation. This latter zone in turn, passes outwards or upwards into the central high grade core of the deposit which has undergone quartz-sericite-chlorite-biotite alteration with associated magnetite-molybdenite-chalcocopyrite ore enclosed within an outer shell of pyrite-chalcocopyrite (also high-grade) hosted by phyllic altered rocks. It should be noted that slightly altered rocks with abundant chlorite contain 4 to 6 times more economic ore than severely altered sericite rocks. The high-grade stockwork core is surrounded by an outer zone of medium grade copper ore in phyllic and propylitic rocks, towards and away from the QMP stock respectively. Propylitically altered rocks predominantly host a pyrite-chalcocopyrite-sphalerite-galena assemblage represented by disseminations and rare veinlets. This latter assemblage is Au-bearing and locally contains calaverite, crenoirite, matildite, hessite, acanthite, aikinite, native gold and silver, with ore-grade mineralisation present as cross-cutting quartz, carbonate, barite and anhydrite veins and veinlets. Feldspar alteration increases with depth.

The paragenesis of ore mineralisation veinlet development within the ore stockwork is represented by a succession of mineral assemblages (from older to younger), as follows: i). barren grey stockwork quartz with hematite, K feldspar and disseminated molybdenite; ii). quartz-magnetite; iii). quartz-pyrite-molybdenite-chalcocopyrite with gold-I (the most productive phase accounting for 90% of the contained gold); iv). quartz-carbonate-polysulphide with gold-II (the remaining 10% of the gold); v). zeolite-anhydrite; and vi). carbonate and barite.

The affect of hydrothermal alteration on host rock compositions is illustrated by (Table 5). Table 6 lists the characteristics of the ore in both Kal'makyr and Dalnee.

**Table 6: Principal characteristics of un-diluted ores from the Dalnee and Kal'makyr deposits** (after Shayakubov, 1983)

Ore	Characteristics	Kal'makyr	Dalnee
Primary sulphide	Grade, %:		
	Cu	0.54	0.37
	Mo	0.0051	0.004
	S (sulphide)	1.81	1.26
	Mineral content, %:		
	Pyrite	2.40	1.66
	Chalcopyrite	1.46	1.06
	Metal contents, ppm:		
	in chalcopyrite	Se - 75.2 Te - 10.6	Se - 109.0 Te - 7.0
	in molybdenite	Re - 961	Re - 1433
in pyrite	Se - 51.6	Se - 68.2	
Total amount of sulphide ore, %	96	99	
Pyrite: chalcopyrite ratio	1.64	1.57	
Major ore minerals	Chalcopyrite, pyrite, magnetite	Chalcopyrite, pyrite, magnetite	
Major gangue minerals	Quartz, anhydrite	Quartz, anhydrite, calcite	
Subordinate minerals	Tetrahedrite, galena, sphalerite, hematite, mushketovite	Bornite, tetrahedrite, molybdenite, sphalerite, galena, hematite	
Secondary sulphide	Cu grade, %	Up to 4, average 1.5	Zone of secondary sulphide enrichment is virtually absent
	Total amount of secondary ore, %	3.0	-
	Major ore minerals	Chalcocite, cuprite, bornite, covellite, malachite	-
Oxidised	Cu grade, %	0.86 (from 0.3 to 3.0)	0.36
	Total amount of oxidized ore, %	1.0	1.0
	Major ore minerals	Malachite, azurite, chrysocolla, Cu-halloysite, ehfite, libethenite	Malachite, azurite, chrysocolla

### Kal'makyr

The Kal'makyr deposit is distributed around and within the outer margins of a central plug of Late Carboniferous quartz monzonite porphyry (QMP) intruding earlier Carboniferous monzonite and diorite. The deposit straddles the Kal'makyr Fault and extends southwards toward the Burgundy Fault (Fig. 5). The main volume of the block defined by these two faults is occupied by monzonite and diorite, although remnants of Devonian volcanic and carbonate rocks are locally preserved.

The majority of the ore at Kal'makyr (65 to 75%) is present in the form of stockwork veins and veinlets, while 30 to 35% occurs as disseminations. The distribution of the ore stockwork and the intensity of veining is controlled by the density of fracturing and brecciation related to both the intrusion of the QMP stocks and dykes, and to linear fracture zones associated with the Kal'makyr and Karabulak faults. As a result, the stockwork is represented by a downward expanding cone (or "inverted cup-shaped" shell) surrounding and capping the quartz monzonite porphyry plug, with a barren core corresponding with the centre of the plug.

The stockwork occurs within a network of fractures which have been healed by quartz veinlets, and less frequently by calcite or anhydrite, which contain large segregations of the ore sulphides, including pyrite, chalcopyrite, chalcocite, pyrrhotite, molybdenite and tetrahedrite. The veinlets vary in thickness from fractions of a millimetre to 3 or 4 cm, and are from a few to a few tens of cm in length. The interval between the veinlets if occupied by lesser disseminated pyrite, chalcopyrite, magnetite and occasionally other sulphides.

The stockwork zone is elongated in a northwest direction, with maximum surface dimensions of approximately 3520 x 1430 m and a maximum vertical extent of 1240 m. The inner annulus of high-grade ore is substantially smaller, with outer dimensions of approximately 1740 x 500 m and a maximum vertical thickness of 450 m. The most intense fracturing and the highest grade ore are related to the intersections of porphyry contacts with the east-west and northeast trending faults and tend to form a broken annulus within the monzonite and diorite wall rocks immediately surrounding the QMP. The grade rapidly decreases inwards to the barren core in the QMP plug. In contrast the high

**Table 7: Au content in major sulphides and its correlation with other elements** (after Golovanov, 1978)

Deposit	Average Au content, ppm		Coefficient of pair correlation			
	Chalcopyrite	Pyrite	Au-Cu	Au-S (sulphide)	Au-Ag	Ag-Cu
Dalnee	24 (7)	7.3 (32)	+0.64	+0.05	+0.31	+0.34
Kal'makyr	22 (20)	3.5 (30)	+0.57	+0.04	+0.19	+0.32

Note: Numbers of samples are in parentheses.

grade annulus is surrounded by a broad halo of medium grade ore before passing into a lower grade periphery. At depth the ore stockwork becomes less continuous and lenses-out downwards via a series of tongues.

The primary Kal'makyr ore contains Cu, Mo, Au, Ag and admixtures of Se, Te, Re, Bi, and In. The Mo-rich orebodies, as defined by a 0.008% Mo cut-off, are located at the periphery of the Cu ore-stockwork. As at the Dalnee deposit, the distribution of gold is controlled by the copper mineralisation. According to Golovanov (1978), the only significant positive coefficient of correlation between elements was established for the Cu-Au pair (Table 7). Hence, chalcopyrite is the main concentrator of gold (or more precisely, the native gold inclusions are closely associated with chalcopyrite). The contribution of pyrite-related gold is insignificant. In the central part of the deposit and at lower levels, the Au-bearing orebodies defined by

0.4 and 0.6 g/t Au contours closely coincide with the Cu orebodies. On the flanks of the Cu deposit, gold related to quartz-polysulphide veins and veinlets, forms a wide low grade halo enveloping the Cu ore.

The upper sections of the ore deposit were subjected to oxidation and supergene enrichment, best developed in areas of more intense fracturing on the QMP contacts and along zones of fault related fracturing. The degree of oxidation, leaching and supergene enrichment varied across the deposit, from oxide to secondary sulphide to mixed oxide-sulphide zones, although the supergene sulphide enrichment was only weakly developed. Oxidation was developed to a maximum depth of 65 m, averaging around 20 m, while leaching, where it replaced *in situ* oxidation, persisted over a similar thickness. The principal mineral within the oxide zone was malachite, with chrysocolla and turquoise being locally important. Where present,

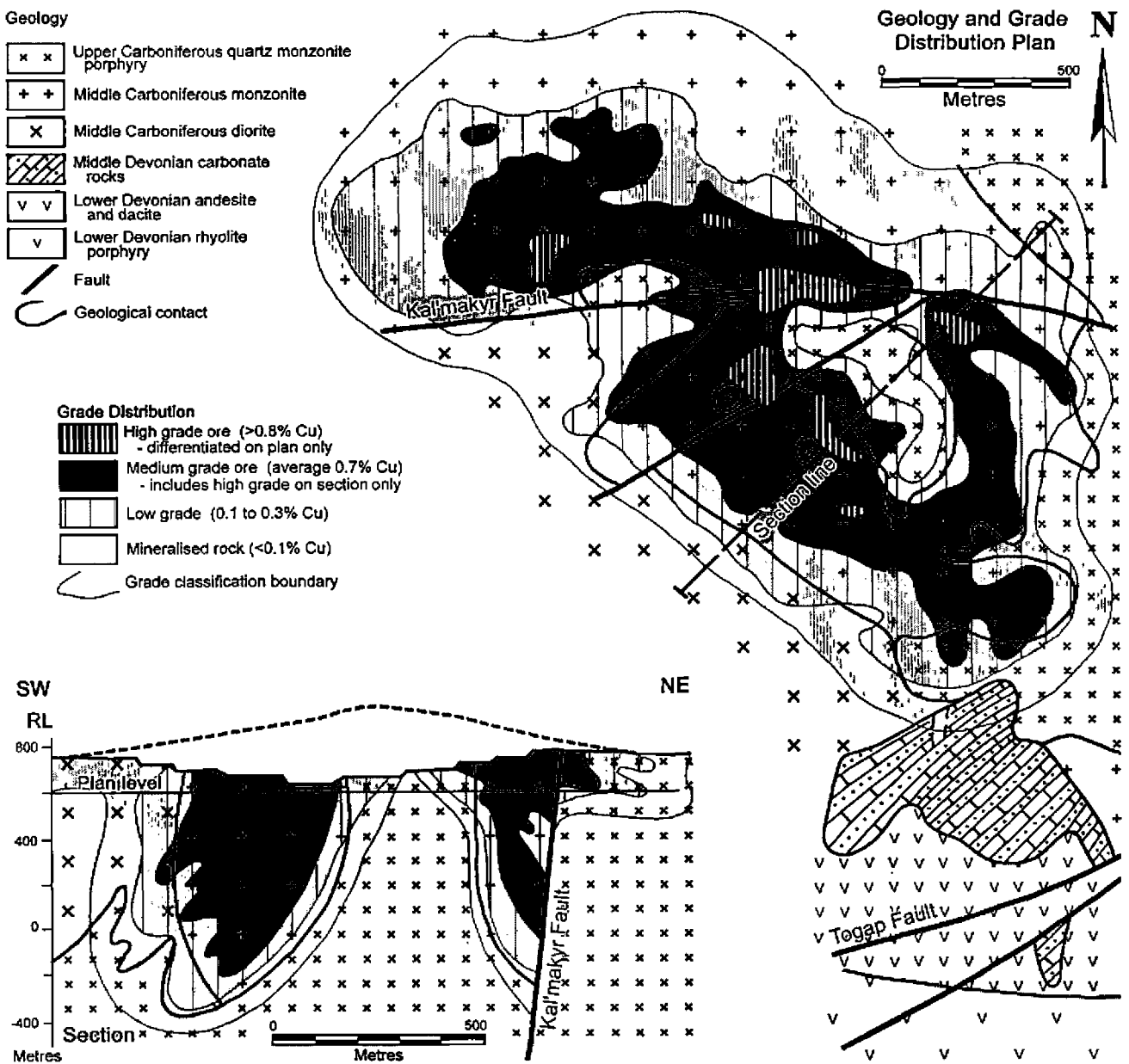


Figure 5: Schematic geological and grade distribution map (right) and cross section (bottom left) through the Kal'makyr porphyry Cu-Au deposit. The grade distribution is after Samonov and Pozharisky (1977), updated by Sokolov (1995) and comprises a representative horizontal slice through the deposit in the upper mined levels.

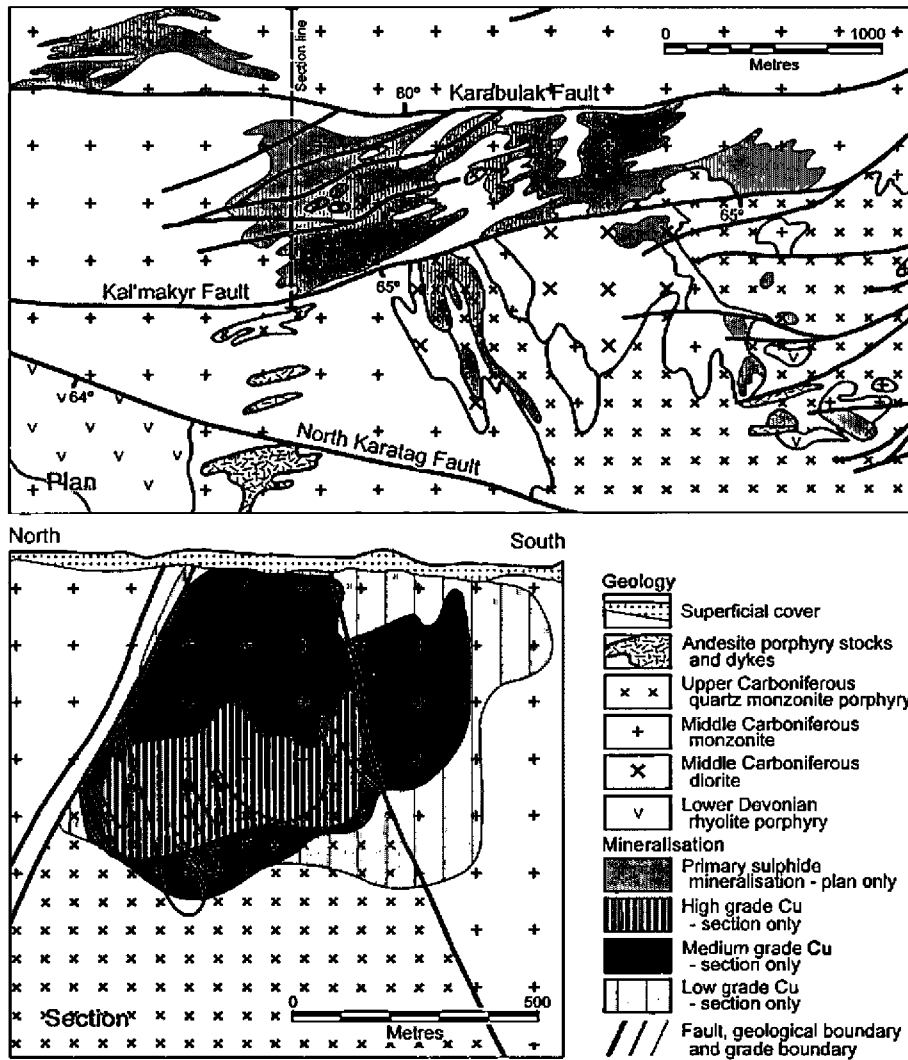


Figure 6: Schematic geological map (top) and cross section (bottom) through the Dalnee porphyry Cu-Au deposit. The fault zone on the northern side of the section is the Karabulak Fault, while the south-dipping structure near the centre is a fault intermediate between the Karabulak and Kal'makyr Faults, the latter being to the south of the section. The geological map is after Rakhubekov (unpublished), and the cross section is after Golovanov et al., (1988).

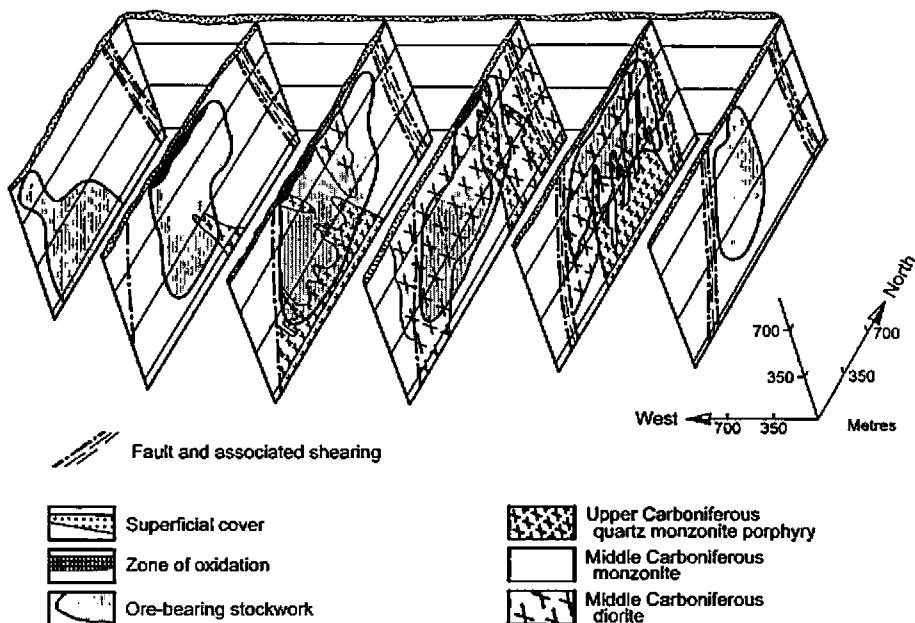


Figure 7: Schematic diagram showing the 3D structure in Central area of the Dalnee deposit. After V. Fedotushkin and A. Rakhubekov (unpublished), in Shayakubov et al., (1999); see Fig. 3 for location).

**Table 8: Distribution of Se, Te, and Re (ppm) in the ore and major ore minerals at the Dalnee deposit (after Shayakubov *et al.*, 1983)**

Material	Se	Te	Re
Ore	3.2	0.3	0.09
Chalcopyrite	141 (62.7)	6.9 (31.8)	0.3 (5.5)
Molybdenite	164 (0.3)	6.8 (6.1)	1186 (80.8)
Pyrite	76 (31.1)	14.0 (59.3)	0.8 (13.7)

Note: Numerals in parentheses denote the contribution of specific minerals to the bulk content in ore (wt %).

supergene sulphide enrichment, principally as chalcocite and covellite, had a maximum thickness of 70 m, averaging 19 m, while a mixed 'complex' oxide-supergene sulphide zone, where developed, also averaged 19 m in thickness. The best accumulations of supergene sulphides were restricted to the Kal'makyr Fault and two northeast trending conjugate structures, forming three broken, lens-like, steeply dipping bodies with lengths of 200 to 2500 m and widths of no more than 60 m (Samonov and Pozharisky, 1977 and references cited therein).

### Dalnee

The Dalnee group of deposits are a west to northwest, down-plunge continuation of Kal'makyr at deeper levels. The >0.1% Cu outline unites these deposits into a common ellipsoidal sub-economic mineralised mass in plan view (Fig. 3). However, post-mineral normal and sinistral strike-slip displacement on both the Karabulak and Kal'makyr faults dissected the ellipse into three blocks. The northern Karabulak block is displaced by 2 km to the west and the Central block (the main Dalnee deposit) for 0.5 km to the west of the southern block and Kal'makyr. The northern block encompassing Karabulak is the least eroded, while the deepest exhumation has affected the southern block and Kal'makyr.

The main Dalnee deposit in the Central area is located within a downward widening tectonic wedge between the Karabulak and Kal'makyr faults which have truncated the mineralised system and displaced ore on the flanks of the underlying QMP. Approximately 58% of the ore in the deposit is hosted by the monzonite, 35% by the diorite and 7% by the QMP. The stockwork is elongated parallel to the east-west direction of faulting and widens downward due to the outward dip of the bounding faults (Figs. 6 and 7), while the base of mineralisation closely follows the apical surface of the underlying QMP stock. The average vertical extent of mineralisation is about 700 m with a maximum of 1200 m on some sections. The higher grade Cu mineralisation occurs below a depth of 150 to 200 m, while the highest grade core is at a depth of 500 to 600 m. The Mo grade maxima lies below the Cu peak at a total depth of 300 to 900 m, where the molybdenite mineralisation is hosted by the diorite, the diorite/monzonite contact, and the upper margin with the QMP stock. Mo mineralisation is virtually absent in the upper levels of the deposit (ie. above 100 to 150 m). The Karabulak deposit to the north is the least economically important of the Dalnee deposits. Drill holes intersected 'high-grade' Cu mineralisation extending along the Karabulak Fault at depth, associated with a small stock of quartz monzonite porphyry (QMP).

Cu, Au and Ag mineralisation contours reflect a coincident pattern of distribution, although the halo of Au mineralisation is generally shifted towards the supra-ore zone and flanks of the Cu deposit. The best development of Au mineralisation is related to the Karabulak Fault. The distribution of Ag approximates that of Au, although it forms a broader halo on the flanks of the deposit with a maxima which is shifted upwards further than the Au peak. The distribution of Se, Te and Re in the ore and the major ore minerals at the Dalnee deposit is outlined in Table 8.

### Sarycheku

The Sarycheku deposit is related to the hanging wall of the Miskan Fault, with the ore grade mineralisation being confined to the tectonic wedge between the Miskan and Sargalam faults. The host rocks are represented by Devonian rhyolite porphyry, which is cut by Late Paleozoic porphyry intrusion. The oxidised and chalcocite ores have virtually been exhausted, while the underlying hypogene sulphide ore is concentrated within a zone which is 1160 m long and has been traced to a depth of 340 m.

### Acknowledgements

This paper is based on a chapter in the excursion guidebook on gold, silver and copper deposits of Uzbekistan (Shayakubov *et al.*, 1999), supplemented by new and additional information and observations. It is reproduced with the kind permission of the IGCP-373 project on "Ore-bearing granites of Eurasia" and IAGOD, and is a contribution to the IGCP-473 project on "GIS metallogeny of Central Asia". Fruitful discussions with Elena Nikolaeva, Mikhail Kazhikhin, Vertrees M. "Mac" Canby, Rustam Koneev, Farkhad Islamov, Vitaly Shatov, Victor Popov, Dmitry Konopelko, Alexander Yakubchuk, and many others are appreciated. The authors thank specifically Sergei Dabisha and Alexander Tadjiev (Almalyk Mining Metallurgical Combine, AGMK) for inspiring comments, their continuous support, and access to data and samples from the mining district that allowed continuous research over many years. Nurmukhammad Akhmedov and Bahtyar Isakhodaev, State Committee on Geology and Mineral Resources, IMR Tashkent, is thanked for facilitating this collaborative study. The paper has benefited from the editorial input, design assistance and review comments of Mike Porter.

### References

- Askarov, F.A., Bigaeva, V.V. *et al.*, 1975 - Absolyutnaya geokhronologiya magmacheskikh obrazovaniy Uzbekistana (Absolute geochronology of igneous rocks in Uzbekistan), Tashkent: Fan, 1975, 247p. (*In Russian*).
- Badalov, S.T., 1970 - The provenance of some components in endogenic sulphate-sulphide and quartz-gold deposits in the Kurama Mountains, *in* K voprosu ob istochnike veshchestva endogennykh rudnykh mestorozhdenii (Provenance of Matter in Endogenic Ore Deposits), Alma-Ata, 1970, pp. 36-54 (*in Russian*).

- Dalimov, T.N. and Ganiev, I.N., 1995 - Northern margin of the Turkestan oceanic basin, *Izv. VUZov Respubliki Uzbekistan*, 1995, no. 1.
- Golovanov, I.M., 1978 - *Medno-rudnye formatsii Zapadnogo Tyan'-Shanya* (Copper mineralisation in the western Tien Shan), Tashkent: Fan, 1978, 239p. (In Russian).
- Golovanov, I.M., Nikolayeva, E.I. and Kazhikhin, E.I., 1986 - Geological and structural conditions of localization of the high-grade ores of porphyry copper deposits; in Friedrich, G.H., et al., (Eds.), *Geology and Metallogeny of Copper Deposits*, Springer-Verlag, Berlin, Heidelberg 1986, pp. 261-270.
- Golovanov, I.M., Nikolaeva, E.I. and Kazhikhin, M.A., 1988 - *Kompleksnaya prognozno-poiskovaya model medno-porfirovoi formatsii* (Integral model for the forecasting and prospecting of porphyry copper deposits), Tashkent: Fan, 1988, 197p. (In Russian).
- Grauch, R., (Ed.), 1996 - *Investment opportunities in mining and minerals in Uzbekistan*, US Trade and Development Agency in cooperation with GOSCOMGEOLOGIYA. Denver, 1996, 150p.
- Isakhojaev, B.A., 1998 - The state of art and problems of applied science on gold geology, Abstr. Sci. Conf., *Gold deposits of Uzbekistan: Geology and Economic Types*, Tashkent, 1998, pp. 14-17 (In Russian).
- Islamov, F.I., 1998 - Specific types of volcanogenic Au-Ag deposits in Paleozoic belts: prospecting guides and forecasting: a case of the Beltau - Kurama volcanoplutonic belt), *DSc Thesis*, St. Petersburg: VSEGEI Institute, 1998 (In Russian).
- Kashirsky, S.A. and Turesebekov, A.Kh., 1999 - Mineral resources of the Almalyk Mining and Metallurgical integrated works, *Gornyi Zhurnal*, 1999, no. 2 (In Russian).
- Kremenetsky, A.A., Minzer, E.F. and Islamov, F.I., 1996 - Evolution of ore-magmatic systems as a basis of forecasting, prospecting, and evaluation of gold-rare-metal deposits, *Razved. Okhr. Nedr*, 1996, no. 8, pp. 29-34 (In Russian).
- Kudrin, V.S., Solov'yev, S.G., Stavinskiy, V.A. and Karabdin, L.L., 1990 - The gold-copper-molybdenum-tungsten ore belt of the Tien Shan, *International Geology Review*, 1990, v. 32, pp. 930-941.
- Lyashenko, V.I., Kremenetsky, A.A., et al., 1998 - Geological and geophysical study of the deep structure of the Angren ore district along the geotraverse Asht - Uchkyz - Kochbulak - Kyzylalma - Kaprel, *Report of the Kochbulak Detachment on results of works in 1991-1998*, Eshonguzar, 1998 (unpublished) (In Russian).
- Meshchaninov, E.Z., 1970 - Some features of gold mineralization in the Almalyk district, in *Geologiya, mineralogiya i geokhimiya rudnykh polei Uzbekistana* (Geology, mineralogy, and geochemistry of ore fields in Uzbekistan), Tashkent: Fan, 1970, pp. 37-44 (In Russian).
- Nikolaeva E.I., Kazhikhin, M.A. and Golovanov, I.M., 1991 - Ore potential of porphyry copper ore-magmatic systems, *Otech. Geol.*, 1991, no. 1, pp. 28-34 (In Russian).
- Samonov, I.Z. and Pozharisky I.F., 1977 - Deposits of copper, in Smirnov, V.I., (Ed.), 1977 - Ore Deposits of the USSR; Pitman Publishing, v. 2, pp. 106-181.
- Seltmann, R. and Porter, T.M., 2005 - The Porphyry Cu-Au/Mo Deposits of Central Eurasia: 1. Tectonic, Geologic & Metallogenic Setting and Significant Deposits; in Porter, T.M. (Ed.), *Super Porphyry Copper & Gold Deposits: A Global Perspective*; PGC Publishing, Adelaide, pp 467-512.
- Shayakubov, T.Sh., 1999 - The mineral potential of the Republic of Uzbekistan and problems of its development, *Geologiya i mineral'nye resursy Uzbekistana*, 1999, vol. 1, pp. 2-7 (In Russian).
- Shayakubov, T.Sh. and Dalimov, T.N., (Eds.), 1998 - *Geologiya i poleznye iskopaemye Respubliki Uzbekistan* (Geology and mineral resources of the Republic of Uzbekistan), Tashkent: Publ. Tashkent State Univ. (In Russian).
- Shayakubov, T.Sh., Dalimov, T.N., Arapov, V.A. et al., 1988 - *Vulkanizm Zapadnogo Tyan'-Shanya* (Volcanism of the western Tien Shan), Tashkent: Fan, 1988. 328p. (In Russian).
- Shayakubov, T.Sh., Golovanov, I.M. and Rakhubenkov, A.T., 1983 - *Medno-porfirovye mestorozhdenie Dal'nee* (The Dalnee porphyry copper deposit), Moscow: Nedra, 1983 (In Russian).
- Shayakubov, T., Islamov, F., Kremenetsky, A. and Seltmann, R., (Eds.), 1999 - Au, Ag, and Cu deposits of Uzbekistan, International field conference of IGCP-373, Excursion B6 of the *Joint SGA-IAGOD symposium*, London-Tashkent, 27 August - 4 September, 1999, 112p.
- Sokolov, A.L., 1995 - The regional and local controls on giant-scale copper and gold mineralisation, Uzbekistan; in Clark, A.H. (Ed.), *Giant Ore Deposits II. Controls on the scale of orogenic magmatic-hydrothermal mineralisation*. Proceedings of the second giant ore deposits workshop, Kingston, Ontario, Canada, April 25-27, 1995. *Dept. of Geological Sciences, Queen's University*, Kingston Ontario, pp. 450-474.
- Tulyuganov, Kh.T., (Ed.), 1974 - *Medno-porfirovye mestorozhdeniya Almalyka* (The Almalyk porphyry copper deposits), Tashkent: Fan, 1974 (In Russian).
- Zakirov, T.Z., 1959 - The distribution of copper mineralization versus the composition of host rocks, in *Trudy SAZPI* (Trans. Central Asian Polytechnical Institute), 1959, vol. 6, pp. 24-29 (In Russian).
- Zav'yalov, G.E. and Islamov, F.I., 1995 - Geodynamic environments of Late Paleozoic metallogeny of the Kurama tectonic zone, *Otech. Geol.*, 1995, no. 6, pp. 31-37 (In Russian).





## ERDENETIIN OVOO PORPHYRY COPPER-MOLYBDENUM DEPOSIT IN NORTHERN MONGOLIA

Ochir Gerel and Baatar Munkhsengel

*Department of Geology, Mongolian University of Science & Technology, Ulaanbaatar, Mongolia.*

**Abstract** - Erdenetiin Ovoo, the largest porphyry copper-molybdenum deposit in Mongolia (1.78 Gt @ 0.62% Cu, 0.025% Mo), is exploited by the Erdenet mine. It is located within the Orkhon-Selenge volcano-sedimentary trough which was developed on an active continental margin. The geodynamic evolution of the trough involves an early intra-continental stage, comprising rifting of a shallow continental shelf, accompanied by the emplacement of sub-aerial Permian mafic and felsic, and Triassic mafic volcanics. The Permian volcanics are predominantly alkali-rich trachyandesites, occurring as interlayered flows and pyroclastics of the Khanui Group, overlying a Vendian (late Neoproterozoic) to early Cambrian basement with Palaeozoic (Devonian) granitoid intrusions, and Carboniferous sediments. Plutons, ranging in composition from diorite to granodiorite, quartz syenite and leucogranite intrude the Permian volcanic succession and exhibit similar compositional trends as the host volcanics. This suggests the intrusions are related to, and possibly coeval with, the volcanic rocks. The Triassic Mogod Formation volcanics, which are largely composed of trachyte flows, trachyandesite and basaltic-trachyandesite, directly overlie the Permian sequence. Early Mesozoic porphyritic subvolcanic and hypabyssal intrusions, which are genetically associated with the trachyandesite volcanics, are related to a continental collisional setting. These include syn-mineral granodiorite-porphyry intrusions which form shallow bodies, occurring as elongated dykes or small, shallow stocks. These porphyries vary from quartz diorite through granodiorite to granite in composition. They are characterised by porphyritic textures (up to 40% phenocrysts) with plagioclase phenocrysts set in a fine-grained groundmass of K feldspar, and are found in the core of the hydrothermal systems, where they are associated with high-grade ore.

Three principal alteration zonations are developed within the Erdenet deposit (Kominek *et al.*, 1977, Khasin *et al.*, 1977), from the core to the periphery, namely: i) sericitic (quartz-sericite) and late siliceous, ii) intermediate argillic (chlorite-sericite), and iii) propylitic (chlorite and epidote-chlorite).

Researchers have progressively evolved an understanding of the paragenesis of mineralisation at Erdenet since the mid 1970s. The most recent observations (Gavrilova *et al.*, 1990) suggest: i) pre-ore quartz-sericite; followed by the ore stages of ii) quartz-chalcopryrite-pyrite; iii) quartz-pyrite-molybdenite-chalcopryrite; iv) quartz-chalcopryrite-tennantite; v) quartz-pyrite-galena-sphalerite; vi) over-printing bornite-chalcocite-covellite; and post-ore vii) gypsum-calcite with pyrite. The first two ore stages are dominated by vein stockworks, while the succeeding three phases are localised by dykes and associated fracturing. All of these phases however, overprint, and largely obliterate, an earlier weak potassic alteration with associated chalcopryrite. The early potassic phase occurs as secondary biotite and magnetite, followed by pink feldspar veining, and is only encountered as remnants in the less fractured, deeper, central sections of the deposit.

The hypogene stage is characterised by chalcopryrite, bornite, covellite and minor chalcocite, and the oxidation stage by Cu carbonates, oxides, phosphates and sulphates, native Cu and ferrimolybdenite. The oxide zone overlies a 30 to 300 m thick supergene enrichment blanket where secondary chalcocite replaces hypogene chalcopryrite and bornite-covellite assemblages in stockworks and sheeted veins.

The proposed magmatic model for the Erdenet district involves multiple partial melting of upper mantle material, a changing level of melting and vertical movement of the magma chamber. In the late crustal phase, large chambers of dioritic magma formed, cooling and fractionating to produce the full spectrum of subvolcanic and shallow porphyries ranging in composition from diorite to granite.

### Introduction

The Erdenetiin Ovoo deposit, at the Erdenet mine, is located in northern Mongolia, 240 km northwest of the capital, Ulaanbaatar. The deposit was discovered in 1964 and first explored by E. Kominek, G. Sanduijav, I. Popousek and later studied by V.S. Kalinin, L.I. Yakimov, I.D. Davydov, E.V. Mikhailov and A.E. Shabolovsky, (Geology of Mongolia, 1977), Khasin *et al.*, (1977), Sotnikov *et al.*,

(1974), Berzina and Sotnikov (1989), Sotnikov and Berzina (1989), Koval, Gerel *et al.*, (1985), Koval and Gerel (1986),

This paper has been prepared for both this volume and for "Seltmann, R., Gerel, O. and Kirwin, D., (Eds.), 2005 - Geodynamics and Metallogeny of Mongolia with a Special Emphasis on Copper and Gold Deposits; SEG- IAGOD Field Trip, 14-16 August 2005, 8th Biennial SGA Meeting. IAGOD Guidebook Series 11: CERCAMS/NHM London. It is included here under a joint copyright arrangement between PGC Publishing and both IAGOD and CERCAMS at the Natural History Museum, London.

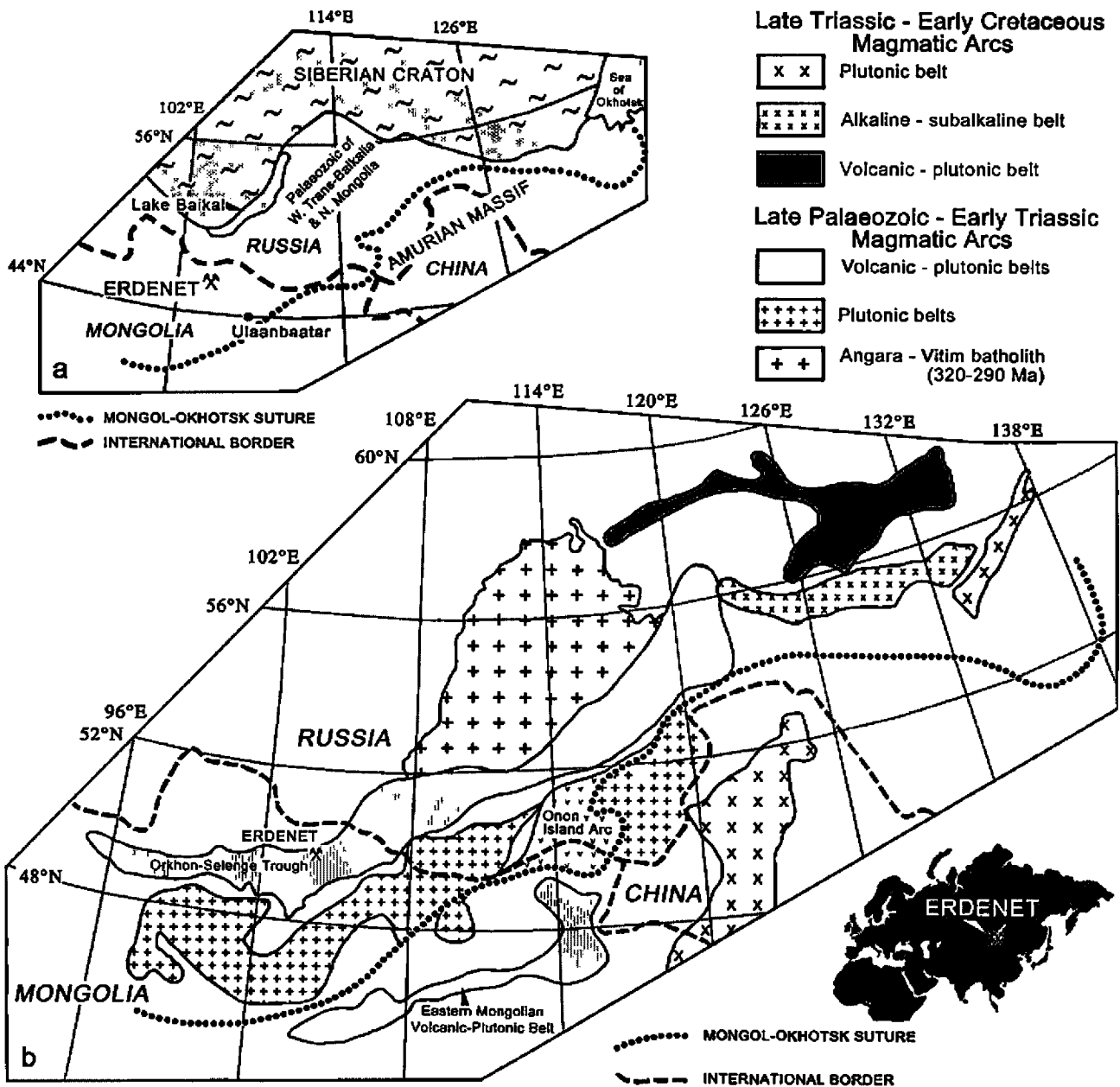
Gavrilova *et al.*, (1985), Gavrilova and Maksimyyuk (1990) and others. The Erdenet mine is the largest Cu-Mo porphyry deposit in Mongolia, with estimated metal reserves calculated in 1991 of 7.6 Mt Cu and 216 600 t Mo in approximately 1490 Mt of ore @ 0.509% Cu and 0.015% Mo (Erdenet Mining Corp., 2002). Estimated mineral resources in 2004 are 2370 Mt @ 0.38% Cu and 0.013% Mo. Projected reserves of deeper ore are estimated to be 1.4 Mt of contained Cu and 37 000 t of Mo. Published mining reserves in 2002 were 766.7 Mt @ 0.61% Cu containing 4.7 Mt of copper (Erdenet Mining Corp., 2002).

The Erdenetiin Ovoo deposit has been mined since 1978 at an annual rate of approximately 20 Mt of ore from an open pit which currently covers an area of 2500 x 1150 m. The initial head grade in 1978 was 0.87 to 0.96% Cu. In 2002 25.8 Mt of ore at a head grade of 0.647% Cu was mined, to produce 131 705 tonnes of copper and 1590 tonnes of

molybdenum in concentrate from a joint Mongolian-Russian ore dressing plant (Erdenet Mining Corp., 2002). Metallurgical recovery in 2002 averaged 83.25% for Cu and 33.06% for Mo in concentrates. The composition of the copper concentrate is: 27-35% Cu, 50-60 g/t Se, 50-70 g/t Ag, 8-9 g/t Te and 0.3-0.5 g/t Au. The molybdenum concentrate from Erdenet contains: 47-54% Mo, 450 g/t Re, 90 g/t Se and 15 g/t Te. A small but increasing amount of tungsten is also produced.

The Erdenet mine is of great importance to the Mongolian economy, accounting for over half of the country's income and export earnings. The mine achieved international production quality standards in 1993. Geotechnical and hydrogeological mining conditions are simple.

The largest porphyry Cu-(Mo-Au) deposits are associated with subduction related magmas, and occur sporadically within magmatic arcs throughout the world. Late



Palaeozoic volcanism in northern Mongolia, which reflects coeval subduction, started in the early Permian, with peak activity in the late Permian-Triassic, corresponding to the closure of the Mongol-Okhotsk Ocean (Tectonics of Mongolia, 1974). Porphyry Cu-Mo deposits occur within the late Palaeozoic Orkhon-Selenge trough and formed under tensional and shear stress conditions. The geologic history of the Mongol-Okhotsk Ocean is still controversial.

In this paper we review earlier investigations conducted while Erdenet was being explored and developed with an emphasis on the intrusive history of the ore-bearing system.

## Regional Geology

The Erdenet deposit occurs within the Selenge terrane of Badarch *et al.*, (2002) and Tomurtogoo (2002), which overlaps the cratonic Tarvagatay terrane and the Orkhon-Selenge trough of Mossakovsky and Tomurtogoo (1974). This overlap terrane is dominated by Permian to lower Triassic volcano-sedimentary and intrusive rocks and upper Triassic to lower-mid Jurassic volcanics and sedimentary cover. The Orkhon-Selenge trough is part of the larger Mongol-Okhotsk fold belt which stretches over 3000 km from west to east, from the Khangay highlands in central Asia, to the Pacific Ocean (Zonenshain *et al.*, 1990). The fold belt is divided into eastern, central and western segments. In the eastern and western segments, it is up to 300 km wide, but narrows in the centre.

The Mongol-Okhotsk fold belt is situated between the Siberian craton and accreted late Palaeozoic blocks of western Transbaikalia and northern Mongolia (together comprising "Siberia") on one side, and the central Mongolian blocks to the south. The central Mongolian blocks comprise three massifs of Precambrian rocks of different composition and character to those of the Siberian Shield, intruded by Palaeozoic batholiths and overlain by Palaeozoic sequences. During the Mesozoic, these three massifs were amalgamated to comprise the single large, ENE elongated, Amurian Massif (see Fig. 1). The northern boundary of the Amurian Massif, is very sharp, marked by the Mongol-Okhotsk Suture which separates it from Siberia. The southern boundary is more diffuse, due to reworking of the basement and the accretion of Palaeozoic magmatic arcs and continental blocks in southern Mongolia, including those hosting the Devonian Oyu Tolgoi porphyry copper-gold deposit (Zonenshain *et al.*, 1990a; Perello *et al.*, 2001).

The Amurian Massif is believed to have originally been separated from Siberia by the Mongol-Okhotsk Ocean, which was subducted northward below the Siberian Craton during the late Palaeozoic to Mesozoic, closing in a west to east scissor-like fashion (Lamb and Cox, 1998; Watanabe and Stein, 2000).

A structural reconstruction of the margin of the Mongol-Okhotsk Ocean during the Middle Palaeozoic indicates subduction and collision of microplates and their subsequent amalgamation. During the Carboniferous and Permian, a volcano-plutonic belt formed on the margin of the Mongol-Okhotsk Ocean. This was terminated in the late Triassic to early Jurassic with the collision of western

Amuria and Siberia, to be replaced by the Mongol-Okhotsk fold belt which formed in the area now occupied by the Khangay and western Khentey mountains. The subsequent history of the Mongol-Okhotsk belt was dominated by the continuing collision between the North China and Siberian continents. Many elements of the island arc and back arc system that had existed on the continental margin were either consumed or tectonically reworked during subsequent subduction and collision (Zonenshain *et al.*, 1990).

Palinspastic data indicate that the majority of the Mongol-Okhotsk Ocean within Mongolia had closed by the middle Jurassic and only the sections in the Far East oceanic basin remained open and still undergoing subduction. Subduction and collision during the late Palaeozoic to early Mesozoic resulted in the uplift of the Khangay and Khentey highlands flanked by depressions, which included the Orkhon-Selenge trough and eastern Mongolian volcanic-plutonic belt, each with a different style of magmatism and mineralisation (Fig. 1). Porphyry copper systems dominated in the north, within the Orkhon-Selenge trough, while polymetallic mineralisation is characteristic of the Eastern Mongolian volcanic-plutonic belt in the south (Gerel, 1990).

The Erdenet deposit is hosted by a late Permian to early Triassic intrusive complex (Fig. 2) which forms part of the extensional volcano-plutonic belt within the Orkhon-Selenge trough. The Orkhon-Selenge trough is the largest of the late Palaeozoic to early Mesozoic structures within the region, stretching for over 200 km in an east-northeast direction, with a width of 30-40 km, filled by Permian and early Mesozoic volcano-sedimentary rocks. Mid to upper Triassic and Jurassic volcanics are widespread throughout the trough, occurring in tectonic grabens and overlapping onto upper Palaeozoic sequences (Tectonics of Mongolia, 1974). Permian rocks overlie Caledonian folded basement composed of upper Riphean (Neoproterozoic) metamorphics, lower Palaeozoic volcanic-terrigenous sequences, Devonian granitoids and non-intrusives, and in the southern part, Carboniferous rocks also. The Permian volcanics belong to the Khanui Group, which is as much as 10-20 km thick in the core of the trough, and up to 5 km on its periphery. The Khanui Group is composed of four conformable formations. The lowest comprises mafic and intermediate volcanics and has a limited distribution. It is overlapped by felsic volcanics of the succeeding formation, which are overlain in turn by volcanoclastics of the third. The fourth and uppermost of the formations is composed of mafic volcanics.

According to Mossakovsky and Tomurtogoo (1976), the Khanui Group's age varies from lower Permian in the west, to upper Permian in the east of the trough. The group is characterised by a sub-alkalic composition, with elevated K alkalinity and a bimodal nature (Kepezhinskas, Lutschitsky, 1973). It exhibits a lateral variation in character, with a volcanic suite in the western peripheral part of the Orkhon-Selenge trough, grading to a volcano-plutonic association (Yashina, Matrenitsky, 1978). Early Permian intrusions occur as a series of parallel dykes within felsic volcanics or as shallow stocks. Doleritic sills, associated with upper Permian basalts, form elongated belts

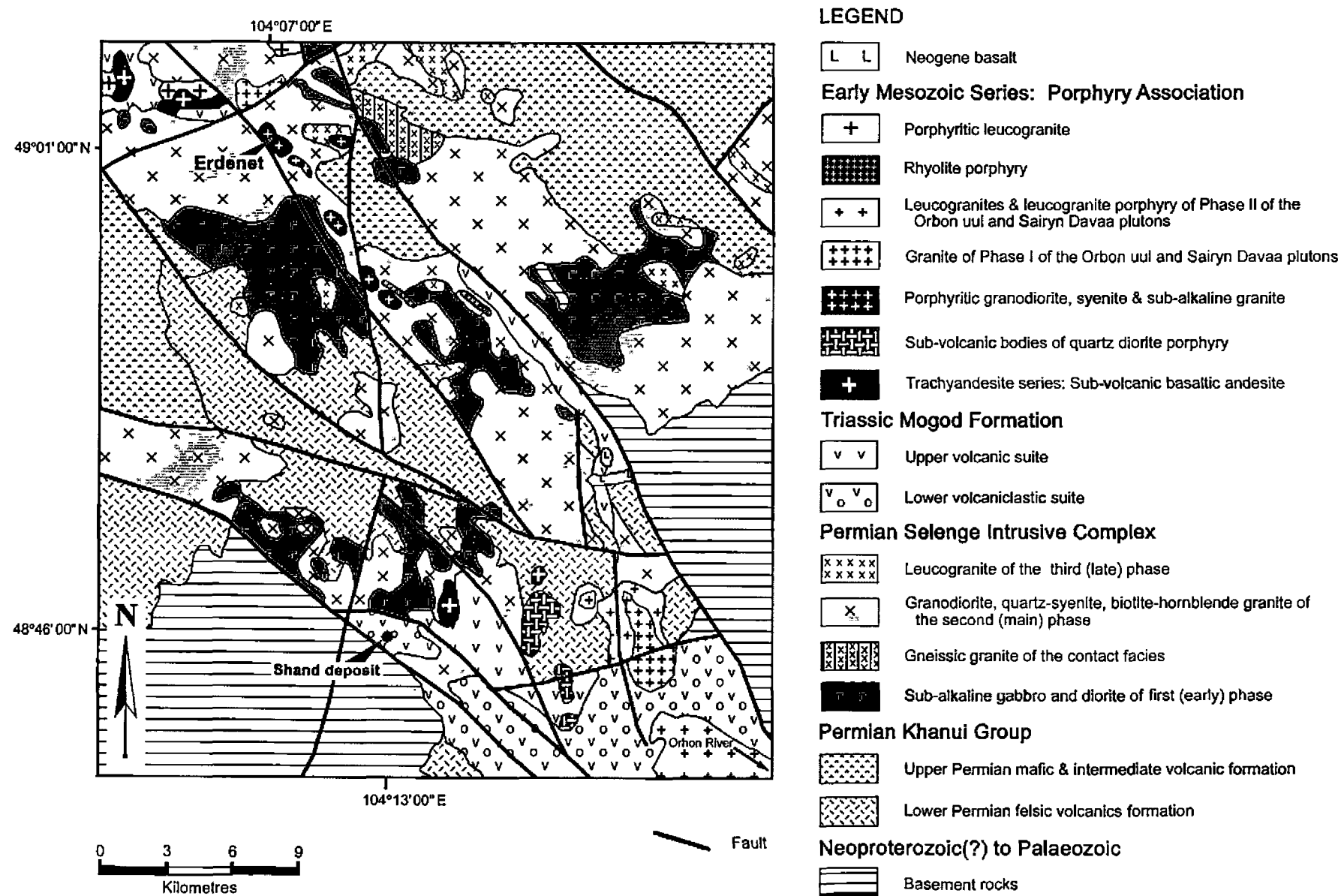


Figure 2: Geological map of the Erdenet ore field (Koval et al., 1985)

in the central part of trough, while late Permian intrusive rocks, which include gabbro-syenite and younger granite-granosyenite associations known as the Selenge Intrusive Complex, are also found in the centre and on the uplifted peripheries.

The main faulting directions are northwest, northeast and sub-latitudinal, creating the mosaic structure of the Orkhon-Selenge trough, whose current geometry has been attributed to post-accretionary disruption and dislocation by extension and or strike-slip faulting. The main deformation age is mid Jurassic (Mossakovsky, 1975).

## Intrusive Magmatism

The Erdenetiin Ovoo deposit is a cylindrical body of quartz-sulphide stockwork veins hosted by an ore-bearing stock which is centred on the multiphase pre-ore Erdenet Pluton of the Selenge Intrusive Complex (Figs. 3 and 4) (Khasin *et al.*, 1977).

The Selenge Intrusive Complex, which occupies an area of around 2800 km<sup>2</sup> (Koval *et al.*, 1982), includes multiple, mainly hypabyssal and shallow intrusions, each covering a few km<sup>2</sup> to 1000 km<sup>2</sup> (Geology of Mongolia, 1973). The individual intrusives have variable textures and compositions with K-Ar ages of intrusion that range from 250 to 210 Ma (Geology of Mongolia, 1973; Koval *et al.*, 1982). Three separate phases are distinguished. The first ranges from diorite to monzonite, the second includes granodiorites, granites, leucogranites and sub-alkaline granites, and the third leucogranites and granites.

The *first (early) phase* comprises gabbrodiorites, diorites, syenodiorites, monzonites and quartz-monzonites which have either fine-grained or mainly porphyritic textures within a mono-crystalline groundmass. Phenocrysts are composed of plagioclase (An<sub>50-65</sub> to An<sub>35</sub>) and K feldspar, as well as hornblende and rare biotite, and clinopyroxene in the gabbrodiorites. Accessory minerals include magnetite, apatite and sphene. The association of plagioclase and hornblende, sometimes with clinopyroxene, K feldspar and biotite is characteristic of these rocks.

The *second (main) phase* is dominated by granitoids, the most common of which are granosyenites, leucocratic granites and granodiorites, with limited syenites and alkaline granites. These granitoids are characterised by miarolitic structures, and hypidiomorphic and micrographic textures. They are composed of K feldspar, plagioclase (An<sub>10-15</sub> to An<sub>25-35</sub>), hornblende, biotite, accessory magnetite, sphene, apatite and zircon.

Dykes and stocks of the *third (last) phase* leucogranites and granites form small bodies of up to 5-10 km<sup>2</sup>, and dyke sets which are widespread throughout the Orkhon-Selenge trough.

The Erdenet Pluton, which surrounds the Erdenetiin Ovoo deposit, is part of the Selenge Intrusive Complex. Like the other plutons of the complex, it is composed of a series of intrusive masses which range in composition from gabbrodiorite to granodiorite and granite. The largest of these is the Erdenet intrusion, which has associated satellites known as the "separate bodies". The earliest phase of the

pluton is composed of amphibole-gabbro and diorite which form large bodies in the peripheral part of the intrusions, or separate bodies of up to a few tens of square kilometres. The main phase is composed of quartz diorite, granodiorite or porphyritic quartz-syenite and granites. Porphyritic granodiorite with feldspar phenocrysts is the dominant lithology, containing ovoid inclusions of quartz-diorite and quartz syenite. This granodiorite is coarse-grained and occurs as cupola-like bodies, which are porphyritic at surface, but become equigranular at depth, and are affected by weak quartz-K feldspar alteration in association with veinlets which sometimes contain chalcopyrite (Gavrilova & Maximyuk, 1989). Within the granite phase, plagioclase is usually rimmed by K feldspar, while micrographic intergrowths in the groundmass are very common, and accessories are magnetite, sphene, apatite and zircon. Some of the rocks within the pluton are characterised by elevated alkalinity and comprise quartz-monzodiorite, monzonite to quartz-syenite and there is a characteristic paragenesis from biotite to amphibole and clinopyroxene. Biotite has a higher Fe content (Gerel, 1990).

A series of mineralisation related dykes and plugs, which are widespread within the Erdenet district and throughout the Orkhon-Selenge trough, was distinguished as the "Porphyry Association" by Koval *et al.* (1985), and Koval and Gerel, (1986) or as the "Porphyry Complex" in the Erdenet ore field (Sotnikov and Berzina, 1985). These intrusives are regarded by the same authors as being separate from, and younger, than the Selenge Intrusive Complex. Koval *et al.*, (1982) regarded these intrusions to be of early Mesozoic age and included them within the Orkhon-Selenge association, which comprises an "earliest" and two main granitoid phases, namely: i) the "earliest" is represented by quartz-diorite, diorite and monzonite, ii) the first main granitoid phase comprises quartz-syenite, hornblende-biotite granite and granodiorite, and iii) the second phase which includes leucogranite and sub-alkaline granite.

Yashina and Matrenitsky (1979), however, includes this "association" within their three separate subdivisions of the Selenge Intrusive Complex, which are: i) gabbro to syenite of middle Permian age; ii) syenite, granosyenite and granite of middle Permian to early Triassic age; and iii) monzogabbro to diorite, syenite, granite, porphyry (Erdenet type) of middle Permian to early Triassic age.

The age of the ore-bearing porphyries and the relationship between these porphyries and pre-mineralisation magmatic associations is interpreted differently by many authors. According to Khasin *et al.*, (1977), the mineralised porphyries are associated with a late phase of the multi-stage Permo-Triassic Selenge Intrusive Complex. If this is the case, the productive association had to be the upper mafic Formation of the Permian Khanui Group and the multiphase Selenge Intrusive Complex (Krivtsov, 1983). Yashina and Matrenitsky (1979) also characterised the granitoid intrusions of the Selenge Complex as Permo-Triassic, although Kuznetsov (1979) described the Selenge Complex as late Hercynian. Sotnikov *et al.*, (1981, 1984), taking into consideration the ore-controlling role of the

porphyry intrusions, and the differences in their appearance when compared to the Selenge Complex, suggested the Porphyry Complex could be post-Selenge, and early Mesozoic in age. Gavrilova *et al.*, (1984) recognised the Porphyry Complex as being Triassic, but older than the intermediate to mafic volcanics of the early Mesozoic Mogod Formation. In this interpretation, there is not a clear

relationship between ore-bearing intrusions and coeval volcanics. Yakovlev (1977) suggested that the ore-bearing porphyries could be related to the Triassic volcanics and that the eruptive breccias of the Erdenet ore field could be facies of these volcanics. Our data (Koval *et al.*, 1982; Koval *et al.*, 1985; Koval and Gerel, 1986) also support this interpretation.

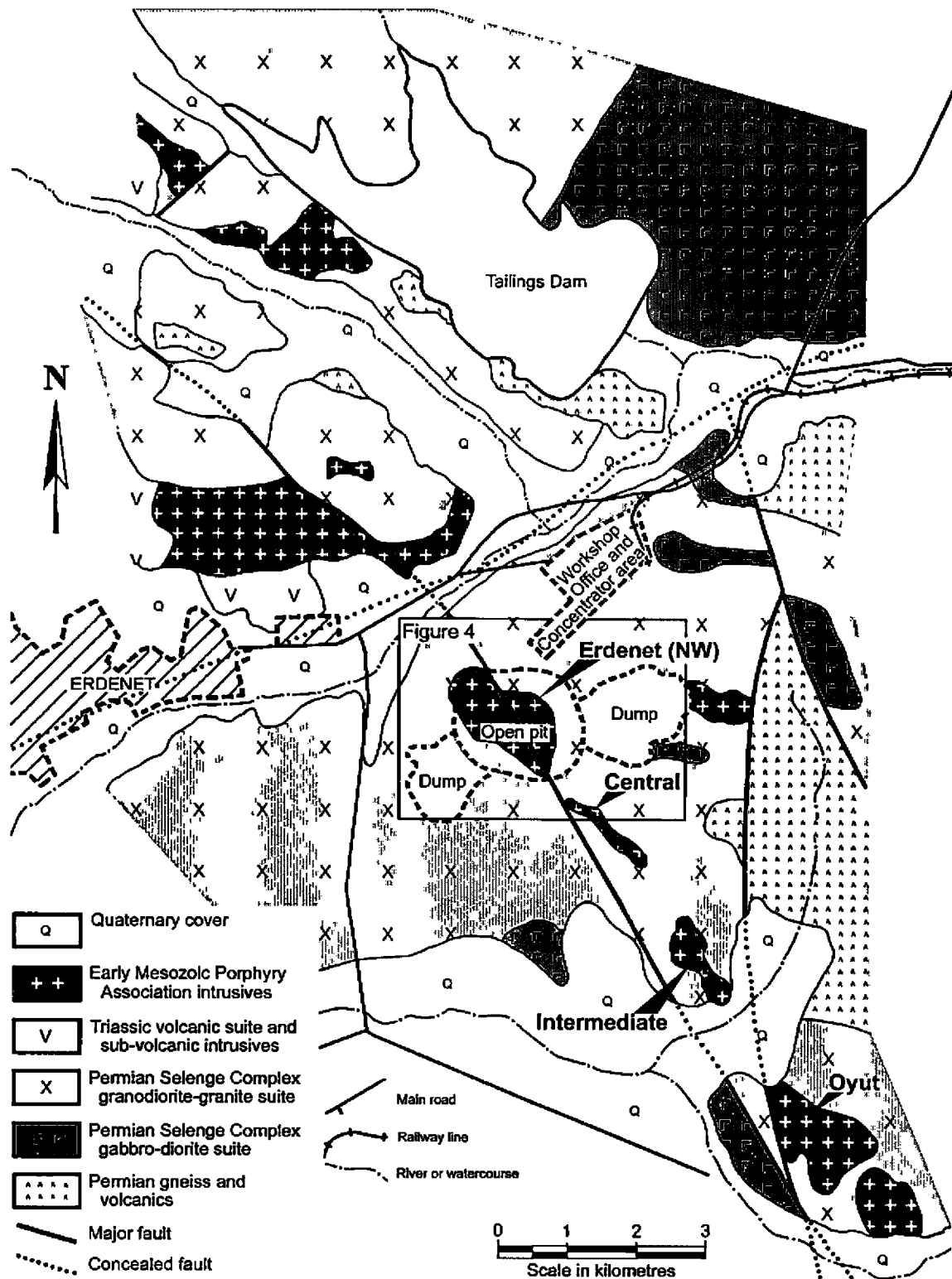


Figure 3: Location plan and geological sketch map of the Erdenet district, northern Mongolia. Topographic and cultural features from satellite image, geology based on Watanabe and Stein (2000) and Fig. 2 (this paper).

## District Geology

The Erdenet ore district is located within a local 20-25 km diameter circular structure which embraces a number of subvolcanic intrusive centres, each of 2 to 2.5 km in diameter, represented by dykes and stocks of altered granodiorite. Four aligned intrusive centres form a northwest trending range of low hills, while a fifth is indicated by geophysical data to be under Quaternary sediment cover of the Erdenetiin Gol River. The five prospects from southeast to northwest are: Oyut, Intermediate, Central, Northwest (the Erdenet mine) and Tsagaan Chuluut (Fig. 3).

The Erdenet ore field porphyries (of the Porphyry Association) and the ore-bearing stockwork are intruded into biotite-hornblende granites, granodiorites and quartz syenites of the Selenge Intrusive Complex. The porphyries crosscut the third phase granites of the Selenge Complex, which in turn cuts the Permian sequence, including the uppermost mafic volcanic formation. Whole rock, amphibole and biotite K-Ar age determinations of the Selenge Intrusive Complex vary from 250 to 210 Ma (Koval, Gerel *et al.*, 1984). The Porphyry Association intrusions (quartz-diorite to granodiorite porphyry and

granite porphyry) post-date the Selenge Intrusive Complex intrusions and therefore can not to be the last member of the Complex. Their typical porphyritic texture and association with eruptive breccias, indicate a totally different and subvolcanic environment for the Porphyry Association. The nearest volcanics of proven early Mesozoic age (Mossakovsky and Tomurtogoo, 1985) occur 35 to 40 km to SSE of the Erdenet deposit, where, at the Shand prospect (Fig. 2), mineralised porphyries cut these volcanics (Koval *et al.*, 1982; Koval, Gerel *et al.*, 1985). In the Khan Kharynam valley (35 km SE of Erdenet, adjacent to the Shand deposit - see Fig. 2), two sequences are distinguished: i) lower volcanic clastics, mainly conglomerate, and ii) upper volcanic basaltic-trachyandesitic. The total thickness is about 1000 m (Yakovlev and Jamsran, in Geology of Mongolia, 1977).

The Porphyry Association includes shallow, subvolcanic and explosive stocks, dykes, necks and sheet-like bodies. They are variable in texture and composition, ranging from porphyritic quartz-diorite and diorite, quartz-syenite, granodiorite to granites and leucogranites, associated with explosive breccia, andesites and trachyandesites, dacites, rhyodacites and rhyolites, trachytes and trachydacites. These rocks are predominantly younger than previously

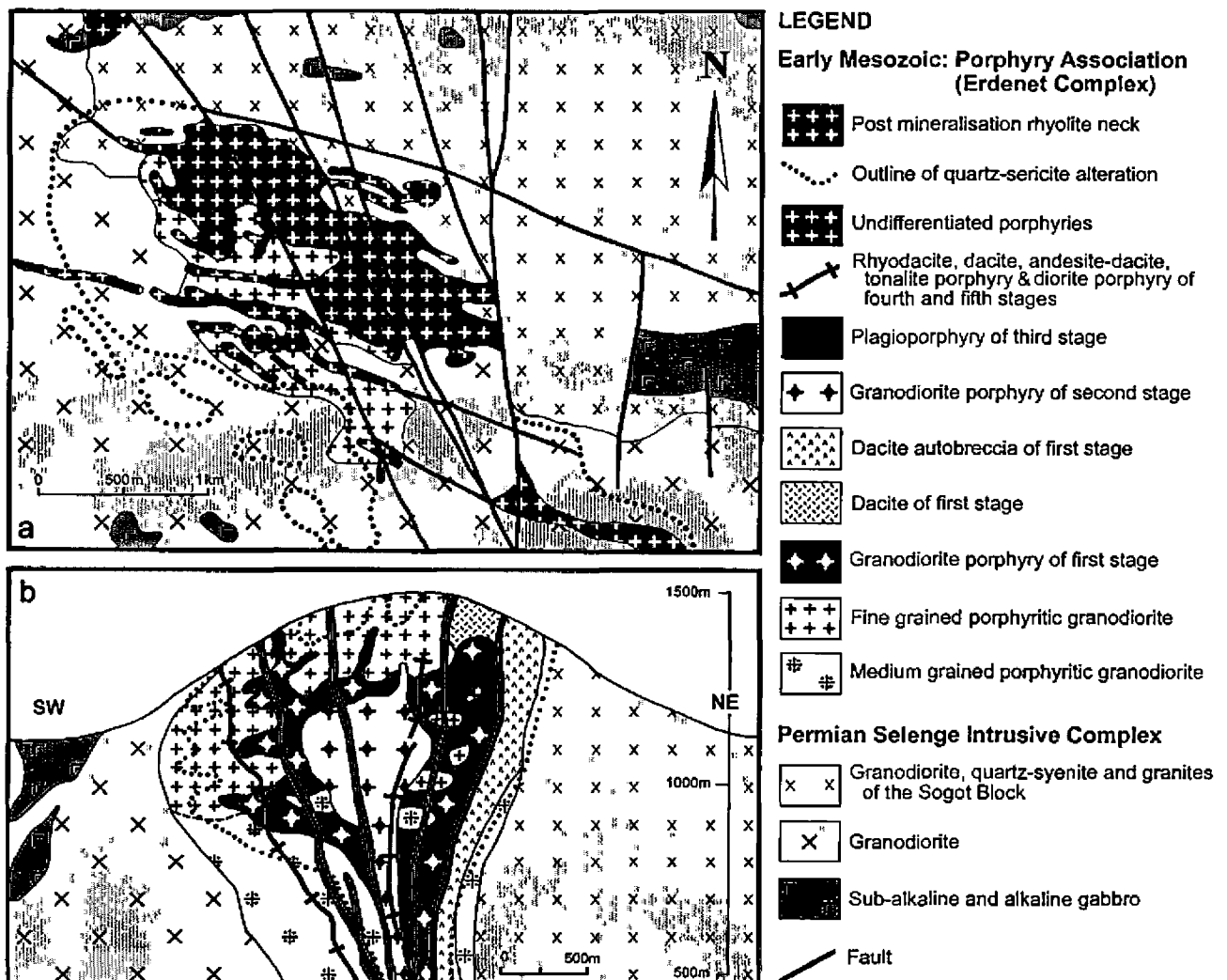


Figure 4: The geology and schematic structure of the Erdenetiin Ovoo (Modified Gavrilova *et al.*, 1990)

a. Surface map of the Erdenetiin Ovoo

b. Schematic cross section



described with K-Ar ages vary from 235 to 185 Ma (Sotnikov *et al.*, 1985). The porphyries are associated with volcanics of a trachyte-trachyandesite-alkaline basalt series occurring in volcanic, subvolcanic and intrusive settings, forming sheets, volcanic cones, dykes and sills.

The evidence of a genetic relationship between the Porphyry Association intrusions and Mesozoic volcanics (Koval, and Gerel, 1986, Koval *et al.*, 1985) can be summarised as follows: i) the crosscutting relation between the Porphyry Association and the third and latest phase of the Selenge Intrusive Complex, showing that the former is the younger; ii) the disruption in the trend of magmatic evolution of the Selenge complex that would be required if the ore-related porphyries were included as members of the complex; iii) the difference in the structural trend of the porphyries and that of the Selenge complex; iv) the difference in the environment of emplacement, between the shallow setting with associated explosive facies that characterise the porphyries, and the deeper hypabyssal conditions of the Selenge complex; v) the up to 40 Ma age difference between the Selenge complex and the porphyries; vi) the presence within the area of Mesozoic volcanics which are compositionally similar to the ore related porphyries; and vii) the intense propylitic, quartz-sericite and silica alteration developed in the both the Mesozoic volcanics and the subvolcanic porphyry bodies. Similar suggestions were presented by Yakovlev (in *Geology of Mongolia*, 1977).

The Erdenetiin Ovoo porphyry copper-molybdenum deposit is associated with, and concentrated within, subvertical, pipe-like intrusive bodies of late Triassic granodiorite porphyry of the Porphyry Association, with diameters of as much as 1.3 to 2.4 km, which drilling indicates to persist over a vertical extent of at least 1000 m. Disseminated, fracture and vein-controlled mineralisation occurs within the intrusive bodies, associated with granodiorite porphyry. The principal ore minerals are chalcopyrite, chalcocite, bornite and tennantite, with associated magnetite, galena, sphalerite and quartz.

There is a well defined mineral zonation within the deposit, from pyrite on the periphery, to a central high-grade core of chalcopyrite-bornite-chalcocite. Weak potassic

alteration, occurring as secondary biotite, was followed by pink feldspar veining where fracturing and veining of the host rock is not intensive. Widespread quartz-sericite and quartz alteration overprints the vein assemblages and is related to major structures and the contact zones of intrusions. A supergene enrichment blanket that ranges from 30 to 300 m in thickness is represented by a bornite-covellite-chalcocite assemblage, overlain by an oxide suite including cuprite, delafossite, malachite, azurite, brochantite, turquoise and native copper.

The Porphyry Association suite includes phaneritic and aphanitic rocks comprising a variable series of intermediate and felsic composition: porphyritic andesites, quartz-diorites, quartz-syenites, granodiorites, dacites, leucogranites and rhyolites. Plagioclase, K feldspar, quartz, hornblende and biotite phenocrysts (45-55 vol.%) are found within a groundmass of granular, subhedral, K feldspar, plagioclase, quartz and rare biotite, with accessory magnetite, apatite, zircon and sphene. Pyroxene is a common component of the quartz syenite. Primary mafic minerals are replaced by sericite, chlorite and carbonate. Plagioclase is characteristically rimmed by K feldspar, while fine hematite dusting of the feldspar causes a pink and reddish colouration. The porphyry suite belongs to a medium and high potassic calc-alkaline series, I-type and magnetite series suites.

The Porphyry Association is represented by a suite with variable intermediate and felsic compositions, from porphyritic quartz-diorite and andesite to leucogranites and rhyolites. There are two petrographic types: i) porphyritic and well crystallised; and ii) more volcanic in character, which are described as shallow or sub-volcanic facies. All display a petrographically very stable association of plagioclase and hornblende. Porphyritic quartz-diorites comprises plagioclase, pyroxene and hornblende, with around 25% phenocrysts of 2-3 x 1 mm, An<sub>50</sub> plagioclase. Feldspar-hornblende porphyry, with subhedral plagioclase, hornblende and biotite phenocrysts, has a granodioritic composition, and constitutes the main mineralised porphyry phase at the Erdenet deposit. Hydrothermal breccias are also present as dykes that are several metres wide, containing irregular quartz veinlet fragments.

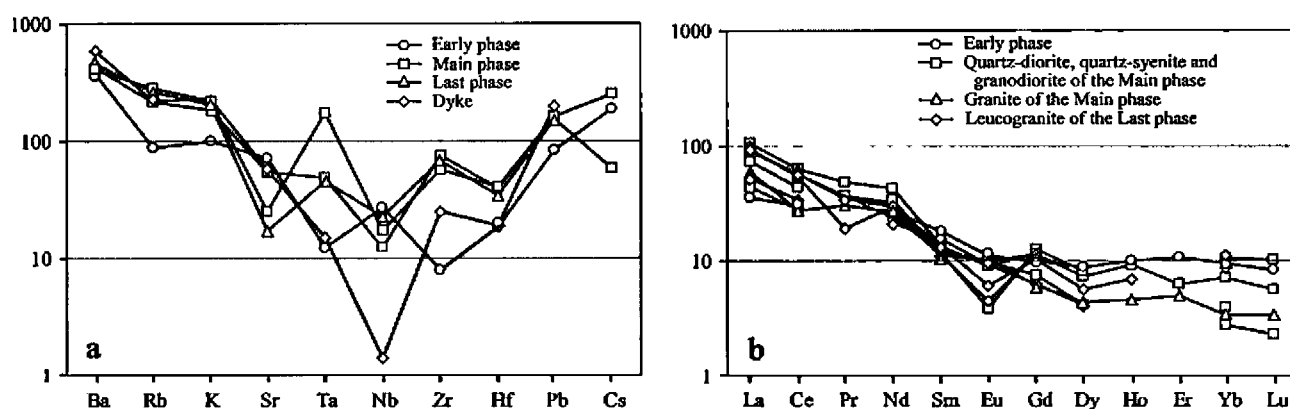


Figure 5: *Selenge Complex samples* - chondrite normalised (Taylor & McLennan, 1985)  
a. Trace element Spider Diagram, and b. REE pattern.

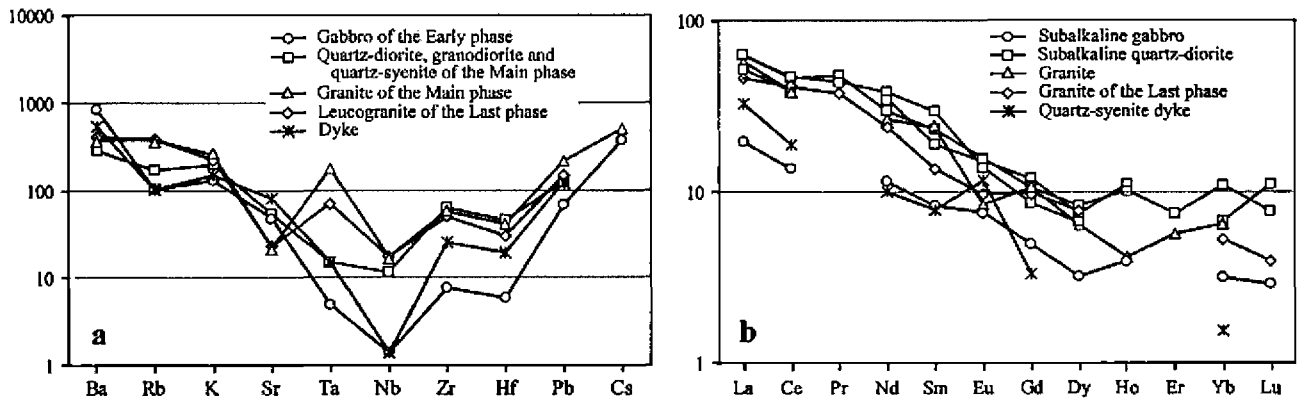


Figure 6: **Erdenet Pluton samples** - chondrite normalised (Taylor & McLennan, 1985)  
 a. Trace element Spider Diagram, and b. REE pattern.

**Age of the Deposit**

Sotnikov *et al.*, (1995), using K-Ar, age dated the host Selenge complex at 290-260 Ma. They had previously K-Ar dated the Erdenet porphyry complex at 235-185 Ma (Sotnikov *et al.*, 1985). Other K-Ar age dates for granites of the Erdenet Pluton yielded 226-245 Ma (Vacl, in Geology of Mongolia, 1977) and 226-221 Ma (Arakelyants, in Geology of Mongolia, 1977). Lamb and Cox (1998) conducted <sup>40</sup>Ar/<sup>39</sup>Ar dating on the sericite from the quartz-sericite alteration zone at Erdenet which yielded 207 Ma, which was thought to reflect the age of mineralisation. More recently, a Re-Os age date on molybdenite from the deposit yielded 240.7±0.8 Ma (Watanabe & Stein, 2000).

**Geochemistry of Magmatic Rocks**

The mineralised porphyry at Erdenet intrudes rocks of the Selenge Intrusive Complex which include a calc-alkaline, medium-K gabbro, granite to high-K monzonite and quartz syenite. These granitoids belong to an I-type, magnetite series (Ishihara, 1981), characterised by an elevated Na-alkalinity, and are enriched in Ba, Sr, Zr, with low contents of Rb and REE (Fig. 5). The REE concentration is characterised by a low fractionated pattern within both the Selenge Intrusive Complex and the Erdenet Pluton, as indicated by Tables 1 and 2. Trace element patterns for

granitoids of the pre-“Porphyry Association” Erdenet Pluton show a very similar distribution, with a more distinct depletion in Nb and Hf (Fig. 6). The REE distribution when compared to granitoids of the Selenge Complex, shows a similar pattern, but without an Eu minimum (Fig. 6).

Early Mesozoic volcanics, coeval with the mineralised porphyries, belong to the sub-alkaline series with high Al<sub>2</sub>O<sub>3</sub>, high to intermediate Mg, enriched in Ba, Rb, REE, Zr, Cr and Ni, and depleted in Nb (Table 3, Fig. 7). The REE distribution for all of the volcanic series is low fractionated, without distinct Eu anomalies. (Fig. 7).

The REE distribution in porphyritic intrusions can be used to distinguish barren from mineralised porphyries. Barren porphyries are enriched in REE, and are poorly fractionated, with a distinct Eu-minimum. Mineralised porphyries are, by comparison, depleted in REE, and more fractionated, without distinct Eu anomalies (Fig. 10). Altered porphyries are depleted in HREE.

Ore-related “Porphyry Association” porphyries contain plagioclase and mafic minerals and are also related to I-type, magnetite series, medium- of high-K, calc-alkaline series rocks (Table 4, Figs. 8, 9). The chondrite normalised pattern shows negative anomalies in Nb, Ta and Ti and a positive anomaly in Pb (Fig. 11). The general enrichment in incompatible elements is characteristic.

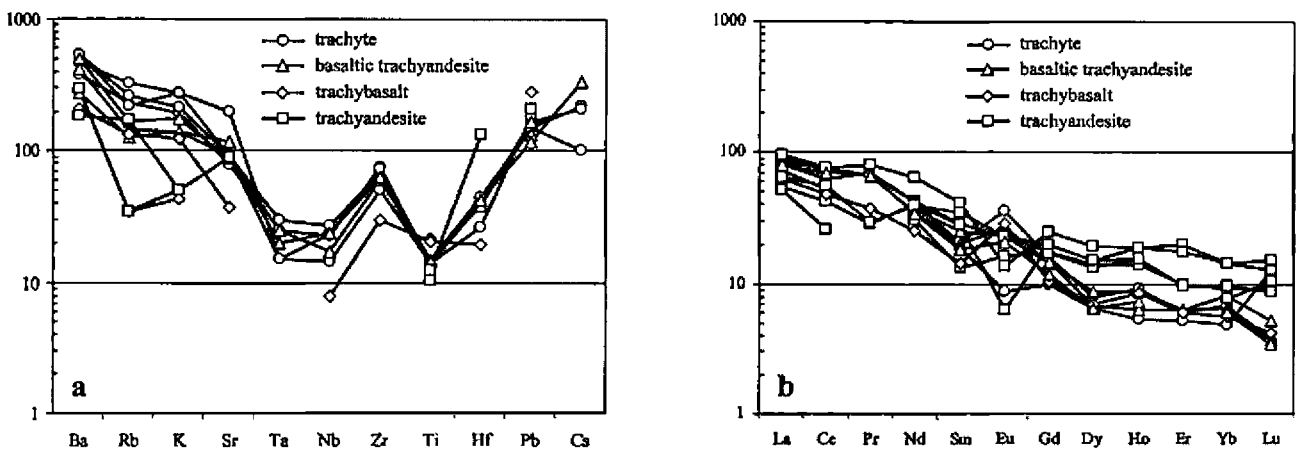


Figure 7: **Volcanic rocks of the Erdenet area** - Chondrite normalised (Taylor & McLennan, 1985)  
 a. Trace element Spider Diagram, and b. REE pattern.

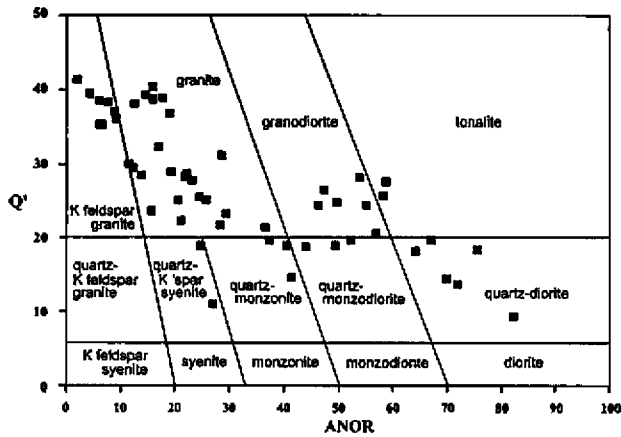


Figure 8. Erdenet Porphyry Association - ANOR - Q' classification diagram (Streckeisen & Le Maitre, 1979). ANOR=100\* An/(Or+An); Q'=Q/(Q+Or+Ab+An).

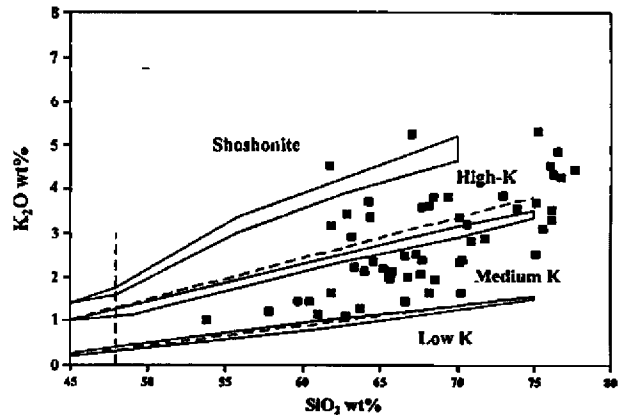


Figure 9. Erdenet Porphyry Association - SiO<sub>2</sub> vs K<sub>2</sub>O diagram (Le Maitre, 1989).

Granites and granodiorites from the Erdenet open pit mine are plotted on a Q'-ANOR diagram in the field of K-feldspar granite (Fig. 12) and in the K<sub>2</sub>O-SiO<sub>2</sub> diagram in the medium- and high K field (Fig. 12).

The distribution of trace elements in granites and granodiorites from the Erdenet open pit mine show depletion in Nb, Sr and Ti which are characteristic for island arc magmas (Fig. 13). Altered granites and porphyries are depleted in LREE (Fig. 13) and enriched in Mo. Enrichment in Al is also very clear (Fig. 14).

### Geophysics

Copper mineralisation is expressed by a zone of lower nT magnetic field values and by a gravity minimum. Induced polarisation surveys over the ore-bearing stock revealed an apparent chargeability anomaly of 3-17% with a maximum of 22.8%, while the resistivity varies from 200 to 800 Ωm.

A radioactive anomaly in the potassium channel alone is detected over the ore-bearing stockworks, accompanied by a noticeable reduction in the thorium and uranium components (Jargalsaikhan *et al.*, 1996).

### Deposit Structure

The ore field coincides with a local, 20 to 25 km long, structurally controlled corridor (Figs. 2 and 3), containing mineralised dykes and stocks of 2 to 2.5 km in diameter, with associated hydrothermal alteration. Zones of propylitisation and tourmalinisation are found within rocks peripheral to these controlling structures.

Four subvolcanic intrusives form a northwest trending ridge, while a fifth is predicted by geophysical data. These sub-volcanic bodies correspond to the main prospects/deposits of the ore field, which are as follows, from southeast to northwest: Oyut, Intermediate, Central, Northwest (Erdenet mine) (Fig.3), and Tsagaan Chuluut.

The Erdenet Pluton and deposit is located at the intersection of NE-SW, NW-SE, N-S and E-W fault trends, which have produced strong fracturing and permeability at their intersection. Sotnikov *et al.*, (1984) suggested these faults structurally controlled the mineralisation and hydrothermal alteration. Dextral movement on the N-S faults is interpreted to be syn-mineralisation, while sinistral movement on the E-W and NE-SW faults is believed to be post-mineralisation (Gavrilova *et al.*, 1989).

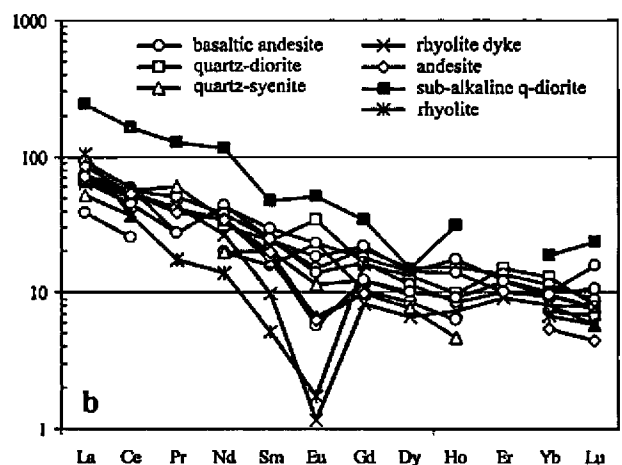
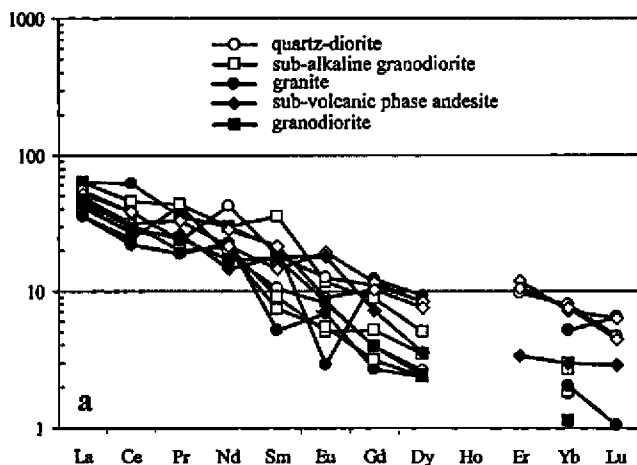


Figure 10: Porphyry Association of the Erdenet Pluton - chondrite normalised (Taylor & McLennan, 1985) a. REE pattern of ore-bearing, and b. Barren samples.

The southwestern and northeastern parts of the Erdenet deposit have steep boundaries intruded by dykes, while N-S and NE-SW trending faults roughly divide the Erdenet Pluton itself, into separate southeastern and northwestern zones, which contain intrusive breccias and mineralised stocks of the Porphyry Association (Gavrilova *et al.*, 1989).

(wt%)	1839	2503	2094	2068	2502	2502/4	1095	1846	1873
SiO <sub>2</sub>	50.20	52.82	67.20	70.33	74.37	73.74		63.74	72.20
TiO <sub>2</sub>	1.42	0.81	0.47	0.36	0.19	0.10		0.70	0.38
Al <sub>2</sub> O <sub>3</sub>	18.50	15.50	15.87	14.55	12.50	13.00		17.76	14.30
Fe <sub>2</sub> O <sub>3</sub>	5.44	2.74	1.52	1.07	1.22	0.51		2.51	1.41
FeO	4.56	4.74	1.94	2.12	1.58	1.71		2.01	1.01
MnO	0.19	0.13	0.05	0.06	0.04	0.09		0.06	0.07
MgO	4.76	6.30	1.11	0.75	0.25	0.30		1.79	0.28
CaO	8.33	9.70	2.65	1.72	0.66	0.60		3.25	0.85
Na <sub>2</sub> O	4.07	3.97	4.69	4.32	3.70	4.29		5.62	5.60
K <sub>2</sub> O	0.73	0.96	3.75	4.19	3.61	4.57		2.73	3.24
P <sub>2</sub> O <sub>5</sub>	0.28	0.20	0.17	0.12	0.06	0.06		0.18	0.06
LOI	1.05	1.58	0.31	0.19	0.21	0.39		0.42	0.43
Total	99.53	99.45	99.73	99.78	98.39	99.36		100.77	99.83
(ppm)									
La	13	16	38	34	33	35	22	27	19
Ce	29	27	60	54	54	51	26	42	32
Pr			6.6	5	4.8	2.6	4.2		
Nd	19	17	30	23	21	21	19	24	15
Sm	4.2	2.8	3.1	2.7	3.1	2.6	2.6	2.7	3.6
Eu	0.97	0.87	0.8	0.34	0.54	0.4	0.91	0.86	0.81
Gd	3.1	3.5	3.6	3.9	3.2	3.5	1.9	2.3	1.95
Dy	3.4	2.8		3.1	2.2		1.7	1.6	1.6
Ho	0.85	0.8			0.6		0.4		
Er	2.7	1.6					1.25		
Yb	2.4	1.8	1	2.6	2.8	2.2	0.85	0.7	
Lu	0.32	0.22		0.39			0.13	0.09	0.85

Note: 1839 - gabbro; 2503 - diorite; 2094 - granite; 2068, 2502, 2502/4 - leucogranite; 1846 - granodiorite; 1873 - granite porphyry.

Table 1: Major element and REE contents of the Selenge Complex granitoids.

(wt%)	1605	1852	2512	1604	1870	1863	2512/2
SiO <sub>2</sub>	49.87	64.07	60.29	66.97	69.32	71.17	66.22
TiO <sub>2</sub>	0.68	0.67	0.69	0.50	0.43	0.29	0.13
Al <sub>2</sub> O <sub>3</sub>	19.70	16.35	16.40	15.80	14.75	14.76	18.70
Fe <sub>2</sub> O <sub>3</sub>	9.32	3.23	1.92	4.05	1.93	1.61	1.00
FeO		2.08	4.31		1.83	1.29	0.72
MnO	0.14	0.11	0.07	0.11	0.06	0.04	0.02
MgO	5.91	1.65	2.40	1.07	0.90	0.49	0.30
CaO	9.40	3.73	4.90	2.33	2.05	1.84	3.70
Na <sub>2</sub> O	3.03	4.80	4.32	5.30	4.24	3.97	5.73
K <sub>2</sub> O	0.76	2.12	2.40	2.68	3.87	3.95	2.76
P <sub>2</sub> O <sub>5</sub>	0.07	0.16	0.21	0.15	0.08	0.07	0.04
LOI	1.10	0.82	1.48	0.82	0.35	0.88	0.38
Total	99.98	99.79	99.39	99.78	99.81	100.36	99.7
(ppm)							
La	7.1	23	19	23	17	21	12
Ce	13	45	37	44	39	37	18
Pr		6		6.5	5.1		
Nd	8.1	27	25	21	17	19	7
Sm	1.9	6.8	4.3	5.3	3.1	5.4	1.8
Eu	0.66	1.2	1.3	1.35	0.84	0.72	1
Gd	1.5	2.6	3.6	3.2	3	3.2	1
Dy	1.2	2.5	2.8	3.1	2.9	2.4	
Ho	0.33		0.94	0.86		0.35	
Er				1.85		1.4	
Yb	0.77	1.65	1.6	2.7	1.3	1.6	0.38
Lu	0.11	0.42		0.29	0.15		

Note: 1605 - gabbrodiorite; 1852 - sub-alkaline granodiorite porphyry; 2512 - sub-alkaline granodiorite; 1604 - quartz-syenite; 1870 - sub-alkaline granite; 1863 and 2512/2 - leucogranite.

Table 2: Major element and REE contents of the Erdenet Pluton granitoids.

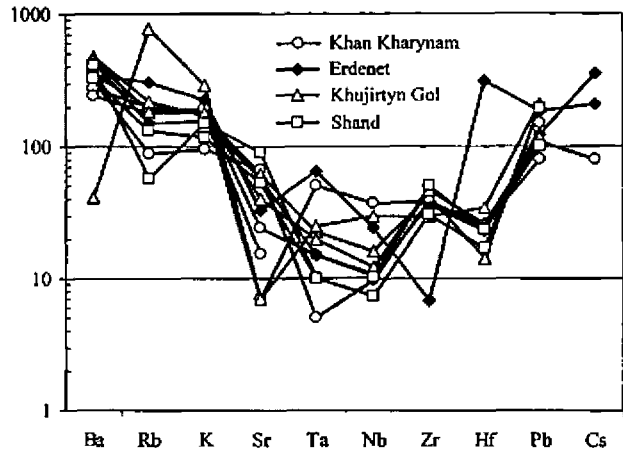


Figure 11: The porphyry association in the Erdenet area - chondrite normalised (Taylor & McLennan, 1985) trace element Spider Diagram.

The southeastern mineralised stock has a pear shape with near vertical contacts at deeper levels. The northwestern stock is horseshoe shaped at surface, with steep but irregular boundaries, which at a depth below 400 m, divides into two steep bodies.

### Ore-related Porphyries

The Erdenetiin Ovoo ore body coincides with "Porphyry Association" porphyry stocks and dykes, and as a result of supergene processes can be divided into three vertical zones, comprising from top to bottom: a leached and oxidised zone, secondary sulphide enrichment, and primary ores. The "Porphyry Association" porphyries can be sub-divided into:

**First stage porphyries** are the main syn-mineral phase, and accompany the introduction of the main economic mineralisation. Intrusives of this stage are dominated by hornblende-biotite granodiorite porphyry with lesser dacite. The granodiorite porphyry has up to 40% phenocrysts, comprising plagioclase (An<sub>28</sub>), hornblende and biotite set in a fine-grained groundmass of quartz, K feldspar and plagioclase (An<sub>14-8</sub>). Dacites have phenocrysts of plagioclase or are aphyric, and are present as veinlets, injections, matrix to the brecciated rocks and within zones of boudinaged granodiorite.

The intrusions of the first stage porphyries was accompanied by explosive activity and brecciation, producing eruptive breccias with granodiorite fragments cemented by granodiorite porphyries, and subsequently by dacites which cemented both brecciated granodiorites and granodiorite porphyries.

Granodiorite porphyries comprise the main mass of the mineralised intrusive stocks, with associated apophyses, satellites and dykes. The first stage porphyries form two connected isometric bodies. The southeastern stock covers an area of 1.0 x 0.8 km and has an inverted pear shape in vertical section, while the northwestern is 0.9 x 0.85 km (Gavrilova and Maksimuk, 1990), and has a horse shoe-shape in plan, with steep NW and sub-horizontal apophyses. At shallow to medium depths the northwestern body maintains a stock-like form, although at depths of 300 to 400 m it splits into two steeply dipping dyke-like bodies (Fig. 4).

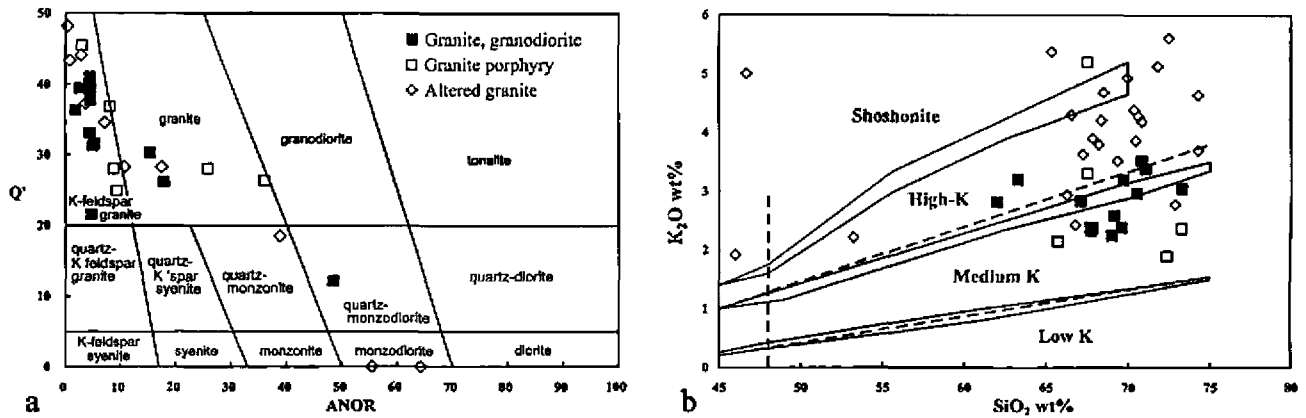


Figure 12: *Granites and porphyries from the Erdenet open pit mine* plotted on a. Q'-ANOR, and b. K<sub>2</sub>O-SiO<sub>2</sub> classification diagrams. Data from K. Naito *et al.*, (1996) included.

Two large explosion pipes up to 250 m across, which are connected at surface, form two isometric bodies, while two relatively large dacite fields, each of about 250 m in diameter are located respectively within the northwestern stock, and as a zone connecting the two stocks, while additional dacitic satellites are peripheral to the stocks.

**Second stage porphyries** are represented by granodiorite and granite porphyries. The granite porphyries are pink-grey and comprise 0.8-5 mm plagioclase (An<sub>10-24</sub>), 3 mm quartz, and rare 0.9 mm hornblende and biotite to 1 mm, as phenocrysts set in fine-grained micropoikilitic, micrographic and spherulitic intergrowths of quartz and K feldspar. K feldspar occurs in spherulitic aggregates as large as 0.7-1.4 mm across. Granodiorite porphyries of the second stage are grey, massive rocks with around 40% phenocrysts of plagioclase An<sub>25-37</sub> (up to 4 mm across),

hornblende (to 265 mm long), chloritised biotite, quartz (to 3 mm) and very rare K feldspar, set in a fine-grained micropoikilitic and micrographic groundmass of K feldspar, plagioclase, quartz and ore minerals. These porphyries crosscut both granodiorite porphyries and dacites of the first stage, and quartz-sericite alteration.

**Third stage porphyries** are represented by biotite-plagioclase, plagiogranite and granodiorite porphyries as well as leucocratic granite porphyries and leucogranitic plagioporphyries (Gavrilova and Maksimiyuk, 1990). These rocks occur within a sub-latitudinal zone up to 1.3-1.4 km wide and crosscut both first and second stage porphyries.

Gavrilova and Maksimiyuk (1990) distinguished both **fourth and fifth stage porphyries**. They observed that the third stage porphyries were crosscut by younger porphyries

(wt%)	2001	2003	2008	2004	1854	2460/30	2460/31	2460/34	2460/36	1866	1864
SiO <sub>2</sub>	58.80	58.60	56.70	55.25	50.55	49.00	46.40	51.56		51.45	56.93
TiO <sub>2</sub>	1.02	1.05	1.10	1.06	1.61	1.53	1.59	1.05		1.68	0.73
Al <sub>2</sub> O <sub>3</sub>	18.95	17.60	17.04	17.88	18.43	17.65	18.70	18.60		16.3	16.58
Fe <sub>2</sub> O <sub>3</sub>	3.66	4.48	5.39	5.34	6.86	7.10	5.80	4.45		7.8	3.87
FeO	1.22	1.15	1.36	1.87	3.88	3.95	5.25	5.20		4.09	1.65
MnO	0.06	0.07	0.10	0.11	0.18	0.21	0.22	0.23		0.21	0.1
MgO	1.63	2.22	3.28	3.00	3.40	4.60	5.70	4.30		3.93	2.74
CaO	4.00	3.82	5.05	5.64	6.41	5.20	9.80	8.70		8.22	4.79
Na <sub>2</sub> O	5.50	5.30	4.99	5.11	5.05	4.05	3.08	3.65		4.9	3.66
K <sub>2</sub> O	3.61	3.86	3.05	2.60	2.23	0.75	0.51	0.31		0.42	2.37
P <sub>2</sub> O <sub>5</sub>	0.25	0.28	0.30	0.36	0.49	0.42	0.44	0.32		0.36	0.28
LOI	1.02	1.41	1.42	1.63	0.50	2.05	2.23	1.65		0.1	6.24
H <sub>2</sub> O											
Total	99.81	99.87	99.81	99.90	99.64	99.57	99.79	100.09		99.46	99.94
(ppm)											
La	30	33	31	35	35	27	20	19	23	24	30
Ce	61	73	73	69	73	50	41	25	46	54	66
Pr	9.5	9		9	11		3.9		5.1	4	
Nd	30	25	26	30	46	30	29	22	18	28	24
Sm	4.3	4.8	5.9	4.7	9.7	6.7	6.4	3.1	3.3	8.1	4.2
Eu	0.76	3.1	2	2.3	1.2	2	0.56	1.4	2.5	2	1.8
Gd	3	4.8	4.4	4.5	7.6	5.4	6.1	5.2	3.2	6	3.6
Dy	2.5	3	3.3	2.6	7.3	5.4	5.8	5.1	2.7	5.8	2.5
Ho	0.45	0.78	0.74	0.54	1.6	1.2	1.3	1.3	0.72	1.6	0.63
Er	1.3	1.5	1.6	1.6	4.9	2.5	2.4		1.5	4.4	
Yb	1.2	1.7	2	1.6	3.6	2.3	2.4	1.9	1.4	3.6	1.5
Lu	0.48	0.14	0.2	0.14	0.57	0.35	0.33	0.4	0.16	0.48	0.13

Note: 2001, 2003-trachyte; 2008, 2004-basaltic trachyandesite; 1854, 2460/30-trachybasalt; 2460/31, 2460/34-basalt; 1866-andesite-dacite; 1864-andesite.

Table 3: *Major element and REE contents of volcanics from the Erdenet Pluton granitoids.*

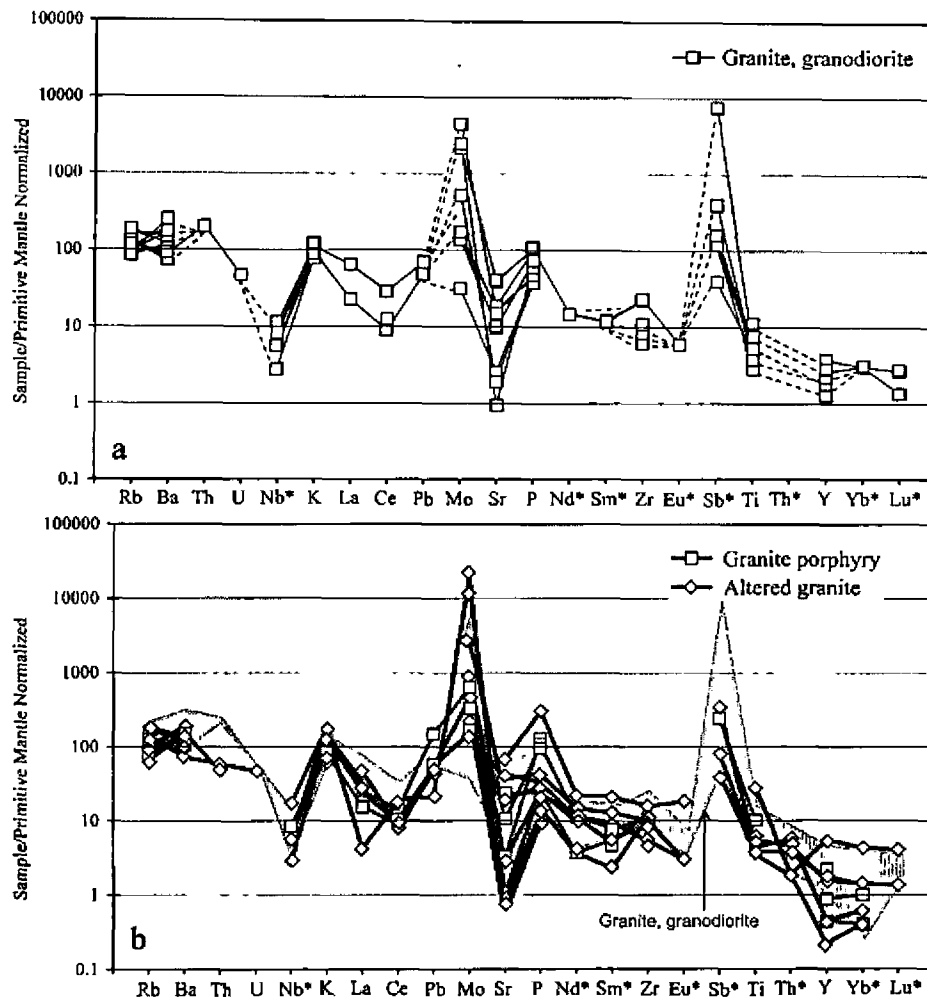


Figure 13. *Granites and porphyries from the Erdenet open pit mine* - spider diagram of a. relatively fresh and b. altered samples. Relatively fresh granites and granodiorites are shown by the grey shading on b. Normalization data after Sun & McDonough (1989).

of fourth stage, represented respectively by leucocratic porphyries and rhyodacites which occur as very rare dykes. The fifth stage porphyries are related diorite porphyries, amphibole-plagioclase andesites and granodiorite porphyries. Propylitic alteration is associated with this stage of intrusion.

*Post-ore stage intrusions* includes dykes and necks of latite, trachyandesite, rhyolite and syenodiorite porphyries, with

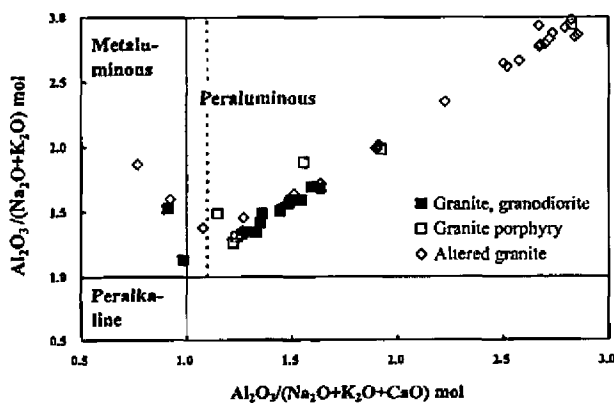


Figure 14: *Relatively fresh and altered granites and porphyries from the Erdenet open pit mine* plotted on a Shand diagram.

mainly sub-latitudinal orientations, dated at 185 Ma by K-Ar techniques (Sotnikov and Berzina, 1990). Dykes of younger basalts, andesites and basaltic trachyandesites have meridional trends.

### Hydrothermal Alteration

Three principal alteration assemblages define a near symmetrical alteration zonation at the Erdenet deposit (Kominek *et al.*, 1977; Yakimov and Davydov, 1988), centred on the granodiorite porphyry intrusion (of the Porphyry Association) and diminishing outward. The alteration zones, from the core to the periphery of the deposit are: i. sericitic (quartz-sericite) with local silicification, ii. intermediate argillic (chlorite-sericite), and iii) propylitic (chlorite and epidote-chlorite) and chloritic (Geology of Mongolia, 1977). The area covered by the total alteration halo (approximately 2.7 x 1.75 to 2.2 km) is more extensive than the porphyritic intrusion, which is around 2.4 x 1.4 km (Gavrilova and Maksimyyuk, 1990).

Quartz-sericite alteration dominates in the core of the deposit, decreasing in intensity towards the periphery. It has influenced between 25 and 45% of the host intrusions at Erdenet. In the central part of the orebody this alteration assemblage may comprise as much as 50 to 60%, and even

(wt%)	2462/25	2462/26	2020	2460/32	2460	2007	2006	2017	1856	2500/14	2066	2065
SiO <sub>2</sub>	53.82	57.90	65.75	66.65	68.24	71.84	67.81	75.65	76.73	63.19	61.92	76.50
TiO <sub>2</sub>	1.07	1.03	0.60	0.58	0.60	0.39	0.58	0.22	0.12	0.74	0.75	0.13
Al <sub>2</sub> O <sub>3</sub>	17.50	16.90	15.16	15.50	14.80	14.14	15.32	12.95	12.38	16.18	16.18	12.71
Fe <sub>2</sub> O <sub>3</sub>	5.07	5.94	3.14	2.30	1.53	1.98	2.45	1.21	0.89	2.78	2.21	0.63
FeO	4.30	1.61	2.08	1.72	2.15	0.65	1.58	0.86	0.72	1.97	2.41	0.68
MnO	0.17	0.13	0.12	0.05	0.05	0.08	0.07	0.05	0.04	0.07	0.08	0.08
MgO	3.49	2.78	1.82	1.10	1.04	0.42	1.31	0.12		2.07	2.12	0.18
CaO	8.76	7.05	3.44	2.80	2.32	1.05	1.85	0.42	0.74	3.03	3.13	0.15
Na <sub>2</sub> O	3.75	4.13	4.75	4.80	4.64	5.44	4.94	4.85	3.72	4.65	4.76	3.11
K <sub>2</sub> O	1.00	1.20	1.95	2.48	3.61	2.85	3.58	3.10	4.26	2.88	3.17	4.85
P <sub>2</sub> O <sub>5</sub>	0.13	0.17	0.11	0.19	0.13	0.08	0.14	0.03	0.01	0.26	0.23	0.02
LOI			0.80	1.88		1.01	0.40	0.52	0.29	1.91	2.68	0.86
H <sub>2</sub> O	1.04	1.07			0.85							
Total	100.10	99.91	99.72	100.05	99.96	99.93	100.03	99.98	99.90	99.73	99.64	99.90
(ppm)												
La	14	24	19	24	27	34	25	26	23	31	88	38
Ce	24	51	35	43	50	57	53	52	48	51	155	35
Pr				3.7		3.7	8.3	5.7	5.8	5.3	17.5	2.4
Nd	14	22	14	31	30	31	24	24	19	24	81	10
Sm	3.6	5.5	4.7	5.7	6.7	5.5	3.9	4.2	2.3	4.6	11	1.2
Eu	2	3	1	1.3	2	1.6	0.58	0.5	0.1	0.55	4.4	0.15
Gd	3.2	4.9	3.8	6.4	5.4	6.6	3	3.8	2.5	3	10.5	4.9
Dy	3.2	5.1	3.7	5.7	5.4	5.4	2.9	3.8	2.5		5.7	
Ho	0.53	0.84		1.3	1.2	1.5	0.4	0.77	0.62		2.6	
Er		3.7		3.4	2.5	3.1		3	2.3			
Yb	1.8	3.2	2	2.8	2.3	2.5	2	2.4	2	1.35	4.6	1.7
Lu	0.26	0.31	0.22	0.34	0.3	0.6	0.3	0.3	0.3	0.17	0.9	0.22

Note: 2462/25, 2462/26 - quartz diorite porphyrite; 2020, 2460/32, 2460, 2006 - granodiorite porphyry; 2007 - sub-alkaline granite porphyry; 2017, 1856 - feldspar porphyry, subalkaline quartz porphyry, rhyolite porphyry; 2500/14, 2066 - subalkaline quartz diorite porphyrite; 2065 - rhyolite porphyry.

(wt%)	2409/10	2000	2449/12	2449/5	1860	1865	1855	2447	1609	1852	1875	2513/23	2513/25
SiO <sub>2</sub>	63.43	63.55	65.65	70.33	67.71	75.23	61.91	59.78	63.80	64.07	65.80	67.40	66.07
TiO <sub>2</sub>	0.69	0.78	0.68	0.48	0.38	0.30	0.83	0.78	0.55	0.67	0.38	0.22	0.30
Al <sub>2</sub> O <sub>3</sub>	15.95	15.00	16.85	16.90	17.14	12.67	16.39	17.70	17.95	16.35	16.70	16.70	16.60
Fe <sub>2</sub> O <sub>3</sub>	2.57	3.20	1.90	1.26	1.77	1.43	3.39	3.42	4.66	3.23	1.51	1.90	1.80
FeO	1.02	3.94	2.69	0.89	0.93	0.72	3.12	2.69		2.08	1.29	1.62	1.71
MnO	0.06	0.20	0.08	0.01	0.04	0.03	0.13	0.12	0.08	0.11	0.13	0.03	0.02
MgO	1.62	1.21	1.65	0.38	0.77	0.21	2.29	2.20	1.52	1.65	1.06	0.90	1.10
CaO	3.20	0.71	0.53	0.45	1.63	0.47	4.53	5.50	4.04	3.73	2.67	2.20	2.40
Na <sub>2</sub> O	5.05	3.94	5.27	4.99	6.45	3.40	4.51	4.96	6.18	4.80	4.90	5.27	5.74
K <sub>2</sub> O	2.20	3.56	1.97	1.61	2.06	5.29	1.63	1.43	1.26	2.12	2.12	2.58	2.65
P <sub>2</sub> O <sub>5</sub>	0.21	0.17	0.13	0.07	0.13	0.04	0.22	0.17	0.18	0.16	0.13	0.15	0.19
LOI	3.94				0.88	0.43	0.69		0.76	0.82	3.22	1.12	1.50
H <sub>2</sub> O		2.21	1.79	2.25				1.20					
total	99.94	98.47	99.19	99.62	99.89	100.22	99.64	99.95	100.98	99.79	99.91	100.09	100.08
(ppm)													
La	13	23	16	13	15	23	20	18	15.5	19	17	29	26
Ce	23	44	30	21	26	59	37	30	26	37	28	45	57
Pr	5.8	5.9	2.7	2.6		4.8	3.2	4.5	3.6		3.3	5.1	7.9
Nd	13	21	15	16	14	21	30	15	10.5	20	12	17	22
Sm	2.4	8.2	2.1	1.2	1.7	4.8	4.2	3.4	4.1	4.9	4	3.9	3.5
Eu	0.71	1	0.44	0.6	0.48	0.25	1.1	1.7	1.55	0.79	0.72	0.45	0.73
Gd	1.2	2.7	1.6	0.82	0.96	3.7	3.4	3.6	2.2	3.1	1.2	1.5	2.2
Dy	1	1.9	1.3	0.9	0.89	3.5	3.2	3.2	1.35	2.9	0.93		
Er							2.4	3	0.84	2.6			
Yb	0.44	0.73	0.45	0.51	0.67	1.3	2	1.8	0.73	1.9	0.28	0.71	0.79
Lu				0.04		0.25	0.18	0.24	0.11	0.17			
Y	3.8	7	7.4	4.1	5	12	20	19	9.4	21	2.9	6.1	7.3

Note: 2449/5 - subalkaline granite porphyry; 2409/10, 2000, 2449/12, 1860, 2447, 1852 - subalkaline quartz diorite porphyrite; 1865 - leucogranite; 1855 - porphyritic andesite; 1609 - quartz diorite porphyrite; 1875, 2513/23, 2513/25 - granodiorite porphyry.

Table 4: Major element and REE contents of volcanics from the Erdenet Pluton granitoids.

up to 90% of the rock mass. It accompanies a stockwork of crosscutting and parallel fractures filled by thin ore bearing quartz veinlets, each fringed by selvages of quartz-sericite altered host rocks. The quartz-sericite vein fringes are from 0.3 to 6 cm wide, representing 5 to 10 times the thickness of the ore veins. Within the stockwork zone, the textures and structure of the original lithology are preserved.

The quartz-sericite alteration grades outwards into intermediate argillic (chlorite-sericite), to a propylitic (chlorite and epidote-chlorite) interval on the peripheries. At a distance of 1 to 1.5 km from the orebody there is no evidence of alteration, except for some tourmalinisation (Gavrilova and Maksimuk, 1990). A second stage of alteration is characterised by brecciation, recrystallisation and sericite-quartz, which overprints the previous stage of hydrothermally altered rocks. Silicification, with very rich chalcopyrite-bornite and molybdenite ores, is a characteristic and important component of this stage.

Quartz-sericite and peripheral intermediate argillic alteration, overprints an earlier phase of K silicate development, comprising quartz-K feldspar, biotite and magnetite. This K silicate alteration is not well developed/preserved at Erdenet, having been overprinted and largely obliterated by up to five subsequent episodes of quartz-sericite and quartz-chlorite. It is only preserved as remnants in the less fractured, deeper, central sections of the deposit

The width of the overall alteration zone tapers downward, e.g. at 1400 m above sea level the zone is 1.12 km wide, diminishing to 0.66 km at 920 m above sea level. The nature of the quartz-sericite alteration also varies with depth, and can be subdivided into two zones.

The deeper of these, between 900 and 1100 m elevation, represents a root zone, comprising separated, pillar-like, steep fracture controlled masses, interpreted on the distribution of elemental concentrations, as representing a zone of vertical/steep angle channels where ore-bearing hydrothermal solutions were focussed (Gavrilova *et al.*, 1989). The upper zone, between approximately 1100 and 1600 m above sea level, represents the main bulk of the ore deposit and appears to be essentially flat lying and occurs within and surrounding all of the Porphyry

Association stocks and satellite intrusions. It varies in thickness from 650 to 700 m in the SW, to 500 to 550 m in the core of the deposit, to 300 to 400 m to the NW. The overall structure of the hydrothermal system is reflected by the distribution of high silica content, which has been traced to a depth of 1600 m below surface.

Separate quartz-sericite alteration and silicification zones are also formed on the margins of the host porphyries, with a 650 m long and 50 to 150 m wide development along the northern contact of the main stock within host granodiorites, while on the southern contact only isolated lenses are recognised.

## Mineralisation

Khasin *et al.* (1977) detailed six stages of alteration and mineralisation as follows: i) pre-ore quartz-sericite, ii) quartz-pyrite, iii) quartz-pyrite-molybdenite, iv) quartz-pyrite-chalcopyrite, v) quartz-pyrite-galena-sphalerite, vi) post-ore gypsum-calcite with pyrite. Hypogene mineralisation is characterised by bornite, chalcocite and covellite, while oxidation produced Cu carbonates, oxides, phosphates and sulphate, native Cu and ferrimolybdenite.

Gavrilova *et al.* (1984) distinguished one pre-ore and five distinct ore stages, namely: Stage I - a quartz-pyrite association, represented by chalcopyrite-pyrite-quartz and molybdenite-quartz veinlets which are 1 to 2 cm, and rarely 3 to 5 cm in thickness; Stage II - quartz-molybdenite veining; Stage III - quartz-chalcopyrite-tennantite, characterised by sphalerite with associated chalcopyrite pyrite-quartz, molybdenite-quartz and pyrite-quartz; Stage IV - quartz-galena-sphalerite, and Stage V - overprinted bornite-chalcocite-covellite (Table 5). Stages IV and V are only poorly mineralised. Coincident magmatic activity, hydrothermal alteration and mineralisation characterise all stages. Only the volume of intrusion differs for each stage, progressively decreasing from stage I to V.

The first two ore stages of Gavrilova *et al.* (1984) are dominated by vein stockworks, while the last three are localised by dykes and associated fracturing. Sulphur isotope studies indicate two hydrothermal phases

Paragenetic Mineral Association	Form of Ore Mineral	Ore & Gangue Mineralogy	Characteristic Trace Elements
I. Quartz-pyrite	Impregnation, veinlets	Pyrite, quartz, sphalerite, chalcopyrite, molybdenite	Se, Ag, Co, Ni, Au
II. Quartz-molybdenite	Impregnation, veinlets	Molybdenite, quartz, pyrite	Mo, Re, Se
III. Quartz-chalcopyrite-tennantite	Impregnation, veinlets, inclusions in minerals	Chalcopyrite, tennantite, pyrite, sphalerite, enargite, galena	Ag, Se, Co, Ni, Au
IV. Quartz-galena-sphalerite (polymetallic)	Veinlets, impregnation	Galena, sphalerite, tennantite, pyrite	Co, Ni, Mo, As, Ag, Bi, Cd
V. Superimposed bornite-chalcocite-covellite	Impregnation, veinlets, inclusions in other minerals	Bornite, chalcocite, covellite	Pb, Zn, Ag, As, Sb

Table 5: Paragenetic mineralogical associations as reported by Gavrilova *et al.* (1984).



(Voinkov *et al.*, 1977). After intensive fracturing the first two ore stages formed the main ore body, dominated by zones of stockwork veining. Then, following a new fracturing, related to the introduction of dykes, further mineralisation was deposited characterised by fracturing and veining. Chalcopyrite accompanied both phases, while molybdenite was also introduced during the first phase.

The increment of the total ore grade introduced in each stage decreased from 0.3-0.8% Cu in stage I, to 0.09-0.19% Cu in stage III. The bulk of the Cu mineralisation is associated with stage I, Mo with stage II and Zn with stage III, while the latter two stages are characterised by high Ag. However, mineralisation is distributed irregularly, with the average Cu grade being 0.7 to 0.8%. Low grade ores contain 0.2 to 0.3% Cu, while the richest are up to 1% Cu (Gavrilova *et al.*, 1984).

Pyrite is the most common hypogene sulphide mineral. Gavrilova and Maksimyuk (1990) distinguished five pyrite associations: i) the earliest in quartz veinlets; ii) in molybdenite-quartz veinlets, iii) in association with chalcopyrite, tennantite and sphalerite; iv) as meta-crystals of pyrite; and v) in association with galena, sphalerite and tennantite. Molybdenite occurs in association with pyrite and quartz, and rarely with chalcopyrite. It forms hexagonal modification 2H, and is sometimes rhombohedral. Chalcopyrite is found in two paragenetic associations, namely: i) quartz-chalcopyrite-tennantite; and ii) with superimposed bornite-chalcocite-covellite. Tennantite also occurs in two associations: pyrite-chalcopyrite-tennantite-sphalerite and tennantite-sphalerite-galena. Enargite is rare, mainly in association with pyrite and quartz. Galena forms impregnations to produce mono-mineral aggregates or veinlets after sphalerite and tennantite. Sphalerite is represented by marmatite and cleiophane.

Hypogene copper mineralisation at the Erdenet deposit is dominated by chalcopyrite and bornite. Late stage covellite is also widespread, while bornite occasionally occurs as intergrowths with chalcocite. Besides Cu and Mo, the ore contain the trace elements: Se, Re, Au, Ag, W, Sn, Ga, Tl, Ge, Bi, Zn, Co, Ni, As and Sb which occur as isomorphic traces in pyrite, chalcopyrite, molybdenite, tennantite, galena and chalcocite (Gavrilova *et al.*, 1984). The most common gangue mineral is quartz.

An upper oxide zone which is up to 70 m in thickness, is characterised by an oxide-sulphide assemblage of cuprite, malachite, azurite, turquoise, brochantite, native copper, delafossite and antlerite. Copper grades in the upper oxidised zone are very variable. No well defined leached cap has been identified.

High grade zones are associated with a 30 to 300 m thick supergene enrichment blanket, where developed, within structurally controlled sheeted veinlets, with supergene chalcocite, which is crystalline, amorphous and collomorphic, replacing hypogene covellite and bornite. Supergene chalcocite is also developed on chalcopyrite within the stockwork zones.

Gavrilova and Maksimyuk (1990) provided additional information on the five stages of mineralisation at Erdenet,

which may be summarised as follows. During stage I, the main ore body formed by the impregnation of quartz-chalcopyrite-pyrite and quartz-molybdenite veinlets within granodiorite porphyry stocks. Stage II is dominated by quartz-chalcopyrite-molybdenite and quartz-molybdenite veinlets with centimetric dimensions, quartz-pyrite and pyrite veinlets which are 1 to 5 cm in thickness, and quartz breccia and quartz veins. All of these veinlets are similar to the A- and B-type veins of Gustafson and Hunt (1975). Stage III represents a regressive event within the deposit, with a characteristic assemblages of sphalerite and galena, but only poor Cu mineralisation (contributing between 0.09 and 0.19% Cu to the grade), and only occupies about 7-8 % of the total orebody's volume as veins similar to the D-type of Gustafson and Hunt (1975). Stages IV and V are late mineralisation phases recognised in drilling data. They consist of veinlets up to a few mm in thickness filled by quartz and sulphides. Alteration comprises sericite, chlorite, epidote and carbonate, with relict biotite, amphibole and plagioclase, while primary textures and pre-existing magnetite are preserved. This latter assemblage represents the propylitic phase of alteration, which is crosscut by the D-type veinlets.

Gavrilova and Maksimyuk (1990) concluded that the Erdenetiin Ovoo deposit had undergone three main alteration events, including: i) an early (pre-ore?) phase of magnetite rich K-silicate alteration (?), now largely obliterated by subsequent over-printing; ii) quartz-sericite (phyllic) and peripheral intermediate argillic sericite-chlorite alteration; and iii) propylitic alteration. Two retrograde stages are developed locally. The relative ages of porphyritic intrusives are determined by field observation of crosscutting relationships between veins and intrusions at intrusive contacts, and by crosscutting relationships between veins of various types.

### Isotopic Study

Tugarinov *et al.*, (1974) studied the sulphur isotopic composition of Erdenet ore. The  $\delta^{34}\text{S}$  value of the sulphides ranged from -3.3 to +2.7‰ with an average value of +0.4‰. Molybdenite is weakly enriched in  $\delta^{34}\text{S}$  (+1 to +1.5‰) compared to copper sulphides and pyrite. The values show no differences in vertical section. Such a homogenous sulphur composition is a result of homogenisation of sulphur before mineralisation. The value of  $\delta^{34}\text{S}$  for the sulphates ranges from +9.1 to +12.5 ‰. The study suggested two stages of hydrothermal ore formation, as detailed above.

### Concluding Remarks

The Erdenetiin Ovoo porphyry-copper-molybdenum deposit is located in the Orkhon-Selenge volcano-sedimentary trough which originally lay on an active Palaeozoic continental margin. The geodynamic evolution of the trough comprises an early intra-continental stage with rifting of a shallow continental shelf accompanied by the emplacement of sub-aerial mafic and felsic Permian and mafic Triassic volcanics (Fig. 2). The Permian volcanics of the Khanui Group largely comprise alkali-rich trachyandesites present as interlayered flows and pyroclastics, overlying a Vendian (late Neoproterozoic) to

early Cambrian basement with Palaeozoic (Devonian) granitoid intrusions, and Carboniferous sedimentary rocks. Plutons, ranging in composition from diorite, to granodiorite, quartz-syenite and leucogranite, intrude the Permian volcanic succession and exhibit similar compositional trends as the host volcanics. This suggests that the intrusions are related to, and possibly coeval with, the volcanics (Geology of Mongolia, 1973). The Triassic Mogod Formation volcanic rocks directly overlie the Permian sequence and are largely composed of trachyte flows, trachyandesite and basaltic-trachyandesite. Porphyritic sub-volcanic and hypabyssal intrusions genetically related to the trachyandesite volcanic series of early Mesozoic age, are related to a continental collision setting (Koval and Gerel, 1986, Gerel, 1990).

The mineralisation of the Erdenet porphyry system is controlled by the shallow-level emplacement of early Mesozoic intrusives. Three mineralisation related alteration phases have been distinguished: i) quartz-sericite with peripheral intermediate argillic (chlorite-sericite), ii) silica-rich; and iii) propylitic. A zonation of alteration is recognised from the deep and central parts of the porphyritic intrusion towards the shallower and outer parts. Early biotite-K feldspar and chalcopyrite are present in the deeper sections, while propylitic alteration occurs distal to a quartz-sericite zone extending beyond the open pit boundary. Propylitic alteration is represented by chloritisation of biotite, with the groundmass replaced by chlorite, epidote, sericite and epidote. Quartz-sericite alteration accompanies high-grade disseminated copper mineralisation. High grade zones have been overprinted by silicification with brecciation, quartz and molybdenite mineralisation.

Gavrilova and Maximyuk (1990) proposed a two level deposit model for Erdenet. The lower level, up to an elevation of 1100 m, coincides with the root zone of the hydrothermal-fluid system. It consists of separate columns and steep fracture controlled bodies. One of these can be clearly recognised as a regular mass with a diameter of about 1 km, which corresponds to the southeast porphyry stock, while a narrow 300 m long fracture zone is found in the southern part of the northwest porphyry stock, and another fracture zone coincides with the southwest satellite. In the interval from 1100-1160 m above sea level, the hydrothermal fluid system structurally changed and the upper level of the system envelops the intrusive stocks, satellites and dykes. This upper, largely flat lying zone varies in thickness from 650-700 m in the southeast, to 500-550 m in the core to 300-400 m in the northwest, and is composed of interlayered intermediate to strongly, to very strongly altered, steep to gently dipping rocks containing the main orebody. This upper level is subdivided into two sub-layers: a lower interval without significant silicification and an upper layer with strong SiO<sub>2</sub> alteration containing visible porphyroblastic quartz and quartz veinlets, and breccias with silica cement. The lower boundary of the quartz rich zone coincides with the lower limit of secondary sulphide enrichment.

The lower level of this deposit model corresponds to vertical and steep structural conduits that facilitated the migration

of ore-bearing hydrothermal fluids to the highly fractured, permeable upper level reservoir, where the fluids accumulated, became saturated, the hosts were hydrothermally altered, and the ore was deposited by boiling of the hydrothermal fluids below a gas cap. The dimensions of the upper reservoir and its shape are controlled by the cupola-like host structure and the encompassing volcanic rocks which formed a screen/cap.

Reliable geochronological data confirm that much of the porphyry alteration and mineralisation formed between 210 and 180 Ma, during the early Mesozoic. There is also evidence of a genetic relation between early Mesozoic volcanics and the Porphyry Association intrusives. A supergene blanket is superimposed within the quartz-sericite alteration interval.

We propose a model of porphyry generation that commences with the emplacement of a hot mafic magma into a parent chamber. Calculations (Gerel, 1990) show that this magma had a sub-alkaline basaltic-andesite composition. The tectonic environment included an active continental margin within continental crust, and the geochemical speciation of andesitic magma. The heterogeneity of the trace element distribution, sometimes even in one suite, antidromous evolution, differences in REE distribution in the volcanics, the high fractionation of REE, normative quartz of all series, and the presence of felsic fractionated members forming small porphyritic and subvolcanic intrusive bodies with a very long fractionation trend (up to 70-75% SiO<sub>2</sub>), can be interpreted to reflect a trend from mafic magmas to porphyritic rocks.

The model also envisages multiple partial melting of upper mantle material, changing levels of melting, and vertical movement of the magma chamber. This process culminated in the late crustal phase to form large chambers of dioritic magma, which cooled and fractionated to produce the full spectrum of sub-volcanic and shallow porphyries ranging from diorite- to granite-porphyry, as observed at Erdenet.

## Acknowledgement

Editorial review by Mike Porter, which has helped to produce the final manuscript, was greatly appreciated.

## References

- Badarch, G., Cunningham, W.D. and Windley, B.F., 2002 - A new terrane subdivision for Mongolia: Implication for the Phanerozoic crustal growth of Central Asia; *Journal of Asian Earth Sciences*, v. 21 (1), pp. 87-110.
- Berzina, A.P., Sotnikov, V.I. and Berzina, A.N., 2001 - H-isotopes in magmatic rocks from Cu-Mo deposits in Siberia and Mongolia; in Piesterzinsky *et al.*, (Eds.), *Mineral Deposits at the Beginning of the 21st Century*, pp. 377-380.
- Dejidmaa, G. and Naito, K., 1998 - Previous studies on the Erdenetiin Ovoo porphyry copper-molybdenum deposit, Mongolia; *Bulletin of the Geological Survey of Japan*. v. 49 (6), pp. 299-309.

- Erdenet Mining Corp., 2002 - EMC Annual Report 2002.
- Gavrilova, S.P. and Maksimyyuk, I.E., 1990 - Stages of formation of the Erdenet molybdenum-copper porphyry deposit (Mongolia). *Geologiya Rudnykh Mestorozhdenii*. No.6, pp. 3-17 (in Russian).
- Gavrilova, S.P., Maksimyyuk, I.E. and Orolmaa, D., 1984 - Features of magmatism and composition of ore of the copper-molybdenum deposit at Erdenetiin Ovoo; in: Endogenic ore formations of Mongolia. *Nauka*. pp. 101-105 (in Russian).
- Geology of Mongolia, 1977 - Volume 3. *Nedra*. 703p. (in Russian).
- Gerel Ochir, 1990 - Petrology, geochemistry and mineralisation of subalkaline Mesozoic magmatism in Mongolia. *Dr. of Science thesis*. Irkutsk, 40p. (in Russian).
- Gerel Ochir, 1995 - Mineral resources of the western part of the Mongol-Okhotsk fold belt; *Resource Geology*, Special Issue, No. 18, pp. 151-157.
- Gustafson, L.B. and Hunt, J.P., 1975 - The porphyry-copper deposit at El Salvador, Chile: *Economic Geology*, v. 70, pp. 857-912.
- Jargalsaikhan, D., Kazmer, M., Baras, Z. and Sanjaadorj, D., 1996 - Guide to the Geology and Mineral Resources of Mongolia; *Ulaanbaatar, GCS Co. Ltd.*, 330p.
- Kepezhinskas, V.V. and Luchitsky, I.V., 1973 - Permian volcanic association; in: Associations of volcanic rocks of Mongolia, their content and stratigraphic position. *M. Nauka.*, pp. 71-93 (in Russian).
- Khasin, R.A., Blagonravov, L.A. and Mikhailov E.V., 1977, in: Geology of Mongolia. *M. Nedra.* pp. 190-195 (in Russian).
- Khasin, R.A., Marinov, N.A., Khurtz, Ch. and Yakimov, L.I., 1977 - The copper-molybdenum deposit at Erdenetiin Ovoo in northern Mongolia; *Geology of Ore Deposits*. No. 6., pp. 3-15 (in Russian).
- Koval, P.V. and Gerel, O., 1986 - Volcanic association of porphyry copper mineralization in the Mongol-Okhotsk intraplate mobile zone; in: Geochemistry of volcanics from different geodynamic settings; *Novosibirsk, Nauka*, pp. 9-93 (in Russian).
- Koval, P.V., Gerel, O. and Smirnov, V.N., 1982 - Association of porphyritic intrusions in the Erdenet area; in: Problems of Geology and Mineral Resources of Central and Eastern Mongolia. *Thesis of IV Kherlen Expedition Symposium. Ulaanbaatar*, pp. 15-17 (in Russian).
- Koval, P.V., Gerel, O., Smirnov, V.N. and Tsenden, Ts., 1985 - Porphyritic intrusion from the Erdenet ore deposit: petrography and chemistry; *Problems of Geology and metallogeny of Mongolia. Ulaanbaatar*, pp. 67-103 (in Russian).
- Koval, P.V., Yakimov, V.M., Naigebauer, V.A. and Goreglyad, A.V., 1982 - Regional petrochemistry of Mesozoic intrusions of Mongolia. *Nauka*, v. 34. 207p. (in Russian).
- Krivtsov, A.I., 1983 - Geological principles of prognosis and exploration of copper-porphyry deposits. *M Nedra*, 256p.
- Kuznetsov, V.A., 1979 - Some problems of Mongolia's metallogeny and distribution of epithermal mineralization related to Mesozoic activation; in: Geology and magmatism of Mongolia. *M. Nauka*, pp. 68-77.
- Lamb, M.A. and Cox, D., 1999 - New  $^{40}\text{Ar}/^{39}\text{Ar}$  age data and implications for porphyry copper deposits of Mongolia; *Economic Geology*, v. 93 pp. 524-529.
- Le Maitre, R.W., Bateman, P., Dudek, A., Keller, J., Lameyre Le Bas, M.J., Sabine, P.A., Schmid, R., Sorensen, H., Streckeisen, A., Wolley, A.R. and Zanettin B., 1989 - A classification of igneous rocks and glossary of terms. *Blackwell*, Oxford.
- Naito, K., Dejidmaa, G., Dorjgotov, D., Nakajima, T. and Sudo, S., 1996 - Geochemical data of granites and ores of Erdenet mine; in Research on exploration and development of mineral resources in Mongolia. *Report of International Research and Development Cooperation ITIT Projects No. 91-1-3*, 1996, pp. 103-135.
- Mossakovsky, A.A., 1975 - Orogenic structures and volcanism of the Paleozoic in Eurasia and its position in the motion of continental crust; *Moscow*, p. 318 (in Russian).
- Mossakovsky, A.A. and Tomurtogoo, O., 1976 - Upper Paleozoic of Mongolia. *M. Nauka*, 127p.
- Perello, J., Cox, D., Garamjav, D., Sanjadorj, S., Diakov, S., Schissel, D., Munkhbat, T.O. and Oyun, G., -2001, Oyu Tolgoi, Mongolia: Siluro-Devonian porphyry Cu-Au-(Mo) and high sulfidation Cu mineralization with a Cretaceous chalcocite blanket; *Economic Geology*, v. 96, pp. 1407-1428.
- Saltykovsky, A.Ya. and Orolmaa, D., 1977 - Late Paleozoic-early Mesozoic volcanism of northern Mongolia and western Transbaikalia. *M. Nauka*, 202p. (in Russian).
- Sotnikov, V.I. and Berzina, A.P., 1989 - Prolonged discrete oriented development of ore-magmatic systems in copper-molybdenum formation; *Geology and Geophysics*. No.1. pp. 41-45 (in Russian).
- Sotnikov, V.I., Berzina A.P. and Bold, D., 1984 - Regularity of distribution of copper-molybdenum mineralisation of Mongolia; in Endogenic ore formations of Mongolia. *Nauka*, pp. 89-101 (in Russian).
- Sotnikov, V.I. and Berzina, A.P., 1985 - On the place of ore porphyries in the scheme for orogenic magmatism of copper-molybdenum ore knots of Mongolia; *Geology and Geophysics*, pp. 3-10 (in Russian).
- Sotnikov, V.I., Panomorchuk, V.A., Berzina, A.P. and Travin, A.V., 1995 - Geochronological boundaries of magmatism in the Cu-Mo porphyry deposit at Erdenetiin Ovoo. *Geology and Geophysics*. v. 36. pp. 79-89 (in Russian).
- Sotnikov, V.I., Ponomarchuk, V.A., Berzina, A.N., Berzina, A.P., Kiseleva, I.P. and Morozova, I.P., 2000 - Evolution of  $^{87}\text{Sr}/^{86}\text{Sr}$  in magmatic rocks from copper-molybdenum porphyry deposits; *Geology and Geophysics*. v. 418, pp. 1112-1123 (in Russian).
- Streckeisen, A. and Le Maitre, R.W., 1979 - A chemical

- approximation to the modal QAPF classification of igneous rocks. *Neues Jahrb. Mineral. Abh.*, v. 136, pp. 169-206.
- Sun, S.-S. and McDonough, W.F., 1989 - Chemical and isotopic systematics of oceanic basalts: implications for mantle composition and processes; in Saunders, A.D. and Norry, M.J., (Eds) *Magmatism in the Ocean Basins. Geological Society, London, Special Publication 42.* pp. 313-345.
- Taylor, S.R. and McLennan, S.M., 1985 - The continental crust: its composition and evolution; *Blackwell, Oxford.*
- Tugarinov, A.I., Voinkov, D.M., Grinenko, L.N. and Pavlenko, A.S., 1974 - Isotopic composition and sources of molybdenum-copper mineralisation of Mongolia; *Geochemistry*, No.2. pp. 173-178 (in Russian).
- Voinkov, D.M., Grinenko, L.N., Garamjav, D. and Jamsran, M., 1977 - About ore stages of hydrothermal origin at the Erdenetiin Ovoo Cu porphyry deposit, Mongolia (by S isotopes); *Izv. VUZ-ov. Geologiya i Razvedka*, No. 1. pp. 77-80 (in Russian).
- Watanabe, Y. and Stein, H.J., 2000 - Re-Os ages for the Erdenet and Tsagaan Suvarga porphyry Cu-Mo deposits, Mongolia, and tectonic implications. *Economic Geology*, v. 95, pp. 1537-1542.
- Yashina, R.M. and Matrenitsky, A.T., 1978 - Petrochemistry of volcanic and intrusive rocks of the Orkhon-Selenge Trough (Mongolia); *Izvestiya AN SSSR., Geol. Series*, v. 10, pp. 26-42 (in Russian).
- Zonenshain, L.P., Kuzmin, M.I. and Natapov, L.M., 1990 - Mongol-Okhotsk fold belt; in: *Tectonics of lithospheric plates of the territory of USSR. Book 1. M. Nedra*, pp. 282-319 (in Russian).
- Zonenshain, L.P., Kuzmin, M.I. and Natapov, L.M., 1990a - Mongol-Okhotsk fold belt; in Page, B.M., (Ed.), *Geology of the USSR: A plate tectonic synthesis; American Geophysical Union, Washington, Geodynamic Series*, v, 21, pp. 97-108.



# ***Biography***

---



## BIOGRAPHIES OF PRINCIPAL AUTHORS - VOLUME 2

---



**Robin Armstrong** currently manages the mining consultancy business at the Natural History Museum in London. His research interests include mineralisation associated with calc-alkaline magmatic systems and the application of GIS to mineral exploration. He graduated from the University of Glasgow in 1994 and then moved to France for a year to complete a DEA in volcanic and magmatic studies. Robin received his PhD from the University of Southampton where he researched ore forming processes in relation to porphyry copper style mineralisation in 1999. The majority of Robin's time is now devoted to the provision of petrological and GIS consultancy from the Natural History Museum.

**Contact details:** Natural History Museum, Department of Mineralogy, Cromwell Road, London SW7 5BD, UK. E-mail: R.Armstrong@nhm.ac.uk

---



**Mark Cloos** graduated from the University of Illinois at Champaign-Urbana in 1976 with a BS degree and from UCLA in 1981 with a dissertation concerning the origin of the Franciscan subduction complex in California. He joined the faculty at the University of Texas at Austin in 1981 as a structural geologist and is now Professor and Getty Oil Company Centennial Chair. His research interests involve all aspects of the geology of convergent plate margins.

**Contact details:** Department of Geological Sciences, University of Texas at Austin, Austin, Texas, 78712, USA. E-mail: cloos@mail.utexas.edu

---



**Kurt C. Friehauf** earned a BSc (Geology) from Colorado State University in 1989 and a PhD (Geological and Environmental Sciences) from Stanford University in 1998. His research has been focused on the evolution of porphyry copper deposits and the geology of Iron-oxide-REE-Cu-Au (IOCG) type ores. His current projects include work on the magmatic-hydrothermal evolution of porphyry copper-gold and skarn mineralization in the Ertzberg-Grasberg district of West Papua (Irian Jaya), Indonesia and Fe-REE mineralisation in the Bayan Obo district, Inner Mongolia, China. He is currently an Associate Professor of Geology in the Department of Physical Sciences at Kutztown University, Pennsylvania.

**Contact details:** Department of Physical Sciences, Boehm Building Room 135, Kutztown University, Kutztown, PA., 19530, USA; Phone: +1 610 683 4446; Fax: +1 610 683 1352; E-mail: friehauf@kutztown.edu

---



**Ochir Gerel** is currently professor and the head of the Department of Geology and Mineralogy, and Director of the Geoscience Centre, at the Mongolian University of Science & Technology in Ulaanbaatar. She graduated with an MSc in Geology and Petrology from the Charles University in Prague, Czech Republic, in 1964, and defended her PhD at the Institute of Earth Crust at the Siberian Branch (in Irkutsk) of the Russian Academy of Science in 1978. She subsequently completed a Doctor of Science degree in 1990 at the Institute of Geochemistry, also at the Siberian Branch of the Russian Academy of Science in Irkutsk. The subject of her Dr. Sc. thesis was "The Petrology and Metallogeny of Sub-alkaline Mesozoic Magmatism in Mongolia". From 1965 she worked at the Mongolian Technical University, now the Mongolian University of Science and Technology. She became the head of the Department of Geology and Mineralogy in 1978, and the Director of the Geoscience Centre in 2001. She is an academician of the International Academy of Higher Education and the Russian Academy of Natural Science. During the period of her leadership at the Department of Geology and Mineralogy, she has established and developed petrological and geochemical education and research in Mongolia. She has been involved in a range of research projects related to magmatism, metallogeny and mineralisation in Mongolia and the surrounding region over a period of several decades. In addition she has supervised MSc and PhD students, worked as a visiting researcher and professor at universities in Russia, Germany and Japan and published over 190 scientific papers since 1966.

**Contact details:** Department of Geology, Mongolian University of Science & Technology, P.O. 46, Box 520, Ulaanbaatar, Mongolia. E-mail: gerel@must.edu.mn





**Igor Golovanov** studied at the Central Asian State University (Tashkent, Uzbekistan) during 1951-1956 and obtained a Diploma with honours in Exploration Geology. From 1956 to 1976 he worked at the Geological Institute of the Academy of Sciences of Uzbekistan, initially as a junior researcher, before being granted a senior research post. From then until the present he has worked at the Institute of Mineral Resources holding such positions as the Head of the Department of Geology of Mineral Resources, the Deputy Director of Science and now as Senior Researcher. His research interests range from mineralogy and geochemistry to geology of ore deposits, and metallogeny of Uzbekistan and Central Asia. Prof. Golovanov undertook research on the oxidation zone of lead-zinc deposits and sulphide ores, metasomatites and the geological-structural specifics of the Almalyk and Muruntau ore regions. He led geological teams during the compilation of metallogenic and prospectivity maps of Uzbekistan and Central Asia. He has also worked as consultant for mining companies such as Barrick Gold, BHP Billiton, Rio Tinto, Oxus and PhelpsDodge during their operations in Uzbekistan and adjacent regions. His current positions at the State Geological Committee of Uzbekistan include: Leading Specialist on Geology of Ore Deposits and Metallogeny, Chairman of the Committee of PhD Degree Accreditation (Geology of Mineral Resources and Metallogeny), Chairman of Scientific-Editing Committee of Uzbekistan on Approval of Geological Maps Prior Their Publication.

**Contact details:** Scientific-Research Institute of Mineral Resources (IMR) of the State Geological Committee of the Republic of Uzbekistan, 11A Shevchenko Street, Tashkent, Uzbekistan;  
E-mails: mineral@cu.uz, golovanov\_i.m@mail.ru

---



**Hou Zengqian** was born in Gaocheng City, Hebei Province, China in 1961. He is an economic geologist and petrologist and was awarded his Ph.D from the China University of Geosciences in Beijing in 1988. He subsequently studied the Kuroko deposits and modern analogues at the Geological Survey of Japan in 1993-1994. He has more than 20 years experience in research on Chinese mineral deposit, including VHMS and porphyry copper deposits in southwestern China, and skarn and Sedex ores in eastern China. He is currently director of the Institute of Mineral Resources, CAGS, and chief-scientist of the national project "Metallogeny in the Tibetan Collisional orogenic Belt".

**Contact details:** Institute of Mineral Resources, Chinese Academy of Geological Sciences, Beijing 100037, China. E-mail: houzengqian@126.com

---



**John T. Paterson** graduated from the University of Montana in 2001 with a B.A. in Mathematics and a B.S. in Geological Sciences. He received an M.S. in Geological Sciences from the University of Texas at Austin in 2004. He did field work in the Grasberg Igneous Complex in June, 2002.

**Contact details:** c/- Department of Geological Sciences, University of Texas at Austin, Austin, Texas, 78712, USA.



**T. Mike Porter** completed a BSc Honours in Economic Geology at the University of Adelaide, South Australia in 1968. He is currently the Principal of Porter GeoConsultancy Pty Ltd, which specialises in arranging and leading professional development courses as the "International Study Tour" series which take industry geologists to mineral deposits and districts around the world. This has taken him to more than 250 of the world's more significant ore deposits. He has also been responsible for designing and arranging the technical program of two major conferences and planning, inviting papers and editing the two "Hydrothermal Iron Oxide Copper-Gold and Related Deposits: A Global Perspective" volumes. Prior to establishing his own company in 1996, he worked as an exploration geologist with CRA Exploration Pty Limited for more than 27 years. In this capacity he was involved in exploration for a range of base and precious metals, in a wide variety of geologic and geographic settings, both in Australia and overseas. He worked in the position of Chief Geologist from 1984 to 1996, principally in conceptual work, information synthesis and project generation, particularly from 1990. This included visits to over 150 significant base, ferrous and precious metal ore deposits on all continents, and subsequent research on their regional and local setting.

**Contact details:** Porter GeoConsultancy Pty Ltd, 6 Beatty Street, Linden Park, SA, 5065, Australia; Phone & Fax: +61 8 8379 7397; Email: [mike.porter@portergeo.com.au](mailto:mike.porter@portergeo.com.au)



**Bruce Rohrlach** spent his formative years in Papua New Guinea, obtained his undergraduate and honours degree in geology from the University of Adelaide in 1987, and worked for 14 years with WMC Resources Ltd – Exploration Division in Australia and the Philippines exploring for sediment-hosted Pb-Zn-Ag, syntectonic Cu, mesothermal lode Au, high and low-sulphidation epithermal, and porphyry ore systems. He completed his PhD (1997-2002) on the Tampakan Cu-Au deposit, Philippines, while on industry-sponsored study leave at the Research School of Earth Sciences, Australian National University. Dr Rohrlach presently works as an exploration consultant, and has undertaken work on projects in Turkey, Iran, Azerbaijan, Mongolia and in the Philippines. His academic experience includes: synthesis and reconstruction of volcanic-arc tectonic histories; application of ELA-ICP-MS zircon  $^{238}\text{U}$ - $^{206}\text{Pb}$ ,  $^{40}\text{Ar}$ - $^{39}\text{Ar}$  and K-Ar geochronology to resolve volcanic/magmatic histories; petrogenesis of metallogenetically fertile calc-alkaline magmas related to the genesis of porphyry and epithermal Cu-Au ore systems; application of ELA-ICP-MS for minor and trace element analysis; quantification of magmatic physico-chemical properties of arc magmas; crustal stress modeling; thermal modelling of magma chambers; and IR spectroscopy of alteration minerals and the application of stable isotope systematics for district-scale palaeohydrological studies.

**Contact details:** Suite C, Swiss Inn 1, Guevarra, Legaspi City, Philippines, E-mail: [brohrlach@hotmail.com](mailto:brohrlach@hotmail.com)



**Rui Zong-yao** was born at Jurong, Jiangsu Province, China in 1935 and graduated from the Nanjing Geological School in 1956, from the Chengdu college of Geology in 1960 and was granted a postgraduate degree from the Chinese Academy of Geological Sciences in 1967. Since then he has continued his research at the Institute of Mineral Resources of the Chinese Academy of Geological Sciences, specialising in the geology and geochemistry of mineral deposits, particularly porphyry copper style ores.

**Contact details:** Institute of Mineral Resources, Chinese Academy of Geological Sciences, 26 Baiwanzhuang Road, Beijing, 100037, P. R. China. E-mail: [ruizy@sina.com.cn](mailto:ruizy@sina.com.cn)



**Reimar Seltmann** graduated from the Technical University (Mining Academy) in Freiberg, Saxony (East Germany) where he specialised in exploration geology. His PhD thesis addressed decision-making criteria during prospecting for rare-metals (Sn, W) in the former Eastern block and aspects of resource evaluation. From 1987 he was a team leader at the Central Institute for Physics of the Earth of the East-German Academy of Sciences specialising in the metallogeny of porphyry breccia pipes. In 1992, at the new GeoResearchCenter (GFZ Potsdam), he shifted his research to granite-related metallogeny and published on textures in rare metal granites. He was a visiting research fellow at the Geological Survey of Canada and at Carleton University Ottawa (1995-1997). Since 1999 he has worked as a petrologist at the Natural History Museum in London (UK), where he initiated and coordinates as Director, the newly formed Centre for Russian and Central EurAsian Mineral Studies (CERCAMS). Reimar was the leader of IGCP project 373 (1997-2002), "Anatomy, textures and magmatic-hydrothermal transition processes of ore-bearing felsic systems in Eurasia" and is the leader of the follow-up IGCP project 473, "GIS metallogeny of Central Asia" (2002-2006), focusing on crustal geotraverses and deposit case studies applying GIS platforms. The project resulted in a series of Geology and Mineral Deposits GIS packages on Central Asia, Mongolia, Afghanistan, Urals and others compiled as collaborative efforts of the CERCAMS network for the mining industry. He has produced a large number of original research papers, monographs, metallogenic maps and reference guidebooks on metal provinces of the former Soviet Union, Mongolia and China and has led field trips to Uzbekistan, Kyrgyzstan, Russia (Urals, Sikhote Alin), Kazakhstan, Xinjiang and Mongolia for IAGOD and SEG.

**Contact details:** Natural History Museum, Department of Mineralogy, CERCAMS (Centre for Russian and Central EurAsian Mineral Studies), Cromwell Road, London SW7 5BD, UK  
Phone: +44 207 942 5042, E-mail: [rs@nhm.ac.uk](mailto:rs@nhm.ac.uk)



**Alireza Zarasvandi** completed his BSc and MSc degrees in the Shahid Chamran and Shiraz Universities respectively in Iran. He was subsequently awarded a PhD in Economic Geology from Shiraz University in 2004. The Title of his PhD thesis was "Magmatic and Structural Controls on the Localisation of the Darreh-Zerreshk and Ali-Abad porphyry copper deposits, Yazd Province, Central Iran. During the preparation of his PhD thesis he spent 8 months at Dalhousie University, Halifax, Canada for a short research program under the supervision of Dr. Marcos Zentilli. He is currently an assistant Professor at Shahid Chamran University at Ahwaz, Iran. His research interests are in the tectono-magmatic controls of porphyry copper deposits and the exploration for these deposits; the geodynamic and metallogenic characteristics of the Urumieh-Dokhtar belt; Ar/Ar and K/Ar geochronology; and fluid inclusions. Several of his papers have been published in international and internal Iranian journals and symposia.

**Contact details:** Department of Geology, Shahid Chamran University, Ahwaz, Iran.  
E-mail: [zarasvandi\\_a@cua.ac.ir](mailto:zarasvandi_a@cua.ac.ir) and [zarasvandi@yahoo.com](mailto:zarasvandi@yahoo.com)

